

# **A novel approach for lithium-ion battery selection and lifetime prediction**

Ph. D Thesis Dissertation

submitted for the degree of Doctor Engineer with International mention

**ELIXABET SARASKETA ZABALA**

Supervisors:

Dr. Jon Andoni Barrena Bruña (MU)

Dr. Lide Mercedes Rodriguez Martinez (IK4-Ikerlan)



Mondragon Goi Eskola Politeknikoa

Thesis defence: 18 September 2014



## **COPYRIGHT**

Attention is drawn to the fact that copyright of this Thesis rests with the author. A copy of this Thesis has been supplied on condition that anyone who consults it is understood to recognise that its copyright rests with the author. No quotation from the Thesis and no information derived from it may be published without appropriately referencing/acknowledging this work.

© Elixabet Sarasketa Zabala, 2014



Grateful thanks to the Ph. D Thesis examiners for accepting to evaluate this work that was carried out between December 2010-June 2014.

### **Ph. D THESIS COMISSION**

---

1. Hilmar Vidarsson, Höganäs AB, Sweden
2. Matthieu Dubarry, Hawaii Natural Energy Institute (HNEI), USA
3. Noshin Omar, Vrije Universiteit Brussel (VuB), Belgium
4. Gurpreet Singh, CIC energiGUNE
5. Ander Goikoetxea Arana, Mondragon Unibertsitatea (MU)
  
6. Jean-Francois Reynaud, CAF Power & Automation
7. Ion Etxeberria Otadui, IK4-Ikerlan
8. Ander Etxeberria Larrazabal, Mondragon Unibertsitatea (MU)

### **INTERNATIONAL Ph. D DISSERTATION REVIEWERS**

---

1. Liya Wang, XG Sciences, USA
2. Maciej Jozef Swierczynski, Aalborg University (AAU), Denmark



*Etxeko neskei*



I would like to thank IK4-Ikerlan for providing me the opportunity to carry out this Ph. D Thesis and Iñaki Goenaga Technological Centres Foundation for the grant given for its development. Thanks to Dr. Igor Villarreal (head of Alternative Generation Systems department) and Dr. Francisco Blanco (Electrical Storage and Thermal Management line manager and Energy Director) for the opportunity given to join the Electrical Storage Systems (ESS) group for performing this work.

I am grateful to my supervisors, Dr. Jon Andoni Barrena Bruña at Mondragon Unibertsitatea (MU) and Dr. Lide Mercedes Rodriguez Martinez for their guidance. My special thanks to Lide for her valuable suggestions and patience during the development of the present work.

I wish to express my gratitude to ISEA (Institute for Power Electronics and Electrical Drives) of RWTH Aachen University (Germany) for welcoming my internship in the Electrochemical Energy Conversion and Storage Systems Group led by Univ.-Prof. Dr. rer. nat. Dirk Uwe Sauer, with the close supervision of Jens Muennix. My sincere thanks to 'Modelling, Analytics and Lifetime Prediction' department for letting me feel as part of your team and for all the support received.

I would like to acknowledge CIC energiGUNE for the collaboration under the ETORTEK 2012 Strategic Program of the Basque Government, specially to Frederic Aguesse for his implication in the post-mortem characterisation. Thanks to Pierre Kubiak and Carmen López for helpful advice related to this work.

I would like to thank Orona and CAF Power & Automation for allowing the use of their applications as niche scenarios of cells selection methodology assessment.

Grateful thanks to all ESS team of IK4-Ikerlan at Arrasate and Miñao for their contribution. I would like to specially acknowledge to all my past and present partners in Batteries Group of Alternative Generation Systems department, whose support and advice have been essential for the development of the present work. Iñigo, Izaro, Isabel, Mikel, Maitane, Egoitz, Maider, Igor eta Lide, eskerrik asko!!

Izaro eta Iñigo, pitxiklista eta Goiuriako dama. Zenbat ordutako eztabaidak, beti adeitsu. Hitz hauekin zuen etengabeko laguntza eta adiskidetasuna eskertzerik ez badago ere, 30 segunduko, gutxieneko!, besarkadak beti edukiko ditut eskaintzeko. Eskerrik beroenak zuri ere Egoitz, lapurtutako ordu guztiengatik. Azken txanpan zure laguntza, beti prest!, ezinbestekoa izan da. Eman errelebua!

Maidier eta Lide, Lide eta Maidier. "Hasta la victoria siempre compañera!", "This way, this other way...", remando junto conmigo. El inicio de este viaje nos regaló nuestra amistad, elkarrekin topo egiteko aukera. Amaierak, egundoko akelarrea egitekoa. Quisiera de algún modo agradeceros de todo corazón vuestra inestimable ayuda y repartiros alegría, mucha alegría.

Eskerrak lankide guztiei. Muchas gracias a tod@s mis compañer@s. Bizikleteroei, a Magdalena. Eskerrak laguntza, animo eta oroimen polit guztiengatik.

Alex and Jens, I can hear "If you are crazy and you know it, clap your hands! ..." at the *keller* office! *Vielen dank* for your great support and every nice moment. Thanks also to the rest of the colleagues in ISEA.

Eskerrak baita ere nolabait Tesi honen itzalean egon zareten han-hemengo guztioi. I do not forget all the friends along the way of this Thesis: Ondarrun; Lekunberriko "piñata" talde guztia; friends in Aachen; Galiza; ...

Mattasunez betetako hurrengo hitzak beti nire alboan egon zaretenoi eskeini nahi dizkizuet, hitzak beti gutxi badira ere. Eskerrak amari, ahizpari, amamari (Aume, preparazu traji?), familia osoari. Amatxo, momentu oro zugandik jasotako indarra eta babes a ezinbestekoak izan dira honaino iristeko. Eskerrik asko nigan uste osoa izateagatik, eskerrik asko nirekin borroka egin eta izarren ditzira beti ikustarazteagatik, eskerrik asko etengabeko bidaian irriparre erraldoi batekin elkarrekin bizitako guztiagatik.

Eta nola ez, eskerrak zeuri ere Señorito, laguntza guztiagatik, pazientzia amaigabeagatik, patata tortila magikoengatik, zeure ta gure troparen babesagatik, ... Duela hile batzuk esan zenidan amestu badezaket, egin dezakedala, ta helmugara iristen lagundu didazu. Mila esker, bihotz-bihotzez.

*No one mentioned, no one forgotten.*

*Eskerrik asko danoi*  
*Muchas gracias a tod@s*  
*Many thanks to all*  
*Vielen dank an alle*

Elixabet

## ABSTRACT

---

There are many lithium battery technologies and their usefulness depends on applications and operating conditions. Even further, within a same battery technology, there are additional factors which depend upon manufacturer and design. The selection of a suitable battery technology and the specific commercial choice is a complex procedure affected by multidisciplinary factors. The available standards and procedures are limited for specific applications, such as electric vehicles (EVs) or consumer electronics, and most of them relate to testing protocols.

The need of a selection procedure for large format storage systems was identified as critical, towards introducing competitive storage solutions into the market by the Electrical Storage Systems Group of IK4-Ikerlan. This Thesis work proposes a robust methodology for lithium-ion (Li-ion) cells selection and lifetime prognosis for a battery to be efficient and reliable in specific applications. It pursues system investment and maintenance costs reduction, and definition of operation strategies for performance efficiency and useful lifetime optimisation.

The strategy of Li-ion cells selection lies in establishing differences among cells. Unsuitable options are rejected gradually, and fewer cells are tested as the experimental analysis deepens in subsequent stages. It aims to be a cost-effective process with broad applicability that can be integrated into the product development system. The analysis focuses on final target applications. Its adaptability to several real scenarios was evaluated for two different applications: residential elevator and catenary-free tramway. It was aimed at evaluating market specifications in various sectors different from automotive applications, where most battery manufacturers and developers focus their activities. The cells selection process comprises several steps: (i) determination of the required cell technical specifications and the real fields of operation, (ii) market research of large format Li-ion technologies, (iii) comparative performance analysis, characterisation and diagnostics of possible cell candidates, and (iv) analysis of lifetime, safety, costs and packaging issues. Not only is the battery pack performance optimisation pursued but also safe, long-lasting and cost-effective operation through the right cell selection and definition of appropriate operation strategies.

Long useful lifetime guarantee is required for target applications and ageing analysis at cell level is a key issue for ESS design. A novel approach is proposed for analysing the complex interaction between ageing processes and operating conditions. It comprises both cycle and calendar ageing but also their interaction in depth analysis. The preliminary step focuses on individually analysing and thoroughly validating both ageing by storage and ageing by working operation (cycling). Initial experimental work is not based on specific end-user profiles, as the methodology targets large applicability to different applications. This way, the main overall objective of this approach includes the development of validation procedures. The ageing analysis enhances the results by adding further steps of dynamic validation (under non-constant impact factors operating schemes) and combining the results of calendar ageing with those from cycling ageing within profiles close to realistic cell operation. The last validation step includes the adaptability of the ageing predictive tool to different targeted end-user scenarios.

The specific procedure for lifetime prognosis developed within this Thesis aims to provide a step ahead. It pursues, on the one hand, the development of quantitative concise algorithms for long-term operation performance predictions, with reduced experimental work. On the other, realistic and scalable widespread of the model to different applications. It provides comprehensive useful life analysis but it also enables distinguishing cell degradation just in the course of the time, which is relevant for many of the most common applications, such as uninterruptible power supplies (UPS) or EVs (*e.g.* a personal car spends about 90-95% of its lifetime in storage mode when parked).

The proposed overall methodology provides a cost-effective route with sufficient accuracy that allows selecting a storage solution and predicts its behaviour in a specific envisaged application with 1-2% root-mean-square error. This method estimates approximately a testing time of three months for the battery preliminary selection and one year for lifetime prediction. The defined procedure for lifetime prognosis has been initially implemented into an extensive platform to evaluate its applicability to other applications and storage technologies.

## LABURPENA

---

Litio baterien barruan hainbat teknologia ezberdin daude, eta bakoitzaren erabilera, aplikazio eta operazio baldintza ezberdinek ezartzen dute. Bateria teknologia berberentzako ere, fabrikatzaile eta diseinuaren arabera zenbait faktore aldatu egiten dira. Bateria teknologia eta bateria komertzial konkretuaren aukeraketa prozesua oso konplexua da, eta jakintza-alor anitzeko faktoreak biltzen ditu. Litio-ioi teknologiek erlazionatutako gaur egungo arau eta prozedurak aplikazio espezifikoetara mugatuak daude, ibilgailu elektrikoa edo kontsumo-elektronikara kasu, eta gehienak proba protokoloetan ardaizten dira.

IK4-Ikerlanen energia elektrikoa biltegitratzeko sistemen ikerketa taldeak produktu lehiakorrek merkaturatzeko, litio-ioi baterientzat aukeraketa prozedura bat garatzeko beharra kritikoa zela identifikatu zen. Doktoretza Tesi honek metodologia sendo bat proposatzen du aplikazio espezifiko baterako litio-ioi gelaxka-aukeraketa eta bizitza-iragarpena egiteko, eta honekin biltegitratzeko sistema soluzio eraginkor eta fidagarriak garatzeko pauso erabakigarri bat ematen du. Inbertsio eta mantenu kostuen murrizketa eta, operazio estrategien definizioa (operazio-efizientzia eta bizitza-erabilgarriaren optimizazioa lortzeko xedearekin) dira garatutako metodologiaren helburu nagusiak.

Litio-ioi gelaxken oinarrizko ezberdintasunak definitzean datza aukeraketa strategiaren funtsa. Gelaxka desegokiak baztertu egiten dira etapetan mailaz-maila, eta era horretan, gelaxka kopurua gutxituz doan heinean analisi esperimentalak sakontzen doa. Aplikazio aunitzeko prozesu errentagarri bat izatea du helburu, eta produktu garapenerako sisteman txertatu daiteke. Analisia jomuga den aplikazioan oinarritzen da, eta bere moldagarritasuna frogatzeko bi aplikazio errealetan saiatu da: etxebizitzetarako igogailuetan eta katenariarik gabeko tranbietan. Bateria fabrikatzaile eta ikerketa talde gehienak automobilgintzan ainguratuta daudenean, lan honetan nahita aukeratu dira ibilgailu elektrikitik haratago doazen sektoreak, garrantzitsua baita giltzarri diren beste sektore hauetan dauden beharrei ere erantzuten jakitea. Gelaxka-aukeraketa prozesua etapa ezberdinetan banatzen da: (i) gelaxken zehaztapen teknikoaren eta operazio profil errealean definizioa, (ii) formatu handiko ioi-litio baterien merkatu-ikerketa, (iii) lehen aukeraketako gelaxken karakterizazio eta diagnostikoa, eta (iv) azterketa bat bizitza erabilgarria, segurtasuna, kostuak eta *battery pack*-aren eraikuntzan egon litezkeen arazo posibleak kontutan

hartzan dituen. Prozesu hau bateriaren errendimenduaren optimizaziotik haratago doa. Helburua funtzionamendu ziurra, iraunkorra eta errentagarria lortzea da gelaxka-aukeraketa zuzena eginez eta estrategia operazio egokiak aukeratzuz.

Bizitza erabilgarri luzea bermatzea eskatzen dute merkatuko aplikazioek, eta horretarako gelaxken degradazioa aztertzea funtsezkoa da energia elektrikoa biltegitratzeko sistemen diseinuan. Ikuspegi berritzaile bat proposatzen du tesi honek zahartze prozesuen eta operazio baldintzen arteko interakzio konplexuak aztertzeko. Ziklatze bidezko degradazioa (operazioan) eta biltegitratze-degradazioa (denborarekin), biak hartzen ditu kontutan, baina era berean, bien arteko interakzioaren analisi sakon bat egiten da. Lehen pausoak banakako analisisian oinarritzen dira, eta zorrozki baliozkotu egiten dira bakoitza bere aldetik, bai biltegitratze-degradazioa, baita ziklatze bidezkoa ere. Hasierako lan esperimental hau ez da profil espezifikoetan oinarritzen, metodologiaren helburua aplikagarritasun zabala lortzea baita. Horregatik, balioztatze prozedurak garatzea ikuspegi honen ataza nagusien artean kokatzen da. Emaitzekin batera osagarri, baliozkotze dinamiko zorrotzak (ikertutako estres-faktoreak denboran konstante ez dituzten profilekin) eta balioztatze konbinatuak egiten dira (gelaxken operazio errealetik gertu dauden profilen ziklatze bidezko degradazioa eta biltegitratze degradazioa konbinatuz). Balioztatzearen azken etapan garatutako iragarpen erremintaren aplikazio aniztasuna ebaluatzen da aplikazio egoera ezberdinak aztertuz.

Litio-ioi baterien bizitza erabilgarriaren pronostikoa egiteko Tesi honetan garatutako prozedura espezifikoak, hainbat abantaila ditu. Alde batetik, bizitza iragartzeko algoritmo kuantitatibo eta laburtuak lortzeko lan esperimentalaren minimizazioa. Bestetik, modeloak errealista eta eskalagarriak dira aplikazio ezberdinetarako. Gainera, metodologiak aldi berean posible egiten du biltegitratze-degradazioa soilki aztertzea, zeina garrantzitsua izan daitekeen adibidez elikatze sistema etengabea (*UPS*) edo ibilgailu elektrikoa bezalako aplikazioetarako (ohizko erabiltzaile baten automobila bere denboraren %90-95 biltegitratuta egongo da, hau da, aparkatuta).

Proposatzen den metodologia orokorrak litio-ioi biltegitratze soluzio baten aukeraketa errentagarri eta efiziente bat ahalbideratzen du, eta %1-2 RMS erroreaz aurreikusten du aplikazio espezifiko batean izango lukeen portaera. Hiru bat hilabete inguruko lan esperimentala eskatzen du gelaxken lehen aukeraketa burutzeko, eta urtebete inguruko bizitzaren iragarpen bat egiteko. Bizitza-iragarpena egiteko prozedura zehaztasun osoz plataforma batean inplementatu da, beste aplikazio eta biltegitratze teknologietan bere aplikagarritasuna ebaluatzeko asmoz.

## RESUMEN

---

Las aplicaciones objetivo y sus condiciones de operación determinan la utilidad de la gran variedad de tecnologías de almacenamiento ion-litio disponibles en el mercado. Incluso para una misma tecnología, hay factores adicionales que dependen de su diseño y del fabricante. La selección de la tecnología adecuada y la batería comercial específica requiere de un proceso multidisciplinar que abarca distintos factores. Las normas y procedimientos vigentes en relación a la tecnología ion-litio están dirigidas a aplicaciones específicas, como el coche eléctrico o la electrónica de consumo, y la mayoría se focalizan simplemente en los protocolos de ensayo.

La necesidad de implementar una metodología de selección de celdas, fue identificada como crítica para la integración en el mercado de productos competitivos basados en baterías de ion-litio, por el grupo de investigación de sistemas de almacenamiento de eléctrico de IK4-Ikerlan. Esta Tesis Doctoral propone una metodología robusta para la selección de celdas ion-litio y predicción de la vida útil de las mismas, como paso decisivo en el desarrollo de soluciones de almacenamiento eficientes y fiables. Los objetivos finales de la metodología desarrollada son la reducción de los costes de inversión y mantenimiento, y la definición de las estrategias de operación de la celda seleccionada, para optimizar el rendimiento en operación y su vida útil.

La estrategia de selección consiste en definir diferencias clave entre las distintas celdas ion-litio. Es un proceso comparativo, en el que las especificaciones de la aplicación final son el criterio de validación. La metodología se basa en el modelo de cascada; las celdas menos adecuadas se van rechazando gradualmente y cada vez son menos las pruebas específicas en etapas subsiguientes. De esta manera, el análisis experimental se profundiza cuanto menor es el número de celdas. El proceso busca la solución final con bajo coste y tiempo, es útil para distintas especificaciones de mercado nicho y puede ser integrado en el sistema de desarrollo de producto. La metodología desarrollada se ha implementado en dos aplicaciones industriales: elevación (ascensor residencial) y tranvía sin catenaria. Debido a que la gran mayoría de los fabricantes de baterías y grupos de investigación centran sus actividades en las distintas topologías del vehículo eléctrico, mediante este estudio se han abarcado aplicaciones distintas de la automoción en respuesta a la demanda industrial existente en otros sectores clave. El

proceso de selección de celdas se divide en varias etapas: (i) definición de las especificaciones técnicas de la celda y perfiles reales de operación, (ii) investigación del mercado de baterías ion-litio de gran formato, (iii) caracterización y diagnóstico de las celdas preseleccionadas, y (iv) análisis de la vida útil, seguridad, costes y posibles problemas relacionados con la construcción del *battery pack*. El alcance de dicho proceso va más allá de la optimización del rendimiento de la batería. Se persigue el funcionamiento seguro, duradero y rentable mediante la correcta selección de la celda y definición de estrategias de operación adecuadas.

Analizar la degradación de la celda es esencial para el diseño de sistemas de almacenamiento de energía, ya que se ha de garantizar una larga vida útil en respuesta a los requerimientos de las aplicaciones del mercado. Por ello, se propone un enfoque novedoso que pretende estudiar la relación compleja entre los procesos de degradación de las celdas ion-litio y las condiciones de operación reales. El análisis comprende la degradación por ciclado (operación) y por paso del tiempo, así como su interacción. Primeramente se centra en el análisis individual y validación exhaustiva de la degradación por ambos modos de operación (ciclado y almacenamiento), sin ensayar perfiles específicos, ya que uno de los objetivos de la metodología es alcanzar una amplia aplicabilidad a distintos supuestos reales. Por ello, este enfoque incluye como tarea principal el desarrollo de los procedimientos de validación. Los resultados se complementan exhaustivamente mediante ensayos de validación dinámica (perfiles en los que los factores de estrés estudiados no son constantes en el tiempo) y la combinación de la degradación por almacenamiento y ciclado mediante perfiles similares, pero no concretos, a la operación real. La última etapa de validación incluye la evaluación de la versatilidad de la herramienta de predicción desarrollada para diferentes escenarios de aplicación.

El procedimiento específico desarrollado en esta Tesis para el pronóstico de vida útil de celdas ion-litio proporciona varias ventajas. Por un lado, la minimización del trabajo experimental para el desarrollo de algoritmos cuantitativos concisos de predicción de vida. Por otro lado, los modelos son realistas y escalables a diferentes aplicaciones para analizar exhaustivamente la vida útil de los sistemas de almacenamiento. Además, la metodología permite analizar, al mismo tiempo, la degradación únicamente por el paso del tiempo, lo cual es relevante para muchas de las aplicaciones industriales como los sistemas de alimentación ininterrumpida o el coche eléctrico (por ejemplo, el coche de un usuario convencional está del 90 al 95% de su vida útil almacenado, es decir, estacionado).

La metodología general propuesta permite la selección de una solución de almacenamiento ion-litio de manera rentable y eficiente, y predice su comportamiento en una aplicación específica con error RMS de sólo 1-2%. Se estiman aproximadamente tres meses de trabajo

experimental para la preselección de la celda y un año para la predicción de la vida mediante este método. El procedimiento para el pronóstico de vida se ha implementado exhaustivamente en una plataforma para evaluar su aplicabilidad a otras aplicaciones y tecnologías de almacenamiento.



## CONTENTS

---

ABSTRACT / LABURPENA / RESUMEN.....	<i>xi</i>
LIST OF FIGURES.....	<i>xxiii</i>
LIST OF TABLES.....	<i>xxxv</i>
SYMBOLS AND ABBREVIATIONS.....	<i>xxxix</i>
GLOSSARY OF TERMS.....	<i>xlvi</i>
<b>Chapter 1</b> .....	<b>1</b>
<b>1. INTRODUCTION</b> .....	<b>3</b>
1.1 FRAMEWORK AND MOTIVATION.....	3
1.2 AIM OF THE THESIS WORK.....	23
1.3 THESIS OUTLINE.....	24
<b>Chapter 2</b> .....	<b>25</b>
<b>2. EXPERIMENTAL TEST PROCEDURES</b> .....	<b>27</b>
2.1. TESTS OF GENERAL USE.....	27
2.2. TESTS FOR LIFETIME PREDICTION.....	35
<b>Chapter 3</b> .....	<b>37</b>
<b>3. DEVELOPMENT OF THE METHODOLOGY FOR CELLS SELECTION</b> .....	<b>39</b>
3.1 TASK 1: PERSPECTIVE AND CRITERIA.....	40
3.1.1 Specific cell parameters related to chemistry choice.....	43
3.1.2 Performance of high power (HP) and high energy (HE) cells related to electrodes processing.....	47
3.1.3 Understanding cell design.....	50
3.1.3.1 Effect of chemistry and construction on performance.....	50
3.1.3.2 Cell manufacturing and casing.....	52
3.1.4 Task 1 conclusions.....	58
3.2 TASK 2: CELLS SELECTION.....	59
3.2.1 Stage 0: emergent electric energy storing market research.....	60

3.2.2 Stage 1: requirements of application and evaluation of available cells .....	60
3.2.3 Stage 2: screening .....	63
3.2.4 Stage 3: detailed analysis of selected cells.....	68
3.2.5 Stage 4: optimisation procedure.....	71
3.3 TASK 3: PROCEDURE FOR CYLINDRICAL CELLS POST-MORTEM ANALYSIS .....	73
3.3.1 Cell disassembly and characterisation methodology .....	75
3.3.1.1 Cylindrical cells disassembly and components extraction .....	77
3.3.2 Physical-chemical and electrochemical characterisation of cell components.....	85
3.3.2.1 Electrodes porous structure characterisation by mercury porosimetry (MIP).....	85
3.3.2.2 Elemental analysis by ICP-OES.....	89
3.3.2.3 Harvested electrodes preparation for half-cells electrochemical measurements.	90
3.3.3 Summary of Li-ion cells post-mortem characterisation methodology .....	93
3.4 SUMMARY AND CONCLUSIONS.....	95
3.4.1 Overview of the methodology for cells selection.....	95
3.4.2 Summary of Chapter 3 and view of the rest of the Thesis work .....	98
<b>Chapter 4 .....</b>	<b>99</b>
<b>4. METHODOLOGY IMPLEMENTATION: CELL SELECTION FOR SPECIFIC APPLICATIONS .....</b>	<b>101</b>
4.1 RESIDENTIAL ELEVATION APPLICATION .....	103
4.1.1 Stage 1: requirements of the application and evaluation of available cells .....	103
4.1.1.1 Requirements of the application.....	103
4.1.1.2 Evaluation of available cells and definition of the optimum operation range .	105
4.1.2 Stage 2: screening .....	109
4.1.2.1 Testing conditions .....	109
4.1.2.2 Results and discussion.....	111
4.1.2.3 Stage 2 summary and general conclusions .....	129
4.2 TRAMWAY APPLICATION.....	132
4.2.1 Stage 1: requirements of the application and evaluation of available cells.....	132
4.2.1.1 Evaluation of available cells and definition of the optimum operation range...	133
4.2.2 Stage 2: screening .....	136
4.3 OVERVIEW OF THE METHODOLOGY IMPLEMENTATION .....	140
4.3.1 Power capability evaluation .....	140
4.3.2 Cells disassembling and design analysis .....	142

<b>Chapter 5</b> .....	<b>145</b>
<b>5. AGEING AND LIFETIME ANALYSIS</b> .....	<b>147</b>
5.1 INTRODUCTION.....	149
5.2 LIFETIME PREDICTION METHODOLOGY .....	155
5.3 CALENDAR LIFETIME.....	161
5.3.1 Experimental .....	161
5.3.1.1 Accelerated calendar ageing tests conditions .....	163
5.3.1.1.1 Calendar ageing and static validation tests.....	163
5.3.1.1.2 Dynamic validation storage tests.....	164
5.3.2 Results and discussions .....	165
5.3.2.1 Cell calendar performance fade evaluation .....	165
5.3.2.2 Calendar ageing predictive model.....	177
5.3.2.3 Real scenarios evaluation .....	181
5.3.3 Calendar ageing main conclusions.....	183
5.4 CYCLE LIFETIME.....	184
5.4.1 Experimental .....	184
5.4.1.1 Accelerated cycling ageing tests conditions.....	185
5.4.1.1.1 Cycle ageing and static validation tests.....	185
5.4.1.1.2 Dynamic validation cycling tests .....	186
5.4.1.2 Post-mortem analysis .....	187
5.4.2 Results and discussions .....	188
5.4.2.1 Cell cycling performance fade evaluation.....	189
5.4.2.2 Cycle ageing predictive model.....	207
5.4.3 Cycle ageing main conclusions.....	220
5.5 COMPLETE LIFETIME MODEL .....	222
5.5.1 Validation approaching real operation .....	224
5.5.1.1 Experimental .....	224
5.5.1.2 Results and discussions .....	226
5.5.2 Validation using realistic profiles .....	229
5.5.2.1 Experimental .....	230
5.5.2.2 Results and discussions .....	233
5.5.2.2.1 Non-symmetric cycling profiles.....	233
5.5.2.2.2 Complex operation conditions.....	234
5.6 REVISION OF THE METHODOLOGY FOR LIFETIME PREDICTION.....	238
5.6.1 Experimental .....	238
5.6.2 Results and discussion .....	239
5.7 SUMMARY AND CONCLUSIONS OF LIFETIME PROGNOSIS APPROACH.....	242

5.8 LIFETIME EVALUATION FOR A RESIDENTIAL ELEVATOR .....	244
5.9 AGEING MODEL APPLICABILITY. FUTURE WORK TO EXTEND THE METHODOLOGY .....	247
<b>Chapter 6</b> .....	<b>251</b>
<b>6. OVERALL SUMMARY AND CONCLUSIONS</b> .....	<b>253</b>
<b>BIBLIOGRAPHY</b> .....	<b>259</b>
<b>APPENDIX A. LITHIUM-ION TECHNOLOGY: FUNDAMENTALS, CELL COMPONENTS AND CONSTRUCTION</b> .....	<b>A5</b>
<b>APPENDIX B. STANDARDS AND MANUALS</b> .....	<b>A23</b>
<b>APPENDIX C. EQUIPMENT AND ANALYTICAL SPECIFICATIONS</b> .....	<b>A27</b>
<b>APPENDIX D. DATABASE OF LITHIUM-ION BATTERIES MARKET. WORLD-WIDE MANUFACTURERS AND TECHNOLOGIES</b> .....	<b>A37</b>
<b>APPENDIX E. SAFETY ANALYSIS FOR CELLS SELECTION</b> .....	<b>A49</b>
<b>APPENDIX F. PUBLICATIONS AND PARTICIPATION IN CONFERENCES</b> .....	<b>A63</b>

## LIST OF FIGURES

---

<b>Figure 1-1.</b> Objectives development in the value chain of electrical ESS at IK4-Ikerlan.....	3
<b>Figure 1-2.</b> Potential range of applications of electrochemical rechargeable battery technologies (Source: Samsung).....	4
<b>Figure 1-3.</b> Distribution of various battery technologies according to their energy and power densities. Specifications at cell level. EDLC: Electric Double-Layer Capacitors; Li-Cap: lithium-carbon capacitor; NiCd: nickel–cadmium; NiMH: nickel–metal hydride; NaNiCl <sub>2</sub> : sodium–nickel chloride (ZEBRA (Zero Emission Battery Research Activities) batteries); Li-ion: lithium-ion.....	5
<b>Figure 1-4.</b> Low temperature battery technologies. Relation between volumetric and gravimetric energy density [10].....	8
<b>Figure 1-5.</b> Stationary energy storage to compliment the renewable energy resources and load levelling for grid integration [11] .....	9
<b>Figure 1-6.</b> Voltage vs. $\text{Li}^+/\text{Li}^0$ of various electrode materials in comparison with the stability window of common liquid organic electrolytes [17].....	14
<b>Figure 1-7.</b> Cost (\$/kWh) analysis of different cell systems [11] .....	14
<b>Figure 1-8.</b> (a) Spiral bound cylindrical cell [22], (b) prismatic cell [23] and (c) pouch cell [22].....	15
<b>Figure 1-9.</b> Main investments of 20 biggest automotive players in Li-ion battery manufacturing [24] .....	17
<b>Figure 1-10.</b> Cathode active materials market share estimation in 2015 extracted after analysis of Table 1-7 and Figure 1-9 .....	17
<b>Figure 1-11.</b> Market analysis on ESS. Schematic compilation of characteristics to take into account when searching for a suitable ESS for the target application.....	21
<b>Figure 2-1.</b> Nominal capacity test (used example: cell with 2.3 A nominal current (1C) and 3.3 V nominal voltage) .....	28
<b>Figure 2-2.</b> Discharging (a) and charging (b) rate capability test for each C-rate and T pair conditions. Each testing condition is repeated 3 times in order to check the repeatability of tests and evaluate average results .....	29
<b>Figure 2-3.</b> Discharge (a) and regen (b) DC IR measurement procedures .....	30
<b>Figure 2-4.</b> Voltage response of a cell to high 17 s (a) discharge and (b) charge pulses. The voltage values used for the assessment of 1s and 17s Direct Current (DC) internal resistance (IR) are indicated in the figures .....	31
<b>Figure 2-5.</b> Hybrid Pulse Power Characterisation (HPPC) test procedure.....	32

<b>Figure 2-6.</b> Hybrid Pulse Power Characterisation (HPPC) Test. Charge and discharge pulses measured within 90-20% SOC range with 10% $\Delta$ SOC intervals (used example: cell with 2.3 Ah nominal capacity and 3.3 V nominal voltage) .....	32
<b>Figure 2-7.</b> Open Circuit Voltage (OCV) test procedure .....	33
<b>Figure 2-8.</b> Close-to-equilibrium Open Circuit Voltage (OCV) test. Cell full discharge at C/5 (used example: cell with 2.3 Ah and 3.3 V nominal capacity and voltage, respectively).....	34
<b>Figure 2-9.</b> Ageing testing procedure.....	36
<b>Figure 3-1.</b> Dominant factors affecting the selection of the Li-ion battery technology .....	40
<b>Figure 3-2.</b> Breakdown of cells design (NOTE that colour code corresponds to the factors identified in Figure 3-1).....	41
<b>Figure 3-3.</b> Battery system costs (cost/kWh) breakdown in 2011 for a 26kWh BEV with NCM-graphite cells -\$777/kWh- [36] .....	42
<b>Figure 3-4.</b> Rest voltage versus SOC curve of (a) NCM/graphite and (b) LCO/graphite commercial cells .....	44
<b>Figure 3-5.</b> Rest voltage versus SOC curves of three different commercial cells containing LFP cathode. Estimated OCV is the mean of rest voltages after charge and discharge operation.....	45
<b>Figure 3-6.</b> The effect of LFP cathode cell voltage plateau and charge-discharge voltage differences on state measurements .....	46
<b>Figure 3-7.</b> Rest voltage versus SOC curve of a LMO/LTO commercial cell .....	47
<b>Figure 3-8.</b> Discharge curves at different C-rates and 25°C for the studied HE (continuous lines) and HP (dotted lines) NCM-based cells.....	49
<b>Figure 3-9.</b> Discharged capacity and specific energy at different C-rates and 25°C for the studied HE and HP NCM-based cells.....	49
<b>Figure 3-10.</b> Ragone plot. Different constant power full discharges of the studied HE and HP NCM-based cells at 25°C.....	50
<b>Figure 3-11.</b> Ragone plots for tested cells from different manufacturers. Different constant power full discharges at room temperature for each type of cell.....	51
<b>Figure 3-12.</b> Thermography images of two prismatic cells with different housing, (a) plastic case and (b) metallic case, at maximum reached temperature during charging at 1C and 25±2°C. Thermography image of a pouch cell (c) at maximum reached temperature during charging at 2C and 25±2°C .....	53
<b>Figure 3-13.</b> A prismatic cell (116x46x183mm) disassembling pictures.....	54
<b>Figure 3-14.</b> Top part, gasket and safety vent of two different commercial 18650 cells (a, b). Top parts (and also the bottom part for the 22650 cell in the right) and insulators for different commercial cells (c) .....	55
<b>Figure 3-15.</b> (a) A HE 18650 cell with a single tab at the end of the wind and a metallic cylindrical mandrel in the middle. (b) A HE 18650 cell with a mandrel in the middle and the positive tab at 19 cm from the inner part. (c) A HP 18650 cell with very thin electrodes rolled using a second negative lead, and a positive tab in the middle of the cathode. (d) A HP 26650 cell with several current collector tabs distributed along the electrodes (no mandrel for the rolling). (e) Different negative (left) and positive (right) current collector tabs.....	56
<b>Figure 3-16.</b> Different components of a cylindrical cell .....	57

<b>Figure 3-17.</b> Flow chart of the defined cells selection methodology stages.....	59
<b>Figure 3-18.</b> (a) Definition of the application, ideal cell and operating conditions. (b) Battery Pack sizing and formation according to the ideally selected cell .....	61
<b>Figure 3-19.</b> Oversizing: (a) new cell and (b) degraded cell .....	63
<b>Figure 3-20.</b> Tests procedure for the purchased cells preliminary characterisation .....	64
<b>Figure 3-21.</b> Costs of owning a battery system. Total Cost of Ownership (TCO) of a system includes the total costs required for building and introducing the system, operating, maintaining and disposing, including lost profits due to e.g. failures ...	70
<b>Figure 3-22.</b> Battery system overview .....	71
<b>Figure 3-23.</b> An example of battery safety layer by layer [48] .....	72
<b>Figure 3-24.</b> Cause and effects of abuse operation conditions .....	72
<b>Figure 3-25.</b> (a) Computed tomography (CT) scan of an 18650 cell [81] (b) Cylindrical cell construction: double-coated electrodes and rolled technology .....	73
<b>Figure 3-26.</b> Pictures of highly aged and damaged harvested anodes, cathodes and separators from different 18650 cells .....	74
<b>Figure 3-27.</b> Two laptop 18650 aged cells (a and b) cell innards (jelly-roll) extraction .....	74
<b>Figure 3-28.</b> Complete general step-wise procedure for cells post-mortem analysis.....	76
<b>Figure 3-29.</b> Cell disassembly methodology development. Options that were tried for cell opening and extraction of cell innards .....	77
<b>Figure 3-30.</b> Extracting 18650 cell innards using nitrogen and hitting the housing.....	78
<b>Figure 3-31.</b> (a) The turning machine designed for cylindrical cells opening. (b) Cylindrical cell top part cutting process using the turning machine. (c) Cell bottom part distorted due to the mechanical force of the three fixing points of the cutting machine. (d) Adapted plastic cell holder for the cutting machine .....	78
<b>Figure 3-32.</b> Top (a) and bottom (b) part cutting of a 18650 Li-ion cell. Housing removal (c) of different cells using pliers after cutting the top part.....	79
<b>Figure 3-33.</b> Summary of the evaluation of the attempted options for cell disassembly .....	80
<b>Figure 3-34.</b> Disassembled fresh cells (unused) from different manufacturers .....	80
<b>Figure 3-35.</b> Different opened parts (i, ii, iv) or just the jelly-roll (iii) for cell centrifuging .....	81
<b>Figure 3-36.</b> (a) A centrifuge container (black with plastic transparent cap) and the inside components. (b) New system for cell centrifuging: plastic container for the opened cells within the container. (c) Electrolyte extraction centrifuging the cell (the crystal container in the right contains the obtained electrolyte. The crystal container in the left contains the electrolyte with the isopropanol, IPA, that was used to clean the centrifuging container).....	82
<b>Figure 3-37.</b> Defined electrolyte collection procedure.....	83
<b>Figure 3-38.</b> Developed methodology for cylindrical cells disassembling and components harvesting. All the steps with the same cell and in Ar-atmosphere .....	84
<b>Figure 3-39.</b> Pore size distribution of anode coating specimens (specimen numbers in the insets) from different similarly aged cells from the same manufacturer .....	87
<b>Figure 3-40.</b> Harvested anode pore size distribution of specimens (specimen numbers in the insets) from different similarly aged cells from the same manufacturer .....	88

<b>Figure 3-41.</b> Half-cell measurements of single-coated and double-coated graphite samples harvested from a 18650 cell.....	91
<b>Figure 3-42.</b> Defined procedure for checking the efficiency of rinsing the electrodes .....	93
<b>Figure 3-43.</b> Lithium-ion cells characterisation methodology (GC-MS: Gas Chromatography with Mass Spectroscopy; ICP: Inductively Coupled Plasma; SEM-EDS: Scanning Electron Microscopy with Energy-Dispersive X-ray Spectroscopy; MIP: Mercury Intrusion Porosimetry; XRD: X-ray Diffraction) .....	94
<b>Figure 3-44.</b> Main steps within Stage 1 (analysis of the application and available cells).....	95
<b>Figure 3-45.</b> Main steps within Stage 2 (screening of preselected cells) .....	96
<b>Figure 3-46.</b> Interactions and relationships between performance (to meet application and installation requirements), costs safety and battery pack issues to consider for the selected cell operating range and control strategies definition .....	97
<b>Figure 3-47.</b> Flow chart and time scale for the main tasks needed for the development of cell selection methodology .....	98
<b>Figure 4-1.</b> Elevator operation. (a) The car travels downward (b) The car travels upstream...	101
<b>Figure 4-2.</b> Comparison of conventional tram and catenary-free tram operation (ACR: rapid charge accumulator). (Source: CAF Power & Automotion) .....	102
<b>Figure 4-3.</b> Residential elevator Li-ion ESS solution developed between IK4-Ikerlan and Orona .....	103
<b>Figure 4-4.</b> Traction and regenerative power profiles <sup>7</sup> for the residential elevation application .....	104
<b>Figure 4-5.</b> Block diagram of a single-phase residential elevator with a Li-ion ESS .....	105
<b>Figure 4-6.</b> Block diagram of battery pack (BP) configuration simulation program showing the inputs and output.....	108
<b>Figure 4-7.</b> Elevator operation charge sustaining profile continuously repeated upon accelerated cycling test. Box in the voltage profile indicates the repetition unit..	109
<b>Figure 4-8.</b> Nominal capacity variation between cells of the same reference. Experimental results of Ref 1, Ref 2 and Ref 3 in blue, red and green open circuits, respectively. Mean value (continuous lines) and 95% Confidence Interval (CI) (dotted lines) of each reference indicated using the same colour. 95% CI of each specimen in grey .....	111
<b>Figure 4-9.</b> Energy efficiency of the references at nominal operating conditions. Experimental results of Ref 1, Ref 2 and Ref 3 in blue, red and green open circuits, respectively. Mean value (continuous lines) and 95% CI (dotted lines) of each reference indicated using the same colour .....	112
<b>Figure 4-10.</b> Most relevant electrical performance results from rate capability tests at: (a) 5°C, (b) 25°C and (c) 45°C.....	114
<b>Figure 4-11.</b> Cell total surface heating after full discharges and charges in CC mode at different operating C-rates and ambient temperature .....	116
<b>Figure 4-12.</b> Depth of Discharge (DOD) for meeting the energy demand of the targeted residential elevator application at normal operating current loads (mean values -diamond-shaped symbols- are indicated for each condition and reference). 60% initial SOC and different ambient temperatures .....	117

<b>Figure 4-13.</b> 17 s Direct Current (DC) internal resistances (IR) as a function of SOC and temperature for different type of cells (10C discharge (DCH) pulses and 1C charge (CHA) pulses with duration of 17 s).....	118
<b>Figure 4-14.</b> Usable energy assessed from power tests that consisted on repeating continuously application operating profile between voltage limits of the cell and ambient T of: (a) 25°C; (b) 5°C.....	120
<b>Figure 4-15.</b> Change in nominal capacities (Q: actual capacity; Q <sub>0</sub> : capacity at the Beginning of Life) as a function of number of cycles (N). Cells cycling under application current profile, 100% initial SOC and 35±5°C .....	121
<b>Figure 4-16.</b> Evolution of the studied three references 1s internal resistance changes upon cycling (IR: actual internal resistance; IR <sub>0</sub> : internal resistance at the Beginning of Life). Direct Current (DC) IR measured at 50% SOC with 10C DCH pulse of 1 s duration .....	122
<b>Figure 4-17.</b> Correlation between Ref 1 power capability loss and capacity loss due to cycling (Q and P: actual capacity and power, respectively; Q <sub>0</sub> and P <sub>0</sub> : capacity and power, respectively, at the Beginning of Life). Power capability was assessed using data from Figure 4-16 .....	123
<b>Figure 4-18.</b> Impedance spectra of Ref 3 measured before and after cycling over 15000 and 45000 cycles. EIS test at 75% SOC and 25°C .....	123
<b>Figure 4-19.</b> Different type of cells thermal power at adiabatic conditions during continuous discharges under application current profile measured before and after cyclic ageing. 20±3°C ambient temperature.....	124
<b>Figure 4-20.</b> Discharge voltage profiles of Ref 1 (a), Ref 2 (b) and Ref 3 (c) during adiabatic calorimetric tests at the BOL and after cyclic ageing .....	125
<b>Figure 4-21.</b> Fitting of capacity loss rate as a function of number of cycles.....	126
<b>Figure 4-22.</b> Fitting of discharge power capability loss as a function of number of cycles.....	126
<b>Figure 4-23.</b> Usable energy assessed from power tests under application operating profile and 25°C after the cells being cycled.....	128
<b>Figure 4-24.</b> Most limiting electrical characteristics at 5°C ambient temperature of the studied three references .....	130
<b>Figure 4-25.</b> Catenary free tramway ESS system developed between IK4-Ikerlan and CAF Power & Automation .....	132
<b>Figure 4-26.</b> Most demanding operating profile for tramway application and other demanded peaks due to unexpected start/stop during catenary-free operation stretch <sup>10</sup> .....	133
<b>Figure 4-27.</b> Stage 1 conclusions. Most relevant characteristics for the purchased cells.....	136
<b>Figure 4-28.</b> Nominal capacity variation between cells of the same reference. Experimental results of Ref T.2, Ref T.6 and Ref T.9 in green, magenta and blue open circuits, respectively. Mean value (continuous lines in the same colour as experimental data) and 95% CI (dotted grey lines). 95% CI of each specimen in grey .....	137
<b>Figure 4-29.</b> Energy efficiency of the references at normal and maximum operating conditions. Experimental results of Ref T.2, Ref T.6 and Ref T.9 in green, red and blue, respectively .....	138
<b>Figure 4-30.</b> Power capability (P) of the three studied cell types at 25°C and usable DOD range to sustain residential elevation application discharge and regeneration requirements .....	141

<b>Figure 4-31.</b> Opening of cylindrical cells from three different manufacturers. Cells analysed for the residential elevation application.....	143
<b>Figure 5-1.</b> Cells selection methodology. Stages and main tasks with Ageing and Lifetime analysis highlighted within Stage 3, as main objective of this chapter .....	147
<b>Figure 5-2.</b> Motivation for lifetime prediction methodology development.....	154
<b>Figure 5-3.</b> Methodology for lifetime prognosis (validation procedures in grey).....	156
<b>Figure 5-4.</b> Controllable factors including changes in cell performance (both while working operation and standing time) when it comes to the battery capacity and internal resistance. Individualisation of stress factors for their effects weighing. This approach pursues to combine calendar and cycling ageing effects to predict cycle ageing at different T and SOC conditions and also to simulate realistic cell complex operation .....	157
<b>Figure 5-5.</b> Chronological scheme of the proposed overall process for lifetime prognosis .....	160
<b>Figure 5-6.</b> Methodology for calendar lifetime prognosis. In grey, activities carried out within this work .....	161
<b>Figure 5-7.</b> Initial and final cell calendar ageing characterisation .....	163
<b>Figure 5-8.</b> Dynamic storage tests. Dynamic T and SOC profiles over time .....	164
<b>Figure 5-9.</b> Charge-discharge curves at 1C and 25°C for the different ageing stages of the cells stored at different SOC and T conditions. Charge-discharge profiles from nominal capacity measurements .....	166
<b>Figure 5-10.</b> DC internal resistance increase ( $IR_{\text{increase}}$ ) and nominal capacity loss ( $Q_{\text{loss}}$ ) adjusted to EOL scale over time (both nominal Q and IR were normalised to initial values). IR measurement by means of 17 s discharge pulse at 10C at 50% cell SOC.....	167
<b>Figure 5-11.</b> Current pulse EPIT results over storage time. (a) DC internal resistance (IR) increase during discharge as a function of 17 s current pulse (10C) applying cell SOC. (b) DC IR increase during charge and discharge at 50% SOC. (a.1 and b.1) storage at 30°C and 70% SOC; and (a.2. and b.2) storage at 40°C and 70% SOC .....	167
<b>Figure 5-12.</b> Relationship between energy loss ( $E_{\text{loss}}$ ) and nominal capacity loss ( $Q_{\text{loss}}$ ) (a), energy loss and internal resistance increase ( $IR_{\text{increase}}$ ) (b) at different storage conditions over time (E, Q and IR were normalised to initial values). IR measurement by means of 17 s discharge pulse at 10C at 50% cell SOC.....	168
<b>Figure 5-13.</b> Charge and discharge rate capability ( $Q_{\text{CHA}}$ and $Q_{\text{DCH}}$ , coloured areas) and cell surface temperature change ( $\Delta T$ , line of columns) on charge at 3C (a) and discharge at 6C (b) at different temperatures at BOL and after storage under different temperature conditions during ca. 20 months. Constant Current (CC) charging time is indicated for each condition in (a) .....	169
<b>Figure 5-14.</b> Reversible time step capacity loss and accumulated capacity loss (both normalised to initial nominal values) of the cells stored at different OC conditions assessed from the nominal capacity test.....	172
<b>Figure 5-15.</b> The influence of SOC (a) and T (b) on cell self-discharge during OC storage. Reversible capacity loss rate (normalised to initial nominal capacity, $Q_0$ ) depending on storing time interval duration ( $\Delta t$ ).....	172

- Figure 5-16.** Close-to-equilibrium C/5 discharge voltage profiles at initial stage for the 2.3 Ah commercial 22650-type cell studied within this work (a,b), and differential voltage (DV,  $dV/dQ$ , c) and incremental capacity (IC,  $dQ/dV$ , d) signatures. Graphite staging phenomena coupled with LFP voltage plateau numbered as 1 to 5..... 174
- Figure 5-17.** Equivalent and representative Differential Voltage (DV) curves, obtained from C/5 discharge voltage profiles, upon storage at different conditions..... 175
- Figure 5-18.** Incremental Capacity (IC) (a) and Differential Voltage (DV) (b) curves for 50°C and 70% SOC test after prolonged storage periods ..... 175
- Figure 5-19.** EIS measurements of the cells stored at 30°C and 70% SOC (a,c) and 50°C and 70% SOC (b,d). EIS measurement at 25°C and two different cell SOC: 30% (a,b) and 70% (c,d)..... 176
- Figure 5-20.** Capacity loss ( $Q_{\text{loss}}$ ) data at different storage static conditions (solid colour markers), fitted calendar degradation model (continuous lines). Open marker (50°C, 90% SOC) corresponds to the test condition used for static validation and the dotted line is the model validation fit..... 178
- Figure 5-21.** Box plot of capacity loss prediction residuals and errors distribution for each storage condition..... 179
- Figure 5-22.** Capacity loss performance (diamond shaped symbols) under dynamic storage conditions for four tests (a-d, plotted in black). The corresponding predictions are represented by green lines..... 180
- Figure 5-23.** Recorded average temperatures of Bangkok, Jizan and Tenerife for each day during one year ..... 182
- Figure 5-24.** Capacity loss prediction for two years of operation at 90% SOC and temperature profiles in Figure 5-23 ..... 182
- Figure 5-25.** quasi-OCV C/5 discharge curve of the studied 2.3 Ah LFP/graphite 22650-type cell. Graphite staging phenomena coupled with LFP voltage plateau numbered as 1 to 5. Cycling ageing testing conditions, middle SOC and SOC range, are depicted in the graph for each DOD ..... 186
- Figure 5-26.** Cycling ageing model dynamic validation. Two tests (a and b) under dynamic both DOD and C-rate over time at 30°C and 50% middle SOC were performed. 187
- Figure 5-27.** (a) Actual nominal capacity (Q) and (b) 17 s discharge DC internal resistance (IR) increase, measured at 50% SOC, upon cycling (1C, 50% middle SOC and 30°C) as a function of Full Equivalent Cycles (FEC), both normalised to initial values ( $Q_0$ : nominal capacity at the Beginning of Life) ..... 189
- Figure 5-28.** Current pulse EPIT results upon cycling (FEC: Full Equivalent Cycles). (a) 17 s DC internal resistance (IR) increase during discharge as a function of the current pulse applying cell SOC. (b) DC IR increase during charge and discharge at 50% SOC. (a.1 and b.1) Cycling at 1C, 100% DOD, 50% middle SOC and 30°C; and (a.2. and b.2) cycling at 1C, 60% DOD, 50% middle SOC and 30°C..... 190
- Figure 5-29.** Illustration of cells performance fade trends for (a)100% DOD and (b) 5% DOD continuous cycling conditions (1C, 50% middle SOC and 30°C). Actual nominal capacity (Q) and 17 s discharge DC internal resistance (IR) increase, measured at 50% SOC, as a function of Full Equivalent Cycles (FEC), both normalised to initial nominal values ( $Q_0$ : nominal capacity at the Beginning of Life) ..... 192

- Figure 5-30.** Ranging of total number of Full Equivalent Cycles (FEC) that the cell could deliver at various DOD levels (1C, 50% middle SOC and 30°C tests) before reaching ca. 90% SOH..... 192
- Figure 5-31.** Wöhler curve. Relationship between DOD and the total number of cycles before reaching ca. 90% SOH ..... 193
- Figure 5-32.** Actual nominal capacity (Q) normalised to initial nominal values ( $Q_0$ ) upon cycling (50% middle SOC and 30°C) as a function of Full Equivalent Cycles (FEC) and time (d-2, e-2 and f-2). C-rate effect on capacity fade at different DOD (a-c) and DOD effect on capacity fade at different C-rate (d-f)..... 194
- Figure 5-33.** Equivalent (same colour) and representative Differential Voltage (DV), obtained from C/5 voltage discharge profiles, curves upon cycling at different DOD levels (1C, 50% middle SOC and 30°C) ..... 196
- Figure 5-34.** (a) Incremental Capacity (IC) and (b) Differential Voltage (DV) curves for 5% DOD test (1C, 50% middle SOC and 30°C) upon cycling after large number of Full Equivalent Cycles (FEC)..... 196
- Figure 5-35.** Differential Voltage (DV) and Incremental Capacity (IC) curves, obtained from C/5 discharge profiles, for 100% DOD test (1C and 30°C) upon cycling ..... 197
- Figure 5-36.** Cycling at 100% DOD (1C, 50% middle SOC and 30°C). (a) Actual nominal capacity (Q) and (b) 17 s discharge DC internal resistance (IR) increase, measured at 50% SOC, as a function of Full Equivalent Cycles (FEC), both normalised to initial values ( $Q_0$  initial nominal capacity) ..... 198
- Figure 5-37.** Impedance spectra measured over different SOH (State of Health) at 25°C and (a) 30% SOC and (b) 70% SOC. 100% DOD (1C and 30°C) tests ..... 199
- Figure 5-38.** Initial photographs of the negative electrode: (a) pristine cell, (b) conditioned cell, (c) BOL cell, (d) two areas along the length of the electrode of the cell cycled for 1521 FEC (93.03% SOH), (e-1) cell cycled for 3276 FEC (79.6% SOH); and (e-2) separator of the cycled cell for 3276 FEC (79.6% SOH). Cycling tests: 100% DOD, 1C and 30°C ..... 200
- Figure 5-39.** Secondary electron SEM images of the negative electrode: pristine cell, conditioned cell, BOL cell, cell cycled for 1521 FEC (93.03% SOH) and cell cycled for 3276 FEC (79.6% SOH). Cycling tests: 100% DOD, 1C and 30°C. The scale is the same for all images ..... 201
- Figure 5-40.** Secondary electron SEM images of graphite electrodes surface (different areas of interest) corresponding to cells cycles for 1521 FEC (a & b) and 3276 FEC (c & d). Cycling tests: 100% DOD, 1C and 30°C..... 201
- Figure 5-41.** Backscattered electron SEM images of the positive LFP electrode: (a) pristine cell and (b) cell cycled for 3276 FEC (79.6% SOH). Cycling tests: 100% DOD, 1C and 30°C. The scale is the same for both images ..... 203
- Figure 5-42.** SEM images of the separator extracted from (a) the pristine cell, (b) the cell cycled for 1521 FEC and (c) the cell cycled for 3276 FEC. Cycling tests: 100% DOD, 1C and 30°C. The scale is the same for all images ..... 203
- Figure 5-43.** X-ray diffraction patterns of the harvested negative electrodes from pristine and BOL cells compared with the ones from 93.03% and 79.6% SOH cells after cycling at 100% DOD, 1C and 30°C ..... 204
- Figure 5-44.** XRD patterns of the LFP positive electrode from a pristine cell and the cell cycled for 3276 FEC (79.6% SOH) at 100% DOD, 1C and 30°C..... 204

- Figure 5-45.** Galvanostatic half-cells cycling of (a) negative graphite and (b) positive LFP harvested electrodes from pristine cell, BOL cell, cell cycled for 1521 FEC (93.03% SOH) and cell cycled for 3276 FEC (79.6% SOH). Cycling tests: 100% DOD, 1C and 30°C..... 205
- Figure 5-46.** Positive and negative electrodes matching from capacity measurements on electrodes harvested from (a) pristine cell, (b) cell cycled for 1521 FEC (93.03% SOH) and (c) cell cycled for 3276 FEC (79.6% SOH). Cycling tests: 100% DOD, 1C and 30°C..... 206
- Figure 5-47.** Illustration of DOD level influence on the total number of Full Equivalent Cycles (FEC) that the cell can deliver. The distinguished two DOD ranges (grey and green areas) and the DOD influence tendency for each of them (black lines). Data: cycling tests under 1C, 50% middle SOC, 30°C and different DOD levels before reaching *ca.* 90% SOH..... 209
- Figure 5-48.** Capacity loss ( $Q_{\text{loss}}$ ) data at different cycling DOD levels (solid colour markers) and fitted cycle ageing model (continuous lines) for cycling at 1C, 50% middle SOC and 30°C..... 210
- Figure 5-49.** Box plot of capacity fade prediction residuals distribution for each modelled cycling condition ..... 211
- Figure 5-50.** Capacity loss experimental data (markers) and predictions (dotted lines) under cycling under different DOD conditions and C-rate conditions: (a) 2C and (b) 3.5C..... 212
- Figure 5-51.** Box plot of capacity loss prediction errors distribution for cycling conditions at C-rates different from modelled 1C condition..... 212
- Figure 5-52.** Capacity loss ( $Q_{\text{loss}}$ ) data (markers) under dynamic cycling conditions (Figure 5-26 (a and b)) and corresponding simulation results (dotted lines). Cycling under dynamic, DOD and C-rate, 50% middle SOC and 30°C..... 213
- Figure 5-53.** Testing procedure for cycling ageing dynamic validation..... 214
- Figure 5-54.** Cycling ageing model dynamic validation II. Four different tests defined under dynamic either DOD (1C) or C-rate (60% DOD), 50% middle SOC and 30°C. Two tests under dynamic DOD (a,b) and other two under dynamic C-rate (c,d). 215
- Figure 5-55.** Capacity loss ( $Q_{\text{loss}}$ ) data (markers) under dynamic DOD cycling conditions (Figure 5-54 (a,b)) and corresponding simulation results (dotted lines). Cycling under 1C, 50% middle SOC, 30°C and dynamic DOD ..... 216
- Figure 5-56.** Capacity loss ( $Q_{\text{loss}}$ ) data (markers) under dynamic C-rate cycling conditions (Figure 5-54 (c,d)) and corresponding simulation results (dotted lines). Fittings are superimposed because the DOD is the same for both tests and the predictions do not include the C-rate effect. Cycling under 60% DOD, 50% middle SOC, 30°C and dynamic C-rate ..... 216
- Figure 5-57.** Cycling ageing dynamic validation III. Additional two tests (a and b) under both dynamic DOD and C-rate over time at 30°C and 50% middle SOC ..... 218
- Figure 5-58.** Capacity loss ( $Q_{\text{loss}}$ ) data (markers) under dynamic cycling conditions (Figure 5-57) and corresponding simulation results (dotted lines). Cycling under dynamic, DOD and C-rate, 50% middle SOC and 30°C ..... 219
- Figure 5-59.** Capacity loss ( $Q_{\text{loss}}$ ) data (markers) under dynamic DOD cycling conditions (Figure 5-54 (a,b)) and corresponding simulation results (dotted lines) using the static ageing acceleration correction factor. Cycling under 1C, 50% middle SOC, 30°C and dynamic DOD. Improvement of the prediction shown in Figure 5-55 ..... 220

- Figure 5-60.** Capacity loss ( $Q_{\text{loss}}$ ) data (markers) under dynamic cycling conditions (Figure 5-26 and Figure 5-57) and corresponding simulation results (dotted lines) using the static ageing acceleration correction factor (Eq. 5-9 and Eq. 5-10). Cycling under dynamic, DOD and C-rate, 50% middle SOC and 30°C. Improvement of the predictions shown in Figure 5-52 and Figure 5-58. Magnification of tests (b-d) in the inset..... 220
- Figure 5-61.** Complete ageing model. Available capacity (Q) and internal resistance (IR) offset prediction in response to time and controllable environmental influences (Eft: Equivalente Full time, EFC: Equivalente Full Cycles) ..... 223
- Figure 5-62** (a). Validation test (I) approaching real operation. Ageing model input impact factors profiles on top and in situ measurable factors in real applications for the marked (dashed grey box) tested time-interval..... 225
- Figure 5-63.** Experimental capacity loss ( $Q_{\text{loss}}$ ) results for the three validation test profiles approaching real operation (Figure 5-62) and the corresponding predictions using the described lifetime prognosis approach..... 227
- Figure 5-64.** Histogram and box plot of the difference between prediction and experimental data values of cell capacity loss induced by profiles approaching real operation. Distribution fit (blue line) in the density plot ..... 227
- Figure 5-65.** Continuation of experimental capacity loss ( $Q_{\text{loss}}$ ) results shown in Figure 5-63 for the three validation test profiles approaching real operation (Figure 5-62). Operation conditions between check-ups are described using the same colour as the corresponding test results. Data showing capacity recovery are shaded in the same colour as the corresponding test results..... 228
- Figure 5-66.** Comparison of capacity loss ( $Q_{\text{loss}}$ ) estimations using the single ageing model (in green) and the simulation platform that includes field measurements conversion and the possibility of simulating real cell operation for each defined time-step ..... 229
- Figure 5-67.** (a) Voltage profile of the validation test simulating elevator operation. (b) Magnification view around day 12 ..... 231
- Figure 5-68.** Real profile testing scheme..... 232
- Figure 5-69.** Experimental capacity loss ( $Q_{\text{loss}}$ ) results (markers) from the most demanding residential elevator profile (Figure 4-6) and the corresponding prediction (dotted line) using the ageing simulation platform (Figure 5-61)..... 234
- Figure 5-70.** Experimental capacity loss ( $Q_{\text{loss}}$ ) results (markers) resulted from residential elevator accelerated operation profile (Figure 5-67 and Figure 5-68) and their estimations (dotted line) using the ageing simulation platform (Figure 5-61). Testing at (a) 30°C ambient T and (b) 40°C ambient T ..... 235
- Figure 5-71.** Differential Voltage (DV) and Incremental Capacity (IC) curves derived from quasi-OCV discharge curves for complex operation test (Figure 5-67 and Figure 5-68) at 30°C ..... 236
- Figure 5-72.** Box plot of capacity loss prediction errors distribution for complex operation test (Validation tests using realistic profiles II in Figure 5-67 and Figure 5-68).. 236
- Figure 5-73.** Change in relative capacity (actual nominal capacity, Q, normalised to initial nominal capacity,  $Q_0$ ) vs. time upon cycling (triangular and square markers) at 1C, different SOCs, different temperatures and DOD: (a) 50% DOD and (b) 30% DOD. Calendar ageing results at equal SOC and T are included (circle markers) as comparative. .... 240

<b>Figure 5-74.</b> Summary of the implementation of the proposed approach for lifetime prognosis. Numbers in the different validation procedures (in green) that were carried out for calendar (model development in magenta), cycling (model development in orange) and complete ageing model (in blue) indicate the order of execution in each case .....	242
<b>Figure 5-75.</b> Real residential elevator one day power profile converted into operating current and SOC at cell level .....	245
<b>Figure 5-76.</b> A residential elevator daily operation capacity loss simulation results for four years .....	245
<b>Figure 5-77.</b> Ageing analysis and lifetime predictive model applicability. Interaction with other activities and the overall outputs (BP: Battery Pack; BMS: Battery Management System; SOH: State of Health; TCO: Total Cost of Ownership)....	247
<b>Figure 5-78.</b> Capacity loss over time, model prediction and prediction corrected to the actual measured SOH.....	248
<b>Figure A-1.</b> Schematic illustration of a $\text{Li}_x\text{C}_6/\text{Li}_{1-x}\text{MO}_2$ lithium-ion cell. During discharge, $\text{Li}^+$ ions migrate through the electrolyte and electrons flow through the external circuit, both moving from the anode to the cathode [18].....	A5
<b>Figure A-2.</b> Different components of main Li-ion batteries.....	A6
<b>Figure A-3.</b> Cathode materials output capacity of Chinese manufacturers [221] .....	A8
<b>Figure A-4.</b> Voltage and specific capacity of different cathode materials .....	A13
<b>Figure A-5.</b> Trade-offs among the five principal cathode Li-ion battery technologies (Note: the farther the coloured shape extends along a given axis, the better the performance along that dimension) [18, 19].....	A13
<b>Figure A-6.</b> Energy released in the decomposition of the different cathodes. Thermal stability [22].....	A14
<b>Figure A-7.</b> Comparison of properties of different materials for cathodes .....	A15
<b>Figure A-8.</b> C/20 discharge curves for graphitic carbon when measured against metallic lithium [67] .....	A16
<b>Figure A-9.</b> Capacity delivery versus charge-discharge cycles of a Sn-C composite electrode [17].....	A17
<b>Figure A-10.</b> Voltage charge-discharge profiles of a LTO anode and of various cathode materials [17].....	A18
<b>Figure A-11.</b> Digatron MCT cell tester (a), tests circuits in it (b) and safety box (c) .....	A27
<b>Figure A-12.</b> DIGATRON EISmeter Impedance Spectroscope.....	A28
<b>Figure A-13.</b> Cylindrical cells typical assembly and connections.....	A28
<b>Figure A-14.</b> Pouch cells connection. Cells with holes in terminals (a) and with short terminals without holes (b) .....	A29
<b>Figure A-15.</b> Prismatic cells connection .....	A29
<b>Figure A-16.</b> CTS climatic chambers.....	A30
<b>Figure A-17.</b> Prebatem climatic chamber.....	A30
<b>Figure A-18.</b> THT EV-ARC Accelerating Rate Calorimeter .....	A30

<b>Figure A-19.</b> FLIR Systems ThermoCAM P25 thermal imaging camera.....	A31
<b>Figure A-20.</b> Sylatech glove-box .....	A31
<b>Figure A-21.</b> SIGMA 2-16 microcentrifuge No. 17140 and centrifuge containers.....	A31
<b>Figure A-22.</b> Thermo Scientific Mercury Porosimeter PASCAL 140 and 440 Series.....	A32
<b>Figure A-23.</b> CD3 and CD3P Dilatometers [230, 231] .....	A32
<b>Figure A-24.</b> ICP Optical Emission Spectrometer VARIAN 725-ES .....	A34
<b>Figure A-25.</b> CEM Mars 5 Microwave Accelerated Reaction System. (a) Oven exterior and (b)Teflon reaction vessel in the support module with control parts assembled....	A35
<b>Figure A-26.</b> Load matrix process [234] .....	A51
<b>Figure A-27.</b> Some root causes of internal short circuits .....	A52
<b>Figure A-28.</b> Processes that take place on the graphite anode-electrolyte interface layer [150]. Reactions of the anode with the electrolyte are considered to be the major source of aging at the negative electrode.....	A53
<b>Figure A-29.</b> Cell failure distributions [22].....	A54
<b>Figure A-30.</b> Instantaneous failure rate curve (a) and cumulative failure distribution of a cell (b) [22] .....	A54
<b>Figure A-31.</b> Lithium-ion cell safety operating window [236] .....	A57
<b>Figure A-32.</b> Reactions occurring on carbon based negative electrode during charge and overcharge [151].....	A58

## LIST OF TABLES

---

<b>Table 1-1.</b> Cell voltages and current costs of various battery technologies at cell level [5] .....	6
<b>Table 1-2.</b> Suitable low temperature secondary technologies for medium-large scale applications .....	12
<b>Table 1-3.</b> Comparison of performance of main Li-ion cells cathodes (the higher the rating, 1:4, the better) [18, 19].....	13
<b>Table 1-4.</b> Negative active material comparison (1: good, 2: better, 3: best) [20] .....	13
<b>Table 1-5.</b> Main properties comparison of the most common commercial batteries [21].....	14
<b>Table 1-6.</b> Properties of different cell mechanical constructions .....	15
<b>Table 1-7.</b> Lithium ion cells market worldwide by main competitors.....	16
<b>Table 1-8.</b> International lithium ion rechargeable battery standards and manuals (see Appendix B).....	19
<b>Table 1-9.</b> Test methods of the main international battery standards and manuals (tests that are similar are coloured in the same way).....	20
<b>Table 3-1.</b> Causes and effects of cell performance.....	42
<b>Table 3-2.</b> Specifications of two pouch cells from the same manufacturer designed with different power to energy ratio (data from manufacturer datasheet).....	48
<b>Table 3-3.</b> Comparison of main components of different HE and HP cells of similar capacity	57
<b>Table 3-4.</b> Functional specifications. The relevance of each of them depend on the application.....	62
<b>Table 3-5.</b> Installation conditions: battery pack (BP) characteristics and restrictions.....	62
<b>Table 3-6.</b> Test description for nominal capacity measurement.....	65
<b>Table 3-7.</b> Description of tests to measure operating charge and discharge capacity .....	66
<b>Table 3-8.</b> Description of DC internal resistance measurement by means of pulses method at different operating SOC and T conditions .....	66
<b>Table 3-9.</b> Description of power tests that evaluate the cells suitability for meeting the application demands.....	67
<b>Table 3-10.</b> Description of the accelerated cycle life test.....	68
<b>Table 3-11.</b> Porosity ( $\epsilon$ ) of anode coating specimens from different cells from the same manufacturer that were similarly aged .....	86
<b>Table 3-12.</b> Harvested anode porous structure characterisation of specimens from different similarly aged cells from the same manufacturer.....	88
<b>Table 3-13.</b> Anode porous structure characterisation of different specimens from a fresh 2 Ah HE NCM/C 18650-type cell.....	89
<b>Table 3-14.</b> Results of a commercial NCM/C 2 Ah 18650-type cell cathode composition measurement in the ICP .....	90
<b>Table 4-1.</b> Residential elevation application installation conditions .....	104

<b>Table 4-2.</b> Most important electric parameters of appropriate cell for the residential elevator application.....	106
<b>Table 4-3.</b> Example of Li-ion cells market analysis. Evaluation of functional energy and power specifications fulfilment.....	106
<b>Table 4-4.</b> Summary of the most representative characteristics of the purchased cells for the residential elevator application evaluation (data from manufacturers).....	107
<b>Table 4-5.</b> Battery pack (BP) sizing for the different types of cells under investigation .....	108
<b>Table 4-6.</b> Definition of the tests conditions in Stage 2 of cells selection methodology for the pursued residential elevator application.....	110
<b>Table 4-7.</b> Capacity and discharge power capability loss fittings .....	127
<b>Table 4-8.</b> Operating DOD range at 25°C according to the application discharge and regenerative power requirements before and after cycling both calculated as a function of the initial capacity (N: number of cycles).....	128
<b>Table 4-9.</b> Dispersion among different specimens of the same reference .....	129
<b>Table 4-10.</b> Comparison of performance of the three studied cells (red: poor; yellow: fair; green: good) .....	131
<b>Table 4-11.</b> Summary of the most representative characteristics of the purchased cells for the tramway application evaluation (data from manufacturers).....	134
<b>Table 4-12.</b> Theoretical evaluation of considered cells for tramway application after initial battery pack sizing (red: poor; yellow: fair; green: good).....	135
<b>Table 4-13.</b> Theoretical cells selection for tramway application.....	135
<b>Table 4-14.</b> Comparison of the estimated operating DOD windows from power test under application conditions and OCV test.....	142
<b>Table 4-15.</b> Comparison of main components of Ref 1, Ref 2 and Ref 3 HP LFP/graphite cells purchased for residential elevator application evaluation. Summary of the most representative cell internal characteristics .....	144
<b>Table 5-1.</b> General energy storage applications requirements (T & D: Transmission and distribution; ISO: Independent System Operator) [3] .....	150
<b>Table 5-2.</b> Overall calendar lifetime prediction worldwide activity.....	151
<b>Table 5-3.</b> Overall cycling lifetime prediction worldwide activity .....	152
<b>Table 5-4.</b> Ageing: effects and causes (compilation from [4]) .....	158
<b>Table 5-5.</b> Test matrix for calendar ageing modelling (static validation highlighted in grey) .	164
<b>Table 5-6.</b> Test matrix for cycling ageing analysis and modelling (static validation highlighted in grey). All the tests were done at 30°C and 50% middle SOC.....	186
<b>Table 5-7.</b> Ah-throughput power values for capacity fade cycling model at different C-rate and DOD conditions.....	212
<b>Table 5-8.</b> Additional cycling tests at 1 C-rate in order to confirm the hypothesis of SOC and T effect on cycle ageing. Tests that were already performed during cycle ageing analysis are marked in grey .....	238
<b>Table 5-9.</b> Cycling tests under different SOC, T and DOD conditions, and the capacity loss ( $Q_{loss}$ ), normalised to initial values, after the same operation time under different conditions used as comparative value of the tests .....	241

<b>Table 5-10.</b> Methodology followed for the analysis of the qualitative and comparative influence of DOD, T and SOC impact factors on cycle ageing, and general stepwise conclusion.....	241
<b>Table A-1.</b> Characteristics of cathode materials [18, 219] .....	A8
<b>Table A-2.</b> Different NCM combinations of $\text{LiNi}_x\text{Mn}_y\text{Co}_{1-x-y}\text{O}_2$ cathode. Theoretical calculations of Ni, Mn and Co metallic constituents proportions and ratios.....	A12
<b>Table A-3.</b> Comparison of properties of the main cathodes [18, 23] .....	A14
<b>Table A-4.</b> Salts used in electrolytes for Li-ion cells [219].....	A19
<b>Table A-5.</b> Summary and titles of all lithium-ion cells standards covered.....	A24
<b>Table A-6.</b> Summary and titles of all lithium-ion cells manuals and reports covered.....	A25
<b>Table A-7.</b> Spanish standards for lithium ion batteries .....	A25
<b>Table A-8.</b> Summary of safety testing protocols and abuse test for Li-ion (covered tests in grey) .....	A26
<b>Table A-9.</b> Specific Technical Data of MCT100-06-10 ME and MCT 50-06-24 ME Digatron cell testers.....	A27
<b>Table A-10.</b> Specifications of type CD3 and CD3P dilatometers [230, 231].....	A32
<b>Table A-11.</b> Specific Technical Data of BaSyTec CTS Standard .....	A35
<b>Table A-12.</b> Li-ion battery market database .....	A38
<b>Table A-13.</b> Selected key failure modes of lithium ion cells [234].....	A55
<b>Table A-14.</b> Lithium battery safety patents .....	A61



## SYMBOLS AND ABBREVIATIONS

---

$A_{cal}$	Calendar ageing
$A_{cyc}$	Cycle ageing
$A_{TOTAL}$	Total ageing. Cell performance deterioration due to real operation (combination of both storage and cycling)
<b>AENOR</b>	“Asociación Española de Normalización y Certificación” (Spanish Association for Standardization and Certification)
<b>ANL</b>	Argonne National Laboratory
<b>ANSI</b>	American National Standards Institute Inc.
<b>ASIC</b>	Application-Specific Integrated Circuit
<b>BATSO</b>	Battery Safety Organisation
<b>BEV</b>	Battery Electric Vehicles
<b>BMS</b>	Battery Management System
<b>BOL</b>	Beginning of Life
<b>BP</b>	Battery Pack
<b>C</b>	Lithiated graphite, $LiC_6$ , anode
	$C_1$ , 1 h capacity, for expressing the battery operating current rate
<b>CC</b>	Constant Current (charging/discharging)
<b>CC-CV</b>	Constant Current charging followed by a Constant Voltage charging
<b>CD</b>	Charge Depleting
<b>CENELEC</b>	European Committee for Electrotechnical Standardization
<b>CHA</b>	Charge
<b>CI</b>	Confidence Interval
<b>CL</b>	Calendar Life
$c_p$	Heat capacity

<b>CR</b>	Internal radius of capillary stem (dilatometer for porosimetry measurement)
<b>C-rate</b>	Charge/discharge current rate, referred to the nominal capacity of the cell
<b>CS</b>	Charge Sustaining
<b>CT</b>	Computed Tomography
<b>CU</b>	Check-up
<b>CV</b>	Constant Voltage
<b>DC</b>	Direct Current
<b>DC IR</b>	Direct Current Internal Resistance
<b>DCH</b>	Discharge
<b>DEC</b>	Diethyl carbonate
<b>DIS</b>	Draft International Standard
<b>DMC</b>	Dimethyl carbonate
<b>DOE</b>	U.S. Department of Energy
<b>DOD</b>	Depth of Discharge
<b>DV</b>	Differential Voltage
<b>ε</b>	Porosity
<b>E</b>	Energy
<b>EDLC</b>	Electric Double-Layer Capacitor
<b>EDS</b>	Energy-Dispersive X-ray Spectroscopy
<b>EFC</b>	Equivalent Full Cycles
<b>EIS</b>	Electrochemical Impedance Spectroscopy
<b>EMC</b>	Ethyl Methyl Carbonate
<b>EN</b>	European Norms (Standards)
<b>EOL</b>	End of Life
<b>EOT</b>	End of Test
<b>EPIT</b>	Electrical Parameters Identification Tests
<b>ESS</b>	Energy Storage System(s)
<b>EV</b>	Electric Vehicle
<b>FCV</b>	Fuel Cell Vehicles

<b>FDIS</b>	Final Draft International Standard
<b>FEC</b>	Full Equivalent Cycles
<b>FEG-SEM</b>	Field Emission Gun-Scanning Electron Microscope
<b>FMEA</b>	Failure Modes and Effects Analysis
<b>GC-MS</b>	Gas Chromatography with Mass Spectroscopy
<b>HE</b>	High Energy
<b>HEV</b>	Hybrid Electric Vehicle
<b>HP</b>	High Power
<b>HPPC</b>	Hybrid Pulse Power Characterisation
<b>IC</b>	Incremental Capacity
<b>ICP</b>	Inductively Coupled Plasma
<b>ICP-OES</b>	Inductively Coupled Plasma-Optical Emission Spectrometry
<b>IEC</b>	International Electrotechnical Commission
<b>IEEE</b>	Institute of Electrical and Electronics Engineers
<b>IL</b>	Ionic Liquid
<b><math>I_n</math></b>	Normalised current rate. It refers to the nominal capacity of the battery
<b>INL</b>	Idaho National Laboratory (DOE National Laboratory operated by Battelle Energy Alliance)
<b>IPA</b>	Isopropanol or isopropyl alcohol
<b>IR</b>	Internal Resistance or Actual Internal Resistance
<b><math>IR_0</math></b>	Initial Internal Resistance
<b>ISC</b>	Internal Short Circuit
<b>ISO</b>	International Organization for Standardization
<b>IT</b>	Information Technology
<b>JIS</b>	Japanese Standards Association
<b>JPL</b>	Jet Propulsion Lab of NASA
<b>LCO</b>	Lithium cobalt oxide, $\text{LiCoO}_2$ (cathode chemistry)
<b>LEV</b>	Light Electric Vehicle
<b>LFP</b>	Lithium iron phosphate, $\text{LiFePO}_4$ (olivine type cathode chemistry)
<b>LIB</b>	Lithium-ion battery
<b>Li-cap</b>	Hybrid lithium-ion capacitors

<b>LIP</b>	Lithium Ion Polymer technology
<b>LLI</b>	Loss of Lithium Inventory
<b>LMO</b>	Lithium manganese oxide, manganese spinel, $\text{LiMn}_2\text{O}_4$ (cathode chemistry)
<b>LMP</b>	Lithium Metal Polymer technology
<b>LNCO</b>	Lithium nickel cobalt oxide, $\text{LiNi}_x\text{Co}_{1-x}\text{O}_2$ (cathode chemistry)
<b>LTO</b>	Lithium titanate, $\text{Li}_4\text{Ti}_5\text{O}_{12}$ (anode chemistry)
<b>MCMB</b>	Mesocarbon microbeads
<b>MIP</b>	Mercury Intrusion Porosimetry
<b>Mnf</b>	Manufacturer
<b><math>m_{\text{sample}}</math></b>	Mass of the specimen
<b>MWCNT</b>	Multi-walled carbon nanotube
<b>N</b>	Number of cycles
<b>n</b>	Number of cells
<b>NiMH</b>	Nickel Metal Hydride battery
<b>NCA</b>	Lithium nickel cobalt aluminium oxide, $\text{LiNiCoAlO}_2$ (cathode chemistry)
<b>NCM</b>	Lithium nickel cobalt manganese oxide cell, $\text{LiNi}_x\text{Co}_y\text{Mn}_z\text{O}_2$ (cathode chemistry)
<b>NEMA</b>	National Electrical Manufacturers Association
<b>NMO</b>	Lithium nickel manganese oxide, $\text{LiNi}_x\text{Mn}_y\text{O}_4$ (cathode chemistry)
<b>NMP</b>	N-Methylpyrrolidone or 1-methyl-2pyrrolidinone
<b>OC</b>	Open Circuit
<b>OCV</b>	Open Circuit Voltage
<b>OMS</b>	Original Equipment Manufacturers
<b>Q</b>	Remaining or actual available capacity
<b><math>Q_0</math></b>	Initial nominal capacity
<b><math>Q/C_0</math></b>	Actual nominal capacity/initial nominal capacity
<b><math>Q_{\text{loss}}</math></b>	Capacity loss
<b><math>Q_{\text{nom}}</math></b>	Nominal capacity
<b>quasi-OCV</b>	Close-to-equilibrium (quasi) Open Circuit Voltage
<b>P</b>	Power

<b>PAU</b>	Pause
<b>PGE</b>	Gel-type polymer electrolyte
<b>PHEV</b>	Plug-in Hybrid Electric Vehicles
<b>PNGV</b>	Partnership for a New Generation of Vehicles
<b>P/P<sub>0</sub></b>	Actual power capability/initial power capability
<b>PPC</b>	Pulse or Peak Power Capability
<b>PNNL</b>	Pacific Northwest National Laboratory
<b>PSOC</b>	Partial State of Charge
<b>RESS</b>	Rechargeable Energy Storage System
<b><math>\rho_{\text{bulk}}</math></b>	Bulk density
<b>RPT</b>	Reference Performance Tests
<b>RT</b>	Room temperature
<b>RUL</b>	Remaining Useful Life
<b>SAE</b>	Society of Automotive Engineers
<b>SEI</b>	Solid Electrolyte Interface
<b>SEM</b>	Scanning Electron Microscopy
<b>SEM-EDS</b>	Scanning Electron Microscopy with Energy-Dispersive X-ray Spectroscopy
<b>SLI</b>	Starting, Lighting and Ignition battery
<b>SNL</b>	Sandia National Laboratories
<b>SOC</b>	State of Charge
<b>SOH</b>	State of Health
<b>T</b>	Temperature
<b>TO</b>	TiO <sub>2</sub> anode
<b>TCO</b>	Total Cost of Ownership
<b>UL</b>	Underwriters Laboratories Inc.
<b>UN</b>	United Nations
<b>UPS</b>	Uninterruptible Power Supply
<b>USABC</b>	U. S. Advanced Battery Consortium
<b>V</b>	Voltage
<b>VRLA</b>	Valve-Regulated Lead Acid battery

<b><math>V_{\text{sample}}</math></b>	Volume of the specimen
<b><math>V_{\text{pores}}</math></b>	Open pore volume
<b>XRD</b>	X-ray Diffraction
<b>ZEBRA</b>	Zero Emission Battery Research Activities

## GLOSSARY OF TERMS

---

### **Actual capacity (Q)**

The quantity of Ampere-hours that can be withdrawn from a battery at that moment. It is also called remaining capacity.

### **Adiabatic calorimetric test**

It consists checking the heat that the battery produces at different operation current profiles. This test enables estimating the thermal power that cells generate in certain operating conditions and the evolution of this value with the temperature. Either the average values of the thermal power can be assessed for a full operating cycle or transient variations of the thermal power for different temperature levels can be estimated. These measurements help evaluating the thermal performance of a cell (new and aged) and sizing the thermal management system of the battery pack containing these cells.

### **Ageing**

Permanent loss of capacity due to either repeated use or passage of time.

### **Ambient temperature**

The average temperature of the surroundings.

### **Anode**

The electrode in an electrochemical cell where the oxidation takes place. It gives up electrons to the external circuit during discharge (negative electrode) and the situation reverses during charge (positive electrode).

### **Apparent density**

The total mass divided by the total volume of the sample excluding open pores, but including closed pores. It is also called skeletal density.

**Balancing**

The process of redistribution in a battery, taking all individual cells to an equal state of charge or voltage level. It is also called equalisation.

**Battery or Battery pack**

One or more electrochemical cells electrically connected in series/parallel to provide the required operating voltage and current levels including, if any, monitors, controls and other ancillary components (fuse, diodes), case, terminals and markings.

**Battery Management System (BMS)**

Any electronic system that manages a rechargeable battery (cell or battery pack), such as by monitoring its state, calculating secondary data, reporting that data, protecting the battery, controlling its environment, and/or balancing it.

**Beginning of Life (BOL)**

The point in time at which life testing begins. A distinction is made between the performance of a battery at this point and its initial performance, because some degradation may take place during early testing before the start of life testing. Analysis of the effects of life testing is based on changes from the BOL performance. Thus, a BOL procedure is foreseen to determine cell characteristics (*i.e.* nominal capacity, internal resistance, etc.) at the beginning of any testing work.

**Boundary Layer**

The volume of electrolyte solution immediately adjacent to the electrode surface in which concentration changes occur due to the effects of the electrode process.

**Bulk density**

Mass of many particles divided by the total volume they occupy in the environment.

**Calendar Life (CL)**

The expected lifetime duration of a cell whether it is in active use or in storage.

**Calorimetry. Calorimetric test**

Calorimetry is the process of measuring the heat of chemical reactions or physical changes as well as heat capacity. A calorimeter is a device used to measure the quantity of heat transferred to or from an object. The instrument determines heat in it by direct measurement of temperature.

In an adiabatic environment, any heat generated by the material sample under test causes the sample to increase the temperature.

The adiabatic calorimetry test enables estimating the thermal power that cells generate in certain operating conditions and the evolution of this value with temperature. Either the average values of the thermal power can be assessed for a full operating cycle or transient variations of the thermal power for different temperature levels can be estimated. These measurements help evaluating the thermal performance of a cell (new and aged) and sizing the thermal management system of the battery pack containing these cells. At the same time, it is useful for the validation of efficiency tests results and internal resistance measurements.

### **Capacitor**

A passive two-terminal electrical component used to store energy electrostatically in an electric field. The forms of practical capacitors, originally known as condensers, vary widely, but all contain at least two electrical conductors (plates) separated by a dielectric (*i.e.* insulator). They are characterised by a single constant value for its capacitance (ratio of the electric charge on each conductor to the potential difference between them, expressed in farads (F) in SI units).

A new type of electrochemical capacitors are electric double-layer capacitors (EDLC) with carbon electrodes or derivatives. They do not have a conventional solid dielectric. There are also hybrid capacitors, such as lithium-ion capacitors (Li-cap)

### **Capacity [Ah]**

The quantity of Ampere-hours that can be withdrawn from a fully charged cell or battery under specified conditions of discharge. Parameters for capacity definition are: procedure of charge, current rate (C-rate) during discharge, cut-off voltage and temperature.

#### ***Available or operating Capacity [Ah]***

The total capacity that will be obtained from a cell or battery at defined discharge rates and other specified discharge or operating conditions. The capacity that can be discharged until discharge cut-off voltage from a completely charged cell.

#### ***Capacity Fade or Irreversible capacity loss***

Gradual loss of capacity of a secondary battery due to ageing processes.

#### ***Capacity Retention [%]***

The fraction of the full capacity available from a battery under specified conditions of discharge after it has been stored for a period of time.

***Nominal capacity [Ah]***

Capacity of the cell or battery, expressed in Ampere-hours, measured at nominal conditions defined by the manufacturer (data-sheet). The actual nominal capacity gives the reference of the irreversible capacity loss over the ageing.

***Reversible capacity loss***

Capacity loss (*e.g.* because of incomplete charge or storage) that can be recovered when the cell is recharged. It represents cell self-discharge.

**Cathode**

The electrode in an electrochemical cell where reduction takes place. During discharge, the positive electrode of the cell is the cathode. During charge, the situation reverses, and the negative electrode of the cell is the cathode.

**Cell or electrochemical cell**

The basic electrochemical unit providing a source of electrical energy by direct conversion of chemical energy. The cell consists of an assembly of electrodes, separators, electrolyte, container and terminals.

**Charge**

The conversion of electrical energy, provided in the form of a current from an external source, into chemical energy within a cell or battery.

***Charge Acceptance***

Ability of a battery to accept charge. It may be affected by temperature, charge rate, and state of charge.

**Check-up (CU)**

A check-up consists on a determined sequence of characterisation tests (Electrical Parameters Identification Testes, EPIT) to periodically check the performance of the battery under test.

**Close-to-equilibrium Open Circuit Voltage (quasi-OCV)**

The Open Circuit Voltage (OCV) curves for an electrochemical cell gives the information on the behaviour of the cell under conditions of zero current flow (see OCV definition below). The quasi-OCV, or also called pseudo-Open Circuit Voltage (ps-OCV), approach is used as a time-efficient method to analyse cell OCV characteristics. A small constant current is passed through the cell to track the cell voltage over cell whole operating range. The current rate needs

to be small enough for observing the transformation processes of cell active materials from voltage measurements.

### **Computed Tomography (CT)**

CT is a technology that uses computer-processed X-rays to produce tomographic images (virtual 'slices') of specific areas of the scanned object. It is a non-destructive scanning system. The CT scanner captures all surfaces, both external and internal, of complex free-form parts and assemblies without harming the object.

### **Conditioning**

Electrical cycle charging and discharging of a battery, before starting the real testing sequence, in order to ensure an adequate stabilisation of the battery or system performance. That is, it consists on the transformation of the active materials into their usable form. Even though the formation cycles, *i.e.* the first controlled charging and discharging cycles for obtaining the right microstructure and contacts between cell components, are carried out at the manufacturer facility, it is necessary to ensure that the passivating SEI layer is stable. It is sometimes indicated when a battery is first placed in service or returned to service after prolonged storage.

### **Constant Current (CC)**

A method of charging/discharging the battery using a current having little variation.

### **Constant Voltage (CV)**

A method of charging the battery by applying a fixed voltage and allowing variations in the current. It is also called constant potential charge.

### **Constant Power Discharge test**

Constant power discharge is very common in all applications where an inverted is coupled with the battery (*e.g.* UPS system). The test consists of battery full discharge at constant power. It provides information about continuous power capability, which is largely limited by the cell heating. Ragone plot can be obtained from this test.

### **Current-rate (C-rate)**

A notation used for expressing the current level relative to battery size to show the performance. It is the discharge or charge current (in Amperes) expressed as a multiple of the rated device capacity (in Ampere-hours). It is used to determine the charging or discharging current values and hence, the time needed to perform a complete charge or discharge. For example, for a

device having a capacity of one Ampere-hour under this reference condition, 5 A charging/discharging would be 5A / (1 Ah) rate or 5C [h<sup>-1</sup>].

**Cumulative runtime**

The collective runtime delivered by the battery over its entire service life.

**Current Density**

The current per unit active area of the surface of an electrode.

**Cut-off Voltage**

The battery voltage at which the discharge is terminated. It is also called end-voltage, minimum voltage, End of Discharge Voltage (EODV) or Discharge Voltage Limit (DVL).

**Cycle**

The discharge and subsequent or preceding charge of a secondary battery such that it is restored to its original conditions.

**Cycle Life**

The number of cycles under specified conditions which are available from a secondary battery before it fails to meet specified criteria of performance.

**Cylindrical cell**

Spirally wound cell which uses the electrode surface made by winding the electrodes and separators into a jelly-roll construction.

**Deep Discharge**

Withdrawal of at least 80% of the rated capacity of a battery.

**Depth of Discharge (DOD) [%]**

The percentage of the rated capacity of a device removed by discharge relative to a fully charged condition, normally referenced to a constant current discharge at the C<sub>1</sub>/1 rate. DOD can be an alternative method to indicate the State of Charge (SOC) of the cell.

**Diffusion**

The movement of species under the influence of a concentration gradient.

**Discharge**

The conversion of the chemical energy of a cell or battery into electrical energy and withdrawal of the electrical energy into a load.

**Double Layer**

The region in the vicinity of an electrode-electrolyte interface where the concentration of mobile ionic species has been changed to values differing from the bulk equilibrium value by the potential difference across the interface.

**Efficiency**

The ratio of the output of a secondary cell or battery to the input required to restore the initial state of charge, under specified conditions. There are different definitions for efficiency:

***Coulombic efficiency ( $\eta Ah$ )***

The ratio of the number of charges that enter the battery during charging compared to the number that can be extracted from the battery during discharging.

$$\text{Coulombic CHA efficiency [\%]} = \text{CHA capacity } (T_b, C\text{-rate}_i) \text{ [Ah]} / \text{DCH capacity (nominal conditions) [Ah]} \cdot 100$$

$$\text{Coulombic DCH efficiency [\%]} = \text{DCH capacity } (T_b, C\text{-rate}_i) \text{ [Ah]} / \text{CHA capacity (nominal conditions) [Ah]} \cdot 100$$

***Voltaic efficiency ( $\eta U$ )***

Voltage difference between the charging voltage and voltage of the battery during discharging.

***Energy efficiency ( $\eta Wh$ )***

A measure of the amount of energy that can be taken from the battery compared to the amount of energy that was charged into the battery beforehand (discharged Wh/charged Wh).

$$\text{Energy efficiency [\%]} = \text{DCH energy } (T_b, C\text{-rate}_i) \text{ [Wh]} / \text{CHA energy } (T_b, C\text{-rate}_i) \text{ [Wh]} \cdot 100$$

**Electrical Parameters Identification Tests (EPIT)**

Sequence of tests to obtain battery parameters usable for different purposes: performance characterisation, modelling, validation, comparison, etc.

**Electrode**

The site, area, or location at which electrochemical processes take place.

**Electrode Potential**

The voltage developed by a single plate either positive or negative against a standard reference electrode. The algebraic difference in voltage of any two electrodes equals the cell voltage.

**Electrolyte**

The medium which provides the ion transport mechanism (charge transfer) between the positive and negative electrodes of a cell.

**End of Life (EOL)**

A condition reached when the device under test is no longer capable of meeting the applicable goals. It may not coincide exactly with the ability to perform the life test profile (especially if cycling is done at elevated temperatures).

**End of Test (EOT)**

Criteria for ageing tests termination. EOT criteria can be based on many monitored test parameters and are generally selected based on the goals of the test.

**Equivalent Circuit**

An electrical circuit that models the fundamental properties of a device (*e.g.* a cell) or a circuit.

**Equilibrium voltage**

Voltage measured at rest in concrete state conditions (temperature, SOC, etc.).

**Error of the estimation**

Relative error of the estimation or prediction.

$$\text{Error of estimation} = ((\text{calculated theoretical value}) - (\text{measured value})) / (\text{measure average value}) \cdot 100$$

**Fade**

How rapidly battery capacity is lost. As batteries fade they have to be recharged more frequently.

**Float Charge**

A method of maintaining a battery in a charged condition by continuous, long-term constant-voltage charging, at a level sufficient to balance self-discharge.

**Formation**

See CONDITIONING.

**Full Equivalent Cycles (FEC)**

The number of complete (100% DOD) cycles corresponding to the amount of Ah-throughout (charged and discharged Ah). FEC is used to compare battery degradation with the same Ah-throughput when the cycling is performed at different DODs inferior to 100% DOD.

**Hybrid Pulse Power Characterisation (HPPC) Test**

It is also called Pulse Power Test (PPT). A test procedure consisting of pulse trains in order to calculate Direct Current (DC) internal resistance (IR) and pulse power and energy capabilities. The objective of pulse power characterisation profile is to demonstrate the discharge pulse power and regenerative charge pulse power capabilities at various SOC. The test protocol uses constant current at levels derived from the suppliers maximum rated pulse discharge and charge current.

**Hysteresis**

Hysteresis of the OCV is a phenomenon that makes the discharging and charging curves not to coincide. It appears as different values for the OCV at a given state of charge (SOC), temperature and age of the battery, caused by different modifications of reaction products that occur during charging and discharging. Consequently, hysteresis also affects the efficiency during cycling.

**Internal Impedance**

The opposition or resistance of a cell or battery to an alternating current of a particular frequency.

**Internal Resistance**

The opposition or resistance to the flow of an electric current within a cell or battery; the sum of the ionic and electronic resistances of the cell components.

**Life**

For rechargeable batteries, the duration of satisfactory performance, measured in years (float life) or in the number of charge/ discharge cycles (cycle life).

**Load**

A term used to indicate the current drain on a battery.

**Maximum Voltage**

The maximum allowed charge voltage value as proposed by the battery manufacturer. It is also called Charge Voltage Limit (CVL) and End of Charge Voltage (EOCV).

**Micro cycle**

Small DOD cycle (up to *ca.* 20% DOD).

**Nominal Voltage**

The characteristic operating voltage or rated typical voltage of the battery given by the manufacturer.

**Nominal capacity test**

This test measures capacity in Ah at constant current discharge rates corresponding to the suppliers rated normally 1C capacity (if not, at the rated one as nominal). 1C is used as reference for static capacity and energy measurement.

**Normalised current ( $I_n$ )**

A notation used for expressing the current level relative to battery size to show the performance. It is the current that can be applied to discharge a fully charged battery completely within  $n$  hours ( $C_n [\text{Ah}] = I_n [\text{A}] \cdot n [\text{h}]$ ).

**Open Circuit Voltage (OCV)**

The difference in voltage between the terminals of a cell under no-load condition (when the circuit is open). It is near to the equilibrium potential.

It is very difficult to measure the equilibrium potential in practical applications due to:

- The accuracy of the voltage monitoring devices.
- Voltage resolution in materials showing voltage plateau.
- Lengthy time for reaching the equilibrium (the state of the battery would be represented by an unique rest cell voltage).

In this context, this Thesis work refers OCV to the cell voltage after 3 hours rest (under no-load conditions).

**Overcharge**

The forcing of current through a battery after all the active material has been converted to the charged state. In other words, charging continued after 100% state of charge is achieved.

**Overdischarge**

Discharge past the point where the full capacity of the battery has been obtained.

**Overvoltage**

The potential difference between the equilibrium potential of an electrode and that of the electrode under an imposed polarization current.

**Parallel**

Term used to describe the interconnection of cells or batteries in which all of the like terminals are connected together. Parallel connections increase the capacity of the resultant battery according to the number of cells connected.

**Passivation**

The phenomenon by which an electrode, although in conditions of thermodynamic instability, remains protected because of its surface condition.

**Power and internal resistance test**

The power and internal resistance test is intended to determine the open circuit voltage (OCV), power capability (discharge and regen) and the ohmic resistance for discharge and charge conditions as a function of State of Charge. This test can be Hybrid Pulse Power Characterisation (HPPC) test.

**Polarisation**

The change of the potential of a cell or electrode from its equilibrium value caused by the passage of an electric current.

***Activation Polarisation***

That part of electrode or battery polarisation arising from the charge-transfer step of the electrode reaction.

***Concentration Polarisation***

That part of electrode or battery polarisation arising from concentration gradients of battery reactants and products caused by the passage of current.

***Ohmic Polarisation***

That part of electrode or battery polarisation arising from current flow through ohmic resistances within an electrode or battery.

**Prismatic Cell**

A cell fabricated with rectangular flat-plate electrodes (it is also called flat-plate cell).

**Ragone plot**

It is an energy density (in Wh/kg) versus power density (in W/kg) graph with logarithmic axes. It shows the influence of the discharge load (power) on the energy that the battery can deliver.

**Rate capability test**

Energy and capacity measurement test at different temperatures and charge and discharge rates. It provides information about the operating capacity, energy efficiency depending on discharge C-rate, charge efficiency for different charging C-rates, etc.

**Rechargeable battery**

A galvanic battery which, after discharge, may be restored to the charged state by the passage of an electric current through the cell in the opposite direction to that of discharge (it is also called both secondary battery and storage battery).

**Reference Electrode**

A specially chosen electrode which has a reproducible potential against which other electrode potentials may be measured.

**Remaining capacity (Q)**

See ACTUAL CAPACITY.

**Remaining useful life (RUL)**

It describes ageing of the battery scaled from the 100% to the EOL. Thus, the RUL would be 100% at the BOL and 0% at the EOL.

**Round trip efficiency**

Ratio between the charged and discharged energy.

**Room temperature (RT)**

25°C ambient temperature. Tests at RT have to be done in temperature chambers.

**Secondary battery**

See RECHARGEABLE BATTERY.

**Self-Discharge**

The loss of the useful capacity of a cell or battery due to internal chemical action. The drop in cell voltage under open-circuit conditions that occurs spontaneously while batteries are left standing.

**Separator**

An ion permeable, electronically nonconductive, spacer or material which prevents electronic contact between electrodes of opposite polarity in the same cell.

**Series**

The interconnection of cells or batteries in such a manner that the positive terminal of the first is connected to the negative terminal of the second, and so on. Series connections increase the voltage of the resultant battery according to the number of cells connected.

**Service Life**

The period of useful life of a battery, expressed in time, before a predetermined end of voltage is reached.

**Shallow cycle**

See MICRO CYCLE.

**Shelf Life**

The duration of storage under specified conditions at the end of which a cell or battery still retains the ability to give a specified performance.

**State of Charge (SOC) [%]**

The ratio between the amount of lithium ions remaining in the negative electrode and the total amount of active lithium ions in the cell system, *i.e.* the sum of lithium ions in the negative and positive electrode. The SOC would be given by cell OCV characteristics ( $SOC = f(OCV)$ ).

In practical applications, SOC is used to represent the amount of available capacity in a battery. In this sense, and according to USABC, a battery SOC is “the ratio of the Ampere hours remaining in a battery at a given rate (residual capacity,  $Q_{res}$ ) to the rated capacity under the same specified conditions ( $Q_{rated}$ )” (thermodynamic aspects would be inherent in this approach).

$$SOC_{USABC} [\%] = (Q_{res} / Q_{rated}) \cdot 100$$

This Thesis work refers to SOC always under 1C operation conditions, as follows:

$$SOC [\%] = (Q_{res} / Q) \cdot 100$$

where  $Q$  is the cell actual nominal capacity (it needs to be updated as the State of Health (SOH) of the cell changes) and  $Q_{\text{res}}$  is calculated as  $Q_{\text{res}} = Q - Ah_{\text{discharged at 1C}}$ , which, alternatively, can be expressed as  $\text{SOC} = 100\% - \text{DOD}$ . This way, the SOC in tests such as HPPC, or middle SOC during cycling, is fixed Ah-based (at 1C).

This definition is used, on the one hand, to distinguish the cycling amplitude from cell cycling window (e.g. 10% DOD between 60-70% SOC) and, on the other hand, because coulomb counting method is used to track the change in charge remaining in the battery at any operating condition (with no chance to fully charge/discharge the battery under the same specific condition).

### **State of Health (SOH) [%]**

It informs of ageing and represents the fraction of performance deterioration remaining (it is an indication of how much of the useful lifetime of the battery has been consumed). There is no absolute definition of how to estimate SOH, so it is defined by the manufacturer or user, but it takes into account any parameter which changes significantly with age, such as charge acceptance, internal resistance, voltage and self-discharge. In a Li-ion battery, SOH is commonly determined by the capacity and/or internal resistance as follows:

$$\text{SOH} (Q) = 100 \% - \Delta Q [\%] \text{ or } \text{SOH} (IR) = 100 \% - \Delta IR [\%]$$

*$\Delta Q$  or  $\Delta IR$ : ratio between capacity or internal resistance of the battery in use and capacity or internal resistance of the unused battery*

### **Stationary Battery**

A secondary battery designed for use in a fixed location.

### **Storage battery**

See RECHARGEABLE BATTERY.

### **Thermal Runaway**

A condition whereby a battery on charge or discharge will overheat and destroy itself through internal heat generation caused by high overcharge or over-discharging current or other abusive condition.

### **Thermography**

Infrared imaging. Thermographic cameras detect radiation in the infrared range of the electromagnetic spectrum (it operates in wavelengths as long as 14000 nm) and produce images of that radiation, called thermograms. The amount of radiation emitted by an object increases

with temperature; therefore, thermography allows seeing variations in temperature. When viewed through a thermal imaging camera, warm objects stand out well against cooler backgrounds. Hence, this technique is useful to study battery heat generation distribution (in the cells and terminals) at different operation conditions.

### **Traction Battery**

A secondary battery designed for the propulsion of electric vehicles or electrically operated mobile equipment operating in a deep-cycle regime.

### **Vent**

A normally sealed mechanism which allows for the controlled escape of gases from a cell.

#### ***Vented cell***

A cell design incorporating a vent mechanism to relieve excessive pressure and expel gases that are generated during the operation or abuse testing of the cell.

### **Voltage (V)**

The theoretical voltage of a cell is a function of the electrode materials, *i.e.* it is an intrinsic property of active materials. It is also dependent on temperature and concentration, as expressed by Nernst equation. OCV is a close approximation of the theoretical voltage.

#### ***Working Voltage***

The voltage of a cell during operation (under load) is always lower than the theoretical voltage: it is given by OCV and overvoltages that take place due to diffusion processes, hysteresis, electrochemical reactions and ohmic resistances. Thus the cell voltage is always above OCV during charging and below during discharging.

$$V_{battery} = OCV - ohmic\ voltage\ drop - reaction\ overvoltage - diffusion\ overvoltage$$



# *Chapter 1*

## INTRODUCTION

---

*This introductory chapter describes why there is need of developing a methodology for battery selection.*



## 1. INTRODUCTION

### 1.1 FRAMEWORK AND MOTIVATION

- **General context**

As the global economy begins to strain under the pressure of high petroleum prices [1] and environmental concerns, sustainable technological evolution has spurred on the development of various types of electrically rechargeable Energy Storage Systems (ESS). It is targeted to meet the growing and critical demands for electrically driven means of transport, power grids and renewable energy integration.

IK4-Ikerlan is involved in introducing competitive rechargeable battery solutions into the market using commercially available cell technologies, as shown within the value chain in Figure 1-1. Development of cell technologies is important, but selecting the most suitable technology is vital for market introduction of the battery. Adequate system integration is essential for the performance and safety. Battery reliability requires a BMS and thermal management system for customer assurance, fulfilling safety, cost and novel application issues. Anyhow, the battery technology is the core driver for creating a competitive battery pack.

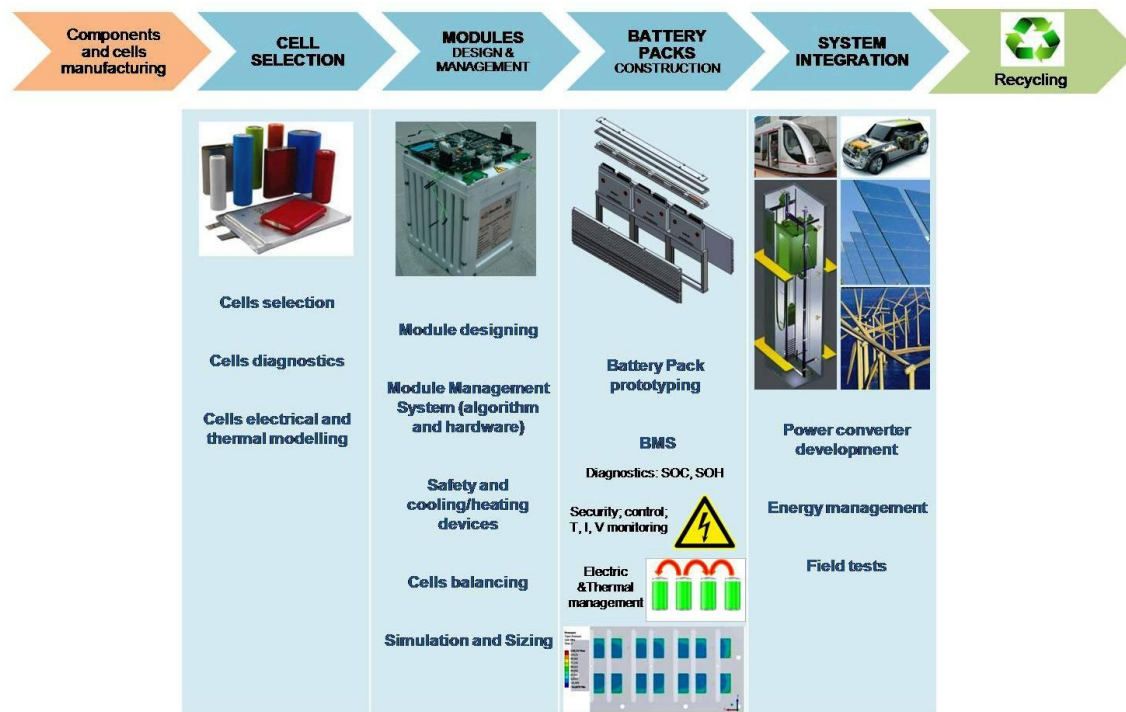


*Figure 1-1. Objectives development in the value chain of electrical ESS at IK4-Ikerlan*

The existing wide range of electrochemical rechargeable battery technologies nowadays can be grouped into lead, nickel, lithium, sodium and flow battery families. New developments based on metal-air (Fe/air, Zn/air, Al/air and Li/air) or lithium-sulphur are in a distant state of development to meet market specifications in various sectors. The state of development of lithium-ion (Li-ion) batteries (LIB) has met global battery market specifications in various sectors, as shown in Figure 1-2: portable and consumer electronic devices, vehicle and other means of traction transport, stationary applications and grid (load levelling, peak shaving, etc.). LIB technology has advanced largely from its first commercialisation in 1991 (Sony and Asahi Kasei), capturing over half of the sales value of secondary consumer market [2]. It is a mature technology for portable equipments that has replaced Nickel Metal Hydride (NiMH) battery in many types of portable equipments, such as laptops and mobile phones. Unfortunately, these Li-ion cells in mass production status do not still fulfil the specified requirements for large-scale potential applications, especially with respect to the lifetime and safety. However, it is a promising candidate due to its large energy and power densities. Intensive commitment of battery world-wide manufacturers and automotive companies to develop ESS based on Li-ion technology for new generations of Hybrid and Electric Vehicles (HEV and EV) is making possible the reduction in manufacturing costs and therefore the continuous development of this technology. However, the long cell lifetime and performance required for industrial applications (e.g. 10-15 years for automotive applications) is still uncertain for LIB. Various types of LIB can be found on the market and their characteristics depend strongly on the active materials combination and also cell design and manufacturing.

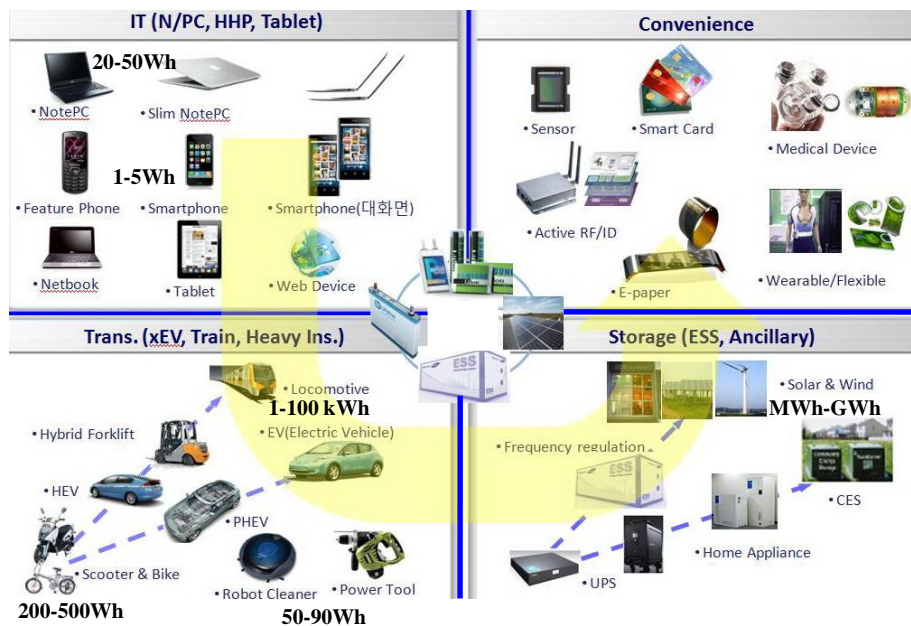
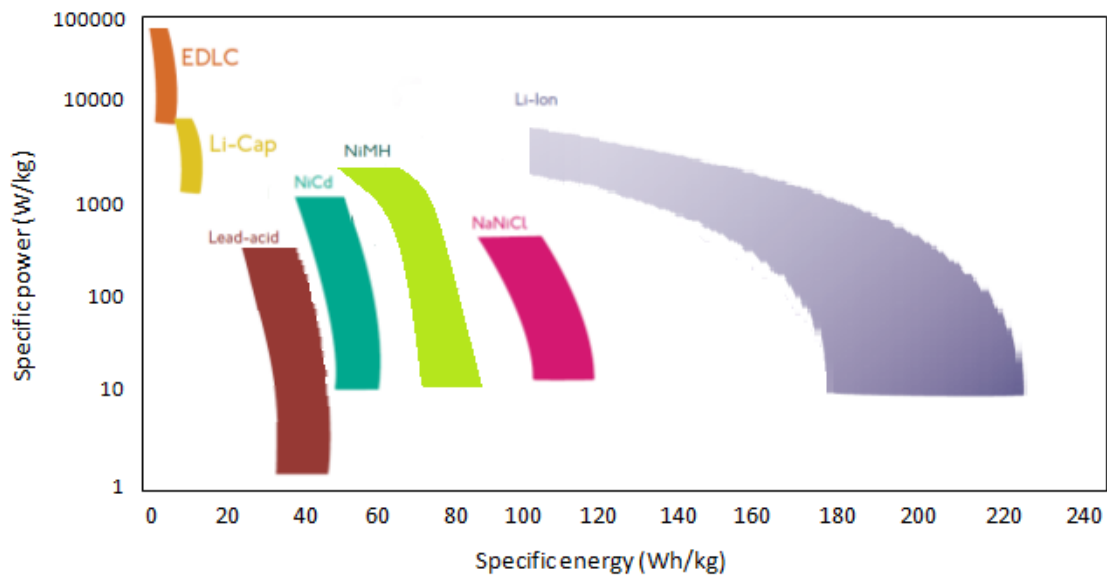


Figure 1-2. Potential range of applications of electrochemical rechargeable battery technologies (Source: Samsung)

Next, the revision of the state of the art related to the most suitable battery technologies for different novel industrial applications is described shortly.

- **Rechargeable battery technologies**

There is a wide range of electrically rechargeable battery technologies. The main assets of these storage systems are their energy densities and technological maturity. Technology capital costs and application benefits are very sensitive to the configuration of the storage system both in terms of power and energy storage capacity [3]. Ragone chart shown in Figure 1-3 plots the specific power and energy delivered by the major electrochemical and electrostatic large format secondary technologies. For consumer cells, Li-ion battery specific energy and power ranges are 190-240 Wh/kg and 4-300 W/kg, respectively [4]. Each type of energy storage technology has its own operating cost parameters. Different cell costs are gathered in Table 1-1. In general, some energy storage systems will not be cost-effective since more technology development is needed to lower the capital costs of such storage systems.



**Figure 1-3.** Distribution of various battery technologies according to their energy and power densities. Specifications at cell level. EDLC: Electric Double-Layer Capacitors; Li-Cap: lithium-carbon capacitor; NiCd: nickel-cadmium; NiMH: nickel-metal hydride; NaNiCl: sodium-nickel chloride (ZEBRA (Zero Emission Battery Research Activities) batteries); Li-ion: lithium-ion

**Table 1-1.** Cell voltages and current costs of various battery technologies at cell level [5]

Technology	Nominal voltage (V)	Costs (€/kWh)
Lead-acid (SLI)	2.0	25–40 for OEM 100–180 for after-market
Nickel-cadmium	1.2	200 – 500 for OEM
Nickel-metal hydride	1.2	275 – 550 for OEM 600 for HEVs
Sodium-nickel chloride	2.5	350 – 600
Lithium-ion (LiCoO <sub>2</sub> )	3.6	200–500 for OEM 400–800 for HEVs
Lithium polymer	3.7	200–500 for OEM 400–800 for HEVs
Lithium-ion (LiFePO <sub>4</sub> )	3.25	200–500 for OEM 400–800 for HEVs
Supercapacitor	2.5–2.8	10,000–20,000
Lithium carbon capacitors	3.8–4	Early market introduction
Lithium-sulphur	2.2	Early market introduction
Rechargeable metal-air batteries	1–4 (depending on technology)	Early research state

SLI: starting, lighting and ignition; OEM: original equipment manufacturer; HEV: hybrid electric vehicle.

Major battery technologies are shortly described below:

#### - Lead-acid (Pb) electrochemical battery

They are by far the cheapest technology with regard to the raw material costs. Other advantages are intrinsic safety and high recycling quotes (more than 95% [5]). The main drawbacks are the low energy density (30-50 Wh/kg with 75-80% efficiency [3]), sulfation and environmental issues (they contain toxic Pb). Further issues are lifetime (500-1500 cycle lifetime [6-8]) and dynamic charge acceptance.

In early stages, nickel-iron (NiFe), nickel-zinc (NiZn) and zinc-chloride (ZnCl<sub>2</sub>) batteries were under development together with lead-acid batteries for electric vehicles, and the latter seemed to just meet market specifications. A new generation step ahead with dramatic improvement is **advanced lead-acid** battery, which incorporates carbon electrode. A supercapacitor carbon electrode is combined with the lead-acid battery negative plate in a single cell to better regulate the flow of energy, thereby extending the power and lifetime. They present the following characteristics: 40-60 Wh/kg with 75-95% efficiency, 4500 cycle lifetime and high specific power (from 150-200 W/kg of lead-acid battery to 2000 W/kg for advanced lead acid) [3].

#### - Nickel-based electrochemical batteries

**Nickel Cadmium (NiCd)** technology shows a slightly higher energy density than lead-acid batteries and a significantly higher power density, but the specific costs are much higher.

**Nickel Metal Hydride (NiMH)** battery is a further development of NiCd batteries, aiming at eliminating toxic cadmium. Voltage profiles of both batteries are very similar. The deep-temperature performance of nickel-metal hydride batteries is rather poor. However,

they approximately double the energy density that nickel–cadmium batteries have, and they are specially characterised by high power density (greater than 1000 W/kg) and long lifetime. Some limitations of this technology are high self-discharge, memory effect and high maintenance requirements.

- **Lithium-ion (Li-ion) electrochemical batteries (LIB)**

Li-ion cells achieve the highest gravimetric energy and power densities of all commercially available rechargeable batteries (Figure 1-3). Their energy efficiency (85-95%) is also very high compared with other battery technologies. Power, low- and high-temperature performances, lifetime and safety characteristics depend strongly on the active materials combination. Further details are given later in this section.

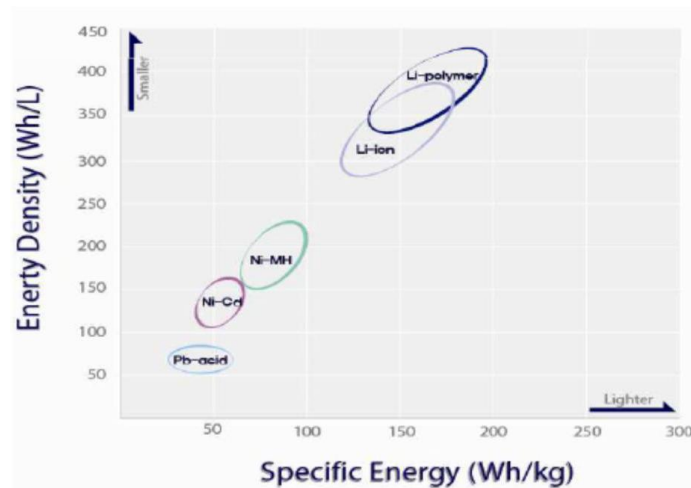
- **Sodium-nickel chloride electrochemical battery** ( $\text{NaNiCl}_2$ , Zero Emission Battery Research Activites, ZEBRA)

It is a high temperature system operating around 300°C, which requires good isolation because cooling-down to ambient temperatures leads to a high thermo-mechanical stress of the ceramic electrolyte. Furthermore, its power capability is limited due to the high internal resistance and it suffers daily 10-15% self-discharge because of high temperature operation. However, it is tolerant of short circuits, it is maintenance free and the material costs are low.

- **Electric double-layer capacitors (EDLC)**. Electromagnetic storage technology.

The energy storage is purely electrostatic, no chemical reaction occurs during charging and discharging. They are, therefore, highly reversible and are capable of working at high current rates, which makes them suitable for boosting and regenerative braking. They have very high power density and excellent cycle lifetime, from 500000 to 1000000 [5, 9], that outperforms nearly all battery technologies. The energy density of EDLC is however much lower than electrochemical batteries. Hence, they can be used only as buffers within a system in combination with other energy storage technology (stored energy in EDLC would be used to ensure service continuity when switching from one source of electricity to another). EDLC energy cost is very high, *ca.* 15000 €/kWh of storage capacity, but the cost of available power is very low, 15 €/kW or less [5].

The advantages of EDLC have been combined with those of Li-ion batteries. Lithium-carbon capacitor or hybrid capacitor (combination of a EDLC and a lithium-battery: **Li-cap**) is the improved technology that has been commercialised recently. It possess a higher power density and cycle lifetime than purely electrochemical batteries.



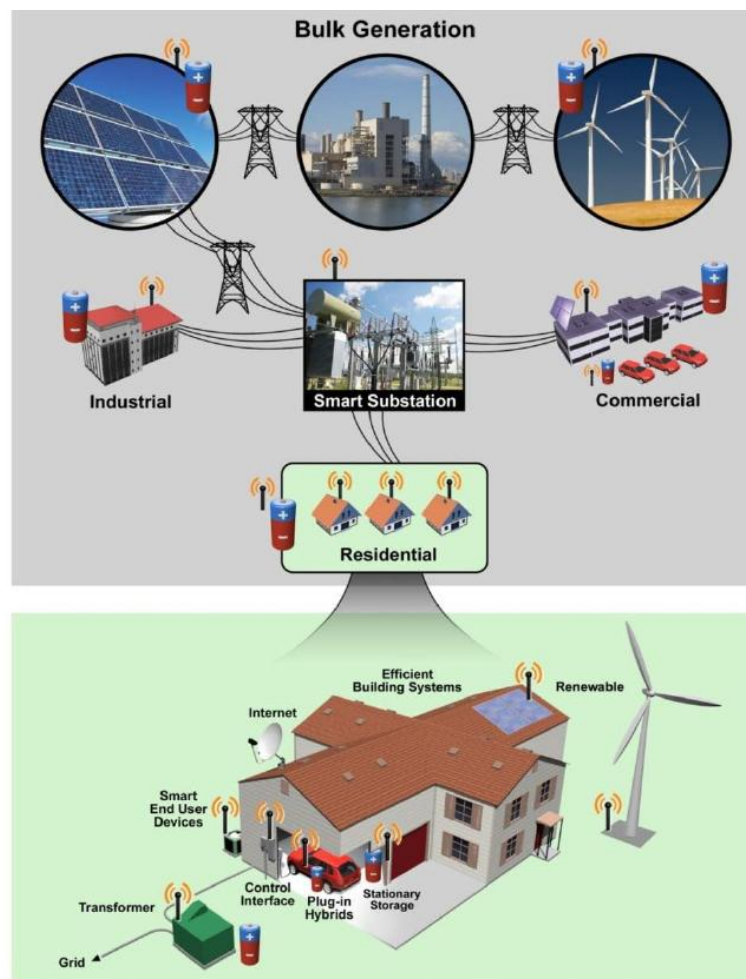
**Figure 1-4.** Low temperature battery technologies. Relation between volumetric and gravimetric energy density [10]

Figure 1-4 illustrates the relationship between gravimetric and volumetric energy density of major low temperature electrochemical rechargeable technologies. Mass and volume of the energy storage capability are other relevant issues for the applications. LIBs weigh around half of NiCd or NiMH batteries of the same capacity. Moreover, their volumetric size is 40-50% and 20-30% smaller than NiCd and NiMH cells have, respectively. Lead-acid technology has the largest volume and weight. The average voltage of a LIB (3.6-3.7 V) is three times that of NiCd or NiMH cell (1.2 V), which reduces significantly the required number of cells to meet application specifications. This way, parallel connection of LIB allows increasing capacity and discharging current rates, which cannot be easily done using NiCd or NiMH cells. LIB charging efficiency (85-95%) and fast charging capability (90% in *ca.* 1.5-2 h) also stand out (*e.g.* for lead-acid technology, the charging efficiency is 70-80% and 90% charging requires *ca.* 6-7 h). Moreover, unlike NiCd and NiMH technology, LIB does not suffer the so called memory effect, which reduces the usable energy and complicates the system maintenance. On the other hand, LIB is the technology that presents lowest self-discharge (2 %/month) and NiMH the largest (15-25 %/month). Anyway, despite the discussion on technical performance indicators, the price of the battery is the main challenge for market introduction. Cost reduction is achieved by technology improvements, but mainly by economy-of-scale effects. Lead-acid technology is the cheapest by far at the market (100-250 €/kWh) and it is the most mature commercial rechargeable battery technology. NiCd is also a mature technology and its cost is low (200-500 €/kWh). The cost of NiMH is slightly larger than NiCd, which is one of the major drawbacks of this technology, but it is still lower than that of LIB (300-800 €/kWh). LIB is relatively new technology with high cost (system costs are enhanced *e.g.* due to control and safety electronics), but it does not require maintenance, while most of lead-acid technologies for

instance does (except for valve-regulated lead-acid, VLRA, battery), and cycle lifetime is larger for LIB, so replacements costs are to be higher for lead-acid than for LIB technology. In addition, the anticipated manufacturing scale will result in lower costs for this promising technology.

- **Applications**

Electric energy storage systems have applications along the entire electric enterprise value chain, as illustrated shortly in Figure 1-5. There are broad types of large scale energy storage applications: system integration (which encompasses applications such as system applications and renewable integration), utility applications, distributed energy storage applications, commercial and industrial applications, residential applications, transport applications, etc. A short review in stationary and transport applications is described below. Stationary applications analysis is based on a EPRI report [3].



**Figure 1-5.** Stationary energy storage to compliment the renewable energy resources and load levelling for grid integration [11]

*System applications* are those in which energy storage provides wholesale market opportunities as well as other benefits such as energy arbitrage, reduced transmission congestion, lower local marginal prices, voltage regulation, and frequency regulation to utilities, customers and society. Electrically rechargeable technology options for system applications include large flow batteries such as zinc-bromine and vanadium redox, large advanced lead-acid battery systems, LIBs, and flywheel systems.

*Renewables integration* need electric energy storage to support electric system balancing and network management (to decouple synchronisation between power generation and consumption), to improve the capacity factor of generation on the system, for transmission reservation, energy arbitrage, ancillary services, and integration cost reduction. Rapid voltage excursions (wind ramps, cloud effects, etc.) present a significant challenge to utilities trying to integrate and manage these resources on their systems. Storage can help by inventorying electricity at night when the demand is low, and act as a shock absorber by smoothing out generation fluctuations. Electrically rechargeable technologies that appear compatible with those requirements include large flow batteries, advanced lead-acid batteries and LIBs. Large photovoltaic applications that may require many cycles and fast response may include EDLC.

In *utility applications* (rural and urban load centres), microgrid peak loads managing is a critical issue for electric enterprise. Improvements options based on electrically rechargeable energy storage technology include lead-acid and advanced lead-acid, sodium-sulfur, vanadium redox, zinc-bromine, Li-ion and metal-air battery systems. *Distributed energy storage applications* involve small energy storage systems (substations) sited on the utility side to support grid peak loads, and the technology options include advanced lead-acid, lithium-ion and flow type batteries. *Commercial and industrial applications* typically require uninterrupted power supply (UPS) or use of back-up generators. Lead-acid batteries have a large global market in UPSs, which require power quality (stored energy is only used for a few seconds). *Residential applications* demand for back-up power, home energy management and, in the future, fast-charging plug-in hybrid and electric vehicles. Technology options in this latter case include lead-acid, advanced lead-acid batteries and LIBs, and potentially small redox systems.

*Transport applications* include bikes and scooters, different automotive (cars and buses) topologies (EV, HEV and Plug-in Hybrid Electric Vehicle (PHEV)), locomotion, forklift or even novel elevators (regenerative systems). A battery for electrified vehicles is always a compromise between a high power (HP) performance, a high energy (HE) storage capability, a low weight, a small volume, a long lifetime and a low price. For each propulsion type, a suitable battery system is needed. NiMH mature technology is the world market leader in HEVs

nowadays (Toyota, Honda, Lexus and many other car manufacturers) and it will be for several years [5], but it is expected that LIBs will overtake this market segment [12], as research activity on today competitive NiMH batteries is relatively low. The use of ZEBRA batteries in private vehicles is difficult because of the low daily mileage and, therefore, the need to compensate thermal losses. They are an interesting option only for fleets, *e.g.* for delivery services in cities. Only two companies are developing ZEBRA batteries worldwide and they seem to focus more on stationary than on automotive applications [5]. At present, the costs for ZEBRA systems are roughly similar to those of LIBs [5]. For automotive applications, the perspectives for LIBs regarding the costs, energy density and handling are better than for ZEBRA, even though there are manufacturers that offer EVs with ZEBRA batteries for niche markets [5]. The starting, lighting and ignition (SLI) battery, which is part of all automotive vehicles, typically is a lead-acid battery, but concepts with LIBs are also under development [13, 14]. Lead-acid batteries are besides used in generating stationary systems for start-up stage. Advanced lead-acid technology is introducing automotive market successfully, but the manufacturing scale is too low for meeting this sector demand. Fully EVs use mainly LIBs owing to high material costs of NiMH. LIB also dominates E-bikes market and it is being introduced in applications where commonly EDLC or NiMH are used, such as E-bus and hybrid power railroad locomotives (traction tramway application).

Table 1-2 summarises main applications for rechargeable electric ESS and the most adequate low temperature technologies. Lead-acid is the only rechargeable mature technology for system applications (in 2010, LIB installations were just 0.02% of worldwide total storage capacity for electrical energy) [3]. Li-ion technology represents a good market value for medium scale stationary applications and it is being gradually introduced. There is almost a consensus that the still emerging Li-ion technology for some applications is the prime candidate to meet the demand of different sectors [15, 16], and large advances in this technology have made possible its applicability to E-mobility and renewable energy storage industries. Near-term traction batteries include NiMH potentially and Li-ion technology. Advanced lead-acid is positioned to become the low-cost automotive alternative in the long-term. Nonetheless, government incentives, commitments of battery manufacturers and automotive companies, and large research activity on Li-ion technology, are enabling a closer approach to industry goals. These are actions leading to the reduction of costs (lower material prices, less expensive battery components and more efficient production processes) for the mass market (increased production capacity especially in the far east and new production capacities in the USA and Europe). Superior especially energy and power characteristics make them the most promising rechargeable technology for vehicle traction power options. It is already a reality for fully EVs

(Nissan Leaf, Mitsubishi i-MiEV, Renault Zoe, Smart, Coda, Fiat 500, Kia Soul, Honda Fit, etc.), HEVs (BMW Active Hybrid 3, Fisker Chevy Spark EV, Infiniti M35H, Honda Civic & CR-Z, Chevy Malibu mild-hybrid, etc.), PHEVs (Chevy Volt, Cadillac ELR, Ford Focus EV, Volvo, Toyota Prius, etc.), hybrid power railroad tramways (Bombardier-Akasol), heavy-duty EVs (hybrid Allison Buses, Proterra, etc.), E-bikes (BionX, Quipplan, BH emotion, Trek, Cannondale, etc.), E-scooters (Yamaha, Suzuki, Motorino, etc.), etc. Lithium resources for meeting worldwide large LIBs demand seems to be sufficient (they are limited to few countries with a core area in South America), but a recycling system for retrieval needs to be established and is ongoing [5].

**Table 1-2.** Suitable low temperature secondary technologies for medium-large scale applications

APPLICATION		TECHNOLOGY
SLI (100 - 600 Wh)	Cars, trucks, buses, lawn mowers, wheel chairs, robots	Lead-acid
VEHICLE TRACTION (20 - 630 kWh)	EV, HEV, PHEV, fork lift trucks, milk floats, locomotives	NiMH, Li-ion
STATIONARY APPLICATIONS (250 Wh - 5 MWh)	Emergency power, local energy storage, remote relay stations, communication base stations, UPS, network management, renewable integration, etc.	Lead-acid, advanced lead-acid, Li-ion, vanadium redox-flow
GRID SYSTEM APPLICATIONS (5 - 100 MWh)	Spinning reserve, peak shaving, load leveling, etc.	Lead-acid, Li-ion, EDLC, vanadium redox-flow

Looking at the perspectives of the available storage technologies, Li-ion battery technology seems to be a good choice for case studies due to its broad properties and applicability in several sectors. For that reason, an overview of this technology is given below.

- **Lithium-ion batteries**

A brief description of the multiple variables that form part of LIB is summarised in terms of materials, cell configuration and market opportunities.

- Materials

The state of the art is summarised in Appendix A. The cathode is the lithium battery component that most limits cell performance. Table 1-3 outlines strengths and weaknesses of main cathode chemistries. Note that the exact composition of the cathode material varies across suppliers and can also be a mix of the described chemistries. Graphite and carbon-based anode materials are dominant but lithium titanium oxide ( $\text{Li}_4\text{Ti}_5\text{O}_{12}$ , LTO), new generation anode, is attractive for

advanced Li-ion batteries [17] maintaining the standard  $\text{LiPF}_6$ -carbonate solvent, liquid electrolyte.

**Table 1-3.** Comparison of performance of main Li-ion cells cathodes (the higher the rating, 1:4, the better) [18, 19]

	<b>LiCoO<sub>2</sub> (LCO)</b>	<b>LiMn<sub>2</sub>O<sub>4</sub> (LMO)</b>	<b>LiNiCoAlO<sub>2</sub> (NCA)</b>	<b>LiNi<sub>x</sub>Co<sub>y</sub>Mn<sub>z</sub>O<sub>2</sub> (NCM)</b>	<b>LiFePO<sub>4</sub> (LFP)</b>
<b>Specific Energy</b>	4	3	4	4	2
<b>Specific Power</b>	2	3	4	3	3
<b>Safety</b>	2	3	2	3	4
<b>Cost</b>	1	3	2	2	3
<b>Performance</b>	3	2	3	3	3
<b>Lifetime (life span)</b>	2	2	4	3	4

**Table 1-4.** Negative active material comparison (1: good, 2: better, 3: best) [20]

	<b>Graphite</b>	<b>Carbon</b>	<b>LTO</b>
<b>Specific Energy</b>	3	2	1
<b>Specific Power</b>	1	2	3
<b>Safety</b>	1	2	3
<b>Low temperature performance</b>	1	2	3
<b>Lifetime</b>	1	2	3

Table 1-4 compares the three anodes. LTO is a safer alternative to the lithiated graphite ( $\text{LiC}_6$ ) anode due to higher potential and therefore intrinsic overcharge protection. In addition, it does not form a passivating layer with the electrolyte, thus giving rise to long lifetime. As shown in Figure 1-6, graphite operates under kinetic stability of common liquid organic electrolytes. Solid Electrolyte Interface (SEI) provides the system extrinsic stability (LTO anodes do not depend on a SEI layer for stability). LTO electrode operates within the stability window of electrolyte, which enables safer and more reliable systems. LTO anode has, however, lower specific capacity (175 mAh/g) and larger operating voltage (1.5 V vs. Li) than graphite (372 mAh/g and ~1 V vs. Li, respectively). LTO-based cells energy density is therefore lower. Costs analysis of different cathode and graphite or LTO combinations is shown in Figure 1-7. Overall cost depends on safety and lifetime of the full cell battery. In order to satisfy the energy requirement of a specific application, LTO packs require more cells and more cathode active material. LTO-based systems are a factor of two larger and heavier than graphite ones and in turn more expensive. On the other hand, LFP-based cell system is slightly more expensive than NCM-based system due to lower potential of LFP cathode. All these comparisons categorised the cathode and anode materials according to their performance of specific property. Table 1-5 summarises the main properties of the most common commercial positive and negative electrodes combinations. It is difficult to find a good solution for all and always a compromise

seems to be the only choice. The decision is probably driven by the application requirements, that will determine which combination is finally adopted.

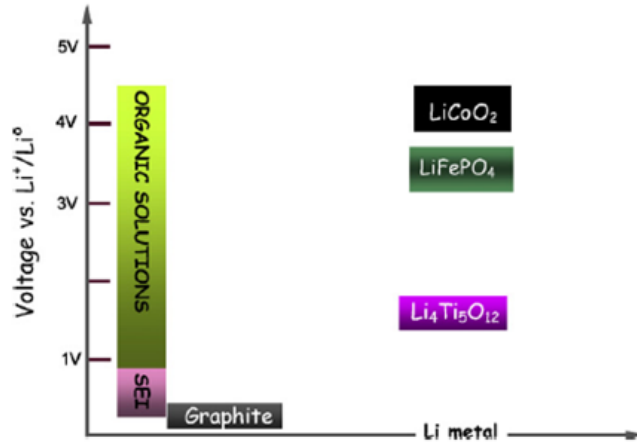


Figure 1-6. Voltage vs.  $\text{Li}^+/\text{Li}^\circ$  of various electrode materials in comparison with the stability window of common liquid organic electrolytes [17]

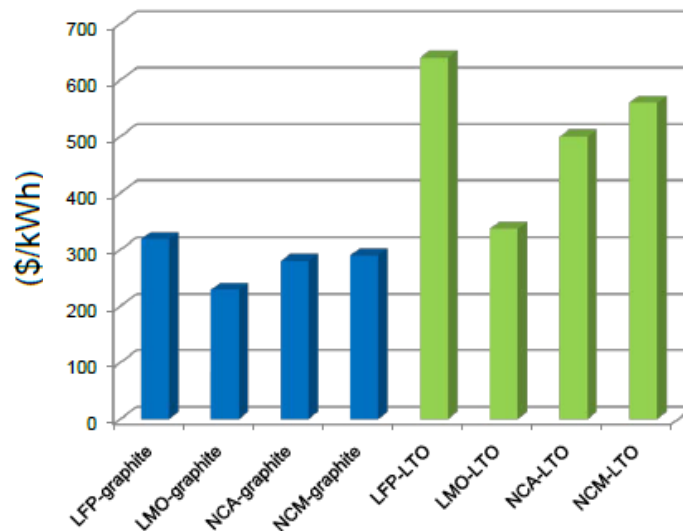


Figure 1-7. Cost (\$/kWh) analysis of different cell systems [11]

Table 1-5. Main properties comparison of the most common commercial batteries [21]

Cathode	Anode	Nominal Voltage	Energy Density	Specific Power	Cycling	Safety	Cost
LCO	Graphite	ca. 3.7 V	High	Fair	Fair	Fair	High
LMO	Graphite	ca. 3.8 V	High	High	Fair	Good	Low
LMO	LTO	ca. 2.3 V	Low	Low	High	Good	High
NCM	Graphite	ca. 3.7 V	High	Fair	Low	Fair	High
NCA	Graphite	ca. 3.7 V	High	High	Fair	Fair	High
LMO-NCM	Graphite	ca. 3.9 V	High	High	Fair	Very Good	Fair
LMO-NCA	Graphite	No data available	High	Fair	Good	Low	High
LFP	Graphite	ca. 3.3 V	Low	High	High	Very Good	Fair
LNO	Graphite	ca. 3.7 V	High	Fair	Fair	Fair	Fair

o Cell configuration

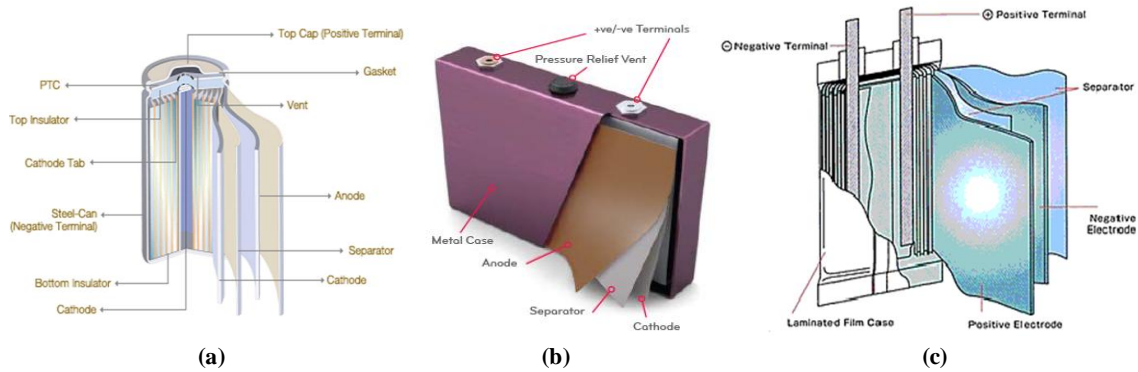


Figure 1-8. (a) Spiral bound cylindrical cell [22], (b) prismatic cell [23] and (c) pouch cell [22]

Li-ion cells are widely available in many sizes and housing ways. Three different Li-ion cell designs are being developed and produced today, as shown in Figure 1-8: cylindrical, prismatic and pouch cells. The case may be simply a robust container made from an aluminium foil, plastic (prismatic) or metal (cylindrical and prismatic), insulated from the electrodes. Table 1-6 summarises the main properties of the three cell mechanical constructions. More details are described in Appendix A. Production experience of cylindrical cells is long but the space utilisation is a main drawback. Pouch cells have higher weight energy density and better heat transfer, but the quality of the welding is an issue even after several years of ongoing development. Prismatic cells are the preferred configuration for automotive application [5] due to the strength of the container compared to pouch cells with case foils, but the latter dominates high power rechargeable lithium cell market [21]. However, from the safety point of view, the prismatic configuration is the best choice, but the thermal characteristics of plastic case prismatic cells are sometimes not acceptable.

Table 1-6. Properties of different cell mechanical constructions

	CYLINDRIC METAL CASE	PRISMATIC METAL CASE	POUCH CELL
<b>Robust</b>	Yes	Yes	No
<b>Packaging efficiency</b>	Bad	Good	Excellent
<b>Ability to scale-up/ Large format</b>	Limited (hard to increase capacity)	Good	Excellent
<b>Manufacturing Cost</b>	Economical (standardised sizes)	Expensive (few standardised sizes)	Economical
<b>Thermal characteristics</b>	Good in small cells Limited in large cells	Good	Very good
<b>Safety</b>	Requires vents. Substantial pressure may cause cell to explode	Good	Intrinsic: swelling, gas generation

NOTE. Colour code means:

GOOD	MODERATE	BAD/NOT ACCEPTABLE
------	----------	--------------------

o Market analysis

Asian manufacturers dominate the Li-ion batteries market. The principal manufacturers are located in Japan (about 80% of the world production), with the exception of BYD in China. The rest is mainly in China, Taiwan and South Korea. Main worldwide high power Li-ion cell producers were examined and they are gathered in Table 1-7 together with the main technologies they work on (for further information see Appendix C). Taking into account the estimated investments of main automotive battery manufacturers shown in Figure 1-9 and chemistry information in Table 1-7, the preferred cathode candidates in 2015 were evaluated and represented as percentages in Figure 1-10.

**Table 1-7. Lithium ion cells market worldwide by main competitors**

MANUFACTURER		CHEMISTRY (mainly graphite anode is used)	PACKAGING DESIGN
Japan	GS Yuasa	LMO, LMO-NCA, NCM, LFP, LCO	Prismatic
	Hitachi	LMO-NCM, NCM	Cylindrical, prismatic
	Panasonic	LNO, LCO, NCM, NCA	Cylindrical, prismatic
	Sanyo	LMO, LMO-NCM, LMO-NCA	Cylindrical, prismatic
	Sony	LCO, LMO, LMO-NCM, LMO-NCA, LFP	Cylindrical, prismatic
	Toshiba	LMO (LTO anode)	Prismatic
China	BAK	LFP	Cylindrical, prismatic, pouch
	BYD	LFP	Prismatic
South Korea	Kokam	NCM, LCO	Pouch
	LG Chem	LMO, LFP, NCM	Cylindrical, prismatic
	Samsung	LCO, NCM, LMO-NCM, LFP	Cylindrical, prismatic
	SK Energy	LMO (graphite and LTO anodes)	Pouch
USA	A123	LFP	Cylindrical, pouch
	AESC	LMO, NCM, LMO-NCM, LMO-NCA	Pouch
	Ener 1	NCM, LMO (hard carbon and LTO anodes)	Pouch
	Johnson Controls (JCI)	NCM, NCA	Cylindrical, prismatic
	Valence Technology	LFP	Cylindrical
Europe	Gaia-LTC (USA)	LCO, NCA, LFP	Cylindrical
	Saft	LFP, NCA	Cylindrical, prismatic
	Varta AG	LMO	Cylindrical, prismatic, pouch
Canada	Electrovaya	NCM	Pouch
	E-one Moli (Molicel) (Taiwan/Canada)	LCO, LMO, NCM, LFP	Cylindrical, prismatic

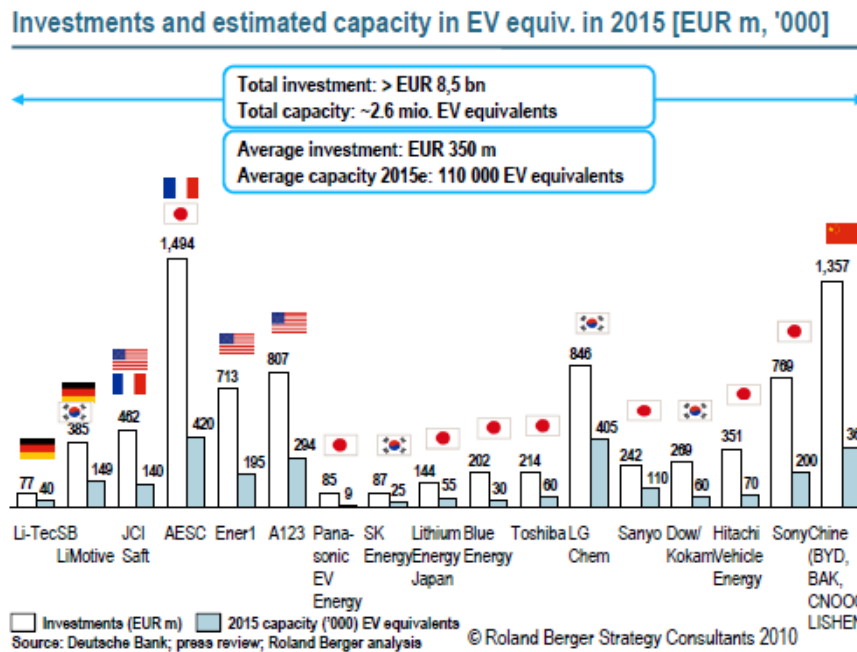


Figure 1-9. Main investments of 20 biggest automotive players in Li-ion battery manufacturing [24]

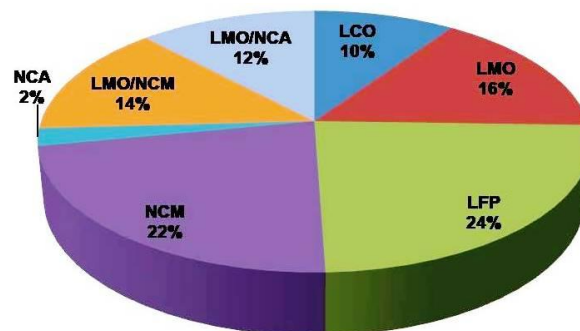


Figure 1-10. Cathode active materials market share estimation in 2015 extracted after analysis of Table 1-7 and Figure 1-9

Leading technologies for high power applications are LFP/graphite and NCM/graphite. However, LTO anode in combination with LMO cathode is also currently used for PHEV/HEV high power applications (Altairnano, Ener1 and Toshiba), since it increases the charge current limit (fast charging speed) [25]. LFP/graphite and NCM/graphite provide semi fast and moderate charging speed, respectively.

- **Review of available standards and testing methodologies**

Main available regulatory and standard requirements are gathered in Table 1-8. In the case of large format batteries, the majority of available standards and manuals refer to automotive

applications. No other transport applications are covered. Standards for stationary applications, which head towards the use of promising novel large format rechargeable Li-ion technologies, are not available either and only some references to manuals are found (PNNL-22010 and SAND 2010-0815). Standards and manuals details are gathered in Appendix B.

The most used standards and manuals are: ISO 12405-1, ISO 12405-2, IEC 62660-1, IEC 61982-2, DOE/ID-11069 (FreedomCAR Battery Test Manual), INL/EXT-07-12536 (DOE Battery Test Manual for Plug-In Hybrid Electric Vehicles). ISO 12405-1 and ISO/FDIS 12405-2 cover basic characteristics, performance, and reliability and abuse testing. The former is focused on high power battery packs, whereas the latter is to be used for high energy battery packs. IEC 62660-1, IEC 61982-4 and the battery test manuals cover performance and life testing. The first two IEC standards are applicable at cell level, while the manuals are focused on battery packs. Table 1-9 gathers together the test contents of these standards and manuals. The tests that are similar are coloured in the same way. This indicates that most testing protocols are introduced in the available standards. Their contents are equivalent and referred mainly to test specific procedures, mostly focused on electrical performance.

**Table 1-8. International lithium ion rechargeable battery standards and manuals (see Appendix B)**

GENERAL		PERFORMANCE TESTING			
STANDARD NUMBER	Scope	STANDARD NUMBER	Scope	MANUAL NUMBER	Scope
IEC 61960	Portable applications	ISO 12405-1	HEV, FCV	INEEL/EXT-04-01986	Automotive application
		ISO 12405-2	BEV		
		IEC 62660-1	BEV, HEV	INL/EXT-07-12536	
NEMA C18.2M.P2	Portable applications	IEC 61982-1	BEV, HEV	DOE/ID-11069	HEV
		IEC 61982-2	BEV, HEV	DOE/ID-11070	42V automotive applications
		IEC 61982-3	BEV, HEV		
ANSI C18.2M	Portable rechargeable cells	IEC 61982-4	BEV, HEV	DOE/ID-10597	HEV
		IEC 61960	Secondary lithium single cells and batteries for portable applications	USABC Battery Testing	EVs
		SAE J2288	EV	UN 38.3	Lithium batteries
SAFETY		SAFETY TESTING			
STANDARD NUMBER	Scope	STANDARD NUMBER	Scope	MANUAL NUMBER	Scope
ISO 6469-1	EV	ISO 12405-3	EV	BATSO 01	LEV (test methods and requirements)
		UL 1642	Primary and secondary user batteries (Power sources in products. Technician-replaceable or user-replaceable applications.)		
ISO 6469-2	EV, Failure	UL 2054	Household and commercial user batteries (Power sources in products. Technician-replaceable or user-replaceable applications.)		
		SAE J2464	EV, HEV		
ISO 6469-3	EV, Protection of persons	UL 2271	LEV		
		UL 2580	EVs		
SAE J2929	EV, HEV	UL 2575	Power tools, heating & lighting appliances	SAND 99-0497	EV, HEV
		IEC 62133	Portable applications		
EN 50272-2	Stationary batteries	IEC 62281	Safety during transport		
		IEC 62660-2	BEV, HEV		
IEC 62133	Portable batteries containing alkaline/non-acid electrolytes	SAE J2464	EV, HEV	SAND 2005-3123	EV, HEV
		UN PIII,38.3	Transportation of dangerous goods		
		IEEE 1625	Portable computing		
		IEEE 1725	Cellular telephones		
		JIS C8714	Portable Electronics Applications		

**Table 1-9.** Test methods of the main international battery standards and manuals (tests that are similar are coloured in the same way)

IEC 62660-1	ISO 12405-1	ISO 12405-2	IEC 61982-4	FreedomCAR battery test manual DOE/ID-11069	DOE test manual for PHEV INL/EXT-07-12536
Capacity and Energy test	Preconditioning test	Preconditioning test	Capacity and Energy density	Static capacity test at various T	Static capacity test at various T
Power test (pulse power profile)	Standard cycle and charge/discharge	Standard cycle and charge/discharge	DCH and regenerative power density (pulse power profile)	Hybrid Pulse Power Characterisation test (HPPC) at various T	Constant Power Discharge Test
Energy efficiency test	Energy and capacity test at RT and other temperatures	Energy and capacity test at RT and other temperatures	Energy efficiency test	Self discharge test	Hybrid Pulse Power Characterization test (HPPC) at various T
Charge retention test	Power and internal resistance test (Pulse Power Characterisation profile)	Power and internal resistance test (Pulse Power Characterisation profile)	Charge retention test at storage	Cold cranking test at various T	Self discharge test
Storage Life test	No load SOC loss test (not for an extended period of time)	No load SOC loss tests (not for an extended period of time)	Storage life test	Energy efficiency test – Round trip efficiency	Cold cranking test at various T
Cycle Life test	SOC loss at storage	SOC loss at storage	Life cycle test (dynamic DCH profile)	Operating Set Point Stability test	Energy efficiency test – Round trip efficiency
	Cranking power at low and high T	Energy efficiency test (fast charging test)		Cycle Life Tests	Cycle Life Tests
	Energy efficiency test - Round trip efficiency (charge balance pulse profile)	Cycle Life		Calendar Life Test	Calendar Life Test
	Cycle Life Test				

• **Need of a standardised cells selection methodology**

The previous sections of this chapter are only a glance of the multiple variables that are present in the energy storage business. In Figure 1-11 it is summarised the initial literature and market research work carried out aiming at finding suitable solutions for different industrial applications. Li-ion technology is a promising solution for new generation medium-large scale ESS. Performance, cost and safety characteristics vary across LIB types on the market. The most important performance aspects are: power density, energy density, energy efficiency, thermal performance and lifetime. These operation characteristics for the different LIB options are not always specified in a clear and comparable way [26-28]. There exist several battery testing procedures defined by different research groups [27, 29-33], but they are often only suited for one type of hybridisation topology (EV, HEV or PHEV), or consumer electronics. The great majority of standards and manuals are also focused on these applications (Table 1-8) and mostly just related to testing protocols (Table 1-9), as it was previously described in this chapter. Besides technical aspects, safety and costs are relevant. The costs depend strongly on the quality of the battery (manufacturing) and application specific requirements. Cells right selection for the different applications means balancing different factors, and the manufacturer plays a decisive role. Hence, a trade-off solution must be achieved. There are many advances in the automotive sector, but there is little defined for applications requiring large-format batteries.

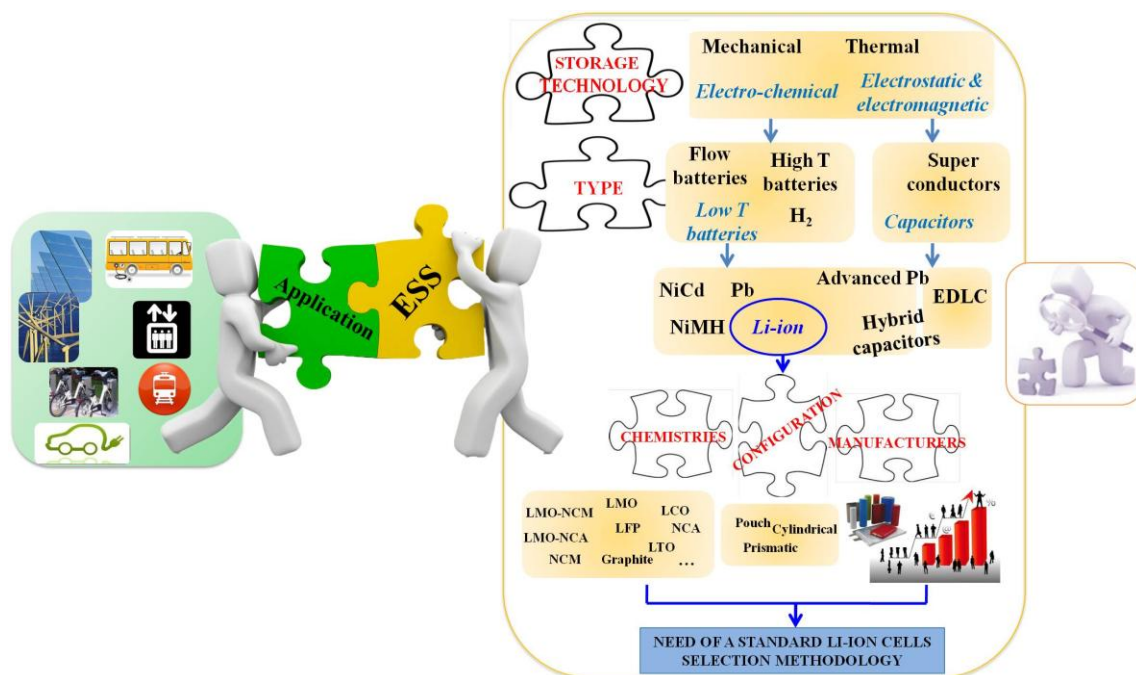


**Figure 1-11.** Market analysis on ESS. Schematic compilation of characteristics to take into account when searching for a suitable ESS for the target application

Overall, the need of developing a systematic way to choose the right large format Li-ion cell for each specific application was identified as a critical step towards introducing competitive storage solutions into the market.

## 1.2 AIM OF THE THESIS WORK

The industry demands procedures to select competitive batteries that must fulfil specific requirements in terms of cost, performance and lifetime. Batteries show a wide variety of choices that depend on many counteractive parameters. This interaction is complex and usually a trade-off is the only possible solution. Finding this trade-off itself is a complex task that requires a multidisciplinary approach with several steps.

The objective of this work is to define a systematic procedure that will allow to match as best as possible the requirements of the final applications with the specifications and properties of available Li-ion commercial cells. This novel methodology should aim at reducing system investment and maintenance costs while optimising the useful lifetime of the battery.

As a starting point, the definition of the methodology will focus on commercial large format Li-ion cells that should meet successfully every demand of the application. This Thesis pursues analysing innovative large scale traction and regenerative applications different from the advanced automotive sector.

This work is initially focused on performing a thorough comparative study of various Li-ion configurations aiming at gaining knowledge of the different technologies. This thorough analysis of available technologies in the state of the art is necessary for the identification of important parameters that are needed for the establishment of successful selection criteria. As extent as possible compilation of existing knowledge in the field would allow a reliable definition of cell selection criteria. This in depth analysis aims at allowing the establishment of a comprehensive stepwise approach that allow screening and reducing progressively the number of choices for the final application.

During the evaluation of the different stages of the selection methodology, special focus is given to the battery lifetime prognosis. This stage is the most challenging as requires deep knowledge of the application operating conditions, which sometimes are difficult to define, requires also a considerable investment of time and therefore, high cost. For this reason, the second main target of the work presented in this Thesis is to develop a reliable and efficient methodology for battery lifetime prediction, able to guarantee the long useful lifetime required for the specific targeted application. This lifetime prognosis method is developed taking as priorities cost-effective solutions with minimum testing time and easy integration of measured parameters into the diagnosis tools for the applications.

### 1.3 THESIS OUTLINE

The contents of this Thesis are divided into six chapters. Besides this introductory chapter, the following chapters are presented:

**Chapter 2** is a compilation of the general testing procedures for cells characterisation. A short description of the general equipment and specific test assemblies designs used in this work are compiled in Appendix C.

**Chapter 3** shows the main activities of the Thesis work. First, it overviews and analyses the overall issues for Li-ion cells right selection. Next, it presents in detail the novel multidisciplinary cells selection methodology developed in this work. Lastly, as necessary tool for in depth lifetime analysis, which is part of the cells selection, a procedure for Li-ion cylindrical cells post-mortem analysis is outlined.

The work described in this chapter involved the compilation of extensive information about Li-ion technology variants and worldwide manufacturing activities. Due to their extension, both subjects are included in Appendix A and Appendix D, respectively. The work described in this chapter also involved the analysis of available standards. Apart from the description given at the introduction, a detailed compilation is included in Appendix B. The last but not least issue that needs addressing during cell selection is safety. A specific compilation of information about safety is given in Appendix E.

**Chapter 4** is about the implementation of the developed cells selection methodology defined in the previous chapter. Two different novel industrial applications are studied: residential elevator and catenary-free tramway. The cells preselection process results and discussions for the elevation application are presented in detail. The second validation of the methodology for tramway application is summarised. After implementing the methodology, further improvements related to the cells selection methodology are suggested.

**Chapter 5** deals with ageing analysis and lifetime prognosis. A novel approach for useful life analysis and validation is proposed. Calendar and cycling ageing detailed studies are presented. Their interactions are also predicted and experimentally validated. The complete model is implemented into a simulation platform and different realistic scenarios evaluations are presented, which validate the developed model. A real residential elevator operation is also simulated and the battery lifetime is predicted under such application environment.

To finalise, **Chapter 6** presents Thesis summary, main conclusions, relevant contributions and future work.

# *Chapter 2*

## EXPERIMENTAL TEST PROCEDURES

---

*A description of general test procedures used in this work.*



## 2. EXPERIMENTAL TEST PROCEDURES

The specifications of the equipment used during this work are shortly described in Appendix C. This section includes a summary of the testing procedures of general use, included in the specific evaluations described in the following chapters. General description and goals of most of the tests is gather in the *Glossary of Terms*.

One of the most important aims of this work is to define specific tests that are needed for cell selection as a function of the application and those other needed to analyse ageing behaviour for further effective evaluation of lifetime prediction. That is why these specific tests will be described within the specific chapters concerned.

### 2.1. TESTS OF GENERAL USE

All the tests were carried out in temperature-controlled environment (climatic chambers, Appendix C) and cells surface temperature upon tests was recorded using Type K thermocouples.

Specific purposes and either details about testing conditions or variations in the procedures are included within the corresponding chapters.

#### 1) Cell conditioning

- *Testing methodology*: 3 full charge (CHA) and discharge (DCH) cycles with 30 min rest period in between to reach a stable condition [ISO 12405-1:2011]. CHA is performed at constant current-constant voltage, CC-CV, mode, and DCH at CC mode until cut-off voltage is reached. CV mode is finished when the current is below 0.05C.
- *Test conditions*: at currents suggested and/or used by the supplier in testing before delivery [ISO 12405-1:2011, ISO 12405-2:2012] and  $25 \pm 2^\circ\text{C}$ .
- *Analysis of results*: voltage CHA and DCH profiles; discharged and charged Ampere hours and energy (in Wh) at each cycle; discharged energy round trip efficiency at each full cycle; coulombic efficiency and CV charging time.

The battery shall be considered as conditioned if the discharged capacity during two consecutive discharges does not change by a value greater than the 3% of the rated capacity [ISO 12405-1:2011, ISO 12405-2:2012].

## 2) Nominal capacity test

- *Testing methodology:* same procedure as for cell conditioning.
- *Test conditions:* nominal operating conditions are established by the manufacturer. In case datasheet does not specify them, 1C and  $25 \pm 2^\circ\text{C}$ .

Figure 2-1 shows, as example, the voltage profile and current during a nominal capacity test carried out in a cell with 2.3 Ah nominal capacity and 3.3 V nominal voltage.

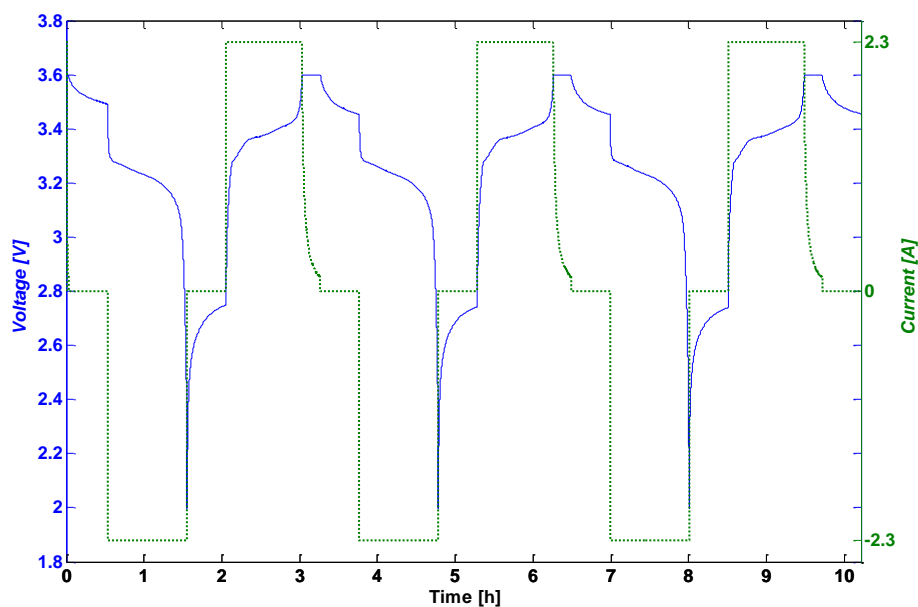


**Figure 2-1.** Nominal capacity test (used example: cell with 2.3 A nominal current (1C) and 3.3 V nominal voltage)

- *Analysis of results:* voltage CHA and DCH profiles; discharged and charged Ampere hours and energy (in Wh) at each cycle; discharged energy round trip efficiency at each full cycle; coulombic efficiency and CV charging time. The average value of the total Ampere-hours discharged in the last two full cycles is considered as the actual nominal capacity.

### 3) Rate capability tests

- *Testing methodology:* 3 CHA and DCH cycles with a rest period in between to reach temperature stable condition (*i.e.* operating  $T$ ). Cells charging performance is evaluated at CC mode as it may be not possible to charge the cell in CC-CV mode during operation in real applications. Figure 2-2 shows the testing procedure.

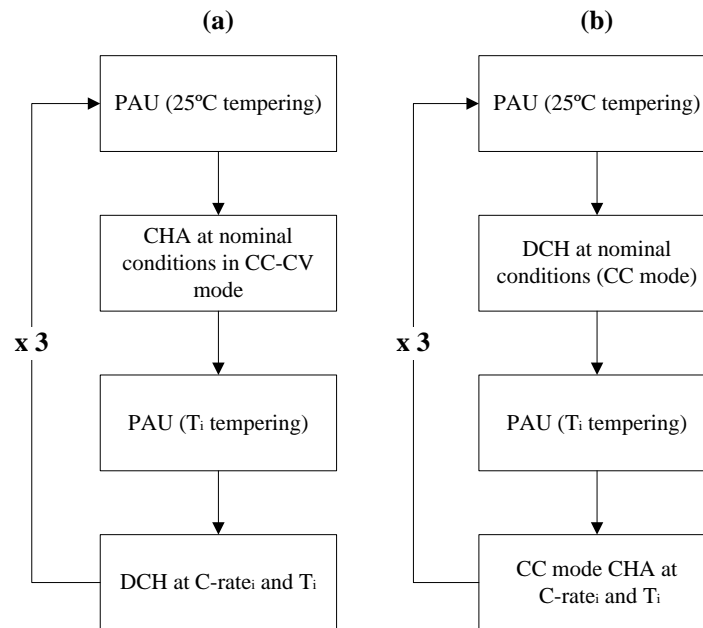


**Figure 2-2.** Discharging (a) and charging (b) rate capability test for each C-rate and  $T$  pair conditions. Each testing condition is repeated 3 times in order to check the repeatability of tests and evaluate average results

- *Test conditions:* nominal CHA and DCH conditions are the same as for the nominal capacity test. Other current loads and temperatures (C-rate<sub>i</sub> and  $T_i$ ) to evaluate rate capabilities are chosen according to either requirements of the targeted application under study or other specific goals (*i.e.* after cell ageing).
- *Analysis of results:* CHA/DCH performance as a function of CHA/DCH velocity and temperature. CHA or DCH voltage profiles; discharged or charged Ampere-hours (operating capacity) and energy (in Wh); CHA or DCH energy round trip efficiency at each full cycle (energy efficiency vs. CHA or DCH C-rates); coulombic efficiency (CHA or DCH capability); Peukert relationships and CV charging time.

#### 4) Internal resistance (IR) test

- *Testing methodology:* Direct Current (DC) IR measurement by pulses method. All either regen or discharge pulses are measured equally, as calculated internal resistance depends on pulse duration and amplitude [34].

- To perform DCH pulses, a fully charged cell at nominal conditions is discharged to a certain SOC ( $SOC_i$ ) at nominal current and specified  $T$  ( $T_i$ ). Afterwards, current pulse is measured applying the appropriate DCH current (it depends on the purpose) for 17 s rise time at the specified  $T$  ( $T_i$ ).

- To perform CHA pulses, a fully discharged cell at nominal conditions is charged to a certain SOC ( $SOC_i$ ) at nominal current and specified  $T$  ( $T_i$ ). Afterwards, current pulse is measured applying the appropriate CHA current (it depends on the purpose) for 17 s rise time at the specified  $T$  ( $T_i$ ).

$\Delta SOC$  (DOD) is Ah-based fixed and is defined according to the cell actual nominal capacity. Figure 2-3 shows the testing procedure.

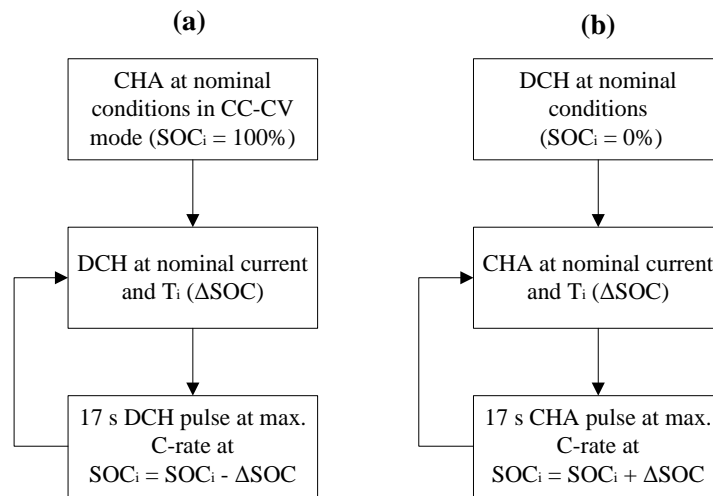


**Figure 2-3.** Discharge (a) and regen (b) DC IR measurement procedures

- *Test conditions:* nominal CHA and DCH conditions are the same as for the nominal capacity test. Pulses measuring SOC<sub>i</sub> and temperatures ( $T_i$ ) are chosen according to either requirements of the targeted application under study or other specific goals (*i.e.* after cell ageing).

- *Analysis of results:* study of electrical performance as a function of ambient temperature and cell SOC. 1 s and 17 s internal resistances are calculated, as expressed in Eq. 2-1 and shown in Figure 2-4, by the difference between the voltage before the pulse during the rest period and the one after specific pulse duration, divided by the pulse current.

$$IR = \frac{\Delta V}{\Delta I} \left\{ \begin{array}{l} IR_{1s} = \frac{V_1 - V_0}{I} \\ IR_{17s} = \frac{V_{17} - V_0}{I} \end{array} \right. \quad \text{Eq. 2-1}$$

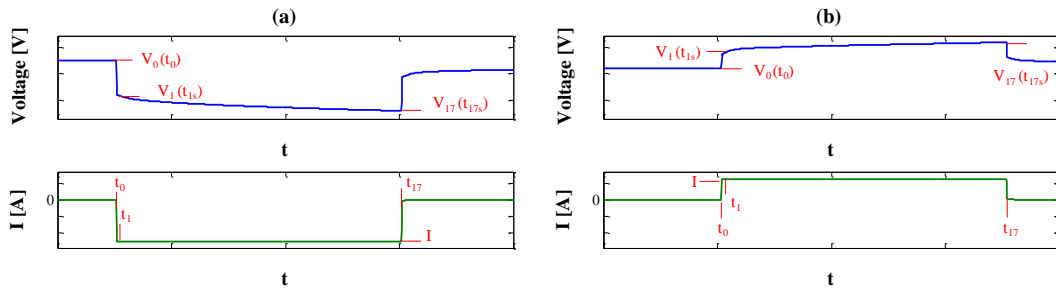


**Figure 2-4.** Voltage response of a cell to high 17 s (a) discharge and (b) charge pulses. The voltage values used for the assessment of 1s and 17s Direct Current (DC) internal resistance (IR) are indicated in the figures

## 5) Hybrid Pulse Power Characterisation (HPPC) Test

- *Testing methodology:* pulse trains at various SOCs. It is carried out according to INL/EXT-07-12536 and DOE/ID-11069 Battery Test Manuals. It differentiates from IR test that both regen and discharge pulses are just measured during the DCH process of the cell (Figure 2-3 (a)) and that the cell discharging between target SOCs is carried out at nominal temperature condition. Regen and discharge pulses are measured one after the other at the same SOC level. Figure 2-5 shows the testing procedure.
- *Test conditions:* Specific conditions (internal resistance measurement SOC intervals ( $\Delta$ SOC), last step SOC, rest periods, etc.) change depending on the purpose of the test and investigated cell.  $\Delta$ SOC (DOD) is Ah-based fixed and is defined according to the cell actual nominal capacity. Figure 2-6 shows, as example, the voltage profile and current during a HPPC test carried out using a cell with 2.3 Ah nominal capacity and 3.3 nominal voltage over cell 90-20% SOC range with 10%  $\Delta$ SOC (DOD) intervals.
- *Analysis of results:* voltage profiles and study of electrical performance as a function of cell SOC. OCV vs. SOC; CHA and DCH internal resistances for 1 s and 17 s voltage drops (Eq. 2-1, Figure 2-4); CHA and DCH internal resistance vs. SOC; DCH power density vs. SOC and peak power capability determination; and CHA power density vs. SOC and peak regen power capability determination.  
It makes possible to define the cell operating window for each application.

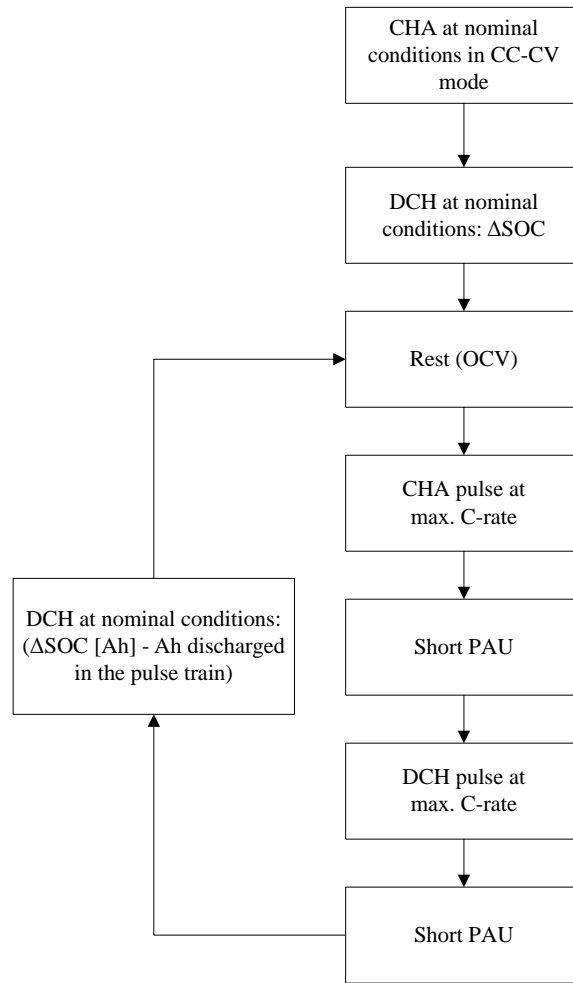


Figure 2-5. Hybrid Pulse Power Characterisation (HPPC) test procedure

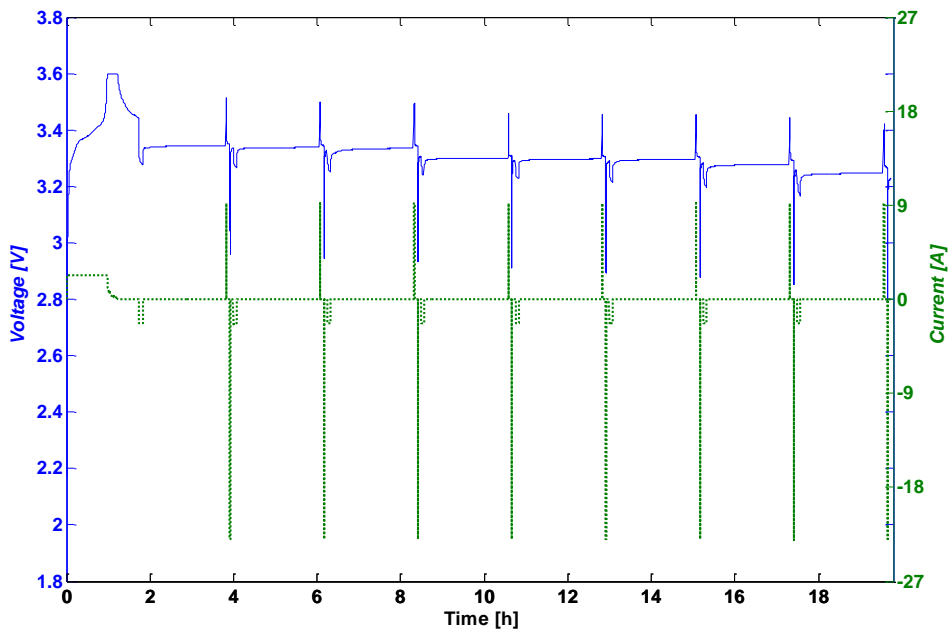
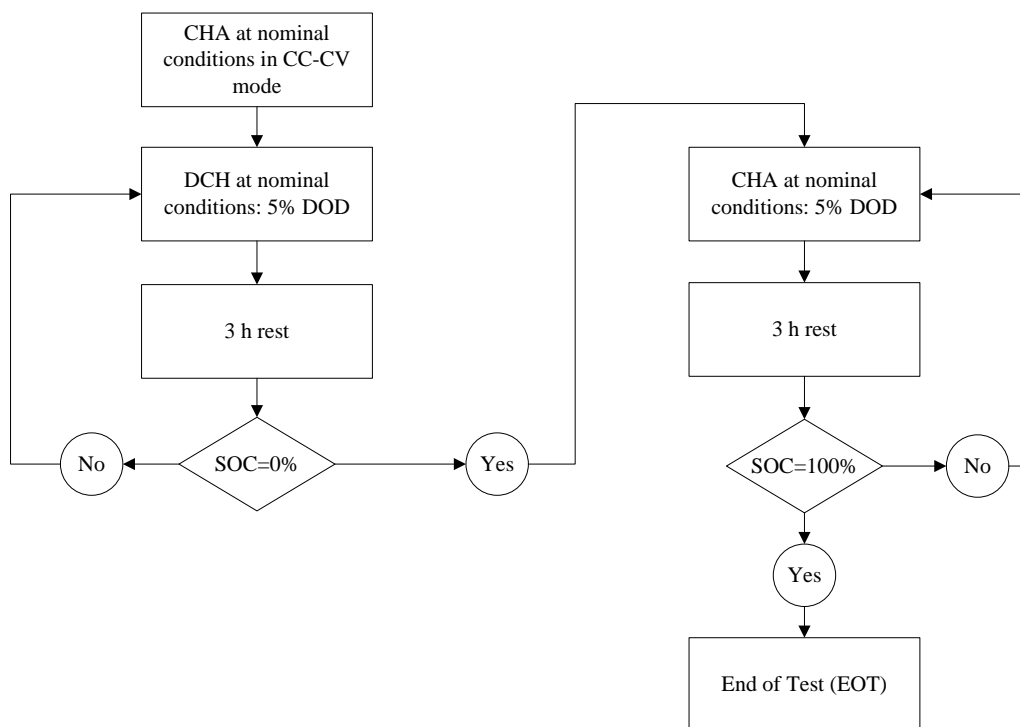


Figure 2-6. Hybrid Pulse Power Characterisation (HPPC) Test. Charge and discharge pulses measured within 90-20% SOC range with 10%  $\Delta$ SOC intervals (used example: cell with 2.3 Ah nominal capacity and 3.3 V nominal voltage)

## 6) Open Circuit Voltage (OCV) test

OCV characteristics can be assessed from HPPC tests, but specific tests were carried out for obtaining charge and discharge voltage curves as a function of SOC under no-loaded conditions after 3 h rest time. The aim of this test was to evaluate cell intrinsic properties.

- *Testing methodology:* fully charged cells (in CC-CV mode and at nominal conditions) are discharged in 5% DOD intervals with 3 h rest period at each SOC. Once at 0% SOC, charging OCV curve is assessed following the same procedure.  $\Delta$ SOC charging/discharging process is carried out at nominal conditions. Figure 2-7 shows the testing procedure.
- *Test conditions:* nominal operating conditions are established by the manufacturer. Test is carried out at  $25 \pm 2^\circ\text{C}$ .
- *Analysis of results:* determination of OCV vs. SOC cell characteristics.



**Figure 2-7.** Open Circuit Voltage (OCV) test procedure

## 7) Close-to-equilibrium Open Circuit Voltage (quasi-OCV) measurements

- *Testing methodology:* fully charged cells (in CC-CV mode) are fully discharged at low C-rates in order to analyse galvanostatic voltage profiles.

- *Test conditions:* C/5 discharge rate and room temperature. 0.2 C-rate was chosen for being the largest cell discharging current (aiming at minimising test duration) that enabled observing the phase changes of the active materials on the voltage response of the cell. Figure 2-8 shows, as example, the voltage profile and current during a quasi-OCV test carried out using a cell with 2.3 Ah nominal capacity and 3.3 nominal voltage.

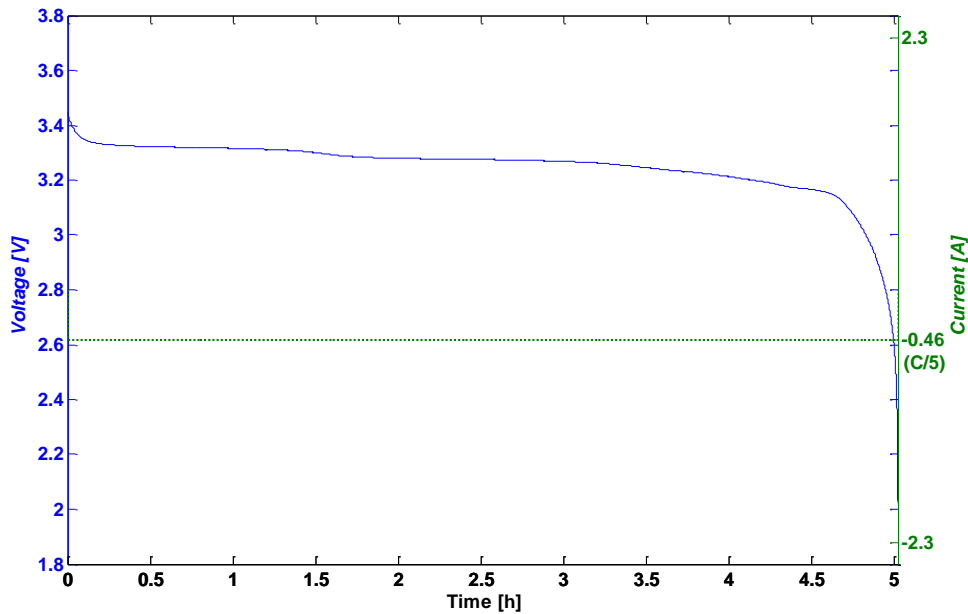


**Figure 2-8.** Close-to-equilibrium Open Circuit Voltage (OCV) test. Cell full discharge at C/5 (used example: cell with 2.3 Ah and 3.3 V nominal capacity and voltage, respectively)

- *Analysis of results:* quasi-OCV characteristics over cell DOD, voltage profile its derivatives: incremental capacity (dQ/dV) and differential voltage (dV/dQ) curves.

## 8) Constant power discharge tests

- *Testing methodology:* fully charged cells (in CC-CV mode and nominal conditions) are discharged at constant power until the cut-off voltage is reached. The test is repeated several times at different discharge powers ( $P_1$ ).
- *Test conditions:*  $P_1$  between the maximum and minimum power that the cell can deliver continuously when fully discharging ( $P_{\max} = I_{\max} \cdot V_{\min}$  and  $P_{\min} = I_{\min} \cdot V_{\max}$ ) and room temperature.
- *Analysis of results:* continuous power capability evaluation (it is largely limited by the heat effects that occur during current flow). Power vs. energy (ragone plot, *i.e.* evaluation of the influence of the discharge load on the energy that can be delivered by a battery) and energy efficiency vs. energy density.

## 2.2. TESTS FOR LIFETIME PREDICTION

Figure 2-9 shows the flow chart for ageing testing procedure including both State of Health (SOH) controlling steps and accelerated ageing tests. The ageing tests and related aspects (boxes in grey) are described in the corresponding chapters.

Intermittent Electrical Parameters Identification Tests (EPIT) execution depended on the purpose of the ageing analysis. They are planned at room temperature (25°C) as follows:

- a) **Actual nominal capacity measurement**
- b) **Close-to-equilibrium Open Circuit Voltage (quasi-OCV) measurements**
- c) **Actual Direct Current (DC) IR measurement by HPPC** (specific testing conditions are described in the corresponding chapters)
- d) **Impedance change evaluation by EIS measurements**

EPIT occasionally included EIS measurements. They were carried out in galvanostatic mode (2 A) using frequency range from 0.1 Hz to 6.5 kHz at room temperature (RT). The cell SOC for the measurements was different depending on the type of ageing, so it will be specified within each specific chapter and section concerned.

Both initial and final characterisation tests at End of Test (EOT) included different tests depending on the type of ageing test and its purpose. These tests can be: rate capability test, EIS measurement and calorimetric test (heat generation measurement at adiabatic conditions). These tests are to be described in detail within each specific chapter and section concerned.

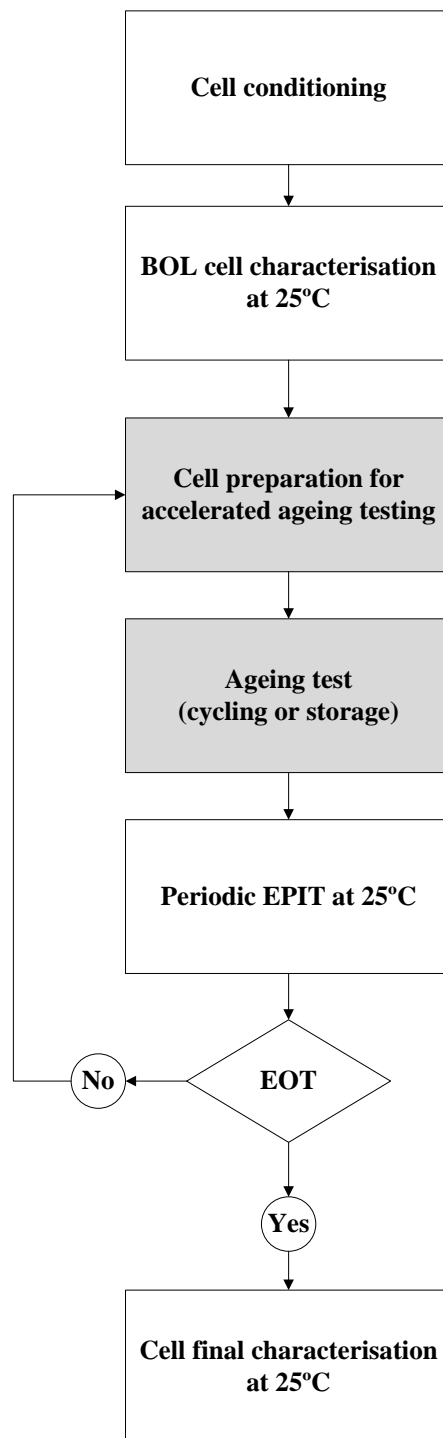


*Figure 2-9. Ageing testing procedure*

# *Chapter 3*

## DEVELOPMENT OF THE METHODOLOGY FOR CELLS SELECTION

---

*This chapter includes all the necessary literature searches (compiled in the Appendixes) and the experimental work to define a robust method for battery cell selection as a function of the application.*



### 3. DEVELOPMENT OF THE METHODOLOGY FOR CELLS SELECTION

The procedure and planning for cells selection definition was structured into four main tasks:

- *The preliminary task* deals with the study of scientific and technical works evolution in the field so as to keep the research at the forefront through the analysis of the difficulties and hitting upon the aspects that must be deeply understood.
- *Task 1* pursues understanding the different variants on Li-ion cells (section 3.1). Theoretical and experimental analyses of different Li-ion technologies factors (comparative study) were necessary to gain base knowledge for a proper definition of the cells selection methodology. The aim was to lay down guidelines for suitable cells detection and definition of cells performance tests to be carried out throughout the methodology.
- *Task 2* was the development of the standard multidisciplinary methodology for cells selection and the definition of the necessary tests (section 3.2).
- *Task 3* deals with a necessary tool for post-mortem analysis. Within cells selection methodology, the need of cells lifetime performance analysis was identified. Post-mortem characterisation provides physical evidence of ageing phenomena so that degradation modes and cell performance can be related over time. Such analysis required developing a methodology for a safe cells disassembling and components harvesting, and defining protocols for components characterisation (section 3.3).

### 3.1 TASK 1: PERSPECTIVE AND CRITERIA

The key issue for creating a competitive battery pack is the battery technology selected. Indeed, this right selection means balancing several factors and reaching a trade-off solution. Figure 3-1 shows the variants of Li-ion cells that have to be studied. As shown briefly at the introduction, there are multiple parameters involved in Li-ion technology. A summary of fundamentals, materials and components to be taken into account for developing selection criteria is included in Appendix A. All size, shape and materials used in the construction of a cell affect its ultimate performance. Figure 3-2 shows an outline of Li-ion cells structure. It summarises all analysed factors observed in Figure 3-1. Both figures show the same colour schemes for a better understanding of their relationships. Figure 3-2 depicts the effect of the cell design (both the construction and active materials composition) on the factors to be taken into account when selecting a technology. That is to say, all cell performance, safety, cost and dimensions (size and weight) are under the influence of the cell chemistry. Overall, chemistry seems to be the dominant factor for Li-ion technology selection. Internal construction and manufacturing are the most important factors when it comes to make decisions [35].

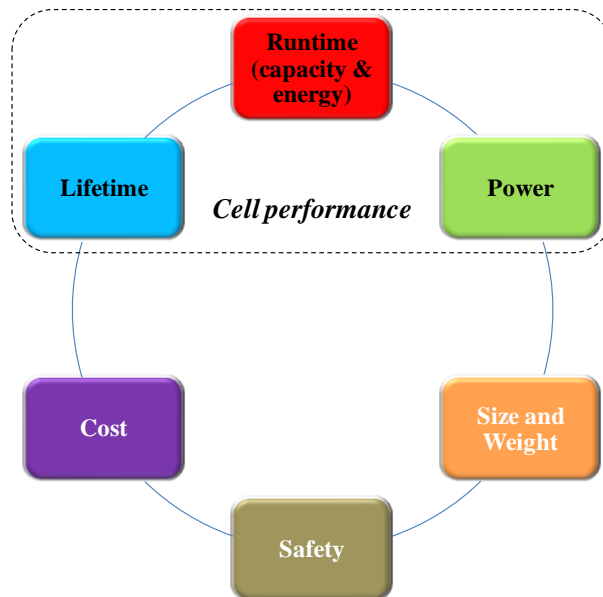


**Figure 3-1.** Dominant factors affecting the selection of the Li-ion battery technology

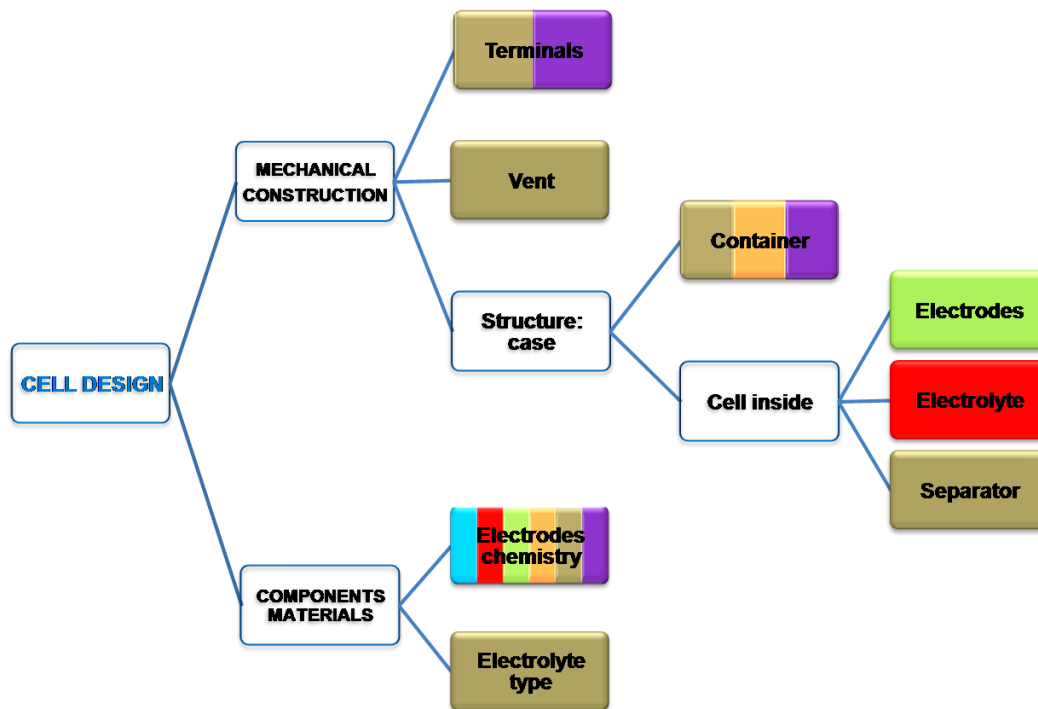


**Figure 3-2.** Breakdown of cells design (NOTE that colour code corresponds to the factors identified in Figure 3-1)

Batteries have the potential to be dangerous if they are not carefully designed (chemistry and construction) or appropriately used within its safe operating window. Stability and safety domains of all components must be studied. Moreover, unsuitable cell design for the application (even though it is a good battery) can provoke failure. Both initial cost and Total Cost of Ownership (TCO) including depreciation and maintenance need to be taken into account so as to sustain a long-term cost-effectiveness of a battery system. Reduction of initial costs need to be pursued in terms of both materials and manufacturing. Figure 3-3 shows Li-ion battery pack (using a NCM-graphite cell) costs forecasts. Mechanical construction of the cell contributes to cell and modules manufacturing cost as well as pack assembly cost and packaging efficiency (volume and weight). Raw materials impact on battery efficiency and the usable energy considering the degradation for the estimated lifetime, which also influences the oversizing of the battery packs.

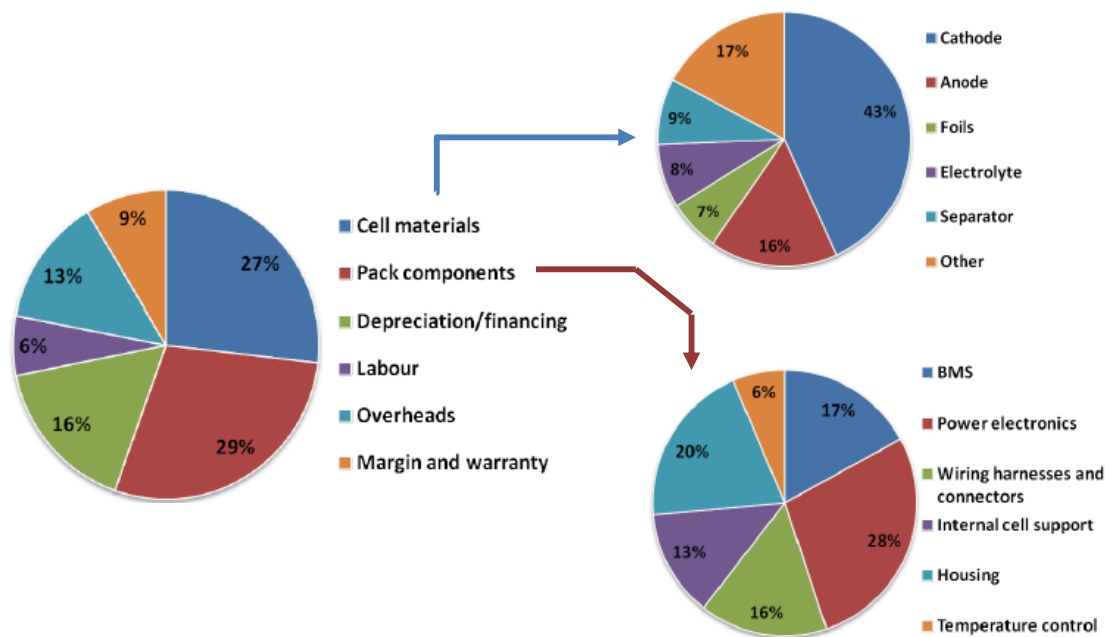


**Figure 3-3.** Battery system costs (cost/kWh) breakdown in 2011 for a 26kWh BEV with NCM-graphite cells - \$777/kWh- [36]

Table 3-1 summarises all the factors that affect cell performance [37]. All chemical materials and their processing, cell assembly, size and casing influence on cell runtime, power capability, lifetime and safety. Voltage and capacity are significant properties of cell chemistry. Power is controlled by the area and morphology (e.g. grain sizes and distribution) of the electrodes. Internal impedance of the cell depends on the conductivity of the electrolyte as well as the layout and resistance of the components in the current path. The thickness of the active electrode materials conditions the lithium insertion processes, being less favourable as the cell is being charged [38]. Performance and lifetime expectancy also depend on cell design.

**Table 3-1.** Causes and effects of cell performance

PERFORMANCE DEFINING FACTORS	INFLUENCE ON / DIRECT RELATIONSHIP WITH
CHEMISTRY (active elements)	Intrinsic properties: theoretical capacity and voltage
ELECTRODES PROCESSING (active surface: grain size distribution and additives)	Rate capability (HE, HP) and cycle lifetime
CASING	Design and geometry
CELL MANUFACTURING (electrode processing + casing)	- $\Delta$ rate capability (kinetics factors) - $\Delta$ resistance - $\Delta$ capacity (due to difference in amount of active material, or in polarisation resistance, or other kinetics factors originated from electrode processing) - $\Delta$ weight

Next, cell performance defining factors gathered in Table 3-1 are evaluated for gaining insight for an adequate development of the cells selection methodology.

### 3.1.1 SPECIFIC CELL PARAMETERS RELATED TO CHEMISTRY CHOICE

A short introduction of cell active materials was presented in *Chapter 1*. The state of the art was also summarised in Appendix A. Specific capacity and voltage are intrinsic properties of electrodes chemistry. Capacity is governed by the weight of the active chemicals. Cell voltage is controlled by the cell chemistry. The relation between batteries State of Charge (SOC) and Open Circuit Voltage (OCV) is a specific feature of electrochemical battery technologies. Active materials that perform a two-phase transition during charge and discharge demonstrate special voltage characteristics. Strong interactions between the embedded lithium and the host lattice during lithium insertion and extraction process lead to a phase separation [39, 40]. Due to the occurrence of at least two different material phases, the electrode electrochemical potential remains almost constant during charge or discharge of the cell. Thus, a typical voltage plateau between lithiated and delithiated states and high differential capacity at a certain electrode voltage can be observed [41]. Both LFP cathode and LTO anode comprise one wide potential plateau that represents a two-phase transition of the active material during lithium insertion and extraction process. In contrast, the graphite anode performs several two-phase transitions [39, 42, 43]. Electrode materials that perform a two-phase transformation can undergo thermodynamical entropic effects, mechanical stress and microscopic distortions that influence voltage characteristics, showing marked differences between charge and discharge voltages. This effect can be critical for reliable state estimation issues, which is a critical task for the model-based state estimation as a part of a Battery Management System (BMS) [39].

OCV measurement tests with commercial cells of different chemistries were carried out aiming at evaluating voltage properties of different electrode combinations (test procedures are described in *Chapter 2*). It was observed that the difference between charge and discharge voltages is almost negligible on cells with nickel or manganese-based and LCO cathodes, as shown in Figure 3-4 for a couple of studied cells. They only exhibited a slight gradient in the rest cell voltage curves because of the high gradient in the specific SOC to voltage relation. However, the difference is marked for the cells with LFP cathode, as shown in Figure 3-5 for three tested cells from different manufacturers. In the voltage plateau part, it may be related to the need to overcome the activation energy of phase transition. The impact is different depending on the cell (Figure 3-5 (a-c)), which could be also due to different materials chemistry, structure and conductivity modifications. But there might still be different charge and

discharge resistance influences even after cell rest at open circuit for 3 h (measurements after 8 h rest were similar).

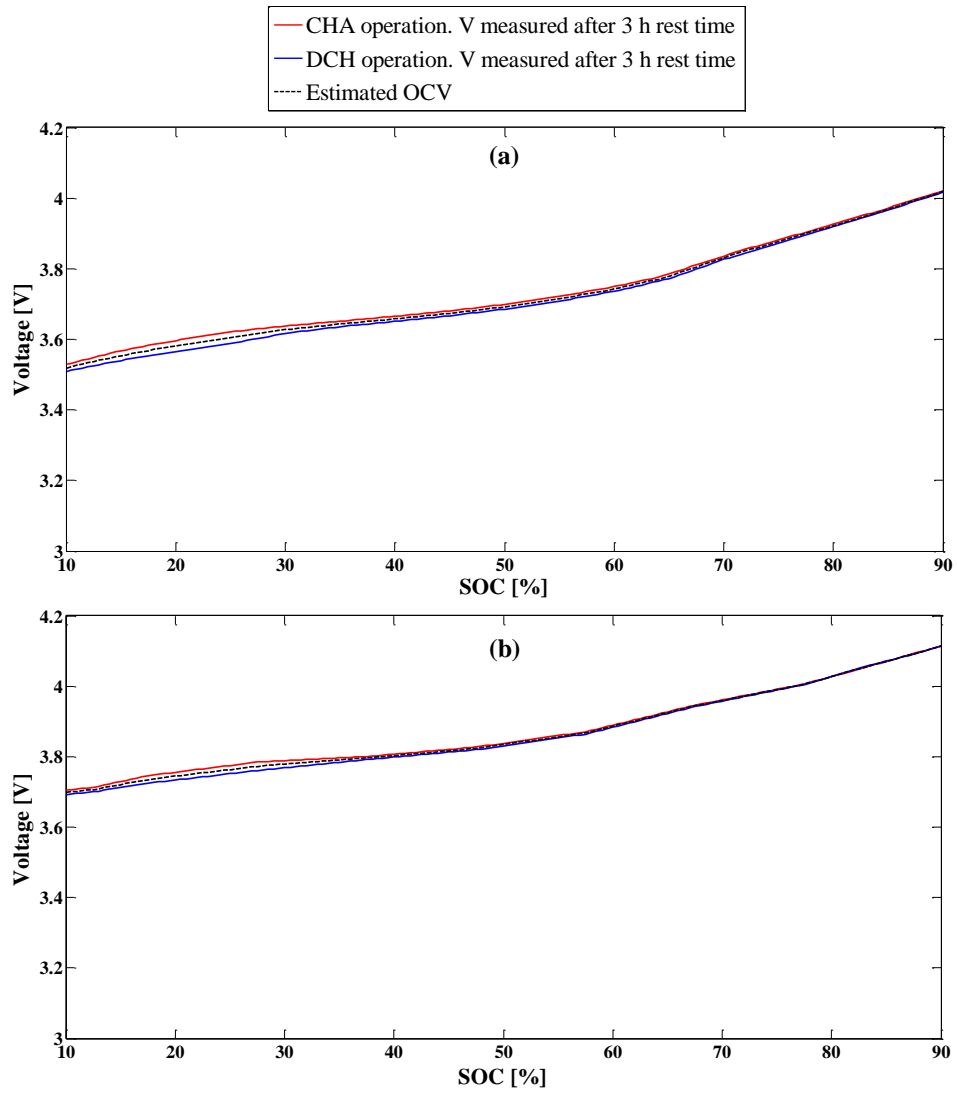


**Figure 3-4.** Rest voltage versus SOC curve of (a) NCM/graphite and (b) LCO/graphite commercial cells

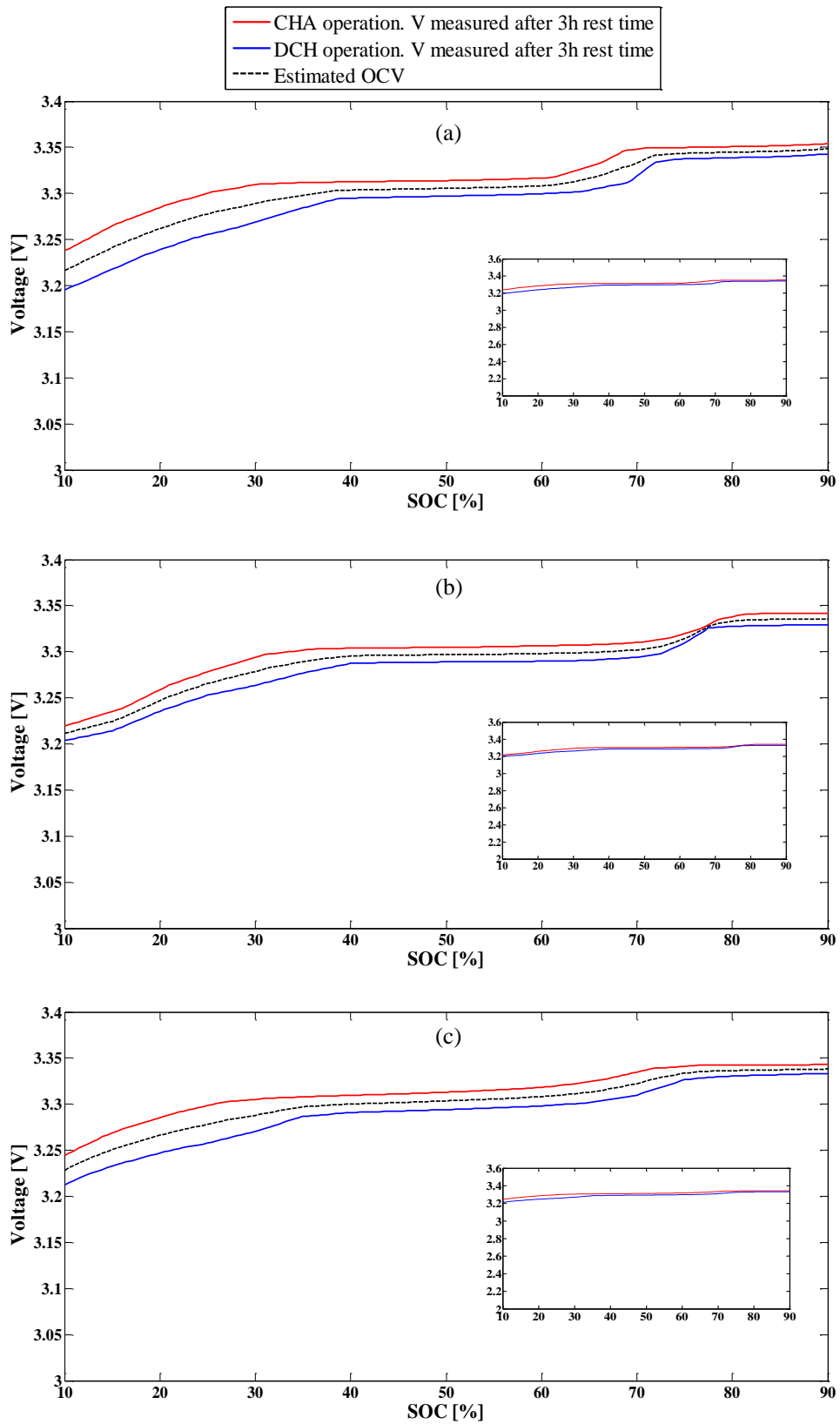


**Figure 3-5.** Rest voltage versus SOC curves of three different commercial cells containing LFP cathode. Estimated OCV is the mean of rest voltages after charge and discharge operation

The differences between charge and discharge voltages causes drawbacks with respect to the accuracy of the measurements and control strategies, as is emphasised in Figure 3-6 (magnification of Figure 3-5 (a)):

- i) For a specific SOC, different voltage values can be measured depending on the beforehand charge or discharge process (indicated in magenta).
- ii) For a specific voltage value, the SOC can change significantly depending on the beforehand charge or discharge process (indicated in grey).
- iii) In a voltage plateau, a slight variation in the voltage could lead to a remarkable change in the SOC (indicated in green) and unacceptable errors in SOC algorithms consequently.

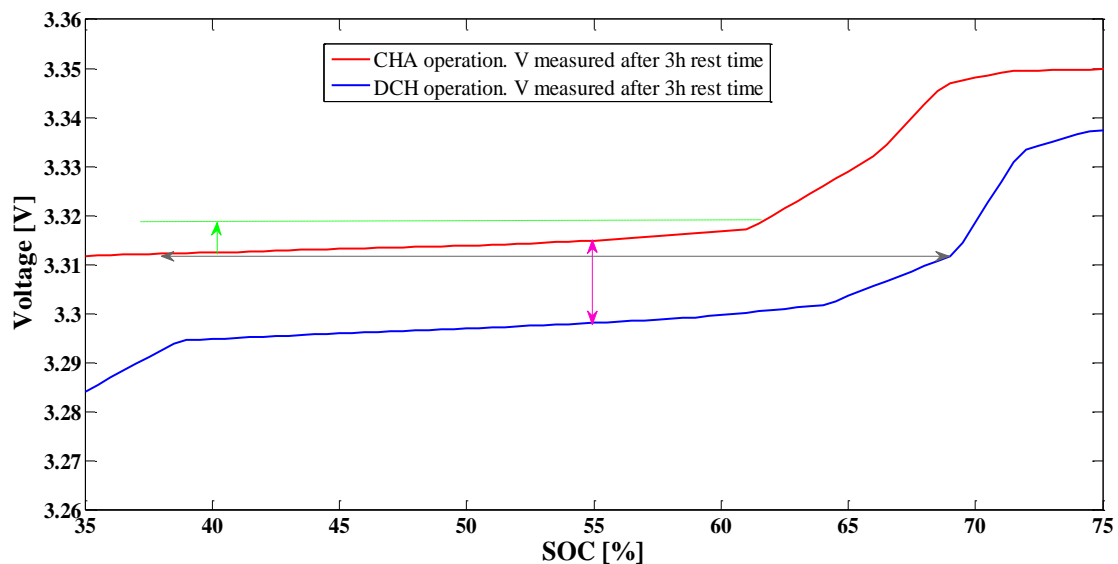


**Figure 3-6.** The effect of LFP cathode cell voltage plateau and charge-discharge voltage differences on state measurements

Figure 3-5 (a-c) showed two-phase transitions over typical single wide potential plateau of LFP cathode that corresponds to  $\text{FePO}_4\text{-LiFePO}_4$  phase transformation (see Figure A-4 in Appendix A). Hence, the anode in these cells should be lithiated graphite, as this anode material shows different plateaus on the charge-discharge potential profile that represent the coexistence of lithiated graphite at different  $\text{Li}_x\text{C}_6$  transformation processes (see Figure A-8 in Appendix A).

LTO-based batteries were also analysed, which are promising for certain niche applications that require high rate capability, long cycle life, wide operating temperature range and safety. Even though LTO anode is compatible with any of the cathodes, it is generally used in conjunction with manganese based materials due to their high potential vs.  $\text{Li/Li}^+$ . Figure 3-7 shows the potential curve of a commercial LMO cathode and LTO anode cell that was obtained

approaching equilibrium conditions. The typical voltage plateau for this tested cell was observed between 60 and 70% SOC corresponding with a cell voltage of *ca.* 2.35 V.

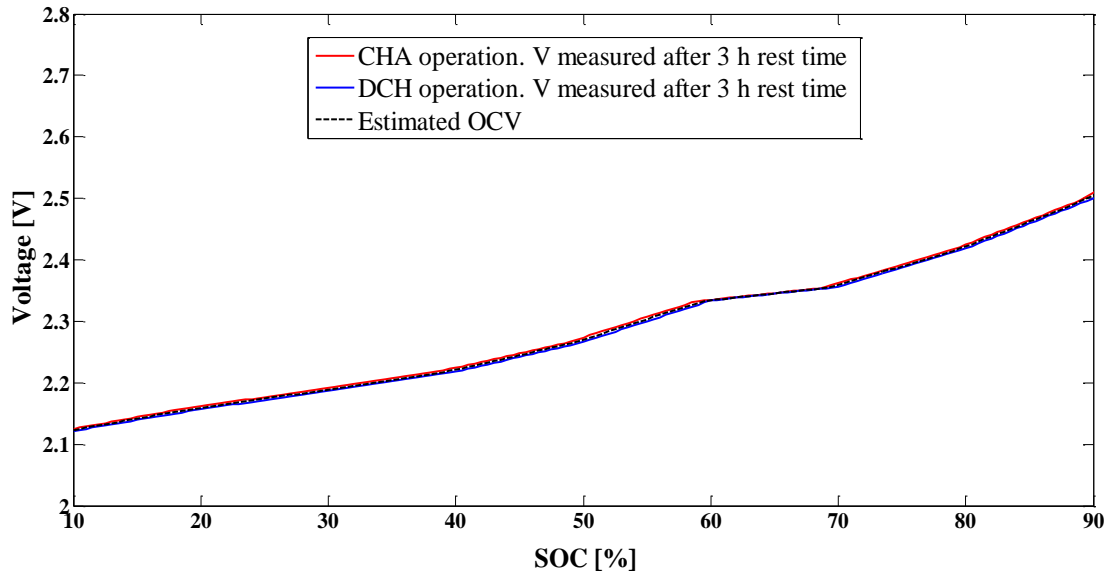


*Figure 3-7. Rest voltage versus SOC curve of a LMO/LTO commercial cell*

### 3.1.2 PERFORMANCE OF HIGH POWER (HP) AND HIGH ENERGY (HE) CELLS RELATED TO ELECTRODES PROCESSING

Large format Li-ion batteries are optimised either for High Power (HP) or High Energy (HE) applications. In some cases, it is also pursued the balance between power and energy density. Increasing the surface area of the electrodes enhances the cell current handling capability, enabling the more power delivery and faster charging. Increasing the mass of electrode active materials in the cell improves the cell energy storage capacity. HP cells require as thin as possible electrodes with a large surface active area and enlarged current collectors. The thickness of the active electrode materials conditions the charge density. Lithium ions diffusion process within the electrode is rate-determining. Typical electrodes thicknesses are around 50  $\mu\text{m}$  for HP cells and 150  $\mu\text{m}$  for HE cells [44].

The rate capability and the amount of available energy depend on the cell design, which effect on cells performance is investigated in this section. Table 3-2 shows the specifications of two cells from the same manufacturer designed to have different power capability and energy density. A comparative performance study was carried out discharging the cells at different constant currents (rate capability test) and constant power (testing procedures are described in Chapter 2).

**Table 3-2.** Specifications of two pouch cells from the same manufacturer designed with different power to energy ratio (data from manufacturer datasheet)

		CHARACTERISTIC	UNIT	HE type cell	HP type cell
<b>INTRINSIC PROPERTIES</b>		Chemical composition of the cathode	---	NCM	NCM
		Geometry	---	Pouch	Pouch
		Internal resistance	<b>mΩ</b>	< 0.9	< 0.8
		Maximum weight	<b>kg</b>	0.885	1.03
		Maximum volume	<b>mm<sup>3</sup></b>	441824	508336
<b>CHARACTERISATION</b>	<b>NOMINAL CHARACTERISTICS</b>	Capacity	<b>Ah</b>	40 (0.2C CHA; 0.5C DCH)	41 (0.2C CHA; 0.5C DCH)
		Nominal voltage	<b>V</b>	3.7	3.7
	<b>CHA CONDITIONS</b>	Charge cut-off voltage	<b>V</b>	4.15	4.15
		Maximum charge current	<b>A</b>	80A (2C)	120 (3C)
		Charge temperature range	<b>°C</b>	10 - 45	10 - 45
	<b>DCH CONDITIONS</b>	Discharge cut-off voltage	<b>V</b>	3	3
		Maximum discharge current	<b>A</b>	200 (5C)	320 (8C)
		Discharge temperature range	<b>°C</b>	(-10) - 55	(-20) - 55
	<b>LIFETIME</b>	Cycle life	<b>N</b>	1000 (1C CHA-DCH; 100% DOD)	1000 (1C CHA-DCH; 100% DOD)

Figure 3-8 shows the results of the rate capability tests that were carried out using the two types of cells. At low discharge rates (0.5 and 1C), both cells performance were similar: almost 100% of their nominal storing capacity was obtained. At higher current rates, however, the discharge curves changed: the voltage drop was enhanced in the case of the energy cell, obtaining as a result no more than 80% of the charged Ampere-hours when operated at the highest allowed C-rate (the cut-off voltage was reached faster). This is because the total resistance of HP cells is lower than the total resistance of HE cells. Hence, there is evidence that the rate capability is improved for HP cells.

Figure 3-9 shows the Peukert curve (capacity vs. C-rate) to compare the rate capability of the two types of cells (HE and HP), and also exhibits their energy densities at different discharge rate conditions. The energy density was larger for HE cell except when it was discharged at the maximum acceptable C-rate. A decrease in the energy was observed as a result of capacity loss and voltage drop (Figure 3-8).

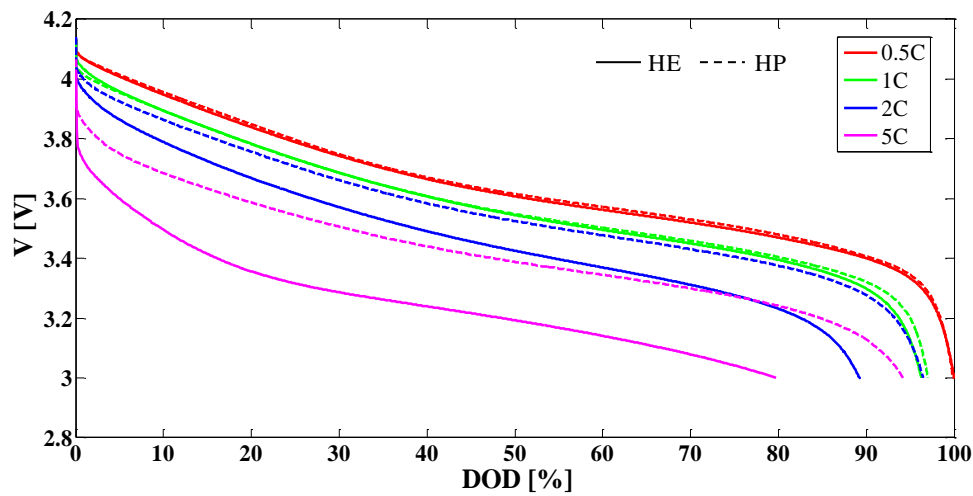


Figure 3-8. Discharge curves at different C-rates and 25°C for the studied HE (continuous lines) and HP (dotted lines) NCM-based cells

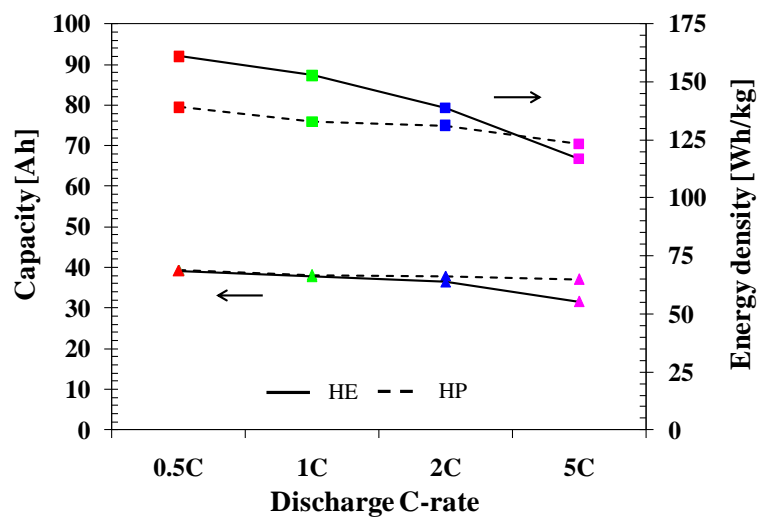


Figure 3-9. Discharged capacity and specific energy at different C-rates and 25°C for the studied HE and HP NCM-based cells

The results from constant power discharge tests were used to evaluate total energy withdrawal under each power condition and represent a normalised curve for making real comparisons between the cells. Figure 3-10 is the Ragone plot of the studied HE and HP cell types, which reveals the trade-offs of specific power related to specific energy (W/kg vs. Wh/kg). HP cell kept good power to energy ratio, *i.e.* it showed high energy efficiency. There was only a loss of 20 Wh/kg (meaning less than the 15% of the total available energy) between maximum and minimum power output. On the contrary, HE cell improved its performance in terms of higher specific energy at low power and provided power at the expense of low energy. As a consequence, in the case of HE cell, it is necessary to reach a compromise for defining the operative energy to power ratio, which may be within the constant power regime near to the

plateau portion of the curve (a small shift in the position on the graph would have a huge impact on the measured performance). If the two cells are compared in terms of maximum specific energy and power, both HP and HE cells operated similarly with maximum specific energy, but maximum specific power for continuous discharge was stated larger for the HP cell. Hence, the specific performance of HP cells compared to HE cells is improved in terms of increased power at high energy.

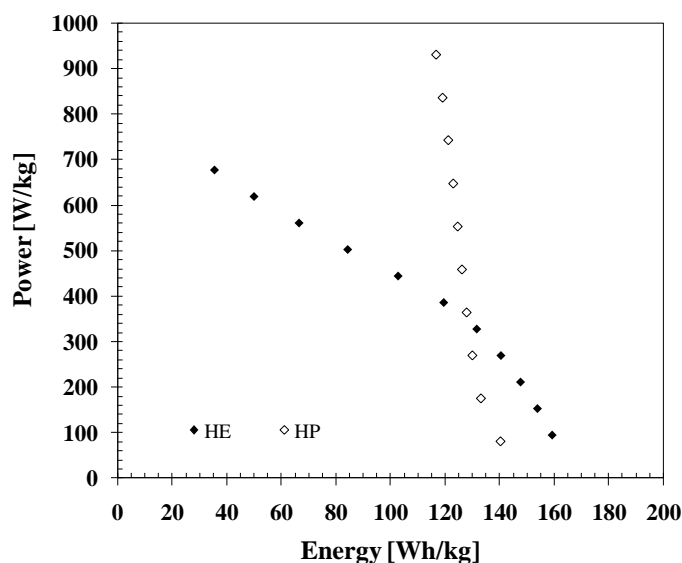


Figure 3-10. Ragone plot. Different constant power full discharges of the studied HE and HP NCM-based cells at 25°C

### 3.1.3 UNDERSTANDING CELL DESIGN

#### 3.1.3.1 EFFECT OF CHEMISTRY AND CONSTRUCTION ON PERFORMANCE

Ragone plots were also used as a way to compare batteries of different chemistries, shapes, sizes and weights. Twelve different cells from ten different manufacturers were discharged under different constant power values using the same procedure as in previous section (constant power discharge test described in *Chapter 2*). Figure 3-11 gathers the discharged specific energy data under different constant specific power values for the different cell types. It shows trade-offs between high-rate discharges and lower-rate discharges on the energy delivery.

HE and HP cells can be identified clearly enough in the plot (Figure 3-11): Manufacturer (Mnf) 2 NCM/C cell and Mnf 7 LFP/C cell are the only HE cells, which construction is different. The former is a pouch cell, whereas the latter is prismatic. Cylindrical cells are commonly HP cells: spiral construction of the electrodes maximises active surface area increasing current handling capability and therefore reducing the internal impedance. The

energy efficiency is larger for Mnf 7 HE LFP/C cell, *i.e.* it kept good power to energy ratio. Mnf 2 HE NCM/C cell is only able to optimise its performance to either energy or power.

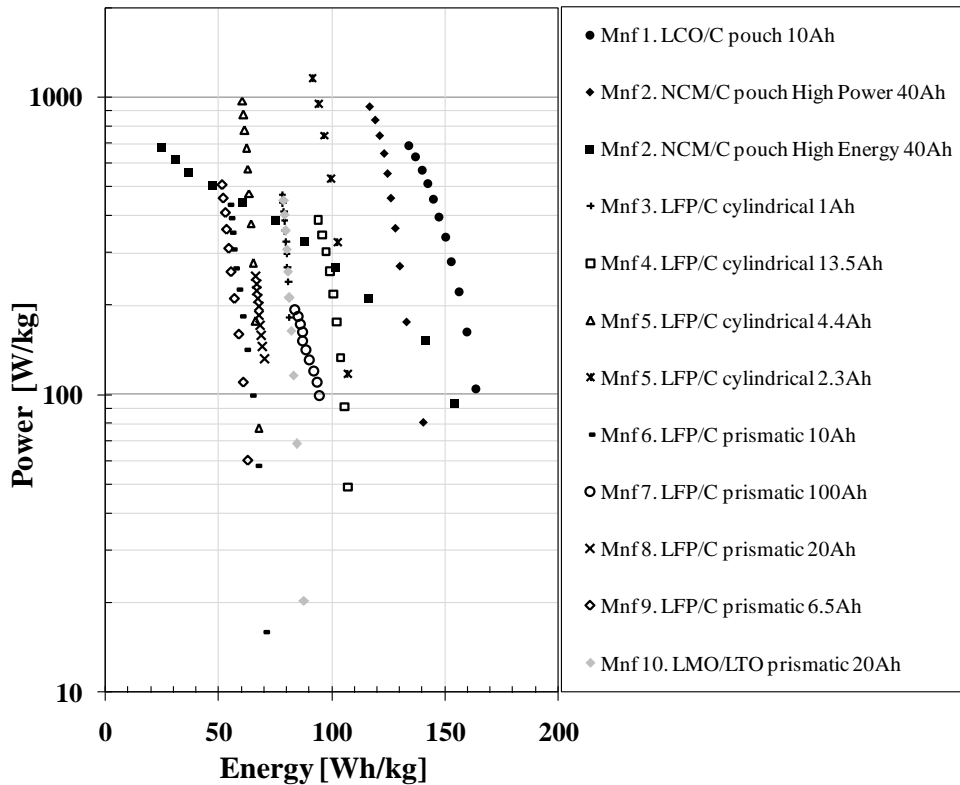


**Figure 3-11.** Ragone plots for tested cells from different manufacturers. Different constant power full discharges at room temperature for each type of cell

When comparing electrodes chemistry, energy and power density of two graphite-based cells were examined. NCM cathode cells are preferable for applications that require high energy storage capacity, whereas LFP cathode cells are appropriate for power demanding applications, such as regenerative and traction applications. Anyway, the power to energy ratio of the analysed HE NCM/C cell (Mnf 2) is remarkable. LCO-based (Mnf 1) cell also showed very good power performance. Regarding the LMO/LTO cell (Mnf 10), its specific power and energy performance is moderate. Despite its fast charging capability, its specific energy is similar to that of other HP cells with graphite anode.

Tested LFP/C HP cells results may also show cell design and geometry issues. Some LFP/C cells are cylindrical (Mnf 3, Mnf 4 and Mnf 5) and others prismatic (Mnf 6, Mnf 8, and Mnf 9). Even though the prismatic ones delivered less energy density in general, there is no clear evidence of it: the differences were not remarkable and if the same tests were carried out with similar cells from other manufacturers, the results would probably also differ. Anyway, the selection of the battery design should take into consideration the specifications of the pursued application.

### 3.1.3.2 CELL MANUFACTURING AND CASING

Weak mechanical design, inadequate pressure seals and vents and improperly specified tolerances can be responsible for many potential failures. Terminals may be also studied for connections either to the external circuit or between the cells. Cell design issues that may cause failure and the possible effects are summarised in Appendix E. Low power cells have relatively simple mechanical structures. Thermal design can be however a source of weakness for high power cells (getting the excess heat out of the cell can be a problem). In smaller cells, the most likely problem would be leakage of the electrolyte. Larger cells are more prone to cracking or splitting, which also cause leakage or distortion. Different cell design issues are analysed in the following a-d sections.

Thermograph images were taken to analyse cell and terminals heating up, which depend on the construction and case material. Cell opening and disassembling is also interesting to analyse cell design, but computed tomography (CT) is also an effective technique for scanning cell assembly without harming it. Initial visual inspection of active materials packaging and cell components can be useful for a general cell inspection. Post-mortem analysis of different cell configurations was carried out at ISEA-RWTH Aachen University (Germany) during the internship (July-Dec. 2012) under the supervision of Univ.-Prof. Dr. rer. nat. Dirk Uwe Sauer. Part of that work is presented in this section.

#### **a) Construction design and housing materials: thermal performance**

A short introduction of cell construction was introduced in *Chapter 1* and further information was also summarised in Appendix A. Cell housing way affects strongly the thermal performance. Heat development in the core of the cell under different operation conditions and heat distribution affect cell performance, ageing and safety. The temperature increases as the charging or discharging current increases. The rate at which heat is removed increases linearly but the rate at which heat is produced increases exponentially. Continuous large current and temperature building up can distort the battery case (prismatic cells with plastic case) or lead to swelling (pouch cells). Terminals heating up due to wiring and system internal resistance can also be large and it depends on terminals materials. Thermal performance depends strongly on cell design. Pouch cells are characterised for having good heat dissipation, but the quality of the welding may influence on terminals heating up. Prismatic cells are similar in shape but with robust container, which material (plastic or metallic) influences the thermal characteristics. Aiming at a qualitative thermal performance comparison of these configurations, thermograph images were taken during the operation of three different cells. Figure 3-12 shows thermograph

images of two prismatic cells with different housing, plastic (Figure 3-12 (a)) and metallic (Figure 3-12 (b)), that were taken during 1C charge at room temperature at natural convection heat transport conditions. Figure 3-12 (c), in turn, shows the thermograph of a pouch cell that was taken in the same conditions but during 2C charge. All these pictures correspond to the cell maximum heating up state.

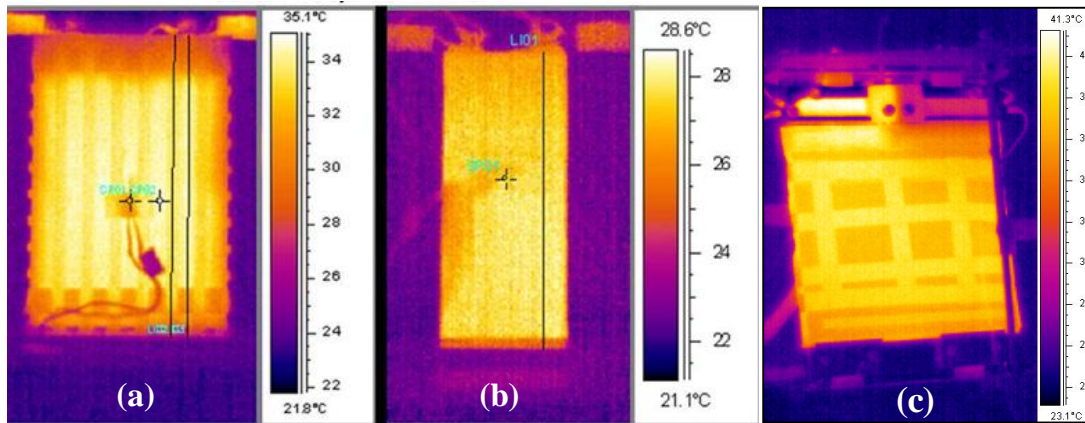


**Figure 3-12.** Thermography images of two prismatic cells with different housing, (a) plastic case and (b) metallic case, at maximum reached temperature during charging at 1C and  $25\pm 2^\circ\text{C}$ . Thermography image of a pouch cell (c) at maximum reached temperature during charging at 2C and  $25\pm 2^\circ\text{C}$

The prismatic cell with plastic case in Figure 3-12 (a) did not show large heating up of external terminals ( $30\text{--}31^\circ\text{C}$ ). Its maximum temperature was measured in the central part ( $33\text{--}34.5^\circ\text{C}$ ) and temperature decreased towards the edges of the cell, close to terminals ( $25^\circ\text{C}$ ) and bottom part ( $28^\circ\text{C}$ ). This thermal behaviour was related to cell inner design. The cell construction of other cell with apparently same configuration is shown in Figure 3-13. There is not electrochemically active mass in the upper part. There is space between the active areas and the plastic case for a better cooling down. In addition, the electrodes are smaller than the case and specially in height-size. These are apparently the reasons why cell heating up is much lower in the upper part than in the core of the cell, as is clearly visible in the thermograph image (Figure 3-12 (a)). The small temperature increase in the upper part may correspond to current collector tabs due to the internal resistance increase as consequence of the current path.

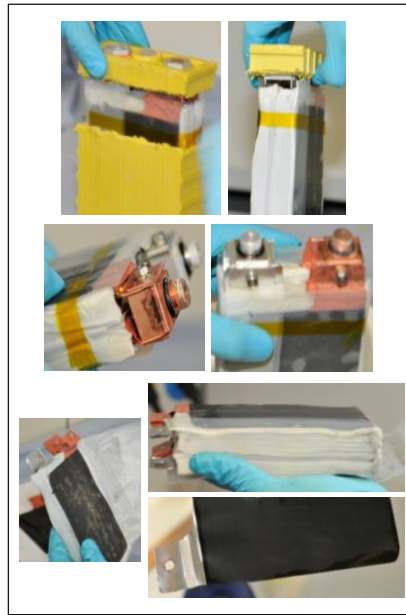


**Figure 3-13.** A prismatic cell (116x46x183mm) disassembling pictures

Figure 3-12 (b) prismatic cell with metallic case showed very low and homogeneously distributed heating up, even though the temperature increase was slightly larger in the central-bottom part. The heat dissipation was excellent and the terminals did not show additional heating up.

Pouch cell lacks of external robust terminals and the current collectors suffered larger temperature impact (Figure 3-12 (c)), specially the one of the positive electrode. While the maximum temperature detected for the negative copper terminal was 31°C, it was 41°C for the positive aluminium terminal. Except for the terminals area, the temperature distribution was homogeneous and it was 39°C in the centre of the active masses.

Overall, the analysis of cell design is of high importance not only for the battery pack mechanical design but also for the thermal conditioning system (normally refrigeration).

**b) Header designs and safety devices**

The header is the component that varies a great deal between different cylindrical cells manufacturers. The designs and safety devices are widely different, as it can be observed in Figure 3-14 (a, b) for two different similar commercial cells that were opened. Figure 3-14 (c) also shows different commercial cells top parts and both bottom and top part insulators. There are cells without any safety device, which is the case for a 22650-type cell which top and bottom parts are the first ones from the right in Figure 3-14 (c, iv). In addition, the case of this

cell was made of aluminum and it was used as positive terminal. However, the typical Ni-plated steel case is commonly used as negative terminal.

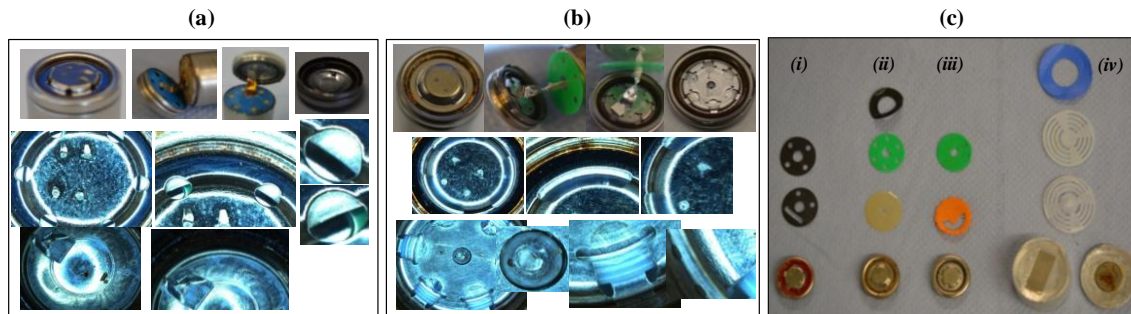


**Figure 3-14.** Top part, gasket and safety vent of two different commercial 18650 cells (a, b). Top parts (and also the bottom part for the 22650 cell in the right) and insulators for different commercial cells (c)

### c) Current collection and rolling procedure

It is important to take into account the packaging procedure, number of current collector tabs and their distribution along the electrodes, etc. for cell thermal and current distribution simulations. Cylindrical cells often use a metallic mandrel for the jelly-roll manufacturing. That is, the stack is obtained by winding the electrodes and separators around a cylindrical mandrel (it is  $\pm 2.8$  mm in diameter for 18650 cells). Aiming at increasing the current collection capability and distribution, HP cell designs often replace the mandrel with an additional tab. Different commercial cylindrical cells were opened to analyse this cell type designs. Figure 3-15 shows the pictures of a couple HE (a, b) and HP (c, d) cells. HE 18650 cell-type in Figure 3-15 (a) contains single positive and negative tabs at the end of the wind to connect the current collectors to the terminals. The positive tab is not however always at the end of the wind but sometimes more inside, as shown in Figure 3-15 (b). Figure 3-15 (c) shows a HP cell which thin electrodes are not rolled using a mandrel, but a second negative lead instead, which is welded to the bottom part of the can together with the lead in the outer part (*i.e.* 2 tabs at both ends of the wind are used to connect the Cu current collector to the terminal). In this specific case (Figure 3-15 (c)), the positive tab is not at the end of the wind, it is placed at the middle of the length of the positive electrode instead. The HP 26650-type cell in Figure 3-15 (d) neither uses any cylindrical mandrel and it employs several tabs along the length of both positive and negative electrodes, aiming at reducing the resistance associated with the current collection system during high current-rates. Figure 3-15 (e) gathers different opened cells current collector tabs.

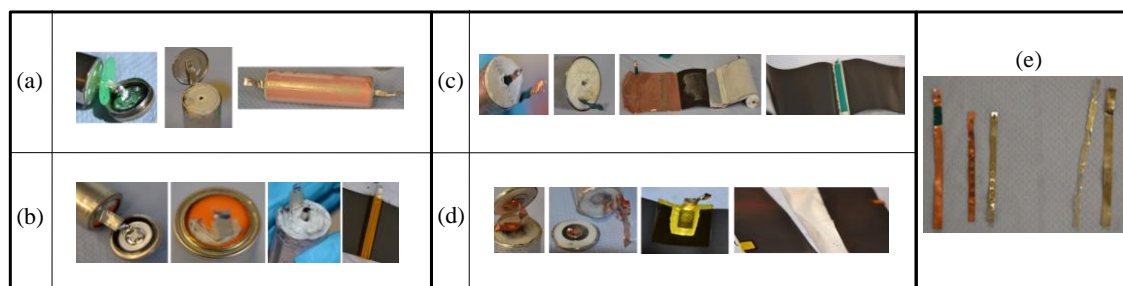


**Figure 3-15.** (a) A HE 18650 cell with a single tab at the end of the wind and a metallic cylindrical mandrel in the middle. (b) A HE 18650 cell with a mandrel in the middle and the positive tab at 19 cm from the inner part. (c) A HP 18650 cell with very thin electrodes rolled using a second negative lead, and a positive tab in the middle of the cathode. (d) A HP 26650 cell with several current collector tabs distributed along the electrodes (no mandrel for the rolling). (e) Different negative (left) and positive (right) current collector tabs

#### d) Mass and dimensions

The evaluation of the different components of the cell and their materials proportion provide insight towards the performance differences between the manufacturers. In addition, it enables estimating cells initial cost breakdown. Similar cell designs can be different in:

- i) Active masses proportion.
- ii) Ratios of positive to negative active material masses.
- iii) Surface to volume ratios (thickness factor) of the materials used.

Components of a typical cylindrical cell are shown in Figure 3-16. It is not always possible to calculate separately the mass of the anode, cathode and separator, since the separator appears to become very sticky with the cell ageing. For different cylindrical cells that were opened, large portions of the electrode coatings stuck to the separator during cell disassembly (cylindrical cells opening and disassembly methods are described in detail in section 3.3). In some cases, the separator had anode coating in one side and cathode coating on the other side. For highly aged cells, the copper current collector was also sometimes found to be totally destroyed in the outer part of the jelly-roll and the graphite delaminated. On the other hand, it is not trivial assessing the amount of electrolyte in these systems, as part of it is evaporated at the moment of cell opening and it is also immersed in the active materials.

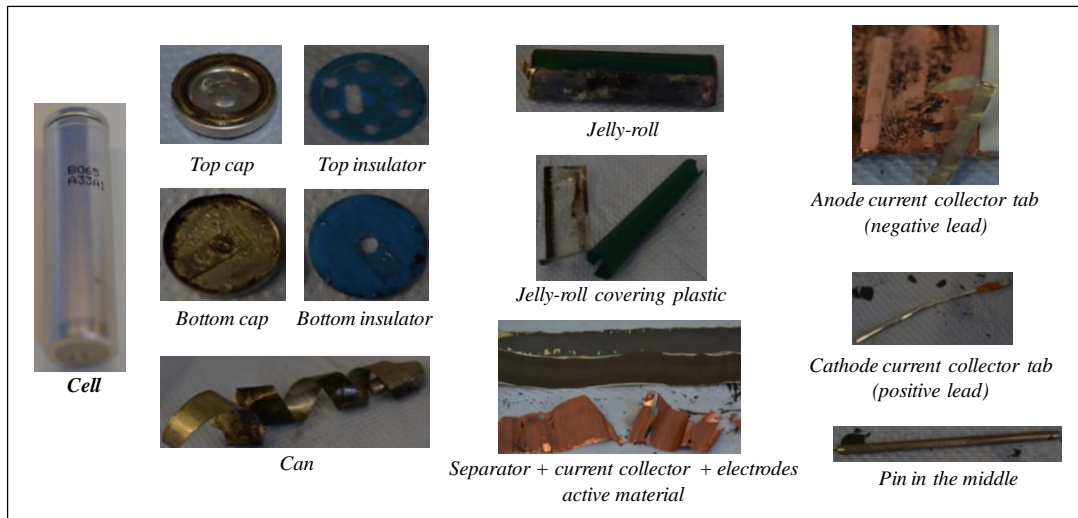


**Figure 3-16.** Different components of a cylindrical cell

The mass and dimensions of the components of different opened commercial cells were assessed. Table 3-3 summarises the main differences between HE and HP cells with similar nominal capacity. Even though the gathered measurements are rough values, the thickness of the anode coating for the HP cell was roughly the half of that of HE cell with same nominal capacity. The cathode electrode thicknesses of both cell types were in the same range. The effective surface area of the HP cell electrodes could have been therefore increased by making its surface more porous and using materials with very fine particle size. On the other hand, the length of the coating part of HP electrodes was more than the double in comparison to the electrodes of HE cells.

**Table 3-3.** Comparison of main components of different HE and HP cells of similar capacity

		NMC/C 2 Ah <b>HE</b> non-used cell	NMC/C 2.2 Ah <b>HE</b> highly aged cell	LFP/C 2.2 Ah <b>HP</b> non-used cell
CELL	Dimensions	18650	18650	22650
	Mass [g]	42.25	44.01	75.49
SEPARATOR	Total wt. [%]	4.24	4.68	6.52
	Length [mm]	850-870	820-835	1860
	Thickness [ $\mu\text{m}$ ]	15	20	22
ANODE	Electrode wt. [%]	27.57	32.56	29.54
	Electrode thickness [ $\mu\text{m}$ ]	135	165	93
	Cu thickness [ $\mu\text{m}$ ]	17	20	15
	Coating length [mm]	732-682	670	1820
CATHODE	Electrode wt. [%]	41.23	37.18	32.15
	Electrode thickness [ $\mu\text{m}$ ]	138	175	137
	Al thickness [ $\mu\text{m}$ ]	16	25	25
	Coating length [mm]	690	620	1765

Dismantling cells with different specifications and from several manufacturers becomes an useful method for an insightful analysis of cell manufacturing. Cell providers may offer similar cells in design but with markedly different performance characteristics, costs, safety guarantees, etc. Internal and external components analysis and assessment can serve to set a root of such differences and to understand the whereabouts of measured cell characteristics.

### 3.1.4 TASK 1 CONCLUSIONS

Chemistry, geometry and design are fundamental parameters for the different applications, but cell performance depends strongly on the manufacturing. Hence, commercial references from battery suppliers must be studied individually.

Chemistry option, *i.e.* most suitable cathode and anode combination, is governed by energy, power, lifetime and safety requirements. Nonetheless, BMS issues ought to be also taken into account, as, for instance, inherent OCV properties of chemistries may hinder SOC-SOH estimations and, consequently, control strategies.

Cell design and casing are factors that affect meaningfully cell thermal behaviour and current correction. Thermal behaviour is related to cell inner design and also to housing material, especially in the case of prismatic cells. Terminals of pouch cells and current collector tabs in cylindrical cells determine cell internal resistance and current handling capability. Cylindrical cells header design is specially an issue for system safety. System power demand specifications (power peaks and continuous battery power rating) will define the required HP or HE cell design. System size (weight and volume) will depend on active materials proportion and electrodes structure. Electrodes combination and the usable energy, as it relates to SOC, need to be also evaluated. Indeed, careful evaluation of operating window and strategies will make possible to identify the highest-value Li-ion solution to meet the requirements of the application, ultimately helping to reduce the costs.

### 3.2 TASK 2: CELLS SELECTION

There is no single battery type that is appropriate for all applications. The cells selection methodology developed within this work is therefore focused on satisfying the requirements related to every individual application.

The cells selection methodology was divided into four main stages, as it is depicted in Figure 3-17. The *preliminary stage (Stage 0)* searches for the emergent Li-ion cells market and aims to create a cells database to be used in the next stage. *Stage 1* focuses on the application thorough analysis and appropriate cells detection for different battery pack designs by means of developing simulation tools with the information provided by the different manufacturers. *Stage 2* tests the preselected cells and checks cells performance, manufacturing quality and capacity for meeting the application demands. It is a screening and fast experimental analysis for rejecting the cells that either show anomalies or are unsuitable for the application. *Stage 3* aims to analyse thoroughly the remaining cells taking into account several aspects:

- i) Lifetime (lifetime prognosis is then necessary)
- ii) Battery pack issues and management: refrigeration system, BMS, etc.
- iii) Costs

Lastly, *Stage 4* aims to build business models and takes also overall system safety into account so as to determine the operating control strategies for the battery pack.

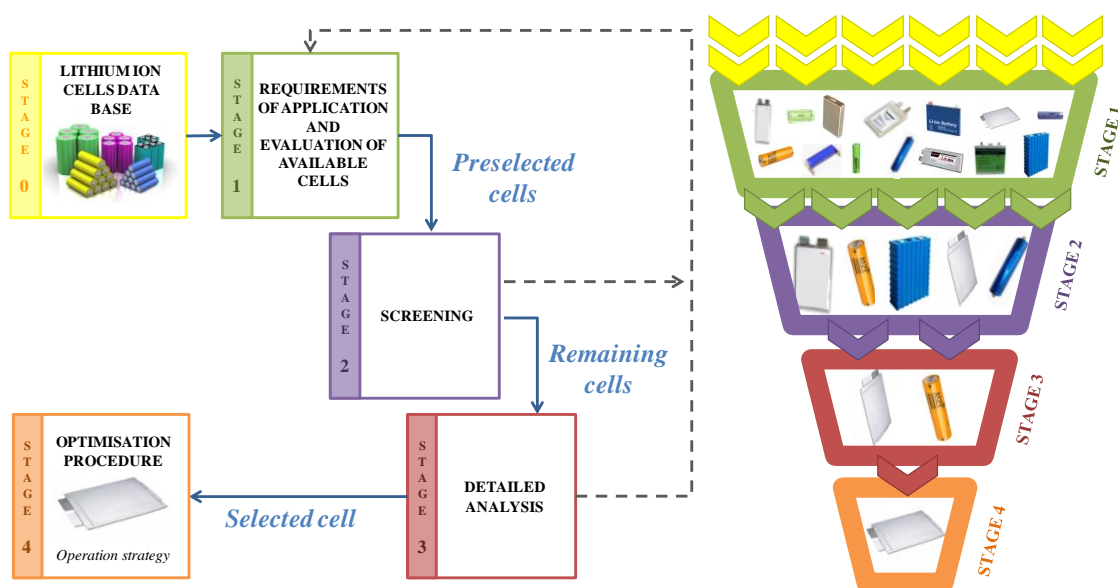


Figure 3-17. Flow chart of the defined cells selection methodology stages

The defined cells selection methodology is based on the waterfall model, *i.e.* it is structured on multiple phases and the selection process progresses systematically from one phase to the next only when the previous one has been completed. Nevertheless, iterative processes can be done and considering returning back to previous stages is acceptable when:

- i)* other or more cells ought to have been tested;
- ii)* decisions made previously are no longer correct according to the obtained results in latter stages.

The strategy firstly just lies in establishing differences among cells so that unsuitable ones can be rejected gradually and fewer cells are tested as the experimental analysis deepens in subsequent stages. Besides, its integration into product development system (Figure 1-1) is possible so that competitive battery packs for different applications can be designed. Furthermore, not only is the battery pack performance optimisation pursued but also safe, long-lasting and cost-effective operation. The full integration into a real application of the finally selected cell is considered during the whole process.

### **3.2.1 STAGE 0: EMERGENT ELECTRIC ENERGY STORING MARKET RESEARCH**

A Li-ion cell market database has been created during this work and summarised in Appendix D. The Table A-12 is a summary of the exhaustive compilation that was done trying to include information about worldwide manufacturers, the technologies they work on and some of their key customers.

### **3.2.2 STAGE 1: REQUIREMENTS OF APPLICATION AND EVALUATION OF AVAILABLE CELLS**

Stage 1 is divided into two main tasks as shown in Figure 3-18. First task deals with in depth analysis of the application (Figure 3-18 (a)) and, the second, with theoretical assessment of suitable cells technical specifications using developed mathematical tools (Figure 3-18 (b)).

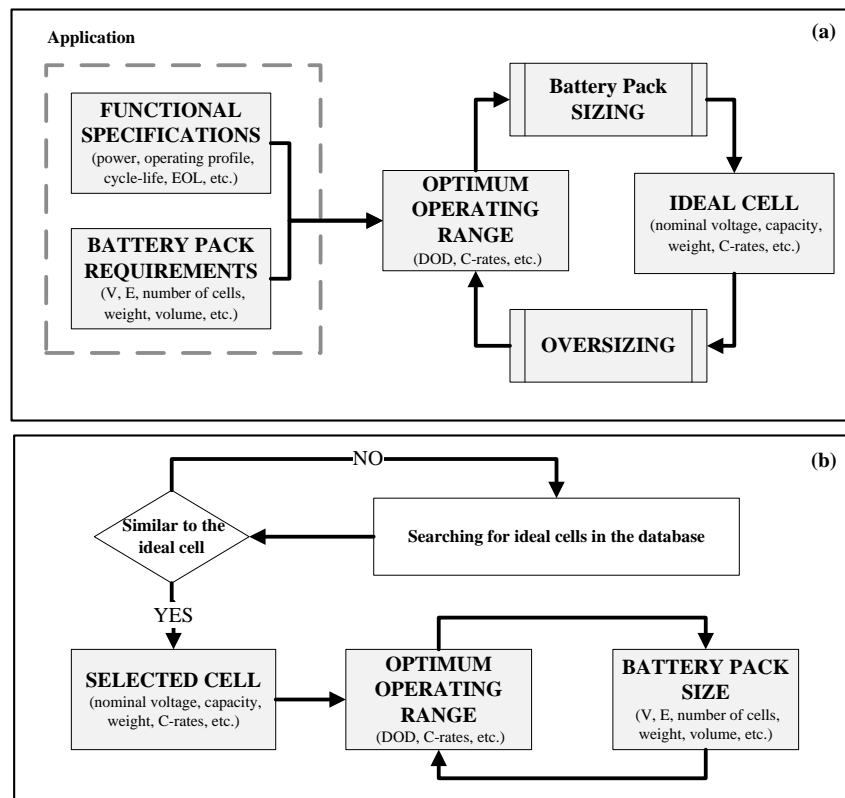


**Figure 3-18.** (a) Definition of the application, ideal cell and operating conditions. (b) Battery Pack sizing and formation according to the ideally selected cell

- **Analysis of the application**

Functional specifications, *i.e.* user requirements, and installation conditions, *i.e.* battery pack requirements, have to be carefully studied so as to determine the operating conditions ( $I(t)$ ,  $V(t)$ ,  $T(t)$  and  $SOC(t)$ ), which in turn depend on the system design, the selection of the size and type of cell, the demanded energy and time availability for battery recharging, and the operating regime [45]. Table 3-4 shows functional specifications that are necessary to take into account to meet user requirements and Table 3-5 the battery pack design restrictions in order to meet installation conditions. The battery pack size needs to meet the application most demanding power and energy conditions. The voltage limitation and, in turn, the minimum number of cells depend on the converter typology. On the other hand, the larger the number of cells, the more complex the control of the battery pack and BMS configuration will be.

**Table 3-4.** Functional specifications. The relevance of each of them depend on the application

FUNCTIONAL SPECIFICATIONS (USER REQUIREMENTS)	
Energy and power demands	Normal discharge power requirements and duration
	Maximum discharge power requirements and duration
	Normal charge power requirements and duration
	Maximum charge power requirements and duration
Calendar lifetime	Years of application
Cycle lifetime	Number of cycles
End of Life (EOL)	Percentage of energy

**Table 3-5.** Installation conditions: battery pack (BP) characteristics and restrictions

INSTALLATION CONDITIONS	
Total voltage	$U_{min.} < U < U_{max.}$ [V]
Total energy	$E_{min.} < E < E_{max.}$ [Wh]
Number of cells	$n \text{ cells} < n \text{ cells}_{max.}$
Total weight of the cells	$W < W_{max.}$ [kg]
Total weight (cells and electronics altogether)	$W < W_{max.}$ [kg]
Cells total volume (vol.)	$vol. < vol_{max.}$ [m <sup>3</sup> ]
BP dimensions	x [m], y [m], z [m]
Temperature restrictions (T management)	$T_{min.} < T < T_{max.}$ [V]
Charger characteristics and requirements	—

Appropriate cells specifications are assessed according to a battery pack configuration. For an appropriate battery pack sizing and operation at cell level, it is necessary determining:

- Application power requirements, both during normal operation and during more demanding events (“Consecutive charges and discharges” in Figure 3-19).
- Application energy demand in all possible operation conditions.

Only a portion of the battery capacity can be used when the ESS is in operation. Hence, as shown in Figure 3-19, it is necessary to consider the usable energy that the battery yields. Batteries have lower discharge power capability at low SOC and lower regenerative power capability at high SOC [46], which translates into unusable energy at certain operating conditions. Not usable DOD range then corresponds to the percentage of the regenerative energy that the cell is not able to store or, in turn, to the stored energy that it is not possible to withdraw to meet application power requirements.

The issue of ageing needs to be also addressed, as the usable DOD range is lower as the cell ages. Battery capacity reduces and internal resistance increases, so voltage limits are reached faster, yielding to lower available energy and power capability. Batteries must be able to produce and retain certain amount of discharge and regenerative power, respectively (acceleration and braking in transport means), over their lifetime, which translates into a pre-determined extra amount of usable energy necessary to meet application energy demands

(“Buffer for ageing” in Figure 3-19). It is therefore necessary to oversize the battery pack or to consider a limited lifetime for it.

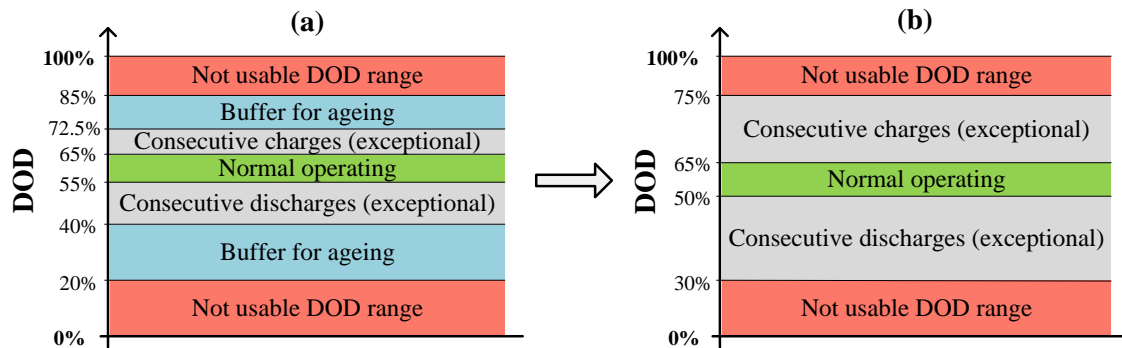


Figure 3-19. Oversizing: (a) new cell and (b) degraded cell

- **Searching for appropriate cells and optimum operation range**

The appropriate cells are identified by consulting the cells database and taking into account the defined cell optimum operating conditions. Lastly, the battery pack configuration is checked and resized in order the cell to operate within the admitted range (fulfilling both user requirements and installation conditions) and to optimise the system. For this, the information provided by the different cell manufacturers is used.

Cells that do not ideally meet the defined demands, even if the battery pack has been oversized, are rejected. Otherwise, cells are at first selected and the defined battery pack configuration is validated.

Last but not least, cells supplying capacity and delivery service of battery manufacturers as well as cells initial cost have to be taken into account.

### 3.2.3 STAGE 2: SCREENING

Own testing procedures were defined founded on standards and manuals in force (see Table 1-8 and Appendix B). First of all, it is necessary to carry out tests that enable deciding whether it is worth going any further with the purchased cells. **Validation tests** consist of:

- Cells preliminary characterisation. Analysis of variability and reliability of cells (*i.e.* fulfilment of the datasheet provided by the manufacturers).
- Different power tests. Evaluation of cells suitability for meeting the application demands by means of different power tests.

Cells that pass both steps of the validation undergo an **accelerated ageing test** at severe cycling conditions, which aims to check degradation tendencies that enable highlighting the most important differences among cells for making further distinctions.

## a) VALIDATION TESTS

### a.1) TESTS FOR CELLS PRELIMINARY CHARACTERISATION

The tests defined for cells preliminary characterisation are, as shown in Figure 3-20: nominal capacity test, rate capability tests and DC internal resistance measurement tests. These tests are described thoroughly in Table 3-6, Table 3-7 and Table 3-8, respectively. The objectives for each test in this section are the specific pursued outcomes for the cells selection.

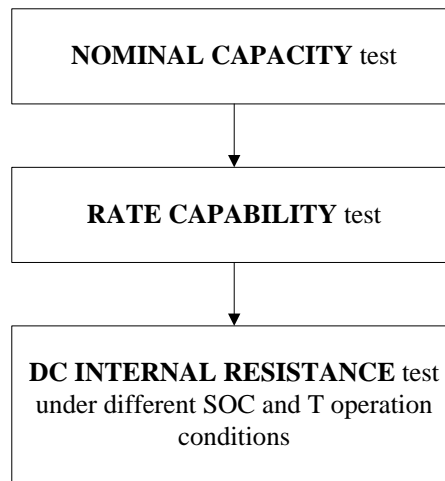


**Figure 3-20.** Tests procedure for the purchased cells preliminary characterisation

**Table 3-6.** Test description for nominal capacity measurement

<b>NOMINAL CAPACITY TEST</b>	
<b>OBJECTIVE</b>	To measure the nominal capacity and energy efficiency of the cell under nominal temperature and current load conditions.
<b>METHODOLOGY</b>	<ul style="list-style-type: none"> <li>• Test procedure defined in <i>Chapter 2</i>.</li> <li>• Number of specimens: the minimum number of cells per manufacturer is 3. Nevertheless, 5 cells of each battery type should be used for calculating the standard deviation between tested batteries [30]. Then, as many cells as possible ought to be tested.</li> </ul>
<b>EVALUATION</b>	<ul style="list-style-type: none"> <li>• The difference between the measured nominal capacity and the nominal capacity value reported by the manufacturer (datasheet). Average discharged Ampere-hour (Ah) data from second and third cycle is compared directly with the nominal capacity data from the manufacturer.</li> <li>• The energy efficiency of references in nominal operating conditions.</li> <li>• The dispersion among different specimens of the same reference.</li> </ul>
<b>VALIDATION CRITERIA</b>	<ul style="list-style-type: none"> <li>• The discharged capacity during two consecutive discharges cannot change by a value greater than 3%. If so, the cell is not even conditioned [ISO/DIS 12405-1:2011].</li> <li>• The measured capacity should be larger than the minimum specified by the manufacturer.</li> </ul> <p><i>NOTE:</i> If the nominal capacity obtained during testing differs more than 5% from the manufacturer specification, this measured nominal capacity shall be used as rated capacity and shall be the basis value for all further current requirements, <i>i.e.</i> the C-rate calculation shall be based on the measured nominal capacity. [ISO/DIS 12405-1:2011]</p>

**Table 3-7.** Description of tests to measure operating charge and discharge capacity

<b>RATE CAPABILITY TEST</b>	
<b>OBJECTIVE</b>	To measure the CHA & DCH capacity and energy efficiency of cells under different temperatures and current load conditions. T recording for cell heating evaluation.
<b>METHODOLOGY</b>	<ul style="list-style-type: none"> <li>• Test procedure defined in <i>Chapter 2</i>.</li> <li>• C-rate<sub>i</sub>: application normal and maximum current loads during both CHA and DCH operation.</li> <li>• T<sub>i</sub> [°C]: minimum T defined for the application, 25°C and maximum T defined for the application.</li> <li>• Number of specimens: minimum 3 cells per manufacturer.</li> </ul>
<b>EVALUATION</b>	<ul style="list-style-type: none"> <li>• Charging and discharging coulombic efficiency and energy efficiency.</li> <li>• Safety boundary conditions of the cell: manufacturer specifications and application requirements.</li> <li>• Analysis of the cell performance within the temperature range of the pursued application.</li> </ul>
<b>VALIDATION CRITERIA</b>	<ul style="list-style-type: none"> <li>• According to EN 61960:2011 standard, the DCH capacity at high current rates and 20 ± 5°C ought to be larger than 70% of the nominal capacity value specified by the manufacturer.</li> <li>• According to EN 61960:2011 standard, the DCH capacity at very low operating temperature (-20°C) cannot be lower than 30% of the nominal capacity value specified by the manufacturer.</li> </ul> <p>The minimum testing temperature is to be probably significantly larger than the one reported by this standard, since it is not expected the system to be working on such ambient conditions or, in such a case, it should have a temperature conditioning system. Hence, the measured DCH capacity at the defined operating conditions ought to be similar to the nominal capacity value.</p>

**Table 3-8.** Description of DC internal resistance measurement by means of pulses method at different operating SOC and T conditions

<b>DC INTERNAL RESISTANCE (IR) TESTS</b>	
<b>OBJECTIVE</b>	To measure the DC internal resistance by means of regen and discharge pulses at different SOC and operating T.
<b>METHODOLOGY</b>	<ul style="list-style-type: none"> <li>• Test procedure defined in <i>Chapter 2</i>.</li> <li>• SOC<sub>i</sub>: minimum SOC defined for the application, 50% SOC and maximum SOC defined for the application.</li> <li>• T<sub>i</sub> [°C]: minimum T defined for the application, 25°C and maximum T defined for the application.</li> <li>• Number of specimens: 1 per reference.</li> </ul>
<b>EVALUATION</b>	<ul style="list-style-type: none"> <li>• Regen and discharge DC internal resistance at different operating conditions.</li> <li>• Impedance as a function of SOC.</li> <li>• Impedance as a function of T.</li> </ul>
<b>VALIDATION CRITERIA</b>	<p>Power capability against the power required by the application. The results can be compared with the energy efficiency results from operating capacity test. Energy loss due to internal resistance is given by Eq. 3-1:</p> $E_{loss} = R_i \cdot I^2 \cdot t$ <p style="text-align: right;"><b>Eq. 3-1</b></p>

### a.2) POWER TESTS UNDER APPLICATION CONDITIONS

One critical attribute that has a significant impact on battery suitability for the application is how much usable energy a battery yields. The usable energy of the battery is the range of SOC between the points where the discharge and regeneration curve meet or exceed the application power requirements. Table 3-9 explains how to assess the cells usable SOC range by performing tests under application operating power conditions.

*Table 3-9. Description of power tests that evaluate the cells suitability for meeting the application demands*

<b>POWER TESTS UNDER APPLICATION CONDITIONS</b>	
<b>OBJECTIVE</b>	To estimate roughly the operating SOC range of cells to meet the application requirements at different operating temperatures.
<b>METHODOLOGY</b>	<ul style="list-style-type: none"> <li>• Testing:               <ul style="list-style-type: none"> <li><i>DCH power tests:</i> <ul style="list-style-type: none"> <li>i) Cell full charging.</li> <li>ii) Application DCH power profile running until the cut-off voltage is reached.</li> </ul> </li> <li><i>CHA power tests:</i> <ul style="list-style-type: none"> <li>i) The charging process starts at minimum operating SOC determined in DCH power test.</li> <li>ii) Application CHA power profile running until the maximum voltage is reached.</li> </ul> </li> </ul> </li> <li>• Number of specimens: 1 per reference.</li> </ul>
<b>EVALUATION</b>	<ul style="list-style-type: none"> <li>• <i>DCH power tests:</i> determination of the minimum operating SOC according to the application DCH power profile capability.</li> <li>• <i>CHA power tests:</i> determination of the maximum operating SOC up to which the cell can be charged in regenerative mode (application braking power capability). This SOC will limit the subsequent discharges.</li> </ul> <p>Assessment of usable energy and power capability.</p>
<b>VALIDATION CRITERIA</b>	<ul style="list-style-type: none"> <li>• Application charging and discharging requirements.</li> <li>• Application energy requirements.</li> </ul>

### b) ACCELERATED CYCLE LIFE TEST AT SEVERE OPERATION CONDITIONS

Table 3-10 describes the cycle life test defined to fast screen the degradation tendency of the cells being compared so as to make a preliminary estimation of the cycle life.

By this stage, both validation tests and accelerated ageing tests should allow to reject several options of cells and still keep some that require a non detailed analysis of suitability for the application (Stage 3).

**Table 3-10.** Description of the accelerated cycle life test

<b>ACCELERATED CYCLE LIFE TEST AT SEVERE OPERATING CONDITIONS</b>	
<b>OBJECTIVE</b>	To analyse the degradation tendency of cells due to cycling in as short as possible time and minimum possible tests for cell screening.
<b>METHODOLOGY</b>	<ul style="list-style-type: none"> <li>• Test procedure defined in <i>Chapter 2</i>.</li> <li>• Ageing test: continuous cycling at real current operating profile.</li> <li>• EPIT: nominal capacity test and HPPC test. Besides, occasional EIS measurements.</li> <li>• BOL and EOT tests: EPIT, EIS, power test under application conditions and calorimetric test.</li> <li>• Number of specimens: 2-3 per reference. At least two cells are cycled at each condition to improve the robustness of the results [47].</li> </ul>
<b>EVALUATION</b>	<ul style="list-style-type: none"> <li>• Capacity loss</li> <li>• Power capability loss</li> <li>• Heat generation</li> </ul> Comparison of different cells ageing behaviour.
<b>VALIDATION CRITERIA</b>	The EOL defined according to the application energy and power demands.

### 3.2.4 STAGE 3: DETAILED ANALYSIS OF SELECTED CELLS

The cell selection has to be focused on different aspects, as it was described previously. The factors that are under investigation in Stage 3 are: ageing, safety, cost and battery pack issues. Lifetime and, in turn, Life Cycle Cost of batteries are the bottlenecks for widespread integration of batteries. It is important to find the best trade-off solution between application requirements and financial justification. On the one hand, both (i) performance and lifetime, and (ii) reliability and safety must be satisfied. On the other hand, the real cost of purchasing the whole battery pack as well as the TCO must be taken into account.

#### a) LIFETIME: AGEING AND SAFETY

*Calendar ageing*, which simulates mainly the standing time (shelf life), and *cycle ageing*, which simulates the working operation of the battery (use), need to be evaluated. Hence, accelerated tests (i) storing cells at different conditions and (ii) using different loads are required for the analysis of cell ageing behaviour. Accurate lifetime predictive semi-empirical models will enable:

- i) Extrapolating the useful lifetime.

- ii) Defining a preliminary cell operation range that meets application requirements, takes into account safety operation boundaries, and system and operating costs.

Operating at certain conditions can cause failure modes to become more prevalent and therefore reduce the reliability. A summary of operation conditions that can lead to uncontrolled cell performance and most common failure modes are included in Appendix E. Specific safety testing protocols and abuse tests are gathered in Appendix B.

Post-mortem analysis for understanding ageing or failure reasons will help:

- i) Identifying specific mechanisms causing performance degradation. It establishes physical basis so that cell performance and degradation modes can be related over time. This way, more reliable and accurate ageing predictive models can be developed and the impact of particular operating schemes on the lifetime of the battery system can be assessed.
- ii) Identifying and characterising processes that limit cell performance and lifetime, aiming at a reliable system. It makes possible abuse tolerance and failures identification and evaluating TCO.
- iii) Determining cell ageing accelerating factors.

Hence, ex-situ destructive ageing characterisation will also provide valuable information for defining the operating and control strategies in a later stage.

Due to the complexity and extension of analysing battery lifetime, there is a dedicated *Chapter 5* exclusively to crucial requirement within Stage 3 of the selection procedure.

## **b) COST**

The real cost of a battery is composed of initial investment cost, replacement cost, preventive maintenance cost and unexpected downtime (system failure) or malfunctions (many defects that cannot be corrected: high internal resistance, electrical short, elevated self-discharge, etc.) cost. As shown in Figure 3-21, initial purchase cost represents only a small portion of the TCO.

The goal of every industry is to obtain the best return on investment. Hence, cycle life cost is an important tool in purchasing decision to establish the most cost-effective solution. This way, the tasks in this part of Stage 3 should be:

- To define a scale of relevance of different cost factors according to the requirements of the application. Cells purchasing cost is already taken into account in Stage 1.

- To identify the factors influencing the Life Cycle Cost and qualitatively quantify their impact on the TCO.

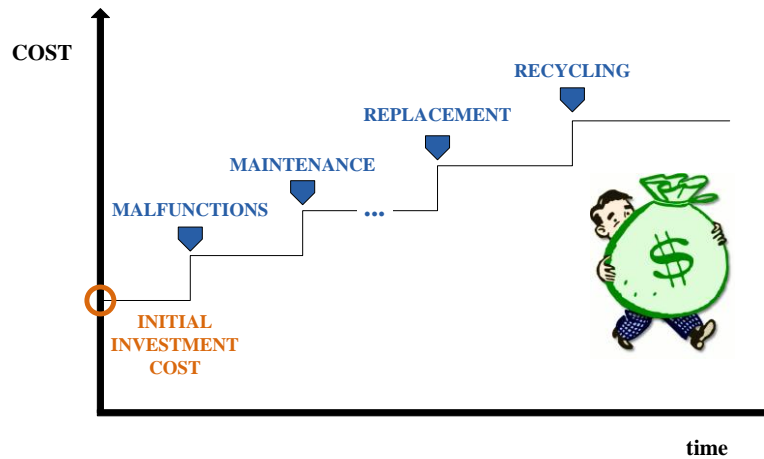


**Figure 3-21.** Costs of owning a battery system. Total Cost of Ownership (TCO) of a system includes the total costs required for building and introducing the system, operating, maintaining and disposing, including lost profits due to e.g. failures

### c) BATTERY PACK ISSUES

Several factors concerning cells, modules and packs must be considered at the design stage for the construction of battery packs. Battery system, as shown in Figure 3-22, consists of many parts [48]. The basic building block is the battery cells. To monitor and control cells, modules and pack (voltage, current and temperature), the system has a master BMS, often in combination with one or several slave management systems (e.g. one per module). Cells must be actively balanced so that they are in equal states and must be maintained within an efficient and safe temperature range, so control of cooling and heating is required (Thermal Management System). As an independent means of electrical safety, the battery often has one or several fuses, for short-circuit protection. Contactors are also placed inside the battery pack in order to connect and disconnect the battery to the rest of the system.

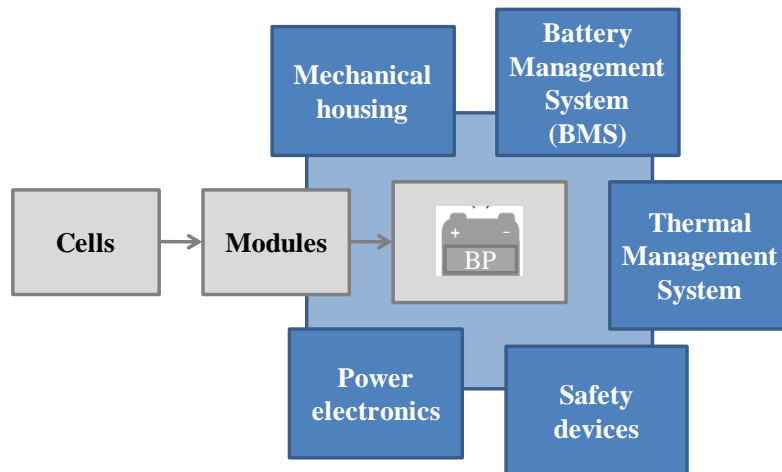


**Figure 3-22.** Battery system overview

Some of the aspects to take into account for selecting a viable cell are:

- i) Mechanical housing: packaging, electrochemical aspects, temperature conditioning system, etc.
- ii) BMS and Thermal Management System: diagnostics (SOC-SOH), cells balancing, thermal management, etc.
- iii) Safety devices.

A deep analysis of battery pack prototyping is beyond the scope of the cells selection methodology, but all these aspects must be accounted for the evaluation and final selection of the most suitable storage solution for the specific application.

### 3.2.5 STAGE 4: OPTIMISATION PROCEDURE

The battery reliability is ensured by adding safety layer by layer, as schematically shown in Figure 3-23. Unexpected battery failure is unacceptable, since it can result in complete either premature failure of the system or loss of facility. The real TCO could be therefore very high. Thus, it is important to carry out Failure Modes and Effect Analysis (FMEA) so as to delimit the operating range of the application to a safe operating window (Figure A-27 in Appendix E). Figure 3-24 summarises schematically the cause and effects of severe operating conditions and the corresponding outcome (for further information see Appendix E, where relevant information for the creation of this Figure 3-24 is included). The FMEA matrix needs to consider, for each failure mode: failure location, cause of failure, effects, relevance, priority and boundary conditions. Abuse tests are also necessary to define some failure modes (see Appendix B).

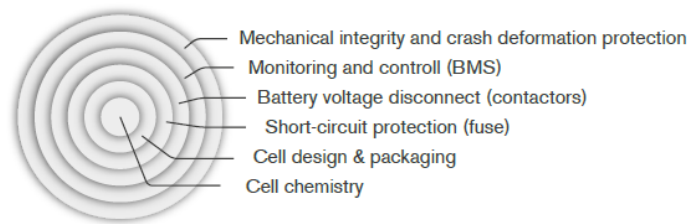
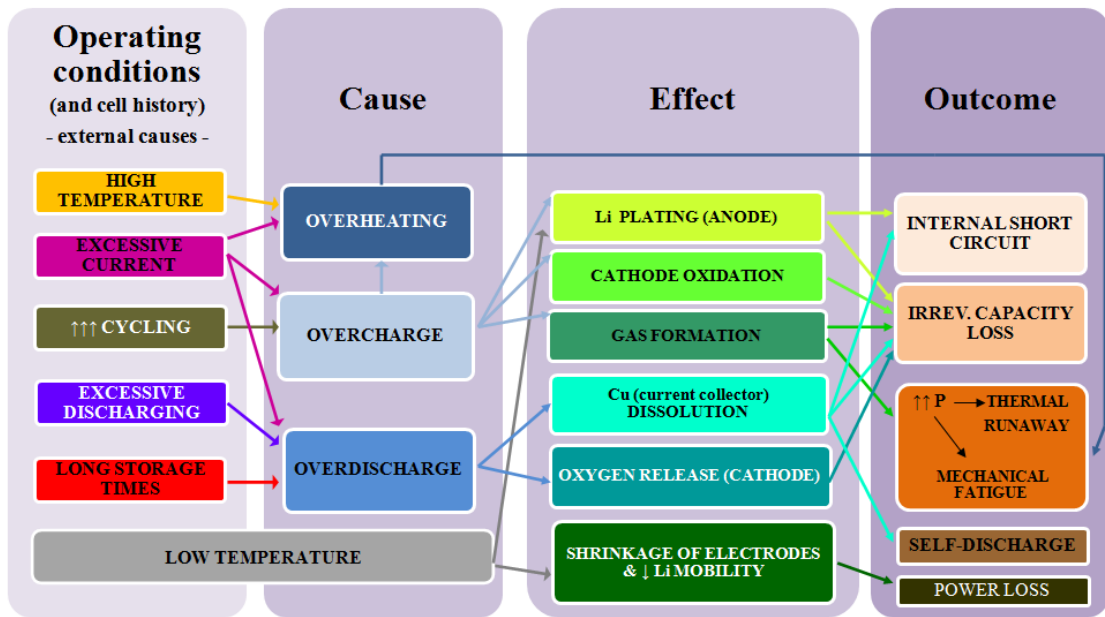


Figure 3-23. An example of battery safety layer by layer [48]



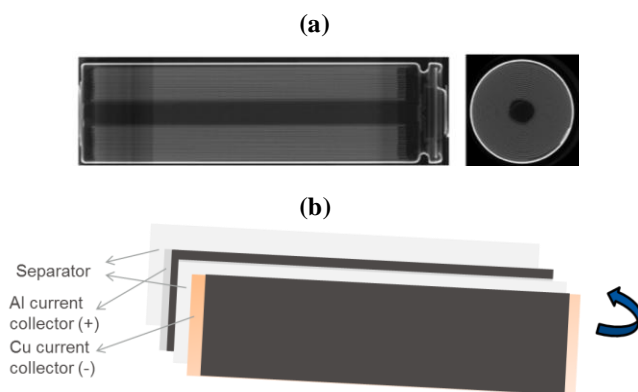
\* External short circuits (overcharge -> overheating).

Figure 3-24. Cause and effects of abuse operation conditions

Stage 4 aims at developing a performance model for the cell selected at the previous stages and lastly, a business model for determining cost-effective solutions. The final goal is to define safe and long-lasting operating strategy taking into account cell performance, lifetime, safety, costs and battery pack issues. The operating range definition might require redesigning the battery pack configuration defined at the first beginning (Stage 1).

### 3.3 TASK 3: PROCEDURE FOR CYLINDRICAL CELLS POST-MORTEM ANALYSIS

Identifying the contributions to cell power and capacity fade, which means understanding performance degradation mechanisms, is critical to both (i) work on cell concepts (involving both chemistries and constructions issues) that can meet the target lifetimes and (ii) establish precise algorithms for long-term performance predictions based on short-term cell test data. The evaluation of degradation mechanisms involves the examination of the nature and extent of physical, chemical and structural changes in the cell and cell components that resulted from accelerated ageing. Several research groups [49-83] are working on post-mortem analysis of Li-ion cells aiming at identifying ageing processes. Nevertheless, cylindrical cells analysis is especially an issue due to its complex configuration, as shown in Figure 3-25, while it is a very common technology in the market for different applications, such as it was selected, for instance, for the residential elevator.



**Figure 3-25.** (a) Computed tomography (CT) scan of an 18650 cell [81] (b) Cylindrical cell construction: double-coated electrodes and rolled technology

Some authors [50, 52, 54, 60, 61, 63, 66, 67, 70, 72, 76, 78-83] worked on cylindrical cells post-mortem analysis with different purposes. However, they did not published the procedure for cells disassembly and harvested components analysis. Argonne National Laboratory (ANL) [58] and D. Aurbach *et al.* (Bar-Ilan University, Israel) [80] just showed few guidelines. In this sense, the first trial and error step was opening different highly aged cells. The important aspects of cells components and design needed to take into consideration during the cells selection were already included in section 3.1.3.2. Figure 3-26 shows pictures of unraveled cell electrodes and separators that show several effects: delaminating of anode, destruction of the current collectors in the outer part of the jelly-roll, mechanical alteration of the cathode due to the fabrication process (pressure of the cylindrical mandrel), sticky separator due to probably binder degradation, discoloration of the separator, etc. The argument enters about the source of these effects, whether they are due to either electrochemical cell ageing or cell disassembling process. Figure 3-27 shows two equivalent cells opening that are aged

apparently at different level. In the case of the cell in Figure 3-27 (a), the extracted cell components were damaged, whereas cell in Figure 3-27 (b) seemed to be a fresh cell. The more aged the cell, the more difficult the disassembly is. But, how large is the influence of the disassembling on the components degradation? The issued challenge is components harvesting without significant degradation, as a first and crucial point to extract later significant and reliable information about degradation.

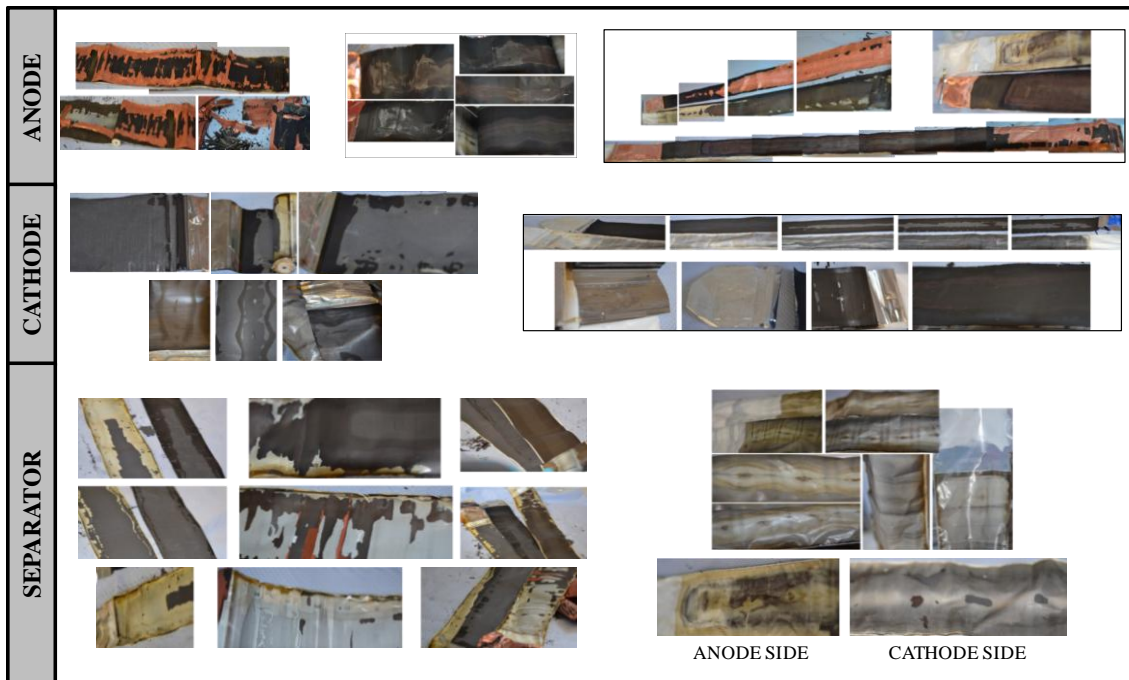


**Figure 3-26.** Pictures of highly aged and damaged harvested anodes, cathodes and separators from different 18650 cells



**Figure 3-27.** Two laptop 18650 aged cells (a and b) cell innards (jelly-roll) extraction

The need to develop a methodology for opening and disassembling the cells safely without significant additional degradation of the components was identified. This work required experimental screening and optimisation, deep analysis and time effort to set a robust methodology. Some physical-chemical and electrochemical characterisation techniques for fresh and aged cell components comparison were also evaluated. The goal of this second task was to define the procedures for obtaining significant characterisation results. All this post-mortem analysis work was carried out at ISEA-RWTH Aachen University (Germany) during the

internship (July-Dec. 2012) under the supervision of Univ.-Prof. Dr. rer. nat. Dirk Uwe Sauer. This six month work assisted the establishment of a reliable method for cell opening and disassembly, currently used at ISEA and also at CIC energiGUNE through an ETORTEK (Strategic Program of the Basque Government) collaboration. It also helped to set the basis for a post-mortem characterisation routine as described in this section. Due to the extent of this work, the post-mortem activity of this Thesis was specially focused on establishing these methodologies, rather than performing extensively actual post-mortem analysis.

### 3.3.1 CELL DISASSEMBLY AND CHARACTERISATION METHODOLOGY

Figure 3-28 shows, in general terms, the proposed methodology for cells post-mortem analysis. External assessment consists on measuring dimensions and mass of the cell and taking pictures before disassembling. That is, removal of the metallic housing for extracting cell innards (jelly-roll). Electrolyte has to be also collected for its physical characterisation. However, this is not an easy task because this type of configuration does not contain electrolyte in excess, solvents evaporate while cell opening/disassembling and the active materials contain a large proportion of it in the porous structure. Once the jelly-roll is weighed, it has to be unwrapped. A scalpel type knife is used for cutting/opening its covering plastic. Unraveling of the components needs to be done smoothly in order to minimise alteration of the cell components and keeping the electrodes as a whole, since, for instance, the separator appears to become sticky with cell age. Visual inspection and taking pictures of electrodes and separators is the next step. This initial examination of inner components is critical in focusing diagnostic effort. Working out the mass and dimensions of the different parts is also very useful for evaluating the proportion of active and inactive materials in the cell. The last step is active materials electrochemical and physical-chemical characterisation. The former is helpful in directing physical-chemical diagnostic studies.

The entire cell disassembly and electrodes harvesting process must be done in Argon (Ar) dry atmosphere within a glove-box, without any contact with ambient atmosphere. The methodology for cells disassembly and components (electrolyte and jelly-roll) extraction is described in the next section 3.3.1.1. Aspects related to some experimental techniques and procedures for cell components characterisation are described in section 3.3.2.

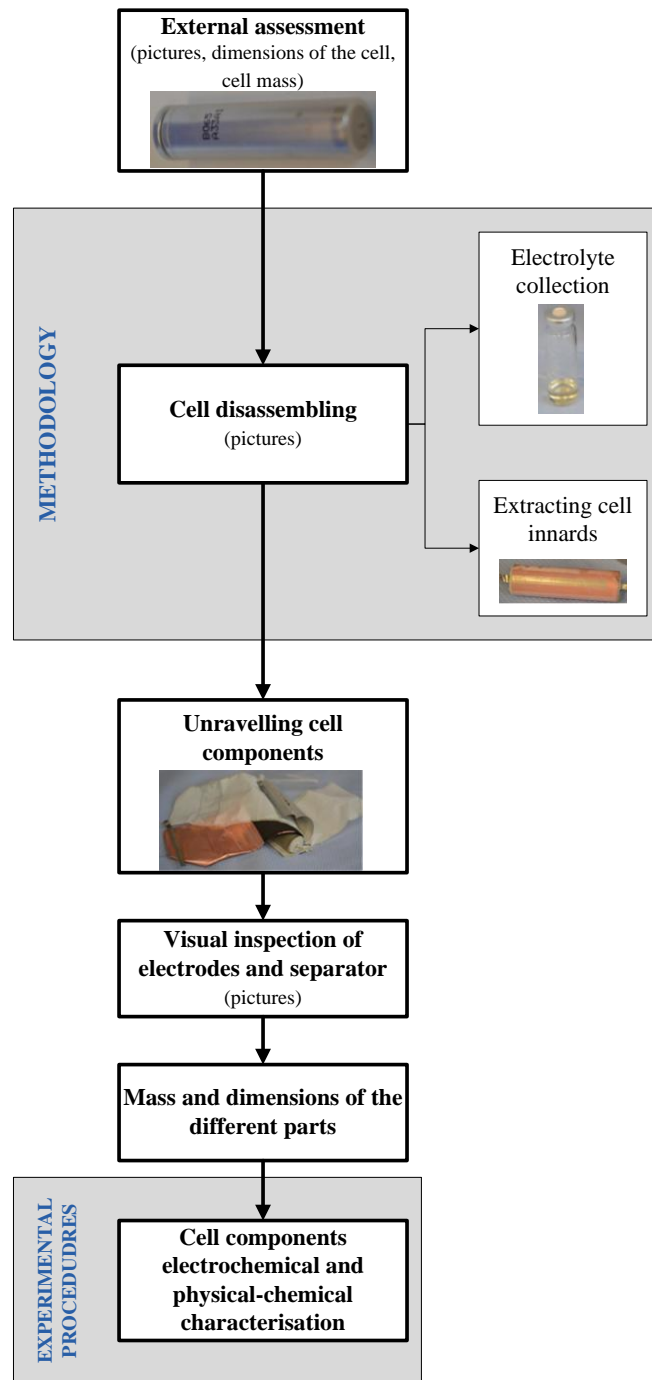


Figure 3-28. Complete general step-wise procedure for cells post-mortem analysis

### 3.3.1.1 CYLINDRICAL CELLS DISASSEMBLY AND COMPONENTS EXTRACTION

This section summarises all the aspects and different attempts during cells disassembly and electrolyte collection process development<sup>1</sup>. The approach taken and level of effort needed for various steps are highly dependent on the type of the electrolyte used in the technology [58].

#### a) Methodology for cell disassembly

Attempted options for cell disassembly are outlined in Figure 3-29 and are described as follows:

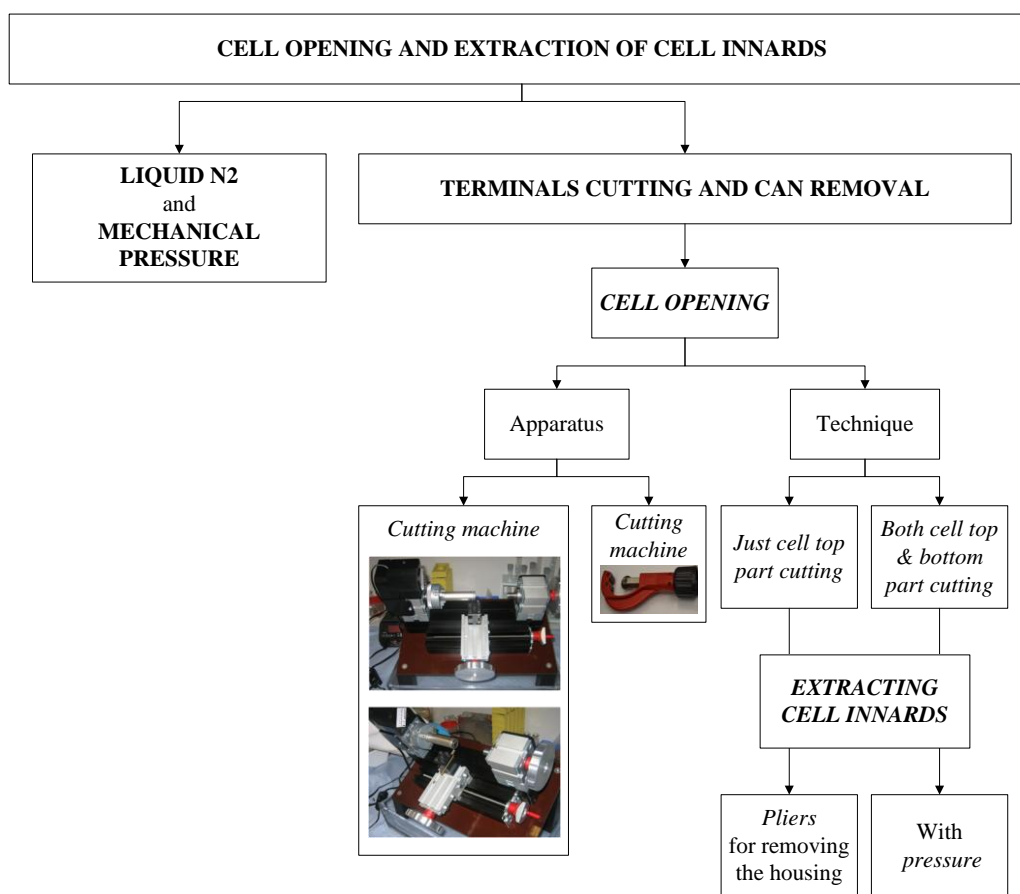


**Figure 3-29.** Cell disassembly methodology development. Options that were tried for cell opening and extraction of cell innards

#### a.1. Cell housing removal cooling down the cell with liquid nitrogen (N<sub>2</sub>) and hitting it with a hammer

The jolly-roll was shrunk (volume change due to low temperature) and the can was broken with pressure, which was totally destroyed. Moreover, the cell was damaged and even burnt in

<sup>1</sup> The procedure was developed out of the glove-box within the extractor hood and disassembling the cells at overdischarged state (~ 0V) so that any safety risk was avoided.

some cases, as it can be observed in Figure 3-30. Hence, it is not an efficient and safe way to obtain the cell innards.

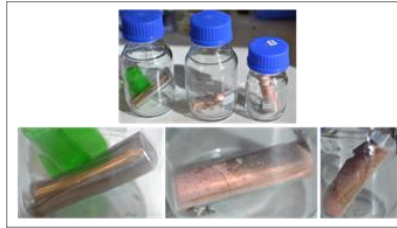


**Figure 3-30.** Extracting 18650 cell innards using nitrogen and hitting the housing

## a.2. Terminal cutting and can removal

### 1. Pipe cutter / Cutting machine

The cell is opened from the top and, if necessary, also from the bottom part either manually using a **pipe cutter** or with a **cutting machine** designed for this purpose. The automatic cutting system consists of, as shown in Figure 3-31 (a):

- a turning machine where the cell is placed within metallic fixing points and rotated automatically.
- a blade that can be adjusted both horizontally and vertically to cut the cell in the desired position. A cell top part cutting is shown in Figure 3-31 (b) step by step, as example.

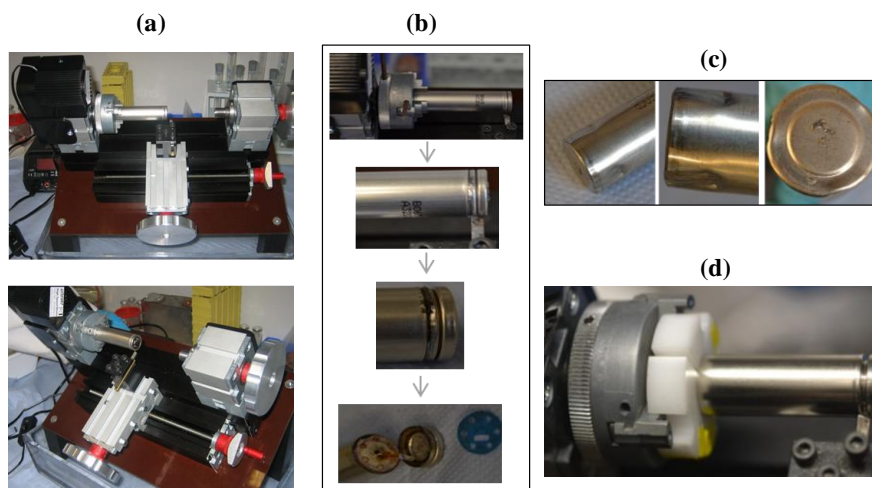


**Figure 3-31.** (a) The turning machine designed for cylindrical cells opening. (b) Cylindrical cell top part cutting process using the turning machine. (c) Cell bottom part distorted due to the mechanical force of the three fixing points of the cutting machine. (d) Adapted plastic cell holder for the cutting machine

For cutting the top part, using a pipe cutter or the cutting machine is similar but doing it manually with the pipe cutter is much faster. However, the machine should be used due to safety reasons (charged cells with fire risk in hands should be avoided).

On the other hand, cutting machine distorts the cell in the bottom part in some cases, as shown in Figure 3-31 (c), due to holding mechanical forces (there are three fixing points), even reaching to break/cut the metallic can when its material is soft (especially when it is made of aluminum). As a consequence, the cell innards are damaged and it is troublesome to extract them (jelly-roll).

A plastic holder which would cover the whole cell diameter, which is shown in Figure 3-31 (d), was designed to sort out this problem. Nevertheless, it did not work out because the fixing was not good enough and, in addition, the new holder was slippery. Therefore, the cell was moving horizontally while being rotated, which did not make possible to cut it just in one position, and it ended up expelled out from the system in all cases.

## 2. Cutting just the top part / Cutting both top & bottom part

Figure 3-32 shows pictures of the top part (Figure 3-32 (a)) and bottom part (Figure 3-32 (b)) cutting of a cell. If pliers are to be used for removing the housing, it is better just to cut the top part, as shown in Figure 3-32 (c). Cutting also the bottom part induced further damaging of cell innards. So it is recommended cutting just the top part.

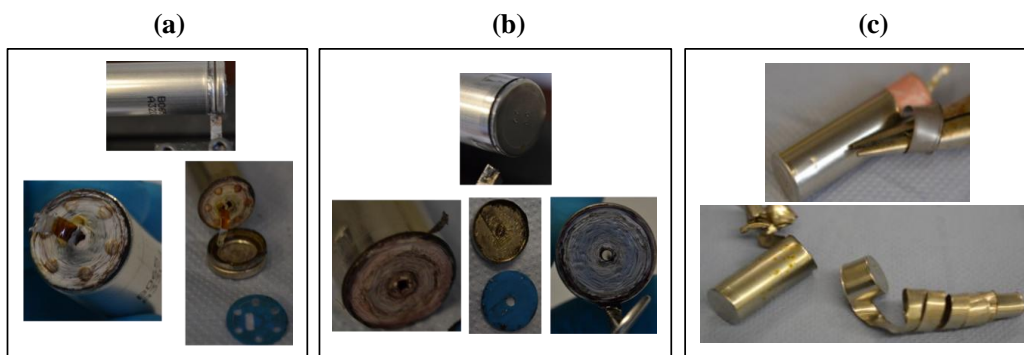


**Figure 3-32.** Top (a) and bottom (b) part cutting of a 18650 Li-ion cell. Housing removal (c) of different cells using pliers after cutting the top part

It was also tried to take out the jelly-roll with pressure, for which it was necessary to cut both top and bottom parts in advance. The pressure was applied manually but there was no result but distorting the can and the jelly-roll. Thus, a tool would be necessary for this procedure to be possible.

Overall, Figure 3-33 shows in short the results of different evaluated options for cells opening and extraction of cell innards.

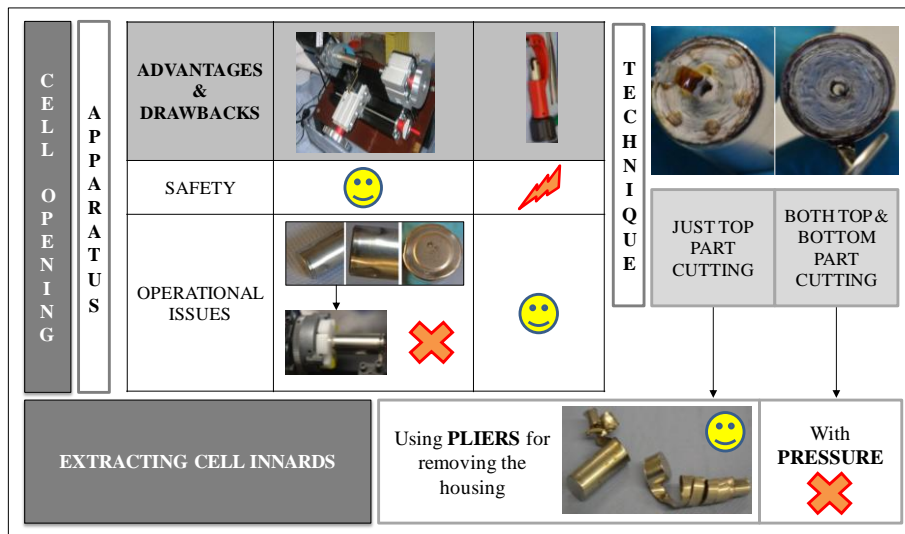


Figure 3-33. Summary of the evaluation of the attempted options for cell disassembly

Highly aged cells were opened to check the different options that were described. When disassembling the cells, different degradation effects, such as graphite delamination or current collector ripping, were observed. Nevertheless, it was uncertain whether it was due to electrochemical ageing or the disassembling process itself. Moreover, it was not possible to evaluate how large the influence of the disassembling on the degradation of components was. For this reason, fresh cells from different cell manufacturers were opened following the same procedure. As it is shown in Figure 3-34, cell innards were obtained with no apparent degradation. Hence, the developed disassembling procedure was validated and defined as follows:

1. Cut only the top part of the cell using a pipe cutter.  
 Non isolated pipe cutter was found in the market. Nevertheless, it should be looked for some similar tool that may be useful for this task since opening cells at high SOC could enhance safety risks.
2. Remove the housing using isolated pliers (and other tools for cutting the edges in the top part).



Figure 3-34. Disassembled fresh cells (unused) from different manufacturers

Following the defined procedure, different manufacturers new and aged cells were successfully opened at different SOCs.

**b) Methodology for electrolyte extraction**

A hole in the cell is needed for collecting the electrolyte either in vapor or liquid form. Thus, it was carried out after cutting the top part of the can and even by puncturing the cell in the bottom middle part (which top part would be cut after collecting electrolyte for extracting the cell innards). It was not punctured the top part as the safety vent of the cell (with a gap) is placed there.

The electrolyte in liquid form was extracted by centrifuging cells with the top part opened in a SIGMA 2-16 microcentrifuge No. 17140 (in Appendix C) at the maximum possible centrifuging both speed, *ca.* 4000 rpm, and duration, 15 min, taking into account system balancing issues. For that, the equipment had to be modified and the extraction technique improved (highly aged cells were used to develop the methodology of extracting the electrolyte). Attempted options for collecting the electrolyte are described as follows:

- Centrifuging of aged cells: (i) without the top cap; (ii) without both the top and bottom cap, (iii) without the can, and (iv) puncturing the cell, as shown in Figure 3-35.

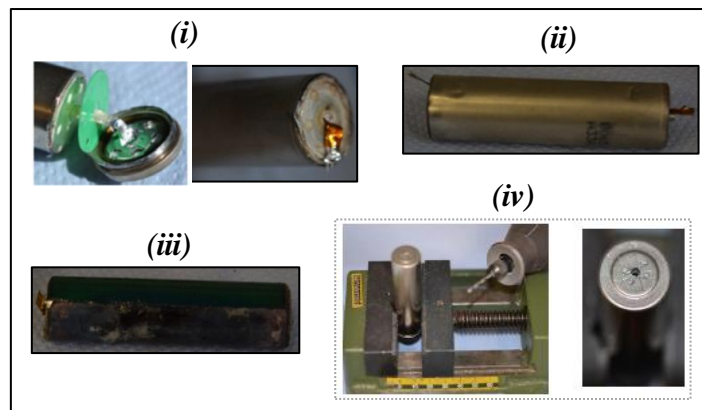


**Figure 3-35.** Different opened parts (i, ii, iv) or just the jelly-roll (iii) for cell centrifuging

It did not work regardless the specimen part introduced or the centrifuging time (they were centrifuged several times for 15 min -due to equipment limitations-). Besides, the glass tube within the centrifuge containers (Figure 3-36 (a)) was broken due to the sharp edges of the cut cell. Hence, neither the electrolyte extracting technique nor the available equipment seemed to be suitable for the pursued task.

- Centrifuging of heated up aged cells with the top part cut

The cells were heated up and kept at 50°C for several hours for altering the viscosity of the electrolyte. The top part of the cell was cut in Ar atmosphere afterwards and immediately introduced in a plastic container, shown in Figure 3-36 (b), for the centrifuging process. Note that:

i) The heating must be long enough so that the cell temperature is homogeneous and does not change during the cutting and centrifuging process, which may entail more than 2 hours. The electrolyte collection was not successful within this time frame. Thus, the cells were left overnight in the climatic chamber at the set temperature for assuring the efficiency of the overall process.

The storing time should be long enough for altering electrolyte viscosity but at the same time it should not cause further degradation of cell components.

ii) The containers of the centrifuge had to be fully emptied so that the new cell plastic container could be introduced (Figure 3-36 (b)).

The entire process was conducted taking special care that the electrolyte and the electrodes were never exposed to ambient atmosphere (the sample plastic holder and the centrifuge container were carefully sealed. Additionally, they were introduced in the globe-box at least 12 hours before their use so that the humidity they could contain was removed). After 15 min at *ca.* 4000 rpm, *ca.* 1 ml of electrolyte was extracted, as shown in Figure 3-36 (c). Thus, the technique of centrifuging was efficient and cutting just the top part of the cell was sufficient. This way, the procedure was also more effective, since it was fast and the least electrolyte was lost in the process of cell opening.

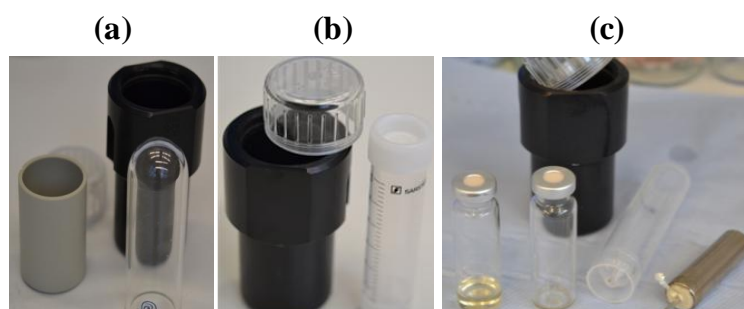


**Figure 3-36.** (a) A centrifuge container (black with plastic transparent cap) and the inside components. (b) New system for cell centrifuging: plastic container for the opened cells within the container. (c) Electrolyte extraction centrifuging the cell (the crystal container in the right contains the obtained electrolyte. The crystal container in the left contains the electrolyte with the isopropanol, IPA, that was used to clean the centrifuging container)

- Extraction of electrolyte from new cells at 0% SOC

Once defined the methodology for extracting the electrolyte, it was repeated using new cells. Nevertheless, it was not necessary to heat them up, since there was sufficient electrolyte in the system that was possible to be collected at the first centrifuging attempt. The electrolyte was colorless when initially extracted.

In conclusion, two processes that alter the electrolyte need to be taken into account:

- i) Highly aged cells may not contain sufficient free electrolyte, *i.e.* the system is dry or poorly wet due to the underwent ageing processes. Besides, the aged electrolyte turns into yellowish/brown color, which may be related to an increase of the solvent viscosity.
- ii) Overdischarging the cells (to 0 V) and taking the electrolyte out of its stability window makes not possible to collect it. There might take place some decomposition processes, such as gassing, that alter the good condition of the electrolyte.

Figure 3-37 summarises the developed methodology for electrolyte collection. First, if the cell is highly aged, it is necessary heating it up for electrolyte extraction. Next step is cell top part cutting within the glove-box using the pipe cutter (cell puncturing would mean additional work, as the cell top part needs to be cut anyway for cell disassembling). Immediately, the rest of the cell has to be introduced in a plastic container and then within the container of the centrifuge (check right sizes), sealing them properly in order to avoid any contact with ambient atmosphere when taking it out from the glove-box for centrifuging (in case it is not possible to ensure inert atmosphere throughout the whole process, the centrifuge should be within the glove-box). The last step is centrifuging at maximum possible velocity and the electrolyte sample is to be collected, again within the glove-box, diluting it in dimethyl carbonate (DMC) solvent once within the glove-box again. Inductively Coupled Plasma (ICP) technique can be used for determining metals concentration in the electrolyte, and Gas Chromatography with Mass Spectroscopy (GC-MS) for solvents and salts (organic components) analysis.

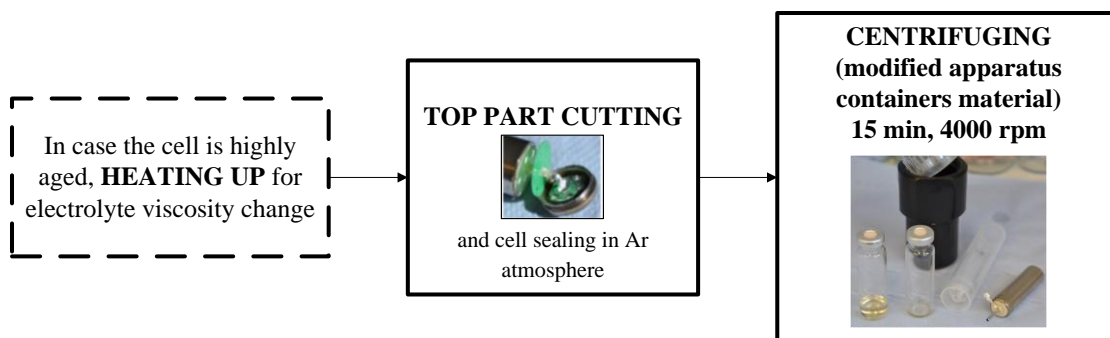


**Figure 3-37.** Defined electrolyte collection procedure

Other option for analysing the electrolyte is collecting electrolyte solutions using solvents (isopropanol, IPA, or DMC) or even collecting the wet separator into sealed containers, right after cell components unravelling, for the volatile components examination using GC-MS technique. A couple of possibilities for electrolyte solutions collection using solvents are: rinsing (inner part of the can, jelly-roll outside part or wet electrode surfaces) and immersion of the jelly-roll (different exposure times).

**c) Overall methodology for cell components harvesting**

After several trials with fresh, old discarded cells as well as specifically aged cells, Figure 3-38 shows the summary of the procedure optimised for a safe cell opening and disassembling, and a subsequent harvested components post-mortem characterisation. Cell components harvesting process can be divided into 4 main steps: (i) cell top part cutting using a pipe cutter, (ii) cell centrifuging for electrolyte collection, (iii) extracting of the cell innards using isolated pliers (or similar tool) and (iv) unraveling the cell components. The methodology was developed and verified at 0V and 0-100% SOC for 18650 and 22650 cells without any contact of inner cell components with ambient atmosphere. Cylindrical cells of up to a diameter of 100 mm can be disassembled using this methodology.

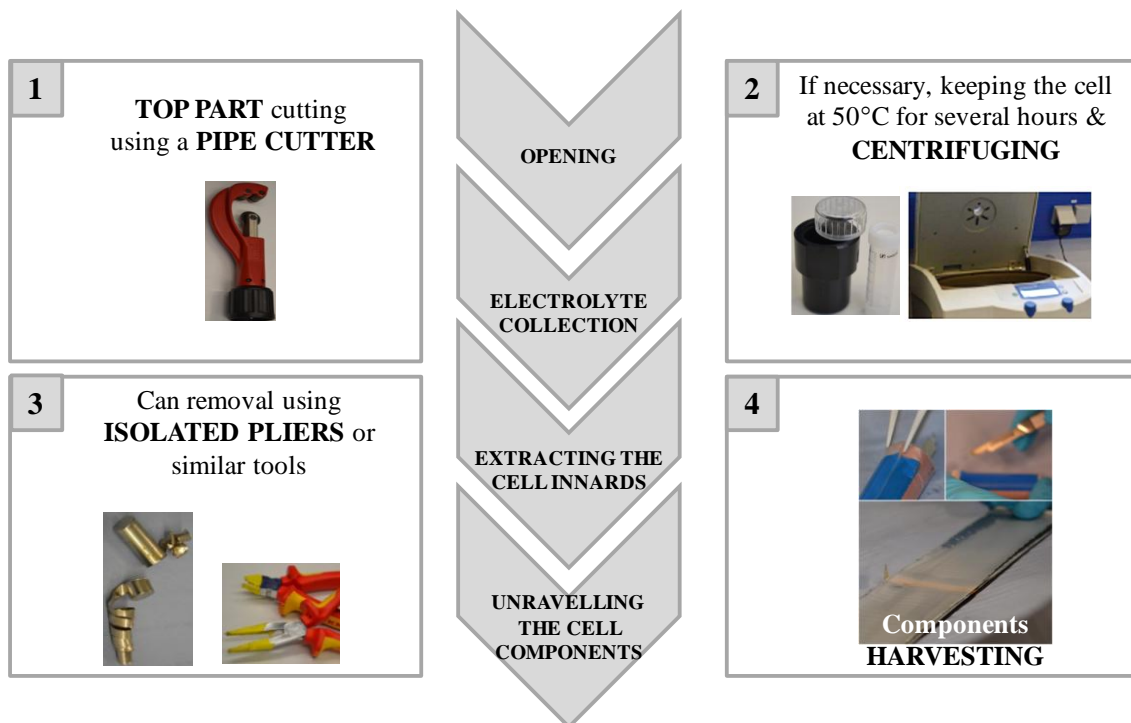


*Figure 3-38. Developed methodology for cylindrical cells disassembling and components harvesting. All the steps with the same cell and in Ar-atmosphere*

### 3.3.2 PHYSICAL-CHEMICAL AND ELECTROCHEMICAL CHARACTERISATION OF CELL COMPONENTS

The performance of porous solids such as battery electrodes is dependent on their pore structure. While higher porosity is advantageous from the standpoint of Li-ion diffusion, it is detrimental to the electrical conductivity of the electrode. Porous structure characterisation involves the determination of the pore size distribution as well as the porosity, which is defined as the ratio of total pore volume of the accessible pores and voids to the total volume occupied by a given amount of the solid [84]. Many different methods have been developed for the characterisation of pore materials. Mercury Intrusion Porosimetry (MIP) is one of the most used ones, where the pores are filled with mercury under pressure. This method is suitable for many materials with pore diameters in the range of 0.003  $\mu\text{m}$ -400  $\mu\text{m}$  [84].

Inductively Coupled Plasma-Optical Emission Spectrometry (ICP-OES) was used for multi-element analysis of metallic compounds of the electrodes, *i.e.* for the positive electrode composition determination. In addition, this analytical technique is also generally used for electrolyte metals and impurities detection, *i.e.* for evaluating the present active lithium and checking the presence of traces of soluble metal contaminants from the electrodes.

The last analytical work carried out was harvested electrodes samples preparation for half-cells electrochemical measurements. Reference electrode cells were prepared to determine the relative contributions of the positive and negative electrodes to the cell ageing (capacity fade and impedance rise). It should be noted that, even though material preparation and cell assembly were carried out in Ar-atmosphere glove-box, all measurements obtained with harvested electrode cells have an inherent uncertainty associated with the cell disassembly process. Besides, there must be variations since electrode stack pressure, gas environment, electrolyte composition and electrode surface films are different from those in the original cells [58].

#### 3.3.2.1 ELECTRODES POROUS STRUCTURE CHARACTERISATION BY MERCURY POROSIMETRY (MIP)

##### a) Specimens preparation: electrode coating layers and entire harvested electrodes

Scraping the electrodes to remove the coating and measure the porosity does not work since a powdered specimen is obtained, which does not correspond anymore with the coated structure. The anode coating was exfoliated and delaminated in some cases. It was also easy to remove in pieces in other cases. Cathode coating was collected with difficulty, since it remained stuck to the aluminum current collector in most of the cases. In the case of highly aged cells, cathode

coating was also largely found in the sticky separator. It was tried to measure the few NCM coating specimens available but there were some unknown reactions that caused measurement failure. Anode active material porosity was possible to measure without any copper current collector on it. The goodness of the results is uncertain, but data was used to evaluate the reproducibility of the measurements. It was thereafter possible to compare the obtained coatings porosity results with the ones corresponding to the whole electrode.

Film harvested electrode material was sampled by cutting strips to fit the appropriate sample holder. Anode was successfully measured, whereas there were some reactions in the case of NCM positive electrode. Nevertheless, even though there is no clear explanation for that, the cathode porosity was finally measured.

#### b) Repeatability of the measurements

After measuring several specimens of anode coatings from different aged cells that were opened, and obtaining apparently acceptable results (porosity range from 20 to 30%), the repeatability was checked using similarly aged cells of the same manufacturer (all of them were from the same battery pack). Random sampling, from both different cells and the electrode of the same cell, was carried out and the corresponding porosity and pore size distribution results are gathered in Table 3-11 and Figure 3-39, respectively. The assessed average porosity value was  $27.89 \pm 1.80\%$  (95% confidence interval, CI). The measurements were therefore repeatable in most cases. The median pore diameter changed between 1000 and 2000 nm and the pore surface area was 2-5 m<sup>2</sup>/g. The variations in the measurements were attributed to the specimens preparation.

**Table 3-11.** Porosity ( $\epsilon$ ) of anode coating specimens from different cells from the same manufacturer that were similarly aged

	$\epsilon$ [%]	Specimen No.
Cell 1	26.25	1
Cell 2	28.15	2
	28.50	3
	27.05	4
Cell 3	29.55	5
Cell 4	28.24	6
	27.49	7

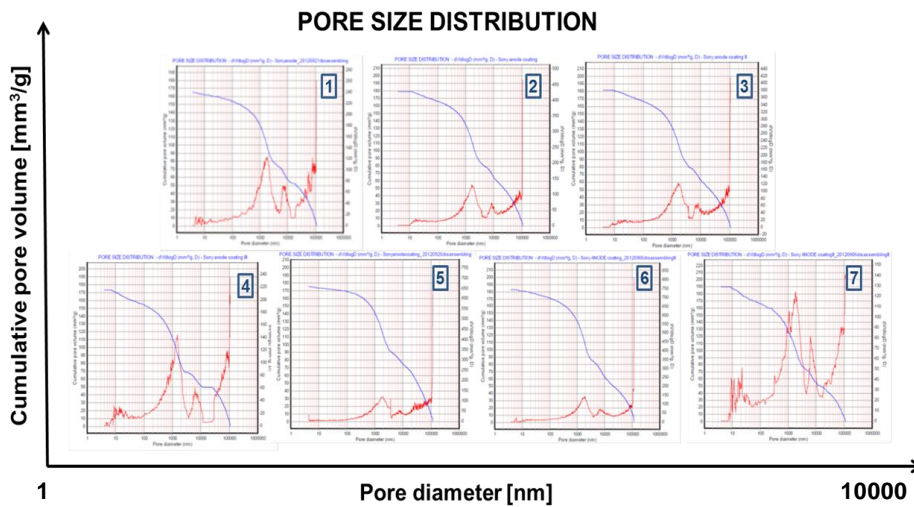


**Figure 3-39.** Pore size distribution of anode coating specimens (specimen numbers in the insets) from different similarly aged cells from the same manufacturer

### c) Coating vs. whole harvested electrodes measurement

To compare results, the same anode of a cell used for checking the repeatability of the measurements (Cell 4) was used for testing samples of the whole anode. The calculations provided by mercury porosimeter (Appendix C) must be corrected when full electrodes are measured, since the current collector is a non-porous solid material. The mass ( $m_{\text{sample}}$ ) and volume ( $V_{\text{sample}}$ ) of the sample must be then recalculated (taking away the mass and volume, respectively, of the current collector) for thereafter assess the final values of density and porosity (Appendix C).

Anode electrode main porous structure characteristics are gathered in Table 3-12, together with the corresponding corrected final porosity and density values, and Figure 3-40. As expected, the whole electrode porosity and apparent density values are lower than for only the coating, since when getting the coating sample the porous structure of the material was somehow modified. Nevertheless, the difference is not so large, *ca.* 4%, so it may be an acceptable error related mostly to the sampling procedure. The pore size distribution of the samples from whole electrodes is, however, uniform, which indicates that measuring just the coating does not provide reliable pore size results (sampling procedure modifies the structures under investigation).

**Table 3-12.** Harvested anode porous structure characterisation of specimens from different similarly aged cells from the same manufacturer

	Specimen No.	Measured			Corrected			
		$\epsilon$ [%]	$V_{\text{pores}}^{\text{[mm}^3]}$	$V_{\text{sample}}^{\text{[cm}^3]}$	$V_{\text{sample}}^{\text{[cm}^3]}$	$\epsilon$ [%]	$\rho^{\text{bulk}}^{\text{[g/cm}^3]}$	$\rho^{\text{apparent}}^{\text{[g/cm}^3]}$
Cell 4	8	20.83	0.027	0.130	0.117	23.18	1.334	1.737
	9	21.66	0.045	0.210	0.187	24.26	1.364	1.801

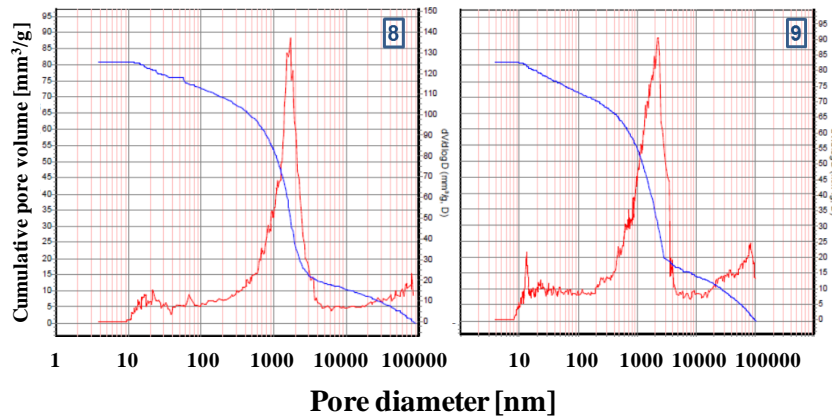


**Figure 3-40.** Harvested anode pore size distribution of specimens (specimen numbers in the inserts) from different similarly aged cells from the same manufacturer

**d) Quantity of sample optimisation**

The importance of the specimen size (mass and volume) for obtaining representative results was evaluated. The volume and mass of the sample to be measured ought to be between 0.4-1.5 cm<sup>3</sup> and 0.625-2.25 g, respectively, taking into account the following:

- 0.5 cm<sup>3</sup> is the maximum test filling volume.
- Eq. A-1 and Eq. A-2 (Appendix C). Using 25-90% of stem is the optimal for the analysis.
- Assumption: porosity of 30% and 1.5 g/cm<sup>3</sup> bulk density for green electrodes.

Optimal specimen size assessment tests were carried out using a 2 Ah HE NCM/C 18650-type cell. At the same time, cells manufacturing reproducibility and active materials homogeneity along the length of electrodes was evaluated. Anode pristine electrode samples of two fresh cells were evaluated using specimen sizes of 0.2-0.3 g (Cell 1), on the one hand, and 0.6-0.8 g (Cell 2), on the other. Table 3-13 shows a summary of the results. It is observed that the results are closer from 30% porosity expected for green electrodes when testing samples of 0.6-0.7 g. Porosity of 31.75±1.92% (95% CI) with 0.77% standard deviation ( $s_{n-1}$ ) was measured along the length of the negative electrode. Results from different specimens collected along the length of the electrode showed not only similar porosity but also similar pore size distribution, mainly

1000 nm diameter pores. This preliminary quantitative analysis hence indicates that anode porous structure is apparently homogeneous in the different exposure areas, considering a finite number of cells and samples.

**Table 3-13.** Anode porous structure characterisation of different specimens from a fresh 2 Ah HE NCM/C 18650-type cell

Specimen		$m_{\text{sample}}$ [g]	Measured $\epsilon$ [%]	$V_{\text{pores}}$ [mm <sup>3</sup> ]	Corrected $\epsilon$ [%]
Cell 1	Anode outer part	0.299	22.29	0.036	25.04
	Anode inner part	0.207	21.57	0.026	24.89
Cell 2	At 9 cm from the outset part	0.619	27.61	0.094	31.21
	At 30 cm from the outset part	0.759	27.44	0.111	31.41
	At 50 cm from the outset part	0.772	28.75	0.124	32.64

Once the procedure for porosimetry measurements was defined, the porous structures of different fresh cathode samples from 2 Ah HE NCM/C 18650-type cell were analysed. They showed  $25.32 \pm 2.06\%$  (95% CI) porosity, 1000 nm pore diameter and  $2.77 \pm 0.19 \text{ g/cm}^3$  (95% CI) bulk density.

### 3.3.2.2 ELEMENTAL ANALYSIS BY ICP-OES

ICP was used for multi-element analysis of metallic compounds of the positive electrodes (composition determination).

Samples submitted for ICP analysis must be fully prepared and should match the acidity of the calibration standards. A mismatch in the acidity can lead to a difference between the viscosities of the samples and the standards. The viscosity (and other factors) affects the nebulisation properties of a solution, which has a significant impact on the accuracy of the analysis. Samples digestion was carried out cutting *ca.* 0.2 g specimens in small pieces for their dissolution in aqua regia (1:3 HNO<sub>3</sub>: HCl. 3 ml HNO<sub>3</sub> (65%) and 9 ml HCl (37%)) by microwaving at 160°C and 300 W for 15 min in *CEM Mars 5 Microwave Accelerated Reaction System*. Different dilution factors were used for preparing the solutions, thus further reducing the matrix and reducing the interference effect whilst maintaining the analyte signals at instrument intensities above background resolution. This way, the prepared analytes had different emission sensitivity.

Different LFP and NCM commercial cathodes were measured aiming at defining the procedures for successful measurements, which comprise issues related to: calibration standards (differences in acceptance range of the solutions from 5 to 10 mg/L), dilution factors of the samples and blank measurement of a diluted acid matrix sample, etc. Element concentrations (in

ppm, *i.e.* mg/L) of trace metals from active materials, Li and Al (from current collector), as well as contaminants such as Cu (from the anode current collector), were analysed. For an overall study of metals concentration in the cell system and evaluating migration of cathode metals, it would be also interesting to examine aged anodes and contaminated electrolyte.

Table 3-14 summarises the ICP results of a cathode sample from a 2 Ah HE NCM/C 18650-type cell, as example. According to the assessed theoretical values for different NCM cathodes (Table A-2 in Appendix A), its composition may be NCM-111 ( $\text{LiNi}_{0.33}\text{Mn}_{0.33}\text{Co}_{0.33}\text{O}_2$ ) which elemental mass percentages are: 34.01% Ni, 31.84% Mn and 34.15% Co. The experimental deviations from the expected theoretical values due to measurements error or other external uncontrolled processes are still an issue, since it was not possible to find any correlation between measured and expected values regardless of the number of repetitions in each test of different similar tested specimens.

**Table 3-14.** Results of a commercial NCM/C 2 Ah 18650-type cell cathode composition measurement in the ICP

Average elemental concentration ( $s_{n-1}$ ) [mg/L]	NCM total [mg/L]	NCM elemental wt% [%]
Li	48840.24 (1165.61)	–
Co	150415.80 (267899)	37.22
Mn	120873.24 (2324.93)	29.91
Ni	132844.77 (2297.43)	32.87
Al	164319.21 (2738.67)	–

### 3.3.2.3 HARVESTED ELECTRODES PREPARATION FOR HALF-CELLS ELECTROCHEMICAL MEASUREMENTS

#### a) Coating: single/double sided electrodes

The coating on one side of the double-sided electrode laminate was removed before electrochemical measurements. All the process, coating-removal and half-cells assembly, was conducted in Ar-atmosphere glove-box to obtain reproducible data.

One side of the coating was dabbed with solvent gently (to minimise material damage) by rubbing with blotting paper. Dabbing was repeated until the coating peeled off the current collector. The most commonly used solvents for PVdF<sup>2</sup> (polyvinylidene fluoride polymer)

<sup>2</sup> There are manufacturers that use other binders: copolymer polyvinylidene fluoride-hexafluoropropylene (PVdF-HFP), aqueous base-SBR (Styrene Butadiene Rubber), polytetrafluoroethylene (Teflon<sup>TH</sup>), polytetrafluoroethylene (PTFE), potassium titanate and neoprene latex. The most typical ones are PVdF, PVdF-HFP and SBR. In some cases, PVdF is used for the cathode and SBR for the anode, the latter one not being so efficient as PVdF (no so sticky).

binder (the most common binder for electrodes) are dimethyl acetamide and NMP (N-Methylpyrrolidone/1-methyl-2-pyrrolidinone)<sup>3</sup>. NMP is a very powerful solvent and it was very effective for destroying the PVdF binder. However, it was aimed at looking for another alternative solvent because the NMP solvent is very harmful for the health. Using acetone worked out in some cases, but not at all times. It could be also checked whether the anode is an aqueous-based electrode (SBR, Styrene Butadiene Rubber, binder), trying to wash away the graphite coating using water. In that case, the use of hazardous NMP may be avoided.

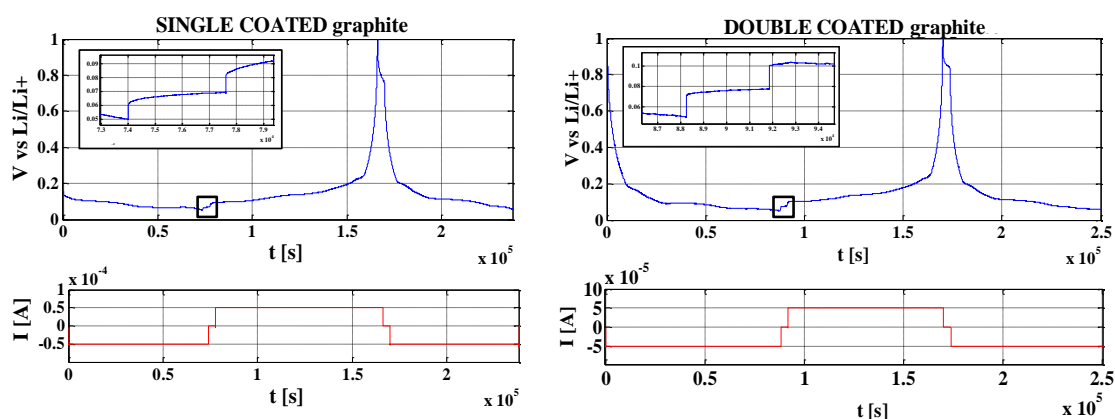


**Figure 3-41.** Half-cell measurements of single-coated and double-coated graphite samples harvested from a 18650 cell

Half-cell measurements with single- and double-sided electrode samples from the same harvested graphite electrode were carried out aiming at comparing both systems (*i.e.* single- and double-sided electrodes). Reference electrode half-cells were prepared using coin cell configuration. Coin cells (CR2024-type<sup>4</sup>) were assembled with 2.01 cm<sup>2</sup>-area (16 mm diameter) punched electrode samples (positive side in the coin cell), lithium-metal counter electrode of the same area (negative electrode), fresh Celgard® 2400 (polypropylene, PP, with 25 μm thickness) 18mm-diameter separator and 100 μL fresh electrolyte. For half-cell testing a BaSyTec Test system was used. The cycling profile of the experiments with single- and double-sided electrodes is shown in Figure 3-41. Double-sided graphite cell resistance was twice the valued of single-sided electrode cell one (insets in Figure 3-41). Double-sided electrodes showed significant voltage drop during discharge and charge due to large ohmic resistance. Electrochemical Impedance Spectroscopy (EIS) measurements would help further analysing the contribution of the double coating to cell resistance and the resulting performance.

<sup>3</sup> Besides, Dimethyl Formamide, Tetramethyl Urea, Dimethyl Sulfoxide and Triethyl Phosphate can be also used, but their solvency efficiency is very low at ambient. NMP has very good solvency properties and it is especially used in the field of polymers and resins.

<sup>4</sup> Cr2025 case with 20 mm diameter and 2.4 mm thickness.

**b) Washing electrodes**

The aim of rinsing harvested electrodes is removing organic layers formed on electrodes so that the source of electrode degradation can be evaluated. In case the original capacity of the harvested electrodes is restored, it means that capacity loss results from pore-clogging or isolation of particles by electronically insulating surface films, whereas the original structure remains unchanged.

The best way for washing electrodes was examined, as part of the procedures for cell harvested electrodes preparation and subsequent electrochemical characterisation. The rinsing solvent should be carefully chosen since electrode performance degradation is affected by the rinse solvent polarity according to D. P. Abraham *et al.* [58, 82]. They consider that dimethyl carbonate (DMC) is the best rinsing solvent. The result of washing depends mainly on the rinsing time, which is specially a tricky matter for carbonaceous anode materials covered by partially soluble layers (SEI layer. See Appendix A, section A.2.3.). In order to evaluate the efficiency of the rinsing process, electrode samples were washed using different methods and ICP was used as analytic technique. The defined procedure is depicted in Figure 3-42. Similar electrode specimens were washed using the same amount of DMC solvent in two different ways: (i) manual shaking and (ii) immersion for several hours. All washed (2,3), unwashed (1) and rinsing solvent (4,5) were analysed in the ICP in order to establish a comparison. The goodness of the measurements and the interpretation of the results are still an issue. Digestion process efficiency (proper dissolution of metals) and accuracy of the digest dilution may have, among others, affected significantly ICP results. Anyway, it can be clearly concluded that shaking procedure even for such a short times is more efficient than the immersion for prolonged times. However, the former is not a gentle technique, since the coating was scattered and damaged. Overall, immersion procedure seems to be more appropriate from the point of view of keeping the integrity of the harvested electrodes. It should be therefore repeated for different longer times to meet the optimal rinsing time. On the other hand, before the chemical analysis, the electrodes should be dried to remove the remaining solvent, preferably in vacuum conditions.

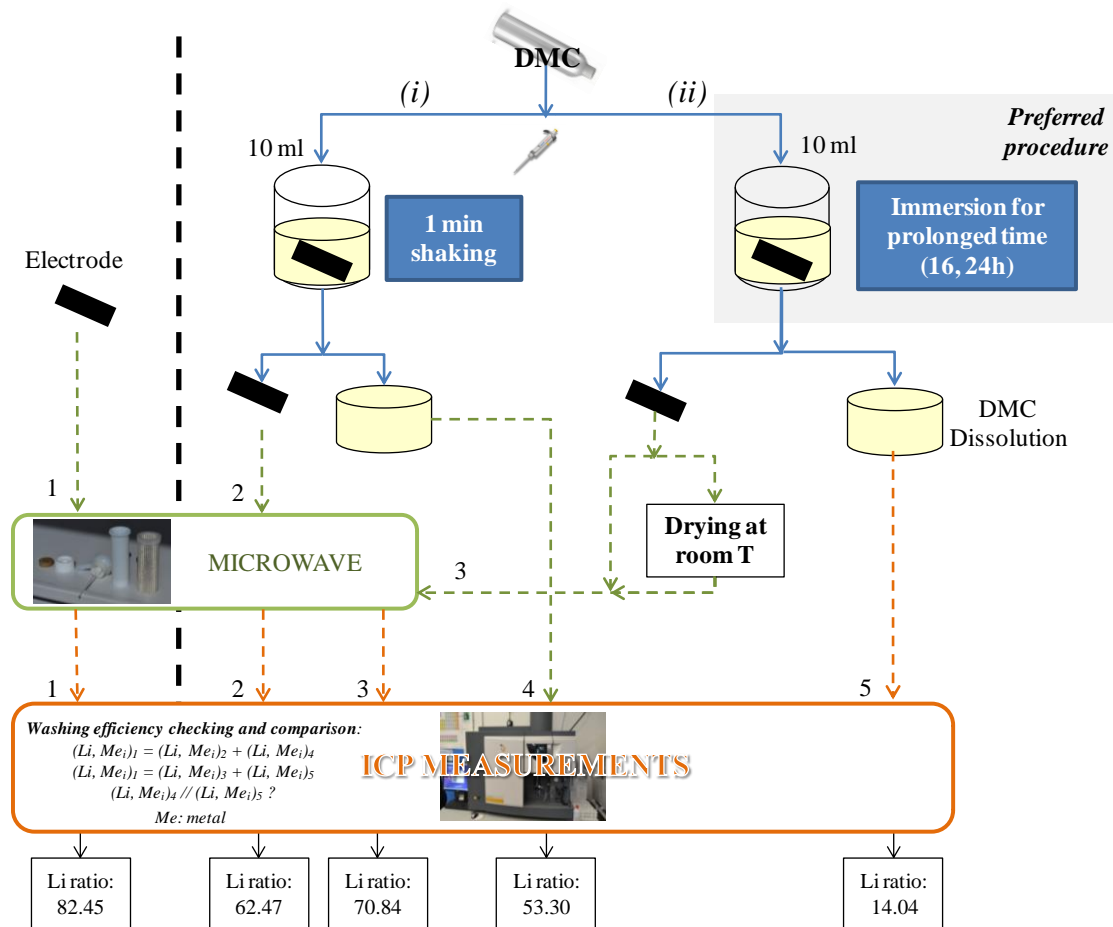


Figure 3-42. Defined procedure for checking the efficiency of rinsing the electrodes

Washing is beneficial but the details of the procedure need to be further defined. The rinsing efficiency could be also evaluated using other methods: (i) Raman spectroscopy to check the SEI layer evolution or (ii) half-cell measurements with washed (different rinsing times) harvested samples and no addition of electrolyte, but just using solvents, for the cell assembly. In this case, if the cell can be charged-discharged, there is ionic conductivity and it means that there is remaining electrolyte in the electrodes. On the other hand, the influence of drying the washed electrodes drying should be checked, both for the rinsing efficiency evaluation and for subsequent electrochemical measurements. Other solvents washing capability, such as dichloromethane or pentane, could be also tried.

### 3.3.3 SUMMARY OF LI-ION CELLS POST-MORTEM CHARACTERISATION METHODOLOGY

Overall process for Li-ion cells post-mortem analysis is shown in Figure 3-43. Aiming at understanding cell design and relative contributions of cell components to ageing, a

methodology for cylindrical cells disassembly was developed. Some analytical techniques were checked and procedures for samples preparation were defined for a comparative post-mortem diagnosis of Li-ion cells. Additional techniques are also proposed in Figure 3-43 for physical and structural characterisation, such as *X-ray Diffraction (XRD)* for grain size analysis and structure determination, *Raman Spectroscopy* for atomic level structural variations detection, *Laser microscope* for particle sizes analysis and *Scanning Electron Microscopy with Energy-Dispersive X-ray Spectroscopy (SEM-EDS)* for microstructure and quantitative chemical analysis.

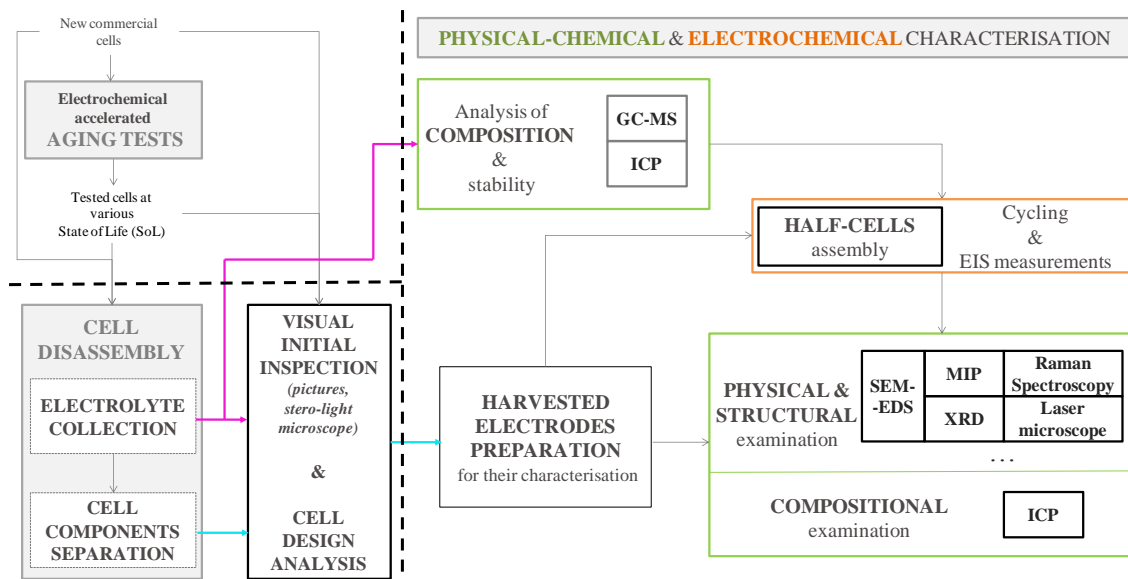


**Figure 3-43.** Lithium-ion cells characterisation methodology (GC-MS: Gas Chromatography with Mass Spectroscopy; ICP: Inductively Coupled Plasma; SEM-EDS: Scanning Electron Microscopy with Energy-Dispersive X-ray Spectroscopy; MIP: Mercury Intrusion Porosimetry; XRD: X-ray Diffraction)

### 3.4 SUMMARY AND CONCLUSIONS

#### 3.4.1 OVERVIEW OF THE METHODOLOGY FOR CELLS SELECTION

Developed cells selection methodology comprises steps between market research, application analysis, cells preselection and thorough evaluation, and the definition of the operating range and control strategies for the selected cell. Figure 3-44 and Figure 3-45 summarise in flow charts the Stage 1 (analysis of the application and available cells) and Stage 2 (screening of preselected cells), respectively. Figure 3-46 gathers the relationships between all the aspects to take into account for operating range and control strategies definition for the target application: cell performance, lifetime, safety, battery pack issues and costs. The implementation of Stages 1 and 2 of the methodology are described in *Chapter 4*. The definition of ageing and lifetime analysis and their implementation are fully reported in *Chapter 5*.

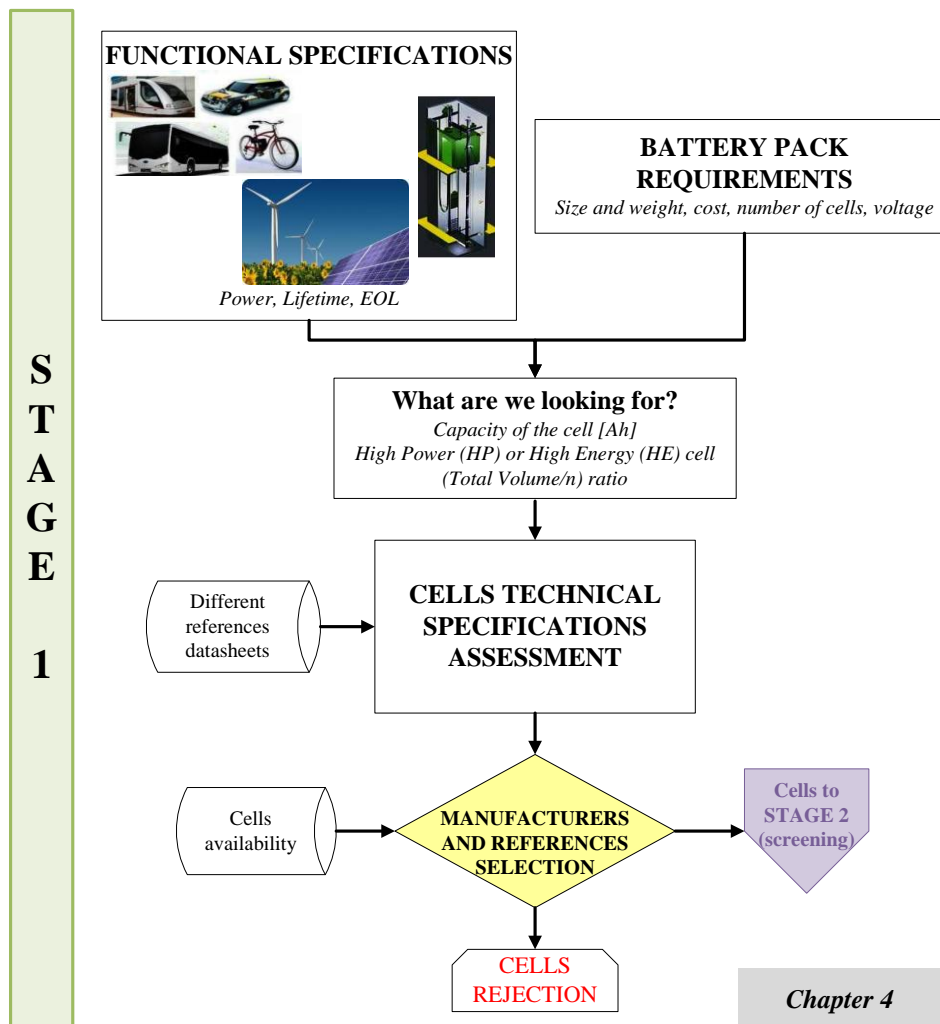


Figure 3-44. Main steps within Stage 1 (analysis of the application and available cells)

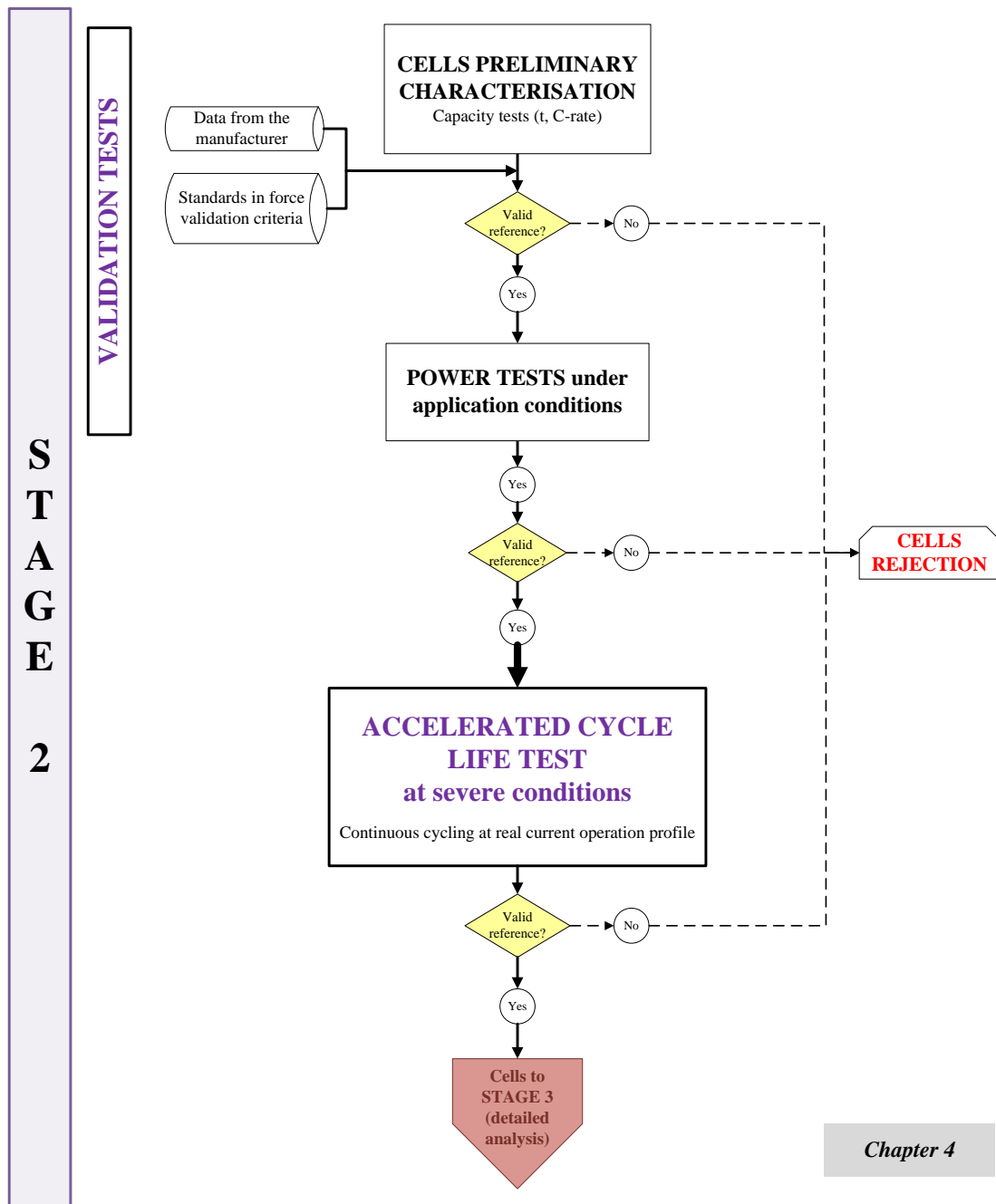
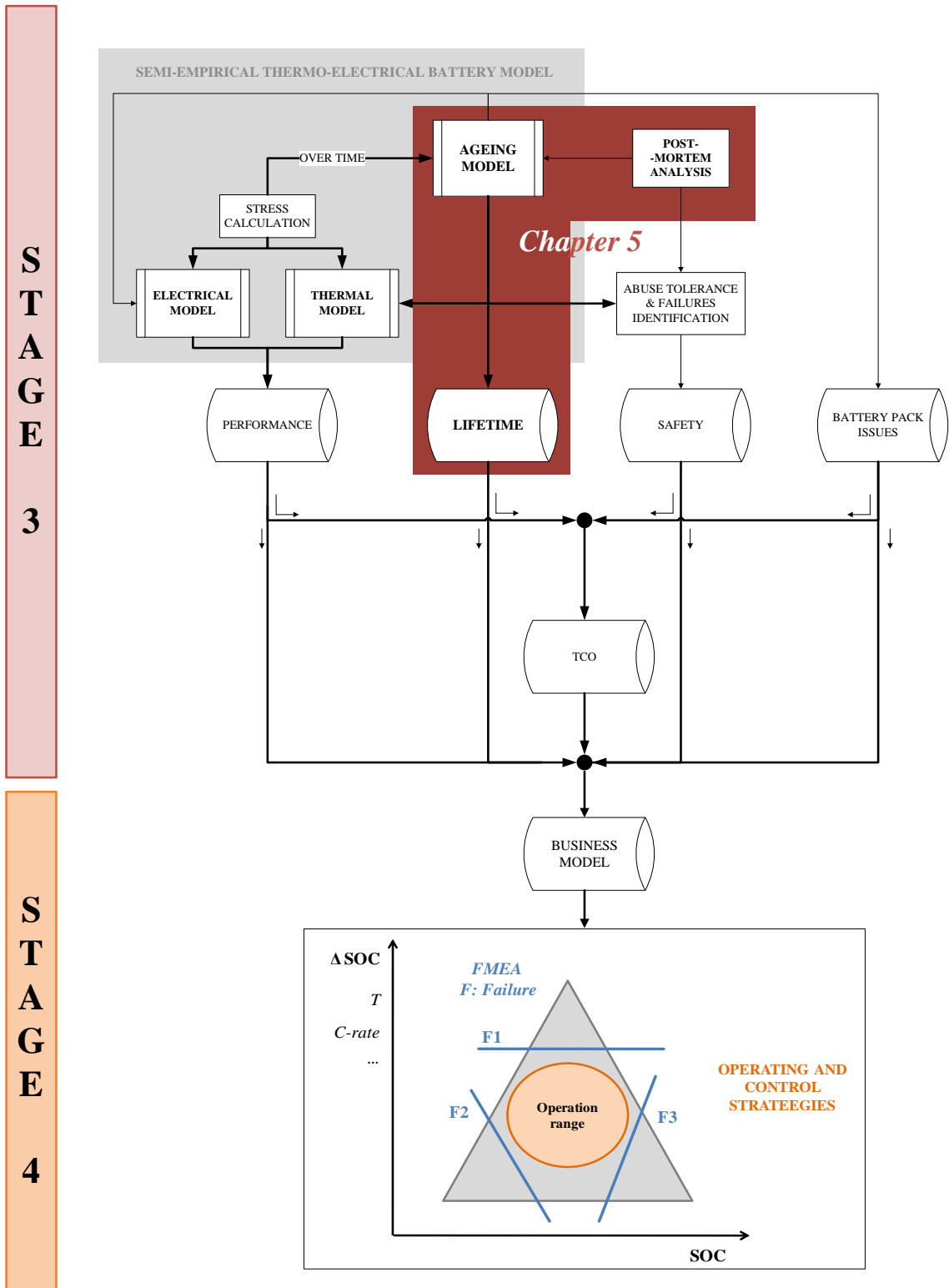


Figure 3-45. Main steps within Stage 2 (screening of preselected cells)



**Figure 3-46.** Interactions and relationships between performance (to meet application and installation requirements), costs safety and battery pack issues to consider for the selected cell operating range and control strategies definition

### 3.4.2 SUMMARY OF CHAPTER 3 AND VIEW OF THE REST OF THE THESIS WORK

The development of the preliminary Task and Tasks 1 to 3 described at the beginning of this chapter have been successfully accomplished. The overall view of these tasks in perspective with subsequent work is given in Figure 3-47.

Figure 3-47 illustrates qualitatively this Thesis work schedule and the dependency relationships between the main activities. The preliminary task, *i.e.* getting up-to-date information on different key issues, is to be kept over the entire research work. Cell selection methodology needs to be defined beforehand for a later specific applications research. Nevertheless, it might be learnt from the implementation, leading to a feedback to the previous task. Then, cell selection methodology could be improved iteratively. The here defined cell selection methodology is implemented and improved in *Chapter 4*, where the cell selection procedure for two different applications is assessed.

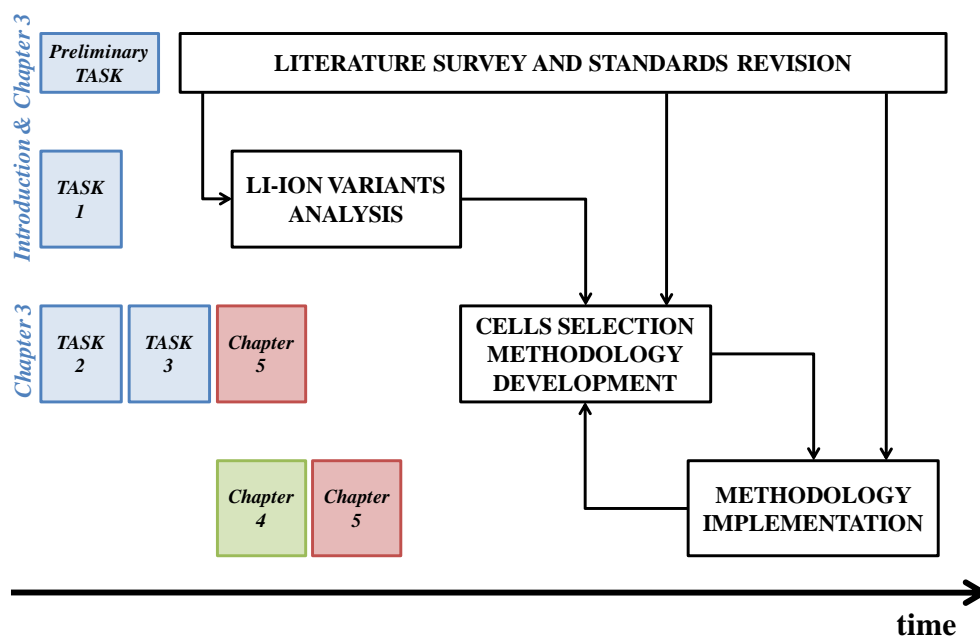


**Figure 3-47.** Flow chart and time scale for the main tasks needed for the development of cell selection methodology

# *Chapter 4*

## METHODOLOGY IMPLEMENTATION: CELL SELECTION FOR SPECIFIC APPLICATIONS

---

*The cell selection methodology defined in Chapter 3 is implemented in two separate applications: a residential elevator and a catenary-free tramway. After those case scenarios analysis, some improvements of the cell selection method are also proposed.*



#### 4. METHODOLOGY IMPLEMENTATION: CELL SELECTION FOR SPECIFIC APPLICATIONS

Transitioning to sustainable technologies, energy independence, operation efficiency increase, and cost and environmental saving goals require the integration of energy storage solutions. Several large format transport and stationary applications pursue integrating batteries with recharging capability and global market looks towards promising Li-ion technologies. There are many possible cell types and manufacturers, hence, aiming at a cost-effective trade-off solution, it is evident the need of implementing the developed cells selection methodology.

In this chapter, the cells preselection process for a residential elevation application is carried out in detail. Moreover, the developed methodology is validated with another case study: catenary-free tramway application.

In residential elevators, one common energy-saving eco-function is the reduction of standby power consumption (*e.g.* automatic illumination shutoff function). Still, the electrical usage can be reduced, saving for instance the braking energy. Figure 4-1 illustrates an elevator operation. If the elevator car travels loaded downward, the force of gravity causes the engine to generate energy (Figure 4-1 (a)). Similarly, when the elevator car travels empty or lightly loaded upstream, the counterweight goes down by gravity and the motor generates power (Figure 4-1 (b)). The energy generated by the elevator could be stored in an ESS (regenerative operation) and used during traction operation, and such energy exploitation would mean a considerable energy saving. It is pursued *ca.* 90% peak power grid demand reduction by means of the implementation of such an ESS.

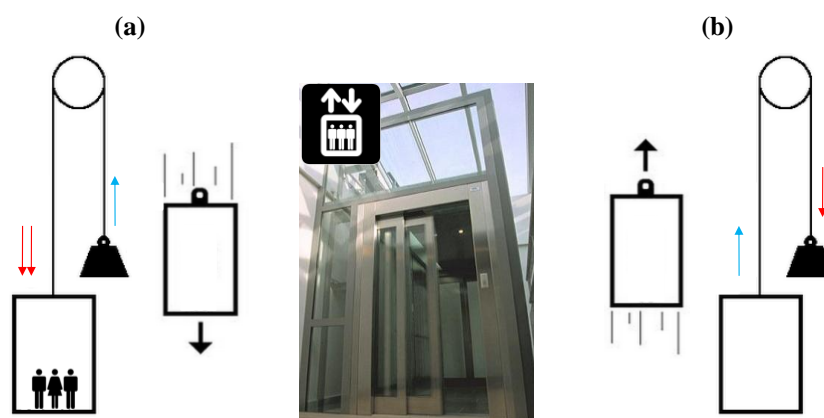


**Figure 4-1.** Elevator operation. (a) The car travels downward (b) The car travels upstream

In catenary-free trams, the on-board ESS stores the braking energy, allowing the tram to run without catenary between stops and, at the same time, as the braking energy is recovered, to save 20-30% of the energy. Freedrive operation of the tram is shown in Figure 4-2. Whilst the tram travels from one stop to another, the storage system powers the traction system. During the braking process, the kinetic energy produced is fully recycled to the storage system, which is recharged partially. When the tram stop, the storage system recharging process is completed.

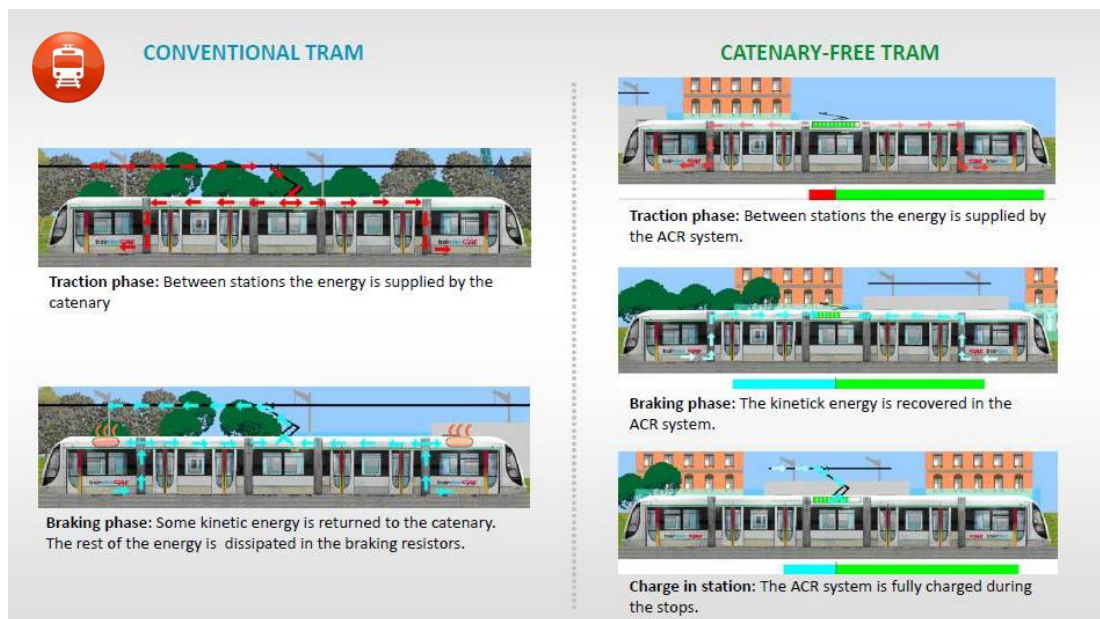


**Figure 4-2.** Comparison of conventional tram and catenary-free tram operation (ACR: rapid charge accumulator). (Source: CAF Power & Automotion)

## 4.1 RESIDENTIAL ELEVATION APPLICATION

### 4.1.1 STAGE 1: REQUIREMENTS OF THE APPLICATION AND EVALUATION OF AVAILABLE CELLS

#### 4.1.1.1 REQUIREMENTS OF THE APPLICATION

The goals of integrating a Li-ion rechargeable ESS into the target application are:

- i) System energy efficiency improvement by storing regenerative braking energy from the traction driving motor (energy generated by the elevator itself when it goes up with no passengers or goes down loaded). Electric energy consumption is, at the same time, reduced, as the stored energy is used in the system during traction operation.
- ii) Cost saving by reducing the energy consumption and power peaks demanded from the electricity grid.
- iii) Autonomous rescue functionality by providing stored energy to the system in case of power failure.

Figure 4-3 shows a Li-ion ESS (battery pack) designed for a residential elevator between IK4-Ikerlan and Orona.



**Figure 4-3.** Residential elevator Li-ion ESS solution developed between IK4-Ikerlan and Orona

#### - Functional specifications<sup>5</sup>

Typical traction and regenerative profiles (energy and power demands) for the residential elevation application are shown in Figure 4-4. The working operation of the elevator can

---

<sup>5</sup> Specific values are confidential information from the application provider.

change; regenerative braking may be repeated without any traction power demand or vice versa. The elevator requires high power for the start-up (short period, less than 2 s, of battery discharge) and it generates a high charging power peak (less than 2 s duration) when it stops (when it goes down loaded with users). The energy balance of the ESS operating under the profile shown in Figure 4-4 is negative. However, the energy stored in the system need to be sufficient for performing an autonomous rescue operation in case of power failure. It is therefore necessary to charge the battery pack from the grid when its stored energy is below the set threshold for meeting the application demands (this occasional charge is not shown in Figure 4-4). There is also a maximum SOC limit that cannot be overtaken and needs to be taken into consideration during the charge from the grid, since the amount of continuous regenerative brakes should not be limited either. There is a crowbar for overvoltage protection but the regenerative energy should be stored as much as possible.

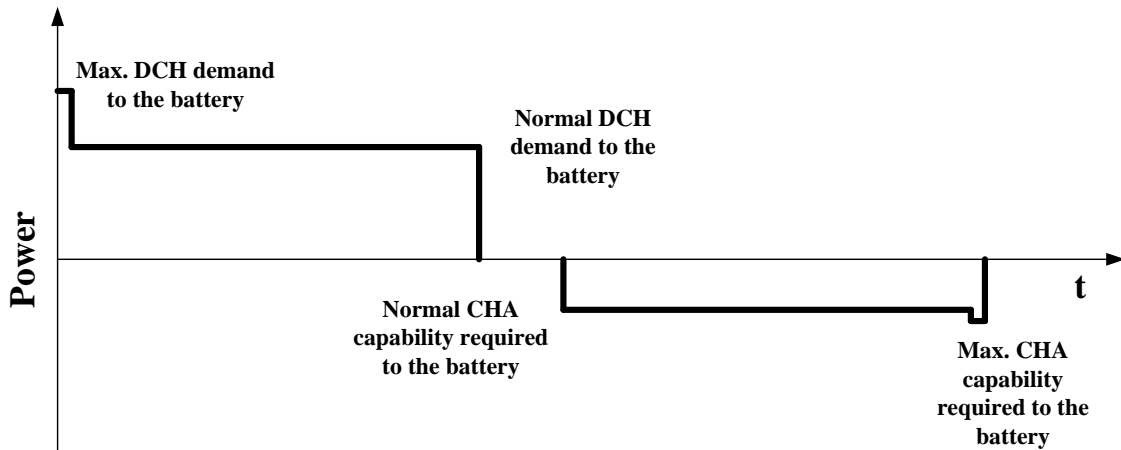


**Figure 4-4.** Traction and regenerative power profiles<sup>7</sup> for the residential elevation application

The lifetime requirements for the ESS are 10 years (calendar lifetime) and 150000 cycles (cycle lifetime).

- Installation conditions

Table 4-1 gathers the battery pack requirements for the residential elevator application.

**Table 4-1.** Residential elevation application installation conditions

<b>INSTALLATION CONDITIONS</b>	
Total voltage	< 300 V
Total energy	550 Wh
Battery pack maximum current handling	< 60 A
Size	15 cm (h) x 30 cm (w) The length is not limited
Temperature restrictions	(+5) – (+45) °C
Charger characteristics and requirements	2 kW single-phase system

The complexity and cost of the control and electronic systems to be used (*e.g.* the converter) are determined by the number of cells and, at a time, by the current handling requirements of the system. Besides, the maximum allowable current should not be larger than the specified in Table 4-1 in order to avoid excessive heating of the system and consequent energy loss of the battery and the converter. Anyway, if necessary, the battery pack will include a temperature conditioning system so as to limit the operating temperature of the cells and thus prevent their accelerated ageing and failure. The length of the battery pack is not restricted, as it will not be located within the elevator but in the elevator shaft.

Figure 4-5 shows in a block diagram a single-phase residential elevator motor, electronics and electricity management system with a Li-ion storage system.

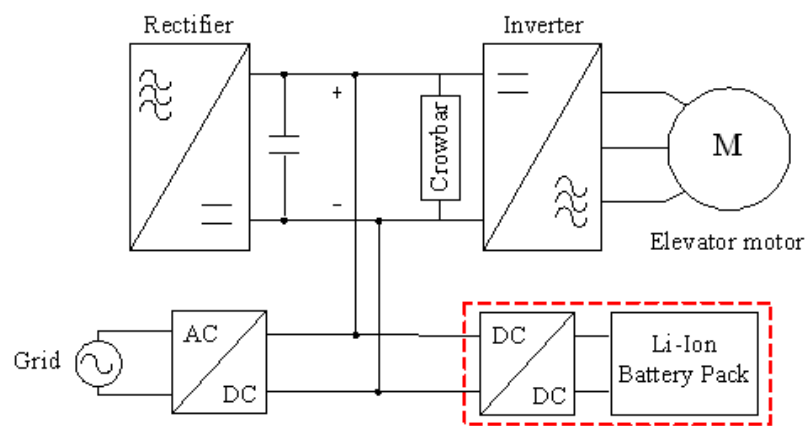


*Figure 4-5. Block diagram of a single-phase residential elevator with a Li-ion ESS*

#### 4.1.1.2 EVALUATION OF AVAILABLE CELLS AND DEFINITION OF THE OPTIMUM OPERATION RANGE

The appropriate cell type was defined taking into account various parameters (related to the battery pack): the number of cells, voltage and maximum current handling restriction. The nominal voltage is an intrinsic property of the cell, which is typically between 3 and 3.8 V. In contrast, the cell capacity is defined by the maximum allowable number of cells in the battery pack and its current handling restriction (60 A), which forces the minimum number of cells to be thirty.

Starting with the optimum operating range prerequisites and a given battery pack design, the ideal cell basic characteristics and operating current loads shown in Table 4-2 were obtained following the procedure from Figure 3-18 (a).

**Table 4-2.** Most important electric parameters of appropriate cell for the residential elevator application

IDEAL CELL		
CHARACTERISTICS	Nominal voltage	3 - 3.8 V
	Nominal capacity	1.5 – 4.5 Ah
OPERATING RANGE	Normal discharge current	minimum 7.3 C
	Maximum discharge current	minimum 10.9 C
	Normal charge current	minimum 3.6 C
	Maximum charge current	minimum 4.5 C

Procedure defined in Figure 3-18 (b) was followed to purchase cells and battery pack sizing:

- *Appropriate manufacturers and cells identification*

Going through the cells database (Appendix D), more than thirty Li-ion secondary cell manufacturers were identified as potential suppliers, after analysing the electrical characteristics of their products and other aspects such as cells production experience and the applications they work on. Table 4-3 shows, as example, the first evaluation of some commercial cells, for which the defined ideal cell electric parameters were taken into account (Table 4-2). Mnf 2, Mnf 3, Mnf 5, Mnf 6, Mnf 8 and Mnf 10 were rejected because of their low charge current handling capability (the application demands up to 4.5C charging rate at cell level) and this was the case for most of the cells available in the market (*i.e.* the severe application charging requirements were the limiting factor in cells search). Note that even though Mnf 7 was not able to meet the maximum charging current demand, this could however be easily sorted out by oversizing slightly the battery pack.

**Table 4-3.** Example of Li-ion cells market analysis. Evaluation of functional energy and power specifications fulfilment

<i>Electric parameters</i>	<b>Mnf 1</b>	<b>Mnf 2</b>	<b>Mnf 3</b>	<b>Mnf 4</b>	<b>Mnf 5</b>
Nominal capacity [Ah]	2.2	2.6	2.3	1.05	3
Normal DCH C-rate	10.0	3.8	10	10.0	10.0
Max. DCH C-rate	68.2	19.2	30	15.0	20.0
Normal CHA C-rate	5.0	1.0	4	5.0	1.0
Max. CHA C-rate	5.0	1.9	4	5.0	1.0
	<b>Mnf 6</b>	<b>Mnf 7</b>	<b>Mnf 8</b>	<b>Mnf 9</b>	<b>Mnf 10</b>
Nominal capacity [Ah]	4.4	2.3	2.9	1.4	3.2
Normal DCH C-rate	37.73	30.4	34.5	14.29	20
Max. DCH C-rate	37.73	52.2	34.5	14.29	40
Normal CHA C-rate	30.91	4.3	2.55	4.64	2
Max. CHA C-rate	30.91	4.3	2.55	4.64	2

NOTE. Colour code means:

MEETS THE APPLICATION DEMANDS	DOES NOT MEET THE APPLICATION DEMANDS
-------------------------------	---------------------------------------

The next step consisted of contacting the identified suppliers to get further information regarding the viable cells: detailed technical information (datasheets), costs, delivery service and so on. However, some suppliers did not reply whereas others did not provide the expected

information. In some cases, cells retail was not facilitated, and that caused a serious narrow down of choices.

*- References validation*

The preliminary evaluation was carried out taking into consideration:

- i) Intrinsic properties and performance characteristics of the cells and the application functional specifications to be fulfilled.
- ii) Manufacturers quality and safety aspects (certificates), the information they provide and suppliers delivery service.
- iii) Initial cost of the cell.

For instance, Mnf 6 and Mnf 9 were decided to be rejected because of high initial cell cost of the former and low cycle life of the latter. However, even though Mnf 4 nominal capacity was lower than the calculated one for the ideal cell, which entails a larger battery pack, it was not rejected due to its good performance characteristics according to the datasheet and low initial cell cost. Other suitable cells could not be purchased due to delivery service limitations. Overall, the available Li-ion cells for the studied application were three LFP-based cylindrical LIBs. Their characteristics are gathered in Table 4-4.

**Table 4-4.** Summary of the most representative characteristics of the purchased cells for the residential elevator application evaluation (data from manufacturers)

		CHARACTERISTIC	UNIT	Ref 1	Ref 2	Ref 3
<b>INTRINSIC PROPERTIES</b>		Chemical composition of the cathode	—	LFP	LFP	LFP
		Geometry	—	Cylindrical	Cylindrical	Cylindrical
		Internal resistance	<b>mΩ</b>	8	< 27	8
		Weight	<b>kg</b>	0.078	0.04	0.07
		Dimensions	<b>mm<sup>3</sup></b>	Ø 26.8 mm h: 66.2 mm	Ø 18.3 mm h: 65.3 mm	Ø 25.85 mm h: 65.15 mm
<b>PERFORMANCE CHARACTERISTICS</b>	<b>NOMINAL CHARACTERISTICS</b>	Nominal capacity	<b>Ah</b>	2.2	1.05	2.3
		Nominal CHA & DCH conditions	<b>h<sup>-1</sup></b>	1C CHA 1C DCH	1C CHA 2C DCH	1C CHA 1C DCH
		Nominal voltage	<b>V</b>	3.2	3.2	3.3
		Energy density	<b>Wh/kg</b>	90.3	85	108.43
	<b>CHA CONDITIONS</b>	CHA cut-off voltage	<b>V</b>	3.6	3.65	3.6
		Maximum CHA current	<b>A</b>	11 (5C)	5.25 (5C)	10 (4.3C)
		CHA temperature range	<b>°C</b>	(0)-(+ 45)	(0)- (+ 45)	(- 30) - (+ 60)
	<b>DCH CONDITIONS</b>	DCH cut-off voltage	<b>V</b>	2	1.8	2
		Maximum DCH current	<b>A</b>	22 (10C)	15.75 (15C)	70 (30.4C)
		Maximum DCH current pulse	<b>A</b>	150 (68.2C)	40 (38C, 10 s)	120 (52.2C, 10 s)
		DCH temperature range	<b>°C</b>	(- 20)-(+ 60)	(- 20)-(+ 60)	(- 30)-(+ 60)
	<b>LIFETIME</b>	Cycle life	<b>N</b>	2000 (1C, 80% DOD)	1500 (10C, 100%DOD)	1000 (10C, 100%DOD)

*- Battery pack configuration analysis and sizing*

During this work, a simulation program for battery pack sizing was developed using MATLAB-Simulink software. It combines:

- i) voltage*
- ii) number of cells*
- iii) power and energy requirements of the application*

This program, which is depicted using a black box in Figure 4-6, was validated for different applications and thereafter used for the studied regenerative application.

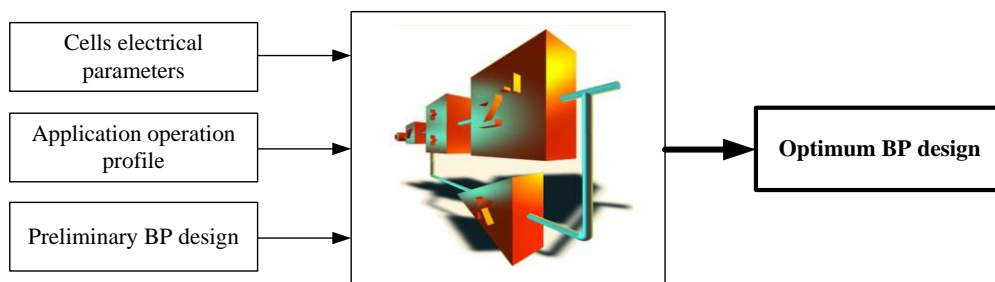


**Figure 4-6.** Block diagram of battery pack (BP) configuration simulation program showing the inputs and output

The best final battery pack configuration (number of cells in series/parallel connection) using each of the reference cells are shown in Table 4-5. Moreover, references operating current loads were assessed in order to plan tests in Stage 2.

**Table 4-5.** Battery pack (BP) sizing for the different types of cells under investigation

	<b>BATTERY PACK (BP) CONFIGURATIONS</b>		
	using <b>Ref 1</b> cells	using <b>Ref 2</b> cells	using <b>Ref 3</b> cells
Total Voltage	268.8 V	275 V	277.2 V
Total Energy	591.36 Wh	550 Wh	637.56 Wh
Total number of cells	84	172	84
Connection	$_{84}S$	$_{86}S_{2P}$	$_{84}S$
Total weight of cells	6.55 kg	6.88 kg	6.38 kg

Table 4-5 shows that the three configurations are similar except for the number of cells and their connections. Ref 2 cells have a capacity *ca.* 45% lower than the others and, therefore, require double number of cells to reach similar specifications. The total voltage of the battery pack could not be larger than 300 V, so two components with 86 cells in each of them ought to be connected in parallel. Consequently, the battery pack initial investment cost would be considerably increased and the safety level would be reduced. It is not recommended to use parallel connections excessively since the system tries to equalise every cell voltage: the cells with larger either voltage or internal resistance are less charged and, when the battery pack is

not working, a current flow that is directly related to the voltage difference, and is inversely proportional to the total internal resistance, is produced. For this reason, in case a cell is overdischarged or is at 0 V (faulty cell), the cell that is connected in parallel to it might be short-circuited.

Overall, Stage 1 allowed a critical and systematic analysis of both the application and LIBs market, obtaining, relatively fast, 3 reference cells that were initially valid for the target application. In addition, the battery pack was sized for each cell using a mathematical program that was developed within this work. This tool will also be extensive for other applications and assessed in traction application as a second case scenario.

#### 4.1.2 STAGE 2: SCREENING

##### 4.1.2.1 TESTING CONDITIONS

Table 4-6 shows the conditions for cells screening tests defined in *Chapter 3* (section 3.2). The experimental procedures are described in *Chapter 2*. The profiles used for screening tests are shown in Figure 4-7.

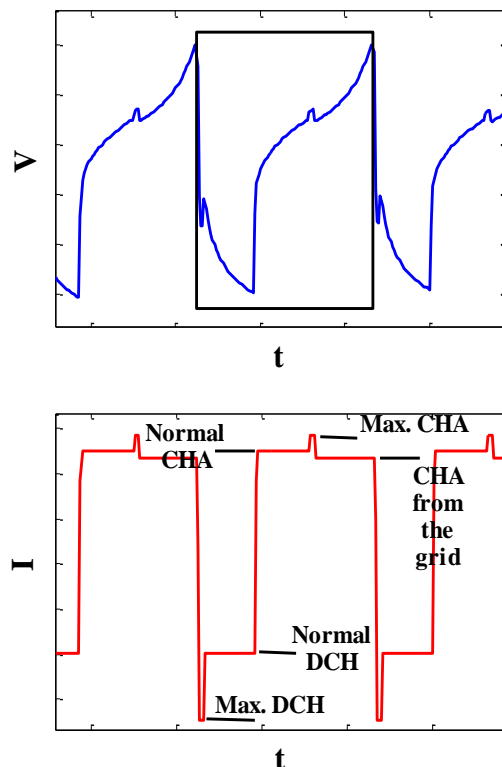


**Figure 4-7.** Elevator operation charge sustaining profile continuously repeated upon accelerated cycling test. Box in the voltage profile indicates the repetition unit

**Table 4-6.** Definition of the tests conditions in Stage 2 of cells selection methodology for the pursued residential elevator application

TEST		TESTING CONDITIONS				VALIDATION CRITERIA													
<b>VALIDATION TESTS</b>	<b>CELLS PRELIMINARY CHARACTERISATION</b>	<b>NOMINAL CAPACITY</b>	Table 4-4 shows the C-rates used by the manufacturer for nominal capacity assessment.				Nominal capacity value specified by the manufacturer (Table 4-4). It should be larger than the value specified as minimum.												
		<b>RATE CAPABILITY</b>	<ul style="list-style-type: none"> <li>Nominal T [°C]: 25 ± 2.</li> <li>Other operating temperatures [°C]: T<sub>1</sub> = 5, T<sub>2</sub> = 25 and T<sub>3</sub> = 45.</li> <li>C-rates: <table border="1" style="margin-left: 20px;"> <thead> <tr> <th colspan="2">Normal</th> <th colspan="2">Maximum</th> </tr> <tr> <th>CHA</th> <th>DCH</th> <th>CHA</th> <th>DCH</th> </tr> </thead> <tbody> <tr> <td>3-4C</td> <td>7-8C</td> <td>4-5C</td> <td>9-11C</td> </tr> </tbody> </table> </li> </ul>				Normal		Maximum		CHA	DCH	CHA	DCH	3-4C	7-8C	4-5C	9-11C	<ul style="list-style-type: none"> <li>Standards in force [EN 61960:2011]</li> <li>Safety boundary conditions of the cell.</li> </ul>
		Normal		Maximum															
		CHA	DCH	CHA	DCH														
	3-4C	7-8C	4-5C	9-11C															
<b>DC INTERNAL RESISTANCE MEASUREMENT</b>	<ul style="list-style-type: none"> <li>SOC [%]: SOC<sub>1</sub> = 25, SOC<sub>2</sub> = 50 and SOC<sub>3</sub> = 75.</li> <li>10C DCH and 1C CHA pulses (so that it is possible to use the same C-rate for all the cells) with duration of 17s.</li> <li>Operating temperatures [°C]: T<sub>1</sub> = 5, T<sub>2</sub> = 25 and T<sub>3</sub> = 45.</li> </ul>				Power capability against the power required by the application.														
<b>POWER TESTS UNDER APPLICATION CONDITIONS</b>	<ul style="list-style-type: none"> <li>Operating temperatures [°C]: 5 and 25.</li> <li>Application power profile (DCH &amp; CHA) schemed in Figure 4-4.</li> </ul>				Comparison of operating SOC ranges of the different references.														
<b>ACCELERATED CYCLE LIFE TEST AT SEVERE OPERATING CONDITIONS</b>		<ul style="list-style-type: none"> <li>Ageing testing procedure described in <i>Chapter 2</i>, Figure 2-11.</li> <li>Testing profile: continuous cycling under application operation profile (Figure 4-4) including charge from the grid, as shown in Figure 4-7. 5% DOD, 5.5C mean C-rate, 97.5% middle cycling SOC and 35 ± 5°C.</li> <li>EPIT: nominal capacity test and HPPC test every 5000 cycles. Occasional EIS measurements. HPPC test conditions: 10C DCH and 5C CHA pulses of 5s of duration, with 5s pause between pulses, at 50 and 75% SOC.</li> <li>BOL and EOL detailed characterisation include: <ul style="list-style-type: none"> <li>EIS at 75% SOC</li> <li>Calorimetric measurement testing the operating DCH current profile (Figure 4-7) 10 times, with 10s rest period after each cycle. Initial SOC: 75%.</li> </ul> </li> </ul>				EOL was defined according to the application functional specifications to be fulfilled: <ol style="list-style-type: none"> <li><b>Power and energy:</b> <ul style="list-style-type: none"> <li>Maximum DCH power and energy requirements at 50% SOC.</li> <li>Both safety energy margin and energy for traction operation must be guaranteed. Assuming that it is possible to fully CHA the cells, when cells Q<sub>loss</sub> is ca. 55%, the EOL would be reached.</li> </ul> </li> <li><b>Lifetime:</b> 150000 cycles (N), which corresponds with ±8000 FEC.</li> </ol>													

### 4.1.2.2 RESULTS AND DISCUSSION

#### a) VALIDATION TESTS

##### a.1) TESTS FOR CELLS PRELIMINARY CHARACTERISATION

- **Nominal capacity tests**

Nominal capacity tests were run using as many specimens of each reference as possible. Figure 4-8 and Figure 4-9 show some of the discharge capacity and energy efficiency results, respectively, of at least 5 specimens of each reference [30], with the corresponding statistical analyses carried out using Minitab software. These figures also show 95% reliability Confidence Intervals (CI) of both each specimen (in Figure 4-8, considering the capacity of each cycle) and the reference itself, which are plotted in grey and with dotted lines, respectively, together with the overall mean values in continuous lines.

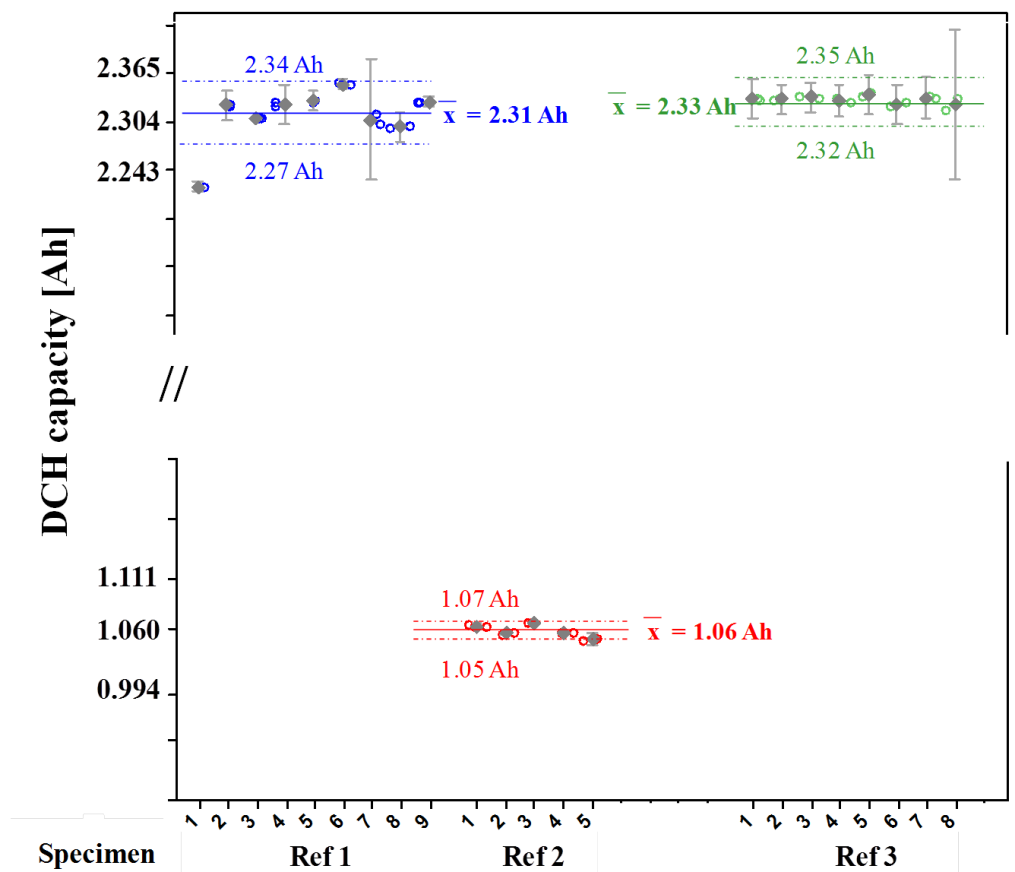


**Figure 4-8.** Nominal capacity variation between cells of the same reference. Experimental results of Ref 1, Ref 2 and Ref 3 in blue, red and green open circuits, respectively. Mean value (continuous lines) and 95% Confidence Interval (CI) (dotted lines) of each reference indicated using the same colour. 95% CI of each specimen in grey

Regarding energy efficiency, Ref 3 showed superior performance, although in all cases it was larger than 90%. The energy efficiencies for some specimens in some of the discharge cycles

were below the calculated lower confidence levels. Nevertheless, this was not a criterion for rejecting the cells, since they were still able to meet the pursued nominal characteristics.

Thermal performance in nominal conditions was acceptable in all cases. The surface of the studied specimens was barely heated up ( $\Delta T < 1^\circ\text{C}$ ) during charging, and the temperature difference was lower than  $3.5^\circ\text{C}$  when discharging.

The dispersion among different specimens of the same reference was also evaluated. Ref 1 showed the largest dispersion with respect to the assessed mean capacity and energy values. Nonetheless, the different measured data were randomly distributed and not grouped.

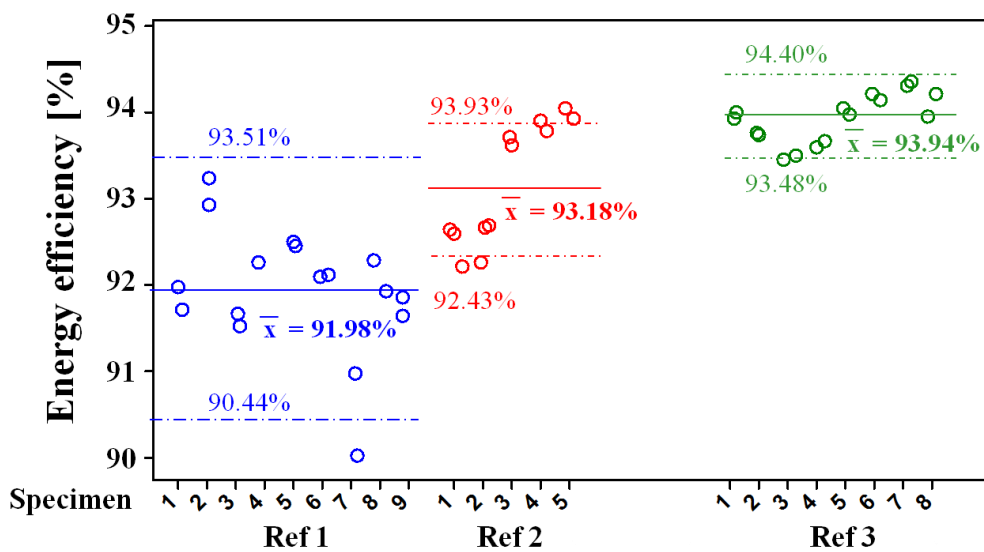


**Figure 4-9.** Energy efficiency of the references at nominal operating conditions. Experimental results of Ref 1, Ref 2 and Ref 3 in blue, red and green open circuits, respectively. Mean value (continuous lines) and 95% CI (dotted lines) of each reference indicated using the same colour

- **Rate capability tests**

Rate capability tests were carried out at constant current so that operating capacity at different application conditions could be assessed. It should be noted that the cells are discharged at constant power conditions in the real application. Therefore, the testing C-rates are rough values, as they were calculated using the cells nominal voltages. Thus, the results are just for guidance and useful for analysing the different references performance.

Electrical performance. Figure 4-10 shows a comparison of charge and discharge characteristics under both application normal and maximum demanding current loads operating conditions and at different temperatures.

- *Operating capacity*

At normal current loads defined for the elevation application, it was possible to withdraw almost the 100% of the Ampere-hours stored in Ref 2 and Ref 3 type cells. The coulombic efficiency of Ref 1 was lower unless the ambient temperature was high. At 5°C, Ref 1 was not able to provide more than the 90% of its stored capacity.

At maximum current load operating conditions, the coulombic efficiencies of the three references were similar to those obtained with lower current rates, except for when they were discharged at 45°C. At this ambient temperature, the discharged capacity reduced in *ca.* 10 and 15% for Ref 2 and Ref 3, respectively. In these cases, as it is to be explained later on (Figure 4-11), the limiting factor was cell temperature, which rose up to the maximum established for safe operation (the cut-off voltage was not reached when the discharge processes were stopped). Thus, had the cells temperature increase been controlled, the cells would have been fully discharged.

Consequently, a temperature conditioning system would be necessary in all cases: (i) To rise ambient temperature during especially night- and winter-time in systems that would use Ref 1. But also, (ii) to limit cells overheating when operating at high ambient temperatures such as 45°C in systems that would use either Ref 2 or Ref 3.

- *Energy efficiency*

Overall, the lowest energy efficiency values correspond to Ref 1. Ref 2 is the best tested technology for meeting the energy demands of the elevation application at low temperatures.

- *CC mode charging*

The operating temperature has a significant influence on cell charging. The lower the temperature, the less Ampere-hours can accept the battery. Hence, ambient temperature rising would optimise every cell charging performance. This is even a more prominent feature at higher C-rates, as it was especially noticed when Ref 1 and Ref 3 were tested. In any case, Ref 1 showed the worst charging capability.

The charging performance is what made the different tested cells types more distinctive between each other. In all cases, it was the limiting factor for meeting the application high current rates regenerative demands.

All these observations indicate that operating at low temperature had a great effect on cells performance. At 5°C, Ref 1 showed the worst performance, hardly being able to charge braking energy. On the contrary, Ref 3 behaved very well and Ref 2 performance was also acceptable.

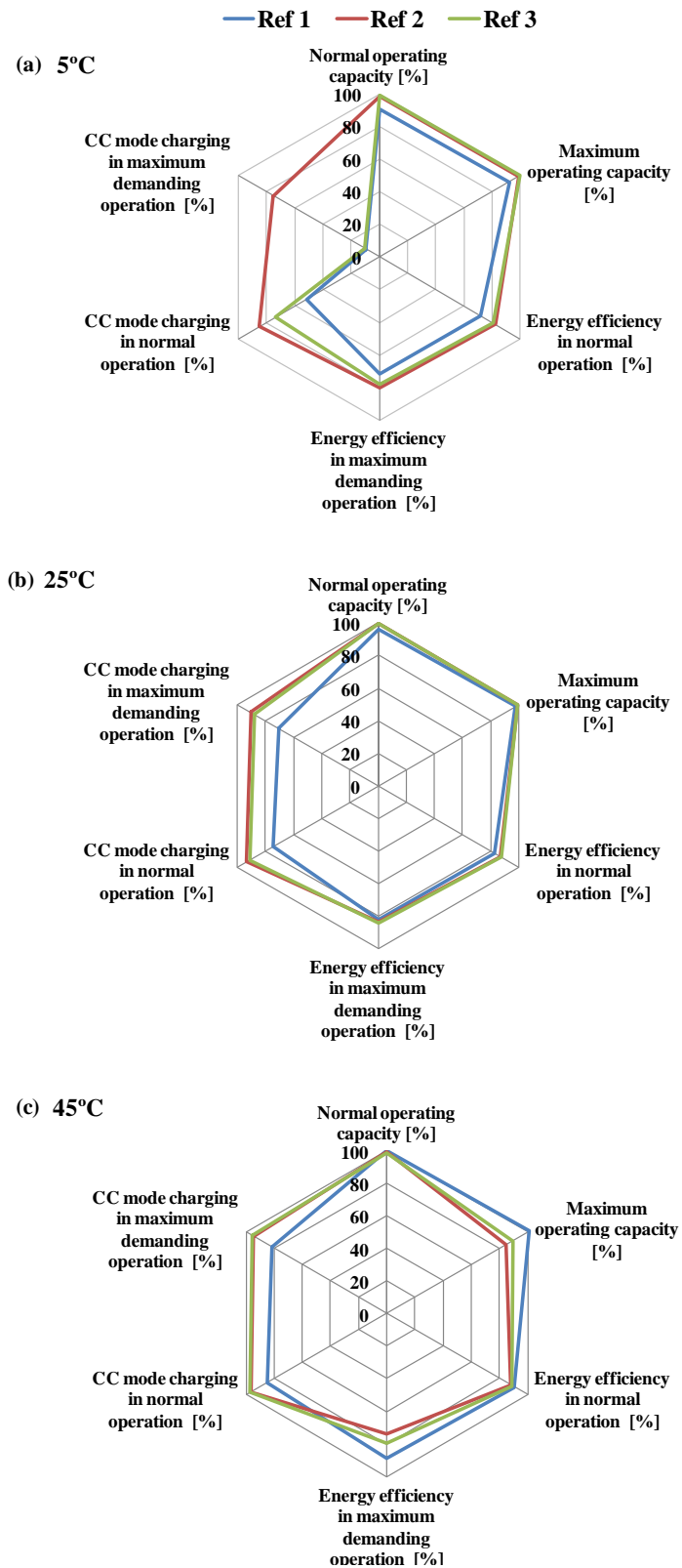


Figure 4-10. Most relevant electrical performance results from rate capability tests at: (a) 5°C, (b) 25°C and (c) 45°C

Thermal performance. Figure 4-11 shows the different cell surface heating at the studied application conditions (cells surface temperature was recorded continuously by Type K

thermocouples, which were placed in the centre of the length of cylindrical cells<sup>6</sup>). When discharging cells at application maximum demanding current loads and 45°C, Ref 2 and Ref 3 reached the maximum discharge temperature defined by the manufacturer (60°C). The discharge process was therefore stopped (safety reasons), which made the energy efficiency to be lower. When cells charging, however, the drawbacks are enhanced at lower temperatures: cells surface temperature increase was larger at 5°C, although it was similar to those when cells charging at 25 and 45°C. In general:

- *The temperature increase was much lower during charge than during discharge.* This is not related to lower operating C-rates during charge, but to lower charging times related to larger internal resistances during charge. Even though the higher the internal resistance, the larger the temperature increase (thermal power:  $P = IR \cdot I^2$ ), higher internal resistance also makes the cells to reach the maximum voltage faster (were the charging period larger, the cells heating up would be larger).
- *During discharge, the temperature increase was lower in all cases as the working ambient temperature increased.* The differences are very low because in all cases almost equal Ampere-hours were discharged (equal working times). However, the higher the temperature, the lower the internal resistance.
- *During charge, the temperature increase was almost constant under normal operation conditions regardless of working ambient temperature.* At low temperature, the charge internal resistance may be very large for Ref 1 and Ref 2, which may have reduced significantly the operating time and the cell heating up was therefore lower. The longer charging time of Ref 3 may be related to lower internal resistance, which may have also made its temperature increase to be similar to the other references.

Overall, Ref 3 showed the largest surface temperature increase both during charging and discharging at different conditions, which may be related to longer operating times and therefore indicates that its internal resistance may be lower.

---

<sup>6</sup> It was considered that the surface temperature was even, although the heat generation in the core of the cell is not homogeneous and its distribution is normally radial, from the inner to the outer part of the jelly-roll. However, this temperature change could not be measured, and the Type K thermocouple was placed in the centre of the length of the cylinder, as the cell heating up is normally localised in the centre of the cell and, this way, the maximum surface temperature may be measured.

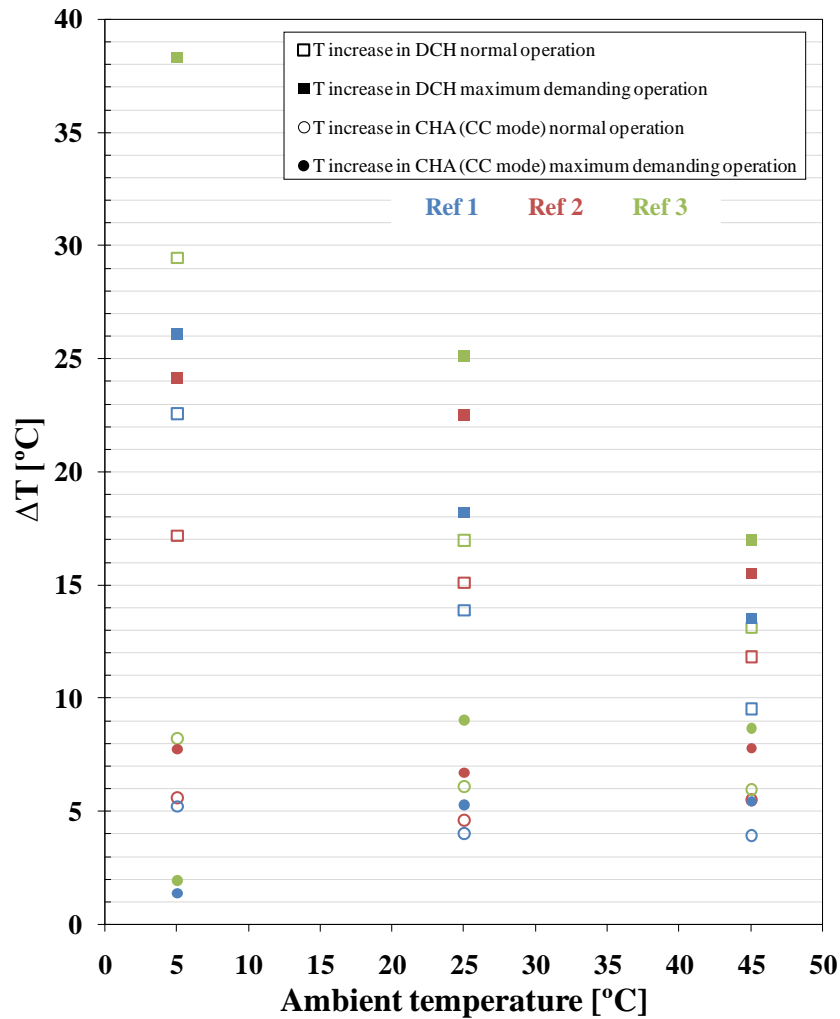
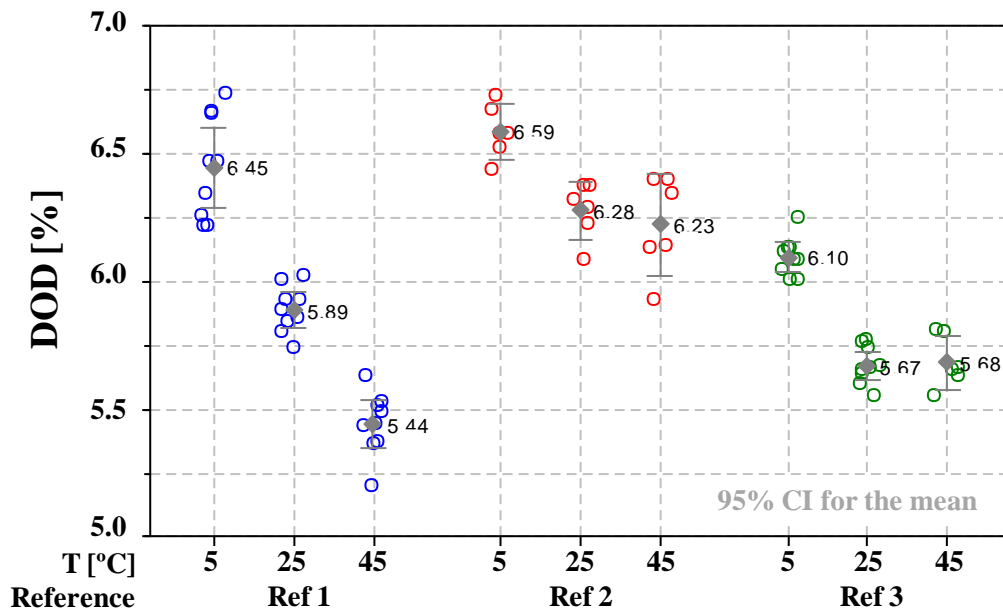


Figure 4-11. Cell total surface heating after full discharges and charges in CC mode at different operating C-rates and ambient temperature

Lastly, the cells were examined taking into account the demands of the application. Thus, Depth of Discharge (DOD) was assessed, as it is an important parameter, specially for battery sizing (it affects, for instance, the cycle life). Figure 4-12 represents the DOD values for several specimens at different temperatures, which were calculated using the results from cells discharging at normal operating conditions and considering the initial operating SOC of 60%. DOD mean values (diamond-shaped symbols) with the corresponding 95% CI are also included in the graph. As expected, DOD is lower with increasing temperature since the operating capacity is larger. However, this dependency was not fulfilled for Ref 2 and Ref 3 at 45°C, since the cells were not fully discharged (cells were heated up very fast to maximum allowable discharge temperature).



**Figure 4-12.** Depth of Discharge (DOD) for meeting the energy demand of the targeted residential elevator application at normal operating current loads (mean values -diamond-shaped symbols- are indicated for each condition and reference). 60% initial SOC and different ambient temperatures

In conclusion, even though the three references seem to be able to meet the application demands at first glance (Figure 4-12), the performance of Ref 1 was limited in terms of both coulombic and energy efficiency, as well as charging performance in CC mode at any ambient temperature.

- **DC internal resistance measurement tests**

The aim of this test in the specific case of Ref 1, Ref 2 and Ref 3 is just to evaluate the internal resistance of these cells under different conditions, since it is not meaningful comparing the internal resistances of: (i) 18650 (Ref 2) and 26650 (Ref 1 and Ref 3) type cylindrical cells and, (ii) cells with significant difference on the stored capacity (Ref 2 is half the size, in Ampere-hours, of both Ref 1 and Ref 3). Figure 4-13 gathers the regenerative and discharge internal resistances measured by the pulses method as a function of SOC and temperature. In general, the largest internal resistance was measured for Ref 2, whereas the lowest was for Ref 3. However, during low temperature discharge, the performance of Ref 2 was the best. These results are not comparable with the ohmic resistance data reported by the cell manufacturers, since the latter are measured by EIS, which means that they are pure ohmic impedance values, whereas those obtained by the pulses method also contain other side reaction effects from polarisation phenomena.

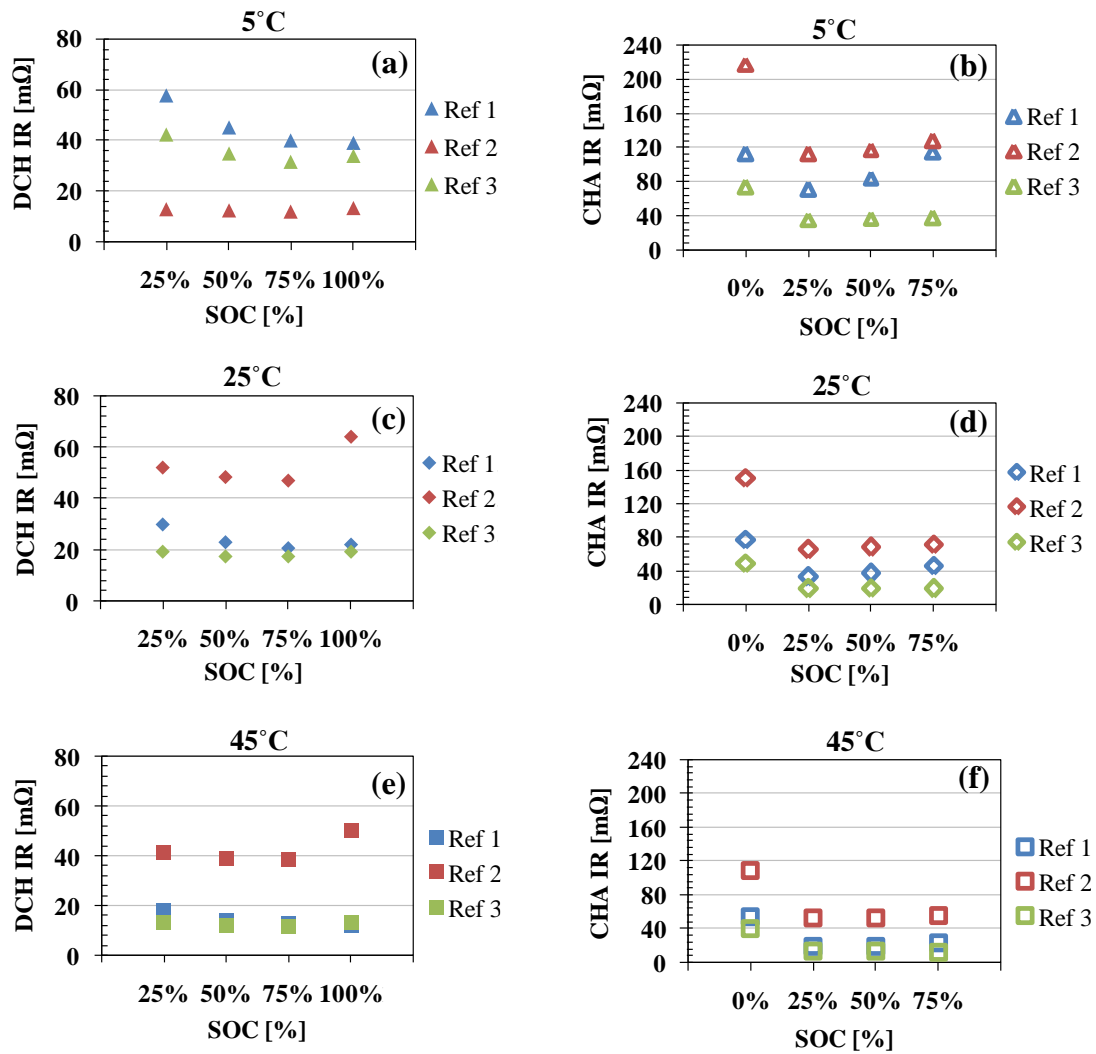


**Figure 4-13.** 17 s Direct Current (DC) internal resistances (IR) as a function of SOC and temperature for different type of cells (10C discharge (DCH) pulses and 1C charge (CHA) pulses with duration of 17 s)

The internal resistance increases at lower temperature (since the conductivity of the electrolyte is reduced) as well as at low and high SOC (Figure 1-6). The influence of SOC was more marked in the case of Ref 2 at any temperature, and it was larger for all the references at lower temperature. The internal resistance remained almost constant in the SOC range between 25 and 75% at 25 and 45°C, whereas at 5°C, it was larger when reducing the SOC within the same range.

The discharge and regenerative resistances remained approximately constant for Ref 3 regardless the SOC (25-75%) and temperature. In the case of Ref 1 and Ref 2, the charge internal resistance was larger than the discharge one, especially at low temperature. In those cases, there was a change in the internal resistance with SOC: discharge resistance was increased whilst regenerative resistance reduced with lower SOC within 25-75% range.

Overall, Ref 3 showed less impedance variations at any application condition and, in general, the lowest values as well. Ref 1 and Ref 2 main drawback lay in the internal resistance increase at low temperature, which could lead to hindering regenerative power loads [85]. In view of the poor performance of Ref 1 in rate capability tests and high internal resistance during discharge at 5°C, its power capability and resultant usable SOC range need to be analysed carefully.

### **a.2) POWER TESTS UNDER APPLICATION CONDITIONS**

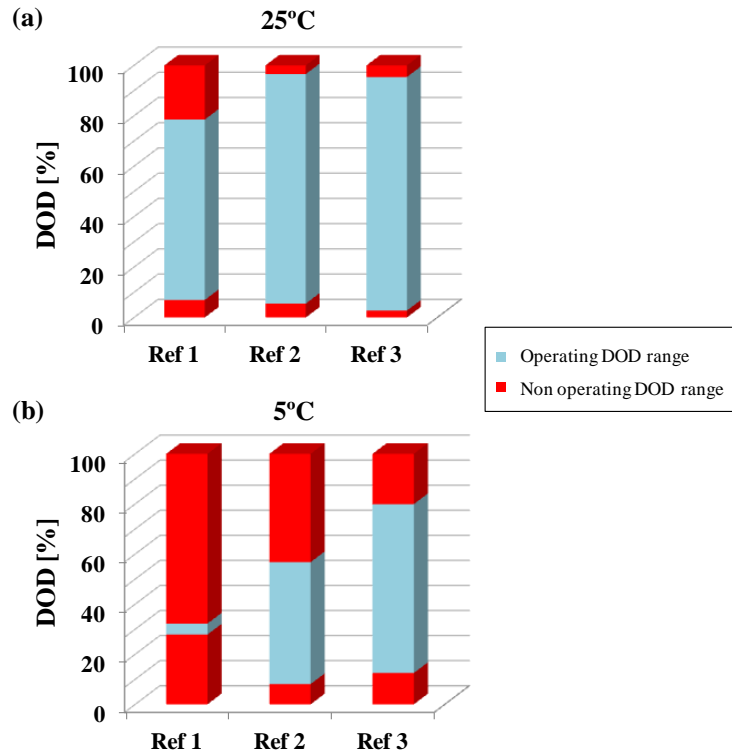
Cell usable DOD range was assessed discharging and charging the cells by applying continuously the real traction and regenerative power profiles of the application (Figure 4-4) between voltage limits of the cell. This approach takes into consideration both power and energy requirements of the application. The power tests under application charge/discharge conditions were run at 25°C (reference temperature) and 5°C, since, as observed from previous results, regenerative power loads could be significantly hindered at low temperatures due to the internal resistance increase. At 45°C, cell power capability should improve in comparison to its performance at 25°C, since cell internal resistance is lower at higher temperatures.

Figure 4-14 illustrates the cell operating window, which indicate the amount of usable energy the cell may yield at 25 and 5°C at the Beginning of Life (BOL) of the three cell types. The measured usable DOD range ensures the cells reliable power performance according to the application charge and discharge requirements.

At room temperature, Ref 2 and Ref 3 could operate almost within the whole cell voltage range. However, Ref 1 regenerative power capability was lower, which would not make possible to operate at SOC higher than *ca.* 80%. When the ambient temperature was 5°C, the usable DOD range reduced significantly because the upper operating SOC limit was reduced in all cases. Hence, the braking energy storage was the limiting factor. The least impact was observed on Ref 3, which operating DOD window at 5°C would be similar to that of Ref 1 at 25°C. Ref 2 charging power capability decreased to the half. The very worst case was the loss of most of the regenerative power capability of Ref 1, which in turn would not be able to provide even one full discharge under application profile conditions unless it was previously charged from the grid with a very low power supply.

All in all, Ref 1 must be rejected at first. Nevertheless, its poor performance at low temperatures could be sorted out by using a temperature conditioning system that would heat up the cells to room temperature (20-25°C). Hence, it was decided to go ahead with the three references and to carry out the degradation test with all of them, after which, the available operating range was

planned to be analysed again. This way, it is possible to validate the decision made previously (Ref 1 rejection) and the methodology development could be more robust. The evaluation of long-term performance may inform whether this stage would be sufficient for reliable battery selection.



**Figure 4-14.** Usable energy assessed from power tests that consisted on repeating continuously application operating profile between voltage limits of the cell and ambient  $T$  of: (a) 25°C; (b) 5°C

## b) ACCELERATED CYCLE LIFE TEST AT SEVERE OPERATION CONDITIONS

The ageing analysis in this section aims at comparing the cycling performance of different type of cells under a specific testing profile. It is an initial useful lifetime screening test, so as to evaluate capacity and power fade trends. This way, it is pursued to assess the cycling capability and operating time for each cell at the EOL defined for meeting the application demands (energy and power).

The cells were cycled continuously using application current operating profile at initial 100% SOC and  $35 \pm 5^\circ\text{C}$ . The SOH was studied by means of capacity and internal resistance measurements every 5000 cycles. Besides, the dispersion due to ageing among different specimens of the same reference was evaluated. Three cells of Ref 1 and Ref 3, and 2 cells in the case of Ref 2, were tested under the same conditions in order to get statistic relevance

(capacity loss and internal resistance increase variation with ageing between different specimens of the same reference).

Figure 4-15 shows the nominal capacity loss as a function of the number of cycles at the specified conditions (realistic profile cycles). Capacity fade depends on time in an exponential way: all the cells showed a greater capacity loss at first cycles, and particularly Ref 1 and Ref 2 (they lost *ca.* 20% of their initial nominal capacity during the first 20000 cycles, whereas the nominal capacity of Ref 3 just decreased by 6% after the same number of cycles). The same cycle ageing tendency for the specimens of each reference can be observed. However, Ref 1 showed the largest dispersion, whereas all tested specimens of Ref 3 behaved similarly. The worst coefficient of variations (CV)<sup>7</sup> upon cycling were 7%, 3% and 1% for Ref 1, Ref 2 and Ref 3, respectively. At the BOL, CV values were in the range of 1.59%, 0.28% and 0.41%, respectively. Hence, the variability among different aged specimens increased the most for Ref 2 in proportion to the deviations at the BOL. In any case, it was the largest for Ref 1.

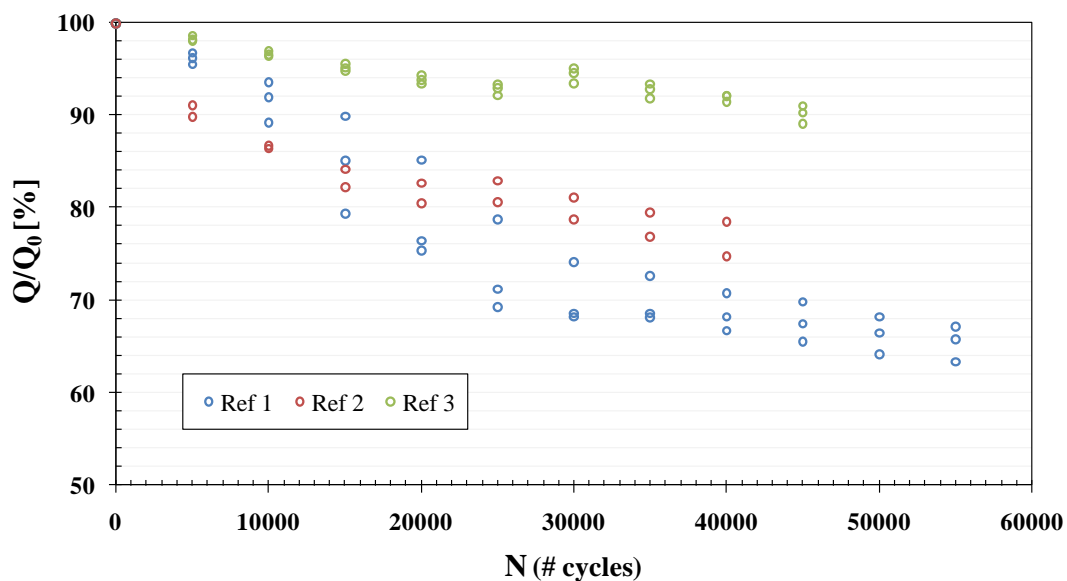


**Figure 4-15.** Change in nominal capacities ( $Q$ : actual capacity;  $Q_0$ : capacity at the Beginning of Life) as a function of number of cycles ( $N$ ). Cells cycling under application current profile, 100% initial SOC and  $35\pm 5^\circ\text{C}$

DC internal resistance measurements showed that both regenerative and discharge resistance evolutions were similar, regardless of different pulse amplitude (*i.e.* calculated after 1 s or 5 s). Larger internal resistance increase rates with cycling were measured at 50% SOC than at 75% SOC. Figure 4-16 shows DC discharge internal resistance changes as a function of the number

<sup>7</sup> Coefficient of variation (CV): ratio of the standard deviation to the mean. It is the normalised measure of dispersion and shows the extent of variability in relation to the mean.

of cycles, which were measured with 10C and 1s pulses at 50% SOC (chosen as the worst case) and  $25 \pm 2^\circ\text{C}$  ambient temperature.

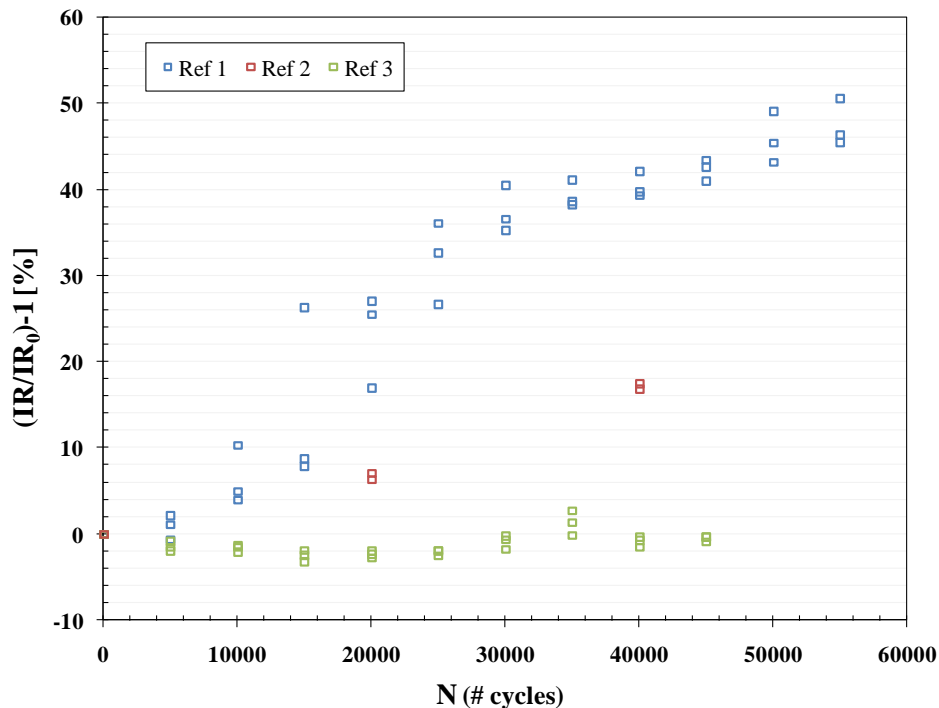


**Figure 4-16.** Evolution of the studied three references 1s internal resistance changes upon cycling ( $IR$ : actual internal resistance;  $IR_0$ : internal resistance at the Beginning of Life). Direct Current (DC) IR measured at 50% SOC with 10C DCH pulse of 1 s duration

Ref 1 and Ref 2 total impedance increased with cycling, which was supposed it to be related to SEI layer growth and electrolyte degradation [86-89]. This effect was more pronounced in the case of Ref 1, which showed 40% internal resistance increase after 40000 cycles, whilst it changed by 18% for Ref 2. However, Ref 1 impedance rise stabilised after 35000 cycles. Aiming at studying the contributions of capacity and internal resistance to this cell type performance fade, the relationship between power capability and capacity loss upon cycling was analysed, as shown in Figure 4-17 (power capability was assessed using DC internal resistance data measured at 50% SOC with 10C DCH pulse of 1 s duration). They showed linear relationship, so capacity and internal resistance increase might have the same origin for Ref 1.

Ref 3 impedance evolution upon cycling is surprisingly different. Contrary to expectations, it decreased during the first 25000 cycles and it kept its initial internal resistance after 40000 cycles. Other investigations with Li-ion cells [90, 91] have found the same tendency. So as to understand Ref 3 internal resistance decrease over cycling, EIS measurements were performed at room temperature and 75% SOC in galvanostatic mode using a frequency range from 0.1 to 6.5 kHz. The obtained impedance spectra, shown in Figure 4-18, proved that the ohmic resistance did not change with cycling (intersection with the real axis), whereas the reaction

resistance was reduced after 15000 cycles but it thereafter increased (first semi-circle, which is typically associated with SEI formed during cycling [92]).

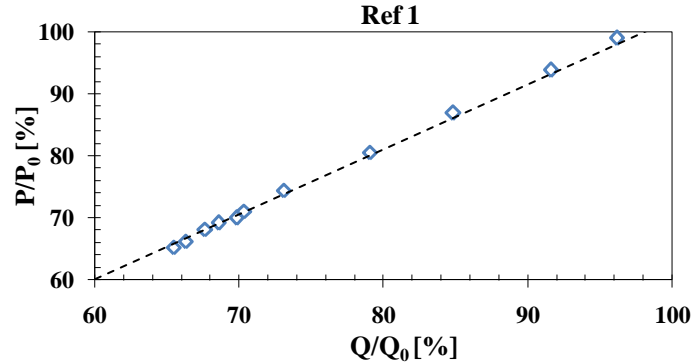


**Figure 4-17.** Correlation between Ref 1 power capability loss and capacity loss due to cycling ( $Q$  and  $P$ : actual capacity and power, respectively;  $Q_0$  and  $P_0$ : capacity and power, respectively, at the Beginning of Life). Power capability was assessed using data from Figure 4-16

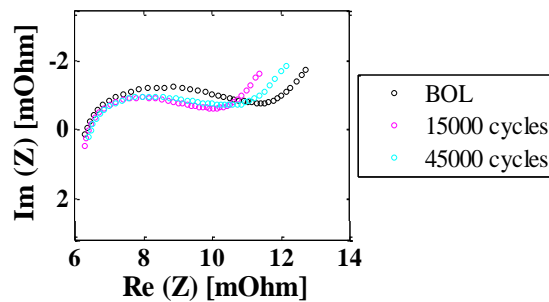


**Figure 4-18.** Impedance spectra of Ref 3 measured before and after cycling over 15000 and 45000 cycles. EIS test at 75% SOC and 25°C

The reduction of the internal resistance could be explained by lithium insertion/extraction processes into electrodes that may lead to active particles mechanical fracture [44, 91, 93]. Finer particles size increases the effective surface area, thus reducing the reaction resistance. This way, the cell can provide higher power capability.

The effect of the impedance change was also observed in the measurements carried out at adiabatic conditions. Previous to calorimetric tests, the heat capacity ( $c_p$ ) of specimens was evaluated at adiabatic conditions using a 2.25 W electrical resistance. It was measured for Ref 3, which  $c_p$  was 1.08 kJ/(kg·K). Thermal power<sup>8</sup> in the following was assessed assuming that the  $c_p$

<sup>8</sup>  $P = (\sum m \cdot c_p) \cdot \Delta T / \Delta t$

where  $m$  is the mass corresponding to all materials within the testing space (cell assembly -Cu plates, screws, Teflon slab-, cell, etc.),  $c_p$  is the heat specific capacity of each of the materials or components (Cu, Teflon, stainless steel, cell and so on),  $\Delta T$  is the temperature increase during the calorimetry test and  $\Delta t$  is the duration of the calorimetry test.

Thermal power can also be assessed as:  $P = IR \cdot I^2$

was  $1 \text{ kJ}/(\text{kg}\cdot\text{K})$  for every studied cell. Calorimetric tests run at the BOL and after cycling shown in Figure 4-19 indicated that the thermal power increased after cycling for Ref 1 and Ref 2. It is directly related to the measured internal resistance increment given that the power depends directly on it<sup>8</sup>. Aged Ref 3 showed thermal power reduction, in agreement with the measured initial internal resistance diminution and no overall internal resistance change for this type of cell. The measurements at adiabatic conditions need to be however optimised, as the mass of each cell is much lower than the other materials (power supply circuit cables, assembly and so on) within the calorimeter. This means that the cell thermal power estimation might be distorted owing to the contribution of the other elements. The tests ought to have been carried out using more than one cell in order to obtain more reliable results. Despite this, the shown relative results are good enough for comparing the thermal behaviour of each cell type before and after ageing.

Discharge voltage profiles from calorimetric tests in Figure 4-20 showed clearly that the internal resistance of Ref 1 and Ref 2 increased. The shape of the curves remained unaltered but shifted to quite lower voltages. On the contrary, in the case of Ref 3, both voltage profiles before and after 45000 cycles were overlapped. Hence, it is clear that the impedance of the latter did not change. On the other hand, a more pronounced voltage drop was measured at the end of the discharge process for every aged cell, which is related to the capacity loss due to cycling. Besides, this effect was more pronounced for Ref 1 and Ref 2, since they were not able to provide ten consecutive discharges after the cycling test.

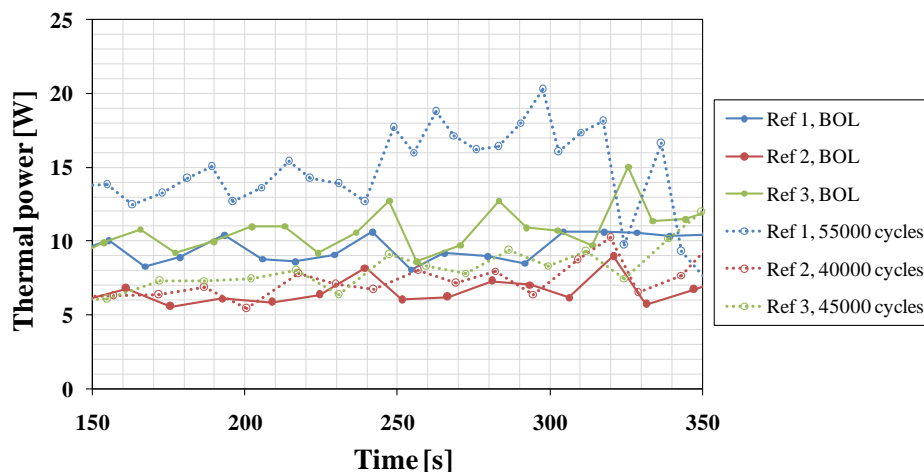


**Figure 4-19.** Different type of cells thermal power at adiabatic conditions during continuous discharges under application current profile measured before and after cyclic ageing.  $20\pm 3^\circ\text{C}$  ambient temperature

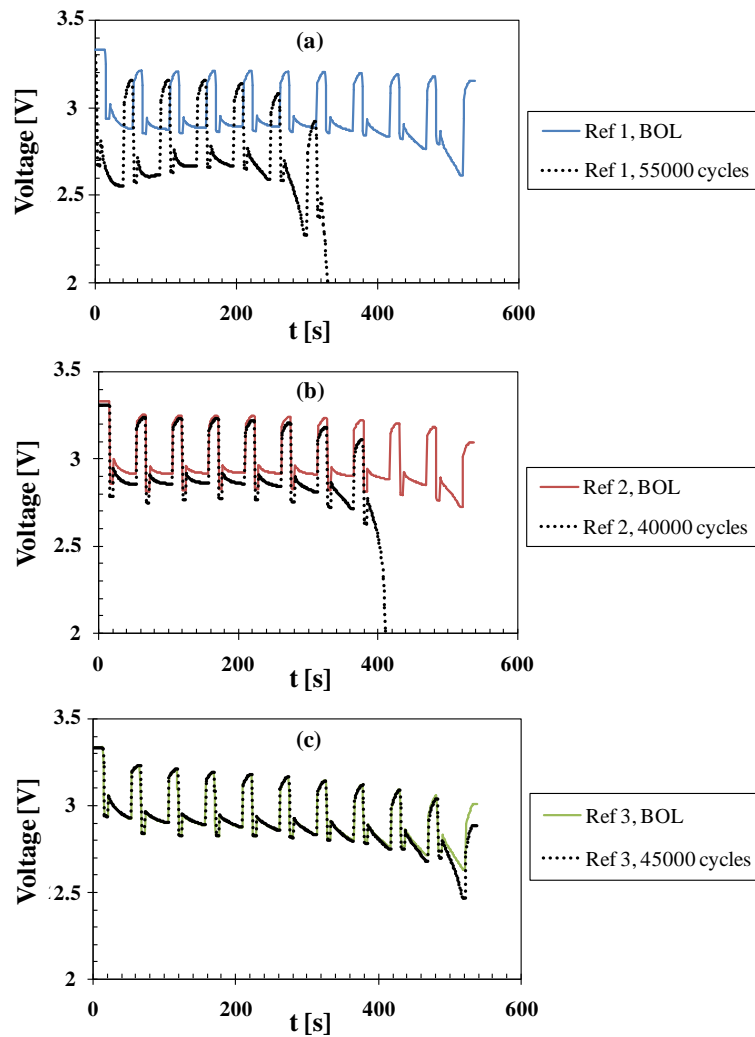


**Figure 4-20.** Discharge voltage profiles of Ref 1 (a), Ref 2 (b) and Ref 3 (c) during adiabatic calorimetric tests at the BOL and after cyclic ageing

Capacity loss and DC internal resistance increase (from HPPC test) average values data were used to evaluate the evolution and quantify the capacity fade and power capability loss rate. Figure 4-21 and Figure 4-22 show the nominal capacity and discharge power capability loss prediction, respectively, for the three references. It must be noted that the fitting of Ref 2 power capability loss was not assessed as there was not enough data for reliable estimations. Regarding Ref 3, as observed for the impedance change (Figure 4-16 and Figure 4-18), the power capability increased at the beginning and it almost recovered its initial value after 45,000 cycles, so it seems that it will be kept approximately constant over cycling.

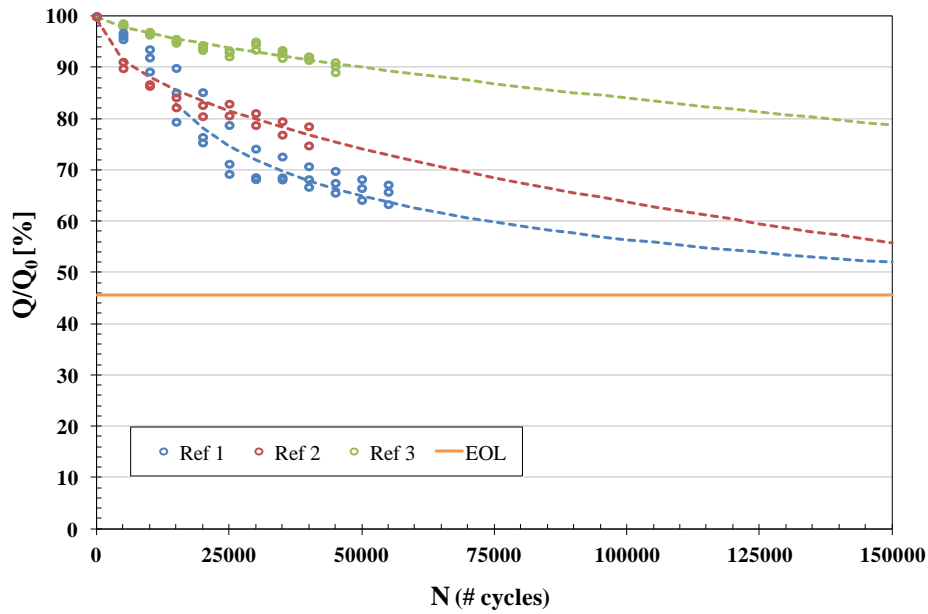


Figure 4-21. Fitting of capacity loss rate as a function of number of cycles

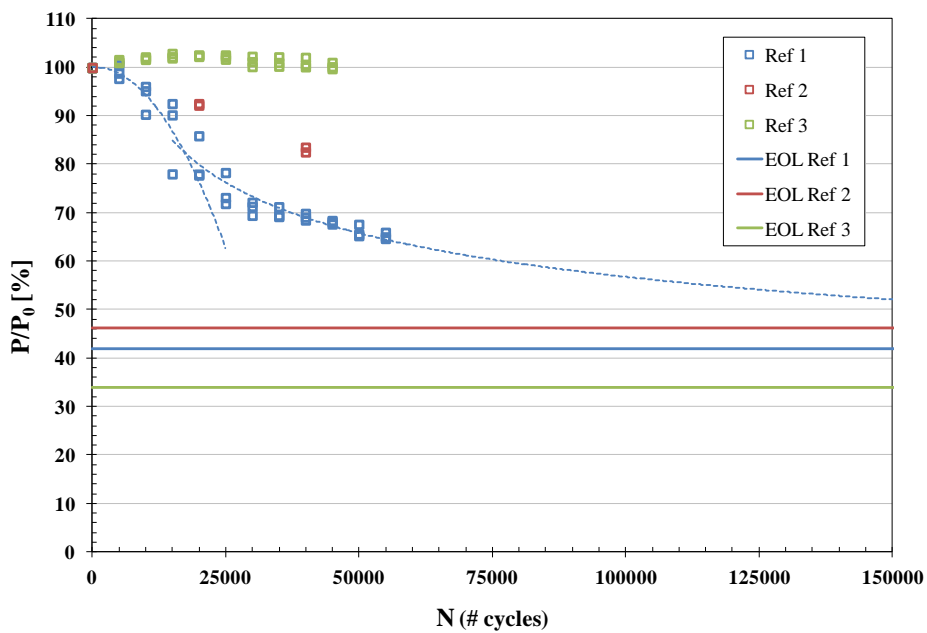


Figure 4-22. Fitting of discharge power capability loss as a function of number of cycles

Table 4-7 gathers mathematical fittings that relate the capacity and power capability loss with the number of cycles for the studied conditions (continuous cycling under the application current profile with *ca.* 5% DOD, *ca.* 100% SOC and *ca.* 33°C). These mathematical relationships show ageing tendencies that enabled making rough predictions with reference to the EOL.

**Table 4-7. Capacity and discharge power capability loss fittings**

Cell type	AGEING PREDICTIONS DUE TO CYCLING	EOL
Ref 1	$Q/Q_0 [\%] = 583.72 N^{-0.203}$ <i>Eq. 4-1</i> ( $R^2 = 0.95$ )	N = 150000 → Q/Q <sub>0</sub> = 51.94 % EOL → N = 283165
	$P/P_0 [\%] = 657 N^{-0.213}$ <i>Eq. 4-2</i> ( $R^2 = 0.96$ )	N = 150000 → P/P <sub>0</sub> = 46.35 % EOL → N = 411080
Ref 2	$Q/Q_0 [\%] = 100 - 0.11 N^{0.5}$ <i>Eq. 4-3</i> ( $R^2 = 0.97$ )	N = 150000 → Q/Q <sub>0</sub> = 57 % EOL → N = 227209
Ref 3	$Q/Q_0 [\%] = 100 - 0.01 N^{0.7}$ <i>Eq. 4-4</i> ( $R^2 = 0.94$ )	N = 150000 → Q/Q <sub>0</sub> = 78.76% EOL → N = 577733

**Ref 1** cycle lifetime seems to be limited by the capacity loss, although both power and capacity fade show similar trends. Its lifetime might be *ca.* 283000 cycles at tested conditions. Consequently, Ref 1 may be able to meet the application demands ( $N \geq 150000$ ,  $Q/Q_0 \leq ca. 45\%$  and  $P/P_0 \leq ca. 42\%$ ). Nevertheless, cycle ageing at other operating conditions has to be also analysed so that the influence of every variable is fully assessed. It is also a must to evaluate the calendar life as 10 years of lifetime are pursued.

Ref 1 demonstrates a two-regime fading pattern (different degradation tendency was observed before and over 15000 cycles). The fast performance fade in the first stage could be explained by side reactions that consume active lithium to the SEI film formation on the graphite/electrolyte interface [17]. Figure 4-16 showed that capacity and internal resistance increase might have the same origin for Ref 1, which may be arisen from SEI layer growth that also increase the interfacial resistance of the anode. The side reaction rate could have gradually decay as the cell was cycled more, because the gradually growing SEI film on the anode will partially impede further occurrences of SEI film forming [94]. In this stage the limiting electrode is usually the graphite negative electrode [94]. The observed performance fade evolution could also result in anode active material loss [95], which is common for LFP/graphite cells [96].

**Ref 2** capacity loss trend followed square root of time dependency, which, according to the literature [97, 98], is typically related to Li-consuming SEI layer growth over time that causes capacity decline and cell polarisation resistance increase (due to increase in film layer thickness). The DC internal resistance increase rate was even higher after 20000 cycles (Figure 4-16), so the dominant degradation mechanism may have changed and there may be additional contributions to the loss of active lithium.

Regarding **Ref 3**, power capability influence on cycle lifetime cannot be evaluated. Power loss might be observed in longer testing times but there is not enough data for making predictions yet. Were Ref 3 cycle lifetime limited by the intrinsic capacity loss, it would be

ca. 578000 cycles at tested conditions. Then, Ref 3 seems to provide the longest lifetime at first. However, as mentioned before, cycle life ageing has to be carefully analysed under different conditions and likewise the shelf life.

The evolution of the usable energy (operating SOC range) deterioration was also considered necessary due to the observed power capability loss. It was appropriate to check Ref 1 usable SOC range due to its poor performance at BOL. For those reasons, the power tests under application conditions were carried out after ageing cells over some cycles. The operating DOD results at 25°C (assessed using the initial nominal capacity in both cases) are gathered in Table 4-8 together with the values obtained at the BOL. Figure 4-22 shows, for the three cycled references after the indicated number of cycles, the actual operating window under the residential elevation application charge and discharge demands at 25°C. Similarly to Figure 4-14, they were assessed from power tests that consisted on repeating continuously the application operation profile between voltage limits of the cell. In Figure 4-22 it is also shown the capacity fade,  $Q_{loss}$ , in purple, as guidance of the total energy of each cell, for evaluating the available energy and the portion of the battery capacity that can be used at such ageing state condition.

**Table 4-8.** Operating DOD range at 25°C according to the application discharge and regenerative power requirements before and after cycling both calculated as a function of the initial capacity (N: number of cycles)

	<b>Ref 1 operating DOD [%]</b>	<b>Ref 2 operating DOD [%]</b>	<b>Ref 3 operating DOD [%]</b>
<b>BOL</b>	71.55	91.05	92.65
<b>Over cycling</b>	39.6 (N = 35000)	63.9 (N = 40000)	87.06 (N = 15000)

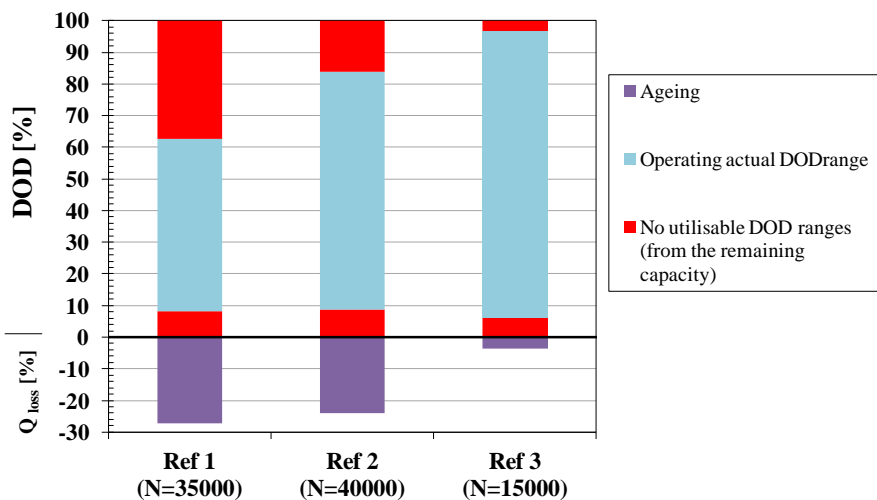


**Figure 4-23.** Usable energy assessed from power tests under application operating profile and 25°C after the cells being cycled

It was not necessary to carry out the tests at 5°C, since Ref 1 operating DOD after 35000 cycles already at room temperature was only *ca.* 40% (considering the initial cell nominal capacity). In view of the results obtained at the BOL (Figure 4-14), Ref 1 could not operate at low temperatures. Ref 2 usable energy at 25°C reduced by 30% over 40000 cycles, whereas Ref 3 operating DOD did not change significantly after 15000 cycles. Despite the uneven number of cycles for the three references, the results observed are consistent with the trends from capacity and power losses (Figure 4-21 and Figure 4-22).

#### 4.1.2.3 STAGE 2 SUMMARY AND GENERAL CONCLUSIONS

Stage 2 focused on cell testing for their characterisation and determination of their suitability for the studied regenerative application. Indeed, it was looked for the aspects that make the cells that were being compared different and the limiting factors for meeting the application demands. These are summarised as follows:

- *Cell variability and tests reproducibility*

Table 4-9 summarises the coefficient of variations of the nominal capacity values assessed for each reference (considering just the specimens tested in the accelerated cycle life test at severe operation conditions). Ref 1 showed much variation in the different measurements, which was even increased when the cells were cycled. On the contrary, Ref 3 different specimens behaved similarly and even the dispersion increased with ageing, the variations among cells kept steady with the number of cycles.

**Table 4-9.** Dispersion among different specimens of the same reference

	Coefficient of variation (CV) of the nominal capacity [%]		
	BOL	Average values over cycling	Maximum values over cycling
Ref 1	1.59	3.94	6.89
Ref 2	0.28	1.83	3.46
Ref 3	0.41	0.60	1.10

- *Electric and thermal performance*

According to the tests carried out at different ambient temperatures, operating at 5°C had a great effect on cells performance. Most relevant characteristics overview at low temperature is depicted in Figure 4-24. Ref 1 showed the lowest usable energy and operating SOC range and it was hardly able to charge braking energy at low temperature. Ref 3 showed excellent behaviour and Ref 2 performance was also acceptable for the application.

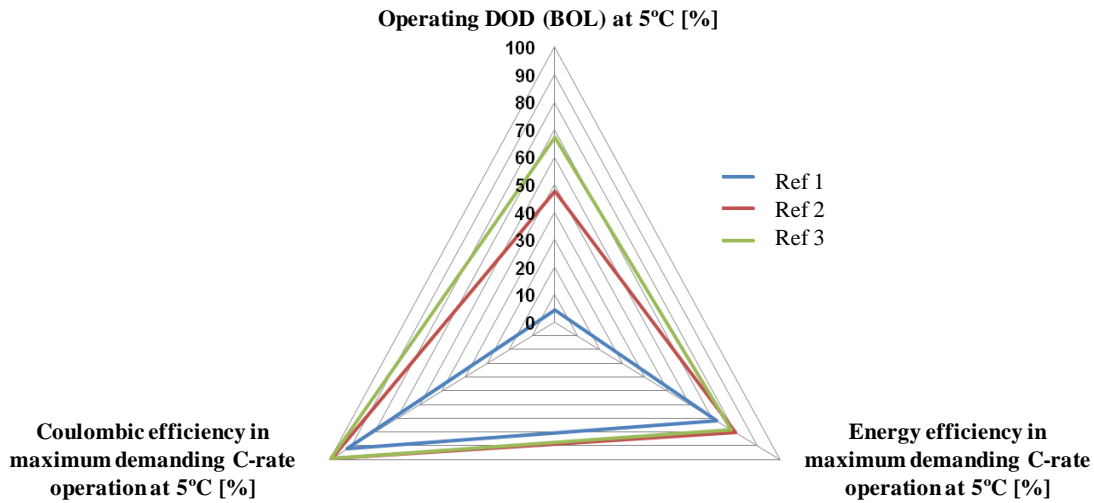


**Figure 4-24.** Most limiting electrical characteristics at 5°C ambient temperature of the studied three references

- *Ageing tendency at severe cycling conditions*

No reference seems to reach the application EOL according to the calculated capacity loss tendencies. However, Ref 2 might not be able to meet the application discharge power capability requirements.

In the long term, Ref 2 seems to lose most of its rated capacity. However, it is more pronounced for Ref 1 after 150000 cycles. Ref 3 shows the best cycling capability, with no increase in the internal resistance and with an estimated cycle lifetime of more than 500000 cycles at tested conditions.

With regards to the operating DOD range over cycling, it was the lowest for Ref 1: just the 40% (considering the initial capacity) at 25°C after 35000, whereas the application requires a lifetime of 150000 cycles. Hence, even though it seems to keep its nominal capacity above the minimum required for the application, the usable energy was considerably deteriorated after 35000 cycles and it might not be able to provide the required total energy. Ref 3 seems to be the only cell type that may have enough usable energy for the application (it still seems to exceed the energy demand after 15000 cycles at 25°C).

Table 4-10 summarises some relevant characteristics of the compared three cells. For a more reliable lifetime analysis, calendar ageing ought to have been also investigated, as cell degradation in the course of the time represents an important factor for cell stability, and may even limit cell useful lifetime. However, it was not considered in this cells preselection stage that aims at the comparison of different references, since storage tests would take long. Overall,

Ref 3 is the most promising candidate for the pursued application. Ref 1 was rejected mainly because of:

- i) Large variability presented among its different cells, which would involve considerable difficulties for cells balancing in the battery pack.
- ii) Poor electrical performance and impedance increase at both low temperatures and during cycling (besides, internal resistance is expected to have even larger impact during storage [99]).
- iii) Large usable energy deterioration over cycling.

On the other hand, it was decided not to carry on with Ref 2 in the subsequent stage due to:

- i) Its large regenerative DC internal resistance at low temperatures, as it could lead to hindering braking power loads.
- ii) The large amount of number of cells that were required because of its low energy density, which would hinder the battery pack construction. Its performance was not good enough to take on that drawback.

**Table 4-10.** Comparison of performance of the three studied cells (red: poor; yellow: fair; green: good)

<b>VARIABILITY</b>		<b>Ref 1</b>	<b>Ref 2</b>	<b>Ref 3</b>
<b>USABLE DOD RANGE</b>	Ambient operating T (fresh cell)	Yellow	Green	Green
	Low operating T (fresh cell)	Red	Yellow	Green
	After ageing	Red	Red	Green
<b>CYCLE AGEING</b>		Red	Yellow	Green

Hence, the only suitable cell for the application would be Ref 3. The battery pack configuration should be optimised to the performance of this cell. A new battery pack sizing can lead to different cell operating power and energy demands.

Stage 3 and Stage 4 are to be developed jointly in this specific case, as in Stage 2 the optimal cell solution was already chosen. In the following, the Thesis work was focused on in depth ageing analysis of Ref 3, which will be described in detail in *Chapter 5*.

## 4.2 TRAMWAY APPLICATION

The proposed cell selection methodology was also implemented for a catenary-free tramway application. This section is a short summary of the methodology implementation for this second validation scenario.

### 4.2.1 STAGE 1: REQUIREMENTS OF THE APPLICATION AND EVALUATION OF AVAILABLE CELLS

Energy storage devices in tramways are required to deliver and accept high-power pulses during tramway acceleration (rapid discharge capability) and braking (rapid charging capability), respectively. Rechargeable technologies specially designed for HP applications are then necessary. Li-ion battery technology shown in Figure 4-25 or its hybridisation with EDLC (for pulse power), in case the Li-ion battery has a low power density, are both viable options. The objective of introducing lithium-based batteries is to increase the efficiency of the system by recovering the braking energy from the traction motor and reducing the energy demanded from the catenary (optimisation of the system in terms of performance and cost). Moreover, it is aimed at driving the railway vehicle in catenary-free areas (autonomy without overhead power cables). Other goals of introducing a ESS in tramways are removing the catenary in some track sections in city centres, for reducing visual impact and infrastructure investments.



*Figure 4-25. Catenary free tramway ESS system developed between IK4-Ikerlan and CAF Power & Automation*

ESS for this application is demanded to provide up to 1400 metres in catenary-free operation (the autonomy depends on battery pack sizing and tram topology), with approximately 20-30% of the overall system energy saving. Most demanding traction and regenerative profiles for the tramway application are shown in Figure 4-26. Normal charge of the battery corresponds to stretches of tramway with catenary, normal discharge demands to catenary-free stretches and maximum discharge demand to unexpected start/stop when driving in catenary-free stretches. The battery needs to meet applications energy and power demands at both normal and most demanding operating conditions (traction peaks).

The battery pack requirements for tramway application are<sup>9</sup>:

- Nominal voltage of the battery pack: 300-500 V
- Number of cells: < 240
- Total weight of the battery pack: 240 kg

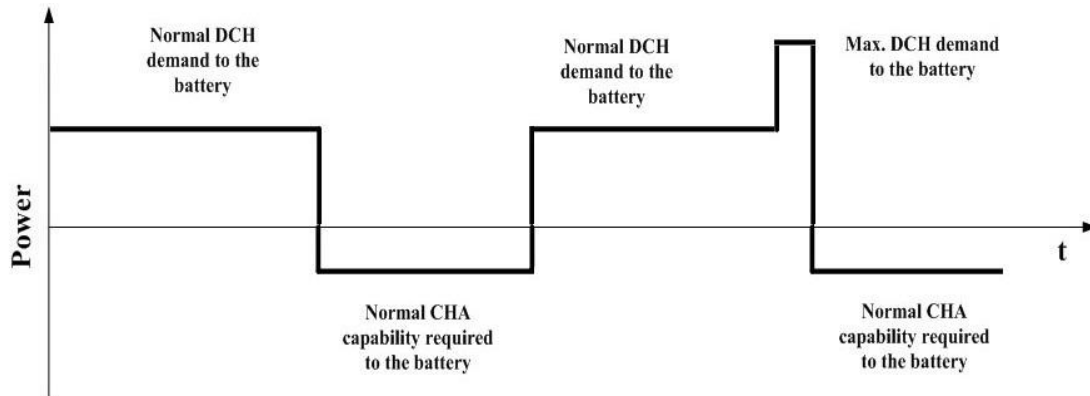


*Figure 4-26. Most demanding operating profile for tramway application and other demanded peaks due to unexpected start/stop during catenary-free operation stretch<sup>10</sup>*

#### 4.2.1.1 EVALUATION OF AVAILABLE CELLS AND DEFINITION OF THE OPTIMUM OPERATION RANGE

Going through the Li-ion technology market database (Appendix D), nine possible cells were found to be suitable for meeting the applications requirements. Their characteristics are gathered in Table 4-11. Once the information provided by the manufacturers was analysed in depth (technical data, details in datasheets, certifications, etc.), real fields of cell operation were determined as a function of most demanding application requirements, using nominal data from the datasheets. The aim in this stage was just to obtain valuable data for the comparison of different configurations and, this way, make first decisions. Hence, at first, it was considered that all the cells in the battery pack would be connected in series so as to calculate more easily all important operating parameters and characteristics. Table 4-12 shows a summary of the appraisal for each evaluated reference (cells T.1 to T.9).

<sup>9</sup> Additional data and more specific values are confidential information from the application provider.

**Table 4-11.** Summary of the most representative characteristics of the purchased cells for the tramway application evaluation (data from manufacturers)

		CHARACTERISTIC	UNIT	Ref T.1	Ref T.2	Ref T.3	Ref T.4	Ref T.5
<b>INTRINSIC PROPERTIES</b>		Cathode	—	LFP	NCM	LFP	NCM	LFP
		Geometry	—	Prismatic	Pouch	Pouch	Pouch	Prismatic
		Internal resistance	<b>mΩ</b>	< 2	< 0.8	< 2	-	< 1.5
<b>PERFORMANCE CHARACTERISTICS</b>	<b>NOMINAL CHARACTERISTICS</b>	Nominal capacity	<b>Ah</b>	40	40	18.5	42	60
		Nominal voltage	<b>V</b>	3.2	3.7	3.65	3.2	3.2
		Energy density	<b>Wh/kg</b>	102	135	159	133	87
	<b>CHA CONDITIONS</b>	CHA cut-off voltage	<b>V</b>	3.8	4.2	4.1	3.65	3.6
		Max. CHA current	<b>A</b>	-	120 (3C)	-	42 (1C)	30 (0.5C)
		CHA temperature range	<b>°C</b>	0 - (+ 45)	10 - (+ 45)	-	(- 20) - (+ 35)	0-(+50)
	<b>DCH CONDITIONS</b>	DCH cut-off voltage	<b>V</b>	2.5	2.7	2.5	2.5	2.5
		Max. DCH current	<b>A</b>	400 (10C)	320 (8C)		90 (2C)	180 (3C)
		Max. DCH current pulse	<b>A</b>	-	-	485 (25C, 10 s)	200 (4.75C, 10 s)	300 (5C, 30 s)
		DCH temperature range	<b>°C</b>	(- 10) - (+ 35)	(- 20) - (+ 55)	(- 25) - (+ 52)	(- 40) - (+ 60)	(- 10) - (+ 60)

**Table 4-11.** Summary of the most representative characteristics of the purchased cells for the tramway application evaluation (data from manufacturers) (continued)

		CHARACTERISTIC	UNIT	Ref T.6	Ref T.7	Ref T.8	Ref T.9
<b>INTRINSIC PROPERTIES</b>		Cathode	—	LFP	LFP	LFP	LFP
		Geometry	—	Prismatic	Prismatic	Prismatic	Prismatic
		Internal resistance	<b>mΩ</b>	> 1	< 2	< 2	< 1
<b>PERFORMANCE CHARACTERISTICS</b>	<b>NOMINAL CHARACTERISTICS</b>	Nominal capacity	<b>Ah</b>	100	60	45	20
		Nominal voltage	<b>V</b>	3.4	3.2	3.2	3.2
		Energy density	<b>Wh/kg</b>	110	96	90	80
	<b>CHA CONDITIONS</b>	CHA cut-off voltage	<b>V</b>	3.6	3.8	3.65	3.65
		Max. CHA current	<b>A</b>	300 (3C)	180 (3C)	-	20 (1C)
		CHA temperature range	<b>°C</b>	0 - (+ 55)	0 - (+55)	0 - (+ 60)	0 - (+45)
	<b>DCH CONDITIONS</b>	DCH cut-off voltage	<b>V</b>	2	2.5	2	2
		Max. DCH current	<b>A</b>	400 (4C)	180 (3C)	450 (10C)	500 (25C)
		Max. DCH current pulse	<b>A</b>	1200 (12C, 5 ms)	600 (10C, 10 s)	-	500 (25C)
		DCH temperature range	<b>°C</b>	(- 25) - (+ 55)	(- 20) - (+ 65)	(- 30) - (+ 70)	(- 20) - (+ 60)

**Table 4-12.** Theoretical evaluation of considered cells for tramway application after initial battery pack sizing (red: poor; yellow: fair; green: good)

	Data-sheet	Function of Sizing			
		DOD	Voltage	Current	No. of cells, weight and volume
Ref T.1		Considerable	V max. limit exceeded (when it is operated with the current recommended by the manufacturer)	Within the limits	Within the set limit
Ref T.2		Very low	V max. limit exceeded	Within the limits	Series-parallel required (it increases the number of cells)
Ref T.3		Low	Within the set limit	DCH peak exceeds cell maximum DCH current	Series-parallel required
Ref T.4		Considerable	V max. limit exceeded	Within the limits	Series-parallel required
Ref T.5		Low	V max. limit exceeded	Within the limits	Weight limit exceed
Ref T.6		Low	V max. limit exceeded	Within the limits	Weight limit exceed
Ref T.7		Low	V max. limit exceeded	Within the limits	Weight limit exceed
Ref T.8		Low	V max. limit exceeded	Within the limits	Weight limit exceed
Ref T.9		Considerable	V max. limit exceeded	Within the limits	Series-parallel required

Taking into account the characteristics of each cell and the application requirements, the evaluated cells were divided into three different groups according to their suitability for the tramway application. The theoretical initial selection is shown in Table 4-13.

**Table 4-13.** Theoretical cells selection for tramway application

Cells with best features	Cells with acceptable features	Cells with regular features
Ref T.2 Ref T.8 Ref T.9	Ref T.1 Ref T.3 Ref T.4 Ref T.6	Ref T.7 Ref T.5

Despite the technical decision adopted (Table 4-13), finally Ref T.2, Ref T.6 and Ref T.9 were purchased because of initial cells costs and availability of manufacturers. Some of their important characteristics, according to the assessed initial battery pack design, are compared in Figure 4-27. Ref T.8 was dismissed because the company had a very short experience in the production of Li-ion batteries, but it is a possible good option for future studies.

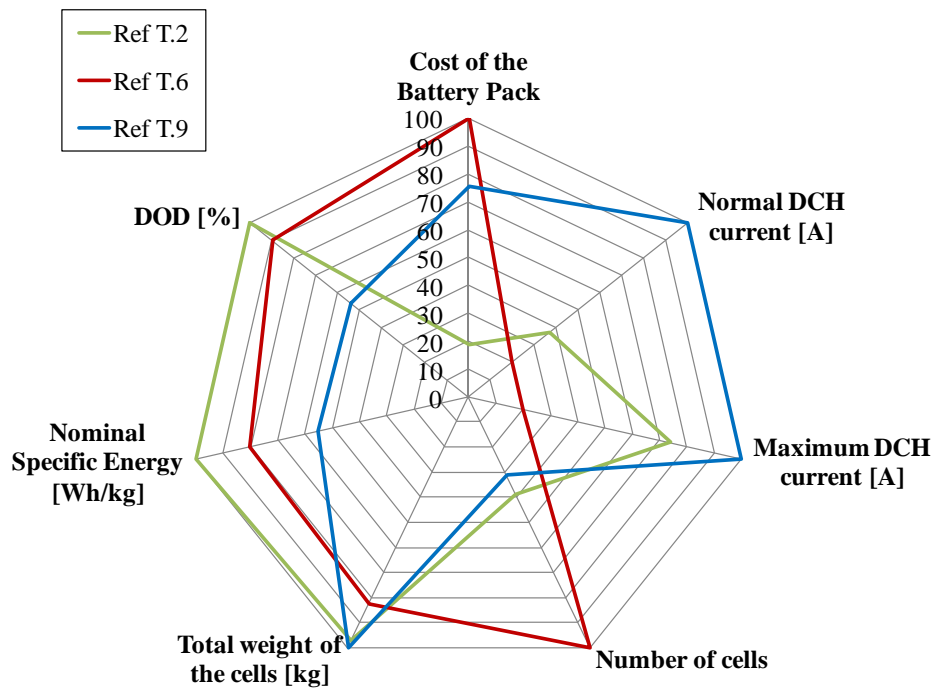


*Figure 4-27. Stage 1 conclusions. Most relevant characteristics for the purchased cells*

#### 4.2.2 STAGE 2: SCREENING

As for the elevator application, nominal capacity, rate capability, DC internal resistance measurement, power under application conditions and an accelerated cycle life test at severe operating conditions were carried out for the three purchased references. In this section, however, only the most relevant experimental results of Stage 2 for the tramway application are shown, as an overview.

- **Nominal capacity tests**

Nominal capacity tests were run using as many specimens of each reference as possible. Figure 4-27 shows the discharge capacity results with the corresponding statistical analysis for each reference, which was carried out using Minitab software. 95% reliability CI of both each specimen and the reference itself, which are plotted in grey and with dotted lines, respectively, and the overall mean values, in continuous lines, are shown. The mean nominal discharge capacity of Ref T.6 was the only one that was larger than the value specified by the manufacturer. However, this reference also showed the largest CI, indicating larger variability among the different specimens of the same manufacturing batch.

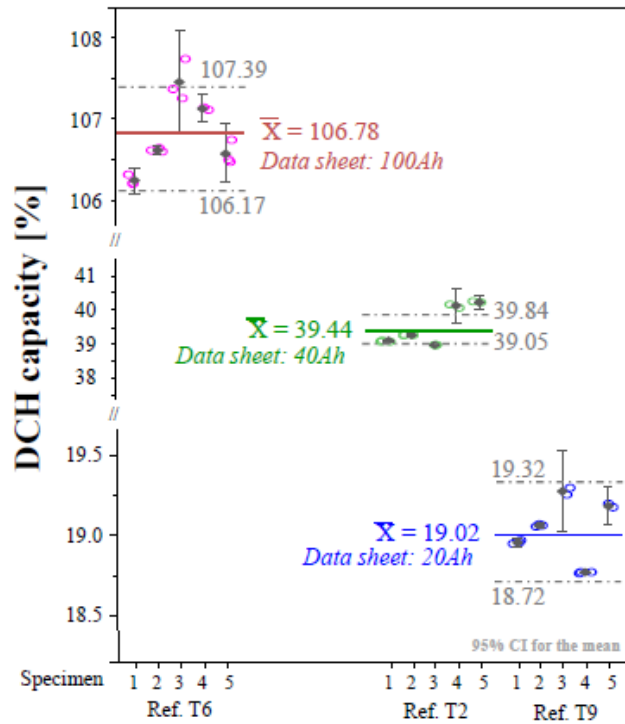


**Figure 4-28.** Nominal capacity variation between cells of the same reference. Experimental results of Ref T.2, Ref T.6 and Ref T.9 in green, magenta and blue open circuits, respectively. Mean value (continuous lines in the same colour as experimental data) and 95% CI (dotted grey lines). 95% CI of each specimen in grey

- **Rate capability tests**

As for the elevator case and described in *Chapter 2*, these tests were carried out at constant current so that operating capacity under different application conditions could be assessed (normal and maximum DCH C-rates). At both normal and maximum loads defined for tramway application, it was possible to withdraw the energy demand of the tramway in all cases. Ref T.2 and Ref T.9 showed a small capacity diminution at 10°C, but it was not remarkable. In the specific case of Ref T.6, it was feasible to discharge at 10°C, 25°C and 45°C almost 100% of the Ampere-hours stored, but at the expense of a huge cell surface temperature increase ( $\Delta T$ ), which could affect its cycle life (at 10°C ambient temperature, the surface temperature increase of Ref. T.6 was *ca.* 26.7°C, while it was around 12°C for Ref T.2 and Ref T.9). Figure 4-29 shows, on the other hand, the energy efficiency of the three references under comparison operating at normal and maximum C-rate conditions. Ref T.2 showed superior performance although in all cases the energy efficiency of Ref T.9 was also larger than the 80%. The variability among different specimens of the same reference was also evaluated under different operation conditions. Ref T.6 showed the largest dispersion against the assessed mean capacity and energy values and Ref T.2 was the reference with the least variance.

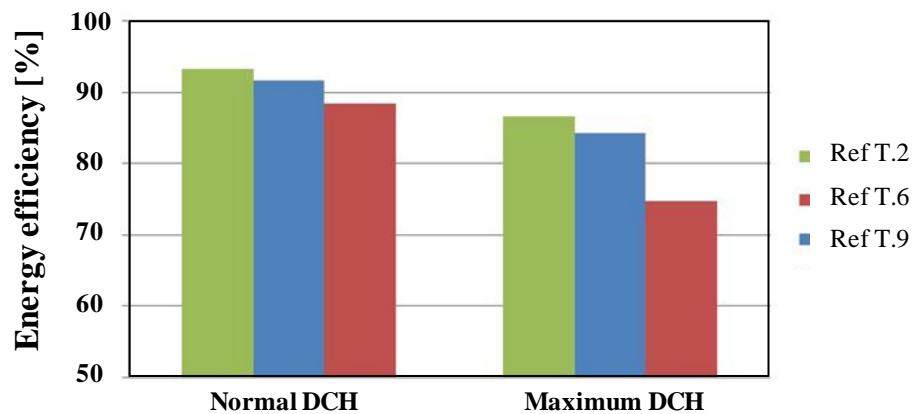


**Figure 4-29.** Energy efficiency of the references at normal and maximum operating conditions. Experimental results of Ref T.2, Ref T.6 and Ref T.9 in green, red and blue, respectively

- **Accelerated cycle life test at severe operation conditions**

The SOH of cells cycled continuously under application current operating profile at 50% middle SOC and  $45\pm 5^{\circ}\text{C}$  was studied by means of periodical capacity and internal resistance measurements. After 560 cycles under application conditions, Ref T.6 was the most aged reference with a capacity loss of approximately 7-8% and 15% internal resistance increase. Ref T.9 and Ref T.2 showed 2.2% and 1.6% capacity loss, respectively, after approximately the same number of cycles (Ref T.9, in turn, underwent around 100 FEC more than the other two references due to the different battery pack sizing in each case, as assessed in Stage 1). The comparatively large degradation of Ref T.6 could be, as mentioned before, the result of the larger heating up upon cycling. Its surface temperature increase was  $2.5^{\circ}\text{C}$  larger than for the other two references.

- **General conclusions**

Overall, **Ref T.2** is the best candidate for the pursued application. Its only drawback is the geometry, as pouch cells assembly in a battery module is more difficult, especially for terminals connection. However, it seems that battery integrators have solved this handicap, as lots of commercial batteries are build using this type of cells.

**Ref T.6** is the less suitable option because of the variability presented among the different specimens of the same manufacturing batch, large heating up when high current rates are demanded and poor performance upon cycling (large capacity fade accompanied by internal resistance increase).

Finally, **Ref T.9** showed similar characteristics to Ref T.2 but its low nominal capacity is an important drawback. It would be necessary to arrange a large number of cells to meet the energy and power demands of the tramway, hindering the battery pack construction and control.

### 4.3 OVERVIEW OF THE METHODOLOGY IMPLEMENTATION

The developed cells selection methodology is an efficient process that enabled finding the best cell solution for the pursued application in a short period of time and with reduced experimental work. It allows battery preliminary selection with a testing time of approximately three months. However, it is worth mentioning some improvements towards optimising the proposed methodology.

#### 4.3.1 POWER CAPABILITY EVALUATION

Power capability and usable DOD range was evaluated under specific application conditions discharging and charging the cells continuously under defined profiles (power test under application conditions). OCV test or HPPC test also enable assessing cell power capability at different SOC, which can be estimated according to Eq. 4-5 and Eq. 4-6, where  $V_{\min.}$  &  $V_{\max.}$  stand for end-of-discharge voltage and maximum charging voltage, and  $IR_{DCH}$  &  $IR_{REGEN}$  are the discharge and regenerative internal resistances measured with the pulses method.

$$P_{DCH(MAX.)} = V_{\min.} \frac{(OCV - V_{\min.})}{IR_{DCH}} \quad Eq. 4-5$$

$$P_{REGEN(MAX.)} = V_{\max.} \frac{(V_{\max.} - OCV)}{IR_{REGEN}} \quad Eq. 4-6$$

From OCV and HPPC tests, regenerative and discharge DC internal resistance can be measured, either from discharge and charge steps for SOC transitions (OCV test) or with pulses method (HPPC test).

Aiming at evaluating the suitability of these tests to evaluate whether the cells could meet the application maximum traction and regenerative power demands, OCV tests were carried out at 25°C for the cells evaluated in the residential elevation application (test procedure is described in *Chapter 2*). The internal resistance was assessed from nominal charge and discharge steps of 15 seconds, and charge and discharge power profiles were assessed according to Eq. 4-5 and Eq. 4-6. Figure 4-30 shows power capability profiles and operating DOD ranges that would make possible meeting application discharge and regeneration power requirements (plotted in dotted lines). The estimated DOD operating windows were compared with the values obtained from power test under application conditions, as shown in Table 4-14. The results are very similar even though the OCV test underestimates slightly the usable DOD range for Ref 1. It establishes the lower limit at *ca.* 20% SOC, whereas it is *ca.* 7% according to the power test.

This difference may however be also related to experimental issues. Hence, similar usable DOD range estimations for different applications can be obtained from OCV and power test under application conditions. Likewise, this conclusion is also valid for HPPC test, as it provides equivalent results to OCV test, as previously mentioned, but more precise internal resistance measurements as voltage drops are enhanced using cell maximum current rates. Besides, if the cells are led to reach the equilibrium state with sufficient rest periods after the pulses at each SOC, cell OCV characteristics could be also assessed from HPPC test.

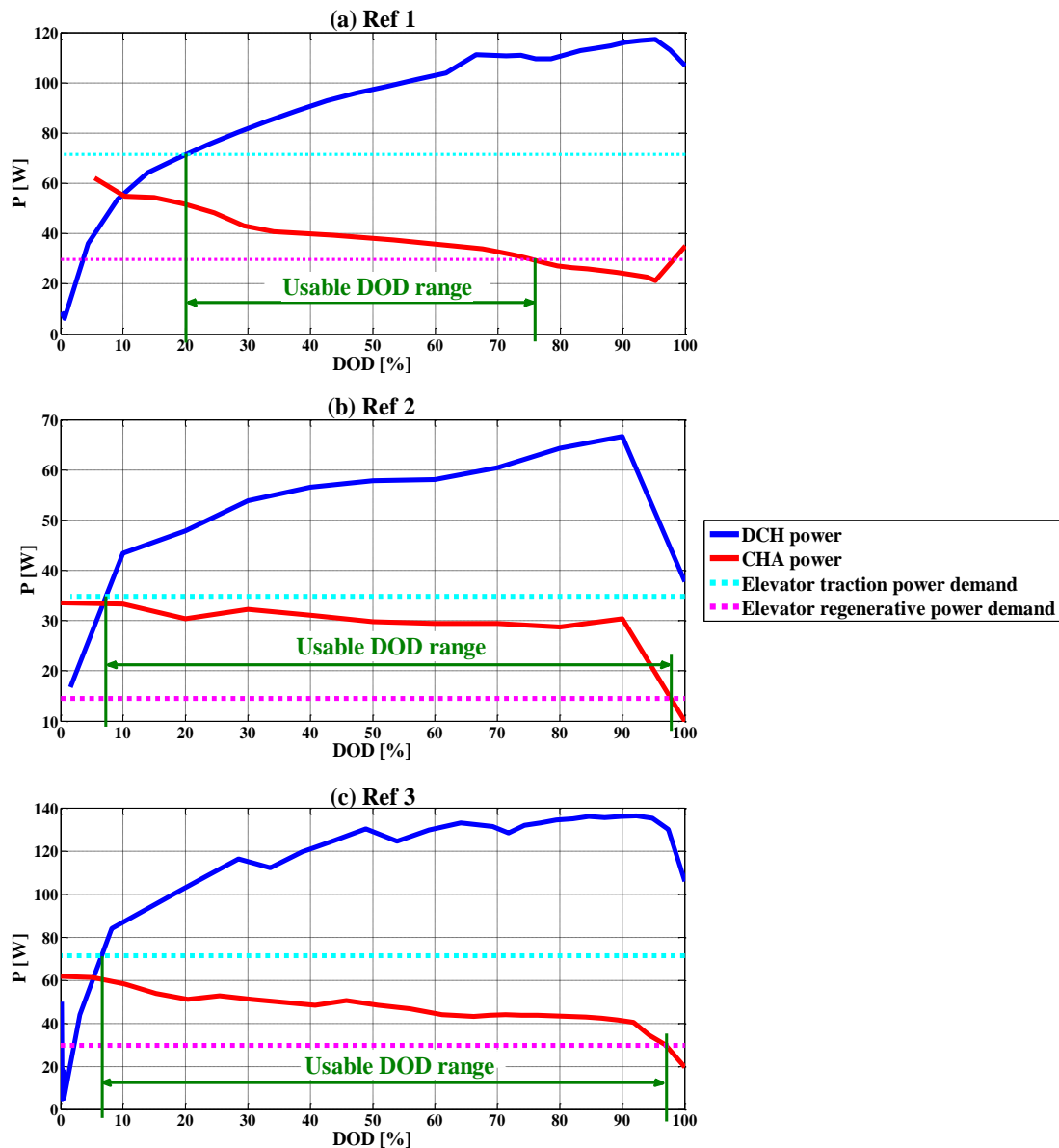


**Figure 4-30.** Power capability (P) of the three studied cell types at 25°C and usable DOD range to sustain residential elevation application discharge and regeneration requirements

**Table 4-14.** Comparison of the estimated operating DOD windows from power test under application conditions and OCV test

USABLE DOD RANGE [%]		
	Power test under application conditions	OCV test
Ref 1	7-79	20-76
Ref 2	5-97	8-98
Ref 3	3-95	7-97

In conclusion, a single HPPC test would provide information about cell OCV characteristics, internal resistance, power capability and usable DOD range. Hence, this test at different temperatures would provide the same information as through three/four tests (OCV test, internal resistance test and power test under application conditions). An specific internal resistance test was defined aiming at measuring the internal resistance at certain SOC, temperature and cell thermodynamic conditions (cell undergoes same electrical and thermal conditions during either charge or discharge previous to the charge or discharge pulses, respectively). However, in case of just comparative purposes, HPPC test could be useful for evaluating the internal resistance at reduced testing time. This way, Stage 2 for cells preselecting could be distinctly simplified depending on the pursued accuracy, which traduces in further time and costs saving, making the methodology more viable and effective.

#### 4.3.2 CELLS DISSASSEMBLING AND DESIGN ANALYSIS

The general post-mortem procedures defined in previous *Chapter 3* for cylindrical cells disassembling (section 3.3) can be applied to perform a comparative evaluation of cylindrical cells. It would enhance the criteria for battery cell selection. The main objective of introducing cells disassembling step within Stage 2 of cells selection methodology would be to gain insight about cell components and design parameters that can affect its performance.

Cells evaluated for the residential elevation application were opened and disassembled following the developed methodology. Figure 4-31 shows top and bottom parts and current collector tabs of the three opened cells. No mandrel is used for rolling any of the three cylindrical cells, as is typical for this type of construction. Ref 1 and Ref 3 in Figure 4-31 (a and c), respectively, are very similar in design. They employ several tabs along the length of both positive and negative electrodes. Ref 2 in Figure 4-31 (b) has a second negative lead instead of a mandrel; 2 tabs at both ends of the wind are used to connect the Cu current collector to the terminal. It has a single positive tab and it is not at the end of the wind but at the middle of the electrode. Several tabs along the length of electrodes may reduce the resistance associated with the current collection system during high C-rates. The internal

resistance results measured at 25°C (Figure 4-13) may be somehow related to this design issue (lithium diffusion processes may be less affected by temperature at 25°C than at low and high, 5°C and 45°C, temperatures). Ref 2 showed largest internal resistance values, and they were very similar for Ref 1 and Ref 3. However, active materials structure plays also an important role, that is enhanced as the cell ages (Figure 4-16).

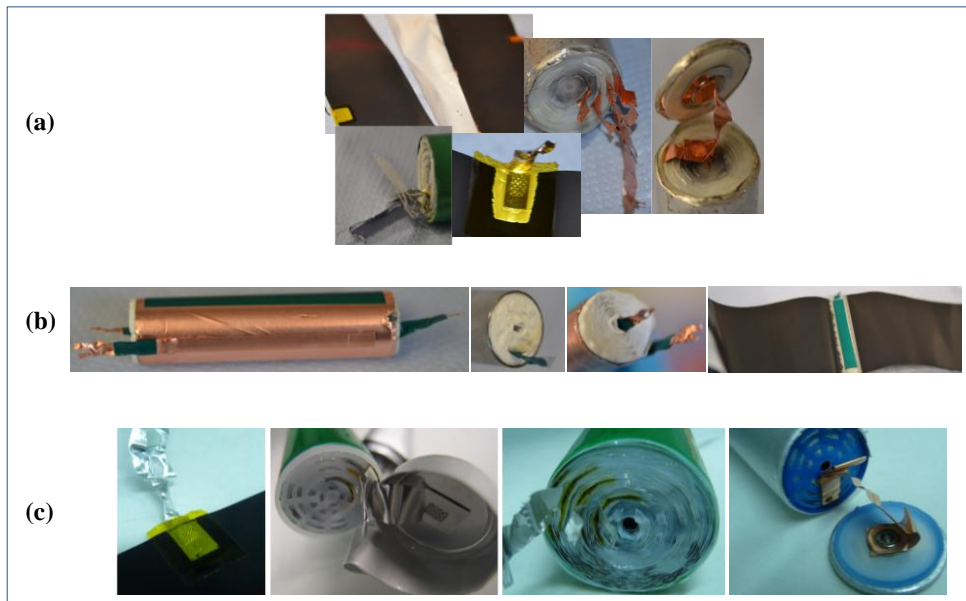


**Figure 4-31.** Opening of cylindrical cells from three different manufacturers. Cells analysed for the residential elevation application

Apart from electrical issues, another aspect to check is, for instance, the amount of electrolyte within the cell, which affects the conductivity. The outer part of Ref 2 jelly-roll was totally dry, whereas electrolyte was spilled out when Ref 1 and Ref 3 opening. Safety aspects are also important, and it attracted special attention that Ref 2 jelly-roll has no covering plastic (Figure 4-31 (b)). Its copper current collector is not protected. Finally, cell different parts materials proportion was evaluated and most relevant information is gathered in Table 4-15. Two Ref 2 cells would be necessary to obtain the capacity the other two 22650-type cells have, and the system weight would be similar (76.6 g). Negative electrodes mass proportions are similar for the three cells. However, Ref 1 has highest graphite active material volume, then Ref 2 (taking into account two cells) and Ref 3 the lowest. However, Ref 3 LFP active material volume is larger than for Ref 1. The coating thicknesses also vary from one cell to the other, and in the case of Ref 1 and Ref 3 cathode and anode coating thicknesses are not comparable. The structure of active materials may hence change significantly from one HP cell to the other.

Overall, in case these preliminary cells design analysis was conducted before the testing, Ref 1 might have been discarded beforehand. It implies doubling the number of cells in the battery pack and at first it shows not outstanding characteristics. What is more, the current collection

may be less efficient than in the other two systems; it has no electrolyte in excess, which may hinder cell performance, specially as it ages; and it seems to be less robust from the active materials packaging point of view.

**Table 4-15.** Comparison of main components of Ref 1, Ref 2 and Ref 3 HP LFP/graphite cells purchased for residential elevator application evaluation. Summary of the most representative cell internal characteristics

		<b>Ref 1 2.2 Ah</b>	<b>Ref 2 1.05 Ah</b>	<b>Ref 3 2.3 Ah</b>
CELL	Dimensions	22650	18650	22650
	Mass [g]	75.5	38.3	71.1
SEPARATOR	Total wt. [%]	6.5	5.4	5.9
	Total Length [mm]	3110	2805	3420
	Thickness [ $\mu\text{m}$ ]	22.0	20.0	15.0
ANODE	Electrode wt. [%]	29.5	29.9	29.1
	Electrode thickness [ $\mu\text{m}$ ]	93	55	75
	Cu thickness [ $\mu\text{m}$ ]	15.0	10.0	10.0
	Coating length [mm]	1820	1350	1583
CATHODE	Electrode wt. [%]	32.2	37.3	44.5
	Electrode Thickness [ $\mu\text{m}$ ]	137	87	170
	Al thickness [ $\mu\text{m}$ ]	25	25	15
	Coating length [mm]	1765	1295	1519

Applying post-mortem disassembly procedure at early stages of the selection process (Stage 2) may help to reduce the number of tests and analysis at later stages of the process. Other systems and applications should be evaluated to validate the relevance of these results.

In summary, the cells selection procedure was successfully implemented to two different industrial applications. Once the methodology has been validated for these specific applications, it is estimated that performing Stage 1 and Stage 2 for another application would take approximately 3 months.

# *Chapter 5*

## AGEING AND LIFETIME ANALYSIS

---

*This chapter deals with ageing and lifetime prognosis, a very important and complex aspect of Stage 3 of the cells selection methodology proposed in Chapter 3. The ageing and lifetime analysis is conducted from a novel perspective, trying to overcome specific needs identified during literature assessment of the state of art (evaluation of worldwide activity). The approach is taking from the development of procedures for both calendar (storage time) and cycling (operation) ageing modelling, and going even further and combining both regimes, analysing their interactions and validating the overall lifetime prognosis proposed. The validation steps are discussed in great detail, as one of the major contributions of this work.*



## 5. AGEING AND LIFETIME ANALYSIS

This chapter is dedicated to the detailed analysis of ageing and lifetime of the cell selected in *Chapter 4* for the elevation application, as part of Stage 3 implementation of the methodology defined in *Chapter 3*. This analysis is necessary for determining if the cell (or cells) preselected in previous stages will be able to fulfil the operation conditions and overall requirements of the application, and during the targeted lifetime. The proposed methodology for cells selection also covers, together with ageing and lifetime, other important aspects such as safety, costs and battery pack issues in Stage 3. The extent of the work presented in *Chapter 5* in perspective with the overall methodology is shown in red in Figure 5-1.

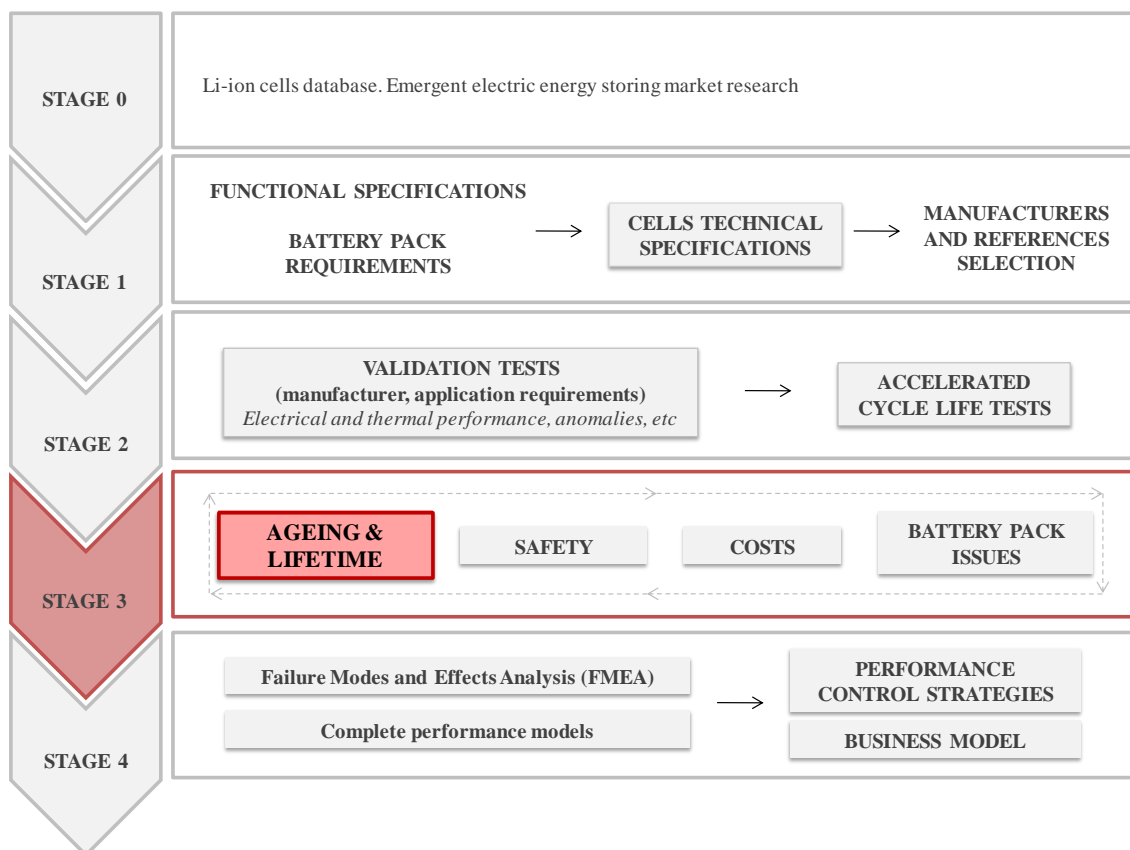


**Figure 5-1.** Cells selection methodology. Stages and main tasks with Ageing and Lifetime analysis highlighted within Stage 3, as main objective of this chapter

This Thesis work proposes a lifetime prognosis methodology that is explained in detail in the next sections. It was implemented for a commercial LFP/graphite 26650-type cell with 2.3 Ah nominal capacity (the cell chosen for the elevation application). LFP cathode based LIBs are, in general, of high interest for high power large scale applications because LFP active material [17, 100-107] possesses:

- Safe performance due to a high thermal stability.
- Low cost and toxicity compared to other cathodes, such as LCO.
- High specific power (LFP cathode has a theoretical capacity of  $170 \text{ mAh}\cdot\text{g}^{-1}$  and redox potential around 3.43 V vs. Li electrode [87]). It is therefore of interest for instance for HEVs, which require batteries to deliver and accept high-power pulses during vehicle acceleration and braking.
- High cycling capability due to stable olivine-type chemical structure.

Even though its low specific energy may be a drawback (*e.g.* for EVs, where the battery cannot be recharged by the generator when driving), it is one of the most capable Li-ion cell type considering safety and production cost [108]. However, the lifetime is still uncertain. LFP-based large size LIBs calendar ageing [51, 62, 87, 109, 110] and cycling ageing [51, 56, 62, 63, 67, 73, 90, 91, 96, 110-121] studies are various in the literature. Several of these research works took into account both calendar and cycling ageing [51, 62, 63, 110], but none of them applied a systematic stepwise multiple validation approach of the models, and this is the main focus of the methodology proposed in this chapter.

## 5.1 INTRODUCTION

Ageing analysis at cell level is one of the key issues for enhancing the integration of Li-ion technology based ESS solutions, as long useful life guarantee is required for target applications and battery lifetime is highly dependent on application conditions. Unfortunately, internal resistance rise and capacity fade of LIBs over calendar- and cycle-life are still a major barrier for novel stationary and transport applications. Automotive and main stationary applications require 10-20 years of calendar life, as shown in Table 5-1, which is still beyond the actual life of available LIBs. It is therefore necessary to study in detail this technology cycling and storage ageing processes and their causes for understanding capacity and power fade over time. A number of ageing processes take however place in parallel due to the complex operation conditions of most of the applications (*e.g.* combination of cycling, rest periods at different SOCs, incomplete charging, wide range of temperatures, etc.), and identifying the factors affecting the lifetime is difficult. One of the few applications that presents one dominant ageing process without no other influences is uninterruptible power supply (UPS) systems, which operate mainly under float charge conditions [122]. For majority of applications, the complex interaction between ageing processes and operating conditions must be analysed. A complete ageing analysis based on real operating conditions is therefore demanding [47, 99]. However, it is not feasible as non-accelerated tests are highly time and cost intensive. Precision of all lifetime predictions models is limited because not all impact factors are taken into account and the exact operating conditions cannot be predicted accurately. Besides, the intrinsic acceleration procedure sometimes affects ageing in a different manner to real operation. For example, small currents or even rest periods can impact on battery lifetime, but their effect investigation by accelerated testing can be a contradiction [122].

Quantitative concise algorithms for long-term operation performance predictions are a necessary tool for the system design. They will determine the optimal sizing of the battery pack for each application. At the same time, the lifetime models will determine the impact of operating conditions aiming at defining operating strategies for an efficient and reliable operation. System safety and economic viability are thus to be addressed. It is intended to develop a tool that can be implemented in different real applications and it is not just focused on either just cell ageing or testing specific end-user profiles that target a single specific application. On the other hand, there are several investigations which analyse separately battery cycling or storage behavior, as is summarised below (calendar ageing and cycling ageing subsections). In most cases, modelling steps do not check dynamic behaviour. However, an accurate lifetime predictive model implies not only understanding calendar and cycling ageing, but their interaction is of particular importance in response to real applications operation. Last, but not least, deep

analyses but simple are required at the same time, so that they can be implemented in real applications. Hence, the approach should be based on on-board measurable parameters. For these reasons, the applicability of precise physic-ageing models available in literature, such as the ones publishes by M. B. Pinsona and M. Z. Bazant [123] or E. Prada *et al.* [124], is largely limited. Moreover, industry might or not be willing to finance such a time demanding and hard computational work. What is important is to ensure that the outcome of lifetime assessment is directly related to benefits for the product development and final end use.

**Table 5-1.** General energy storage applications requirements (T & D: Transmission and distribution; ISO: Independent System Operator) [3]

Application	Description	Size	Duration	Cycles	Desired Lifetime
Wholesale Energy Services	Arbitrage	10-300 MW	2-10 hr	300-400/yr	15-20 yr
	Ancillary services <sup>2</sup>	See Note 2	See Note 2	See Note 2	See Note 2
	Frequency regulation	1-100 MW	15 min	>8000/yr	15 yr
	Spinning reserve	10-100 MW	1-5 hr		20 yr
Renewables Integration	Wind integration: ramp & voltage support	1-10 MW distributed 100-400 MW centralized	15 min	5000/yr 10,000 full energy cycles	20 yr
	Wind integration: off-peak storage	100-400 MW	5-10 hr	300-500/yr	20 yr
	Photovoltaic Integration: time shift, voltage sag, rapid demand support	1-2 MW	15 min-4 hr	>4000	15 yr
Stationary T&D Support	Urban and rural T&D deferral. Also ISO congestion mgt.	10-100 MW	2-6 hr	300-500/yr	15-20 yr
Transportable T&D Support	Urban and rural T&D deferral. Also ISO congestion mgt.	1-10 MW	2-6 hr	300-500/yr	15-20 yr
Distributed Energy Storage Systems (DESS)	Utility-sponsored; on utility side of meter, feeder line, substation. 75-85% ac-ac efficient.	25-200 kW 1-phase 25-75 kW 3-phase Small footprint	2-4 hr	100-150/yr	10-15 yr
C&I Power Quality	Provide solutions to avoid voltage sags and momentary outages.	50-500 kW	<15 min	<50/yr	10 yr
		1000 kW	>15 min		
C&I Power Reliability	Provide UPS bridge to backup power, outage ride-through.	50-1000 kW	4-10 hr	<50/yr	10 yr
C&I Energy Management	Reduce energy costs, increase reliability. Size varies by market segment.	50-1000 kW Small footprint	3-4 hr	400-1500/yr	15 yr
		1 MW	4-6 hr		
Home Energy Management	Efficiency, cost-savings	2-5 kW Small footprint	2-4 hr	150-400/yr	10-15 yr
Home Backup	Reliability	2-5 kW Small footprint	2-4 hr	150-400/yr	10-15 yr

1. Size, duration, and cycle assumptions are based on EPRI's generalized performance specifications and requirements for each application, and are for the purposes of broad comparison only. Data may vary greatly based on specific situations, applications, site selection, business environment, etc.  
2. Ancillary services encompass many market functions, such as black start capability and ramping services, that have a wide range of characteristics and requirements.

There are numerous worldwide activities in the field of battery ageing analysis, modelling and lifetime prediction, which are approached from a wide range of perspectives. The following sections overview these activities and groups them into major degradation causes, that is, cycling operation (cycle life) and standby or storage mode (calendar life). A third section describes the overall lifetime prediction literature revision and starts highlighting the origin of the ageing and lifetime approach proposed in this chapter work.

- **Calendar ageing**

The storage ageing represents an important factor, taking into account that, for instance, a personal car spends about 90-95% of its lifetime in storage mode when parked [109, 125] or that most UPS are only used a few minutes over their lifetime, just when the mains power fail. Hence, investigating cell degradation in the course of the time in storage mode, which is the definition for calendar life in the present work, is of high importance for many applications.

There are several calendar ageing studies in the literature [49-66, 78, 83, 86, 87, 98, 99, 109, 110, 121, 125-149] for different LIB technologies based mainly on: NCM ( $\text{LiNiCoMnO}_2$ ), NCM-LMO ( $\text{LiMn}_2\text{O}_4$ ), NMO ( $\text{Li}(\text{NiMn})_2\text{O}_4$ ), LFP ( $\text{LiFePO}_4$ ), LCO ( $\text{LiCoO}_2$ ), LNCO ( $\text{LiNiCoO}_2$ ) and NCA ( $\text{LiNiCoAlO}_2$ ). Standing period (t), State of Charge (SOC) and temperature (T) are the main factors that affect the calendar lifetime and charge retention of the battery. Degradation processes not only depend on storage conditions but also strongly on electrolyte and electrodes active materials [88, 150, 151]. Table 5-2 shows a literature review of main calendar ageing analyses on several LIB technologies (physical approaches are out of scope and this survey is focused on commercial and prototype batteries). Some authors [98, 126, 127, 132, 133, 136] studied both calendar and cycling individually and compared the corresponding ageing results under similar SOC and T conditions.

**Table 5-2.** Overall calendar lifetime prediction worldwide activity

Type of analysis		Reference
Non-destructive electrical and/or electrochemical characterisation, sometimes including fitting		[52, 55, 58, 59, 62-65, 83, 86, 87, 98, 99, 109, 110, 121, 125-130, 132-149]
Post-mortem analysis		[49-66]
- Understanding of impact factors effect - Studying ageing phenomena		[57, 78, 87, 110, 132, 133, 140, 144, 149]
Dynamic behaviour analysis	Cell voltage	[132]
	Temperature. Model validation	[109]

- **Cycling ageing**

As mentioned earlier, the properties of batteries change with conditions of use (cycle life). There are some applications that require high cycling capability of batteries. The demand on the battery system in a heavy-duty HEV is different compared to a passenger car, since buses and distribution trucks are generally used between ten and fifteen hours per day all year around with high power demands in challenging duty cycles [152, 153]. The challenges are to find a way to cycle the battery system under optimal conditions and, at the same time, save as much fuel as possible. There are also stationary applications which battery would be mainly cycling over time, such as the grid system applications for transmission voltage and frequency regulation to utilities, customers and society.

There are several cycling ageing studies in the literature [47, 51-53, 56, 60-65, 67-78, 91, 95-99, 110, 112-121, 127-129, 132, 133, 136, 139-144, 148, 149, 154-173] for different LIB technologies based mainly on: NCM, LMO, NCM-LMO, NMO, LFP, LCO, LNCO and NCA with graphite as anode; and NCM/LTO (titanate anode). Table 5-3 shows a literature review of main cycling ageing analysis on several LIB technologies (physical approaches are out of scope and this survey is focused on commercial and prototype batteries).

**Table 5-3. Overall cycling lifetime prediction worldwide activity**

<b>Type of analysis</b>	<b>Reference</b>
Non-destructive electrical and/or electrochemical characterisation, sometimes including fitting	[47, 52, 57, 62-65, 67-71, 74-77, 91, 95-99, 110, 112-121, 127-129, 132, 133, 136, 139-143, 148, 149, 154-172]
Post-mortem analysis	[51-53, 56, 60-62, 64, 65, 67-78]
- Understanding of impact factors effect - Studying ageing phenomena	[57, 63, 67, 78, 91, 96, 110, 112, 114, 115, 133, 140, 144, 149, 154, 155, 157, 158, 165, 173]

Some authors analysed cycle life under specific dynamic application conditions and most of them were focused on vehicle operation [95, 115, 116, 157, 163]. S. Peterson *et al.* [116] evaluated differences between dynamic discharge (representing the driving) and constant discharge (energy arbitrage) using statistical analyses. T. M. Bandhauer *et al.* [174] also checked dynamic power profiles apart from constant current tests, but aiming at analysing thermal behaviour. Some studies went a step further away and, in addition to cycling, they analysed: (i) safety issues by means of abuse tests [175], (ii) financial costs associated to different types of cycling [116], (iii) a methodology for factors coupling [117], among others.

- **Lifetime prognosis approach**

Lifetime prognosis is a crucial requirement for successful and reliable integration of the battery into the application requiring an energy storage solution. Ageing tests under real operating conditions are time and cost intensive; accelerated tests are, however, powerful but limited as they can alter and hinder the real cell degradation due to their accelerator factor itself. For this reason, a compromise is needed and models are necessary to be able to perform estimations and extrapolations out of the range of the analysed conditions for modelling, in order to predict the battery lifetime and possible integration into an application. Several model approaches for lifetime predictions reported in the literature are briefly described below.

M. Ecker *et al.* [99] validated the calendar ageing model under static cycling operation, aiming at verifying whether the developed model would be able to predict cycling ageing. They also combined the calendar semi-empirical approach with impedance-based electro-thermal model for a complete lifetime model and checked a realistic current profile for HEV. J. Schmalstieg *et al.* [148] used the calendar and cycling ageing studies to develop a holistic ageing model. Their overall model validation was based on different realistic driving profiles and temperatures. D. Stroe *et al.* [176] showed a methodology for lifetime prediction. They did not either include calendar and cycling single model validation steps and they proposed an application specific mission profile to verify the overall lifetime model. S. Onori *et al.* [173] analysed ageing combining cycling and calendar under specific PHEV profiles. H. Wenzl *et al.* [177] analysed the ageing under complex conditions of use and showed a methodology for ageing prediction at dynamic conditions. Other authors [143, 178-181] used the method of effects weighing (superposition) for degradation analysis.

This work proposes a methodology for lifetime prognosis that comprises both cycling and calendar ageing but also their interaction in depth analysis that suits different applications. The main overall objective of this work includes the development of validation procedures for both ageing types models and the analysis of the applicability of the methodology [182]. The validation process not only consisted in additional tests under other constant operating conditions (static validation), but also under non-constant impact factors operating schemes (dynamic validation), as battery stress conditions in real applications are barely constant and models need to be extrapolated to any arbitrary real profile, which mostly combines several conditions at once. So far, most of the ageing model validations are just based on either static impact factors evaluation [147, 183] or specific application profiles evaluation. It is therefore demanded developing predictive tools that enable evaluating the degradation under different non-constant stress levels operating conditions [109, 147, 184].

All these premises for lifetime prognosis evaluation, including applications requirements and techno-economic viability of the proposed approach, are gathered in Figure 5-2 and constitutes the pillar for this work. That means that the models and predictions developed here should be able to be adapted to any application; should be based on direct measurable parameters and simple models; should be able to predict battery behaviour under cycling and storage conditions and include dynamic operation which approaches real operation conditions.

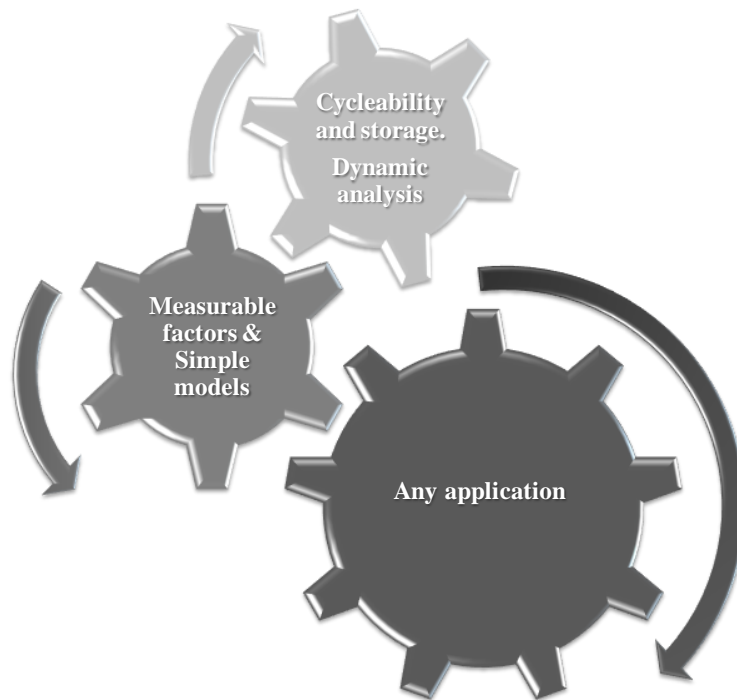


*Figure 5-2. Motivation for lifetime prediction methodology development*

In this sense, taking into account the reasons discussed above and gathered in Figure 5-2, it is pursued a methodology for battery cell useful life analysis that enables lifetime predictive accurate models:

- with low cost. A compromise between the accuracy of the models and time-intensive experimental work (and computational effort) need to be reached.
- that can be implemented in real applications.
- that are scalable (potentially extensible to different operating scenarios and systems).

It is aimed at comprehensively providing useful life analysis that covers both ageing by storage and ageing by working operation (*i.e.* cycling). Besides, the model ought to be able to simulate real operation and it should have broad applicability, being the methodology suitable for either any technology or application.

## 5.2 LIFETIME PREDICTION METHODOLOGY

Figure 5-3 depicts the approach proposed in this work for the ageing model development. A novel methodology for useful lifetime optimisation is proposed which starts with the premise that the ageing model ought to be valid to any real condition and is to be developed based on the analysis of all controllable causes affecting ageing, *i.e.* stress or impact factors: SOC, T, time, DOD, C-rate and Ah-throughput (or number of cycles, N). Their contribution to cell performance has to be simulated in order to control the battery operation and thus the costs (effective ageing). Hence, it is required measuring cells capacity loss ( $Q_{\text{loss}}$ ) and internal resistance (IR) increase, as a mean to quantify loss in dynamic current capability (*i.e.* power fade) and relaxation ability over time. Thus, capacity and internal resistance are to be the ageing metrics for cell performance degradation tracking. Ageing by just storage and ageing by working operation, that is to say, mechanically induced ageing due to volume changes and consequent instability of material, are to be separated and studied individually. Additionally, key calendar and cycling ageing impact factors are to be separated in order to parameterise derived single semi-empirical relationships based on static experimental analysis. Calendar ageing ( $A_{\text{cal}}$ ) is to be analysed at different temperatures (T) and SOC (Eq. 5-1) and cycle ageing ( $A_{\text{cyc}}$ ) as a function of C-rate and DOD (Eq. 5-2). Ageing model is to be developed using a stress factors time-domain and Ah-throughput-domain characterisation method, by capturing the dominant effects on cell performance degradation for fitting each single testing parameter. Effects weighing method is used for battery complete degradation analysis in accordance with the assumption made by other authors [143, 178-181, 185]. This method accepts, as shown in Figure 5-4, that storage and cycling ageing effects can be superimposed and that the effect of SOC and T is the same during storage and operation, and so their effect is taken into account in the calendar ageing model. This approach allows simulating realistic dynamic cell operation for a given system ( $A_{\text{TOTAL}}$ ) through the combination of single calendar and cycling ageing models (Eq. 5-3). This way, cycle ageing can be also predicted under different T and SOC conditions.

$$A_{\text{cal}} = f(\text{SOC}, T, t) \quad \text{Eq. 5-1}$$

$$A_{\text{cyc}} = f(\text{DOD}, \text{C-rate}, \text{Ah-throughput}) \quad \text{Eq. 5-2}$$

$$A_{\text{TOTAL}} = A_{\text{cal}} + A_{\text{cyc}} = f(\text{SOC}, T, t, \text{DOD}, \text{C-rate}, \text{Ah}) \quad \text{Eq. 5-3}$$

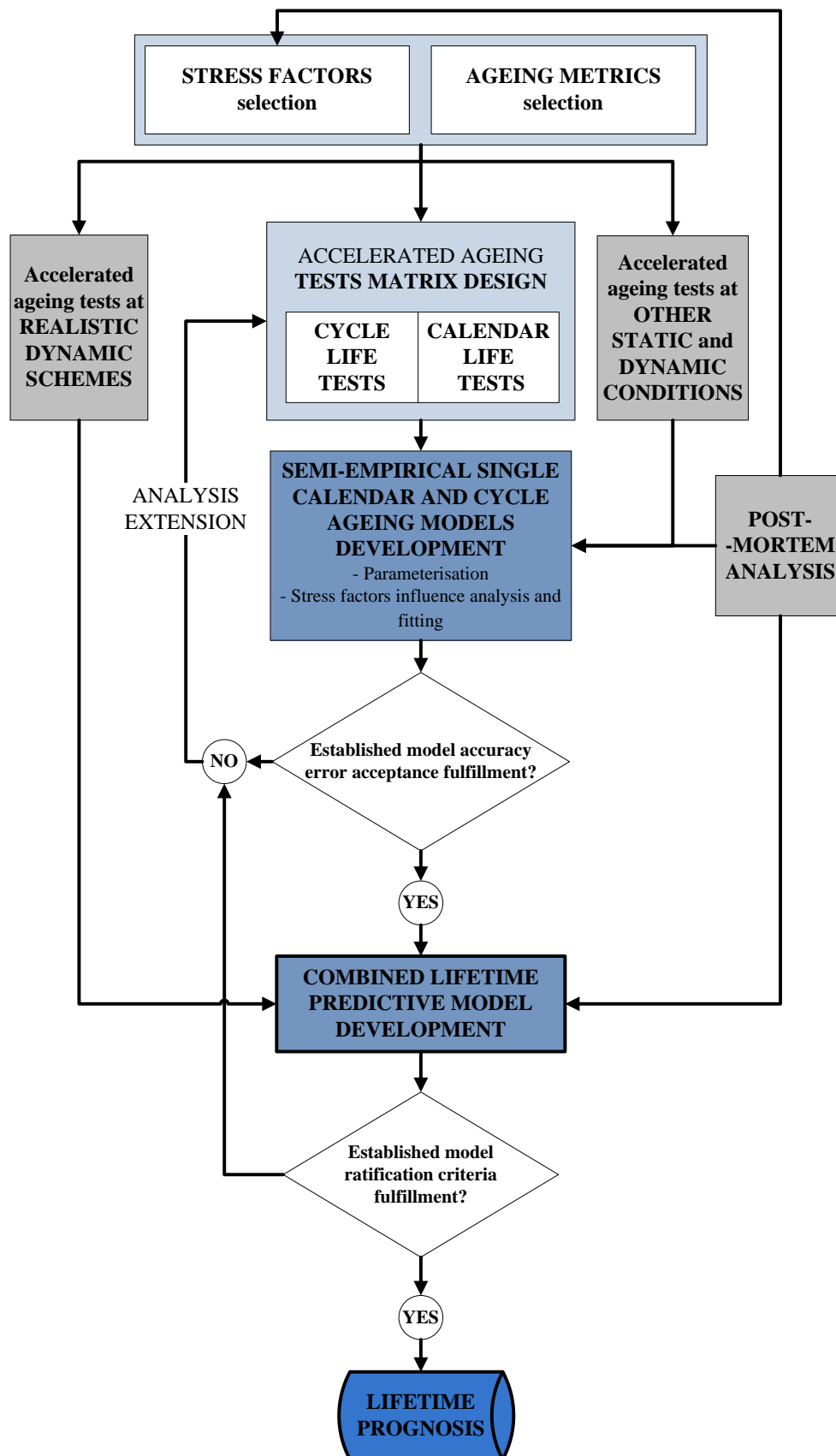
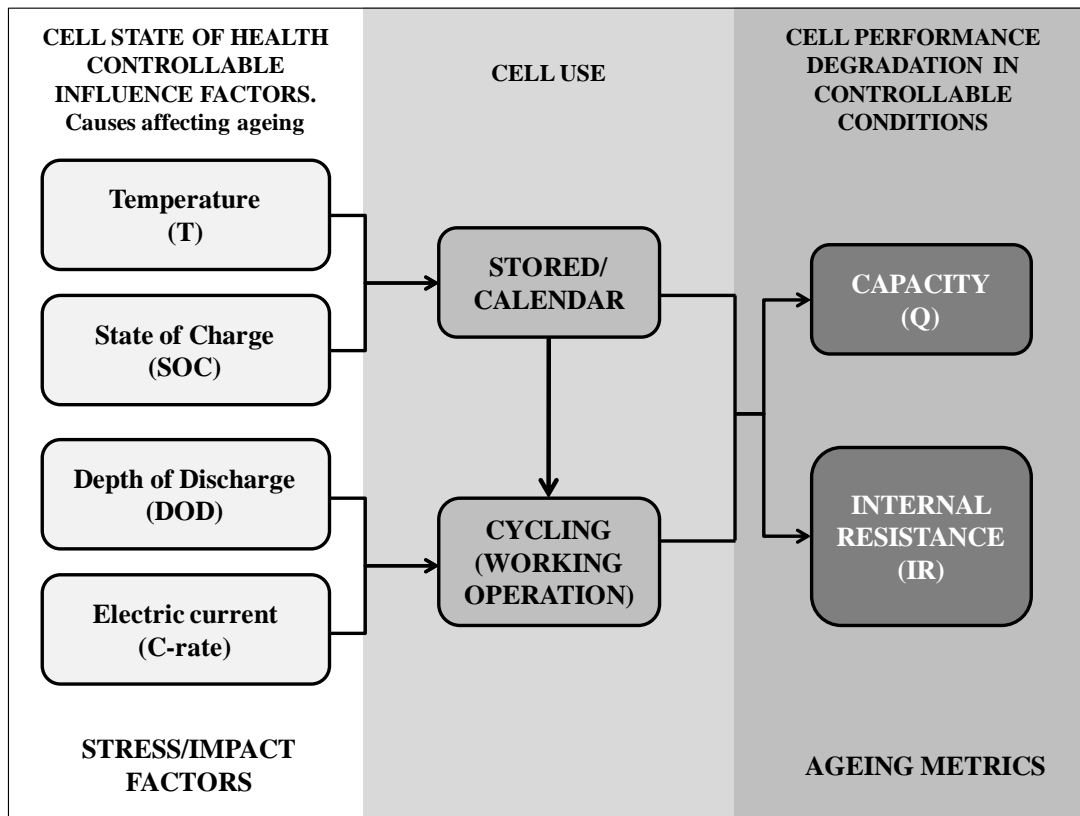


Figure 5-3. Methodology for lifetime prognosis (validation procedures in grey)



**Figure 5-4.** Controllable factors including changes in cell performance (both while working operation and standing time) when it comes to the battery capacity and internal resistance. Individualisation of stress factors for their effects weighing. This approach pursues to combine calendar and cycling ageing effects to predict cycle ageing at different T and SOC conditions and also to simulate realistic cell complex operation

Main impact factors of Li-ion degradation and main mechanisms are summarised in Table 5-4 (see also Table A-13 in Appendix E). The main ageing mechanisms of Li-ion batteries are Loss of Lithium Inventory (LLI) and Loss of Active Material (LAM), which imply consumption of active materials that result in irreversible capacity loss and internal resistance increase [17]. Li-ion cells deterioration depends on the type of active materials, manufacturing process, load conditioning and cell design. Parasitic decomposition reactions of both anode and cathode active materials with electrolyte at electrodes interfaces dominate ageing processes. LLI in batteries with graphite anode mainly arises from the reduction of electrolyte at anode surface that forms of Solid Electrolyte Interface (SEI) layer. Parasitic reactions also lead to Solid Permeable Interface (SPI) formation and organic solvents oxidation on cathode surface. The graphite anode is, however, the most critical electrode because, as shown in Figure 1-6, it is not within the electrochemical stability window of the most common organic electrolytes [17]. Growth of SEI layer due to lithium oxidation on the negative electrode not only results in irreversible capacity loss, but it also increases the electrode impedance, *i.e.* loss of electrical contact within the porous electrode [110], which is directly related to power fade of the cell [86, 150], and also may cause lithium plating (see Figure A-25 in Appendix E). LAM is

mainly a result of structural damage and material loss related to dendrite formation that may increase self-discharge (short circuit risk), particle isolation, crystals growth (reduction of the effective area), electrodes volume changes, electrode delamination, etc. [22, 110, 169]. These effects are specially relevant when graphite is used as anode [96]. Exfoliation and particle cracking due to solvent co-intercalation and electrolyte reduction inside graphite sometimes accompanied with gas evolution would lead to rapid negative electrode deterioration [150]. LAM can also mean material, *e.g.* Fe ions, dissolution, but LFP cathodes are not normally subjected to such ageing phenomenon. Hence, analysing the graphite anode crystalline microstructure, surface and morphology is of great importance as they influence directly the cell performance. While cycling generally damages the materials reversibility, the main ageing phenomena during storage are widely caused by interactions between electrolyte and active materials interface [49, 87, 110, 169]. Reaction rates during cell operation are on an overall view affected by SOC and temperature. Cell performance can change dramatically with temperature and it affects ageing as a long-term effect. According to N. Omar [186], particularly the impact of temperature has a great influence on the battery behaviour during acceleration and regenerative braking events. Discharge rate is the major variable that reduces day to day effective capacity while the battery is in use [18]. Other typical reported ageing effects, related to non active components, are: electrodes binder decomposition; current collector corrosion; separator melting and corrosion; etc.

**Table 5-4. Ageing: effects and causes (compilation from [4])**

<b>AGEING EFFECTS</b>	<b>AGEING CAUSES -degradation mechanisms-</b>	<b>ACCELERATED BY MANY IMPACT FACTORS</b>
<i>Capacity loss (loss of active material, loss of lithium)</i>	<ul style="list-style-type: none"> <li>• Intercalation of solvent</li> <li>• Delamination of graphite</li> <li>• Cracking</li> </ul>	Very high SOC (overcharging)
	Loss of contact active mass particles due to volume change	High C-rate, high DOD
<i>Capacity and power capability loss</i>	<ul style="list-style-type: none"> <li>• Decomposition of electrolyte (cathodic oxidation/anodic reduction)</li> <li>• Dissolution of binder</li> </ul>	High T, high SOC
	<ul style="list-style-type: none"> <li>• Deposition of metallic lithium</li> <li>• Formation of SEI</li> </ul>	High T, high C-rate, bad cells design
<i>Growth of impedance, power capability loss</i>	<ul style="list-style-type: none"> <li>• Growth of SEI</li> <li>• Change of surface porosity</li> </ul>	High C-rate, high DOD
	Decrease of active surface (continuous growth of SEI)	High T, high SOC
	Corrosion of conductor	Low SOC, deep discharge

The most extended End of Life (EOL) criteria, normally for EVs, is defined as when actual nominal capacity is 80% when normalised to initial value [187, 188] or initial internal resistance increases by a factor of two [132]. This criterion is not even defined clearly for other types of

applications. However, these definitions do not necessarily match with the cell performance degradation point where it is no longer usable in its intended application. It is therefore difficult to define the End of Test (EOT) beforehand (at BOL), as it will depend on many specific cell operation conditions. For these reasons, EOL is not included as a performance metric in the protocol and EOT in turn depends on each experiment.

Validation procedures for ageing models in depth analysis were defined. As it is beyond the scope of this lifetime prognosis approach the execution of large-scale experimental work, the goodness of the defined methodology and overall results lie on the validation process that comprises five steps: post mortem analysis, static validation, dynamic validation, analysis approaching real operation and realistic profiles evaluation.

- *Post-mortem analysis* gives physical evidence of the induced ageing effects, which makes possible identifying temporal correlation between performance fade and degradation mechanisms. It is essential to understand ageing modes in order to establish a clear evolution of battery life (*i.e.* to develop precise long-term lifetime prediction algorithms based on short-term cell test data).
- *Static validation.* Developed single (cycling and calendar) models (Eq. 5-1 and Eq. 5-2) need to be checked in other conditions different from the ones used for the modelling process, so additional tests at constant impact factors profiles are necessary. This validation under constant stress conditions informs about the goodness of the developed algorithms within ranges for the considered impact factors. However, in real applications, stress conditions are far from being constant over time.
- *Dynamic validation* of each single (cycling and calendar) model (Eq. 5-1 and Eq. 5-2) is also necessary, as stress factors are not constant for batteries operating in real applications. Hence, it is of high importance to carry out tests changing, within the same test, the impact factors that are under investigation in each case. This dynamic validation evaluates the model capability to adjust to dynamic impact factors operating schemes and simulations precision. Moreover, the effect of changing the sequences of events on ageing may be observed.
- *Overall model dynamic validation (approaching real operation).* The next step is trying to simulate the reality, combining different storage and operating profile periods over time (Eq. 5-3). This model validation aims at checking whether it is possible making realistic predictions analysing beforehand individually calendar and cycling ageing effects. Additionally, this step enables evaluating the hypothesis of SOC and T effects on cycling

when running cells at different temperatures, and also including several middle cycling SOC<sub>s</sub> during different cell charging-discharging periods between random storage intervals.

- *Validation using realistic profiles.* The last task is to evaluate whether the model is useful for simulating real applications operation, and predict the ageing. This way, useful battery life is to be investigated under real conditions.

Overall, as summarised in Figure 5-5, the process for batteries lifetime optimisation is:

- Individualisation and investigation of the battery stress factors for their effects weighing.
- Battery ageing single (cycling and calendar) models development.
- Thorough validation of the cycling and calendar ageing models.
- Combined (overall) battery ageing model development and thorough validation.

The last step would be the useful life analysis and the implementation of the model to meet the pursued goal (e.g. battery pack sizing, TCO estimation, integration of the ageing model in the BMS together with the electrical and thermal performance models, etc.).

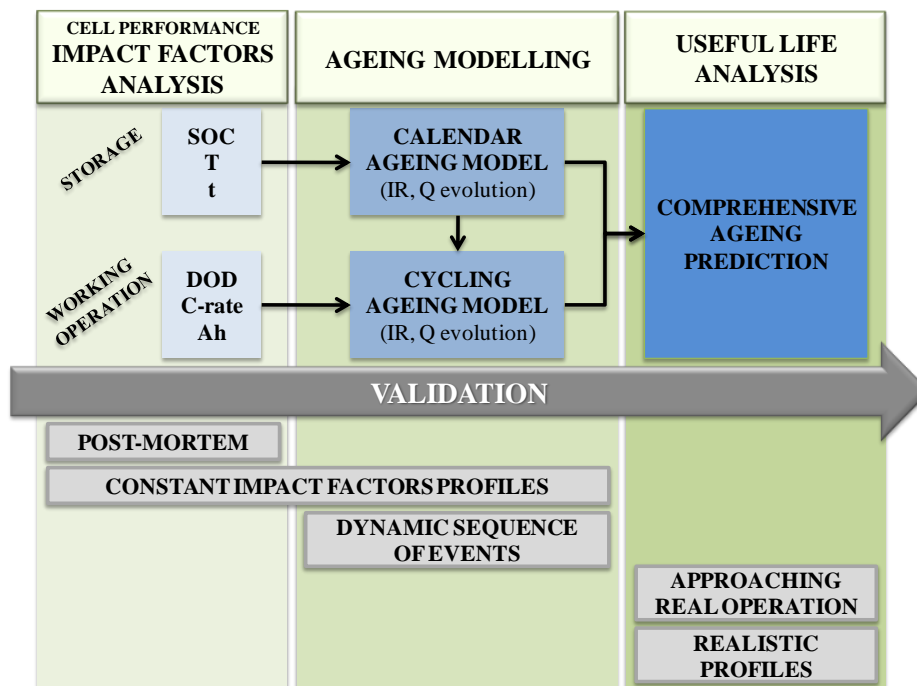


Figure 5-5. Chronological scheme of the proposed overall process for lifetime prognosis

At first, it is pursued the lifetime prognosis for a given system, applicable to any real condition. A further step is the application to other chemical battery systems. This methodology enables analysing not only overall lifetime issues, but also individual calendar and cycling ageing.

### 5.3 CALENDAR LIFETIME

As part of a comprehensive lifetime analysis procedure, this section aims specifically at studying cell performance degradation under different temperature and SOC storage conditions and developing a thoroughly validated semi-empirical calendar ageing predictive model. After reviewing the state of the art, this calendar ageing analysis enhances the results by adding further steps of dynamic validation. The process defined for calendar lifetime analysis is shown in Figure 5-6. The present investigation work covers the steps within the shadowed area. Thus, predictions were performed comparing with experimental data upon storage under variable environment T and/or SOC conditions on the same cells over time (dynamic validation). Finally, the calendar-life performance of the investigated LFP-based cell was also evaluated in a real UPS application.

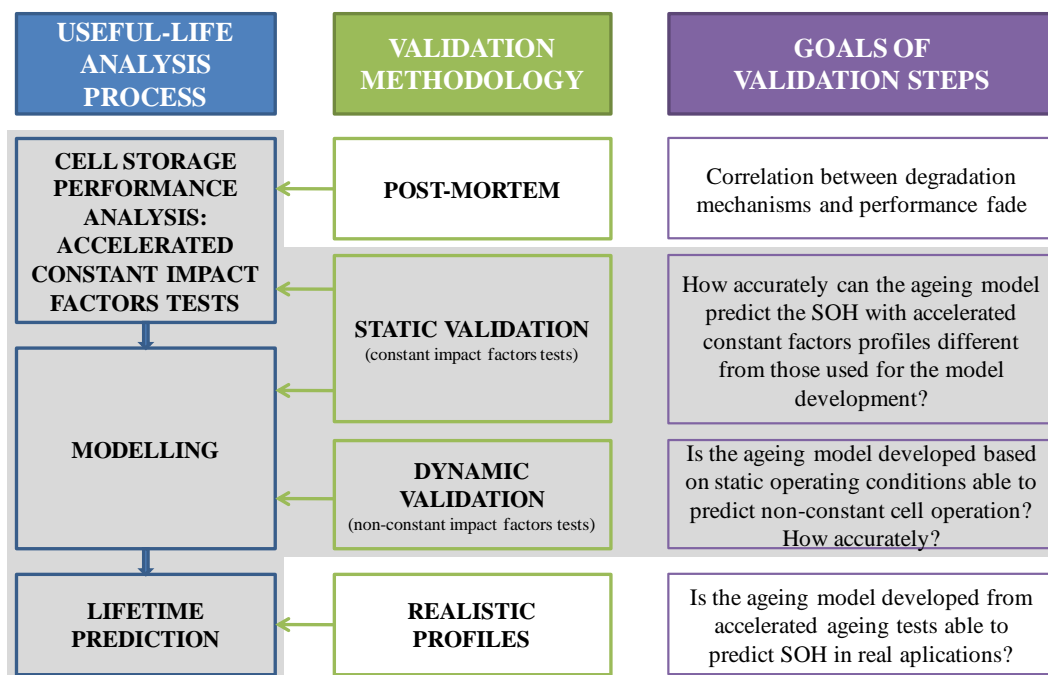


Figure 5-6. Methodology for calendar lifetime prognosis. In grey, activities carried out within this work

#### 5.3.1 EXPERIMENTAL

Single-factorial variation storage experiments were carried out using 26650-type LFP-based cells of the same manufacturing batch with 2.3 Ah nominal capacity and 3.3 V nominal voltage. For each storage test a single cell was used, since:

- The cells reproducibility assessment at the Beginning of Life (BOL) using 74 cells indicated that the true population mean nominal capacity falls within  $2.313 \pm 0.005$  Ah range with 95% certainty.

- In the previous study using the same reference it was measured that the average coefficient of variation upon cycling ageing was just 6% using 3 cells per condition (accelerated ageing test in Chapter 4 -Stage 2 of cells selection for the residential application-). Even lower variation is expected during storage.

The ageing tests were performed in a temperature-controlled environment. CTS and Prebatem climatic chambers were used with this purpose (Appendix C). The periodical check-up (CU) experiments were carried out using Digatron multiple cell tester with data acquisition BTS-600 software (Appendix C). Electrochemical Impedance Spectroscopy (EIS) measurements were conducted using Digatron EISmeter Impedance Spectroscope.

Experimental procedures are described in *Chapter 2*. Both capacity loss and internal resistance increase were measured in order to evaluate cell SOH over time and parameterise battery ageing model. Intermittent Electrical Parameters Identification Tests (EPIT), which were carefully planned so that their impact on cell degradation was as negligible as possible, consisted on:

- *Actual nominal capacity (Q) test*, described in *Chapter 2*.
- *Close to equilibrium Open Circuit Voltage (quasi-OCV) measurement test*, described in *Chapter 2*.
- *Actual Direct Current (DC) internal resistance measurement by HPPC test*: current pulses at cell maximum acceptable charge and discharge C-rates over cell 90-20% SOC range with 10% DOD intervals.

Additionally, both BOL and cell further characterisation tests at EOT included, as highlighted in purple in Figure 5-7:

- *EIS measurements*, as described in *Chapter 2*, at 30% and 70% cell SOC. This test was also included occasionally in EPIT. According to Q.C.Zhuang *et al.* [189], EIS technique is one of the most promising methods for ageing mechanisms investigation for Li-ion batteries (used in automotive applications).
- *Rate capability tests*, as described in *Chapter 2*. The charging and the discharging C-rates were 3C and 6.5C, respectively at 5, 25 and 45°C.

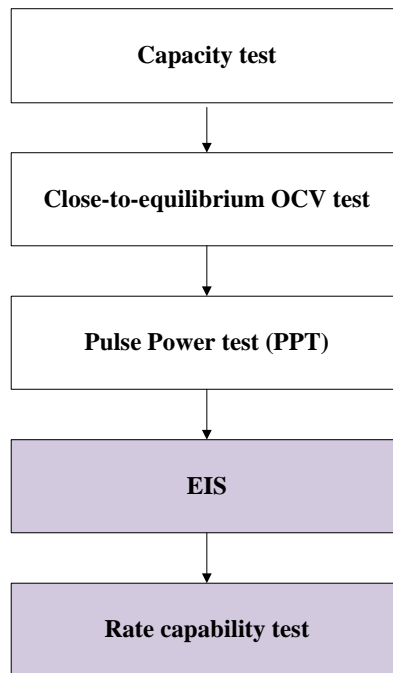


*Figure 5-7. Initial and final cell calendar ageing characterisation*

### 5.3.1.1 ACCELERATED CALENDAR AGEING TESTS CONDITIONS

#### 5.3.1.1.1 CALENDAR AGEING AND STATIC VALIDATION TESTS

Calendar ageing was initially investigated at several but constant T and SOC storage conditions over time on the same cell, as shown in Table 5-5. Five different storage conditions were used for calendar ageing model development and an additional one at 50°C and 90% SOC for the static validation (shaded in Table 5-5). Range limits for the tested external influence factors were chosen within the cell operation window set by the manufacturer. Nonetheless, outer limits were not checked since a real-life application may not operate in such conditions. Ageing tests were carried out correcting the values of set SOC parameter according to cell actual capacity after every EPIT. Cells were stored at open circuit (OC) in order that reversible capacity loss rates could be evaluated as a function of impact factor levels, storing period and accumulated irreversible capacity fade. Even though OC storage mode could in principle imply a drawback for ageing predictive models development, other authors reported that self-discharge is of minor importance below 100% SOC [132]. Even though this latter ageing study was of a NCM-based LIB, self-discharge of Li-ion cells is mostly due to delithiation of graphite and Solid Electrolyte Interface (SEI) formation at graphite surface [190].

**Table 5-5.** Test matrix for calendar ageing modelling (static validation highlighted in grey)

T [°C]	SOC [%]		
	30	70	90
30		X	
40	X	X	X
50		X	X

**5.3.1.1.2 DYNAMIC VALIDATION STORAGE TESTS**

Additional tests under variable environment temperature and/or SOC conditions within each cell were carried out aiming at the validation of the calendar ageing model under different stress levels operating conditions. The tested four operating schemes with non-constant impact factors are shown in Figure 5-8. Temperature was made dynamic upon storage for three of them and SOC in one of the tests (in red).

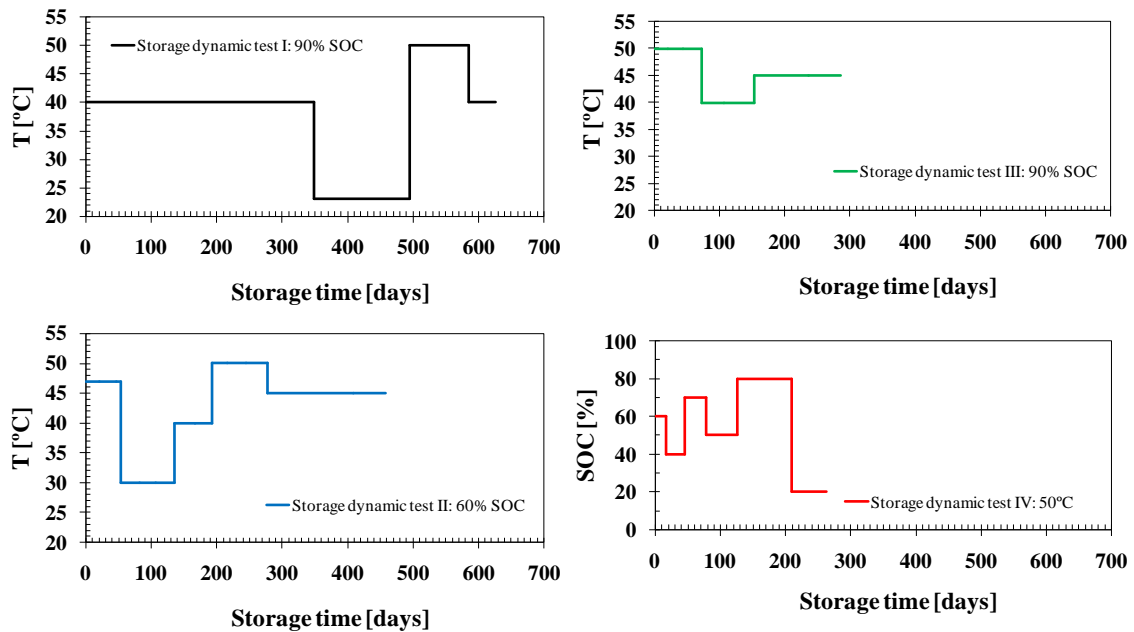


**Figure 5-8.** Dynamic storage tests. Dynamic T and SOC profiles over time

### 5.3.2 RESULTS AND DISCUSSIONS

The results from calendar ageing tests were used to understand cells behaviour upon different storage conditions and to develop a comprehensive calendar lifetime predictive model. Main evaluated parameters are discussed in the following section.

#### 5.3.2.1 CELL CALENDAR PERFORMANCE FADE EVALUATION

- **Analysis of ageing results**

The measured average nominal capacity of all the cells used for storage tests was  $2.331 \pm 0.014$  Ah (95% confidence interval, CI) at the BOL. Charging/discharging voltage responses at different ageing stages were analysed aiming at identifying the contributions of irreversible capacity loss and internal resistance increase. Figure 5-9 shows the charge-discharge curves at 1C and 25°C after similar storage periods under different conditions (Table 5-5). Similarly to reported in [87] for the same cell chemistry, it was observed that calendar-life is more affected by elevated temperature than by SOC (*i.e.* capacity fade increases faster with storage temperature compared with SOC). In general, there is a shift in discharge curves to lower actual capacity values as time increases. The length of the plateau part is shortened, which indicates capacity loss due to loss of active lithium (LLI) [112]. The voltage plateau, which corresponds to the nominal voltage of the cell, was slightly shifted to lower voltages as the cells aged. This is a consequence of the internal resistance increase [67, 112]. Additionally, the duration of CC charge mode time decreased with storage. The SOH of the studied LFP/graphite cell is apparently directly connected with the available active lithium inventory even after large storing periods. Hence, it may be deduced that the main cause of ageing was the decomposition of the electrolyte and the resulting growth of SEI layer due to deposition of decomposition products on graphite anode surface. Additionally, at 50°C and 70% SOC, unlike for the other studied conditions, the contribution of internal resistance factor is more marked after *ca.* 19 months of storage. Hence, the ohmic resistance and charge transfer resistance may have become larger at such high temperature, confirming that electrolyte decomposition is mainly influenced by the temperature [191]. The former internal resistance increase contribution may indicate electrolyte degradation and the latter the progressive increase of the thickness of the passivating layer.

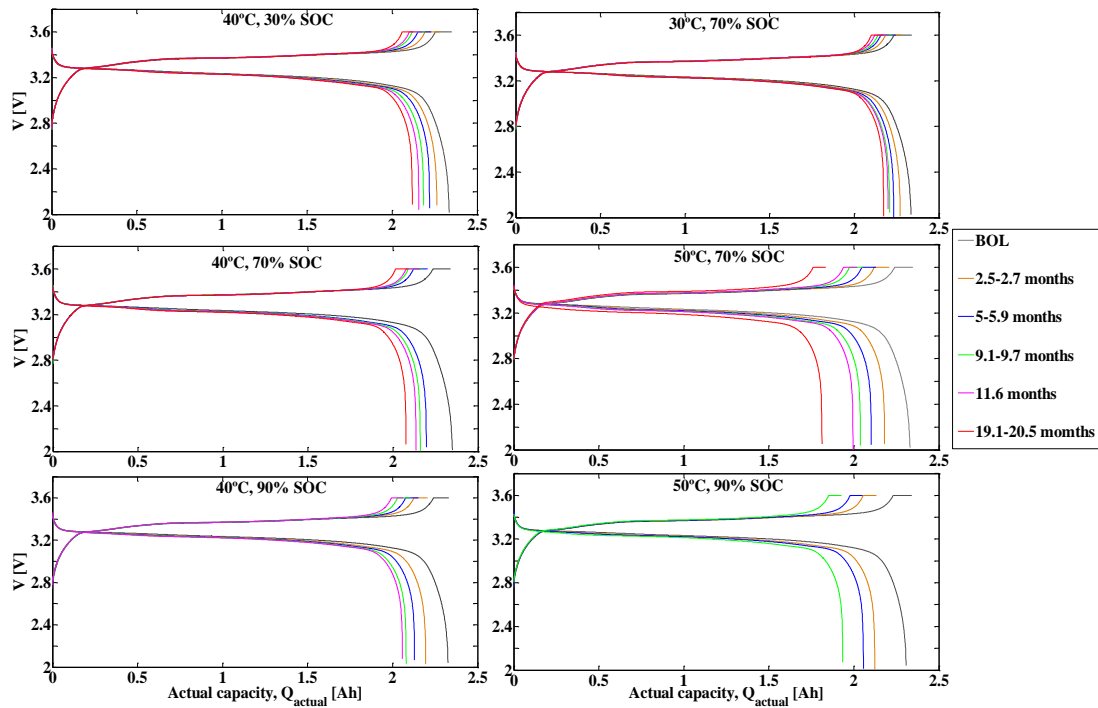


**Figure 5-9.** Charge-discharge curves at 1C and 25°C for the different ageing stages of the cells stored at different SOC and T conditions. Charge-discharge profiles from nominal capacity measurements

Figure 5-10 shows DC internal resistance increase and nominal capacity loss over time during different cell storing conditions, which are represented according to the most extended criteria for the End of Life (EOL) in the literature, *i.e.* 80% SOH (Q) and 200% SOH (IR). That is to say, the measured capacity loss was adjusted to the common scale of the EOL by translating 20% capacity loss to 100% scale so that both ageing metrics could be compared within the useful lifetime of the cell. Area in red in Figure 5-10 represents cell state over this EOL definition. DC internal resistance change evolution during discharge at 50% SOC (17 s pulse) is just used for evaluating cell power performance fade, because, as shown in Figure 5-11 for a couple of tests as example, the measured internal resistance change trend was similar regardless of DC internal resistance testing procedure (HPPC test) (*i.e.* the reference SOC (Figure 5-11 (a)) and charge or discharge current step (Figure 5-11 (b))). The moderate increase of total resistance suggests that bulk transport properties are almost unchanged over storage (absence of structural degradation) [87]. According to [112, 192], if the battery impedance does not increase rapidly compared to capacity loss, the battery behaviour is stable with temperature. However, during 50°C storage (70% SOC), both capacity loss and internal resistance increase evolutions were altered clearly after approximately 500 days of storage ( $Q_{loss}$  tendency change cannot be observed in Figure 5-10 as the measured values were larger than 20%  $Q_{loss}$ ). M. Kassem *et al.* [87] also observed from impedance spectra analysis of a LFP/graphite cylindrical cell that the overall cell resistance strongly depends on storage temperature and that

there is not clear influence of the storage SOC values. Internal resistance increase data in Figure 5-10 agree with the reported observations, but the influence of large SOC level (Figure 5-12 (b)) indicates need of further investigation of this stress factor effect on internal resistance increase.

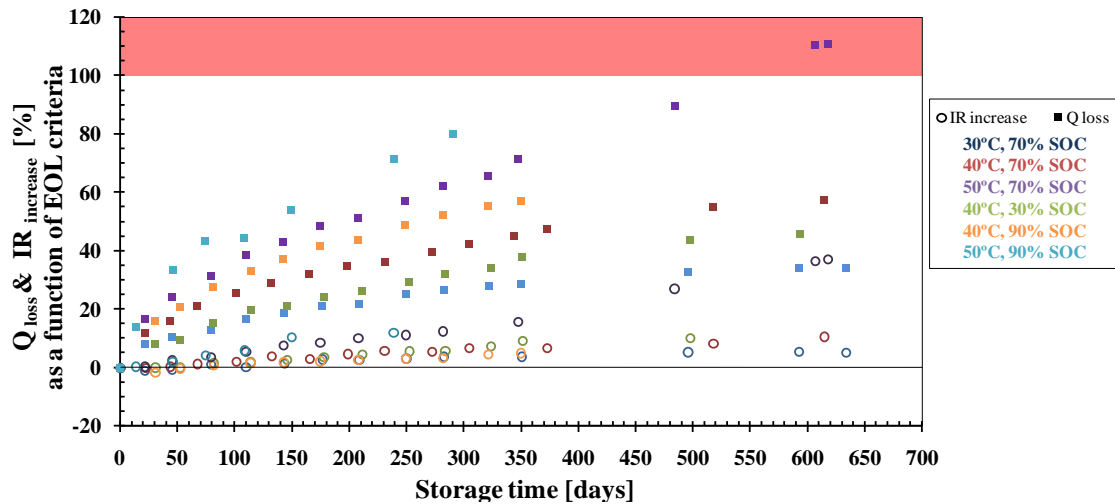


Figure 5-10. DC internal resistance increase ( $IR_{increase}$ ) and nominal capacity loss ( $Q_{loss}$ ) adjusted to EOL scale over time (both nominal  $Q$  and  $IR$  were normalised to initial values).  $IR$  measurement by means of 17 s discharge pulse at 10C at 50% cell SOC

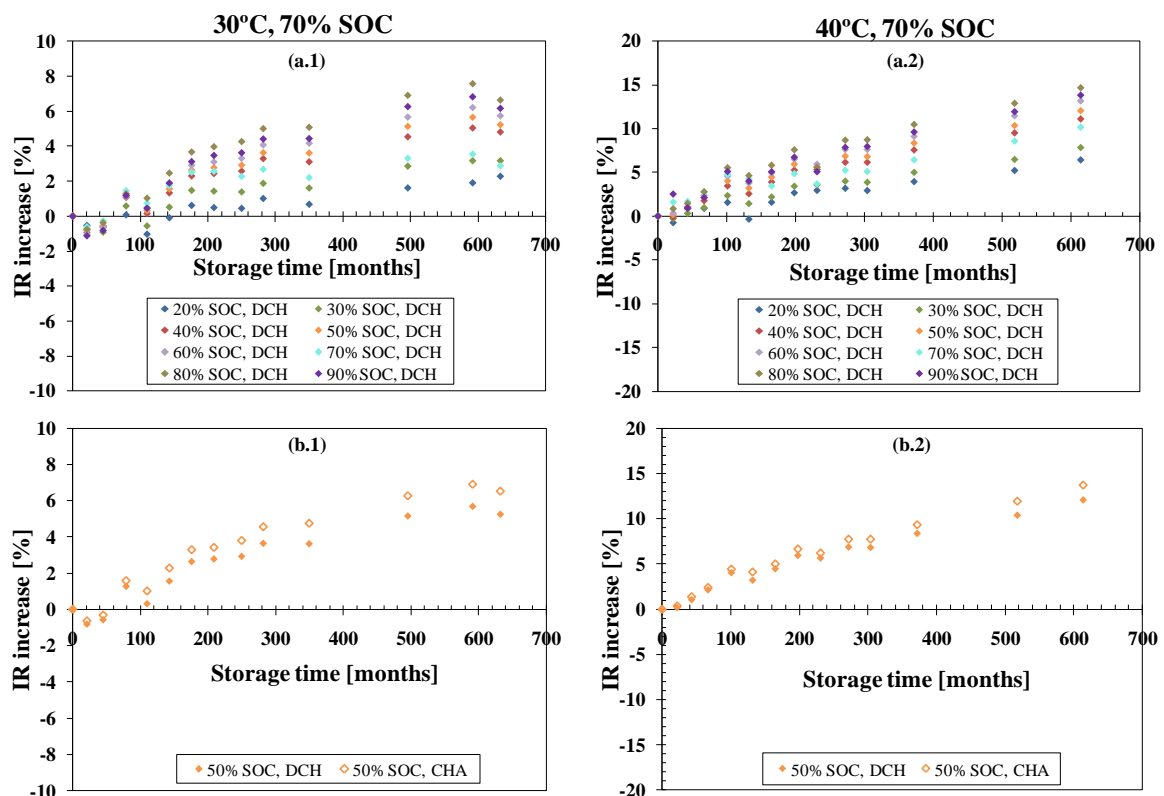
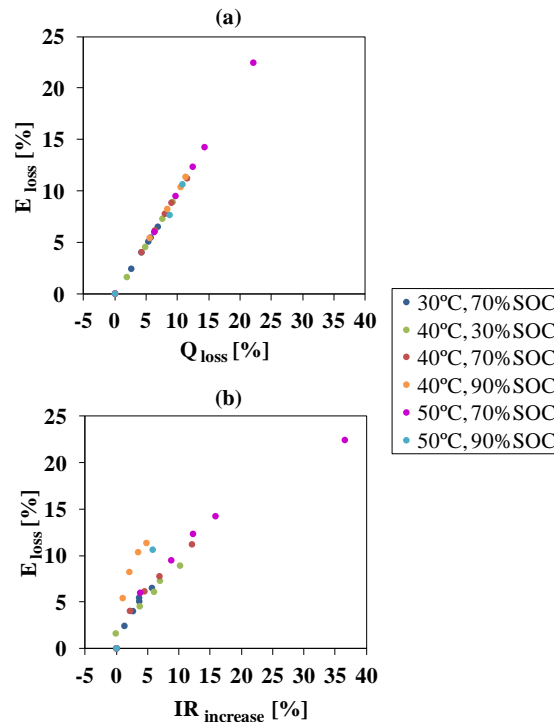


Figure 5-11. Current pulse EPIT results over storage time. (a) DC internal resistance ( $IR$ ) increase during discharge as a function of 17 s current pulse (10C) applying cell SOC. (b) DC  $IR$  increase during charge and discharge at 50% SOC. (a.1 and b.1) storage at 30°C and 70% SOC; and (a.2. and b.2) storage at 40°C and 70% SOC

In order to further check the contribution of capacity loss and impedance change on cell performance fade, their relationship with cell energy loss was examined. Figure 5-12 shows cell energy loss ( $E_{loss}$ ) as a function of capacity fade ( $Q_{loss}$ ) and internal resistance increase ( $IR_{increase}$ ) under different storage conditions (experimental data in Figure 5-12 correspond to the storage times shown in Figure 5-9).  $E_{loss}$  was assessed from nominal capacity tests, referring to the total energy that the cell can provide, normalised to each cell initial energy withdrawn values.  $Q_{loss}$  and  $IR_{increase}$  were also normalised to initial values. An unexpected slight initial decrease of internal resistance was observed (Figure 5-12 (b)), in agreement with other studies with similar cells [90, 110]. For the rest, even after 11-12 months of storage and an energy loss in the range of 10-15%, internal resistance just increased *ca.* 15%. Energy loss, however, fitted proportionally with capacity loss. As described in Eq. 5-4 with 95% CI, they show practically linear behaviour, as also validated for 50°C and 90% SOC storing condition. Hence, the contribution of internal resistance change to energy loss was not significant, regardless its larger impact at high storing SOC (specially at 90%). All in all, Figure 5-9, Figure 5-10 and Figure 5-12 showed that the investigated LFP-based cell was aged primarily due to capacity fade rather than power fade, as also reported by other authors [67, 90, 110]. The slight internal resistance increase (more likely due to SEI layer growth) may not have had influence on capacity loss, as the voltage drop of discharge profiles upon ageing was almost negligible (Figure 5-9).



**Figure 5-12.** Relationship between energy loss ( $E_{loss}$ ) and nominal capacity loss ( $Q_{loss}$ ) (a), energy loss and internal resistance increase ( $IR_{increase}$ ) (b) at different storage conditions over time ( $E$ ,  $Q$  and  $IR$  were normalised to initial values).  $IR$  measurement by means of 17 s discharge pulse at 10C at 50% cell SOC

$$E_{\text{loss}} = (0.97 \pm 0.02) \cdot Q_{\text{loss}}$$

Eq. 5-4

The influence of internal resistance on cell performance was also evaluated by means of charge-discharge rate capability tests at different temperatures at BOL and after different ageing conditions at the EOT. Figure 5-13 aims at evaluating cells rate capability at different SOH due to the storage at different temperatures during the same period of time. Hence, the results corresponding to cells that were stored at 30°C, 40°C and 50°C for *ca.* 21 months are discussed, with a SOH, referred to capacity, of 93%, 88.5% and 77.9%, respectively (actual nominal capacity normalised to the nominal capacity at BOL). Figure 5-13 represents for the selected aged specimens and BOL condition, as reference: (i) the charged capacity at 3C in CC mode (Figure 5-13 (a)) and discharge capacity at 6.5C (Figure 5-13 (b)), both normalised to cell actual nominal capacity (at 1C) (coloured areas), (ii) the charging time in CC mode under different conditions (Figure 5-13 (a)), and (iii) the cell surface temperature total change during charge and discharge measured with Type K thermocouples in each case (line of columns and right axis of abscissas) in both figures. Operating capacity data at 45°C is not shown in Figure 5-13 (b) because the outcomes were not comparable, as all the tested specimens could not be fully discharged (up to the cut-off voltage) due to large surface temperature increase above the maximum temperature safety limit. Operating capacity data, in percentage, already show changes in cell current dependency upon polarisation effects.

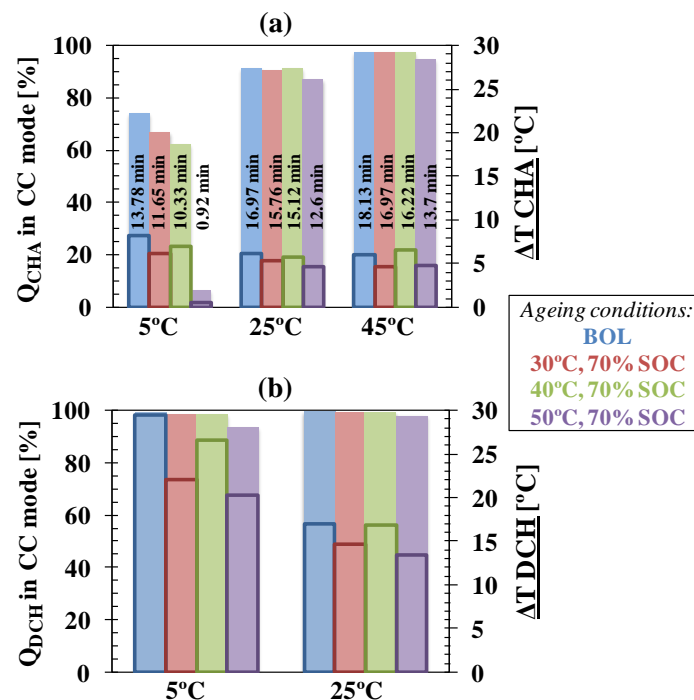


Figure 5-13. Charge and discharge rate capability ( $Q_{\text{CHA}}$  and  $Q_{\text{DCH}}$ , coloured areas) and cell surface temperature change ( $\Delta T$ , line of columns) on charge at 3C (a) and discharge at 6C (b) at different temperatures at BOL and after storage under different temperature conditions during *ca.* 20 months. Constant Current (CC) charging time is indicated for each condition in (a)

The ambient temperature had a significant influence on cell regenerative operation (Figure 5-13 (a)). At 25°C, there was virtually no change in the charging capability among the BOL cell and the aged cells stored at 30 and 40°C. The retention of charge rate capability suggests a negligible increase of cell resistance upon storage, as demonstrated above. The difference between initial state and after ageing at 50°C was very small, the Ampere-hours that the cell could accept just reduced 2.8%. The influence of this cell internal resistance increase on charge capability was not apparently large, as the increase of cell charging percentage was not particularly enhanced, in all cases *ca.* 8%, from 25 to 45°C ambient temperature testing even though elevated temperature favours rate of lithium intercalation-deintercalation kinetics. At 5°C with slow Li-ion diffusion, the operating voltage range was reduced and, therefore, the more aged the cell, the less charge the cell could accept. The temperature change on the most aged cell was so small because it was hardly charged. According to S. S. Zhang *et al.* [85], poor low temperature performance might be related to low lithium diffusivity and high charge-transfer resistance of delithiated graphite upon charging. The ionic conductivity of electrolyte and SEI layer on graphite surface may be especially reduced in the case of the cell that had been stored at 50°C. Hence, its poor regenerative performance at low temperature may be the consequence of high electric polarisation.

At 6.5C current load and 25°C discharge conditions (Figure 5-13 (b)), it was possible to withdraw almost the total Ampere-hours charged in cells that had been stored at 30 and 40°C (99-99.5%). The cell aged at 50°C provided just 1.5% less capacity than the BOL cell reference. The thermal behaviour was similar in all cases because of the lower discharge times to reach the cut-off voltage (the stored capacity was 7%, 11.5% and 22.1% lower for the cells stored at 30, 40 and 50°C, respectively, than BOL cell). The rate capability on discharge might have been maintained due to significant LLI. Lower lithium intercalation into the graphite anode restricts the operation window of LFP electrode (loading mismatch between positive and negative electrode, *i.e.* "reservoir effect"). At lower maximum lithium stoichiometry, the rate capability of the cell is larger [96, 110]. The results demonstrated that at room temperature the discharged capacity barely depends on the C-rate (discharge at 1C and 6.5C was almost equal). At 5°C, cells that had been stored at 30 and 40°C underwent a slight decrease of 0.9-1% in discharged capacity when compared to BOL cell, whereas the difference increased up to 5.9% for the cell that was stored at 50°C. Its charge transfer resistance may have increased and electronic and ionic conductivity modified. The suffered polarisation was remarkably higher in the discharged state of the cell. Charging of a discharged Li-ion battery is more difficult than discharging a charged battery at low temperature [85].

Overall, Figure 5-9, Figure 5-12, Figure 5-10 and Figure 5-13 demonstrate that there was negligible increase of cell resistance upon storage, LLI was dominant ageing phenomenon and LFP electrode might not be degraded. In the case of 50°C and 70% SOC storage condition, after prolonged storage time the LLI was not any more stable (indicating ageing processes modification).

- **Self-discharge**

Total capacity loss of cells stored at OC was evaluated, meaning both irreversible capacity loss and cell reversible capacity loss, as side reactions also lead to self-discharge of the cell. Reversible capacity loss (self-discharge) was analysed for each storage period between EPITs, whereas irreversible capacity loss was considered accumulative over time. Figure 5-14 presents the corresponding results for the different storage conditions (comparative reversible and irreversible capacity loss data). The self-discharge rate is expected to evolve with ageing [126]. However, the reversible capacity loss was approximately constant regardless the irreversible capacity loss increase over time, although it changed depending on storing time step duration ( $\Delta t$ ). It was initially larger than after overall prolonged storing time. The effect of storing temperature and SOC on reversible capacity loss, as shown in Figure 5-15, was also assessed. Self-discharge rate increased with storing SOC (Figure 5-15 (a)). Higher SOC resulted in lowering the anode potential, which causes electrochemical instability on electrolyte material. Intercalated lithium in lithiated graphite tends to diffuse to the edges where it may interact with solvent components [193]. There was no clear temperature dependency on cell reversible capacity loss (Figure 5-15 (b)), even though it is recommended storing batteries below room temperature (ideally 15°C) because of low self-discharge rates and slow ageing processes. On the contrary, both stress factors (SOC and T) effects were appreciable on irreversible capacity loss. The higher both SOC and T, the larger the capacity fade upon storage (Figure 5-14). After ca. 10 months of storage, at 40°C, the irreversible capacity loss was 6.4%, 8% and 10.5% at 30%, 70% and 90% SOC, respectively. At 70% SOC, capacity decreased by 5.3%, 8% and 12.4% at 30°C, 40°C and 50°C, respectively.

The demonstrated low self-discharge rate was related to the stable SEI layer growth (Figure 5-10, before the ageing rate increased at 50°C and 70% SOC), as electrolyte solvents that enable the formation of such surface films cause less self-discharge that is initiated at the negative electrode. Negligible and constant self-discharge indicates that the ageing model based on OC storage mode tests data is as valid as the one based on charge sustaining (CS) mode tests, as assumed when defining the experimental conditions.

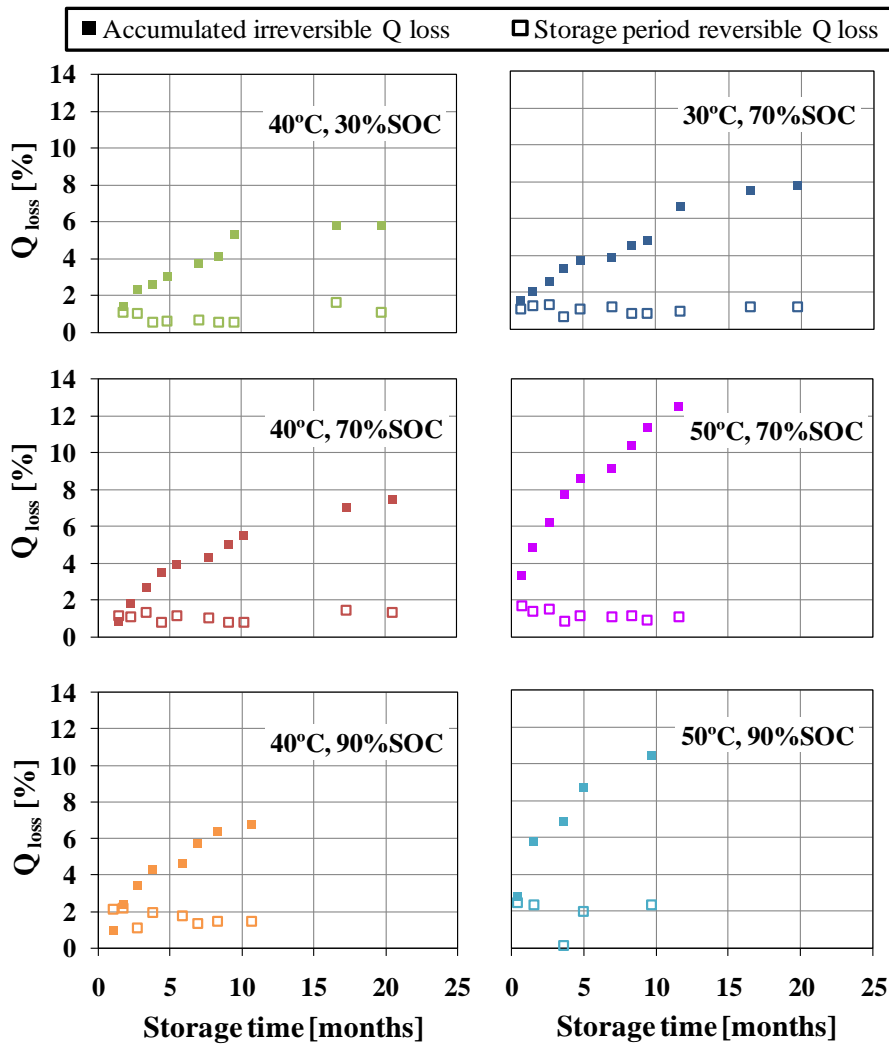


Figure 5-14. Reversible time step capacity loss and accumulated capacity loss (both normalised to initial nominal values) of the cells stored at different OC conditions assessed from the nominal capacity test

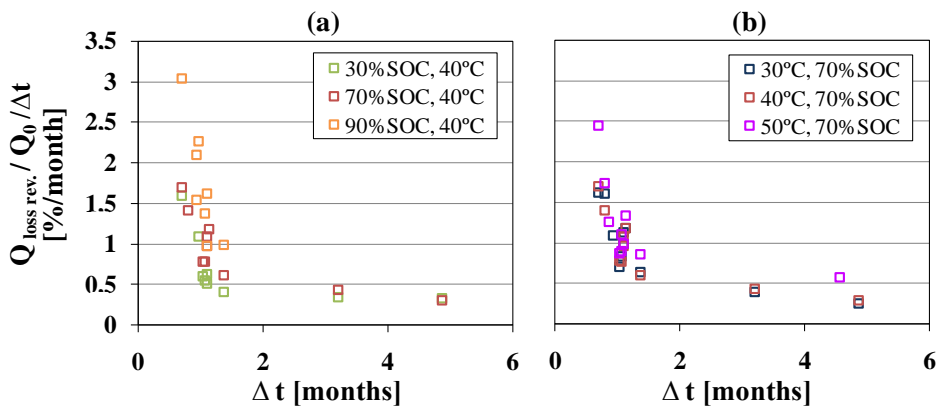
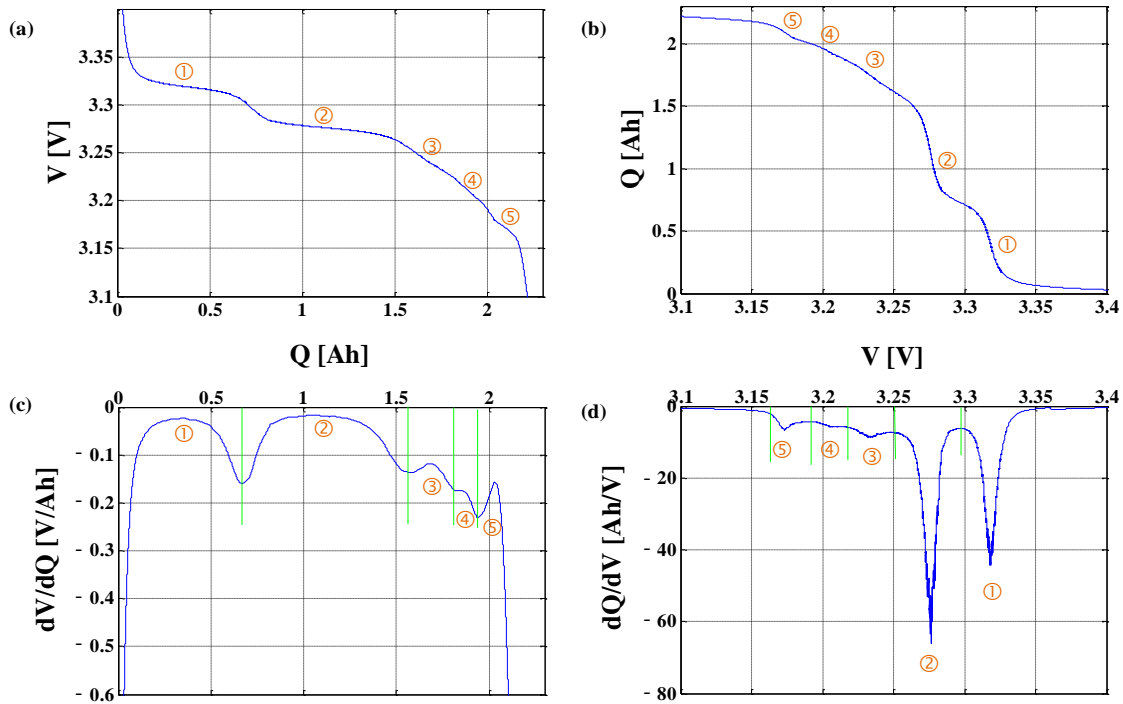


Figure 5-15. The influence of SOC (a) and T (b) on cell self-discharge during OC storage. Reversible capacity loss rate (normalised to initial nominal capacity,  $Q_0$ ) depending on storing time interval duration ( $\Delta t$ )

- **Analysis of ageing mechanisms**

Voltage profiles at different ageing stages and rate capability results indicated that LLI was induced over different storage conditions. LLI degradation mechanism is the result of cell imbalance [109] due to different lithium consumption rate at negative and positive electrode as consequence of reduction of electrolyte and lithium oxidation at the anode surface. At high temperature (50°C, 70% SOC), not only was irreversible capacity loss measured, but also internal resistance increase (slight drop of voltage plateau in Figure 5-9 and internal resistance increase change in Figure 5-10), which may also be the consequence of the growth of the ionic conductive SEI passivation layer that contains complex electrochemically inactive products [86, 150].

Analysis of incremental capacity (IC) and differential voltage (DV) curves derived from quasi-OCV measurements (described in experimental Chapter 2), as shown in Figure 5-16, enabled examining the voltage plateaus of the cell, which represent the capacity involved in the graphite electrode material phase transformation reactions [155, 194], and understanding more in detail the degradation phenomena, as these curves are mainly representative of the graphite negative electrode in the case of LFP-based cell. The voltage curve of LFP presents a single plateau, which corresponds to  $\text{FePO}_4\text{-LiFePO}_4$  phase transformation, that yields a featureless differentiation curve. Graphite, however, shows different plateaus on the charge-discharge potential profile that represent the coexistence of lithiated graphite at different  $\text{Li}_x\text{C}_6$  transformation processes. Even though typically three-staging phenomena are reported for the graphite [50], for the studied LFP cell five of them were detected within graphite intercalation-deintercalation window coupled with LFP potential plateau, in agreement with observations of M. Dubarry *et al.* on LFP cells [96]. They are numbered as 1 to 5 in Figure 5-16. They are revealed as 5 valleys in DV curves in Figure 5-16 (c) (the four peaks, indicated using the green lines, correspond to transitions between five transformation phases in equilibrium) and as 5 peaks in IC curves in Figure 5-16 (d). M. Safari and C. Delacourt [110] reported four of them for the same cell configuration (they did not pay attention to the staging transition marked as 4 in Figure 5-16).



**Figure 5-16.** Close-to-equilibrium C/5 discharge voltage profiles at initial stage for the 2.3 Ah commercial 22650-type cell studied within this work (a,b), and differential voltage (DV,  $dV/dQ$ , c) and incremental capacity (IC,  $dQ/dV$ , d) signatures. Graphite staging phenomena coupled with LFP voltage plateau numbered as 1 to 5

Figure 5-17 represents DV curves for the different storage tests. Reduction of active lithium within the negative electrode at the beginning of cell discharge (graphite delithiation) was observed in all cases. The first valley in DV curves shrank gradually upon storage. This change of the stage 1 lithium-graphite compound most likely correspond to irreversible lithium loss (LLI) [67]. No other changes were particularly highlighted except for the cell stored at 50°C and 70% SOC. Figure 5-18 shows, more in detail, different ageing effects that were gradually detected upon storage on this cell. In this case, all peaks and valleys in IC and DV curves, respectively, somehow faded after prolonged storage even though the first valley in DV curves did not completely disappear. After 10-11 months of storage under 50°C and 70% SOC, first peak in DV curves shifted to higher capacities reducing the distance between peaks. Likewise, not only the intensity of the peak at 3.32 V in IC curves (peak 1) decreased so as for the one at 3.28 V (peak 2). This effect represents loss of graphite active material (LAM), as the distance between any two peaks in DV curves is proportional to the amount of active carbon, *i.e.* capacity involved in the graphite electrode material phase transformation reactions [67, 155, 194]. Hence, loss in graphite available sites for reaction with lithium was induced, which means that graphite could not be lithiated to the same level as it was initially. The staging process would not however change, as none of the valleys in DV curves disappeared at all. Anyway, LLI was highly enhanced before LAM phenomenon was observed,

so graphite LAM did not directly lead to capacity loss (there may be enough storage capacity for the amount of active lithium in the cell [67])[194].

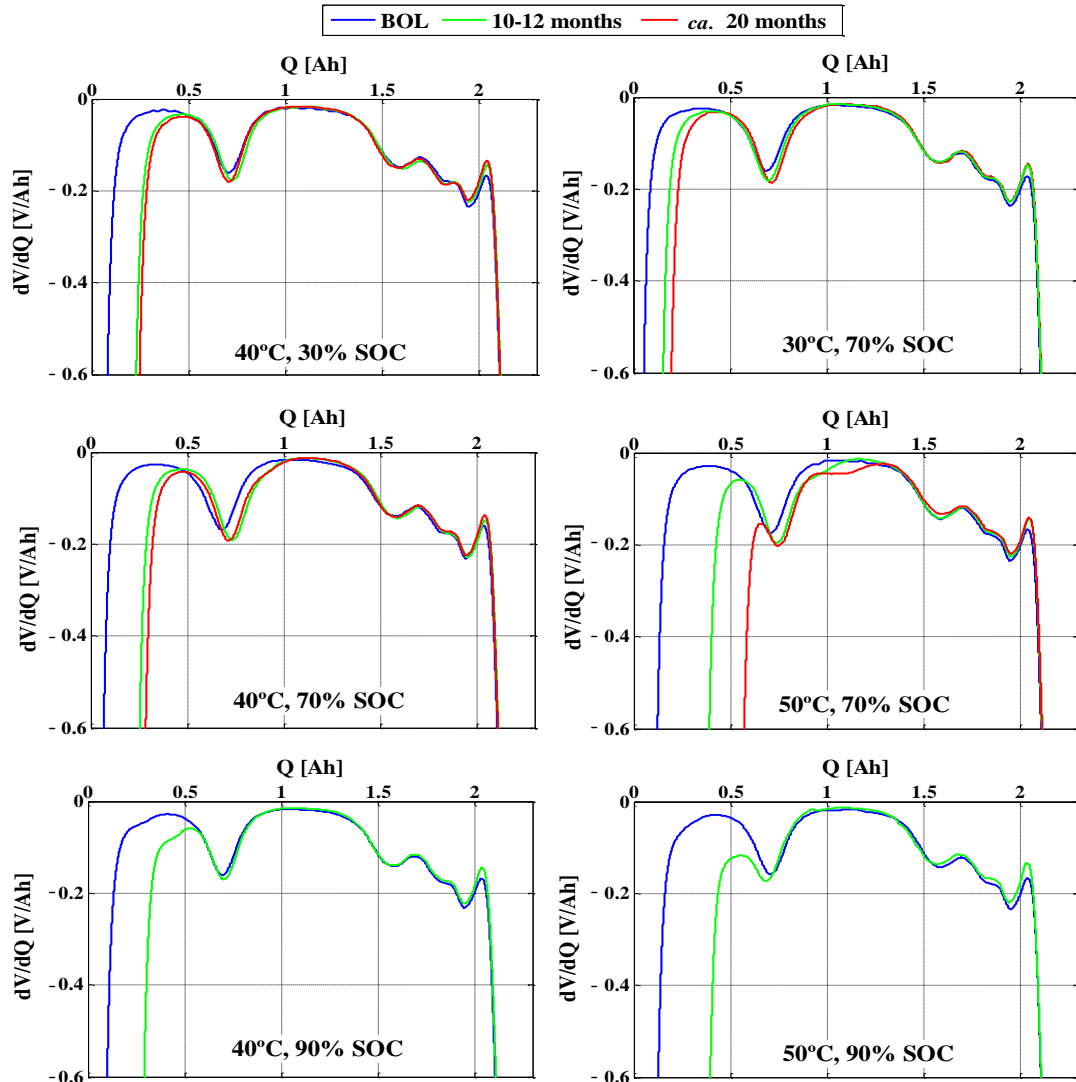


Figure 5-17. Equivalent and representative Differential Voltage (DV) curves, obtained from C/5 discharge voltage profiles, upon storage at different conditions

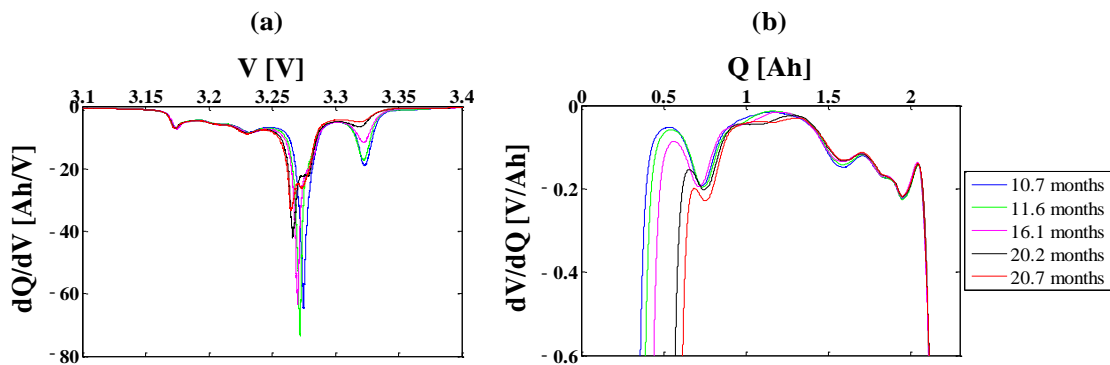


Figure 5-18. Incremental Capacity (IC) (a) and Differential Voltage (DV) (b) curves for 50°C and 70% SOC test after prolonged storage periods

From IC and DC curves it was not possible to find out the reasons for impedance change. EIS measurements were carried out with this purpose. Figure 5-19 shows a comparative study of 50°C (70% SOC) storage condition with other at 30°C (70% SOC), as it was deduced that cell resistance strongly depends on storage temperature. There are plotted EIS spectra measured at two different SOCs, aiming at confirming that the check-up SOC condition is not relevant for analysing cell impedance evolution. The approach for representative ageing effects identification is mainly focused on the impedance real part at high and low frequency. The high frequency intercept with the real axis, related to ohmic resistance, was shifted to larger values, indicating degradation of electrolyte that leads to growth of SEI layer (see Appendix A, section A.2.3.). The shift measured in the cell stored at 50°C after just 3.7 months was similar to the one at 30°C after *ca.* 21 months. It increased *ca.* 2 mOhm and *ca.* 0.5 mOhm at 50°C and 30°C storage, respectively, after *ca.* 21 months. Hence, the ohmic resistance change was highly influenced by cell ageing storage temperature. On the other hand, the semicircle resistance at medium frequency also changed significantly in the highly aged cell at 50°C ambient temperature, in comparison with the one stored at 30°C (*ca.* 21 months of storage). It means that apart from limiting the conductivity of electrolyte upon storage, as a result of its organic deposition on graphite electrode surface, the charge transfer was also limited as the passivating resistive layer got thicker and denser. These EIS observations correlate to DC internal resistance sharp increase at prolonged storing times (Figure 5-10, after the check-up at *ca.* 355 days of storage), as also concluded from quasi-OCV measurements.

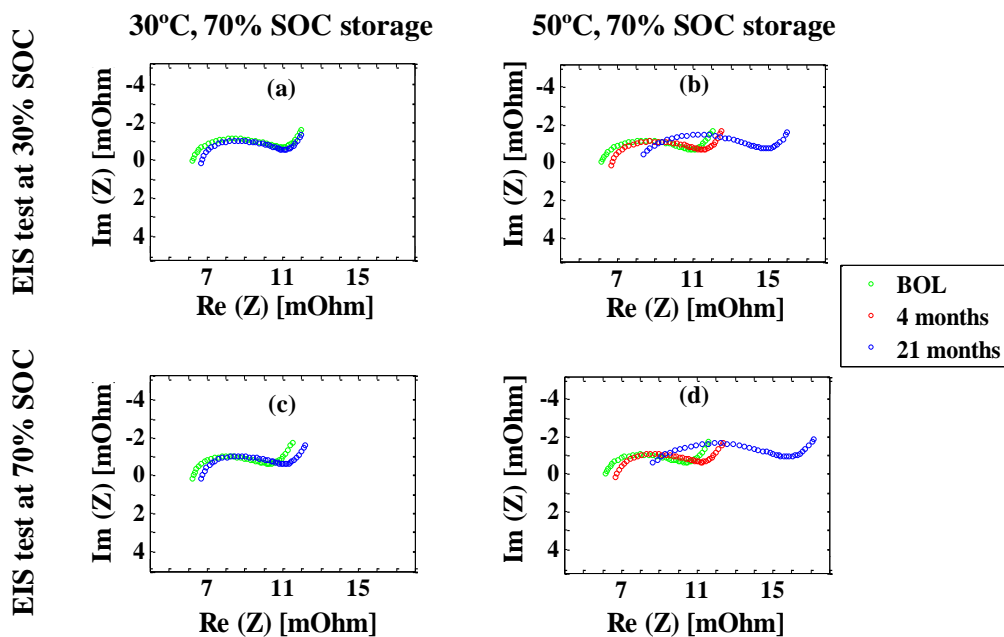


Figure 5-19. EIS measurements of the cells stored at 30°C and 70% SOC (a,c) and 50°C and 70% SOC (b,d). EIS measurement at 25°C and two different cell SOCs: 30% (a,b) and 70% (c,d)

Overall, in agreement with previous studies [63, 110, 195], calendar ageing close to room temperature (*e.g.* 30°C in the present work) does not result in significant degradation of the electrodes. Cell overall performance is limited by the available active lithium. After prolonged storage at high temperature, the results reveal that large LLI also led to LAM associated with graphite electrode and impedance change. LLI was responsible for the majority of ageing processes.

### 5.3.2.2 CALENDAR AGEING PREDICTIVE MODEL

Lifetime of the investigated LFP-based cell, based on results discussed previously, would be restricted by the remaining available capacity (power fade would not be a limiting factor). Hence, the calendar ageing predictive model development is therefore focused on capacity fade evolution. Five different storage conditions were used for modelling and an additional one, at the more severe conditions (50°C and 90% SOC), for the static validation (Table 5-5). A single degradation mode, LLI, was modelled as the appearance of the representative ageing effects changed upon ageing condition. The method of least squares was used for fitting experimental data. Eq. 5-5 shows the overall semi-empiric mathematical model for calendar ageing, where  $\alpha_1$ ,  $\beta_1$ ,  $\alpha_2$  and  $\beta_2$  are constant fitting parameters. Figure 5-20 shows capacity loss experimental results (solid markers) at different accelerated ageing conditions, which were constant upon storage within each test, and the corresponding predictions (lines) resulting from the developed model. The static validation at 50°C and 90% SOC is plotted in the same figure (dotted line). For the 50°C and 70% SOC storage condition, the last 3 check-ups capacity results were not taken into account for impact factors effect quantification, since, as discussed above, there was a change in degradation mechanism, from LLI to a combination of LLI and LAM, later than the CU after 355 days of storage. Detecting the inflection points in experimental data, which indicate transition to sudden fade, is of high importance for defining the EOL. Otherwise, the lifetime would be over-predicted, as it can be observed in Figure 5-20 (shadowed area).

$$Q_{\text{loss}} [\%] = \alpha_1 \cdot \exp(\beta_1 \cdot T^{-1}) \cdot \alpha_2 \cdot \exp(\beta_2 \cdot \text{SOC}) \cdot t^{0.5} \quad \text{Eq. 5-5}$$

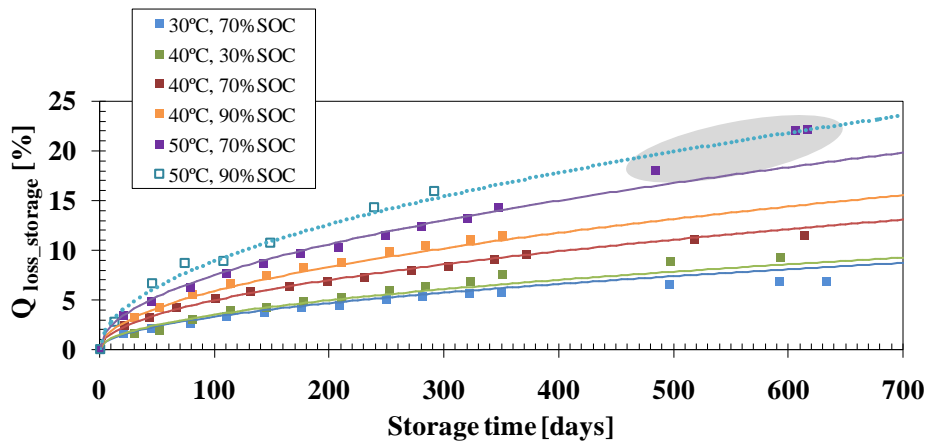


**Figure 5-20.** Capacity loss ( $Q_{loss}$ ) data at different storage static conditions (solid colour markers), fitted calendar degradation model (continuous lines). Open marker (50°C, 90% SOC) corresponds to the test condition used for static validation and the dotted line is the model validation fit

Lithium ions consumption rate, which is inversely proportional to the thickness of the SEI layer, followed the square root of time function as is typical for carbon anode cells [86, 196]. The effect of storage temperature on chemical reactions that led to the growth of non-conductive SEI layer, because temperature influences mainly electrolyte decomposition [191], and the consequent impedance rise was explained by Arrhenius law. This law also takes into account the effect of cell voltage at high temperature and how it increases the rate of lithium loss [135]. The activation energy was  $35.64 \pm 19.35 \text{ kJ}\cdot\text{mol}^{-1}$  (95% CI). Regarding voltage impact on parasitic chemical reactions leading to capacity loss, both linear [197] and exponential [135, 198] evolutions were checked, providing the latter the best fitting in all cases.

Goodness of capacity fit and prediction (validation) was evaluated for all experimental data points, but for data within the shadowed area, at each storage condition. The distribution of residuals is shown in Figure 5-21 in a box plot, which includes the static validation prediction errors (*i.e.* data not used for modelling). Depicting graphically groups of numerical data through their quartiles enabled identifying outliers, which are marked with asterisks (Figure 5-21). They may be due to variability in the measurements or may indicate experimental error. The boxes spacing indicate the degree of dispersion of residuals, the average values are indicated with open circles and the line inside the boxes represent the median. Focusing just on evaluating the modelling accuracy, it was high for the 40°C and 70% SOC condition. At this storing condition the variability was the least, its distribution was negatively skewed and, additionally, the median residual was the lowest. 40°C and 90% SOC storing condition presented the largest median residual but it was similar to that of 40°C and 30% SOC storing condition, which, in addition, exhibited greater variability and mean residual. The latter was assessed including every data (also outliers) and is indicated with spots in Figure 5-21 for each condition. On the other hand, data at 70% SOC and different temperatures (30, 40 and 50°C) showed very similar median

residual: *ca.* 0.2%. Fitting at 30°C exhibited the greatest variability among them with the distribution positively skewed. Its interquartile range was however just about 0.4%. Overall, temperature effect was very accurately quantified and the goodness of SOC impact factor modelling was slightly lower at the conditions that were not considered for temperature effect evaluation (30% and 90% SOC). In any case, even taking into account the variability outside the upper and lower quartiles, which is indicated with lines extended from the boxes (whiskers), the difference between measured data and estimation was not larger than 1%.

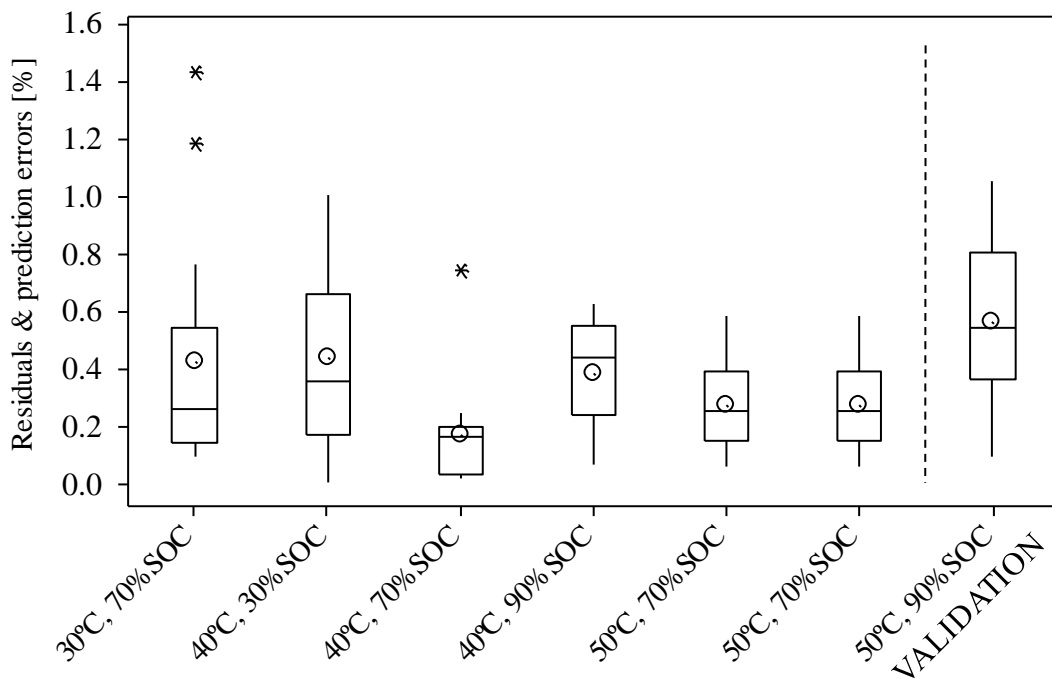


**Figure 5-21.** Box plot of capacity loss prediction residuals and errors distribution for each storage condition

Static validation (50°C, 90% SOC) showed that the largest verified error of the capacity loss predictive model (Figure 5-21) was within the same range, *ca.* 1%. The median prediction error was larger than but similar to the median residual at 40°C and 90% SOC storing condition. Taking into account that the validation consisted in very demanding storing conditions, it was concluded that the model demonstrated high degree of prediction accuracy. Hence, the developed capacity loss model could be used for precise lifetime estimation within the analysed windows of SOC and T factors (Table 5-5), and under constant storage conditions.

- **Model dynamic validation**

As described earlier, the validity of the developed calendar-life predictive model was checked in other conditions different from the ones used for modelling (*i.e.* static validation at 50°C and

90% SOC). Testing at constant operating conditions is not however enough for approaching cell behaviour in real applications, on which the operation and ambient temperature is dynamic. In order to enhance the applicability of the model, additional tests were carried out changing the impact factors within the profile on the same cell (Figure 5-8). Figure 5-22 shows experimental capacity loss data (diamond shaped symbols) of four cells (a-d) that were put to the test under different thermal and SOC profiles (in black lines) and the corresponding predictions using the developed calendar ageing model (in green lines). The method used for predicting the capacity loss at dynamic factors profiles took into account the accumulated ageing by former usage [177, 199]. This way, the residual capacity was used as reference point for further predictions at different operating conditions and not simply the operating time.

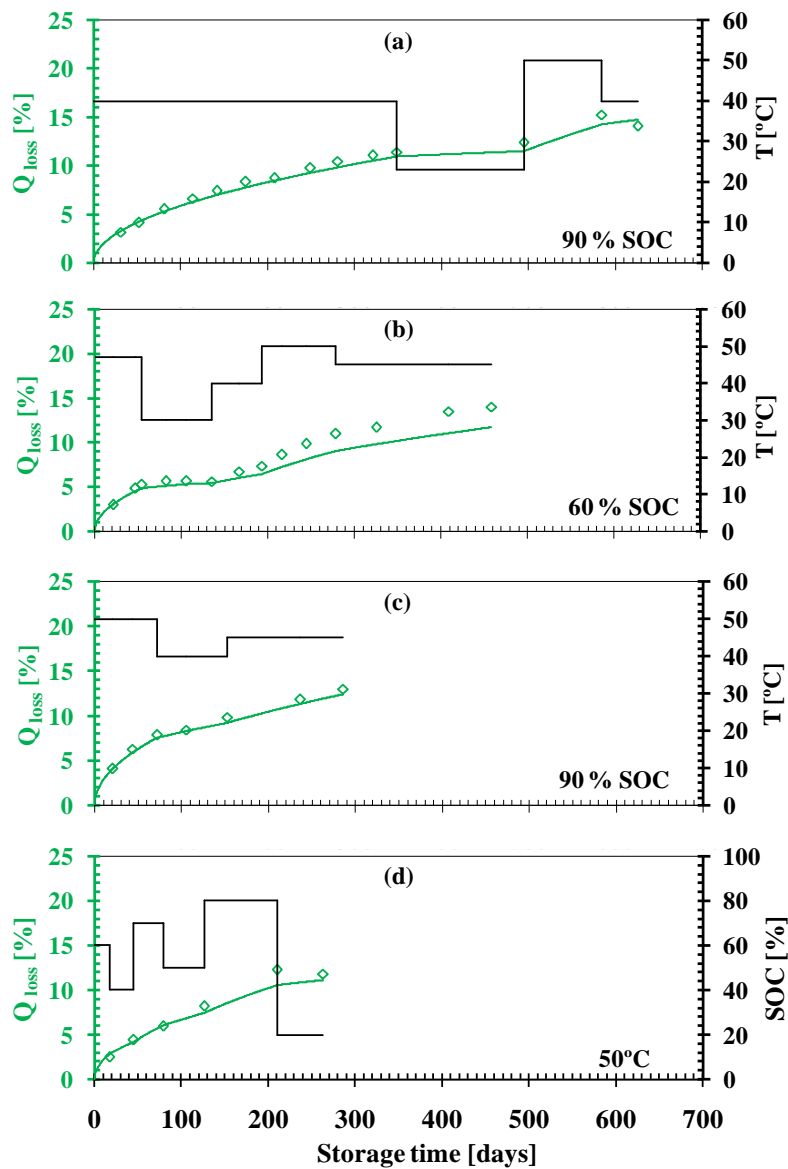


**Figure 5-22.** Capacity loss performance (diamond shaped symbols) under dynamic storage conditions for four tests (a-d, plotted in black). The corresponding predictions are represented by green lines

From Figure 5-21 it was deduced that temperature effect was more precisely quantified than SOC effect in the capacity loss predictive model. The assessed average prediction error for dynamic SOC test profile upon storage on the same cell (Figure 5-22 (d)) was 0.64%, whereas it was 0.70% for dynamic temperature tests (Figure 5-22 (a-c)). In any case, the overall root-mean-square error (RMSE) was just 0.93%, so the forecasting error at non-constant operation conditions was very low. Hence, the calendar ageing predictive tool that was developed considering (i) the model based on capacity loss evolution evolved from constant condition tests and (ii) the ageing by former usage for predictions at random conditions upon storage, is of high accuracy. This way, it was possible analysing calendar-life performance of different real applications. The following section describe further estimations for an UPS application.

### 5.3.2.3 REAL SCENARIOS EVALUATION

The calendar life performance of a cell in worldwide UPS applications was evaluated. Three different scenarios located at Bangkok (Thailand), Jizan (Saudi Arabia) and Tenerife (Spain) were analysed. Average daily temperatures over a year [200-202] were considered as plotted in Figure 5-23. It was supposed that the cell in the UPS would be at 90% SOC, ready to supply large power peaks. The SOC was considered constant upon storage for the predictions, as, after the very short runtime, the cell would be recharged immediately to the initial SOC when the power would turn back. In addition, it was assumed that the activation energy of chemical reactions would not change above 15°C up to 50°C (such as it did barely between 30 and 50°C). Figure 5-24 shows the assessed capacity loss evolution over two years (the profiles in Figure 5-23 were simulated twice). It was assumed that the initial main degradation mechanism (LLI) would not change, in agreement with previous observations. Experimental data at more demanding temperature conditions (40°C and 90% SOC, and 50°C and 90% SOC tests) only showed LLI over a year (Figure 5-18 and Figure 5-20). Furthermore, the model considering this ageing phenomena predicted precisely the capacity loss of a cell at non-constant temperature storage conditions during more than 600 days (Figure 5-20 (a)).

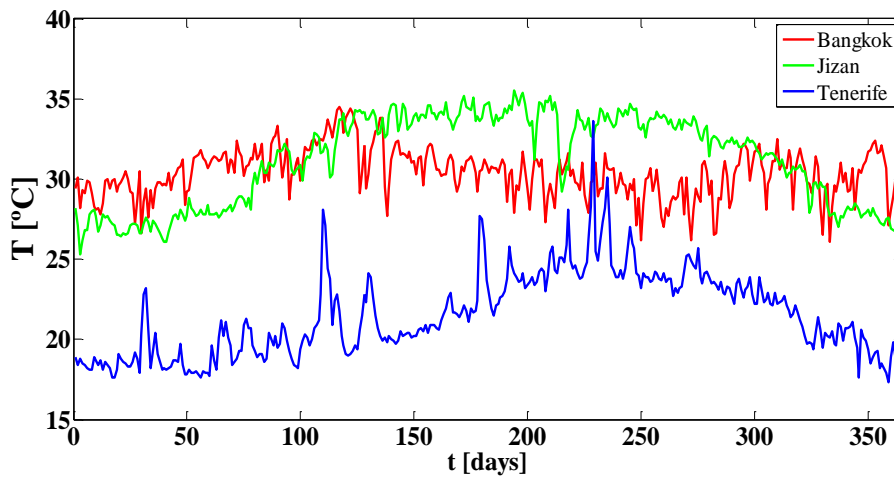


Figure 5-23. Recorded average temperatures of Bangkok, Jizan and Tenerife for each day during one year

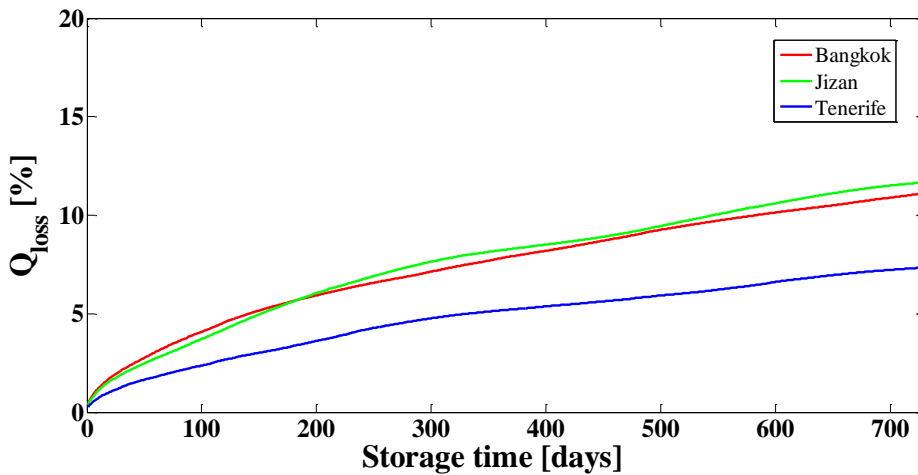


Figure 5-24. Capacity loss prediction for two years of operation at 90% SOC and temperature profiles in Figure 5-23

The capacity loss evolution of the battery stored in Jizan and Bangkok would be very similar as the thermal profiles are in these two cities. The largest average temperature difference between them over the year is 7.2°C. Even though the temperature in Jizan is lower than in Bangkok during the first *ca.* 80 days of the year, the predicted cell capacity loss was larger in Bangkok even during the first 200 days. In agreement with the observed exponential dependence between temperature and evolved capacity loss (Figure 5-20), initial higher storage temperature of just 2.5°C in average would affect more the cell performance than thereafter average temperature difference of 3.5°C during 200 days. After this period, however, for prolonged calendar time, the cell in the UPS of Jizan would be more degraded, even though the compared two thermal profiles change slightly (at the end of the year the temperature in Bangkok is slightly higher). In the case of the cell to be stored between 17 and 33°C under the thermal profile measured in Tenerife, its capacity fade would be 4% lower after two years than for the ones stored between

ca. 25-35°C. The predicted capacity loss in a complete year was 5.2%, 7.9% and 8.3 % at 21°C, 30.5°C and 31.9°C median temperature, respectively. Hence, in this specific case, even though the differences are very low, the higher the median temperature, the larger the cell performance loss in the long-term.

### 5.3.3 CALENDAR AGEING MAIN CONCLUSIONS

The presented semi-empirical model represents successfully the storage behaviour of the cell both at static and dynamic operating conditions. Understanding of degradation was done by the combined analysis of voltage profiles, electric measurements of capacity and internal resistance ageing metric, EIS measurements and IC and DV diagnostics techniques. The identified main ageing mechanism is LLI due to moderate SEI evolution. The SEI formation due to parasitic reactions in anode surface/electrolyte interface increases over time, also leading to cell impedance change. At high temperature and long storing time, additional ageing effects were induced and, as a consequence, the main degradation mechanism, initially LLI, changed to a combination of LLI and LAM. The developed model covers one main degradation mechanism (LLI) and in most cases is able to predict calendar ageing over a wide range of storage conditions.

The calendar ageing results also indicated that the useful life of the investigated LFP-based Li-ion cell is mostly controlled by capacity fade rather than power fade. Hence, SOH monitoring and/or predicting should be based mainly on the actual capacity. This is why the model is based on capacity loss evolution over time. The developed semi-empirical model simulates square-root of time dependency and both exponential state of charge and temperature dependencies showing high goodness of fit with the experimental results. The calculated model residuals are in all cases below 1%. This model was thoroughly validated under different static and dynamic T and SOC conditions, over prolonged times. The estimated RMSE for the dynamic validations is 0.93%, corroborating the high model accuracy under realistic operating schemes.

The simulation of an UPS application has been used to prove that the events order within the dynamic thermal profiles determines the ageing upon storage. The developed model is able to adapt to the history of events.

## 5.4 CYCLE LIFETIME

A further step towards an overall lifetime prognosis is the analysis of cycling performance and the development of a thoroughly validated semi-empirical cycle ageing predictive model. This section deals with cycle ageing analysis as a function of DOD, C-rate and Ah-throughput at both static and dynamic operation schemes. After reviewing the state of the art (Table 5-3), this cycle ageing analysis enhances the results by adding further steps of dynamic validation that do not focus on specific applications. The next step within the lifetime prognosis approach is to combine the results of cycling ageing with those from calendar ageing. The methodology defined for cycle lifetime prognosis is the same as for calendar lifetime analysis shown in Figure 5-6, but in this case, apart from the steps within the shadowed area, an additional validation step was performed: post-mortem analysis.

### 5.4.1 EXPERIMENTAL

Cycling experiments were carried out using 26650-type LFP-based cells of the same manufacturing batch with 2.3 Ah nominal capacity and 3.3 V nominal voltage. Range limits for the actively tested external influence factors were chosen within the cell operation window set by the manufacturer and taking also into account the cell behaviour observed during several initial screening tests. Nonetheless, C-rate outer limits were not checked since a real-life application may not operate in such conditions. For each cycling test a single cell was used in most cases, since, as already mentioned in the calendar lifetime section:

- The cells reproducibility assessment at the Beginning of Life (BOL) using 74 cells indicated that the true population mean nominal capacity falls within  $2.313 \pm 0.005$  Ah range with 95% certainty.
- In the previous study using the same reference it was measured that the average coefficient of variation upon cycling ageing was just 6% using 3 cells per condition (accelerated ageing test in Chapter 4 -Stage 2 of cells selection for the residential application-).

Specific tests were repeated in order to check the reliability of results.

The ageing tests were performed in a temperature-controlled environment. CTS and Prebatem climatic chambers were used for this purpose (Appendix C). Both cycling and periodical check-up experiments were carried out using Digatron multiple cell tester with data acquisition BTS-600 software (Appendix C).

Experimental procedures are described in *Chapter 2*. Both capacity loss and internal resistance increase were measured in order to evaluate cell SOH over time and parameterise battery ageing

model. EPIT, which were carefully planned so that their impact on cell degradation was as negligible as possible, consisted on:

- *Actual nominal capacity test*, described in *Chapter 2*.
- *Close to equilibrium Open Circuit Voltage (quasi-OCV) measurement test*, described in *Chapter 2*.
- *Actual DC internal resistance measurement by HPPC test*: current pulses at cell maximum acceptable charge and discharge C-rates over cell 90-20% SOC range with 10% DOD intervals.

Additionally, both BOL and cell further characterisation tests at EOT included *EIS measurements* at 30% and 70% cell SOC (experimental procedure is described in *Chapter 2*). This test was also occasionally included in EPIT.

#### **5.4.1.1 ACCELERATED CYCLING AGEING TESTS CONDITIONS**

##### **5.4.1.1.1 CYCLE AGEING AND STATIC VALIDATION TESTS**

Cycling ageing was initially investigated at several but constant DOD and C-rate cell operating conditions over time on the same cell. Different ageing processes were analysed in one by one experiments (single factorial experiments). Furthermore, C-rate and DOD binary combinations were analysed at certain chosen levels, which were defined based on capacity. Table 5-6 shows the cycling static accelerated ageing tests matrix. Ten different conditions were used for cycling ageing model development and an additional one at 2C and 100% DOD for the static validation (shaded in Table 5-6). Symmetric charge sustaining cycling performance was analysed. All the cycling tests were performed at 30°C and 50% middle SOC (baseline temperature and voltage cycling conditions), and at CC charging-discharging mode. Figure 5-25 shows the different cycling tests conditions, *i.e.* middle SOC and SOC ranges, in the quasi-OCV curve of the investigated cell (obtained from quasi-OCV test described in *Chapter 2*), illustrating the transformation processes the active materials performed over cycling. Different equilibrium phases of the cell system are numbered in the same figure (1-5). Experiments were carried out correcting set parameters values (SOC and DOD) according to cell actual capacity (Q). In case the cells were tested using always the same values of the impact factors, additional polarisation effects could show up in the data.

**Table 5-6.** Test matrix for cycling ageing analysis and modelling (static validation highlighted in grey). All the tests were done at 30°C and 50% middle SOC

C-rate	DOD [%]					
	5	10	30	50	60	100 <sup>1</sup>
1C	X	X	X	X	X	X
2C		X			X	X
3.5C		X			X	

<sup>1</sup> Cells were cycled between charge and discharge cut-off voltages (3.6-2V), which corresponds with 97% DOD

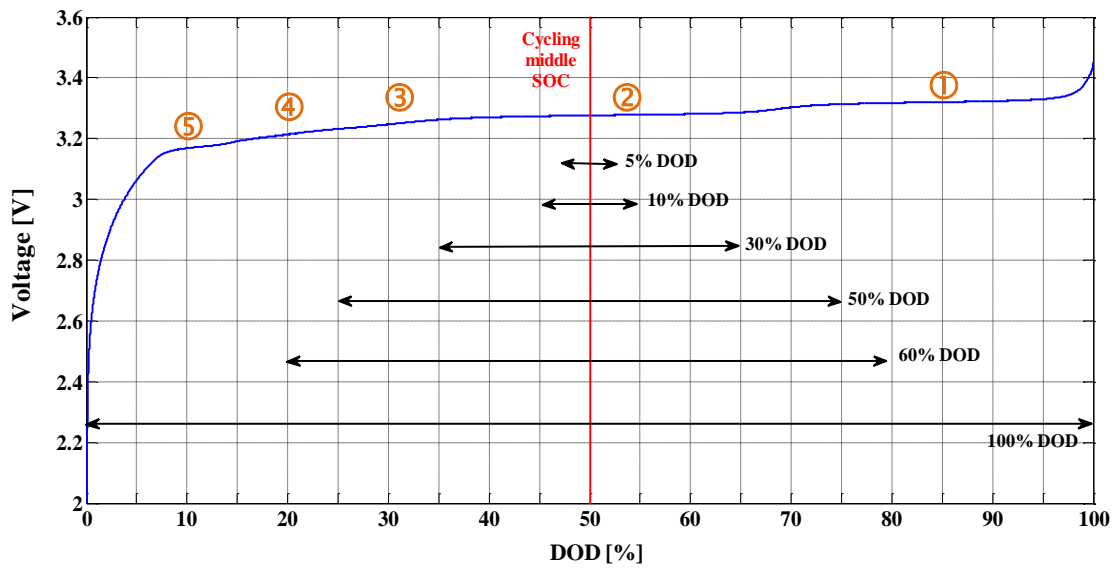


**Figure 5-25.** quasi-OCV C/5 discharge curve of the studied 2.3 Ah LFP/graphite 22650-type cell. Graphite staging phenomena coupled with LFP voltage plateau numbered as 1 to 5. Cycling ageing testing conditions, middle SOC and SOC range, are depicted in the graph for each DOD

#### 5.4.1.1.2 DYNAMIC VALIDATION CYCLING TESTS

Additional tests under variable DOD and C-rate were carried out aiming at the validation of the cycling ageing model under different stress levels operating conditions. Two dynamic impact factors operation schemes that are plotted in Figure 5-26 were planned. Both DOD (in red) and C-rate (in blue) were changed in each of the tests.

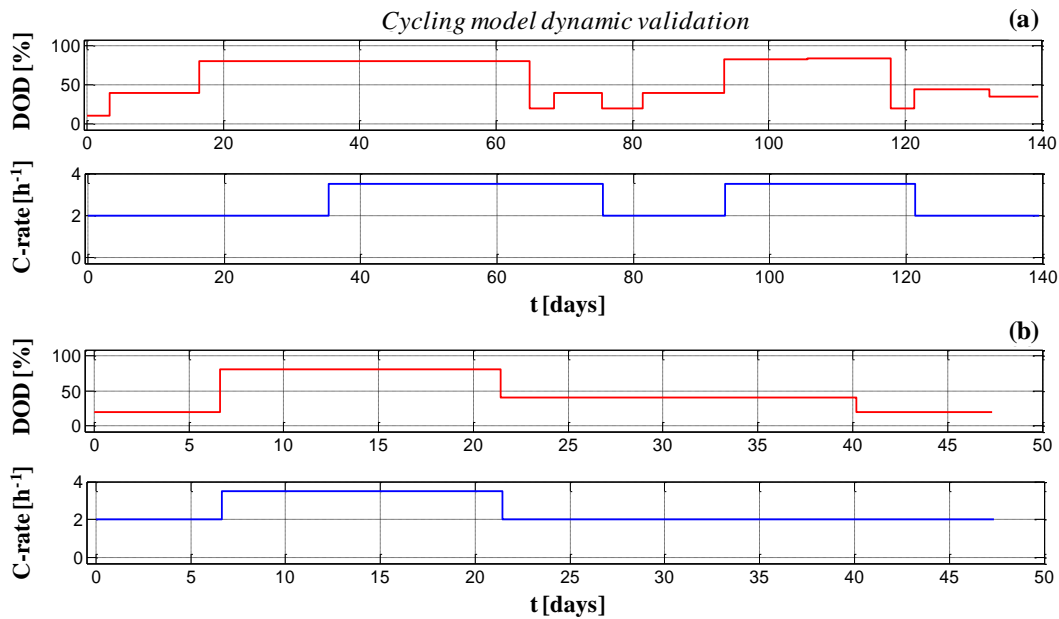


**Figure 5-26.** Cycling ageing model dynamic validation. Two tests (a and b) under dynamic both DOD and C-rate over time at 30°C and 50% middle SOC were performed

#### 5.4.1.2 POST-MORTEM ANALYSIS

Ex-situ destructive diagnosis techniques were used for identifying the main induced degradation mechanisms and failures that cause cell capacity and power fade. Cell components visual, electrochemical and physical-chemical characterisation aimed at validating the ageing processes analysis using non-destructive techniques. This work covers the evaluation of the impact of large DOD stress factor.

This post-mortem analysis work was carried out in collaboration with CIC energiGUNE under the ETORTEK 2012 Strategic Program of the Basque Government. Cell disassembly, components harvesting and initial inspection was performed following the methodology defined in this work (*Chapter 3*, section 3.3). F. Aguesse (CIC energiGUNE) has been responsible for performing the characterisation analysis with the cells aged in this work.

Pristine, conditioned (after formation cycles), BOL aged cells at 93.03% and 79.6% SOH (mid-life and EOT conditions) were opened after discharging them at 25°C and 1C to the cut-off voltage established by the manufacturer (safety reasons). The cell condition after purchase (control experiments), initial state and aged cells under 100% DOD continuous cycling were characterised aiming at a comparative study (these cells cycling is described in section 5.4.1.1.1). Two specimens of each pristine, conditioned and BOL cell conditions were

examined in order to check the reproducibility of cell physical-chemical characteristics and diagnostic results.

The middle and the external area (0.5 cm from the edge) of the electrodes width, jelly-roll height, were selected for harvested electrodes characterisation. Additionally, different samples were collected along the whole electrode length in order to check the ageing inhomogeneities along the jelly-roll (observation of cell design influence on internal temperature, current and SOC distribution) [203, 204]. It was decided not to wash the samples before the different examination steps to prevent alterations of the surface structure and to avoid any changes in the electrode performance due to the rinsing solvent polarity [58, 82].

The coating on one side of the electrode laminate was removed using NMP solvent for half-cells electrochemical measurements. 2016-type coin cells (from Hohsen Corp.) were assembled using commercial 1M  $\text{LiPF}_6$  in 1:1 EC/DMC fresh electrolyte from UBE. Galvanostatic measurements were carried out in a Maccor battery tester at room temperature. Half-cells with LFP electrode were cycled at C/6 between 4.2 and 2.8 V, whereas graphite electrodes were tested between 0.01 and 1 V at C/2. The stability upon cycling and the operating SOC window of the harvested electrodes were analysed.

Harvested electrodes and separators microstructures were examined in a FEI 200 Quanta Field Emission Gun-Scanning Electron Microscope (FEG-SEM) at low vacuum mode at 15 kV. EDS analyses were carried out using EDAX Genesis software. A carbon coating was previously deposited onto the separator samples to avoid electronic charging. Samples in the glove-box were taken to the microscope in a hermetically sealed vacuum container in order to avoid the contact of the sample with air as much as possible.

Both negative and positive harvested electrodes structure was analysed by XRD. Samples were prepared inside the glove-box using a special air-tight XRD holder covered with Kapton tape. A Bruker-D8 diffractometer mounted with a  $\text{Cu-K}\alpha$  radiation source (accelerating power of 30kV x 50mA) was used in the Bragg-Brentano geometry mode. The diffraction patterns were recorded from 15 to 80° in two-theta values. Both negative and positive harvested electrode samples were examined.

## 5.4.2 RESULTS AND DISCUSSIONS

The effect of DOD and C-rate parameters upon cycling is discussed in the following section. Cell cycling behaviour is interpreted by combining the results from cycling ageing tests results

and post-mortem analysis. The cycle lifetime predictive model has been developed by introducing a comprehensive dynamic validation approach.

#### 5.4.2.1 CELL CYCLING PERFORMANCE FADE EVALUATION

- **Analysis of cycling ageing results**

The measured average nominal capacity of all the cells used under cycling examination was  $2.304 \pm 0.009$  Ah (95% CI) at the BOL. The evolution of cell performance ageing metrics when cycled at different DOD conditions are presented in Figure 5-27 as a function of Full Equivalent Cycles (FEC). The evolution of DC internal resistance change during discharge at 50% SOC is just used for evaluating cell power performance fade due to cycling. As shown in Figure 5-28 for a couple of tests as examples, the trend of measured internal resistance was also similar, despite the current pulse testing reference SOC (Figure 5-28 (a)) and charge or discharge current step (Figure 5-28 (b)) during the check-ups.

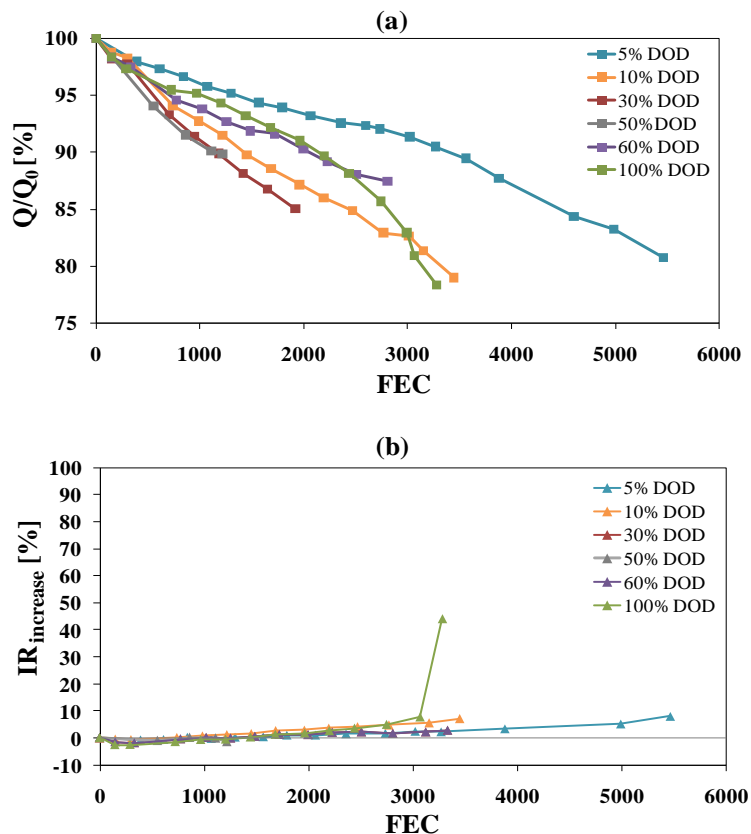


**Figure 5-27.** (a) Actual nominal capacity ( $Q$ ) and (b) 17 s discharge DC internal resistance ( $IR$ ) increase, measured at 50% SOC, upon cycling (1C, 50% middle SOC and  $30^\circ\text{C}$ ) as a function of Full Equivalent Cycles (FEC), both normalised to initial values ( $Q_0$ : nominal capacity at the Beginning of Life)

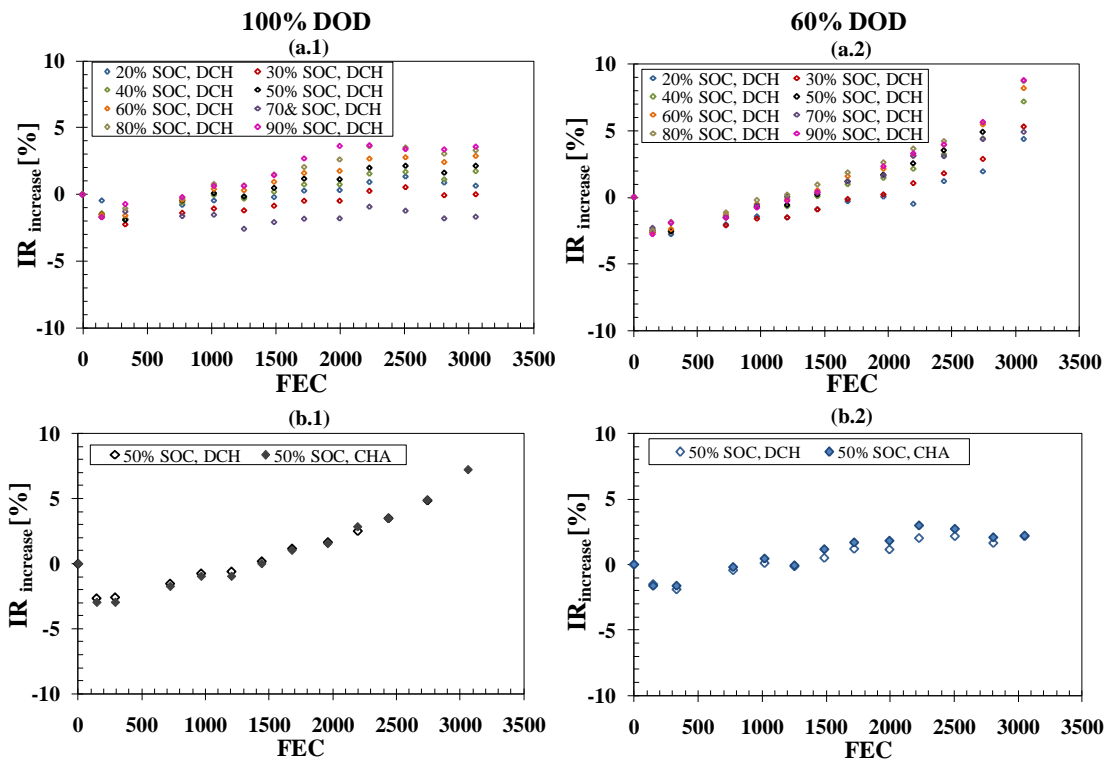


**Figure 5-28.** Current pulse EPIT results upon cycling (FEC: Full Equivalent Cycles). (a) 17 s DC internal resistance (IR) increase during discharge as a function of the current pulse applying cell SOC. (b) DC IR increase during charge and discharge at 50% SOC. (a.1 and b.1) Cycling at 1C, 100% DOD, 50% middle SOC and 30°C; and (a.2. and b.2) cycling at 1C, 60% DOD, 50% middle SOC and 30°C

The comparison of capacity fade (Figure 5-27 (a)) and DC internal resistance increase (Figure 5-27 (b)) at a same DOD cycling condition shows that the cells under cycling lost significantly more capacity than power, alike under cell storage. In addition, initial diminution of internal resistance was observed as well (Figure 5-10). The moderate increase of total resistance (less than 10%) suggests that bulk transport properties are almost unchanged over cycling (absence of structural degradation) [87].

The shape of the capacity loss curves in Figure 5-27 (a) indicates that the capacity loss trend changed upon cycling for 5% DOD and especially for 100% DOD tests, as illustrated in Figure 5-29. Ageing behaviour was no longer linear but parabolic, as is typical for Li-ion technology according to the literature [205], after 2000-2500 FEC at 100% DOD. At the same time, the internal resistance increase tendency was also altered clearly following the same tendency (Figure 5-29 (a)), and especially between the last two EPIT. For 5% DOD, the changes were not so marked (Figure 5-29 (b)), but both capacity loss and internal resistance increase rates changed after *ca.* 3000 FEC. Hence, it suggests that the dominant degradation mode is not the same over the whole cycle lifetime of the battery. As the occurrence of the representative ageing effects changed upon cycling conditions, DOD effect was therefore evaluated just considering the results before cell ageing process apparently changed (at *ca.* 90% SOH for the

two cycling conditions where such change was observed). From data presented in Figure 5-27, Figure 5-30 compares the total FEC the studied cell could run at different DOD levels before the capacity drops to *ca.* 90% of the initial value (lifetime criterion where the ageing state for all the tests was similar). The presented Wöhler curve is just bidimensional (at 25°C, 1C and 50% middle SOC), which shows a non-linear dependency between FEC and cycle depth. Usually an exponential relationship is assumed, but the reference used in this work revealed that the cells cycled under large and small DODs both show the slowest degradation. Even though it is a rule of thumb that deep cycling considerably reduces the cycle lifetime of the battery due to the volume changes in materials (impact on the mechanical stability), experimental data shows that, in this case, 100% DOD level is not the most detrimental to the battery health (it was checked for a couple of cells, in which cell to cell variation was minimal). The cell FEC *vs.* DOD relationship does not show a single tendency either. Short cycles with low 5% DOD led to more than 3500 FEC. At 30% DOD level, the least FEC were measured, but the number of cycles were similar in the 10-50% DOD range. According to the literature, phase changes in the battery materials during operation can lead to considerable mechanical stress [133, 206] because the lattice parameters of materials change depending on predominant phases [207]. Figure 5-25 shows the transformation processes that the studied active materials performed over cycling. At 10, 30 and 50% DOD cycling, the cell provided similar FEC (Figure 5-30). However, the cells were cycled within the same voltage plateau of the graphite (2) in the case of 10 and 30% DOD and, at 50% DOD, there were over phase (1-3) changes. At 60 and 100% DOD the Ah-throughput was also similar (Figure 5-30), slightly larger for the former, and in one case it was cycled over four different phases (1-4) and in the other over the five of them. Hence, there is no clear relationship between cycling and graphite electrode staging phenomena for the studied commercial LFP/graphite cell. Figure 5-30 and Figure 5-25 show, contrary to M. Ecker *et al.* observations [133], that cells cycled in SOC ranges that crossed phase transitions of graphite electrode did not age faster, and that even for the same voltage plateau there is no correlation between ageing behaviour and DOD impact factor. Overall, the damage of cycle depth, staging phenomena itself and calendar ageing may all be superimposed. More data would be needed for deriving a direct correlation. Anyhow, there were demonstrated different DOD effect ranges, 10-50% DOD range making a clear difference.

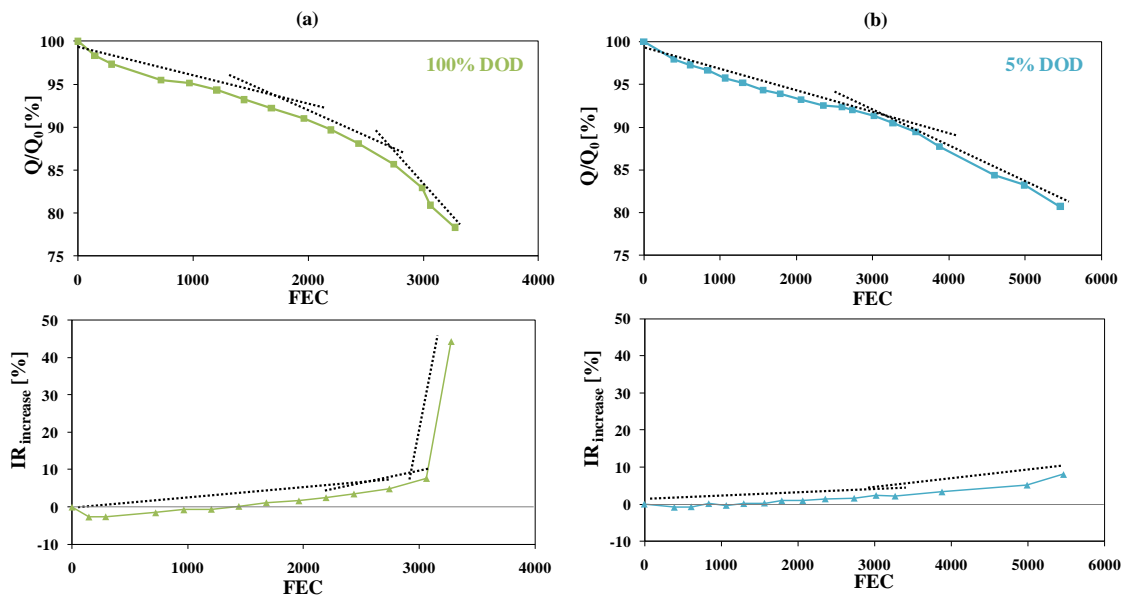


**Figure 5-29.** Illustration of cells performance fade trends for (a) 100% DOD and (b) 5% DOD continuous cycling conditions (1C, 50% middle SOC and 30°C). Actual nominal capacity ( $Q$ ) and 17 s discharge DC internal resistance ( $IR$ ) increase, measured at 50% SOC, as a function of Full Equivalent Cycles (FEC), both normalised to initial nominal values ( $Q_0$ : nominal capacity at the Beginning of Life)

Above cycle ageing modelling purpose, this parameter was further analysed. The influence of DOD on the total number of cycles that the cell can provide was checked, which can serve as hints guidelines for battery pack sizing or control strategies. In this case, experimental number of cycles ( $N$ ) vs. DOD data at *ca.* 90% SOH showed typical Wölher curve tendency, as shown in Figure 5-31 (fitting using least squares method). The best fitting result (dotted line) corresponds to Eq. 5-6, where  $\alpha_5$ ,  $\beta_5$ ,  $\alpha_6$  and  $\beta_6$  are constant fitting parameters.

$$N = \alpha_5 \cdot \exp(\beta_5 \cdot \text{DOD}) + \alpha_6 \cdot \exp(\beta_6 \cdot \text{DOD}) \tag{Eq. 5-6}$$

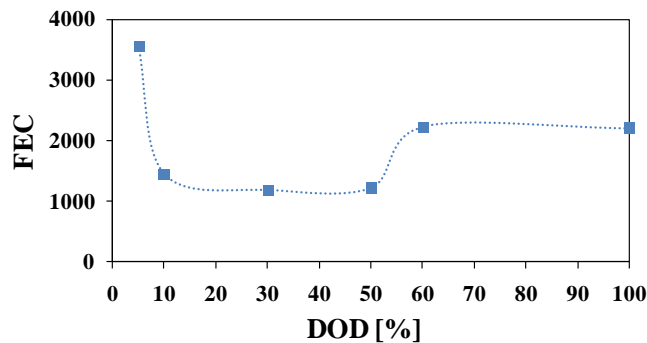


**Figure 5-30.** Ranging of total number of Full Equivalent Cycles (FEC) that the cell could deliver at various DOD levels (1C, 50% middle SOC and 30°C tests) before reaching *ca.* 90% SOH

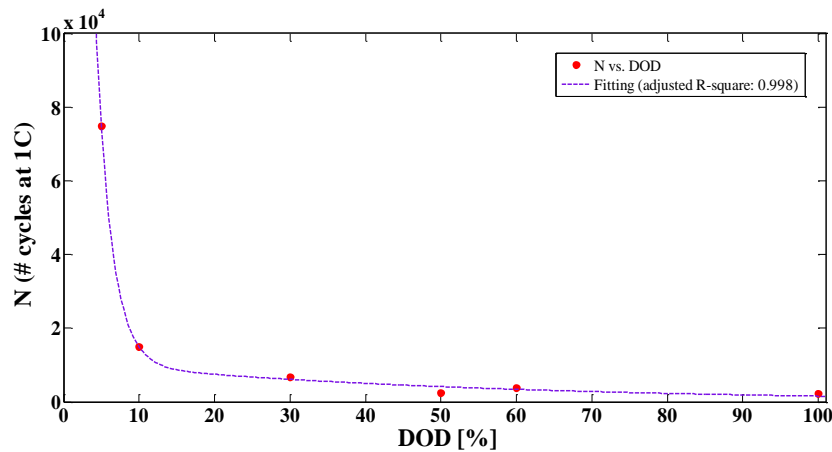


**Figure 5-31.** Wöhler curve. Relationship between DOD and the total number of cycles before reaching ca. 90% SOH

C-rate effect was also analysed. Figure 5-32 shows the influence of DOD (a-c) and C-rate (d-f) parameters on cell capacity retention as a function of FEC and time (d-2, e-2 and f-2). At each C-rate, FEC or, in turn, Ah-throughput, is directly proportional to time, but Ah-throughput parameter enables quantifying and correlating the ageing behaviour for different C-rates. When changing the cycling C-rate from 1C (Figure 5-32 (a)) to 2C (Figure 5-32 (b)), the capacity fade evolution was similar for 10 and 100% DOD levels. At these conditions (Figure 5-32 (d-1, f-1)), the influence of increasing the C-rate from 1C to 2C was negligible. At 60% DOD (Figure 5-32 (e-1)), even though capacity loss evolution was similar at different C-rates during the first 1000 FEC, the stress was afterwards enhanced at intermediate C-rate (2C). The cells cycled at 1C and 3.5C however, behaved similarly (Figure 5-32 (e-1)), but the capacity fade was even lower at 3.5C for a comparable number of FEC. This modification in the capacity retention tendency at 60% DOD revealed a change in the DOD effects comparison at 1C and 2C (Figure 5-32 (a, b)): while at 1C the performance fade was larger under 10% DOD than under 60% DOD (Figure 5-30), at 2C the results were similar regardless of the DOD. At 3.5C (Figure 5-32 (c)), again the capacity loss of the cell cycled at 60% DOD was lower than for the one at 10% DOD. At 10% DOD the degradation rate did not change remarkably with C-rate (Figure 5-32 (d-1)), although the larger the C-rate, the higher the capacity fade for this DOD level.

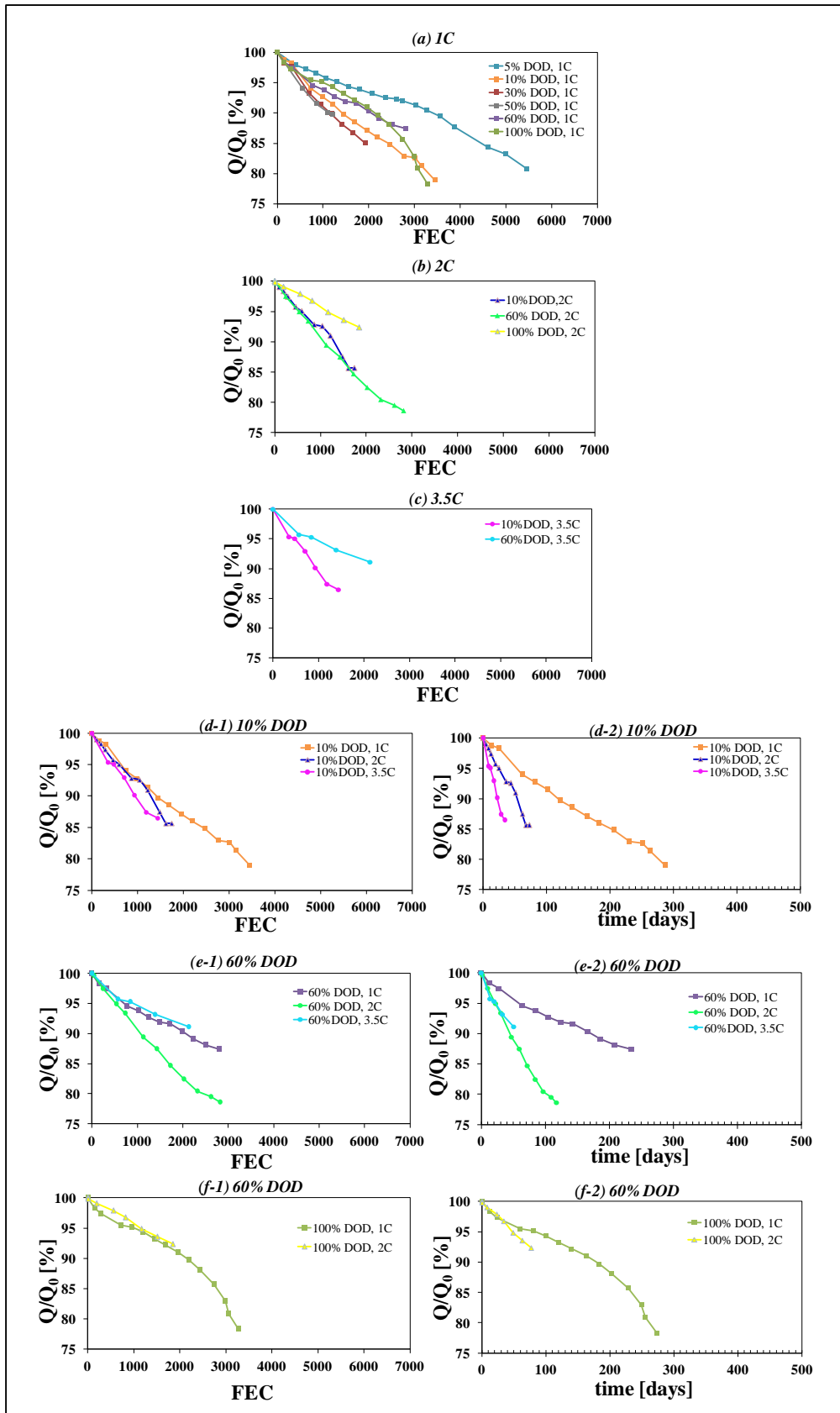


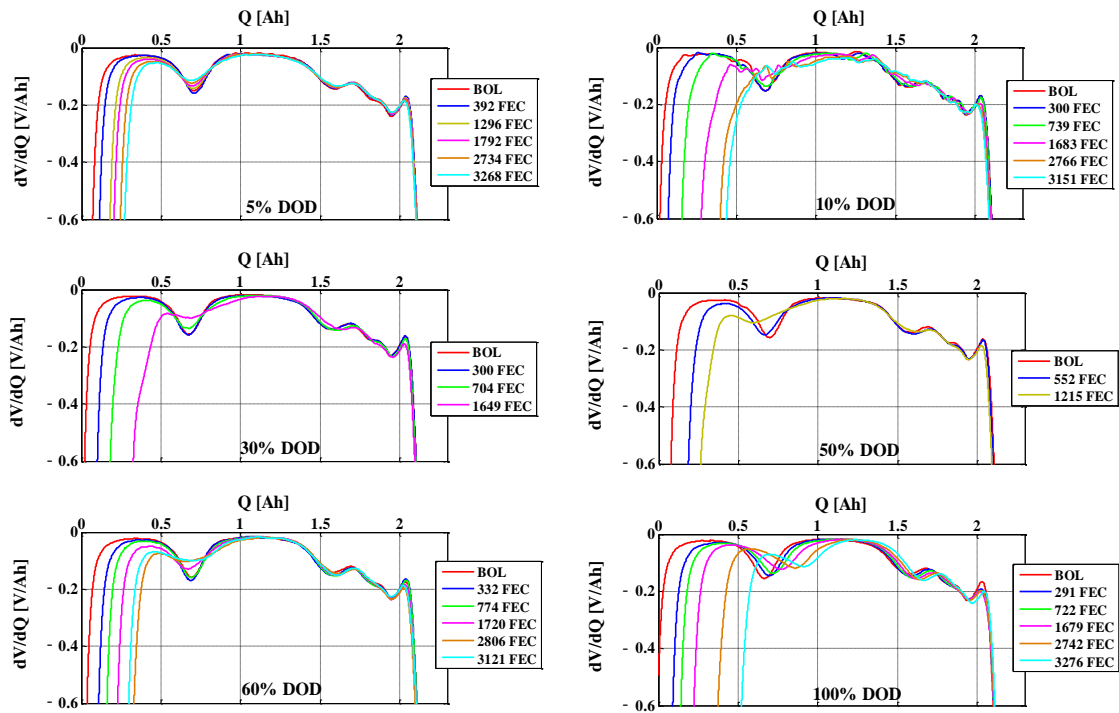
**Figure 5-32.** Actual nominal capacity ( $Q$ ) normalised to initial nominal values ( $Q_0$ ) upon cycling (50% middle SOC and 30°C) as a function of Full Equivalent Cycles (FEC) and time (d-2, e-2 and f-2). C-rate effect on capacity fade at different DOD (a-c) and DOD effect on capacity fade at different C-rate (d-f)

In conclusion, at large 100% DOD cycling, the amount of charge in the system overlaps the C-rate effect. Initially the cycling time (calendar effect) induced the capacity loss more than the operating electric current (Figure 5-32 (f-2)), in agreement with the conclusions of E. Scott *et al.* [208] and also M. Ecker *et al.* [133], who found out that there is strong superposition of calendar ageing in high SOC range cycle depth. However, it seems 2C testing to be more severe over time. At low 10% DOD cycling, the effect of cycling time (or Ah-throughput) is more significant than C-rate, but there is also C-rate influence. At intermediate 60% DOD cycling, the effect of C-rate was enhanced but the trends are not in agreement with the general theory that the degradation rate increases with C-rate, as is fulfilled for 10% DOD test. Contrary to expectations, ageing at this 60% DOD level was largely accelerated at intermediate C-rate, 2C, and 3.5C cycling did not stand out. Hence, there are complex non-linear combined effects of DOD and C-rate, which additionally depend on DOD level (Figure 5-30). More data would be necessary for an in depth interpretation of C-rate impact on cell degradation.

- **Analysis of cycling ageing mechanisms**

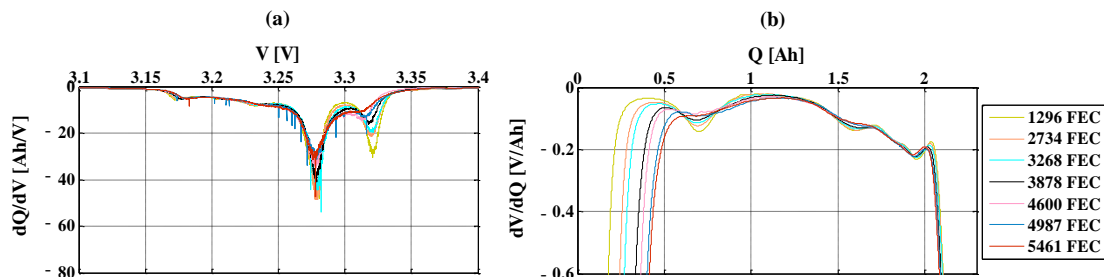
The examination of close-to-equilibrium discharge curves (quasi-OCV EPIT, described in *Chapter 2*), using DV analysis ( $dV/dQ = f(V)$ ), provided insight into degradation phenomena. The main characteristics of such curves were described above when calendar ageing was analysed (Figure 5-16). Figure 5-33 presents DV curves for each cycling condition at different DODs. Equivalent FEC signatures are shown in the same colour and only comparative data are shown (as EOT was not the same in all cases). The signatures for 10% DOD cycling condition indicated that there were measurement errors (test circuit issue at low C-rate), which hinder the identification of transitions from one electrochemically active phase to another.

The first valley shrank gradually in all cases, which demonstrates change of the stage 1 lithium-graphite compound [67] upon cycling. Hence, reduction of active lithium within the negative electrode at the beginning of cell discharge led to LLI. In the particular case of 100% DOD, all DV peaks but the last one moved towards larger SOC, which still requires analysis for further understanding. Barely any other changes were particularly highlighted from DV curves, but 5% DOD condition testing was extended up to *ca.* 5500 FEC, for which an analysis is not included in Figure 5-33. Special attention was drawn to 5% DOD and 100% DOD due to observed ageing metrics tendencies changes (Figure 5-29).



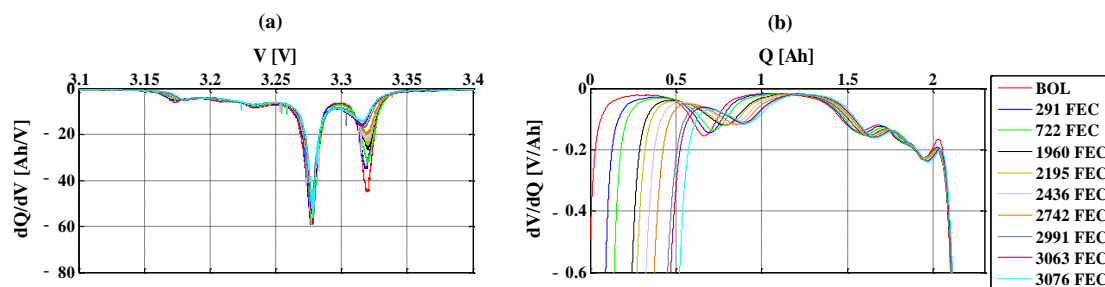
**Figure 5-33.** Equivalent (same colour) and representative Differential Voltage (DV), obtained from C/5 voltage discharge profiles, curves upon cycling at different DOD levels (1C, 50% middle SOC and 30°C)

Figure 5-34 shows more in detail the evolution of DV curves for 5% DOD cycling condition after prolonged operation, complementing the analysis with IC curves. In accordance with the ageing rate tendency change observed (Figure 5-29 (b)), from 3068 FEC onwards peaks at low SOC (*i.e.* 2-5 peaks indicated in Figure 5-16) are also modified, even though the first peak did not disappear at all. Apart from the reduction of active lithium, graphite active material was apparently modified, and this electrode degradation showed up in different graphite staging processes (2-5 peaks intensities significantly reduced and peak 3-4 cannot be virtually distinguished). Hence, even though initially LLI was the main ageing phenomenon, the performance fade of the cell cycled at 5% DOD after prolonged cycling was apparently caused by a combination of LLI and LAM. From the signatures it is difficult to identify impedance changes, as all the IC peaks are notably modified, but its origin may be LLI.



**Figure 5-34.** (a) Incremental Capacity (IC) and (b) Differential Voltage (DV) curves for 5% DOD test (1C, 50% middle SOC and 30°C) upon cycling after large number of Full Equivalent Cycles (FEC)

Figure 5-35 shows minutely (from 1679 FEC on) the evolution of DV curves for 100% DOD cycling condition and also includes IC curves. In IC signatures (Figure 5-35 (a)) the peaks associated with the highest SOC (peak 1, as indicated in Figure 5-16) are significantly more affected than the ones at lower SOC, indicating that LLI was apparently the main degradation mode. The size of the first peak reduced significantly upon cycling. This was also manifested in the respective first valley on DV curves (Figure 5-35 (b)), which corresponds with the reduction of the normalised capacity reduced in *ca.* 5.6% after 3063 FEC. Over the storage effect, mechanical stress during cycling might have enhanced the loss of exchangeable Li, which also apparently affected the electrode structure. All peaks/valleys in IC/DV curves somehow faded after prolonged cycling at 100% DOD, even though the first valley in DV curves (peak 1 in IC curves, as indicated in Figure 5-16) was not completely lost. It was therefore concluded that LAM took place and assumed it to be related to active anode material alteration [194], which means that the graphite could not be lithiated to the same level as it was initially. All the transitions from one equilibrium to the other were affected (DV peaks shifting to larger SOC). The last DV peak barely shifted, with negligible changes in the last valley 5 (peak 5 in IC curves). None of the valleys disappeared at all, even though they changed gradually, so the graphite staging process could apparently be completed upon cycling. Regarding cell impedance changes, even though IC peaks were more or less positioned at the same voltages during nearly the entire cycling test, a shift towards lower voltages of the IC curve after 3063 FEC was detected, in agreement with the sharp DC internal resistance loss measured (Figure 5-27 (b)). From IC and DC curves analysis, however, it was not possible to identify the effect responsible for the impedance change. For this reason, EIS spectra measurements were analysed.



**Figure 5-35.** Differential Voltage (DV) and Incremental Capacity (IC) curves, obtained from C/5 discharge profiles, for 100% DOD test (1C and 30°C) upon cycling

Impedance change evolution for 100% DOD test is shown in Figure 5-37. Impedance measurements were carried out at different SOH for two different cells tested at 25°C and both 30% and 70% SOC, which cell to cell variability upon cycling is shown in Figure 5-36. Even though the resistance at medium frequency changed slightly at different EIS measuring SOC (Figure 5-37 (a, b)), it was considered insignificant and assumed that the influence of SOC on

impedance measurements is negligible, in agreement with DC internal resistance measurements published in Ref. [182]. The high frequency intercepts with the real axis, which represents the resistance related to primarily the electrolyte (besides external leads and connections), is shifted to larger values upon cycling, indicating degradation of electrolyte. Conductivity of electrolyte seems to be therefore limited during cycling, which is a result of organic deposition of the electrolyte on graphite surface (reduction of solvents proportion). This effect may have been enhanced due to high cell voltages (cycling was carried out between cell voltage limits). Higher SOC results in low anode potential, which causes electrochemical instability on electrolyte material [193].

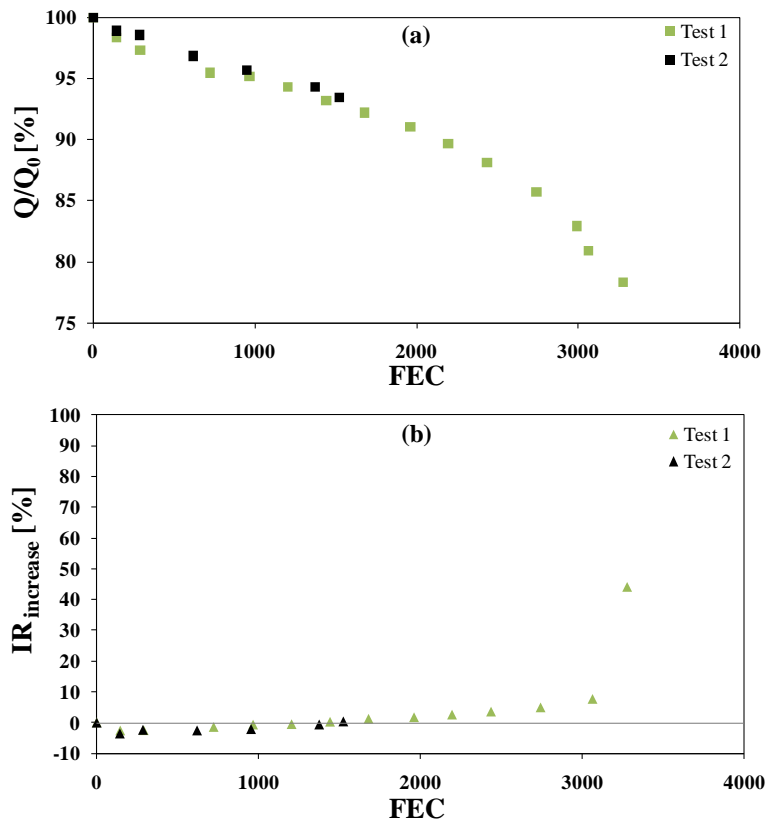


**Figure 5-36.** Cycling at 100% DOD (1C, 50% middle SOC and 30°C). (a) Actual nominal capacity ( $Q$ ) and (b) 17 s discharge DC internal resistance ( $IR$ ) increase, measured at 50% SOC, as a function of Full Equivalent Cycles (FEC), both normalised to initial values ( $Q_0$  initial nominal capacity)

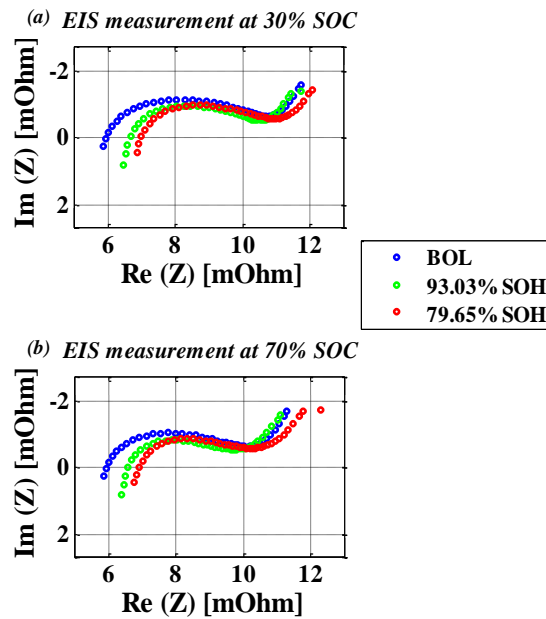


**Figure 5-37.** Impedance spectra measured over different SOH (State of Health) at 25°C and (a) 30% SOC and (b) 70% SOC. 100% DOD (1C and 30°C) tests

Overall, at 5 and 100% DOD cycling conditions, the ageing processes phenomena was a combination of LLI due to progressive growth of SEI layer, LAM and cell impedance change. For the rest of the tests at different DODs, as for the EOT, the ageing state was still governed by LLI. In order to validate these conclusions and aiming at further understanding the cell performance deterioration, post-mortem analysis was carried out for the 100% DOD aged cells.

#### • Validation of the ageing mechanisms using post-mortem analysis

Post-mortem analysis, *i.e.* ex-situ diagnostic evaluation, was carried out to confirm the ageing mechanisms identified with the in-situ electrochemical measurements. The specific behaviour observed for the 100% DOD (1C and 30°C) cycled cells was further analysed using the post-mortem methodology defined during the stage at ISEA-RWTH Aachen University (*Chapter 3*, section 3.3). This part of the work was done in collaboration with CIC energiGUNE that has implemented the developed novel methodology for cell disassembly into their routines for post-mortem characterisation. F. Aguesse (CIC energiGUNE) has been responsible for performing the characterisation analysis. Most important results are described shortly as follows.

*a) Visual inspection and microscopic analysis*

The first step after cell disassembling was the initial visual inspection of the unravelled components. LFP active material was strongly adhered onto the aluminium current collector and no macroscopic changes were indentified. The graphite electrode was not delaminated in any of the cases but its appearance changed, as shown in the images of Figure 5-38. Gold-coloured line in the middle of negative electrodes collected on pristine, conditioned and BOL (Figure 5-38 (a-c)) cells was observed. It is assumed that remaining lithium was present on the graphite electrode even after the cell discharge up to the cut-off voltage. After continuous cycling, the gold-line turned into blue coloration, revealing organic deposition related to the decomposition of the electrolyte (Figure 5-38 (d, e-1)). Moreover, localised areas containing plated metallic lithium (clear bright spots) were detected in the cell at 79.6% SOH (Figure 5-38 (e-1)). In all cases, the negative electrode sides presented the grey colour of graphite indicating less electrode degradation, as also reported by M. Klett *et al.* [62]. These areas apparently remained unchanged upon cycling. Lastly, no apparent physical damage of the separators was detected, despite the coloration change and an electrolyte brownish stain in the middle along the whole length of the jelly-roll, as shown in Figure 5-38 (e-2) for the cell at 79.6% SOH. At this stage, only few drops of liquid electrolyte were collected.

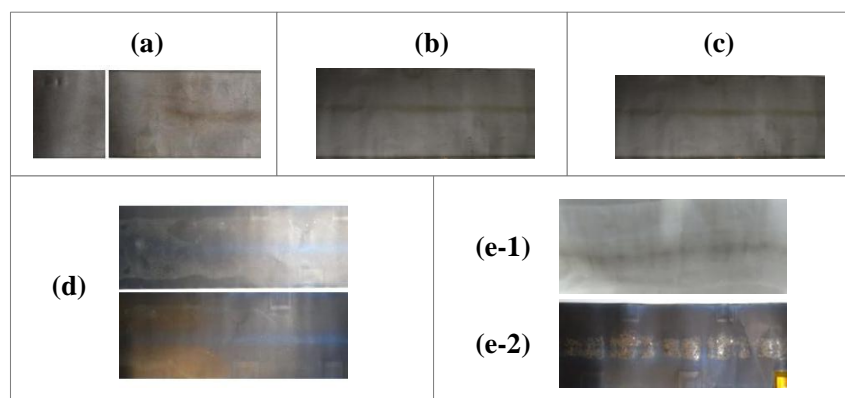


**Figure 5-38.** Initial photographs of the negative electrode: (a) pristine cell, (b) conditioned cell, (c) BOL cell, (d) two areas along the length of the electrode of the cell cycled for 1521 FEC (93.03% SOH), (e-1) cell cycled for 3276 FEC (79.6% SOH); and (e-2) separator of the cycled cell for 3276 FEC (79.6% SOH). Cycling tests: 100% DOD, 1C and 30°C

Backscattered SEM images from different negative electrodes areas are shown in Figure 5-39. No microstructure changes were observed between pristine, conditioned and BOL graphite electrodes, nor on the sides of any of the electrodes, whereas the middle area was altered for cycled electrodes. Hence, apparently the external areas barely took part or did only partially in the electrochemical processes and the negative electrode degradation was concentrated in the middle area, probably as a consequence of inhomogeneous current distribution in the system,

although temperature increase in the core of the jelly-roll and system pressure could also have contributed to it [62].

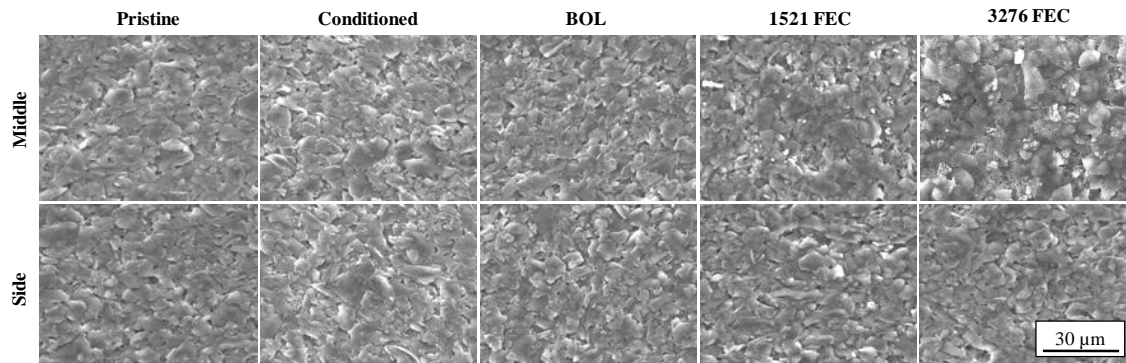


**Figure 5-39.** Secondary electron SEM images of the negative electrode: pristine cell, conditioned cell, BOL cell, cell cycled for 1521 FEC (93.03% SOH) and cell cycled for 3276 FEC (79.6% SOH). Cycling tests: 100% DOD, 1C and 30°C. The scale is the same for all images

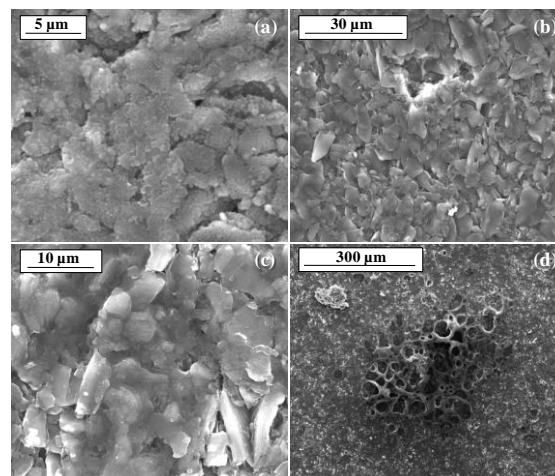


**Figure 5-40.** Secondary electron SEM images of graphite electrodes surface (different areas of interest) corresponding to cells cycles for 1521 FEC (a & b) and 3276 FEC (c & d). Cycling tests: 100% DOD, 1C and 30°C

SEM images of selected representative zones of graphite electrodes middle areas are presented in Figure 5-40. The different images (Figure 5-40 (a-d)) indicate different degradation processes that were induced within the same electrode upon cycling. On the surface of graphite sample cycled for 1521 FEC (Figure 5-40 (a, b)), two ageing phenomena were revealed: partial covering of graphite rough particles (Figure 5-40 (a)), looking like drops), indicating SEI formation, and cavities appearance (Figure 5-40 (b)) that were not observed in pristine, conditioned and BOL negative electrodes. The cavities may indicate loss of cohesion between graphite particles that may have affected the electrical conductivity. Figure 5-40 (c) indicates that the resistive surface layer got thicker and denser upon cycling, and the cavities got larger after 3216 FEC in localised areas, as shown in Figure 5-40 (d). In areas where metallic lithium was visually detected (Figure 5-38 (e-1)), the surface was polymerised and presented large

cavities of up to 10 microns. Hence, the cavities altering the surface layer were the consequence of gas formation due to electrolyte decomposition that reacts with the fresh metallic lithium [209].

Several design parameters dictate the susceptibility to lithium plating: (i) nature of electrolyte crucially affects on lithium intercalation kinetics [210], and (ii) graphite is prone to it due to the proximity of its reversible potential to that of lithium [210, 211]. Strenuous charge conditions implying large exchange currents and low temperatures lead to such a phenomenon that deteriorates radically cell performance. Cells were fully charged at 1C thousands of times, which may have reduced lithium intercalation kinetics at the anode and caused its polarisation. Charge transfer resistance increase due to the progressive growth of the passivating layer may have led to metallic lithium deposition in preference to lithium intercalation. The plated lithium is largely reversible and reoxidises during the subsequent discharge at potentials about 100 mV higher than the lithium deintercalation potentials [210], resulting in a high voltage plateau preceding the usual discharge profile and manifesting low columbic efficiency [212]. If given sufficient time, it can also intercalate into graphite [210]. Unfortunately, it does not disappear entirely. No metallic lithium was observed in the harvested electrode analysed after 1521 FEC (Figure 5-40 (a)), where localised and reversible lithium plating may have occurred. After 3276 FEC, however, there was non-reversible metallic lithium that was largely spread (Figure 5-38 (e.1)). Its reaction with electrolyte degraded graphite surface as observed before (Figure 5-40 (d)), which may have increased largely the internal resistance of the cell, in agreement with EPIT results at the EOT (Figure 5-36). On the other hand, isolated, non-active lithium on graphite surface may have contributed significantly to the enhance capacity loss after *ca.* 2500 FEC (metallic lithium nucleation accelerates the plating). Hence, these lithium plating effects may explain the observed cell performance loss (Figure 5-36) and the dominant degradation mechanism change (LLA) diagnosed from DV and IC curves (Figure 5-35). Close-to-equilibrium OCV measurements did not however enabled detecting metallic lithium.

SEM images of harvested positive electrodes in Figure 5-41 did not show distinctive change of LFP active material microstructure even after more than 3000 cycles and large cell impedance change. Figure 5-42 shows the microstructure of the separator, demonstrating that even after more than 3000 cycles there are no clogged pores, which makes still possible Li-ions transfer. They did not show any macroscopic defect either. EDS analysis of unwashed separator samples indicated presence of lithium hexafluorophosphate,  $\text{LiPF}_6$ , electrolyte salt on the surface (14.3 and 2.32 at% of F and P, respectively), so there might be still free electrolyte that make possible Li-ions conduction.

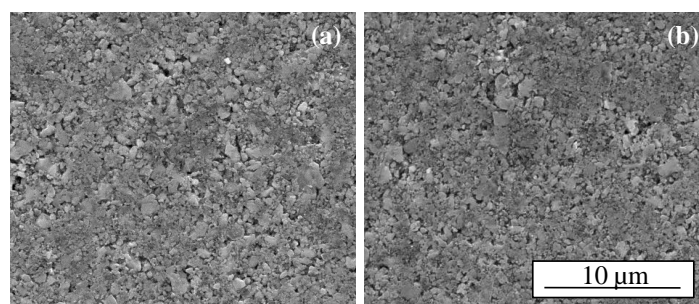


**Figure 5-41.** Backscattered electron SEM images of the positive LFP electrode: (a) pristine cell and (b) cell cycled for 3276 FEC (79.6% SOH). Cycling tests: 100% DOD, 1C and 30°C. The scale is the same for both images

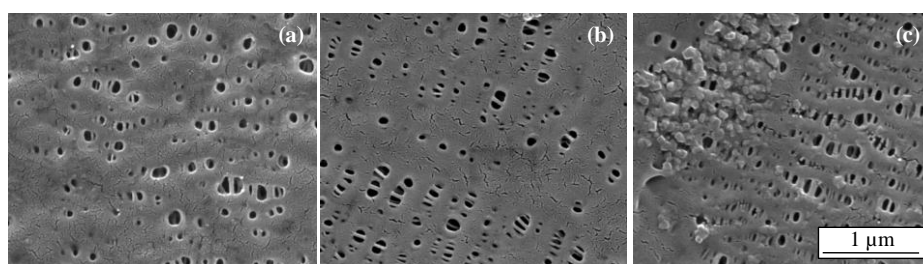


**Figure 5-42.** SEM images of the separator extracted from (a) the pristine cell, (b) the cell cycled for 1521 FEC and (c) the cell cycled for 3276 FEC. Cycling tests: 100% DOD, 1C and 30°C. The scale is the same for all images

#### *b) Structural characterisation*

XRD analyses of graphite negative electrode samples extracted from the centre of the harvested electrodes are shown in Figure 5-43. The most intense peaks correspond to the diffraction lines of graphite and copper (current collector). Additional less intense peaks mainly located between 20 and 40° in two-theta angle are also present. These peaks may be attributed to the crystallisation of organic electrolyte salts, such as  $\text{LiPF}_6$ , and additives (unwashed electrodes were examined). However, (002) characteristic peak of the graphite was not consequently shifted, as it can be observed in the inset of Figure 5-43. The amount of lithium within the graphite layers after the delithiation process is similar at the different ageing stages [58]. Hence, at first, no additional trapped lithium within the graphite structure seemed to have led to lithium loss. However, even though the peak position change is slight and inconsistent, its intensity decreased upon cycling. This reduction of the diffraction of X-rays by scattering could correspond to either a decrease of the crystallinity of the electrode or to a reduction of the crystallite size. The decrease of crystallinity is associated to an increase of the SEI layer on the surface of the electrode, *i.e.* growth of amorphous carbonate compounds on the surface of graphite particles. SEM observations do not show significant morphology changes and with these results combined, the conclusion seems to favour the latter explanation.

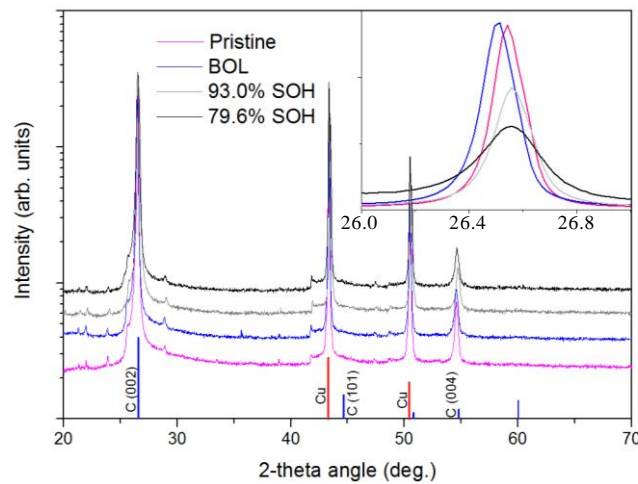


**Figure 5-43.** X-ray diffraction patterns of the harvested negative electrodes from pristine and BOL cells compared with the ones from 93.03% and 79.6% SOH cells after cycling at 100% DOD, 1C and 30°C

XRD patterns of harvested positive electrodes from pristine and the most aged cell are presented in Figure 5-44. The crystal structure of the electrode was identified as olivine-type LFP in the *Pnma* symmetry. Main crystallographic phase of the LFP remained unchanged regardless the cell degradation, but small diffraction peaks at 18.1° and 38.7° appeared (indicated with arrows in Figure 5-44), which reveals a small presence of unlithiated FePO<sub>4</sub> phase [213] after more than 3000 FEC.

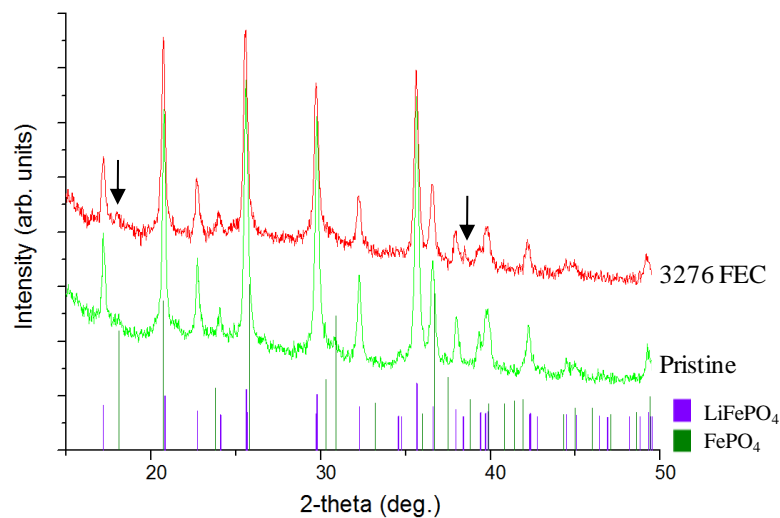


**Figure 5-44.** XRD patterns of the LFP positive electrode from a pristine cell and the cell cycled for 3276 FEC (79.6% SOH) at 100% DOD, 1C and 30°C

*c) Electrochemistry of harvested electrodes*

Galvanostatic half-cells cycling of the negative and positive harvested electrodes using lithium metal as counter electrode are shown in Figure 5-45. Half-cells were cycled repeatedly in order

to evaluate the good cycling capability and the reproducibility of the results. Figure 5-45 shows the first five cycles for selected electrode samples.

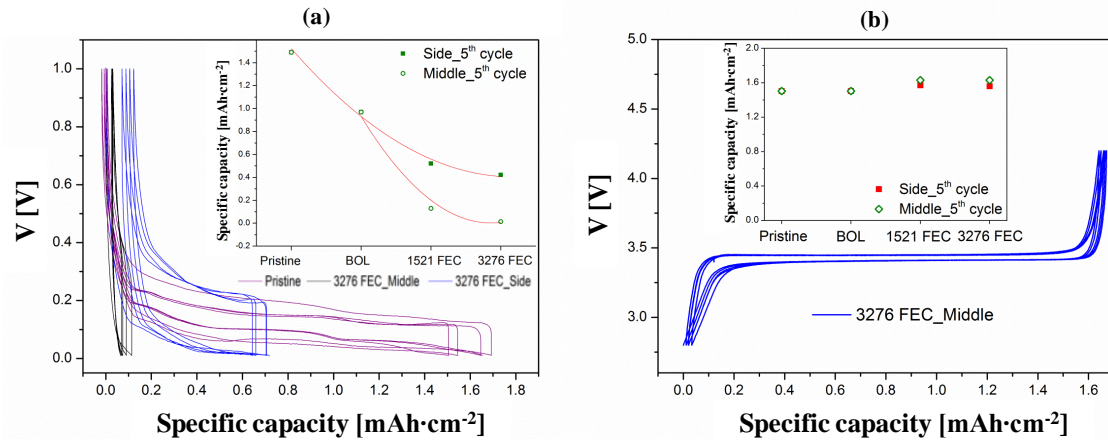


**Figure 5-45.** Galvanostatic half-cells cycling of (a) negative graphite and (b) positive LFP harvested electrodes from pristine cell, BOL cell, cell cycled for 1521 FEC (93.03% SOH) and cell cycled for 3276 FEC (79.6% SOH). Cycling tests: 100% DOD, 1C and 30°C

Figure 5-45 (a) shows cycling profiles of the pristine cell and the cell cycled for 3276 FEC, which performance depended distinctly on the selected electrode area from the original aged cell. Graphite electrode polarisation increased with ageing. Samples harvested from the middle area of the highly aged electrode showed a capacity loss of more than 95%, whereas on the side areas the capacity decreased by 60% on average. The intercalation-deintercalation process could be therefore hardly performed in the middle area and its efficiency was reduced appreciably on the sides. Hence, the passivating layer formed on top of the graphite surface seemed to limit substantially lithium transport from the electrolyte into the graphite. As observed by electron microscopy and already shown in Figure 5-39 (3276 FEC), the SEI layer was more homogeneous and thicker (covering all particles) on the middle of the electrode than on the sides. The inset in Figure 5-45 (a) compares the specific capacity of the graphite from pristine, BOL and aged cells (both studied EOTs: after 1521 and 3276 FEC). For the first two, just the values corresponding to the middle electrode area are shown, as the differences between different areas were not as appreciable as for the aged cells, which proportionally showed the same specific capacity differences between the electrode areas. *In-situ* electrochemical measurements showed large capacity decline for the anode, but data in Figure 5-45 (a) oversteps reasonable values according to the theoretical specific capacity of the half-cells electrode samples. Hence, cell disassembling, electrodes handling and half-cells assembly process may have somehow influenced harvested electrode samples properties, although they were all treated in the same way. The obtained data serves as guidance for ageing process phenomena understanding.

Cycling performance of harvested LFP electrode is shown in Figure 5-45 (b). The voltage profiles, voltage plateau and the specific capacity were similar for all studied samples (pristine, BOL and aged cells, after 1521 and 3276 FEC), so the voltage cycling profiles of a sample from the middle area of the LFP electrode harvested from the most aged cell are shown as example. On the other hand, as presented in the inset of Figure 5-45 (b), the discharge specific capacity did not change regardless the ageing rate or the sampling electrode area. Hence, electrochemical properties of LFP electrode were not altered upon cycling.

All in all, it was concluded that changes in graphite-electrolyte interface were responsible for both the sharp increase of full cell internal resistance after more than 3000 cycles (resistive interfacial layer growth; carbonate polymerisation at the interface due to electrolyte oxidation and impedance increase as consequence; etc.) and overall cell capacity fade (decomposition of electrolyte and lithium consuming SEI growth; metallic lithium deposition; etc.). It was demonstrated that LFP cathode is a robust material that presents good cycling capability with no structural degradation after over 3000 cycles. There was therefore an effect of mismatch between the positive and negative electrodes, and the degree of lithiation of LFP electrode decreased significantly with cell ageing regardless the good performance of LFP electrode: from *ca.* 90% to *ca.* 79% after 1521 FEC, and to *ca.* 70% after 3276 FEC. These results are in good agreement with the unlithiated olivine structure detected from XRD patterns. In consequence, the usable SOC range of LFP electrode and, to the same extent, full cell SOC operation window were reduced upon cycling, as shown in Figure 5-46 for the harvested electrodes middle areas from different fresh and aged electrodes. The cell SOC operation window reduced by 23% after 1521 FEC, and it did by 54% after 3276 FEC.

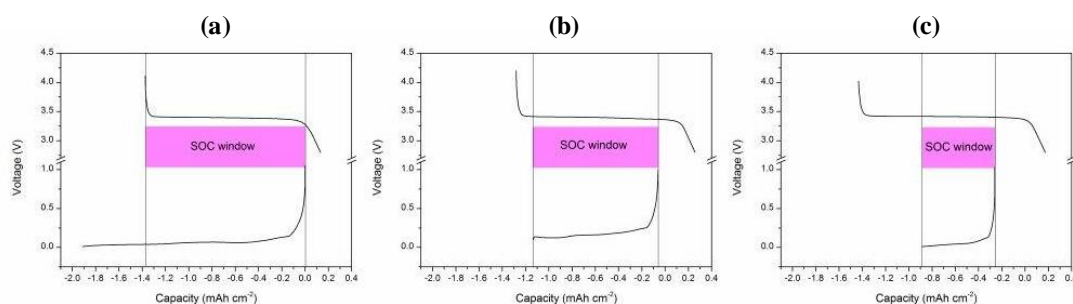


**Figure 5-46.** Positive and negative electrodes matching from capacity measurements on electrodes harvested from (a) pristine cell, (b) cell cycled for 1521 FEC (93.03% SOH) and (c) cell cycled for 3276 FEC (79.6% SOH). Cycling tests: 100% DOD, 1C and 30°C

#### *d) Post-mortem analysis conclusions*

Post-mortem analysis provided conclusive physical evidences that the main cause of ageing was the non-uniform decomposition of the electrolyte and the resulting evolution of SEI layer due to deposition of decomposition products over the graphite anode surface. A non-homogeneous layer was formed progressively consuming active lithium, which also led to loss of conductivity (electrolyte consumption). Its thickness increased gradually, in turn enlarging the charge-transfer resistance. After prolonged cycling Li-ions transport process was apparently blocked in the middle area of the electrode. This effect reduced lithium intercalation kinetics at the negative electrode and may have provoked irreversible metallic lithium deposition, resulting in additional loss of cyclable lithium (LLI) and uneven active material loss (LAM) due to isolated electrode surface. The observed effects agree with the most extended theory for the changes that take place in anode-electrolyte interface, as shown in Figure A-25 (Appendix E). LLI was not due to the lithium intercalation process within the anode (lithium trapping within the host structure of the graphite), but its main cause factor was the side reactions that decomposed the electrolyte on the anode side. Hence, even though initially LLI was the main degradation mechanism, cell performance fade, and especially capacity loss, was afterwards caused by a combination of LLI, reduced active electrode area (LAM) and cell impedance increase (step-wise electrolyte degradation). These conclusions agree with the mainly reported two-stage degradation process of LFP/graphite Li-ion cells [91].

Post-mortem observations are in good agreement with the main ageing processes deduced from in-situ electrochemical examinations. Hence, cell components physical-chemical evaluation was valuable for validating degradation modes for an adequate ageing predictive model development. This analysis also evidenced the heterogeneity of the complex ageing processes inside the cell and showed that it is not possible to set apart the observed mechanisms in order to evaluate their particular dependence on operating conditions. The semi-empirical model would not be able to completely represent the observed ageing phenomena.

#### **5.4.2.2 CYCLE AGEING PREDICTIVE MODEL**

A semi-empirical cycle lifetime model was developed based on the following considerations in the previous section:

##### *1. Ageing metrics: capacity and internal resistance*

The investigated LFP-based cell was primarily aged due to capacity fade rather than internal resistance increase. The cycle lifetime would therefore be limited by available capacity, as it

was the case for calendar lifetime. This way, cycle ageing predictive model was focused on capacity loss evolution.

Instead of using time, Ah-throughput (the amount of charge received and delivered by the battery) was chosen as a parameter for the cycle lifetime modelling (Ah-throughput-domain characterisation method).

## 2. C-rate and DOD effect

C-rate effect was minimal for some of the tests (Figure 5-32) and it was different depending on DOD level. DOD and C-rate effects are combined at certain DOD levels. It would be therefore necessary to simulate the ageing trends due to C-rate for each cycling DOD. No tests were planned for such a study, as it is beyond the scope of this work (it requires to extend test matrixes for in detail evaluation). It is hence aimed at the step-wise implementation and validation of the proposed approach for lifetime prognosis (one of its goals is to minimise the experimental work). Hence, C-rate effect was not taken into account in the cycling ageing model.

The capacity fade fitting would then include data of the conditions in the test matrix at 1C (Table 5-6), containing six different conditions.

Within this framework for cycle ageing modelling, the test planned for the model static validation (2C and 100% DOD) could not be used with the initial purpose (C-rate effect was not modelled). On the other hand, no 1C test was set apart for the static validation, after considering all the data necessary for the modelling.

## 3. DOD and Ah-throughput effect

It was observed that the DOD and Ah-throughput relationship do not follow a single dependency (Figure 5-30), *i.e.* that the DOD impact factor effect for the investigated cell is different depending on the DOD level. As illustrated in Figure 5-47, two influence scale ranges (coloured in grey and green) and a different DOD dependency for each of them (lines), can be distinguished. Hence, it would not be possible to model DOD factor effect with just one fit for the whole DOD range.

## 4. Ageing phenomena

It was confirmed that electrolyte degradation and SEI layer evolution dominates the cycle ageing (LLI), despite the occurrence of other consequential effects. LAM was detected but it was induced after different Ah-throughput depending on the ageing conditions. Hence, it was decided not to consider experimental data after the detected inflexion points (Figure 5-29)

that indicate transition to the combination of different ageing processes, as verified from close-to-equilibrium curves analysis (Figure 5-34 and Figure 5-35).

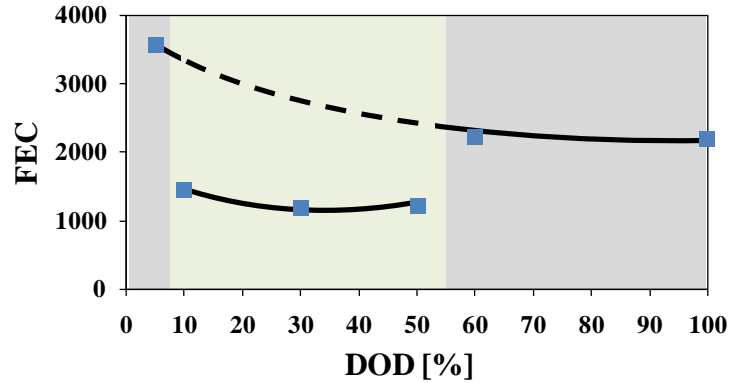


**Figure 5-47.** Illustration of DOD level influence on the total number of Full Equivalent Cycles (FEC) that the cell can deliver. The distinguished two DOD ranges (grey and green areas) and the DOD influence tendency for each of them (black lines). Data: cycling tests under 1C, 50% middle SOC, 30°C and different DOD levels before reaching ca. 90% SOH

As for the calendar ageing model, a single main degradation mode was modelled and least squares fitting method was used. To determine the most appropriate mathematical functionalities that match the conclusions from ageing analysis, illustrated in Figure 5-47, and also to determine the fitting parameters rearranging the terms, a multistep optimisation process was implemented. Different steps also defined the best DOD ranges for the two equations used for capacity fade modelling. Eq. 5-7 and Eq. 5-8 show the overall semi-empiric mathematical model for cycle ageing, where  $\alpha_3$ ,  $\beta_3$ ,  $\alpha_4$ ,  $\beta_4$ ,  $\gamma_1$ ,  $\gamma_2$  and  $\gamma_3$  are constant fitting parameters. Eq. 5-7 fits ageing data in green coloured section in Figure 5-47 (10-50% DOD). Eq. 5-8 fits ageing data in grey coloured sections and also adjusts to the transitions between the two identified DOD ranges, besides permitting extrapolations below 5% DOD ( $10\% > \text{DOD} & \text{DOD} > 5\%$ ). The level of stress was increased due to the charge in the system (Ah-throughput), as for calendar ageing, square root of time capacity fade dependency was observed ( $t^{0.5}$ ). LLI was therefore enhanced due to the mechanical stress during cycling. The cycling performance loss as a function of Ah-throughput was, in addition, different depending on DOD level ( $\text{Ah}^{0.87}$  or  $\text{Ah}^{0.65}$ ).

$$Q_{\text{loss, cycling}} [\%] \quad (10\% \leq \text{DOD} \leq 50\%) = (\gamma_1 \cdot \text{DOD}^2 + \gamma_2 \cdot \text{DOD} + \gamma_3) \cdot \text{Ah}^{0.87} \quad \text{Eq. 5-7}$$

$$\begin{aligned} Q_{\text{loss, cycling}} [\%] \quad (\text{DOD} < 10\% \ \& \ \text{DOD} > 50\%) = \\ = (\alpha_3 \cdot \exp(\beta_3 \cdot \text{DOD}) + \alpha_4 \cdot \exp(\beta_4 \cdot \text{DOD})) \cdot \text{Ah}^{0.65} \end{aligned} \quad \text{Eq. 5-8}$$

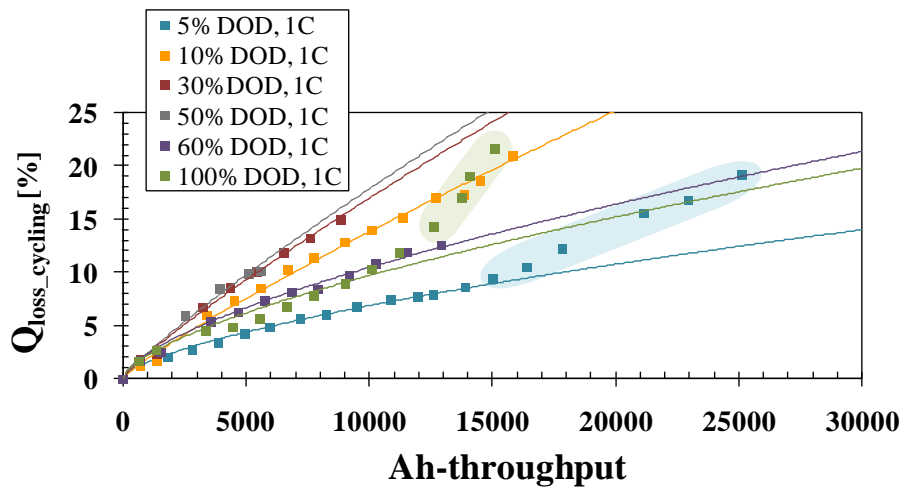


**Figure 5-48.** Capacity loss ( $Q_{loss}$ ) data at different cycling DOD levels (solid colour markers) and fitted cycle ageing model (continuous lines) for cycling at 1C, 50% middle SOC and 30°C

Figure 5-48 shows the capacity loss experimental results at different DOD levels (solid markers) and the corresponding predictions (lines) using the developed model. Data not considered for the modelling, as mentioned above, are shadowed using the same colour as the experimental data solid markers (5% DOD and 100% DOD). For such cases, if the EOL was not defined beforehand, the lifetime would be over-estimated and the ageing phenomena may lead to sudden fade. Goodness of capacity loss fit was evaluated for all experimental data at each cycling condition, except for data within shadowed areas (not considered for the fitting). Box plot in Figure 5-49 shows the distribution of modelling residuals. The average values for each group of data are illustrated with open circles and the median with a line inside the boxes. There was one outlier in 30% DOD experimental data. The fitting accuracy was the highest for 5% DOD cycling condition: its residuals variance was just 0.01%, interquartile range 0.15% and median 0.12%. The model also matched with high precision 30% DOD ageing data (0.05% variance, 0.23% interquartile range and 0.22% median of the residuals). The 60% DOD fittings residuals median is between those for 5 and 30% DOD, but the interquartile range is larger (0.68%). The largest difference between fitting and experimental data was for 100% DOD cycling condition, but the model results were still good. Whiskers showed 0.22% variance and the median was 0.47%, but the residuals showed symmetric distribution. 50% DOD fitting showed the largest median residual value (0.51%), but the sample size at this condition was not representative (N=4). Its interquartile range was equal to that of 10% DOD fitting, but for the latter the residuals distribution was symmetric. The accuracy of the model for each fitted DOD cycling condition (1C, 50% middle SOC and 30°C) is ranged as follows: 5% > 30% > 60% > 10% > > 50% > 100% DOD. All in all, the mean overall fitting residual was just 0.32% and 1.45% the maximum.

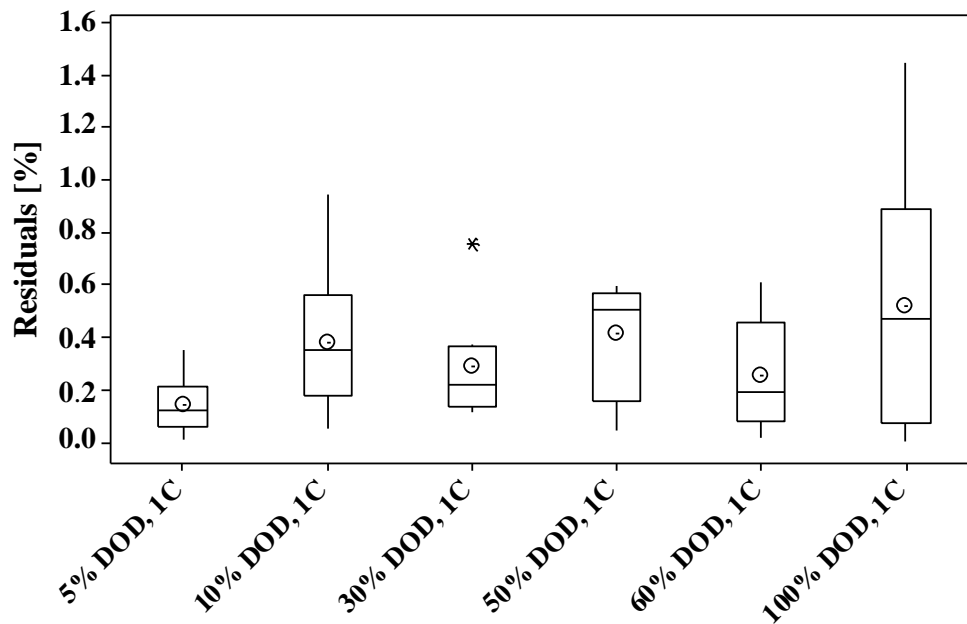


Figure 5-49. Box plot of capacity fade prediction residuals distribution for each modelled cycling condition

The suitability of the developed function for the cycle life model was further assessed against different operating C-rates. Eq. 5-7 and Eq. 5-8 were used to fit capacity loss evolutions at each examined C-rate, as shown in Figure 5-50. Prediction errors are evaluated in Figure 5-51. The mean prediction error was 1.44%, for which the major contribution was coming from 10% DOD and 3.5C cycling condition prediction. The source of the error was not therefore the change of the power law relation, as it changed especially under 60% DOD and 2C cycling condition, in agreement with the observations from Figure 5-32. Table 5-7 shows Ah-throughput power values ( $b$  from  $a \cdot Ah^b$  capacity loss function) at different DOD and C-rate levels. Notice that it is not consistent to assess a single power value for the defined 10% > DOD > 50% range (Figure 5-47) at 2C, although there were two power values (at 60% and 100% DOD), due to the complex non-linear combined effects of DOD and C-rate. Individual prediction errors for 10% DOD and 2C showed the largest variance and the lowest prediction errors median value (0.69%) at the same time. The large variance could be ascribed to experimental measurements. Even though no outliers were identified, the last three data values are away from the ageing tendency followed by this test. The errors median was the largest for 10% DOD and 3.5C (2.72%). For the rest of tests, the prediction error median was quite low, 0.96-1.27%. The overall predictions results, using the model that does not take into account the C-rate impact factor effect, are successful under cycling tests that combine different complex interactions of C-rate and DOD.

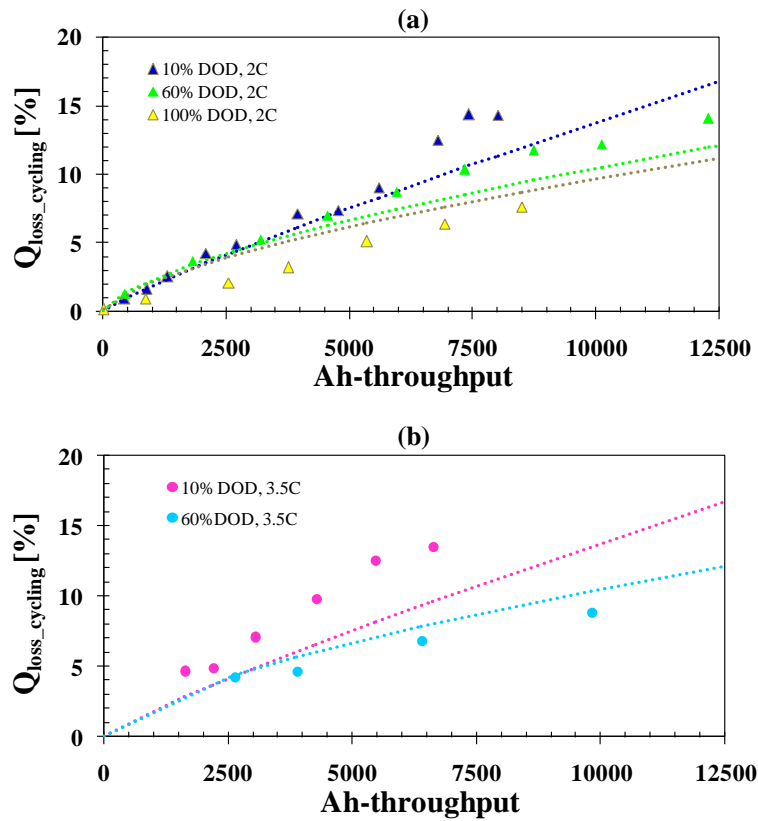


Figure 5-50. Capacity loss experimental data (markers) and predictions (dotted lines) under cycling under different DOD conditions and C-rate conditions: (a) 2C and (b) 3.5C

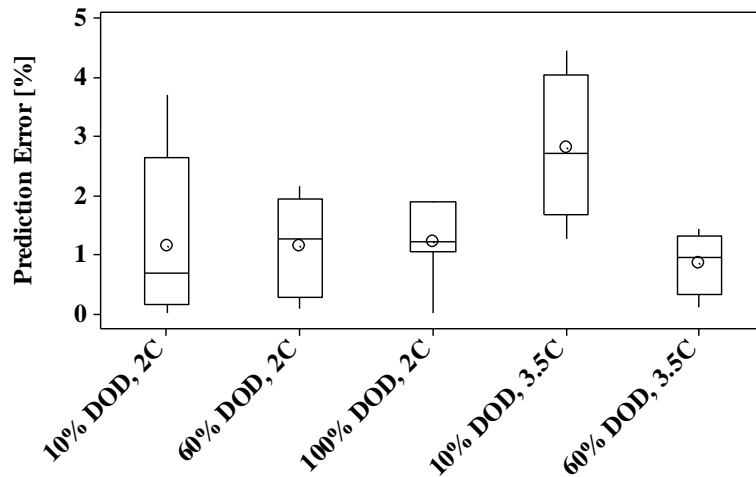


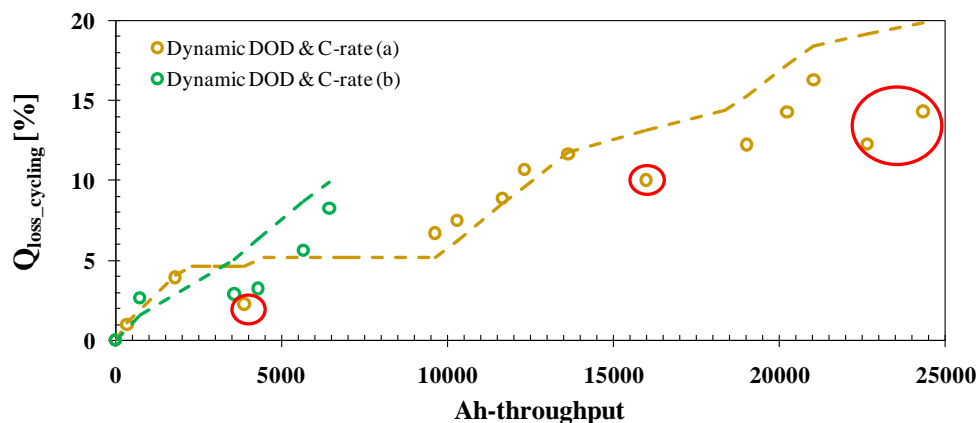
Figure 5-51. Box plot of capacity loss prediction errors distribution for cycling conditions at C-rates different from modelled 1C condition

Table 5-7. Ah-throughput power values for capacity fade cycling model at different C-rate and DOD conditions

$Q_{loss} = a \cdot Ah^b \rightarrow$ Power values (b)					
1C		2C		3.5C	
$10\% \leq DOD \leq 50\%$	0.87	10%	0.91	10%	0.84
$10\% > DOD > 50\%$	0.65	60%	1.04	60%	0.57
		100%	0.61		

- **Dynamic validation**

Additional tests were run in order to check model validity under more realistic conditions, which the model would have to face for predicting lifetime in real applications. These tests consisted of making dynamic upon cycling the controllable cycling ageing impact factors that were considered within this work, *i.e.* DOD and C-rate according to the lifetime prognosis methodology (Figure 5-4). The defined two dynamic validation tests profiles were shown in the experimental section (Figure 5-26). To evaluate the effect of the sequences in the same load collectives shown in Figure 5-26, it was assumed, in agreement with H. Wenzl *et al.* [177], that the degradation caused by a new event is independent of the cell history (previous cycles) that induced accumulated ageing. Figure 5-52 shows capacity loss experimental data (open markers) and the corresponding predictions using Eq. 5-7 and Eq. 5-8 (dotted lines with the same colour as the corresponding experimental data markers). Results showing capacity recovery are encircled in red. In such cases, the level of stress in the cell was reduced due to either the cycling conditions or pause times before and after the check-ups at some time. These data are set apart as the developed capacity loss model is accumulative upon ageing and would never be able to predict cell capacity rise because of reversible phenomena. The prediction methodology under dynamic cycling conditions is the same used for dynamic calendar ageing (section 5.3.2.2): it takes into account the ageing by former usage, so the residual capacity is used as a reference point for further predictions at different operating parameters and not simply the operating time [177, 199]. The total ageing time is the sum of the cycling time periods at different DOD and C-rate conditions. It appears that the general irreversible capacity offset trend is followed. However, it is difficult to describe the relationship between the mathematical correlation and measured cell performance loss, and even to qualitatively understand capacity fading behaviour for the different conditions upon cycling.



**Figure 5-52.** Capacity loss ( $Q_{loss}$ ) data (markers) under dynamic cycling conditions (Figure 5-26 (a and b)) and corresponding simulation results (dotted lines). Cycling under dynamic, DOD and C-rate, 50% middle SOC and 30°C

Initially, two dynamic cycling tests were just planned, as presented in experimental section (Figure 5-26). Different both C-rate and DOD periods were combined at a time, as one of the targets of the lifetime prognosis methodology was to minimise the time consuming and cost-intensive experimental work. However, in view of the complexity of the results (Figure 5-52), it was considered interesting to carry out additional tests and a methodology for cycling ageing dynamic validation was defined, which is outlined in the flow chart in Figure 5-53. After the combined analysis of different cycle ageing impact factors under dynamic conditions (*Dynamic validation I*), in case it were necessary, the methodology would propose to also study individually DOD and C-rate parameters single effects more in depth under non-constant profiles (*Dynamic validation II*). These analyses intend to provide insight into the combined effects analysis (*Dynamic validation I*). However, if believed necessary, more additional tests would be suggested (*Dynamic validation III*) for an in depth understanding of cell ageing behaviour under realistic cycling operation conditions.

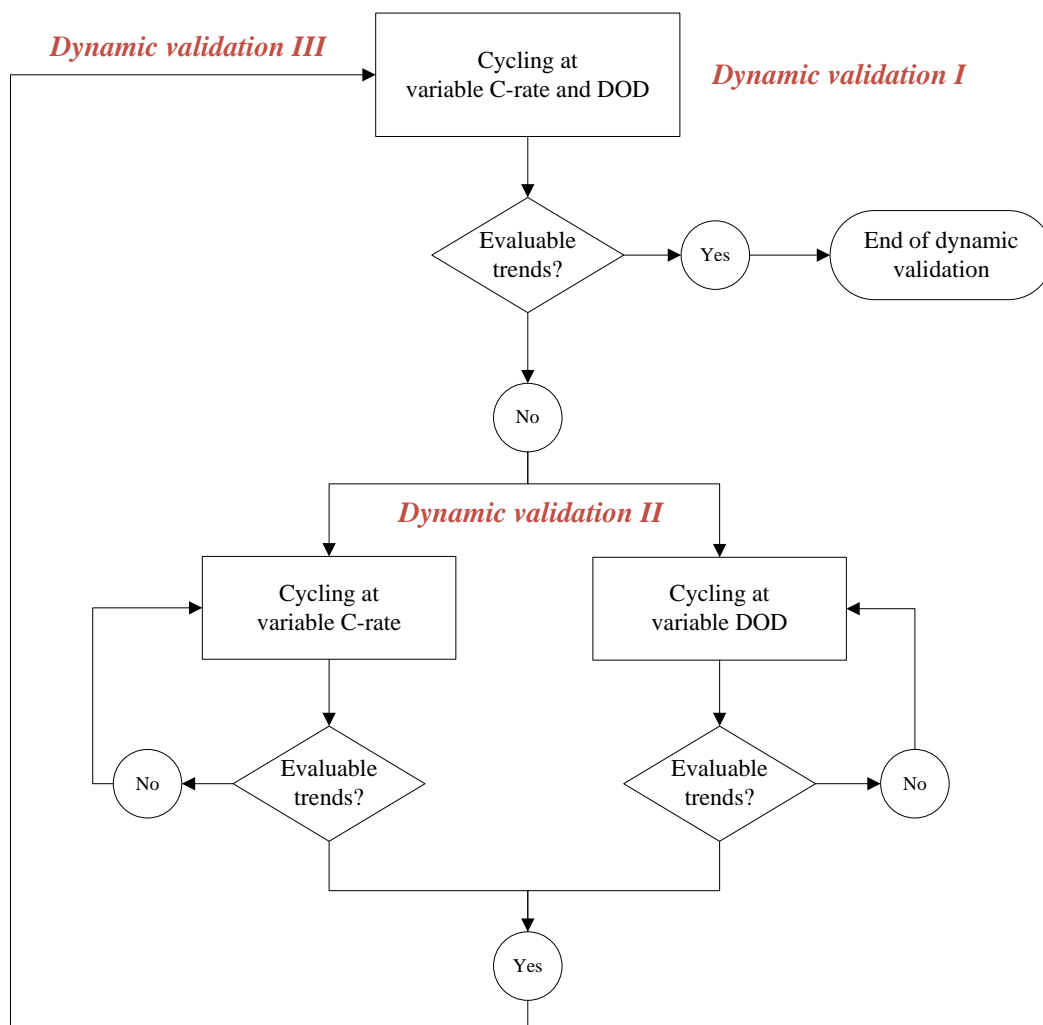
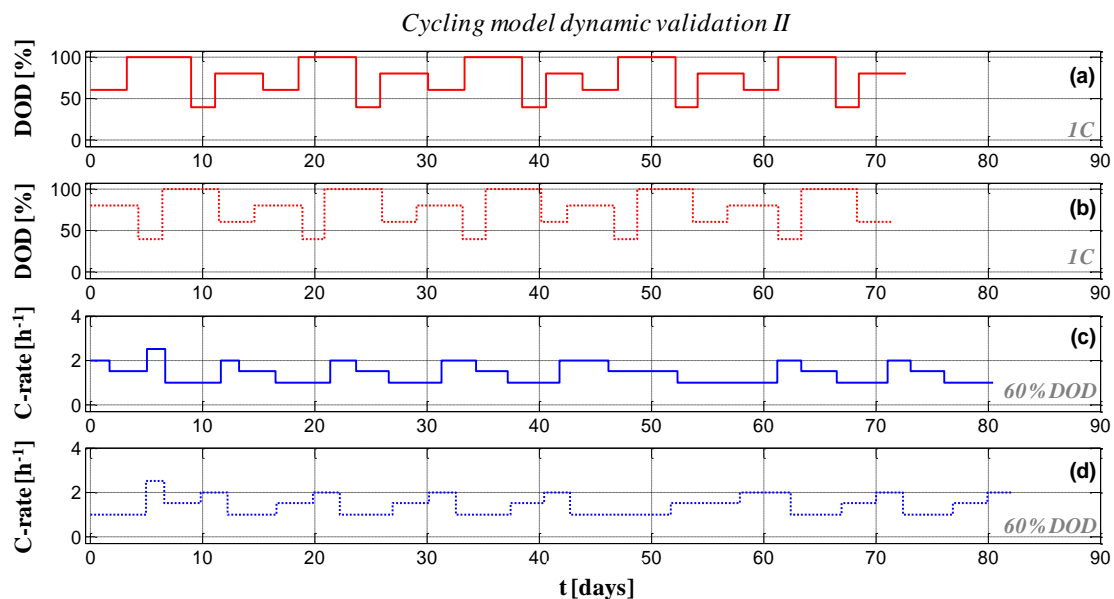
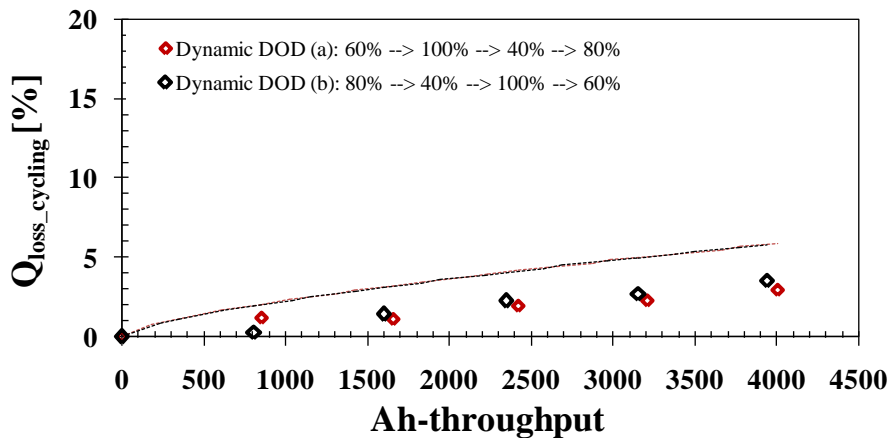


Figure 5-53. Testing procedure for cycling ageing dynamic validation

The first step (cycling at variable both C-rate and DOD) of the dynamic validation methodology was already fulfilled, with no clearly evaluable trends (Figure 5-52). Further tests that were defined for the dynamic validation of individual DOD and C-rate impact factors effects (*cycling model dynamic validation II*), are shown in Figure 5-54. These tests were planned so that it was also possible to explore the effect of different either DOD or C-rate sequences of cycling events in the same test. This way, these parameters alternation sequences between check-ups were planned from lower to higher values in one of the tests (Figure 5-54 (a, c) for dynamic DOD and C-rate evaluation, respectively) and, alternatively, from higher to lower DOD in the other (Figure 5-54 (b, d) for dynamic DOD and C-rate evaluation, respectively). The number of cycles (N) under each either DOD or C-rate condition were approximately the same. Figure 5-55 and Figure 5-56 show experimental results of the dynamic DOD and C-rate cycling tests (markers), respectively, and the corresponding predictions (dotted lines), using the cycling ageing model (Eq. 5-7 and Eq. 5-8) and the previously described methodology for prediction at non-static conditions.



**Figure 5-54.** Cycling ageing model dynamic validation II. Four different tests defined under dynamic either DOD (1C) or C-rate (60% DOD), 50% middle SOC and 30°C. Two tests under dynamic DOD (a,b) and other two under dynamic C-rate (c,d)



**Figure 5-55.** Capacity loss ( $Q_{loss}$ ) data (markers) under dynamic DOD cycling conditions (Figure 5-54 (a,b)) and corresponding simulation results (dotted lines). Cycling under 1C, 50% middle SOC, 30°C and dynamic DOD

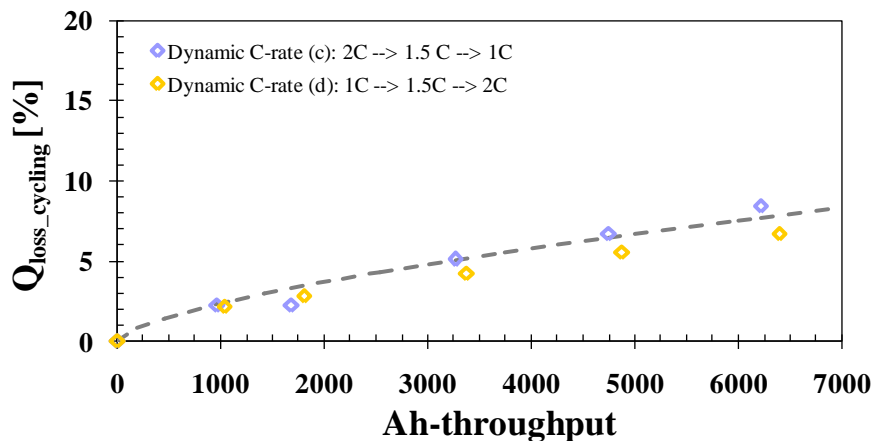


**Figure 5-56.** Capacity loss ( $Q_{loss}$ ) data (markers) under dynamic C-rate cycling conditions (Figure 5-54 (c,d)) and corresponding simulation results (dotted lines). Fittings are superimposed because the DOD is the same for both tests and the predictions do not include the C-rate effect. Cycling under 60% DOD, 50% middle SOC, 30°C and dynamic C-rate

The repetitive dynamic DOD tests sequences, as already shown in the first two tests profiles in Figure 5-54 (a, b), are as follows: (Test a) 60% DOD → 100% DOD → 40% DOD → → 80% DOD and (Test b) 80% DOD → 40% DOD → 100% DOD → 60% DOD. The cycle ageing semi-empirical mathematical model shows that the total capacity loss is independent of any sequence of DOD. Experimental verification in Figure 5-55 however indicates that there is a slight dependence on the sequences, although different DODs lead roughly to the same overall degradation. The results show that the capacity decline is more accelerated going from higher to lower DOD levels (Figure 5-54 (b)) than when going from lower to higher cycling voltage range (Figure 5-54 (a)). These observations need of verifications at larger testing times though, to ensure that the sequence of DOD events will not play a larger role when battery operation changes constantly.

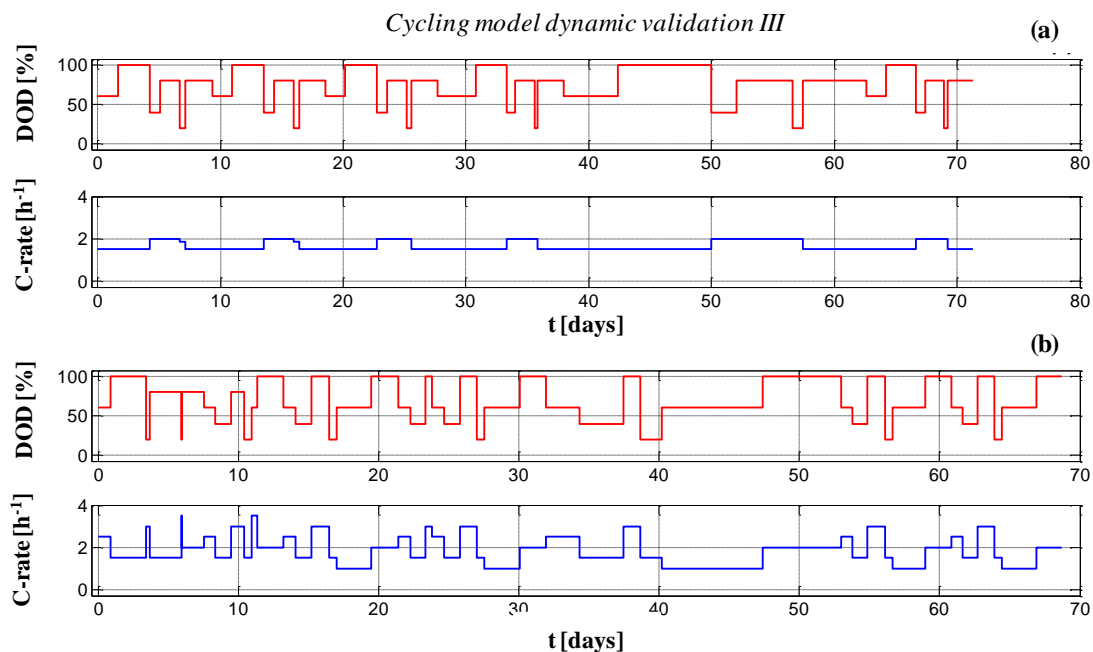
The repetitive dynamic C-rate tests sequences are as follows: (Test c)  $2C \rightarrow 1.5C \rightarrow 1C$  and (Test d)  $1C \rightarrow 1.5C \rightarrow 2C$ . As already shown in the profiles in Figure 5-54 (c, d),  $2.5C$  was also intercalated in the first cycling period. From applied C-rates profiles it can be deduced, as shown in Figure 5-56, that firstly higher C-rate level (Test c) leads to overall slightly larger degradation. However, initially the degradation was not faster and cell ageing overlapping was observed in the third check-up. Figure 5-54 shows that after 32-32.5 days of continuous operation (2400-2600 Ah-throughput), cells underwent additional cycles to the planned sequences, under different conditions in each case. Cell under Figure 5-54 (c) test did it at  $2C$  over 22 h, whereas cell under Figure 5-54 (d) was cycled at  $1C$  for 9 h (afterwards, the tests continued as planned). This alteration may have led to larger degradation of the former cell, which also could have accelerated the degradation rate afterwards. Anyway, the differences do not attract so much attention. Overall, from *cycling model dynamic validation II* it was concluded that cycle ageing depends little on the sequences of the cycles either DOD or C-rate, which confirms the hypothesis adopted for the modelling (degradation independent on cell history). However, it is necessary to verify the degradation that occurs when intercalating events of storage operation between cycling sequences.

Results from cycling the battery under dynamic power profile (Figure 5-56) also showed that the models based on constant-current data at just  $1C$  predict the dynamic performance data well. It suggests that factors affecting capacity fade are similar at low and high charging and discharging rates for a given DOD. The prediction errors were even optimised at dynamic C-rate, so the model adapts even better to more realistic battery behaviour. The mean prediction error was reduced from 1.44% (under static C-rate conditions) to 1.16%. However, prediction accuracy diminished under dynamic DOD continuous cycling conditions (Figure 5-55). Capacity loss predictions were distinctly over measured data, but keeping the same tendency. It seemed that such over-estimation was controlled by a critical factor. This characteristic was revealed for estimations under dynamic DOD conditions and not for dynamic C-rates at a constant DOD. Moreover, after 4000 Ah-throughput the capacity loss under dynamic DOD conditions was in the range of 3-3.5%, whereas it was 4-8.5% under static DOD conditions (Figure 5-48). Therefore, the initial conclusion was that the cell degradation is lessened under dynamic DOD conditions, which means that the ageing acceleration factor for different static DOD tests is larger than that for dynamic DOD tests. The ageing predictive model, which is a function of DOD and Ah-throughput, was developed based on static tests data, and this is apparently why it over-estimates the ageing under dynamic DOD conditions. Going back to the initial cycling model dynamic validation (Figure 5-52), this conclusion could not be clearly demonstrated, as data did not show any marked tendency. Aiming at overcoming the

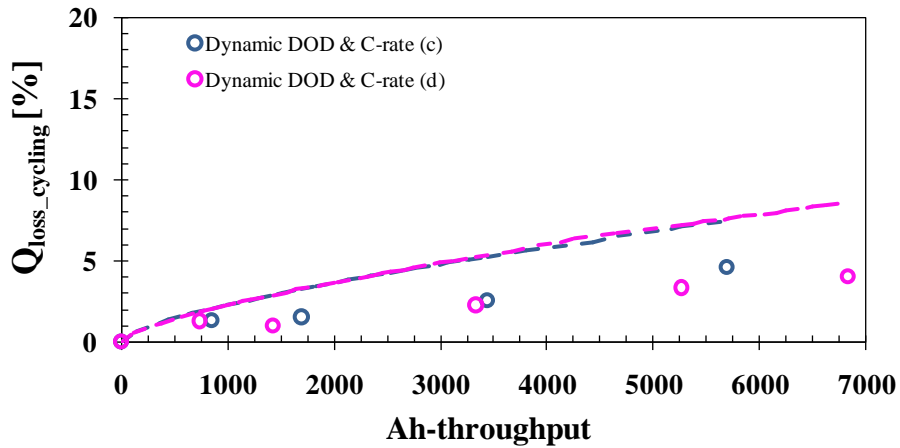
discrepancies between modelling results and experimental data, additional tests under dynamic both C-rate and DOD operation schemes were carried out.

Figure 5-57 shows the defined test profiles for the *cycling model dynamic validation III* step. They covered DOD levels that were not evaluated in the modelling process (such as 20%, 40% and 80% DOD) and the C-rate was also made much more dynamic. This is an attempt to evaluate the C-rate issue under more exigent conditions, as evidenced in the profiles defined in Figure 5-57 (b). Figure 5-58 presents these last C-rate and DOD dynamic validations experimental results (markers) and simulation outputs (dotted lines) based on Eq. 5-7, Eq. 5-8 and the prediction methodology that takes into account the accumulated ageing each time the operating parameters change. This closer examination of both cell ageing behaviour and the established cycle ageing model goodness demonstrated that:

- i) The impact of the C-rate factor is not large and its level of influence on capacity loss rate does not stand out (it is negligible).
- ii) The developed model for 50% middle SOC and 30°C, based on static and symmetric cycling conditions tests results, over-estimates the cell capacity fade under dynamic operation. Continuous cycling at static conditions accelerates the cell ageing more than continuous cycling under dynamic conditions, although the latter tests were also accelerated. The acceleration factor for static ageing continuous conditions is mainly influenced by the DOD factor.



**Figure 5-57.** Cycling ageing dynamic validation III. Additional two tests (a and b) under both dynamic DOD and C-rate over time at 30°C and 50% middle SOC



**Figure 5-58.** Capacity loss ( $Q_{loss}$ ) data (markers) under dynamic cycling conditions (Figure 5-57) and corresponding simulation results (dotted lines). Cycling under dynamic, DOD and C-rate, 50% middle SOC and 30°C

The solution for improving the cycle ageing predictive model was to introduce a correction factor that deals with the ageing acceleration issue. With this purpose, ageing acceleration factors for DOD parameter under static and dynamic ageing conditions were compared. The respond matrix was contrasted with observation data and the best model correction complex factor coefficient, namely  $k$ , was assessed performing the prediction errors analysis. This factor is a function of Ah-throughput.

Figure 5-59 and Figure 5-60 show the predictions using the cycle ageing model with the DOD ageing effect acceleration correction factor implemented for dynamic operation estimations, as indicated in Eq. 5-9 and Eq. 5-10. The predictions RMSE for dynamic DOD cycling improved from 2.20% (Figure 5-55) to 0.88% when implementing the ageing acceleration correction factor (Figure 5-59). It also improved consistently for the predictions of the four tests that combined dynamic both C-rate and DOD events: from 2.79% (Figure 5-52 and Figure 5-58) to 1.75% (Figure 5-60).

$$Q_{loss, cycling} [\%] \quad (10\% \leq \text{DOD} \leq 50\%) = (\gamma_1 \cdot \text{DOD}^2 + \gamma_2 \cdot \text{DOD} + \gamma_3) \cdot k \cdot \text{Ah}^{0.87} \quad \text{Eq. 5-9}$$

where  $k=1$  in case the DOD factor is constant over time

$$Q_{loss, cycling} [\%] \quad (\text{DOD} < 10\% \ \& \ \text{DOD} > 50\%) = (\alpha_3 \cdot \exp(\beta_3 \cdot \text{DOD}) + \alpha_4 \cdot \exp(\beta_4 \cdot \text{DOD})) \cdot k \cdot \text{Ah}^{0.65} \quad \text{Eq. 5-10}$$

where  $k=1$  in case the DOD factor is constant over time

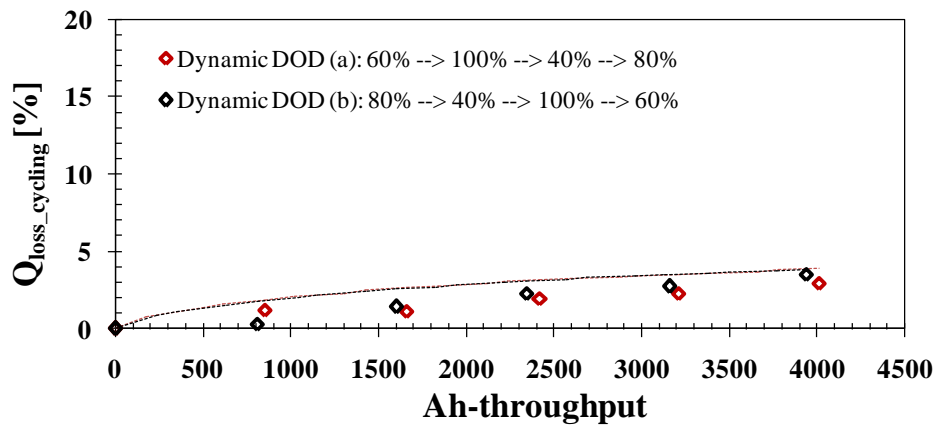


**Figure 5-59.** Capacity loss ( $Q_{loss}$ ) data (markers) under dynamic DOD cycling conditions (Figure 5-54 (a,b)) and corresponding simulation results (dotted lines) using the static ageing acceleration correction factor. Cycling under 1C, 50% middle SOC, 30°C and dynamic DOD. Improvement of the prediction shown in Figure 5-55

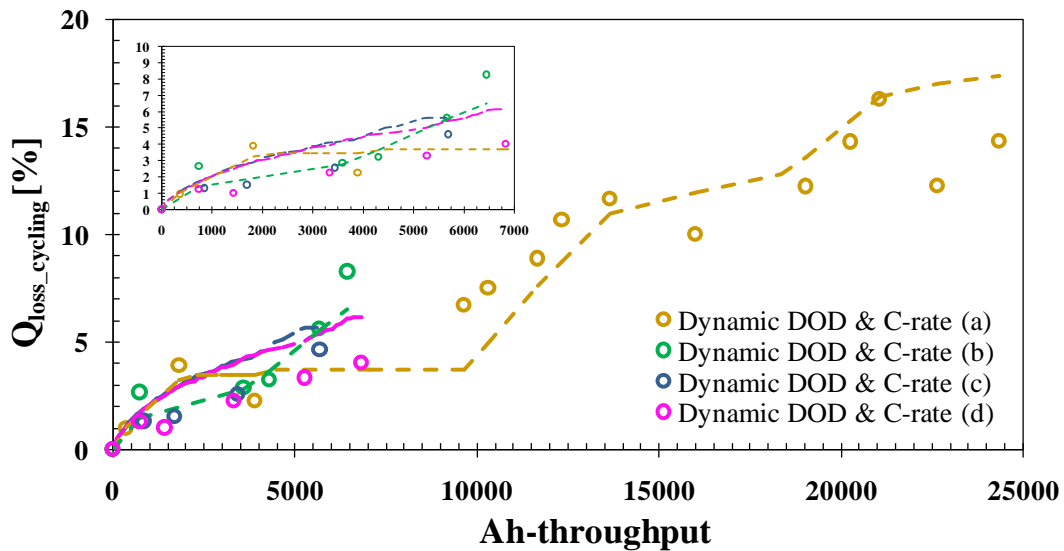


**Figure 5-60.** Capacity loss ( $Q_{loss}$ ) data (markers) under dynamic cycling conditions (Figure 5-26 and Figure 5-57) and corresponding simulation results (dotted lines) using the static ageing acceleration correction factor (Eq. 5-9 and Eq. 5-10). Cycling under dynamic, DOD and C-rate, 50% middle SOC and 30°C. Improvement of the predictions shown in Figure 5-52 and Figure 5-58. Magnification of tests (b-d) in the inset

### 5.4.3 CYCLE AGEING MAIN CONCLUSIONS

Cycling dynamic validations provided many important results regarding C-rate and DOD effects under non-constant schemes for promoting the understanding of cycle ageing phenomena. Overall, eight cycling ageing model dynamic validation tests were carried out, which were defined with different specific goals for an extensive capacity loss evaluation.

The developed model does not include C-rate factor, but it was able to predict precisely its effect as well. This is corroborated by applying the model prediction to different static C-rates operation conditions experiments not used for modelling. Even further tests at dynamic C-rate conditions show better agreement between experimental and model results, validating the proposed cycling model.

Static cycling degrades the cell more than dynamic operation. That means that the prediction based on the static modes underestimates the lifetime. The initial proposed model, which is based on LLI ageing phenomnon, systematically overestimates capacity loss upon more realistic dynamic conditions and therefore a correction factor for ageing acceleration rate was introduced. Taking all this into account, the estimated RMSE was 1.75%.

## 5.5 COMPLETE LIFETIME MODEL

Once cycle and calendar ageing impact factors (Figure 5-4) were quantified separately, and single cycling and calendar ageing models were thoroughly validated, their effects were combined. Different sequences changing constantly between several cycling and standby operation events were analysed. Ageing model (Eq. 5-5, Eq. 5-9 and Eq. 5-10) and the approach outlined for cell complete ageing analysis were implemented into a simulation platform (MATLAB-Simulink framework). Figure 5-61 shows the Simulink block diagram of the lifetime prediction platform, which includes field parameters conversion into ageing model inputs and enables simulating cell real operation for each time-step (in the specific case of the investigated cell, internal resistance increase is not predicted but just the capacity loss). The basis of the complete algorithm is as follows:

- Effects weighing method. Cycle and storage effects were superimposed.
- Hypothesis: SOC and T impact factors effects are the same during storage and cycling operations.
- Assumption that the ageing processes of a new event are independent of the cell history.
- Methodology of predictions: accumulated capacity loss was taken into account for making further predictions at a different cycling or calendar event.

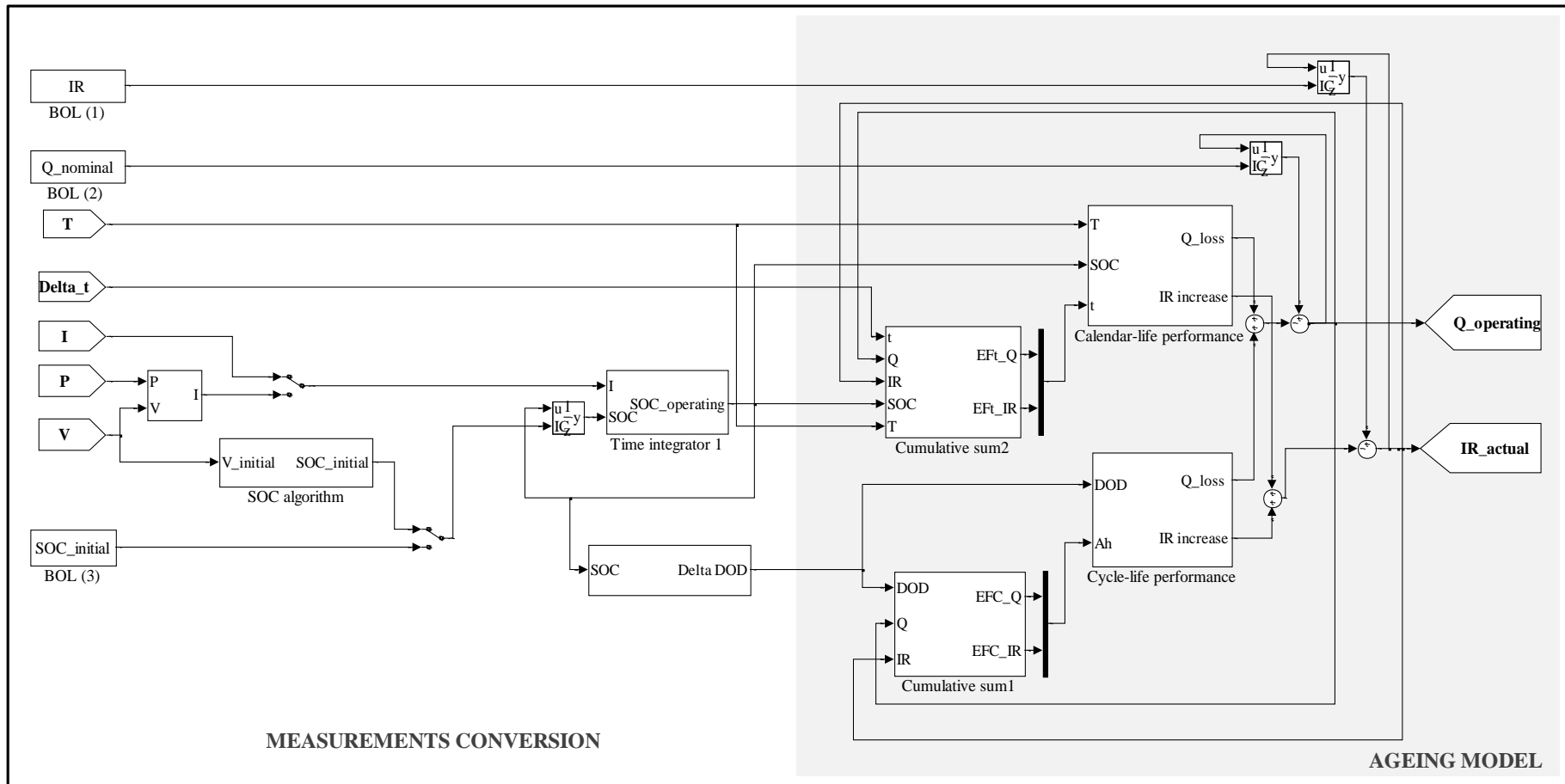


**Figure 5-61.** Complete ageing model. Available capacity ( $Q$ ) and internal resistance ( $IR$ ) offset prediction in response to time and controllable environmental influences ( $Eft$ : Equivalente Full time,  $EFC$ : Equivalente Full Cycles)

### 5.5.1 VALIDATION APPROACHING REAL OPERATION

Different storage and cycling operating events were combined aiming at evaluating:

- i) Such schemes impact on cell capacity loss.
- ii) The possibility of predicting cell capacity loss under such profiles following the proposed approach for lifetime prognosis (basis of the complete algorithm, as described above).

This first complete model analysis is based on symmetric cycling operation, *i.e.* charge sustaining and a single C-rate at each DOD, like cycle ageing was modelled. Further validation steps will comprise the model adaptability to different realistic scenarios, which implies complex cycling operation.

#### 5.5.1.1 EXPERIMENTAL

Figure 5-62 (a), (b) and (c) show different tested validation tests profiles approaching real operation, which combine the effects of SOC, T, DOD, C-rate, time (storage effect) and Ah-throughput (cycling effect). Figure 5-62 (a) also shows the current profile and the voltage response, as well as the cell surface heating during the test. Besides the temperature, Figure 5-62 (a) and (b) profiles are very similar but not exactly the same. After cycling periods at different middle SOC, DOD and C-rate, the cells were kept at the same test temperature and at a defined, but different over time, SOC for different storage periods: 30 min, 4 h and 8 h. They intend to represent a short pause (30 min, *e.g.* EV stop for doing errands in the city centre), overnight or working hours storage (8 h, *e.g.* pause of an office elevator or a personal car parked) and in between brake (4 h, *e.g.* overnight pause of a residential elevator). Moreover, calendar testing periods were also prolonged, aiming at, on the one hand, representing holiday periods *e.g.* for EV used for every-day driving, and, on the other hand, examining the capacity recovery phenomenon, probably related to charge redistribution when there is no lithium intercalation-deintercalation (cell charging-discharging) force acting on the electrodes [125].

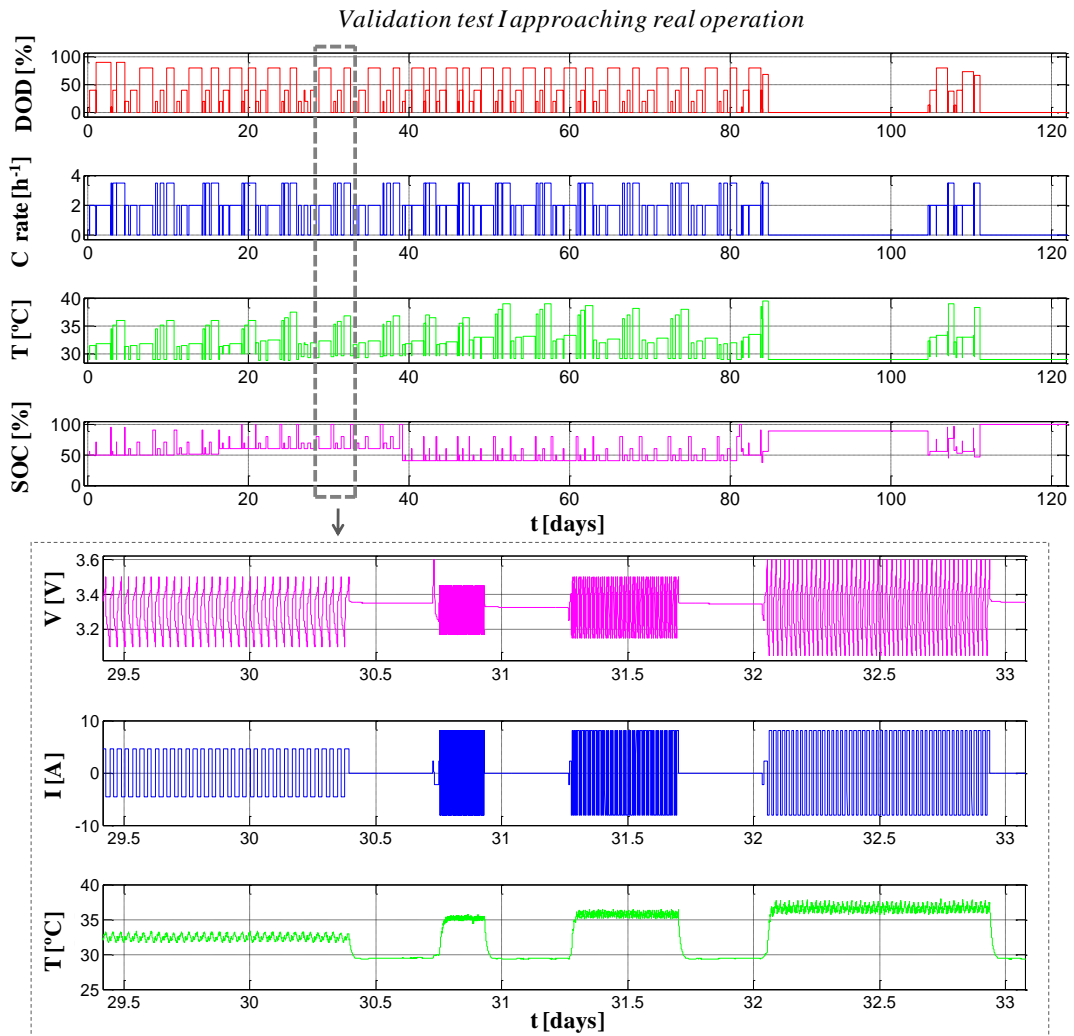


**Figure 5-62 (a).** Validation test (I) approaching real operation. Ageing model input impact factors profiles on top and in situ measurable factors in real applications for the marked (dashed grey box) tested time-interval

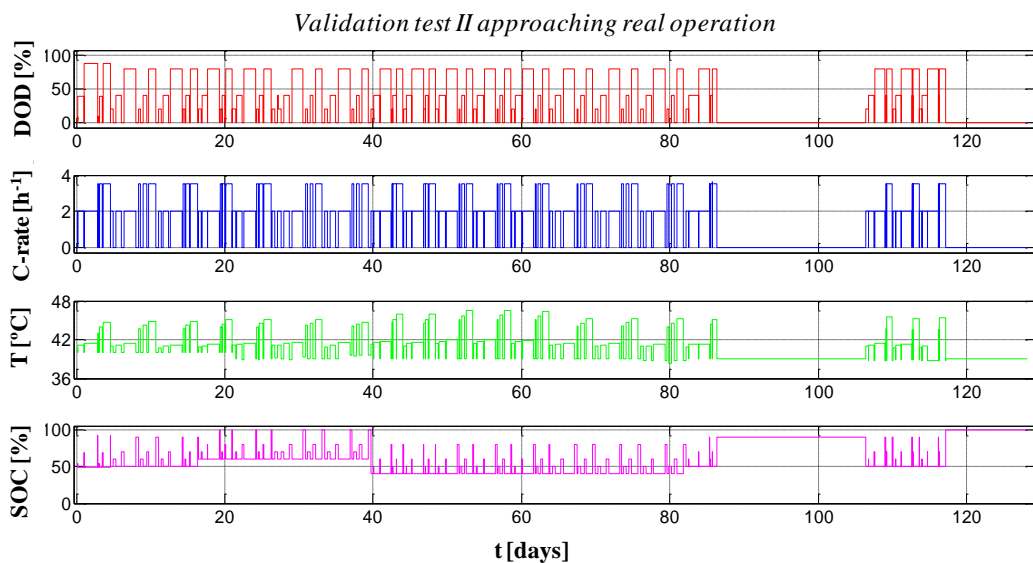


**Figure 5-62 (b).** Ageing model input impact factors profiles from validation test (II) approaching real operation

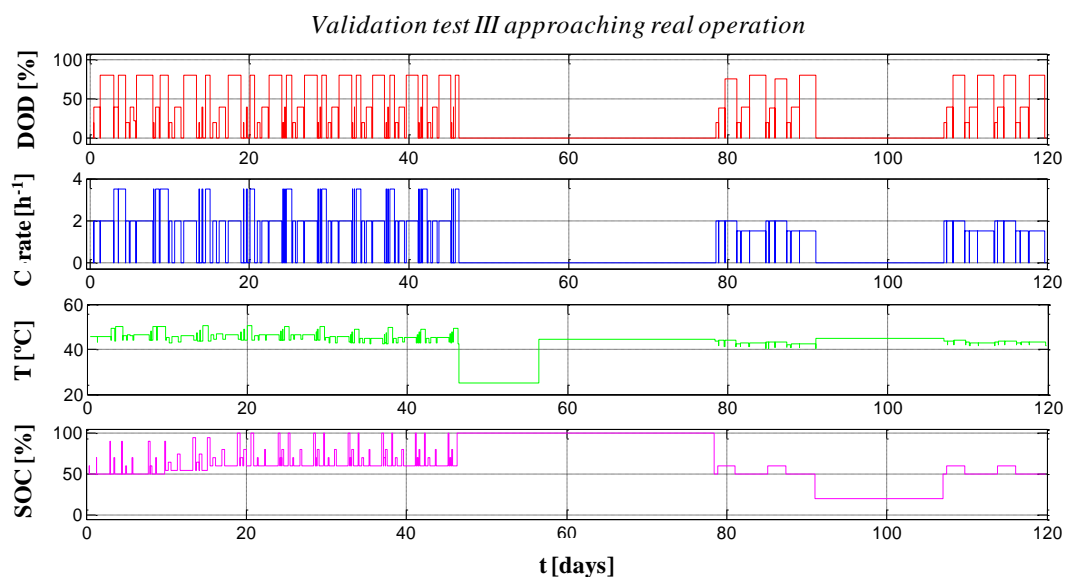


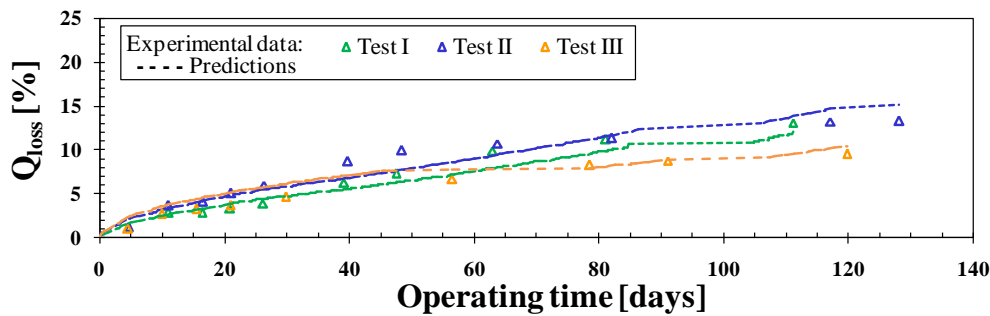
**Figure 5-62 (c).** Ageing model input impact factors profiles from validation test (III) approaching real operation

Experimental procedures are described in *Chapter 2*. The ageing tests and check-up tests were performed in temperature-controlled environments (CTS and Prebatem Climatic Chambers, in Appendix C) and using Digatron multiple tester with data acquisition BTS-600 software (Appendix C). Even though internal resistance increase was not modelled, and these tests pursue model validation, it was also measured to completely evaluate cell SOH over time and to ensure that cell internal resistance increase does not either increase in operating conditions approaching real operation. Intermittent EPIT tests were the same as for calendar and cycling ageing tests. HPPC test and quasi-OCV test were performed just for supervising cell ageing processes. No further characterisation tests were included.

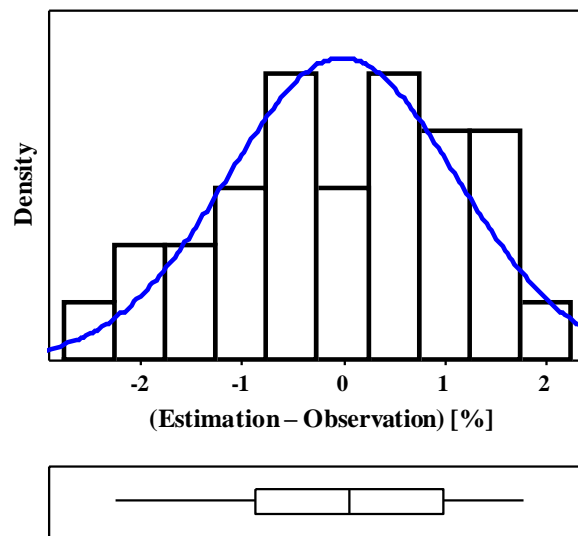
### 5.5.1.2 RESULTS AND DISCUSSIONS

Figure 5-63 shows the capacity changes measured under various experimental conditions during combined cycling and storage continuous operation over 120 days (profiles in Figure 5-62) and includes the predicted values using the algorithm discussed above. These estimations were assessed using just the ageing model and not the complete platform, so the ageing model inputs did not exactly represent instantaneous cell operation but they were, among others, middle SOC and mean temperature for each defined event. The predictions goodness evaluation is illustrated in Figure 5-64. It shows in a histogram the density of differences between measurements (observations) and predictions. The distribution characteristics of such differences are shown in the box plot. The median of the predictions error was just 0.89%. The distribution fitting, shown with a blue line in the histogram, indicates that it was almost normal (p-value = 0.538). Hence,

the null hypothesis for the predictions was accepted. That means that the proposed approach for lifetime prognosis is able to predict with high accuracy cell capacity loss under operation conditions that combine different storage and cycling events. The overall RMSE was 1.11%. It bears mentioning that the internal resistance increase of these tested cells was lower than 1% or even still negative after prolonged operation.



**Figure 5-63.** Experimental capacity loss ( $Q_{loss}$ ) results for the three validation test profiles approaching real operation (Figure 5-62) and the corresponding predictions using the described lifetime prognosis approach



**Figure 5-64.** Histogram and box plot of the difference between prediction and experimental data values of cell capacity loss induced by profiles approaching real operation. Distribution fit (blue line) in the density plot

The capacity recovery phenomenon was also studied, as part of the results of validation tests approaching real operation shown in Figure 5-63. SOC was varied during the combined operation (cycling and calendar) as in real applications it may typically vary depending on specific load profiles. Likewise, it was also varied during the prolonged storage periods for a couple of tests (validation Tests I and II, Figure 5-62). Figure 5-65 shows a continuation of these tests, from 90 days of operating time onwards. These data were not evaluated with the ageing model, as it is a capacity fade accumulative model, which would never predict such a cell behaviour. Data showing capacity recovery are shaded in the same colour as the

experimental data (green, blue or orange, depending on the test). Operating conditions between different check-ups are also indicated in the same chart. Prolonged pause periods (battery at rest) after combined cycling and calendar operation slowed down the ageing. K. L. Gering *et al.* [214] also reported that calendar ageing is cross-dependant on cycling, *i.e.* that calendar ageing rate may be different if the cell was cycled prior to calendar test or in between calendar tests. A. Eddahech *et al.* [215] concluded that the recovery-rate is dependent on resting period SOC and duration, but in this work it was observed that it also strongly depends on cell stress level due to former usage. For the Test III at 40-45°C, a very slight capacity recovery of 0.02% was measured after 16 days of storage at 20% SOC. A. Eddahech *et al.* [215] however concluded that the impact of calendar ageing at high temperature is large at the beginning of ageing and after that stage the rest periods slow down the ageing. For the Test II at 35-40°C, there was no capacity recovery after 11 days of storage at 100% SOC, but the capacity loss increase was also low, 0.09%. However, 0.8% capacity recovery was measured under the same conditions (11 days at 100% SOC) but 30-35°C ambient temperature (Test I). For Test I and Test II the operating electrical profiles previous to these observations were similar, but the electrochemical and degradation processes are strongly influenced by temperature. The results also indicate that the recovery phenomenon is not affected by the ageing state. The SOH of the cells under Test I and Test II (25-30°C and 35-40°C ambient temperatures, respectively) were similar, 13.08% and 13.19% respectively, before the 11 days storage period at 100% SOC.

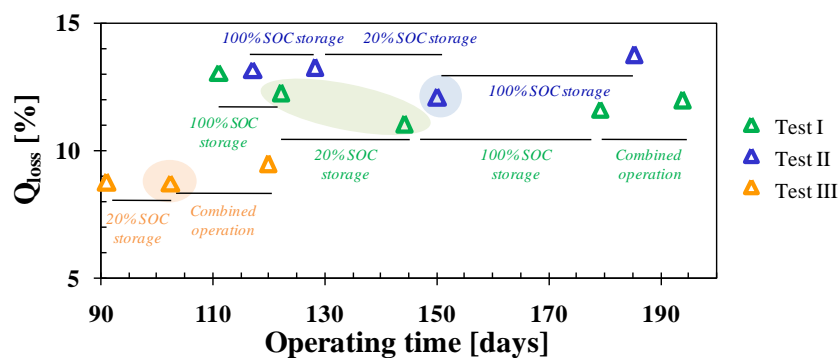


**Figure 5-65.** Continuation of experimental capacity loss ( $Q_{loss}$ ) results shown in Figure 5-63 for the three validation test profiles approaching real operation (Figure 5-62). Operation conditions between check-ups are described using the same colour as the corresponding test results. Data showing capacity recovery are shaded in the same colour as the corresponding test results

Varying the SOC during the prolonged storage periods enabled examining the effect of events order on cell performance. In this case, the effect of SOC alternation. For both validation Test I and Test II (Figure 5-62 and Figure 5-65), when going from higher to lower SOC (from 100% to 20% SOC), cell capacity was recovered, and going from lower to higher SOC (from 20% to

100% SOC) capacity loss was accelerated, vanishing the capacity recovery effect. Same behaviour was observed by S. Käbitz *et al.* [132] with NMC/graphite cells. The capacity recovery phenomenon not only cannot be predicted with the model, as mentioned above, but might be also a source of error for diagnosis in BMS (online calculation of actual capacities).

These initial combined predictions were based on middle SOC<sub>s</sub> (and event average temperature), as is the developed cycle ageing model (Eq. 5-9 and Eq. 5-10). However, the built simulation platform reads instantaneous temperature, voltage and current data, measures SOC and DOD, and can predict the ageing based on real SOC, T, DOD and Ah-throughput for each time step. Aiming at evaluating the differences of using just the ageing model or the complete platform for predicting the capacity loss, profiles in Figure 5-62 were simulated using the platform. Figure 5-66 shows a comparison of both predictions for the worst case scenario: Test II (it showed the largest prediction error using just the model). The prediction error increased in 0.08% using the complete simulation platform for this specific case. The deviations from one prediction to the other (using the complete simulation tool or just the ageing model) include both the modelling error (the fact that is based on middle SOC) and the introduced error with model inputs (real time-step data or assessed mean values for each event).

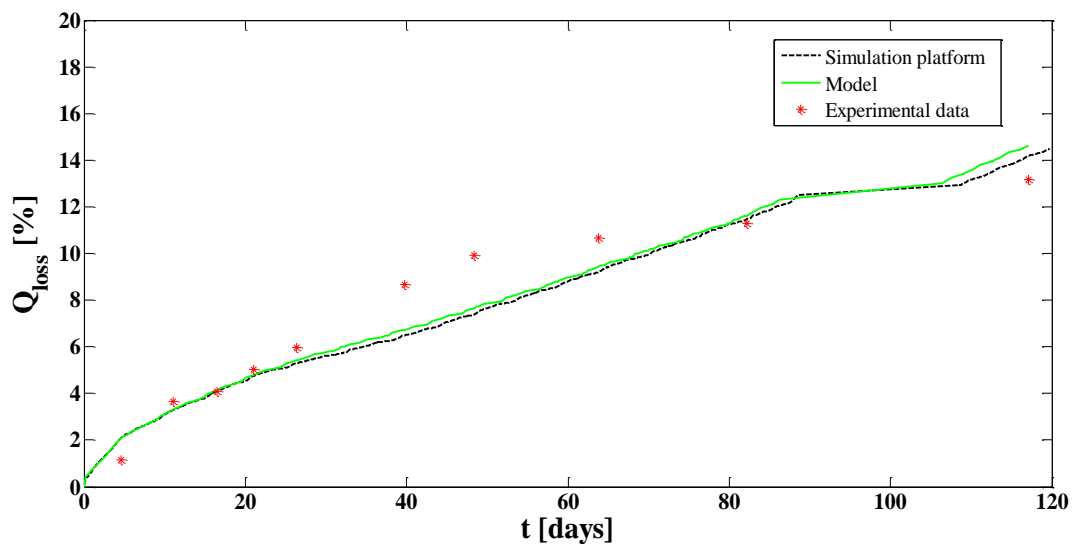


**Figure 5-66.** Comparison of capacity loss ( $Q_{loss}$ ) estimations using the single ageing model (in green) and the simulation platform that includes field measurements conversion and the possibility of simulating real cell operation for each defined time-step

## 5.5.2 VALIDATION USING REALISTIC PROFILES

The last step of the lifetime prognosis methodology (as described in Figure 5-5) was the validation using realistic profiles to evaluate algorithm applicability limitations. This validation

scenario aimed at the simulation of the residential elevator operation as closely as possible. With this purpose, the developed simulation platform tool was used (lifetime prognosis approach with field parameters conversion). This task was performed in two steps:

1. *Validation using realistic profiles I.* Test accelerated by repeating continuously a charge sustaining (CS) profile with no pauses in between. Non symmetric profiles, meaning different charge and discharge C-rates within the same DOD.
2. *Validation using realistic profiles II.* Complex operating conditions combining partial SOC cycling (micro-cycles), charge depleting (CD) cycling (macro-cycles), rest periods at different SOCs, incomplete charging and cell temperature change over time.

### 5.5.2.1 EXPERIMENTAL

*Validation using realistic profiles I* consisted in the most demanding residential elevator profile defined in the implementation of the cells selection methodology. This type of cell ageing was described in *Chapter 4*. Tests conditions are given in Table 4-6 and the profile in Figure 4-6 within *Chapter 4*. Three repetitions were performed under the same profile.

*Validation using realistic profiles II* evaluated the complex operation of a residential elevator, including trips between different floors and pauses. In order to reduce the time under test, the operation profile was accelerated linking all the trips that an elevator performs during a day, but with short rest periods in between that simulate elevators door opening and closing time. Figure 5-67 (a) shows the SOC profile tested at 30 and 40°C, that consist in 3 h of continuous operation followed by a pause of 2 h at different SOC each time, simulating within 5 h a full day of operation highly accelerated. It was pursued to reproduce the operation of a not heavily-trafficked elevator, performing overall daily trips at a time and the overnight pause was also shortened. As shown in Figure 5-67 (b), the macro-discharging itself was composed of a series of micro-discharging cycles (profile rich on discharge, *i.e.* charge depleting) repeated until *ca.* 10% SOC was reached and the macro-charging was a single charging up to 90% SOC representing recharging from the grid. The maximum DOD of micro-cycles was *ca.* 25% (composed of a short high power peak and a subsequent less demanding battery discharging period), which may correspond with the operating scheme of an elevator placed in a skyscraper (trips with large DOD). Figure 5-68 shows the real profile testing chronogram. Experimental procedures are described *Chapter 2*. In this case EPIT were actual nominal capacity test and quasi-OCV test, both described in *Chapter 2*. No additional tests were performed. Internal resistance was not measured in view of the results of previous tests. In case of any significant change of the internal resistance, it would be besides revealed in quasi-OCV profiles analysis.

All these experiments and check-up tests were performed in a temperature-controlled environment (CTS and Prebatem Climatic Chambers, in Appendix C) and using Digatron multiple tester with data acquisition BTS-600 software (Appendix C).

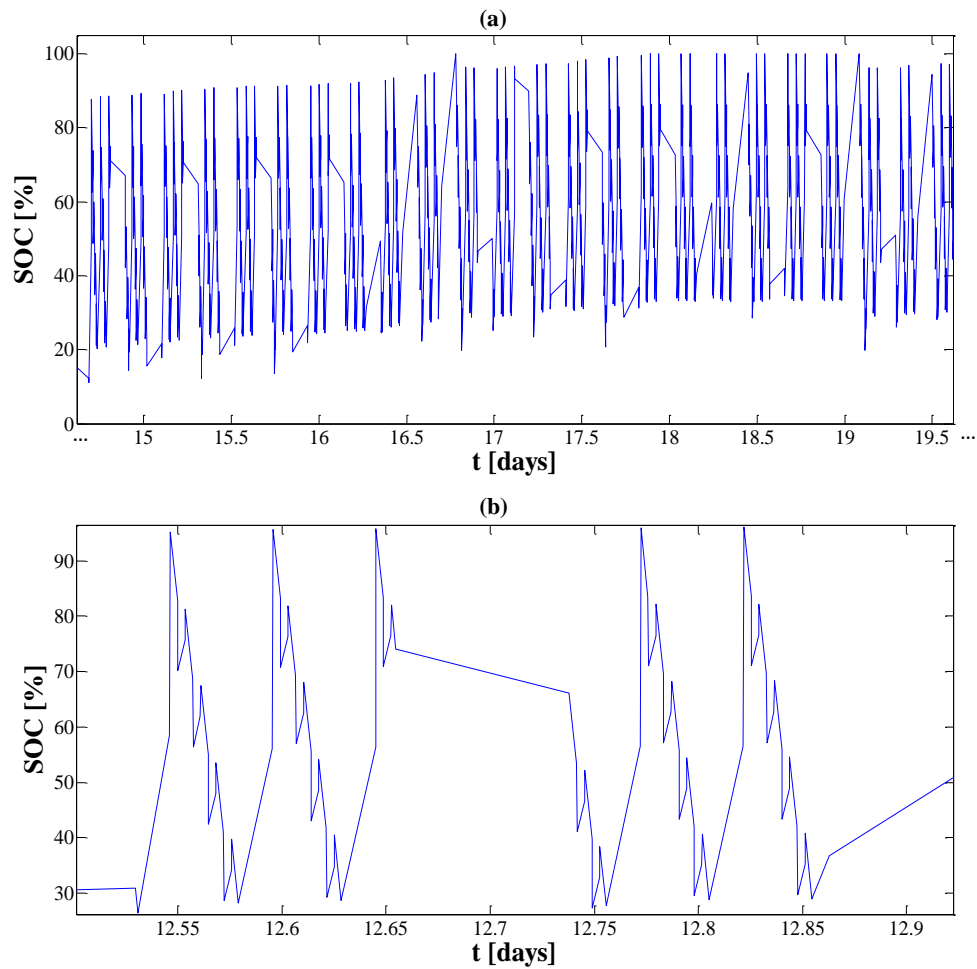


**Figure 5-67.** (a) Voltage profile of the validation test simulating elevator operation. (b) Magnification view around day 12

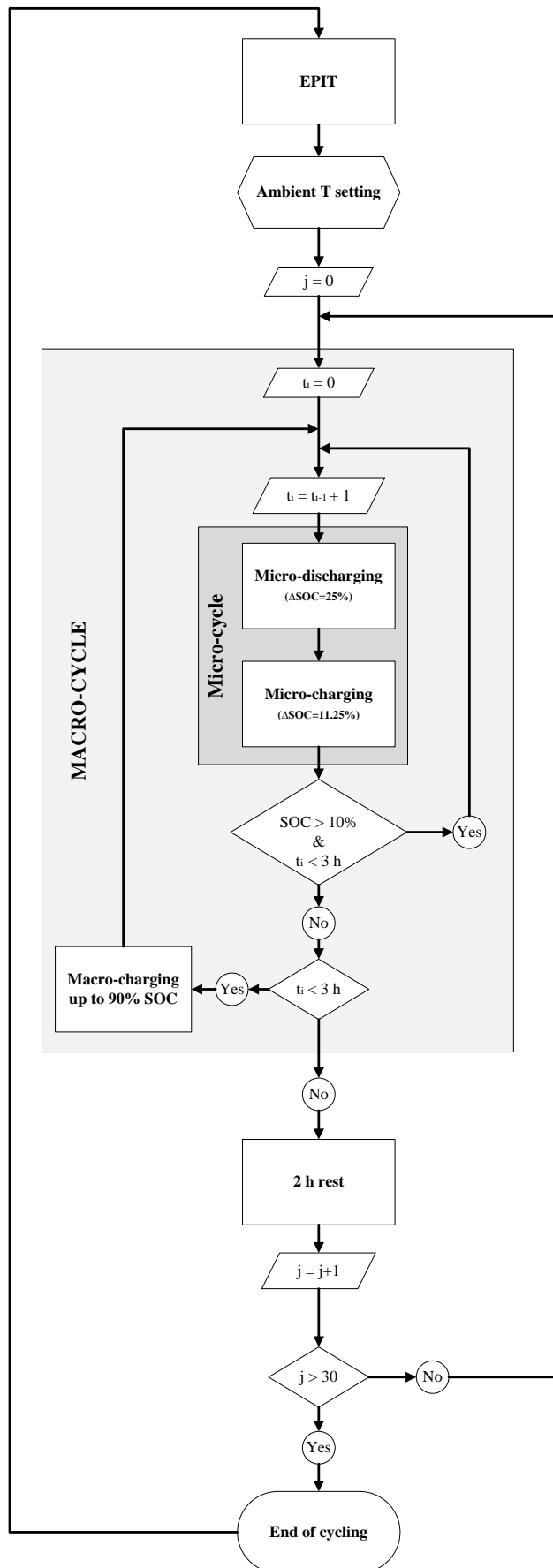


Figure 5-68. Real profile testing scheme

## 5.5.2.2 RESULTS AND DISCUSSIONS

### 5.5.2.2.1 NON-SYMMETRIC CYCLING PROFILES

All ageing analysis results of *Validation tests using realistic profiles I* are gathered in *Chapter 4* (section 4.1.2.2. b) -accelerated cycle life tests at severe operation conditions-). Figure 5-69 shows the capacity loss experimental results of a cell as a function of the time (markers) that were analysed with the simulation platform (prediction in dotted line). In view of the results, it is once again confirmed that the effect of C-rate on capacity fade is of minor importance (it is overlapped by DOD effect). The mathematical capacity loss model suits to different C-rate operation conditions, and lifetime prognosis approach applicability to predict non-symmetric (but repetitive over time) profiles is also validated.

This validation step reveals the fulfilment of two of the goals proposed for lifetime prognosis: the model is accurate under no modelled operation modes, RMSE was just 0.58%, and is scalable. The ageing model was not developed focusing on a specific end-user profile but it is able to predict ageing due to realistic operation. Eq. 4-4 targets the capacity fade prediction of a single specific application (residential elevation) operating in a specific way (Figure 4-6). It is just a function of the number of cycles (in turn, Ah-throughput) and considers DOD and C-rate relationship as a constant value ( $Q_{\text{loss}} [\%] = a \cdot N^b$ ). The power law of this mathematical relationship and that of the ageing model at 5% DOD (corresponding to this test) are equal: 0.7 and 0.65, respectively. The corresponding predictions using Eq. 4-4 and the developed lifetime prognosis approach after 30000 cycles, *i.e.* 33.61 days of continuous cycling, were very similar: 6.84% and 6.69%, respectively. Hence, the presented novel approach has broad widespread to different operation conditions (it was already used to simulate symmetric cycling, simply standby operation, combination of different cycling and calendar ageing events and, distinctly, asymmetric C-rate cycling, which operation mode was not considered for the model development).

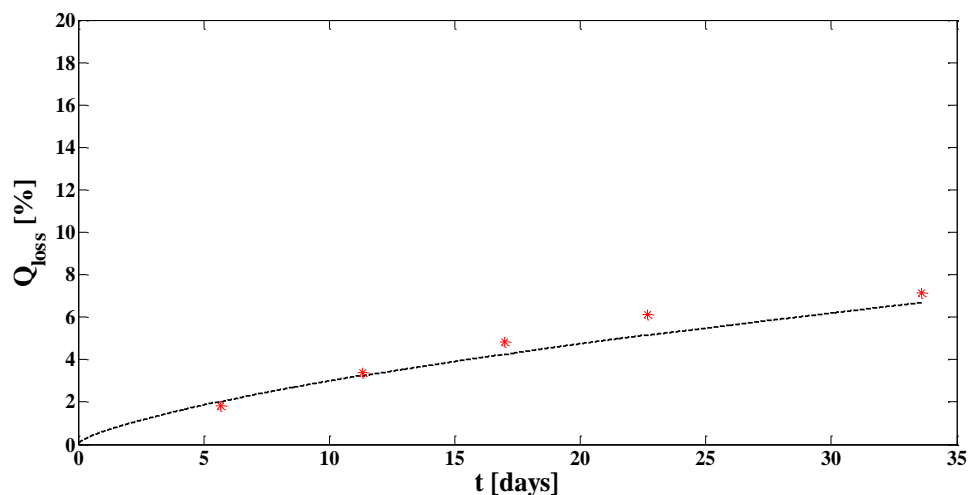


**Figure 5-69.** Experimental capacity loss ( $Q_{loss}$ ) results (markers) from the most demanding residential elevator profile (Figure 4-6) and the corresponding prediction (dotted line) using the ageing simulation platform (Figure 5-61)

#### 5.5.2.2.2 COMPLEX OPERATION CONDITIONS

The measured data and estimations of *Validation tests using realistic profiles II*, i.e. residential elevator accelerated operation profile (Figure 5-67 and Figure 5-68), are presented in Figure 5-70. The evolution of capacity fade prediction at complex operation conditions yielded an overall 1.4% RMSE. The prediction results described more deviation from observations in the case of the cell tested at 40°C (it was 1.15% for Figure 5-70 (a) and 1.6% for Figure 5-70 (b)). It could have been caused by experimental set-up issues, as this cell charge-discharge current was neither controlled nor measured for an almost a whole day between 4<sup>th</sup> and 5<sup>th</sup> CUs. The fact that the two cells age similarly regardless the 10°C temperature difference (after 115-120 days of cycling, the capacity loss was 11.1% at 30°C and 9.5% at 40°C) might be one of the consequences. However, this also happened for the cells under the validation tests approaching real operation tested at the same two ambient temperatures (after 82 days of operation, when Validation test I and II were still almost equivalent, both cells underwent the same capacity loss: 11.2%). It was therefore concluded that there are combined effects that overlap Arrhenius law, i.e. temperature impact on cell ageing is dependent on operation conditions, and that the rule of thumbs "the reaction rate doubles with  $\Delta T = 10^\circ\text{C}$  increase" [135] is just valid for calendar ageing, in which specific conditions of SOC and T also play a role. On the other hand, the ageing phenomena analysis for the complex operation conditions indicates that the ageing processes were modified upon cycling.

Figure 5-71 shows DV (a) and IC (b) curves for the cell tested at 30°C (Figure 5-70 (a)). The first valley in DV curves shrank gradually, as the intensity of the peak 1 at high SOC (at 3.32 V)

decreased over cell complex operation. LLI was apparently the main ageing mechanism during the first *ca.* 100 days of operation. Afterwards, however, not only did the stage 1 lithium-graphite compound undergo changes, but all other peaks (specially at 3.28 V) and valleys also faded. The distinctive changes that worth highlighting are that the first valley in DV curves disappeared almost completely (the signature at high SOC changes in IC curves), and the second also shrunk meaningfully. Hence, either the degradation of graphite electrode active material was considerably induced or the access to active material was blocked and active surface area was decreased (LAM). The ageing model is however applicable for LLI ageing processes (this single effect was modelled), which may have contributed to prediction errors. Anyway, the model follows the trend of these changes in capacity loss evolution and the box plot in Figure 5-72 shows that the median prediction error is not larger than 1% and the variance (dispersion) is 0.57%.

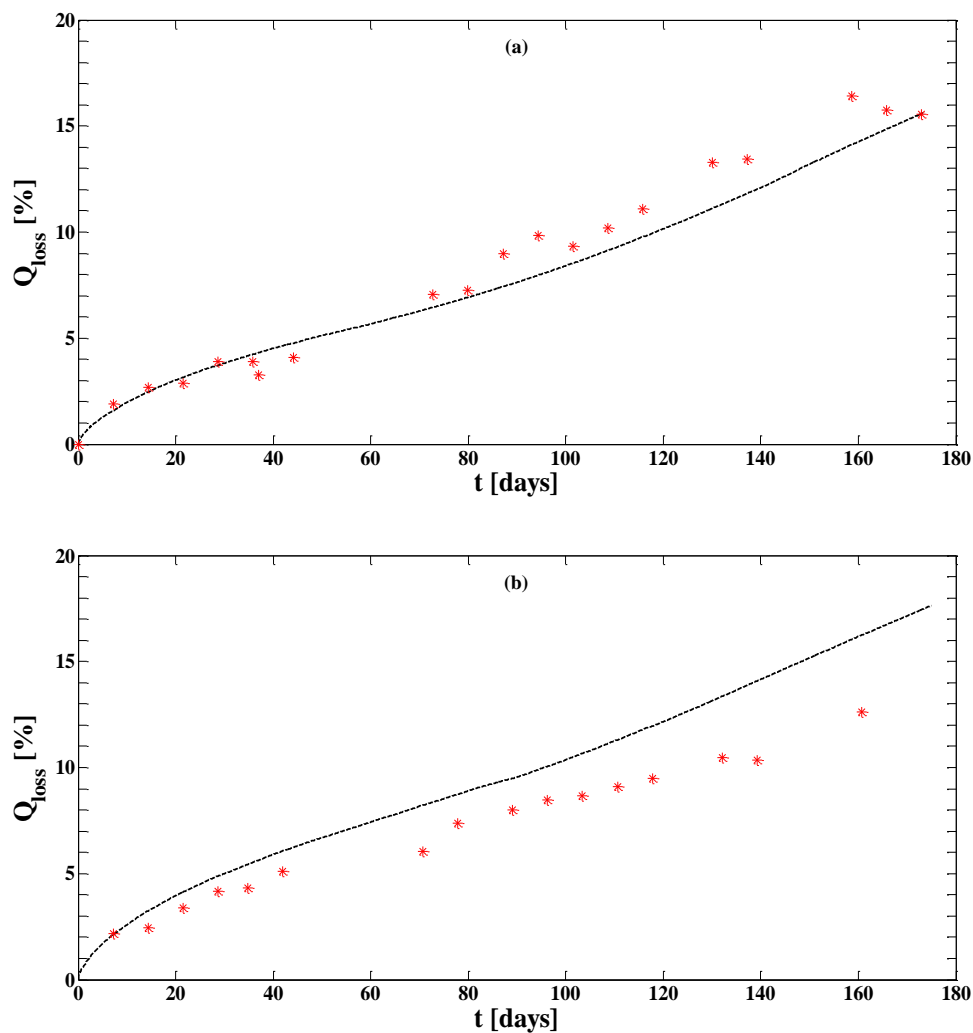


**Figure 5-70.** Experimental capacity loss ( $Q_{loss}$ ) results (markers) resulted from residential elevator accelerated operation profile (Figure 5-67 and Figure 5-68) and their estimations (dotted line) using the ageing simulation platform (Figure 5-61). Testing at (a) 30°C ambient  $T$  and (b) 40°C ambient  $T$

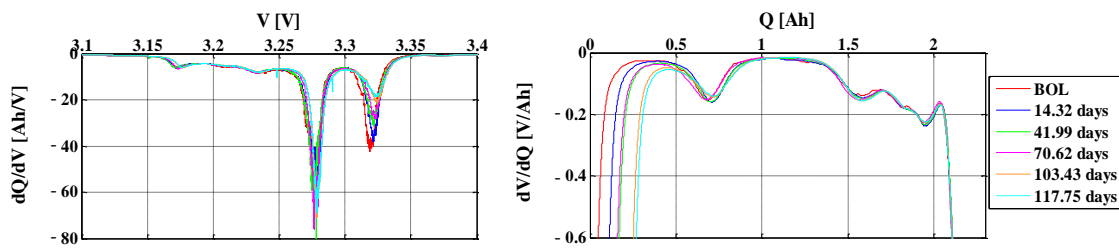


Figure 5-71. Differential Voltage (DV) and Incremental Capacity (IC) curves derived from quasi-OCV discharge curves for complex operation test (Figure 5-67 and Figure 5-68) at 30°C

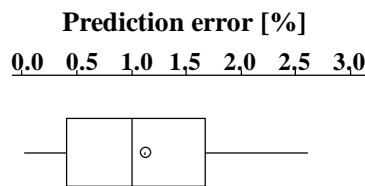


Figure 5-72. Box plot of capacity loss prediction errors distribution for complex operation test (Validation tests using realistic profiles II in Figure 5-67 and Figure 5-68)

This last validation step confirms consistently that the proposed lifetime prognosis approach meets all the initial established goals:

- The predictions are **accurate**: 1.4 % RMSE for complex highly accelerated residential application profile.
- The approach is **scalable** to different scenarios with broad applicability to different operation conditions. Ageing was analysed at accelerated static calendar and cycling conditions, and the ageing model was developed based on that initial analysis (and not on specific conditions). The prediction algorithm was however able to adapt to very different operation modes and predict the ageing with high accuracy (1.18% RMSE for profiles that combined different storage and cycling sequences, 0.58% RMSE for non symmetric cycling profiles and 1.4% RMSE for complex operation profiles).
- The algorithm implemented into a simulation platform is **realistic**. It is based on measurable parameters in real applications (measurements conversion step in the platform). The semi-empirical model uses simple mathematic relationships, so its integration into a BMS for online capacity fade estimations would be feasible. And it is applicable to complex real profiles.

The developed ageing model serves for a single degradation mode (LLI). In order to completely represent the complex ageing processes, a physics-based model would be necessary. Anyway, the model matches with cell overall ageing behaviour and the identification of degradation phenomena change (presence of LAM) would mean the need of a cell replacement action, as it could lead to sudden fade. The degradation phenomena can be

online monitored carrying out cell full discharges at low C-rates from time to time for obtaining IC and DV curves. This diagnosis action can be performed when the battery is at rest, such as in overnight pauses when its use is not demanded [194].

- The approach enables meeting the described objectives and **reducing the costs** at a time. Experimental work was significantly reduced: cycling was checked at a single SOC and T, and cycling and calendar effects were superimposed for obtaining the complete model. In addition, were of interest to check just the impact of, for instance, calendar effect in a real application, it would not be necessary to step back and analyse it afterwards individually, which would entail increasing analysis time and costs. Besides all this, the ageing model is scalable and realistic, which means that this versatile tool makes possible reducing several specific models to different applications into a single one, this way minimising also the costs.

## 5.6 REVISION OF THE METHODOLOGY FOR LIFETIME PREDICTION

Even though model *validation approaching real operation* may inform about SOC and T effect during cycling (the prediction goodness tells about the validity of the approach for their consideration), it was considered interesting to confirm the main premise assumed by the methodology for complete ageing model development. That is, it was aimed at understanding if different cycle ageing processes can be evaluated by superposition of individually analysed ageing effects or if they interact with each other in a nonlinear way. Hence, it would be necessary to further check the cycling performance to confirm the hypothesis that SOC and T effects are the same during both cycling and storage. Additional tests were run this way to analyse the sensitivity of cell ageing to cycling temperature and SOC.

### 5.6.1 EXPERIMENTAL

Single-factorial SOC and T variation cycling experiments were carried out to check, in a fast way, their impact on cycle ageing. Additional cycling tests with this purpose are specified in Table 5-8. Five tests were performed under two different DOD conditions, 50 and 30%, in view of the fact that the effect of DOD is different depending on the DOD range. The DOD levels were chosen within the same DOD range (Figure 5-47), to at least confirm that the conclusions withdrawn are valid in general (within the same DOD range) and do not just depend on specific conditions. The analysis was not extended to other DOD conditions from the different DOD range (Figure 5-47), because the aim was not to characterise in detail SOC and T effects on cycling.

**Table 5-8.** Additional cycling tests at 1 C-rate in order to confirm the hypothesis of SOC and T effect on cycle ageing. Tests that were already performed during cycle ageing analysis are marked in grey

DOD [%]		50			30	
Middle SOC [%]		70	50	30	70	50
T [°C]						
30		X			X	
40		X		X	X	

Experimental procedures are described in *Chapter 2*. All these experiments and check-up tests were performed in a temperature-controlled environment (CTS and Prebatem Climatic Chambers, in Appendix C) and using Digatron multiple tester with data acquisition BTS-600 software (Appendix C). EPIT were the same as for cycle ageing. Quasi-OCV test and HPPC test were performed just for supervising cell ageing processes. No additional characterisation tests were included.

## 5.6.2 RESULTS AND DISCUSSION

Figure 5-73 shows the change in the relative capacity of the cells cycled under different middle SOC, temperature and DOD conditions (50% DOD in Figure 5-73 (a) and 30% DOD in Figure 5-73 (b)). Together with cycling tests results, equal SOC and temperature calendar tests results are depicted as comparison. The capacity loss data showing tendency change accompanied with main degradation mechanism change, are shadowed using the same colour as the experimental data solid markers. These data are not considered for the pursued analysis in this section, as the ageing phenomena is different for the comparative calendar condition, and also because ageing model does not consider such transitions. Were the influence of SOC and T the same during cycling and standby operation, and the effect of calendar and cycling ageing could be superimposed [143, 178-181, 185], the difference between cycling and calendar ageing capacity loss (for the same middle SOC and T), for equal DOD and C-rate cycling conditions, should be the same. That is to say, for the same time of operation:

$$\begin{aligned} & Q_{loss\_cycling}(SOC_i, T_i, DOD_i, C-rate_i) - Q_{loss\_calendar}(SOC_i, T_i) = \\ & = Q_{loss\_cycling}(SOC_j, T_j, DOD_i, C-rate_i) - Q_{loss\_calendar}(SOC_j, T_j) \end{aligned}$$

The influence of Ah-throughput under each specific condition is however noticeable in any of the cases. For instance, there is few difference between 30% middle SOC and 40°C cycling and calendar operation (Figure 5-73 (a)), as is the case of 70% middle SOC and 30°C modes of operation (Figure 5-73 (b)). However, the differences are larger for the rest of the conditions at same DOD and C-rate at equal operating times, and these are even enlarged with lower SOH. On the other hand, this section cycling data shows discrepancies in capacity loss at 30 and 40°C for equal operating times (tests at 70% middle SOC, at both 30% and 50% DOD, in Figure 5-73 (a, b)), while no differences were observed under non-static tests that combined calendar and cycling operation events in the sequences: *Validation tests I and II approaching real operation* and *Validation tests using realistic profiles II*. Hence, there were present inherent complex processes that required deep analysis.

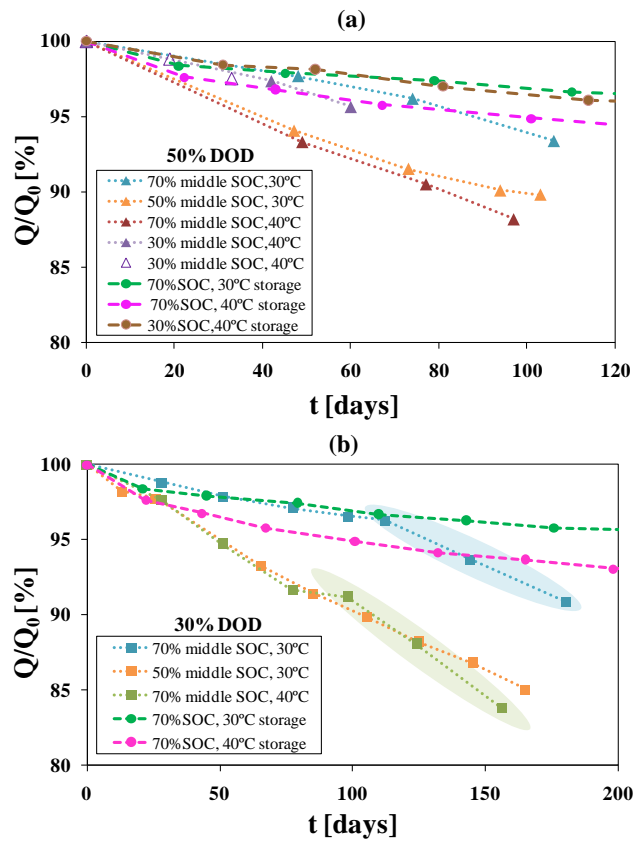


**Figure 5-73.** Change in relative capacity (actual nominal capacity,  $Q$ , normalised to initial nominal capacity,  $Q_0$ ) vs. time upon cycling (triangular and square markers) at 1C, different SOC, different temperatures and DOD: (a) 50% DOD and (b) 30% DOD. Calendar ageing results at equal SOC and  $T$  are included (circle markers) as comparative.

Assumption of equal effect of SOC and  $T$  during storage and cycling is not fulfilled at static operation conditions. Dynamic cycling tests under different SOC and  $T$  should also be checked to determine the validity of such assumption under less severe conditions. From these results, and for the same SOH, as shown in Table 5-9, the general stepwise analysis described in Table 5-10 was performed to examine the influence of SOC,  $T$  and DOD conditions on cycle ageing (static conditions). Overall, as outlined in the same Table 5-10, it was concluded that all analysed impact factors ( $T$ , SOC and DOD) effects are combined upon cycling. Their effect rating was as follows:  $T > DOD > SOC$ . However, deep extended analysis would be necessary for validating these conclusions and for weighing these impact factors effects on cycling operation.

**Table 5-9.** Cycling tests under different SOC, T and DOD conditions, and the capacity loss ( $Q_{loss}$ ), normalised to initial values, after the same operation time under different conditions used as comparative value of the tests

	FACTOR			OUTPUT: $Q_{loss}$ [%] for ca. 74 days of cycling
	SOC [%]	T [°C]	DOD [%]	
Test 1	50	30	50	8.47
Test 2	70	30	50	6.61
Test 3	70	40	50	9.45
Test 4	30	40	50	4.76
Test 5	70	30	30	2.93
Test 6	70	40	30	8.82

**Table 5-10.** Methodology followed for the analysis of the qualitative and comparative influence of DOD, T and SOC impact factors on cycle ageing, and general stepwise conclusion

DATA ANALYSIS	CONCLUSION Factors effects on capacity fade
<b>1. T and SOC influence on cycling</b> (DOD factor made constant) Comparison on Tests 1, 2, 3, and 4	- The higher the T, the larger the degradation - There is no clear evolution of SOC influence
<b>2. T and DOD influence on cycling</b> (SOC factor made constant) Comparison on Tests 2, 3, 5 and 6	- T effect on capacity fade larger than DOD effect
<b>3. SOC and DOD influence on cycling</b> (T factor made constant) Comparison on Tests 1, 2 and 5	- DOD effect on capacity fade larger than SOC effect

Not only are there complex effects combination between DOD and C-rate, as concluded in section 5.4 (cycle lifetime), but also T, DOD and SOC effects are combined upon cycling. Then, the effect of SOC and T is not the same during calendar and cycling, and complex effects combination is not as simply as superimposing the effects of different impact factors. However, the impact level of these cycling ageing effects should be low. Acceptable high accuracy of the predictions along the different validation steps were already showed. Hence, the level of importance of such a detailed analysis will depend on the specific pursued goals.

### 5.7 SUMMARY AND CONCLUSIONS OF LIFETIME PROGNOSIS APPROACH

This work has successfully achieved the goals of developing an accurate, reliable, realistic, scalable and low cost methodology for lifetime prediction. The scheme in Figure 5-74 summarises all the steps analysed during this work. The boxes in orange correspond to the activities for cycle life, the boxes in magenta to calendar life and the blue one is their combination for a complete lifetime model development. The respective validation steps are indicated in green, with the numbers indicating the order of implementation of the procedure in each case (calendar, cycle and complete ageing models).

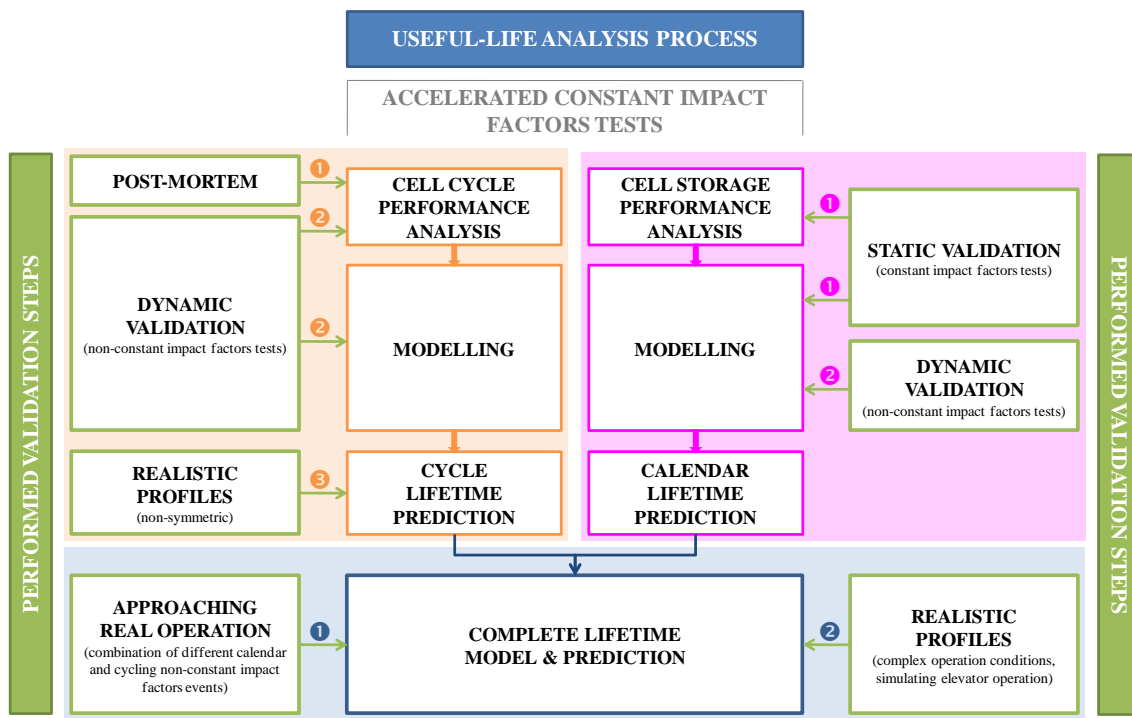


**Figure 5-74.** Summary of the implementation of the proposed approach for lifetime prognosis. Numbers in the different validation procedures (in green) that were carried out for calendar (model development in magenta), cycling (model development in orange) and complete ageing model (in blue) indicate the order of execution in each case

For an optimal ageing analysis, as concluded from previous section, the cycle ageing matrix ought to be extended. However, it is uncertain the number of experiments that would be necessary to thoroughly understand cycle ageing behaviour and to obtain results of high significance that would enable its modelling. It would not be perhaps possible with a simple mathematical model, as the proposed lifetime approach enabled. And, in the end, the improvement of overall results would be uncertain. The accuracy of the predictions is already very high, and there are also other several inherent errors in the overall process that are not evaluated. These errors may be gathered together into three main groups [216]: (i) uncontrollable factors such as cell-to-cell variability (cells standard deviation at BOL was

0.007 Ah), measurement error or ambient conditions (meaning humidity, pressure, etc.); (ii) nuisance factors, for instance EPIT schedule or cycling protocols change due to cell ageing; and (iii) factors that are considered constant: homogeneous temperature along the whole jelly-roll, conditioning procedure and so on. All these factors effect ought to have been determined in order to assign an error to the precision. However, it is beyond the scope of the present research work.

The number of initial experiments was small and in a relatively short period of time (*ca.* 1 year), it is possible to perform a lifetime prognosis of a battery for a specific application. In this particular chapter, several steps further were taken to validate the proposed method and to understand the extent and applicability of the resulting estimations. Once this process is made, validated and understood, the methodology may not require so many validation procedures for further case scenarios. However, if still does so, the prognosis method is still cost and time effective. The benefits of achieving accurate lifetime predictions will be further quantified in future work. And further improvements/extensions of the methodology will raise when applying to other batteries and applications. All in all, this work constitutes a significant step forward to progress in prognosis tools. Future work can be related to the second degradation mechanism occurring at later stages during operation, and produces of a sudden performance loss and failure of the storage system.

## 5.8 LIFETIME EVALUATION FOR A RESIDENTIAL ELEVATOR

Developed ageing model provides cell capacity loss estimations beyond measured and modelled operation range and time, as it was thoroughly validated with excellent results. The real operation of a residential elevator with 630 kg passenger mass (maximum 8 passengers) and 800 kg cabin mass was simulated based on a whole day power profile field measurements reported by E. Bilbao [217]. Figure 5-75 shows the daily current (Figure 5-75 (a)) and SOC (Figure 5-75 (b)) operating profile at cell level, which was assessed based on the battery pack sizing of Stage 1 of the cells selection methodology implementation in *Chapter 4* (Ref 3). Degradation of a cell in a battery pack of a residential house elevator located in Tenerife was evaluated, considering average daily temperatures over a year that are shown in Figure 5-23, and simulating repeatedly the profiles in Figure 5-75. It was assumed that the cell is at ambient temperature (which implies that the elevator shaft is at such temperature and that the cell is not hypothetically heated up during operation). Figure 5-76 shows the predicted capacity loss for four years. The question that arises is how long the predictions are valid for. That is to say, how far the extrapolations are within the cell safe operation timeframe, where the main degradation mechanism is just LLI. In this sense, ageing results from *Validation tests using realistic profiles II*, which reproduced accelerated operation of a residential elevator, were used as reference to evaluate the possible lifetime. Figure 5-71 showed that from *ca.* 100 days of accelerated operation on, the dominant degradation mechanism started to change. Taking into account that 5 h testing simulated one full day of operation (case study), 100-170 days of testing (operating timeframe when ageing phenomenon change was detected) would mean 1.3-2.2 years of real operation. However, the profile was particularly accelerated, both increasing the use rate and with high temperature. In consequence, cell ageing behaviour may be highly influenced. In addition, the real operation profile of an elevator (Figure 5-75) is dominated by standby operation, and calendar ageing testing results indicated that the cell storage ageing tendency just changed at very high temperature (50°C and 70 % SOC) after *ca.* 1 year. In any of the cases, the degradation mechanism change was not observed before 90% SOH, so after 10% capacity loss cell safe operation cannot be ensured from the simulations. After 4 years of daily real residential elevator operation simulation using average daily temperature of Tenerife (a year profile), it was predicted that cell degradation would be precisely 10.98 %. Hence, the lifetime of the LFP-based cell investigated in this work, operating in a residential elevator application under the influence of the conditions previously described, would be four years.

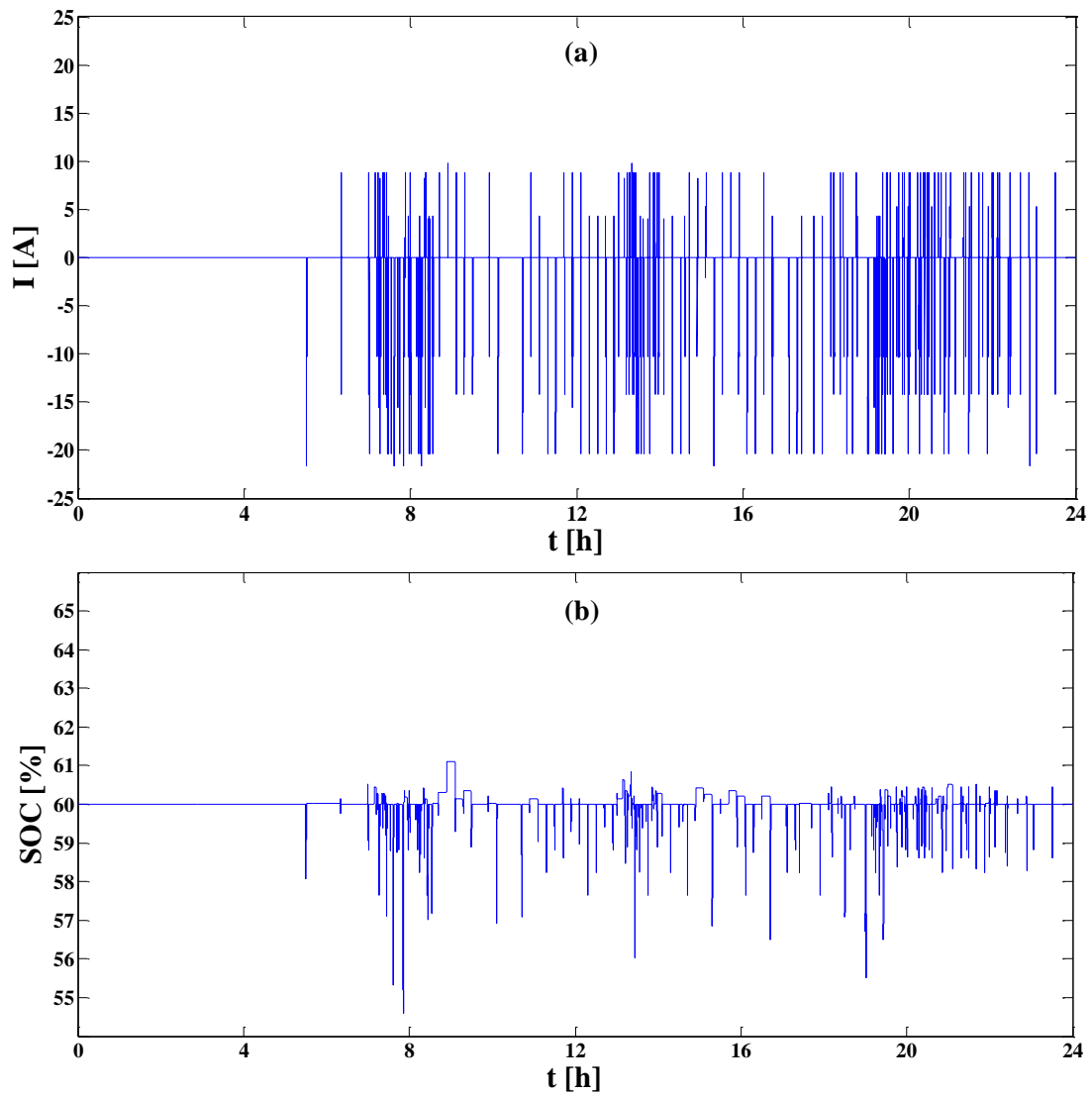


Figure 5-75. Real residential elevator one day power profile converted into operating current and SOC at cell level

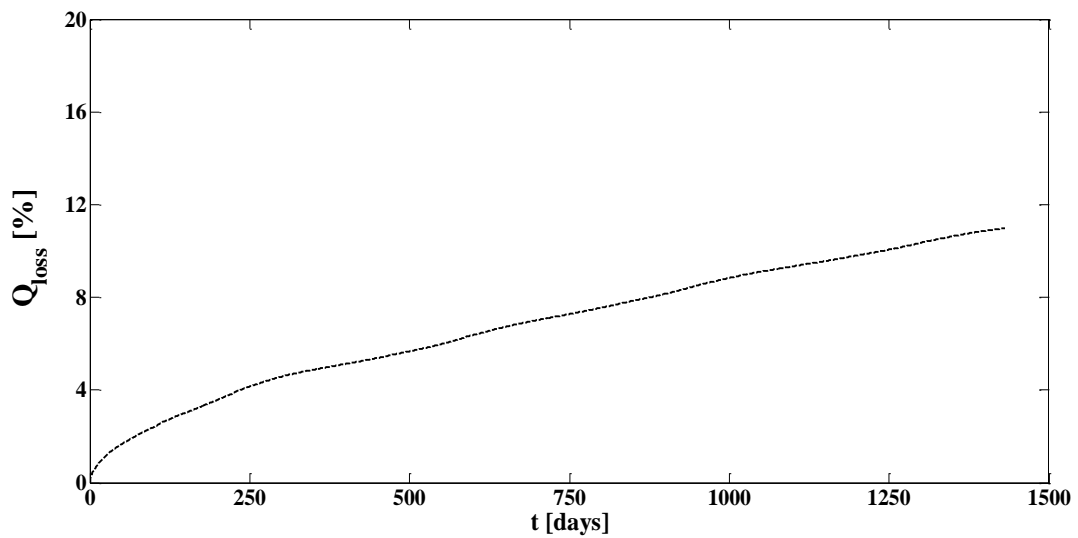


Figure 5-76. A residential elevator daily operation capacity loss simulation results for four years

The presented model, together with the estimated Wöhler curve ( $N$  vs. DOD, Figure 5-31) and the observed relationship between the energy that the cell can provide and store upon cycling (FEC vs. DOD, Figure 5-29), can have broader applicability than just predict the lifetime. These all are key elements for battery pack sizing and for defining operation strategies that ensure safe and required lifetime for different end-user applications.

In case the lifetime was limited to *ca.* 10% SOH, the battery pack size could be optimised based on Figure 5-29 and Figure 5-31 (they are limited to a same main degradation mechanism (LLI) that was considered in the ageing model). The total Ah-throughput the cell can provide depended on the cycling amplitudes. It seems that regardless operating at 10, 30 or 50% DOD, the output is similar. The total FEC that the cell can provide increases at 60 and 100% DOD conditions in *ca.* 1000 FEC, but it is also equal for these two conditions even with such a difference in cell operating SOC utilisations during cycling. A difference of 1000 FEC is representative, it means approximately a third of the entire lifetime, taking into account that the specifications for the residential elevator indicate an approximate cycle life of 150000 cycles, which are 3000 FEC. At 5% DOD, additional 1000 FEC can be obtained. Hence, from the energy point of view, operating at low DOD would be the optimal, but it is key reaching the compromise of minimising costs due to either getting a larger amount of energy or reducing the battery pack size. It might be of interest to divide even by 20 the battery pack capacity (the total energy output range is similar for 60% and 100% DOD conditions, meaning system capacity reduction by a factor of 1/12 and 1/20, respectively, when operated under such conditions instead of at 5% DOD), if it is taken into account, on the one hand, that cell materials and depreciation costs respectively mean 27% and 16% of the TCO (data for an EV battery pack [36]) and, on the other hand, that 10 years of lifetime are required for the pursued residential application. The system oversizing will be always necessary as the usable energy of the cells will be influenced by more factors than ageing, as analysed in *Chapter 3* and illustrated in Figure 3-19. In addition, from post-mortem analysis it was observed that uneven ageing of the cell components is an important issue for cylindrical cells. The inefficient use of active materials requires over-dimensioning the battery system and influences the operating strategies to meet end-user functional specifications.

The observations along the entire ageing and lifetime analysis within the present chapter could be considered for resizing the battery pack predesigned in the Stage 1 of the cells selection methodology, which would lead to an optimised ESS system.

### 5.9 AGEING MODEL APPLICABILITY. FUTURE WORK TO EXTEND THE METHODOLOGY

Back in the initial Figure 5-1, the ageing and lifetime analysis is an important part of Stage 3 from overall cell selection methodology. But this stage needs still to be complemented with other multidisciplinary aspects such as safety, costs and battery pack issues. Addressing these aspects is already beyond the scope of this work, but an overall perspective of the developed ageing model applicability is given in Figure 5-77. It contextualises the role of ageing and lifetime prediction and its relevance towards finding the best ESS solution for specific applications. The useful life predictive model applicability is shortly described below, as a way to conclude this chapter with a wider view of the diagnosis procedure.

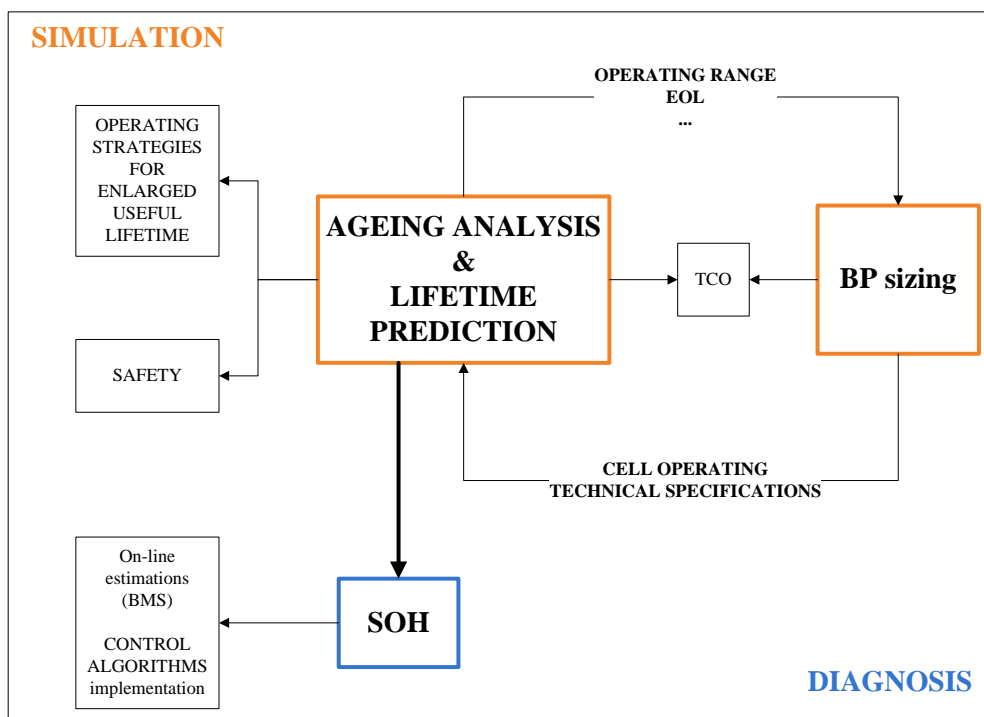


**Figure 5-77.** Ageing analysis and lifetime predictive model applicability. Interaction with other activities and the overall outputs (BP: Battery Pack; BMS: Battery Management System; SOH: State of Health; TCO: Total Cost of Ownership)

- **SOH estimation for BMS**

The model could be implemented into a BMS for on-line SOH estimations. However, the reliability of the estimations would be influenced by model error and other cell performance issues, such as capacity recovery phenomenon. On-line actual capacity calculations would be optimised in case real capacity measuring complementary techniques were used. Were the model updated systematically with real data, as shown in Figure 5-78, the margin of error would be reduced. Hence, using a predictor/corrector framework based on on-board measurements,

battery operating and control strategies could be adjusted guaranteeing reliable battery prognosis.

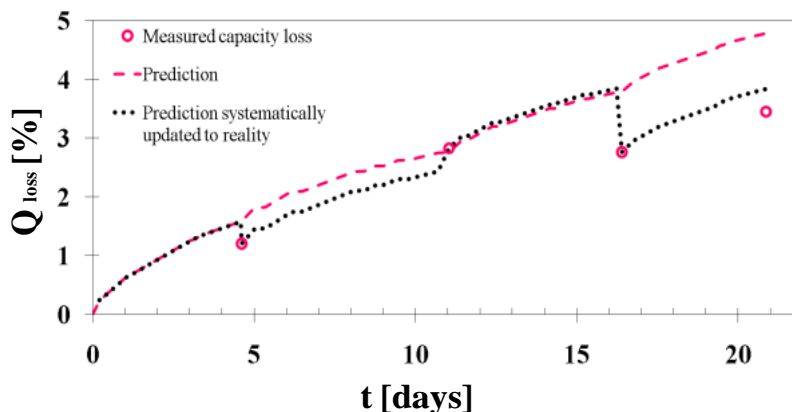


Figure 5-78. Capacity loss over time, model prediction and prediction corrected to the actual measured SOH

- **Battery Pack (BP) sizing**

While looking at new applications and services that ESS could provide in future scenarios, it is clear that at least in the short-term, the price of the systems is a challenging barrier to overcome. Due to this high cost of the batteries, optimising the battery size for each specific application is a really desired objective to achieve. Depending on the selected battery size and the operation conditions, the stress of the battery changes drastically.

Implementing the ageing model into simulating tools makes possible evaluating performance losses due to different sizing and operating conditions and thus determining the best size and operating ranges for the studied stress factors depending on the pursued goal (longest lifespan, reduction of costs, enhancement of safety and so on). The ageing model is in this scenario a core issue to hit the target in the design phase. Moreover, FEC vs. DOD and N vs. DOD curves derived from cycle ageing parameters analysis are key elements for battery pack sizing and operation strategies definition.

- **Business model**

The technical and business deployment of electrical ESS has the great potential to burst substantial revolutions in the field of sustainable transportation and sustainable and intelligent energy systems. Without leaving aside all the technical issues that are to be solved, the deployment of successful innovative business models will be of great importance. The first attempts are on their way in the market: car-sharing solutions like drive2go or DriveNow [218]

are opening a new way of conceiving products and business, battery leasing companies are already a reality, and the secondary battery utilisation is being intensely discussed (*i.e.* using batteries removed from electric car as grid storage).

Battery lifetime and its prognosis, together with battery ageing diagnosis, are clearly some of the enabling analysis tools that will support business models for a completely new market. Implementing the ageing model into an extensive simulation tool that takes into account costs, battery pack sizing, etc., could indeed:

- be of great help to estimate the real potential value of a battery even if its life is partially consumed, and also calculate the resale value when needed.
- allow estimating the first or/and second life of a certain battery in different applications, and choose the most profitable options between many alternatives.
- help typifying pairs of applications that would best match as first/second life followers, and guide new business deployment to start from the most profitable business niches.
- shed light on what is the most adequate point to switch from a first to a second life application.

All in all, those agents in the market, which are able to answer questions connected to ageing, will successfully help designing business models that will drive future energy scenarios. Therefore, ageing models and lifetime prognosis like the one developed in this Thesis will play an important role for innovative business models.



# *Chapter 6*

## OVERALL SUMMARY AND CONCLUSIONS

---



## 6. OVERALL SUMMARY AND CONCLUSIONS

- There are many lithium-ion battery technologies and there is no single battery type that is appropriate for all applications. For a right cell selection, it has to be reached a trade-off solution between several factors: performance (energy and power), lifetime, cell size and weight (battery pack requirements), total cost of ownership (TCO) and safety. Cell ultimate performance is affected by its design: size, shape, housing (can, terminals and safety components), active materials and manufacturing.

Chemistry option is governed by energy, power, lifetime and safety requirements but intrinsic properties, such as OCV characteristics, need to be addressed due to control issues within the battery pack (BMS). Specific performance of HP cells is improved in terms of increased energy at high power conditions, but the energy efficiency of HE cells is reduced under high power operation. Therefore, it is necessary to determine the most efficient operation window in terms of usable energy. This way, the usable energy as it relates to SOC should be considered when determining which Li-ion battery to implement.

Chemistry and geometry are fundamental parameters for the different applications, but cell performance depends strongly on manufacturing parameters such as: (i) active material structure and mass (percentage of active materials within the system); (ii) current collection (number of tabs, distribution and connection to terminals); and, (iii) housing (active materials isolation, shape, case material and terminals), which is especially important for battery pack mechanical design but also for the thermal conditioning. Hence, initially chemistry (intrinsic properties) and configuration might be chosen according to target application requirements, but at the end, specific references of different manufacturers need to be compared, as many differences are encountered among them.

- The applicability of batteries depends on applications and operating conditions. The available standards and procedures are, on the one hand, mostly focused on electric vehicles (EVs) or consumer electronics, and, on the other, most of them just consist of testing protocols. The cells selection methodology developed within this work is focused on satisfying the requirements related to every individual application. The strategy firstly just lies in establishing differences among cells so that experimental analysis deepens just with

fewer preselected cells. Overall, the process pursues meeting end-user performance requirements, but also safe, long-lasting and cost-effective operation, and the cell integration into the final real application is borne in mind during the whole selection process. It also considers an effective solution towards finding the best choice of cell within as short as possible timeframe, providing enhanced value to the implementation of the proposed procedure.

- The defined cells selection process comprises four main stages. A preliminary stage (Stage 0) includes keeping up to date with the most recent advances in technologies and solutions, and it is maintained over time. The other stages consist of applying the cell selection procedure. In this sense, Stage 1 and Stage 2 were successfully applied to the preselection of cells for two different industrial applications: residential elevator and tramway. The latter was used as a validation scenario.

For the residential elevator application, LFP-based cylindrical cells were compared. This was the only technology found in the market able to meet the application functional and battery-pack requirements: HP charge and discharge pulses capability, small size in capacity (1.5-4.5 Ah) and around 3-3.8 V operating voltage. An initial market thorough analysis enabled starting the experimental stage just with three different cells (taking also into account that some of the candidate cells were not purchased due to high initial system investment). It cannot be left behind that some of the identified cells could not be purchased. Three electric and thermal performance tests, *i.e.* capacity test, rate capability test and internal resistance measurement test, enabled indentifying the weaknesses and strengths of the three choices of cells, and the advantages were balanced. A subsequent power test under application conditions was crucial for evaluating cells suitability for meeting applications power and energy demands. However, the methodology revision enabled concluding that a single HPPC test would provide the same information at once and a better use of available time and effort. From this single test at different temperatures, cell internal resistance, OCV characteristics and usable SOC range were successfully evaluated. Lastly, a first insight about the lifetime was achieved with the accelerated cycling test at severe conditions, which made the preselected cell to stand out from the rest. This cell ageing and lifetime analysis was carried out thoroughly as part of the detailed analysis (Stage 3) of cells selection methodology.

For the tramway application, three different LFP-based cells and NCM-based prismatic and pouch cells with nominal capacities ranging from 20 to 100 Ah were compared. One of them was discarded due to high surface temperature increase during initial tests and poor cycling

capability (100 Ah prismatic cell with plastic case). The other two showed good cycling performance but it was decided not to preselect the one with lower capacity due to battery pack construction issues. Lower capacity implies more cells and hence, parallel connection is required for meeting application demands, which increases the complexity of the battery pack assembly and control.

The cells selection methodology developed within this Thesis work estimates approximately a testing time of three months for the battery preliminary selection, taking into account some typical problems that can arise and cause delays.

- In depth ageing and lifetime analysis was considered of high interest as long useful lifetime is required for novel industrial applications. The main objective in this work was to develop a semi-empirical model with broad applicability that would serve as a tool to determine useful lifetime and operating strategies for different real applications. A novel approach was proposed for analysing the complex interactions between ageing processes and operating conditions. The methodology for comprehensive lifetime analysis comprises both cycle and calendar ageing but also the thorough examination of their interaction. The two major assumptions of the ageing analysis procedure are that (i) calendar and cycling ageing effects can be superimposed and that (ii) the effect of SOC and T impact factors is the same during storage and cycling operation. The methodology aims at minimising and optimising the time consuming and cost-intensive experimental work. It was therefore specially focused on models validation. Validation procedures were developed for:
  - i)* Single calendar and cycle ageing models. Dynamic validation stands out. That is, analysis of the degradation under different stress levels operating conditions over time. This is of high novelty within the state of the art reported work.
  - ii)* Complete model, which combines calendar and cycle ageing. The methodology for model construction is checked and based assumptions are evaluated.
  - iii)* Analysing the model applicability to different complex conditions. The model adaptability to realistic conditions is verified.

The proposed ageing and lifetime prediction methodology is based on a systematic stepwise multiple validation approach which covers successful validity assessment of the initial assumptions made.

- Ageing of the LFP-based Li-ion cell preselected for residential elevation application (Stages 1 and 2) was analysed for the defined lifetime prognosis approach implementation,

as part of Stage 3 definition and development. Its useful life is mostly controlled by capacity fade rather than power fade.

Cell performance degradation under different temperature and SOC storage conditions was evaluated. Loss of Lithium Inventory (LLI) was the identified main ageing mechanism due to moderate SEI evolution. The developed model covers one main degradation mechanism and in most cases is able to predict calendar ageing over a wide range of storage conditions. The estimated RMSE for the dynamic validations was 0.93%. The calendar-life performance of the studied reference was also evaluated in a UPS application. These simulations proved that the events order within the dynamic thermal profiles determines the ageing upon storage.

Cycle ageing was initially studied as a function of DOD and C-rate impact factors. For the studied cell, the effect of current is different depending on the charge/discharge range level. DOD effect on cell performance overlaps C-rate effect. The DOD effect depends on the DOD range itself and it was modelled with residuals below 1%. Dynamic validations enabled gaining insight into cell behaviour under more realistic cycling operation. It indicated that DOD effect acceleration rate is larger under static conditions (continuous cycling under the same DOD level), which were used for the model development. Hence, a dynamic operation correction factor for the DOD effect was assessed based on the dynamic validation results. This correction factor depends on Ah-throughput. On the other hand, changing C-rate values upon cycling showed that the developed cycling ageing model, which does not take into account the C-rate effect, predicts cell ageing under its effect with a maximum error of *ca.* 1%. The estimated RMSE for the dynamic validations is 1.6%. In view of the results, it was concluded that DOD effect based model is sufficient to provide an accurate prediction of cell behaviour under a wide range of static, dynamic and realistic conditions. This simplification reduces significantly the experimental work.

Additional cycling tests at different SOC and T values were carried out for confirming the major hypotheses of the methodology. They enabled concluding that all DOD, SOC and T impact factors are combined upon cycling. The effects impact rating is as follows:  $T > DOD > SOC$ . These effects were not however weighed because the methodology for lifetime prediction proposes superimposing calendar and cycling ageing effects, and the former takes into account T and SOC effects.

Complete ageing model was developed following the initially defined methodology. It was validated superimposing all dynamic T, SOC, DOD and C-rate conditions over prolonged times. The estimated overall RMSE was 1.1%, corroborating the high model accuracy under operating schemes approaching real operation. A further step was checking non symmetric

cycling profiles and also complex profiles, *i.e.* a combination of charge depleting mode of operation, micro and macro cycles, storage at different SOC, etc. The model was implemented into a simulation platform with the purpose of performing simulations under specific operation conditions for different applications.

The lifetime prognosis simulation platform calculates real instantaneous SOC (when cell charging or discharging) and predicts the ageing depending on it, while the developed model considered the middle SOC for the cycling. The inputs for this lifetime prognosis tool are parameters that are measurable in real applications (voltage, temperature, current and time) and it converts them into ageing model inputs (SOC, DOD, Ah-throughput, T and t) for precise and concise predictions. The RMSE for charge sustaining but asymmetric cycling profile (different C-rates within the same DOD) was 1.4%. It is within the measured variability of results (max. 0.99 standard deviation for three cells from the same manufacturing batch that were equally aged).

Real but accelerated residential operating profiles were simulated and contrasted against tests results over more than 120 days with outstanding matching results. The RMSE of prediction was also just 1.4%, validating in an overwhelming manner the goodness of the developed lifetime predicting tool and reliability of the ageing model.

The proposed methodology for lifetime prediction potentially provides a cost-effective route with sufficient accuracy. This method estimates approximately one year for lifetime prediction evaluation. Single factorial static tests that were used for calendar and cycle ageing models were run for nearly two years. However, the extensive validation protocols that were defined enabled understanding ageing phenomena and evaluating the applicability and accuracy of the developed ageing predictive model, within a timeframe of half a year. The model simulates a single ageing mechanism (LLI). Were aimed to evaluate dominant degradation mode change over time and the consequent system failure, the EOT would have to be extended until detecting cell performance behaviour change.

- A procedure for cylindrical cells post-mortem analysis was defined, specially focusing on the methodology for a safe cells opening and disassembling and components harvesting, without modifying cell components. It was also focused on defining procedures for obtaining significant physical-chemical and electrochemical characterisation results.

Cylindrical cells disassembling enabled gaining insight about cell design issues that can affect performance and system safety. It was very useful for comparing at first sight cells of similar configuration and performance. On the other hand, post-mortem analysis was defined

and used as a further ageing model validation step. Post-mortem analysis of cells cycled between cell maximum operating SOC range was carried out. Physical-chemical characterisation of harvested cell electrodes verified the degradation mechanisms that were identified from *in situ* cell electrochemical characterisation tests. Hence, the developed semi-empirical model that simulates cell performance fade is indeed in agreement with the ongoing ageing processes.

Overall, this Thesis work has successfully developed a comprehensive methodology for cells selection which is effective in terms of time, cost and applicability. This cell selection has been based in multiple steps, all of which have been started from the right beginning within the IK4-Ikerlan Energy Unit, generating a significant progress with respect to the internal existing know-how. The achievements in the step referred to lifetime prediction methodology have been remarkable, providing an effective and accurate way to estimate lifetime of a Li-ion battery under the specific conditions of the targeted application. The methodology is novel, original and competitive in terms of minimised number of experiments and combined analysis procedures. It demonstrates a significant progress with respect of the state of the art of existing methods in the field. Future work will focus on extending the applicability of the developed lifetime prognosis tool to several industrial sectors for ESS sizing, which will be afterwards integrated into a business model for overall system evaluation. Moreover, its viability will be further explored for other battery technologies.

# ***Bibliography***

---



- [1] <http://www.infomine.com/investment/metal-prices/crude-oil/5-year/>. Last access date: June 2014.
- [2] Monthly battery sales statistics. Machinery statistics released by the Ministry of Economy, Trade and Industry: <http://www.baj.or.jp/e/statistics/02.php>. Last access date: Mar. 2011.
- [3] D. Rastler, Electric Power Research Institute (EPRI), *Electricity Energy Storage Technology Options. A White Paper Primer on Applications, Costs, and Benefits*, Dec. 2010.
- [4] D.U. Sauer, *presentation in 'Storage Systems based on Li-ion Batteries for Stationary Applications' IndustrialPh. D/Course*, Aalborg University, Department of Energy Technology, 1-3 May 2012, Denmark.
- [5] H. Budde-Meiwes, J. Drillkens, B. Lunz, J. Muennix, S. Rothgang, J. Kowal, and D.U. Sauer, *A review of current automotive battery technology and future prospects*, Journal of Automobile Engineering, 2013. 227(5): p. 761–776.
- [6] M.F. Rius and A.F. Iduarte, *Influence of Shallow Cycling on the Ageing of SLI Batteries*, Master Thesis, ISEA-RWTH Aachen.
- [7] P. Van den Bossche, F. Vergels, J. Van Mierlo, J. Matheys, and W. Van Autenboer, *SUBAT: An assessment of sustainable battery technology*, Journal of Power Sources, 2006. 162(2): p. 913-919.
- [8] [http://www.yuasaeurope.com/images/uploads/uk/downloads/shortforms/NP\\_shortform.pdf](http://www.yuasaeurope.com/images/uploads/uk/downloads/shortforms/NP_shortform.pdf). Last access date: June 2014.
- [9] P. Kreczanik, C. Martin, P. Venet, G. Clerc, G. Rojat, and Y. Zitouni, *Constant power cycling for accelerated ageing of supercapacitors*, EPE, 2009, Barcelona, Spain.
- [10] J. Pemberton, *Advances in Lithium Battery Energy Storage Technology*. Zest Energy Pty Ltd and Kokam Co. Ltd in Australian Energy Storage Conference and Exhibition, 8 May, 2014.
- [11] D. Choi, W. Wang, V.V. Viswanathan, and G.Z. Yang, D.o.E. Pacific Northwest National Laboratory, *Low Cost, Long Cycle Life, Li-ion Batteries for Stationary Applications*, Nov. 2, 2010.
- [12] M. Anderman, *In search of the optimal hybrid configuration*, in 13th annual advanced automotive battery conference, 4–8 Feb. 2013, Pasadena, California, USA.
- [13] E. Karden, *Requirements for next generation microhybrid batteries*, in 3rd advanced automotive battery conference, 18–22 June 2012, Mainz, Germany.

- [14] M. Thele, *Evaluation of Li-ion batteries in 14 V architectures*, in 3rd advanced automotive battery conference, 18–22 June 2012, Mainz, Germany.
- [15] <http://www.specchemonline.com/articles/view/where-are-lithium-ion-batteries-headed>.  
Last access date: June 2014.
- [16] K. Franz, R.B.S. Consultants, *Technology and Market Drivers for Stationary and Automotive Battery Systems*, in Batteries 2012 conference, 2012.
- [17] B. Scrosati and J. Garche, *Lithium batteries: Status, prospects and future*, Journal of Power Sources, 2010. 195(9): p. 2419-2430.
- [18] Battery university: <http://batteryuniversity.com/>. Last access date: May 2014.
- [19] *Batteries for Electric Cars. Challenges, Opportunities, and Outlook to 2020*, The Boston Consulting Group, 2010.
- [20] A.J. Hunt, ENER1, *Large Format Lithium Power Cells for Demanding Hybrid Applications*, Joint Service Power Expo, Power to Sustain Warfighter Dominance, 2011.
- [21] S. De-Leon, *High Power Rechargeable Lithium Battery Market*, in IFCBC meeting 2010, 4 Feb 2010.
- [22] Electropaedia, Energy Sources and Energy Storage, Battery and Energy Encyclopa: <http://www.mpoweruk.com/>. Last access date: Apr. 2011.
- [23] Axeon Guide to Batteries: <http://www.axeon.com/>. Last access date: Apr. 2011.
- [24] *Powertrain 2020. L-ion batteries-the next battery ahead?*, Roland Berger Strategy Consultants, Munich/Dhangai/Detroit, Feb. 2010.
- [25] P. Van-den-Bossche, *The Electric Vehicle Charged by the Grid*, in PHEV-09, Sept. 28 to 30, 2009, Canada.
- [26] P. Bai, G. Tian, and Q. Chen, *Capacity Loss in Different Charge/Discharge Cycles of Lithium Ion Batteries*, in EVS24 International Battery, Hybrid and Fuel Cell Electric Vehicle Symposium, May 13-16, 2009, Stavanger, Norway.
- [27] F.P. Tredeau and Z.M. Saleme, *Evaluation of Lithium iron phosphate batteries for electric vehicles application*, in IEEE Vehicle Power and Propulsion Conference, 7-10 Sept., 2009, Dearborn.
- [28] J.P. Fellner, G.J. Loeber, and S.S. Sandhu, *Testing of lithium-ion 18650 cells and characterizing/predicting cell performance*, Journal of Power Sources, 1999. 81-82: p. 867-871.

- [29] A.F. Burke, *Batteries and ultracapacitors for electric, hybrid, and fuel cell vehicles*, Proceedings of the IEEE, 2007. 95(4): p. 806-820.
- [30] N. Omar, B. Verbrugge, G. Mulder, P. Van Den Bossche, J. Van Mierlo, M. Daowd, M. Dhaens, and S. Pauwels, *Evaluation of performance characteristics of various lithium-ion batteries for use in BEV application*, in Vehicle Power and Propulsion Conference (VPPC), 2010 IEEE, 1-3 Sept. 2010, Lille, France.
- [31] G. Mulder, N. Omar, S. Pauwels, F. Leemans, B. Verbrugge, W. De Nijs, P. Van Den Bossche, D. Six, and J. Van Mierlo, *Enhanced test methods to characterise automotive battery cells*, Journal of Power Sources, 2011. 196(23): p. 10079-10087.
- [32] A. Burke and M. Miller, *Performance characteristics of lithium-ion batteries of various chemistries for plug-in hybrid vehicles*, in EVS24 International Battery, Hybrid and Fuel Cell Electric Vehicle Symposium May 13-16, 2009, Stavanger, Norway.
- [33] N. Omar, M. Daowd, B. Verbrugge, G. Mulder, P.V.d. Bossche, J.V. Mierlo, M. Dhaens, S. Pauwels, and F. Leemans, *Assessment of Performance Characteristics of Lithium-Ion Batteries for PHEV Vehicles Applications Based on a Newly Test Methodology*, in EVS25 International Battery, Hybrid and Fuel Cell Electric Vehicle, 5-9 Nov., 2010, Shenzhen, China.
- [34] O.O. Hans-Georg Schweiger, Oliver Komesker, André Raschke, Michael Schiemann, Christian Zehner, Markus Gehnen, Michael Keller and Peter Birke, *Comparison of Several Methods for Determining the Internal Resistance of Lithium Ion Cells*, Sensors, 2010. 10: p. 5604-5625.
- [35] A.F. Burke and M. Miller, *The UC Davis Emerging Lithium Battery Test Project*, UCD-ITS-RR-09-18, 2009.
- [36] *Cost and performance of EV batteries*, Element Energy Limited, Final report for The Committee on Climate Change, 2012.
- [37] M. Dubarry, N. Vuillaume, and B.Y. Liaw, *Origins and accommodation of cell variations in Li-ion battery pack modeling*, International Journal of Energy Research, 2010. 34(2).
- [38] T.F. Fuller, M. Doyle, and J. Newman, *Simulation and optimization of the dual lithium ion insertion cell*, Journal of the Electrochemical Society, 1994. 141(1): p. 1-10.
- [39] M.A. Roscher, O. Bohlen, and J. Vetter, *OCV Hysteresis in Li-Ion Batteries including Two-Phase Transition Materials*, International Journal of Electrochemistry, 2011. 2011: p. 6.
- [40] M.D. Levi and D. Aurbach, *Frumkin intercalation isotherm - a tool for the description of lithium insertion into host materials: a review*, Electrochimica Acta, 1999. 45(1): p. 167-185.

- [41] M.A. Roscher, J. Vetter, and D.U. Sauer, *Characterisation of charge and discharge behaviour of lithium ion batteries with olivine based cathode active material*, Journal of Power Sources, 2009. 191(2): p. 582-590.
- [42] M. Winter, J.O. Besenhard, M.E. Spahr, and P. Novák, *Insertion electrode materials for rechargeable lithium batteries*, Advanced Materials, 1998. 10(10): p. 725-763.
- [43] D. Aurbach, B. Markovsky, I. Weissman, E. Levi, and Y. Ein-Eli, *On the correlation between surface chemistry and performance of graphite negative electrodes for Li ion batteries*, Electrochimica Acta, 1999. 45(1-2): p. 67-86.
- [44] J. Christensen, *Modeling diffusion-induced stress in Li-ion cells with porous electrodes*, Journal of the Electrochemical Society, 2010. 157(3): p. A366-A380.
- [45] H. Wenzl, I. Baring-Gould, R. Kaiser, B.Y. Liaw, P. Lundsager, J. Manwell, A. Ruddell, and V. Svoboda, *Life prediction of batteries for selecting the technically most suitable and cost effective battery*, Journal of Power Sources, 2005. 144(2): p. 373-384.
- [46] G. Denomme, *Usable Energy: Key to Determining the True Cost of Advanced Lithium Ion Battery Systems for Electronics Vehicles*, Battery Power, Jan.-Feb. 2012.
- [47] J. Wang, P. Liu, J. Hicks-Garner, E. Sherman, S. Soukiazian, M. Verbrugge, H. Tataria, J. Musser, and P. Finamore, *Cycle-life model for graphite-LiFePO<sub>4</sub> cells*, Journal of Power Sources, 2011. 196(8): p. 3942-3948.
- [48] B. Sandén and P. Wallgren, *Systems Perspectives on Electromobility*, Chalmers University of Technology, 2014, 978-91-980973-9-9.
- [49] M. Kassem and C. Delacourt, *Postmortem analysis of calendar-aged graphite/LiFePO<sub>4</sub> cells*, Journal of Power Sources, 2013. 235: p. 159-171.
- [50] D.P. Abraham, J. Liu, C.H. Chen, Y.E. Hyung, M. Stoll, N. Elsen, S. MacLaren, R. Twisten, R. Haasch, E. Sammann, I. Petrov, K. Amine, and G. Henriksen, *Diagnosis of power fade mechanisms in high-power lithium-ion cells*, Journal of Power Sources, 2003. 119-121: p. 511-516.
- [51] K. Amine, J. Liu, and I. Belharouak, *High-temperature storage and cycling of C-LiFePO<sub>4</sub>/graphite Li-ion cells*, Electrochemistry Communications, 2005. 7(7): p. 669-673.
- [52] K. Amine, C.H. Chen, J. Liu, M. Hammond, A. Jansen, D. Dees, I. Bloom, D. Vissers, and G. Henriksen, *Factors responsible for impedance rise in high power lithium ion batteries*, Journal of Power Sources, 2001. 97-98: p. 684-687.

- [53] D. Aurbach, B. Markovsky, A. Rodkin, E. Levi, Y.S. Cohen, H.J. Kim, and M. Schmidt, *On the capacity fading of LiCoO<sub>2</sub> intercalation electrodes: The effect of cycling, storage, temperature, and surface film forming additives*, *Electrochimica Acta*, 2002. 47(27): p. 4291-4306.
- [54] R.P. Ramasamy, J.W. Lee, and B.N. Popov, *Simulation of capacity loss in carbon electrode for lithium-ion cells during storage*, *Journal of Power Sources*, 2007. 166(1): p. 266-272.
- [55] Q. Zhang and R.E. White, *Calendar life study of Li-ion pouch cells*, *Journal of Power Sources*, 2007. 173(2 SPEC. ISS.): p. 990-997.
- [56] M. Safari and C. Delacourt, *Simulation-based analysis of aging phenomena in a commercial graphite/LiFePO<sub>4</sub> cell*, *Journal of the Electrochemical Society*, 2011. 158(12): p. A1436-A1447.
- [57] I. Bloom, J. Christophersen, and K. Gering, *Differential voltage analyses of high-power lithium-ion cells 2. Applications*, *Journal of Power Sources*, 2005. 139(1-2): p. 304-313.
- [58] D.P. Abraham, Argonne National Laboratory, U.S. Department of Energy, *Diagnostic Examination of Generation 2 Lithium-Ion Cells and Assessment of Performance Degradation Mechanisms*, ANL-05/21, July 2005.
- [59] T. Yoshida, M. Takahashi, S. Morikawa, C. Ihara, H. Katsukawa, T. Shiratsuchi, and J.-i. Yamaki, *Degradation Mechanism and Life Prediction of Lithium-Ion Batteries*, *Journal of Electrochemical Society*, 2006. 153(3): p. A576-A582.
- [60] X.V. Zhang, P.N. Ross, R. Kostecki, F. Kong, S. Sloop, J.B. Kerr, K. Striebel, E.J. Cairns, and F. McLarnon, *Diagnostic Characterization of High-Power Lithium-Ion Batteries For Use in Hybrid Electric Vehicles*, *Journal of the Electrochemical Society*, 2001. 148(5): p. A463-A470.
- [61] S. Bourlot, P. Blanchard, and S. Robert, *Investigation of aging mechanisms of high power Li-ion cells used for hybrid electric vehicles*, *Journal of Power Sources*, 2011. 196(16): p. 6841-6846.
- [62] M. Klett, R. Eriksson, J. Groot, P. Svens, K. Ciosek Högström, R.W. Lindström, H. Berg, T. Gustafson, G. Lindbergh, and K. Edström, *Non-uniform aging of cycled commercial LiFePO<sub>4</sub>/graphite cylindrical cells revealed by post-mortem analysis*, *Journal of Power Sources*, 2014. 257: p. 126-137.

- [63] T.G. Zavalis, M. Klett, M.H. Kjell, M. Behm, R.W. Lindström, and G. Lindbergh, *Aging in lithium-ion batteries: Model and experimental investigation of harvested LiFePO<sub>4</sub> and mesocarbon microbead graphite electrodes*, *Electrochimica Acta*, 2013. 110(0): p. 335-348.
- [64] D. Aurbach, B. Markovsky, Y. Talyossef, G. Salitra, H.-J. Kim, and S. Choi, *Studies of cycling behavior, ageing, and interfacial reactions of LiNi<sub>0.5</sub>Mn<sub>1.5</sub>O<sub>4</sub> and carbon electrodes for lithium-ion 5-V cells*, *Journal of Power Sources*, 2006. 162(2): p. 780-789.
- [65] B. Stiaszny, J.C. Ziegler, E.E. Krauß, J.P. Schmidt, and E. Ivers-Tiffée, *Electrochemical characterization and post-mortem analysis of aged LiMn<sub>2</sub>O<sub>4</sub>-Li(Ni<sub>0.5</sub>Mn<sub>0.3</sub>Co<sub>0.2</sub>)O<sub>2</sub>/graphite lithium ion batteries. Part I: Cycle aging*, *Journal of Power Sources*, 2014. 251(0): p. 439-450.
- [66] S. Watanabe, M. Kinoshita, and K. Nakura, *Capacity fade of LiNi<sub>(1-x-y)</sub>CoxAlyO<sub>2</sub> cathode for lithium-ion batteries during accelerated calendar and cycle life test. I. Comparison analysis between LiNi<sub>(1-x-y)</sub>CoxAlyO<sub>2</sub> and LiCoO<sub>2</sub> cathodes in cylindrical lithium-ion cells during long term storage test*, *Journal of Power Sources*, 2014. 247(0): p. 412-422.
- [67] P. Liu, J. Wang, J. Hicks-Garner, E. Sherman, S. Soukiazian, M. Verbrugge, H. Tataria, J. Musser, and P. Finamore, *Aging Mechanisms of LiFePO<sub>4</sub> batteries deduced by electrochemical and structural analyses*, *Journal of the Electrochemical Society*, 2010. 157(4): p. A499-A507.
- [68] R.S. Rubino, H. Gan, and E.S. Takeuchi, *A Study of Capacity Fade in Cylindrical and Prismatic Lithium-Ion Batteries*, *Journal of Electrochemical Society*, 2001. 148(9): p. A1029-A1033.
- [69] K. Maher and R. Yazami, *A study of lithium ion batteries cycle aging by thermodynamics techniques*, *Journal of Power Sources*, 2014. 247(0): p. 527-533.
- [70] G. Ning, B. Haran, and B.N. Popov, *Capacity fade study of lithium-ion batteries cycled at high discharge rates*, *Journal of Power Sources*, 2003. 117(1-2): p. 160-169.
- [71] P.L. Moss, G. Au, E.J. Plichta, and J.P. Zheng, *Study of capacity fade of lithium-ion polymer rechargeable batteries with continuous cycling*, *Journal of the Electrochemical Society*, 2010. 157(1): p. A1-A7.
- [72] S. Muto, Y. Sasano, K. Tatsumi, T. Sasaki, K. Horibuchi, Y. Takeuchi, and Y. Ukyo, *Capacity-Fading Mechanisms of LiNiO<sub>2</sub>-Based Lithium-Ion Batteries: II. Diagnostic Analysis by Electron Microscopy and Spectroscopy*, *Journal of Electrochemical Society*, 2009. 156(5): p. A371-A377.

- [73] M.J. Plancha, C.M. Rangel, B. Rodrigues, and F. Azevedo, *Degradation of Lithium Iron Phosphate-based Cathode in Lithium Ion Batteries: a Post-mortem Analysis*, *Ciência e Tecnologia de Materiais*, 2011. 23: p. 59-66.
- [74] J. Shim, R. KostECKI, T. Richardson, X. Song, and K.A. Striebel, *Electrochemical analysis for cycle performance and capacity fading of a lithium-ion battery cycled at elevated temperature*, *Journal of Power Sources*, 2002. 112(1): p. 222-230.
- [75] D. Aurbach, E. Zinigrad, H. Teller, and P. Dan, *Factors Which Limit the Cycle Life of Rechargeable Lithium (Metal) Batteries*, *Journal of Electrochemical Society*, 2000. 147(4): p. 1274-1279.
- [76] D. Zhang, B.S. Haran, A. Durairajan, R.E. White, Y. Podrazhansky, and B.N. Popov, *Studies on capacity fade of lithium-ion batteries*, *Journal of Power Sources*, 2000. 91(2): p. 122-129.
- [77] J. Cannarella and C.B. Arnold, *Stress evolution and capacity fade in constrained lithium-ion pouch cells*, *Journal of Power Sources*, 2014. 245(0): p. 745-751.
- [78] I. Bloom, J.P. Christophersen, D.P. Abraham, and K.L. Gering, *Differential voltage analyses of high-power lithium-ion cells: 3. Another anode phenomenon*, *Journal of Power Sources*, 2006. 157(1): p. 537-542.
- [79] C.J. Mikolajczak, T. Hayes, M.V. Megerle, and M. Wu, in *IEEE International Conference on Portable Information Devices. PORTABLE07, 25-29 May 2007*.
- [80] D. Aurbach, B. Markovsky, A. Rodkin, M. Cojocar, E. Levi, and H.-J. Kim, *An analysis of rechargeable lithium-ion batteries after prolonged cycling*, *Electrochimica Acta*, 2002. 47(12): p. 1899-1911.
- [81] C. Mikolajczak, M. Kahn, K. White, and R.T. Long, *Fire Protection Research Foundation, Lithium-Ion Batteries Hazard and Use Assessment*, 1100034.000 A0F0 0711 CM01.
- [82] D.P. Abraham, J.L. Knuth, D.W. Dees, I. Bloom, and J.P. Christophersen, *Performance degradation of high-power lithium-ion cells-Electrochemistry of harvested electrodes*, *Journal of Power Sources*, 2007. 170(2): p. 465-475.
- [83] E.V. Thomas, H.L. Case, D.H. Doughty, R.G. Jungst, G. Nagasubramanian, and E.P. Roth, *Accelerated power degradation of Li-ion cells*, *Journal of Power Sources*, 2003. 124(1): p. 254-260.
- [84] ISO15901-1, *Evaluation of pore size distribution and porosimetry of solid materials by mercury porosimetry and gas adsorption – Part 1: Mercury porosimetry*. 2005.

- [85] S.S. Zhang, K. Xu, and T.R. Jow, *The low temperature performance of Li-ion batteries*, Journal of Power Sources, 2003. 115(1): p. 137-140.
- [86] M. Broussely, S. Herreyre, P. Biensan, P. Kasztejna, K. Nechev, and R.J. Staniewicz, *Aging mechanism in Li ion cells and calendar life predictions*, Journal of Power Sources, 2001. 97-98: p. 13-21.
- [87] M. Kassem, J. Bernard, R. Revel, S. Pélissier, F. Duclaud, and C. Delacourt, *Calendar aging of a graphite/LiFePO<sub>4</sub> cell*, Journal of Power Sources, 2012. 208: p. 296-305.
- [88] M. Broussely, P. Biensan, F. Bonhomme, P. Blanchard, S. Herreyre, K. Nechev, and R.J. Staniewicz, *Main aging mechanisms in Li ion batteries*, Journal of Power Sources, 2005. 146(1-2): p. 90-96.
- [89] J. Zhou and P.H.L. Notten, *Studies on the degradation of Li-ion batteries by the use of microreference electrodes*, Journal of Power Sources, 2008. 177(2): p. 553-560.
- [90] J. Groot, *State-of-Health Estimation of Li-ion Batteries: Cycle Life Test Methods*, Master Thesis, Chalmers University of Technology 2012.
- [91] M. Dubarry, C. Truchot, and B.Y. Liaw, *Cell degradation in commercial LiFePO<sub>4</sub> cells with high-power and high-energy designs*, Journal of Power Sources, 2014. 258(0): p. 408-419.
- [92] D. Andre, M. Meiler, K. Steiner, C. Wimmer, T. Soczka-Guth, and D.U. Sauer, *Characterization of high-power lithium-ion batteries by electrochemical impedance spectroscopy. I. Experimental investigation*, Journal of Power Sources, 2011. 196(12): p. 5341-5348.
- [93] P.A. P. Gyan, J. Hafsaoui, F. Sellier, S. Bourlot, S. Zinola, F. Badin, *Experimental assessment of battery cycle life within the SIMSTOCK research program*, in Les Rencontres Scientifiques d'IFP Energies Nouvelles - Int. Scient. Conf. on hybrid and electric vehicles, 6-7 Dec.2011, RHEVE.
- [94] Q. Zhang and R.E. White, *Capacity fade analysis of a lithium ion cell*, Journal of Power Sources, 2008. 179(2): p. 793-798.
- [95] P. Gyan, P. Aubret, J. Hafsaoui, F. Sellier, S. Bourlot, S. Zinola, and F. Badin, IFPEN, *Experimental assessment of battery cycle life within the SIMSTOCK research program*, in Les Rencontres Scientifiques d'IFP Energies Nouvelles - Int. Scient. Conf. on hybrid and electric vehicles – RHEVE 2011, 6-7 Dec. 2011.
- [96] M. Dubarry and B.Y. Liaw, *Identify capacity fading mechanism in a commercial LiFePO<sub>4</sub> cell*, Journal of Power Sources, 2009. 194(1): p. 541-549.

- [97] I. Bloom, S.A. Jones, E.G. Polzin, V.S. Battaglia, G.L. Henriksen, C.G. Motloch, R.B. Wright, R.G. Jungst, H.L. Case, and D.H. Doughty, *Mechanisms of impedance rise in high-power, lithium-ion cells*, Journal of Power Sources, 2002. 111(1): p. 152-159.
- [98] J. Belt, V. Utgikar, and I. Bloom, *Calendar and PHEV cycle life aging of high-energy, lithium-ion cells containing blended spinel and layered-oxide cathodes*, Journal of Power Sources, 2011. 196(23): p. 10213-10221.
- [99] M. Ecker, J.B. Gerschler, J. Vogel, S. Käbitz, F. Hust, P. Dechent, and D.U. Sauer, *Development of a lifetime prediction model for lithium-ion batteries based on extended accelerated aging test data*, Journal of Power Sources, 2012. 215(0): p. 248-257.
- [100] H. Joachin, T.D. Kaun, K. Zaghbi, and J. Prakash, *Electrochemical and thermal studies of carbon-coated LiFePO<sub>4</sub> cathode*, Journal of the Electrochemical Society, 2009. 156(6): p. A401-A406.
- [101] A.K. Padhi, K.S. Nanjundaswamy, and J.B. Goodenough, *Phospho-olivines as Positive-Electrode Materials for Rechargeable Lithium Batteries*, Journal of Electrochemical Society, 1997. 144(4): p. 1188-1194.
- [102] A. Yamada, S.C. Chung, and K. Hinokuma, *Optimized LiFePO<sub>4</sub> for Lithium Battery Cathodes*, Journal of Electrochemical Society, 2001. 148: p. A224-A229.
- [103] N. Ravet, Y. Chouinard, J.F. Magnan, S. Besner, M. Gauthier, and M. Armand, *Electroactivity of natural and synthetic triphylite*, Journal of Power Sources, 2001. 97-98(0): p. 503-507.
- [104] H. Huang, S.C. Yin, and L.F. Nazar, *Approaching theoretical capacity of LiFePO<sub>4</sub> at room temperature at high rates*, Electrochemical and Solid-State Letters 2001. 4(10): p. A170-A172.
- [105] Z. Chen and J.R. Dahn, *Reducing Carbon in LiFePO<sub>4</sub>/C Composite Electrodes to Maximize Specific Energy, Volumetric Energy, and Tap Density*, Journal of Electrochemical Society, 2002. 149(9): p. A1184-A1189.
- [106] S.Y. Chung, J.T. Bloking, and Y.M. Chiang, *Electronically conductive phospho-olivines as lithium storage electrodes*, Nature Materials, 2002. 1(2): p. 123-128.
- [107] S. Franger, F.L. Cras, C. Bourbon, and H. Rouault, *LiFePO<sub>4</sub> Synthesis Routes for Enhanced Electrochemical Performance*, Journal of Electrochemical Society, 2004. 151: p. A1024-A1027.
- [108] A. Ritchie and W. Howard, *Recent developments and likely advances in lithium-ion batteries*, Journal of Power Sources, 2006. 162(2): p. 809-812.

- [109] S. Grolleau, A. Delaille, H. Gualous, P. Gyan, R. Revel, J. Bernard, E. Redondo-Iglesias, and J. Peter, *Calendar aging of commercial graphite/LiFePO<sub>4</sub> cell - Predicting capacity fade under time dependent storage conditions*, Journal of Power Sources, 2014. 255: p. 450-458.
- [110] M. Safari and C. Delacourt, *Aging of a Commercial Graphite/LiFePO<sub>4</sub> Cell* Journal of Electrochemical Society, 2011. 158(10): p. A1123-A1135.
- [111] H. Guo, J. Jiang, J. Wang, T. Lou, and X. Li, *Characteristic on internal resistance of lithium-ion power battery*, Beijing Jiaotong Daxue Xuebao/Journal of Beijing Jiaotong University, 2011. 35(5): p. 119-123.
- [112] M. Dubarry, B.Y. Liaw, M.S. Chen, S.S. Chyan, K.C. Han, W.T. Sie, and S.H. Wu, *Identifying battery aging mechanisms in large format Li ion cells*, Journal of Power Sources, 2011. 196(7): p. 3420-3425.
- [113] F. Todeschini, S. Onori, and G. Rizzoni, *An experimentally validated capacity degradation model for Li-ion batteries in PHEVs applications*, in 8th IFAC Symposium on Fault Detection, Supervision and Safety of Technical Processes (SAFEPROCESS), 29-31 August, 2012, Mexico City, Mexico.
- [114] Y. Zhang, C.Y. Wang, and X. Tang, *Cycling degradation of an automotive LiFePO<sub>4</sub> lithium-ion battery*, Journal of Power Sources, 2011. 196(3): p. 1513-1520.
- [115] N. Omar, M.A. Monem, Y. Firouz, J. Salminen, J. Smekens, O. Hegazy, H. Gualous, G. Mulder, P. Van den Bossche, T. Coosemans, and J. Van Mierlo, *Lithium iron phosphate based battery - Assessment of the aging parameters and development of cycle life model*, Applied Energy, 2014. 113: p. 1575-1585.
- [116] S.B. Peterson, J. Apt, and J.F. Whitacre, *Lithium-ion battery cell degradation resulting from realistic vehicle and vehicle-to-grid utilization*, Journal of Power Sources, 2010. 195(8): p. 2385-2392.
- [117] Z. Li, L. Lu, M. Ouyang, and Y. Xiao, *Modeling the capacity degradation of LiFePO<sub>4</sub>/graphite batteries based on stress coupling analysis*, Journal of Power Sources, 2011. 196(22): p. 9757-9766.
- [118] X.-Y. Zhou, Y.-L. Zou, G.-J. Zhao, and J. Yang, *Cycle life prediction and match detection in retired electric vehicle batteries*, Transactions of Nonferrous Metals Society of China, 2013. 23(10): p. 3040-3045.

- [119] L. Lam, *A Practical Circuitbased Model for State of Health Estimation of Li-ion Battery Cells in Electric Vehicles*, Master Thesis, Electrical Engineering, Mathematics and Computer Science Faculty, University of Technology Delft, 2011.
- [120] D. Anseán, M. González, J.C. Viera, V.M. García, C. Blanco, and M. Valledor, *Fast charging technique for high power lithium iron phosphate batteries: A cycle life analysis*, *Journal of Power Sources*, 2013. 239(0): p. 9-15.
- [121] C. Delacourt and M. Safari, *Life Simulation of a Graphite/LiFePO<sub>4</sub> Cell under Cycling and Storage*, *Journal of Electrochemical Society*, 2012. 159(8): p. A1283-A1291.
- [122] D.U. Sauer and H. Wenzl, *Lifetime Prediction*, Elsevier B. V., 2009.
- [123] M.B. Pinson and M.Z. Bazant, *Theory of SEI Formation in Rechargeable Batteries: Capacity Fade, Accelerated Aging and Lifetime Prediction*, *Journal of the Electrochemical Society*, 2012. 160(2): p. A243-A250.
- [124] E. Prada, D. Di Domenico, Y. Creff, J. Bernard, V. Sauvant-Moynot, and F. Huet, *Physics-based modelling of LiFePO<sub>4</sub>-graphite Li-ion batteries for power and capacity fade predictions: Application to calendar aging of PHEV and EV*, in 2012 IEEE Vehicle Power and Propulsion Conference, VPPC 2012, 9-12 October 2012, Seoul, South Korea.
- [125] A. Eddahech, O. Briat, E. Woirgard, and J.M. Vinassa, *Remaining useful life prediction of lithium batteries in calendar ageing for automotive applications*, *Microelectronics Reliability*, 2012. 52(9-10): p. 2438-2442.
- [126] R.P. Ramasamy, R.E. White, and B.N. Popov, *Calendar life performance of pouch lithium-ion cells*, *Journal of Power Sources*, 2005. 141(2): p. 298-306.
- [127] R.B. Wright, C.G. Motloch, J.R. Belt, J.P. Christophersen, C.D. Ho, R.A. Richardson, I. Bloom, S.A. Jones, V.S. Battaglia, G.L. Henriksen, T. Unkelhaeuser, D. Ingersoll, H.L. Case, S.A. Rogers, and R.A. Sutula, *Calendar- and cycle-life studies of advanced technology development program generation 1 lithium-ion batteries*, *Journal of Power Sources*, 2002. 110(2): p. 445-470.
- [128] I. Bloom, B.W. Cole, J.J. Sohn, S.A. Jones, E.G. Polzin, V.S. Battaglia, G.L. Henriksen, C. Motloch, R. Richardson, T. Unkelhaeuser, D. Ingersoll, and H.L. Case, *An accelerated calendar and cycle life study of Li-ion cells*, *Journal of Power Sources*, 2001. 101(2): p. 238-247.
- [129] R.G. Jungst, G. Nagasubramanian, H.L. Case, B.Y. Liaw, A. Urbina, T.L. Paez, and D.H. Doughty, *Accelerated calendar and pulse life analysis of lithium-ion cells*, *Journal of Power Sources*, 2003. 119-121: p. 870-873.

- [130] K. Asakura, M. Shimomura, and T. Shodai, *Study of life evaluation methods for Li-ion batteries for backup applications*, Journal of Power Sources, 2003. 119-121: p. 902-905.
- [131] B. Markovsky, Y. Talyossef, G. Salitra, D. Aurbach, H.J. Kim, and S. Choi, *Cycling and storage performance at elevated temperatures of LiNi<sub>0.5</sub>Mn<sub>1.5</sub>O<sub>4</sub> positive electrodes for advanced 5 V Li-ion batteries*, Electrochemistry Communications, 2004. 6(8): p. 821-826.
- [132] S. Käbitz, J.B. Gerschler, M. Ecker, Y. Yurdagel, B. Emmermacher, D. André, T. Mitsch, and D.U. Sauer, *Cycle and calendar life study of a graphite|LiNi<sub>1/3</sub>Mn<sub>1/3</sub>Co<sub>1/3</sub>O<sub>2</sub> Li-ion high energy system. Part A: Full cell characterization*, Journal of Power Sources, 2013. 239(0): p. 572-583.
- [133] M. Ecker, N. Nieto, S. Käbitz, J. Schmalstieg, H. Blanke, A. Warnecke, and D.U. Sauer, *Calendar and cycle life study of Li(NiMnCo)O<sub>2</sub>-based 18650 lithium-ion batteries*, Journal of Power Sources, 2014. 248(0): p. 839-851.
- [134] Q. Zhang and R.E. White, *Calendar life study of Li-ion pouch cells. Part 2: Simulation*, Journal of Power Sources, 2008. 179(2): p. 785-792.
- [135] R. Arunachala, *Development of an Aging Model for Lithium Ion Batteries based on Calendar Aging Tests*, Master Thesis, RWTH Aachen university, 2011.
- [136] I. Bloom, S.A. Jones, V.S. Battaglia, G.L. Henriksen, J.P. Christophersen, R.B. Wright, C.D. Ho, J.R. Belt, and C.G. Motloch, *Effect of cathode composition on capacity fade, impedance rise and power fade in high-power, lithium-ion cells*, Journal of Power Sources, 2003. 124(2): p. 538-550.
- [137] B.Y. Liaw, E.P. Roth, R.G. Jungst, G. Nagasubramanian, H.L. Case, and D.H. Doughty, *Correlation of Arrhenius behaviors in power and capacity fades with cell impedance and heat generation in cylindrical lithium-ion cells*, Journal of Power Sources, 2003. 119-121(0): p. 874-886.
- [138] Y. Mita, S. Seki, N. Terada, N. Kihira, K. Takei, and H. Miyashiro, *Accelerated Test Methods for Life Estimation of High-Power Lithium-Ion Batteries*, Electrochemistry Communications, 2010. 78(8): p. 384-386.
- [139] G. Sarre, P. Blanchard, and M. Broussely, *Aging of lithium-ion batteries*, Journal of Power Sources, 2004. 127(1-2): p. 65-71.
- [140] I. Bloom, L.K. Walker, J.K. Basco, D.P. Abraham, J.P. Christophersen, and C.D. Ho, *Differential voltage analyses of high-power lithium-ion cells. 4. Cells containing NMC*, Journal of Power Sources, 2010. 195(3): p. 877-882.

- [141] I. Bloom, B.G. Potter, C.S. Johnson, K.L. Gering, and J.P. Christophersen, *Effect of cathode composition on impedance rise in high-power lithium-ion cells: Long-term aging results*, Journal of Power Sources, 2006. 155(2): p. 415-419.
- [142] J.P. Christophersen, C.D. Hoa, C.G. Motloch, D. Howell, and H.L. Hess, *Effects of Reference Performance Testing during Aging Using Commercial Lithium-Ion Cells*, Journal of Electrochemical Society, 2006. 153(7): p. A1406-A1416.
- [143] B. Lunz, Z. Yan, J.B. Gerschler, and D.U. Sauer, *Influence of plug-in hybrid electric vehicle charging strategies on charging and battery degradation costs*, Energy Policy, 2012. 46(0): p. 511-519.
- [144] M.C. Smart, B.V. Ratnakumar, L.D. Whitcanack, F.J. Puglia, S. Santee, and R. Gitzendanner, *Life verification of large capacity Yardney Li-ion cells and batteries in support of NASA missions*, International Journal of Energy Research, 2010. 34(2): p. 116–132.
- [145] B.Y. Liaw, R.G. Jungst, G. Nagasubramanian, H.L. Case, and D.H. Doughty, *Modeling capacity fade in lithium-ion cells*, Journal of Power Sources, 2005. 140(1): p. 157-161.
- [146] E.V. Thomas, E.P. Roth, D.H. Doughty, and R.G. Jungst, Sandia National Laboratories, *Experimental Design and Analysis for Accelerated Degradation Tests with Li-ion Cells*, SAND2003-2897, 2003
- [147] E.V. Thomas, I. Bloom, J.P. Christophersen, and V.S. Battaglia, *Statistical methodology for predicting the life of lithium-ion cells via accelerated degradation testing*, Journal of Power Sources, 2008. 184(1): p. 312-317.
- [148] J. Schmalstieg, S. Käbitz, M. Ecker, and D.U. Sauer, *A holistic aging model for Li(NiMnCo)O<sub>2</sub> based 18650 lithium-ion batteries*, Journal of Power Sources, 2014. 257(0): p. 325-334.
- [149] M. Dubarry, C. Truchot, B.Y. Liaw, K. Gering, S. Sazhin, D. Jamison, and C. Michelbacher, *Evaluation of commercial lithium-ion cells based on composite positive electrode for plug-in hybrid electric vehicle applications. Part II. Degradation mechanism under 2C cycle aging*, Journal of Power Sources, 2011. 196(23): p. 10336-10343.
- [150] J. Vetter, P. Novák, M.R. Wagner, C. Veit, K.C. Möller, J.O. Besenhard, M. Winter, M. Wohlfahrt-Mehrens, C. Vogler, and A. Hammouche, *Ageing mechanisms in lithium-ion batteries*, Journal of Power Sources, 2005. 147(1-2): p. 269-281.

- [151] P. Arora, M. Doyle, and R.E. White, *Mathematical modeling of the lithium deposition overcharge reaction in lithium-ion batteries using carbon-based negative electrodes*, Journal of the Electrochemical Society, 1999. 146(10): p. 3543-3553.
- [152] B.Y. Liaw and M. Dubarry, *From driving cycle analysis to understanding battery performance in real-life electric hybrid vehicle operation*, Journal of Power Sources, 2007. 174(1): p. 76-88.
- [153] E. Jobson, *Hybrid technology for buses*, in European Fleets Conference, 2010, Örebro, Sweden.
- [154] J. Groot, *Statistic Method for Extraction of Synthetic Load Cycles for Cycle life Tests of HEV Li-ion Batteries*, in EVS24 International Battery, Hybrid and Fuel Cell Electric Vehicle Symposium, May 13-16, 2009, Stavanger, Norway.
- [155] X. Han, M. Ouyang, L. Lu, J. Li, Y. Zheng, and Z. Li, *A comparative study of commercial lithium ion battery cycle life in electrical vehicle: Aging mechanism identification*, Journal of Power Sources, 2014. 251(0): p. 38-54.
- [156] A. Eddahech, O. Briat, H. Henry, J.Y. Delétage, E. Woïrgard, and J.M. Vinassa, *Ageing monitoring of lithium-ion cell during power cycling tests*, Microelectronics Reliability, 2011. 51(9-11): p. 1968-1971.
- [157] M. Dubarry, V. Svoboda, R. Hwu, and B.Y. Liaw, *Capacity and power fading mechanism identification from a commercial cell evaluation*, Journal of Power Sources, 2007. 165(2): p. 566-572.
- [158] M. Dubarry, V. Svoboda, R. Hwu, and B.Y. Liaw, *Capacity loss in rechargeable lithium cells during cycle life testing: The importance of determining state-of-charge*, Journal of Power Sources, 2007. 174(2): p. 1121-1125.
- [159] T. Sasaki, T. Nonaka, H. Oka, C. Okuda, Y. Itou, Y. Kondo, Y. Takeuchi, Y. Ukyo, K. Tatsumi, and S. Muto, *Capacity-Fading Mechanisms of LiNiO<sub>2</sub>-Based Lithium-Ion Batteries: I. Analysis by Electrochemical and Spectroscopic Examination*, Journal of Electrochemical Society, 2009. 156(4): p. A289-A293.
- [160] J. Shim and K.A. Striebel, *Characterization of high-power lithium-ion cells during constant current cycling: Part I. Cycle performance and electrochemical diagnostics*, Journal of Power Sources, 2003. 122(2): p. 188-194.
- [161] U. Tröltzsch, O. Kanoun, and H.-R. Tränkler, *Characterizing aging effects of lithium ion batteries by impedance spectroscopy*, Electrochimica Acta, 2006. 51(8-9): p. 1664-1672.

- [162] K. Takei, K. Kumai, Y. Kobayashi, H. Miyashiro, N. Terada, T. Iwahori, and T. Tanaka, *Cycle life estimation of lithium secondary battery by extrapolation method and accelerated aging test*, Journal of Power Sources, 2001. 97-98: p. 697-701.
- [163] Y. Zhang and C.Y. Wang, *Cycle-life characterization of automotive lithium-ion batteries with LiNiO<sub>2</sub> cathode*, Journal of the Electrochemical Society, 2009. 156(7): p. A527-A535.
- [164] S.S. Choi and H.S. Lim, *Factors that affect cycle-life and possible degradation mechanisms of a Li-ion cell based on LiCoO<sub>2</sub>*, Journal of Power Sources, 2002. 111(1): p. 130-136.
- [165] M. Dubarry, V. Svoboda, R. Hwu, and B.Y. Liaw, *Incremental capacity analysis and close-to-equilibrium OCV measurements to quantify capacity fade in commercial rechargeable lithium batteries*, Electrochemical and Solid-State Letters, 2006. 9(10): p. A454-A457.
- [166] S.-W. Eom, M.-K. Kim, I.-J. Kim, S.-I. Moon, Y.-K. Sun, and H.-S. Kim, *Life prediction and reliability assessment of lithium secondary batteries*, Journal of Power Sources, 2007. 174(2): p. 954-958.
- [167] R.B. Wright, J.P. Christophersen, C.G. Motloch, J.R. Belt, C.D. Ho, V.S. Battaglia, J.A. Barnes, T.Q. Duong, and R.A. Sutula, *Power fade and capacity fade resulting from cycle-life testing of Advanced Technology Development Program lithium-ion batteries*, Journal of Power Sources, 2003. 119–121(0): p. 865-869.
- [168] J.-W. Lee, Y.K. Anguchamy, and B.N. Popov, *Simulation of charge–discharge cycling of lithium-ion batteries under low-earth-orbit conditions*, Journal of Power Sources, 2006. 162(2): p. 1395-1400.
- [169] J.R. Belt, C.D. Ho, T.J. Miller, M.A. Habib, and T.Q. Duong, *The effect of temperature on capacity and power in cycled lithium ion batteries*, Journal of Power Sources, 2005. 142(1–2): p. 354-360.
- [170] J.P. Christophersen, C.G. Motloch, C.D. Ho, D.F. Glenn, R.B. Wright, J.R. Belt, T.C. Murphy, T.Q. Duong, and V.S. Battaglia, Idaho National Engineering and Environmental Laboratory & Bechtel BWXT Idaho (LLC) *DOE Advanced Technology Development Program for Lithium-Ion Batteries: INEEL Interim Report for Gen 2 Cycle-Life Testing*, 2002
- [171] M.M. Joglekar and N. Ramakrishnan, *Cyclic Capacity Fade Plots for aging studies of Li-ion cells*, Journal of Power Sources, 2013. 230(0): p. 143-147.

- [172] S. Brown, K. Ogawa, Y. Kumeuchi, S. Enomoto, M. Uno, H. Saito, Y. Sone, D. Abraham, and G. Lindbergh, *Cycle life evaluation of 3Ah LixMn2O4-based lithium-ion secondary cells for low-earth-orbit satellites: I. Full cell results*, Journal of Power Sources, 2008. 185(2): p. 1444-1453.
- [173] S. Onori, P. Spagnol, V. Marano, Y. Guezennec, and G. Rizzoni, *A new life estimation method for lithium-ion batteries in plug-in hybrid electric vehicles applications*, Journal of Power Electronics, 2012. 4(3): p. 302 - 319.
- [174] T.M. Bandhauer, S. Garimella, and T.F. Fuller, *Temperature-dependent electrochemical heat generation in a commercial lithium-ion battery*, Journal of Power Sources, 2014. 247(0): p. 618-628.
- [175] S.W. Eom, M.K. Kim, I.J. Kim, S.I. Moon, Y.K. Sun, and H.S. Kim, *Life prediction and reliability assessment of lithium secondary batteries*, Journal of Power Sources, 2007. 174(2): p. 954-958.
- [176] D. Stroe, M. Swierczynski, A.-I. Stan, and R. Teodorescu, *Accelerated lifetime testing methodology for lifetime estimation of Lithium-ion batteries used in augmented wind power plants*, in Energy Conversion Congress and Exposition (ECCE), 2013 IEEE, 15-19 Sept. 2013, Denver, CO.
- [177] H. Wenzl, A. Haubrock, and H.P. Beck, *Degradation of lithium ion batteries under complex conditions of use*, Zeitschrift fur Physikalische Chemie, 2013. 227(1): p. 57-71.
- [178] F. Herb, A. Jossen, S. Reiff, and M. Wöhr, *Investigation of Li-battery and fuel cell aging in FC hybrid car model*, in Eleventh Grove Fuel Cell Symposium, 23 Sept. 2009, London.
- [179] C. Günther, A. Jossen, and V. Späth, *Lifetime Models for Lithium-ion Batteries*, in Advanced Battery Technologies for Automobiles and Their Electric Power Grid Integration, 2nd Technical Conference, 1-2 February 2010, Rheingoldhalle, Mainz.
- [180] K. Smith, T. Markel, G.H. Kim, and A. Pesaran, *Design of Electric Drive Vehicle Batteries for Long Life and Low Cost* in ICCV NRCL/PR-5400-40933, Oct. 2010.
- [181] C. Guenther, B. Schott, W. Hennings, P. Waldowski, and M.A. Danzer, *Model-based investigation of electric vehicle battery aging by means of vehicle-to-grid scenario simulations*, Journal of Power Sources, 2013. 239: p. 604-610.
- [182] E. Sarasketa-Zabala, I. Laresgoiti, I. Alava, M. Rivas, I. Villarreal, and F. Blanco, *Validation of the methodology for lithium-ion batteries lifetime prognosis* in EVS27, Nov. 17-20, 2013, Barcelona, Spain.

- [183] K.J. Chung and C.C. Hsiao, *Accelerated Degradation Assessment of 18650 Lithium-Ion Batteries* in International Symposium on Computer, Consumer and Control (IS3C), 4-6 June 2012, Taichung, Taiwan.
- [184] E.V. Thomas, I. Bloom, J.P. Christophersen, and V.S. Battaglia, *Rate-based degradation modeling of lithium-ion cells*, Journal of Power Sources, 2012. 206: p. 378-382.
- [185] F. Herb, *Alterungsmechanismen in Lithium-Ionen-Batterien und PEM-Brennstoffzellen und deren Einfluss auf die Eigenschaften von daraus bestehenden Hybrid-Systemen*, Ph. D Thesis, Fakultät für Naturwissenschaften der Universität Ulm 2010.
- [186] N. Omar, *Assessment of rechargeable energy storage systems for plug-in hybrid electric vehicles*, Ph. D Thesis, Vrije Universiteit Brussel, 2012.
- [187] E. Wood, M. Alexander, and T.H. Bradley, *Investigation of battery end-of-life conditions for plug-in hybrid electric vehicles*, Journal of Power Sources, 2011. 196(11): p. 5147-5154.
- [188] J. Neubauer and A. Pesaran, *The ability of battery second use strategies to impact plug-in electric vehicle prices and serve utility energy storage applications*, Journal of Power Sources, 2011. 196(23): p. 10351-10358.
- [189] Q.C. Zhuang, T. Wei, L.L. Du, Y.L. Cui, L. Fang, and S.G. Sun, *An electrochemical impedance spectroscopic study of the electronic and ionic transport properties of spinel LiMnO*, Journal of Physical Chemistry, 2010. 114: p. 8614-8621.
- [190] T. Utsunomiya, O. Hatozaki, N. Yoshimoto, M. Egashira, and M. Morita, *Influence of particle size on the self-discharge behavior of graphite electrodes in lithium-ion batteries*, Journal of Power Sources, 2011. 196(20): p. 8675-8682.
- [191] D. Chalasani, J. Li, N.M. Jackson, M. Payne, and B.L. Lucht, *Methylene ethylene carbonate: Novel additive to improve the high temperature performance of lithium ion batteries*, Journal of Power Sources, 2012. 208(0): p. 67-73.
- [192] G. Gachot, S. Grugeon, G.G. Eshetu, D. Mathiron, P. Ribière, M. Armand, and S. Laruelle, *Thermal behaviour of the lithiated-graphite/electrolyte interface through GC/MS analysis*, Electrochimica Acta, 2012. 83: p. 402-409.
- [193] R. Yazami and Y.F. Reynier, *Mechanism of self-discharge in graphite-lithium anode*, Electrochimica Acta, 2002. 47(8): p. 1217-1223.
- [194] M. Dubarry, C. Truchot, and B.Y. Liaw, *Synthesize battery degradation modes via a diagnostic and prognostic model*, Journal of Power Sources, 2012. 219: p. 204-216.

- [195] M. Hellqvist Kjell, S. Malmgren, K. Ciosek, M. Behm, K. Edström, and G. Lindbergh, *Comparing aging of graphite/LiFePO<sub>4</sub> cells at 22 C and 55 C - Electrochemical and photoelectron spectroscopy studies*, Journal of Power Sources, 2013. 243: p. 290-298.
- [196] H.J. Ploehn, P. Ramadass, and R.E. White, *Solvent Diffusion Model for Aging of Lithium-Ion Battery Cells*, Journal of The Electrochemical Society, Journal of Electrochemical Society, 2004. 151(3): p. A456-A462
- [197] F. Herb, A. Frank, C. Nitsche, and A. Jossen, *Optimization of fuel cell and battery control in relation to component aging of fuel cell power train*, Optimierung der regelung zwischen brennstoffzelle und batterie in bezug auf komponentenalterung, 2009. 57(1): p. 40-47.
- [198] A. Barré, B. Deguilhem, S. Grolleau, M. Gérard, F. Suard, and D. Riu, *A review on lithium-ion battery ageing mechanisms and estimations for automotive applications*, Journal of Power Sources, 2013. 241: p. 680-689.
- [199] M. Lepiorz, W. Weydanz, D. Most, and A. Jossen, *Ah-throughput versus residual capacity method for prediction of capacity loss of Li-ion batteries at alternating temperatures*, in 5th Advanced Battery Power 26-27 Feb. 2013, Aachen, Germany.
- [200] <http://www.tutiempo.net/clima/BANGKOK/2013/484550.htm>. Last access date: 24/04/2014
- [201] <http://www.tutiempo.net/clima/Gizan/2013/411400.htm>. Last access date: 24/04/2014
- [202] [http://www.tutiempo.net/clima/Tenerife\\_Sur/2013/600250.htm](http://www.tutiempo.net/clima/Tenerife_Sur/2013/600250.htm). Last access date: 24/04/2014
- [203] M. Fleckenstein, O. Bohlen, M.A. Roscher, and B. Bäker, *Current density and state of charge inhomogeneities in Li-ion battery cells with LiFePO<sub>4</sub> as cathode material due to temperature gradients*, Journal of Power Sources, 2011. 196(10): p. 4769-4778.
- [204] G. Zhang, C.E. Shaffer, C.Y. Wang, and C.D. Rahn, *Effects of non-uniform current distribution on energy density of li-ion cells*, Journal of the Electrochemical Society, 2013. 160(11): p. A2299-A2305.
- [205] R. Spotnitz, *Simulation of capacity fade in lithium-ion batteries*, Journal of Power Sources, 2003. 113(1): p. 72-80.
- [206] R. Deshpande, Y. Cheng, M.W. Verbrugge, and A. Timmons, *Journal of Electrochemical Society*, 2011. 158(6): p. A718-A724.
- [207] J.R. Dahn, *Phase diagram of Li<sub>x</sub>C<sub>6</sub>*, Physical Review B, 1991. 44(17): p. 9170-9177.

- [208] E. Scott, J. Brown, C. Schmidt, and W. Howard, *A practical Longevity Model for Lithium-Ion Batteries: De-coupling the Time and Cycle-Dependence of Capacity Fade*, in 208th ECS Meeting 16-21 October 2005, Los Angeles, California.
- [209] C.M. López, J.T. Vaughey, and D.W. Dees, *Insights into the role of interphasial morphology on the electrochemical performance of lithium electrodes*, Journal of the Electrochemical Society, 2012. 159(6): p. A873-A886.
- [210] B.V. Ratnakumar and M.C. Smart, *Lithium plating behavior in lithium-ion cells*, ECS Transactions, 2010. 25(36): p. 241-252.
- [211] M. Lanz and P. Novák, *DEMS study of gas evolution at thick graphite electrodes for lithium-ion batteries: The effect of  $\gamma$ -butyrolactone*, Journal of Power Sources, 2001. 102(1-2): p. 277-282.
- [212] W.S. Kim and W.Y. Yoon, *Observation of dendritic growth on Li powder anode using optical cell*, Electrochimica Acta, 2004. 50(2-3 SPEC. ISS.): p. 541-545.
- [213] A.S. Andersson, B. Kalska, P. Eyob, D. Aernout, L. Häggström, and J.O. Thomas, *Lithium insertion into rhombohedral  $\text{Li}_3\text{Fe}_2(\text{PO}_4)_3$* , Solid State Ionics, 2001. 140(1-2): p. 63-70.
- [214] K.L. Gering, S.V. Sazhin, D.K. Jamison, C.J. Michelbacher, B.Y. Liaw, M. Dubarry, and M. Cugnet, *Investigation of path dependence in commercial lithium-ion cells chosen for plug-in hybrid vehicle duty cycle protocols*, Journal of Power Sources, 2011. 196(7): p. 3395-3403.
- [215] A. Eddahech, O. Briat, and J.M. Vinassa, *Lithium-ion battery performance improvement based on capacity recovery exploitation*, Electrochimica Acta, 2013. 114: p. 750-757.
- [216] W. Prochazka, G. Pregartner, and M. Cifrain, *Design-of-experiment and statistical modeling of a large scale aging experiment for two popular lithium ion cell chemistries*, Journal of the Electrochemical Society, 2013. 160(8): p. A1039-A1051.
- [217] E. Bilbao, *Energy Management Strategies Based on Dynamic Programming for Applications with Energy Storage Capacity*, Ph. D Thesis, École polytechnique fédérale de Lausanne EPFL, 2013.
- [218] <http://www.iceventure.de/blog/business-development/business-model-aspects-of-battery-leasing-and-secondary-utilization.html>. Last access date: June 2014.
- [219] T.B. Reddy, *Linden's Handbook of Batteries*. 3th edition, McGraw-Hill, 2002, ISBN 0-07-135978-8.

- [220] Battery Blog: battery news, views and education. <http://batteryblog.ca/>. Last access date: Apr. 2011.
- [221] Global and China Rechargeable Lithium Battery Industry Report 2009-2010. <http://www.researchinchina.com/> Last access date: Apr. 2011.
- [222] L. Gautier, *Umicore Specialty Oxides & Chemicals, New developments in cathode materials for Lithium-Ion Batteries*, in Materials Valley Workshop, Jan. 2006, Hanau, Germany.
- [223] P.G. Bruce, *Energy storage beyond the horizon: Rechargeable lithium batteries*, *Solid State Ionics*, 2008. 179(21–26): p. 752-760.
- [224] J. Hassoun, P. Realea, and B. Scrosati, *Recent advances in liquid and polymer lithium-ion batteries*, *Journal of Materials Chemistry*, 2007. 17: p. 3668-3677.
- [225] A. Varzi, C. Täubert, M. Wohlfahrt-Mehrens, M. Kreis, and W. Schütz, *Study of multi-walled carbon nanotubes for lithium-ion battery electrodes*, *Journal of Power Sources*, 2011. 196(6): p. 3303-3309.
- [226] D. Claus, The Minerals, Metals & Materials Society (TMS), *Materials and Processing for Lithium-ion Batteries*, <http://www.tms.org/pubs/journals/jom/0809/daniel-0809.html>.
- [227] B.A. Johnson and R.E. White, *Characterization of commercially available lithium-ion batteries*, *Journal of Power Sources*, 1998. 70(1): p. 48-54.
- [228] D. Aurbach, *Review of selected electrode–solution interactions which determine the performance of Li and Li ion batteries*, *Journal of Power Sources*, 2000. 89(2): p. 206-218.
- [229] *Harding Battery Handbook For Quest® Rechargeable Cells and Battery Packs*: <http://www.hardingenergy.com>.
- [230] *Thermo Scientific Mercury Porosimeter PASCAL 440 Series Instruction Manual*. PN 317 130 30, Revision April 2009.
- [231] ISO 15901-1. *Evaluation of pore size distribution and porosimetry of solid materials by mercury porosimetry and gas adsorption – Part 1: Mercury porosimetry*. 2005.
- [232] *Thermo Scientific Mercury Porosimeter PASCAL 140 Series Instruction Manual*. PN 317 130 26, Revision Apr. 2009.
- [233] M. Tabaddor, Underwriters Laboratories Inc. (UL), *Safety standards for lithium-ion cells*, 2011.

- [234] P. Gollob, U. Wiedemann, B. Kaltenecker, K. Denkmayr, V. Hennige, H. Hick, T. Li, R. Schneider, and F. Zieher, *Reliability & Safety of Lithium Battery Packs*, in A3PS Conference, 19.11.2010 Vienna.
- [235] H.P. Jones, J.T. Chapin, and M. Tabaddor, *Critical Review of Commercial Secondary Lithium-Ion Battery Safety Standards*, in Making Safety Matter, IAASS, European Space Agency Publications- ESA SP, 2010.
- [236] L. Lu, X. Han, J. Li, J. Hua, and M. Ouyang, *A review on the key issues for lithium-ion battery management in electric vehicles*, *Journal of Power Sources*, 2013. 226(0): p. 272-288.
- [237] H.J. Chung, T.S. Earmme, H. Kim, and M. Lee, *Over-discharge Protection in Li-ion Batteries: Part I. Approach for Overcharge Protection Method* in 210th ECS Meeting, 29 Oct.-3 Nov. 2006, Cancun, Mexico.
- [238] H.F. Li, J.K. Gao, and S.L. Zhang, *Effect of Overdischarge on Swelling and Recharge Performance of Lithium Ion Cells*, *Chinese Journal of Chemistry* 2008. 26(9): p. 1585-1588.
- [239] P. Arora, R.E. White, and M. Doyle, *Capacity Fade Mechanisms and Side Reactions in Lithium-Ion Batteries*, *Journal of Electrochemical Society*, 1998. 145(10): p. 3647-3667.



# *Appendix*

---



## APPENDIX CONTENTS

---

<b>APPENDIX A. LITHIUM-ION TECHNOLOGY: FUNDAMENTALS, CELL COMPONENTS AND CONSTRUCTION .....</b>	<b>A5</b>
A.1. CELL FUNDAMENTALS .....	A5
A.2. CELL COMPONENTS .....	A6
A.2.1. CATHODE.....	A7
A.2.1.1. COMPARISON OF CATHODES PROPERTIES .....	A13
A.2.2. ANODE.....	A15
A.2.3. ELECTROLYTE .....	A18
A.3. CELLS CONSTRUCTION .....	A20
A.3.1. CYLINDRICAL METAL CASE CELLS .....	A20
A.3.2. PRISMATIC CASE CELLS .....	A21
A.3.3. POUCH CELLS .....	A21
<b>APPENDIX B. STANDARDS AND MANUALS .....</b>	<b>A23</b>
<b>APPENDIX C. EQUIPMENT AND ANALYTICAL SPECIFICATIONS .....</b>	<b>A27</b>
<b>APPENDIX D. DATABASE OF LITHIUM-ION BATTERIES MARKET. WORLD-WIDE MANUFACTURERS AND TECHNOLOGIES.....</b>	<b>A37</b>
<b>APPENDIX E. SAFETY ANALYSIS FOR CELLS SELECTION.....</b>	<b>A49</b>
E.1. FAILURE MODES AND EFFECTS ANALYSIS (FMEA) [10] .....	A51
E.1.1. FAILURE MODES .....	A51
E.1.2. CAUSES AND EFFECTS.....	A55
E.1.2.1. CELL DESIGN .....	A55
E.1.2.2. UNCONTROLLED OPERATING CONDITIONS .....	A56
E.1.2.3. MECHANICAL FATIGUE .....	A60
E.1.2.4. SELF-DISCHARGE .....	A60
E.2. TESTS AND PATENTS .....	A60
<b>APPENDIX F. PUBLICATIONS AND PARTICIPATION IN CONFERENCES.....</b>	<b>A64</b>



## APPENDIX A. LITHIUM-ION TECHNOLOGY: FUNDAMENTALS, CELL COMPONENTS AND CONSTRUCTION

### A.1. CELL FUNDAMENTALS

Li-ion cells have lithium intercalating compounds as positive and negative materials. That is, lithium ions are exchanged between positive and negative electrodes: they are inserted or extracted from interstitial space between atomic layers within the electrochemically active materials. Figure A-1 shows an illustration of a Li-ion cell operation. The cathode material is typically a metal oxide (with a layered or tunnelled structure), on an aluminium foil current collector. The anode material is normally a graphitic carbon (with layered structure) on a copper current collector. The electrodes are electrically isolated by a microporous separator film in cells that employ liquid or gel-polymer electrolyte [219]. Separators are electrical insulators that allow the diffusion of lithium ions while the cell is charging or discharging.

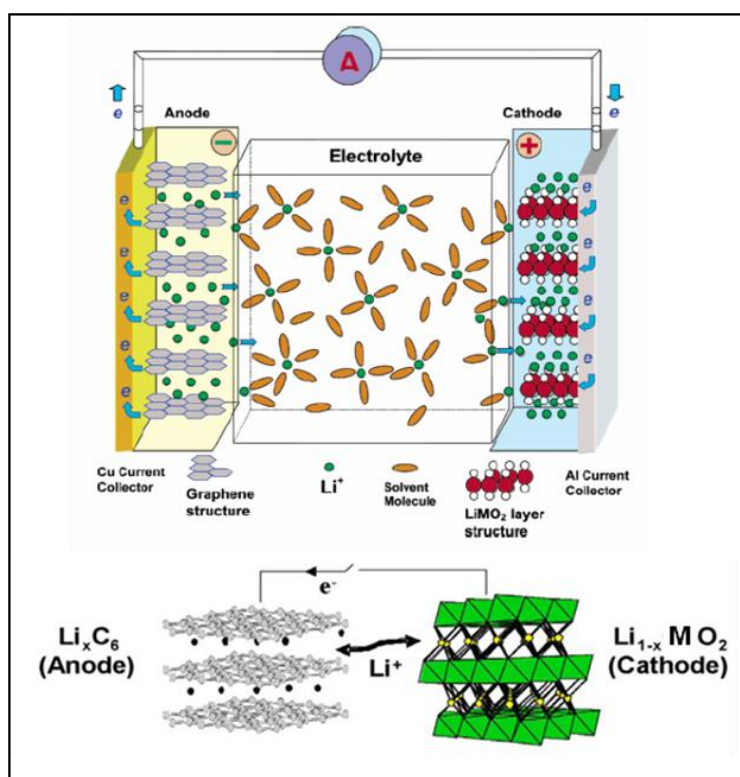


**Figure A-1.** Schematic illustration of a  $\text{Li}_x\text{C}_6/\text{Li}_{1-x}\text{MO}_2$  lithium-ion cell. During discharge,  $\text{Li}^+$  ions migrate through the electrolyte and electrons flow through the external circuit, both moving from the anode to the cathode [18]

When a Li-ion cell is charged, the positive material (cathode) is oxidised and the negative material (anode) is reduced. Electrode and redox reactions in a Li-ion cell that combines a metal oxide ( $\text{Li}_{1-x}\text{MO}_2$ ) cathode and graphite or carbon anode are the following:



Most common cathode materials are synthesised at discharged state (*i.e.* fully lithiated) and they are the only source of lithium within the cell upon construction. After construction the first charge is called the formation charge, where the cathode is slowly delithiated to form the Solid Electrolyte Interface (SEI) layer against the typically carbon anode. The SEI layer is formed from components in the electrolyte and lithium from the cathode. Additional lithium ions are also irreversibly lost into the carbon anode itself, for a total irreversible first charge capacity loss of 20% or more [220].

## A.2. CELL COMPONENTS

Figure A-2 shows different configurations of Li-ion batteries according to their components.

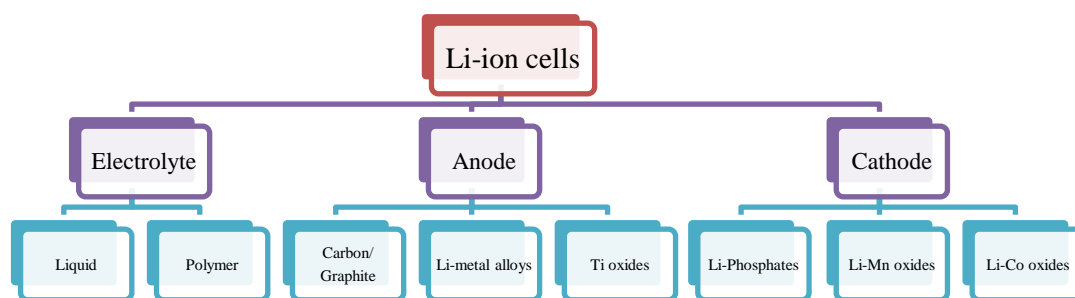


**Figure A-2.** Different components of main Li-ion batteries

Regarding the current collector materials, the most common are: copper for the anode and aluminium for the cathode. In addition, other metals, such as nickel and stainless steel, have been also tested.

All size, shape and materials used in the construction of a cell affect its ultimate performance:

- Cell voltage is controlled by the cell chemistry.
- Capacity is governed by the weight of the active chemicals.

- Power is controlled by the area and morphology (*e.g.* grain sizes and distribution) of the electrodes.
- Internal impedance of the cell depends on the conductivity of the electrolyte as well as the layout and resistance of the components in the current path.

### A.2.1. CATHODE

The energy of the battery is limited by the specific capacity of the electrodes, and the cathode in particular (it is the lithium battery component that most limits the performance) [23]. Thus cathode materials research is one of the most challenging aspects of Li-ion battery development today, holding the majority of the potential for improvement in terms of cell energy density, electrical performance, safety and cost.

Requirements that Li-ion positive electrode materials must satisfy are [219]:

- High free energy of reaction with lithium.
- Ability to incorporate large quantities of lithium in order to enable high current capability.

The needed highly electronegative cathode material makes it to contain high level of oxygen bonded in various structures with: (i) metal atoms, such as cobalt, nickel, vanadium, chromium, aluminium, titanium or manganese; or (ii) in the form of a metal phosphate, such as iron phosphate. The large amount of oxygen atoms makes Li-ion cell hazardous and risky of fire or explosion [220].

Another strong oxidising agent is sulphur, which can be used in high energy density lithium-sulphur systems. These are currently being developed by a few American companies such as Sion Power, Polyplus and Oxis Energy. The main drawback of a sulphur based cathode is that some of the intermediary  $\text{LiS}_x$  compounds are solvent in the electrolyte, causing the cathode and electrolyte to deteriorate [220].

- Reversible exchange of lithium without volume change, so that long life and high efficiency are possible.
- High lithium ions diffusivity.
- Good electronic conductivity, so that the process of charge and discharge (electrons are removed or returned to the cathode) can occur at high rate.
- Insoluble in the electrolyte.
- Prepared from inexpensive reagents.
- Low cost synthesis.
- Compatibility with the other materials in the cell.

These factors guide the selection and development of positive electrode materials.

Depending on the cathode material, Li-ion family is divided into three major battery types: lithium-ion-cobalt ( $\text{LiCoO}_2$ , LCO), lithium-ion-manganese ( $\text{LiMn}_2\text{O}_4$ , LMO) and lithium-ion-phosphate ( $\text{LiFePO}_4$ , LFP). Other oxides, such as lithium-ion-nickel-cobalt ( $\text{LiNi}_x\text{Co}_{1-x}\text{O}_2$ , LNCO), lithium-ion-nickel-manganese ( $\text{LiNi}_x\text{Mn}_y\text{O}_4$ , NMO) and lithium-ion-nickel-cobalt-manganese ( $\text{LiNi}_x\text{Co}_y\text{Mn}_z\text{O}_2$ , NCM) are also used. The voltage and capacity characteristics of most common cathode materials are summarised in Table A-1.

**Table A-1.** Characteristics of cathode materials [18, 219]

MATERIAL	Specific capacity [mAh/g]	V vs. Li (at 0.05C)	Advantages or Disadvantages
$\text{LiCoO}_2$	140-155	3.88	Most common commercially (Co is expensive)
$\text{LiMn}_2\text{O}_4$	100-120	4.00	Mn is inexpensive, low toxicity, least exothermic decomposition
$\text{LiFePO}_4$	150	3.3	Long life, good safety, higher self-discharge

The materials of main interest for battery manufacturers are manganese-based compounds (LMO or NMO) and olivine lithium metal phosphates (LFP) [17]. Cell manufacturers from USA and China (A123 and BYD are the leaders, respectively) are strategically investing in LFP because of its safe performance. Japan is, however, focusing on manganese cathodes, LMO, which are widely manufactured and are therefore more robust and cheaper.

Japan and Europe are currently the leading manufacturers of cathodes: Umicore and Nichoia have 50% of the market altogether (30% and 20%, respectively). Other important producers are Toda Kogyo, SEIMI and SEIDO. The main suppliers in China are Beijing Easpreing Shanshan Co. and Holding Company. Figure A-3 shows the different cathodes used by various Chinese companies, which cathode production capacity is between 35000-40000 tonnes/year [221].

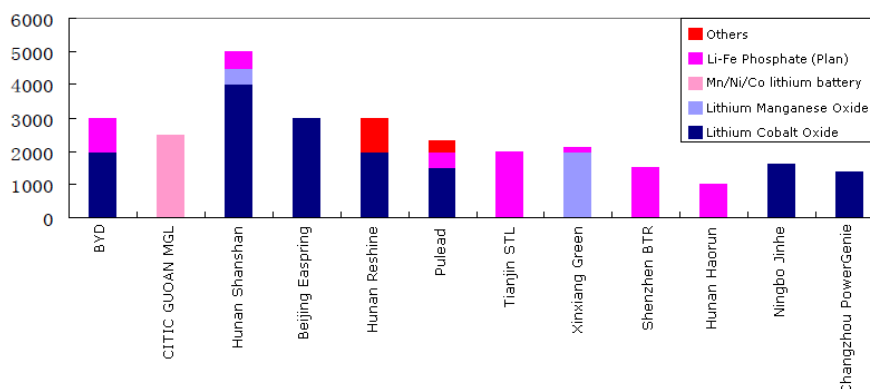


**Figure A-3.** Cathode materials output capacity of Chinese manufacturers [221]

- **LiCoO<sub>2</sub> (LCO)**

Lithium Cobalt Oxide has been the most widely used cathode material in Li-ion batteries, typically for use in laptops and mobile phones, for many years. It was successfully commercialised for the first time by Sony in 1990.

LiCoO<sub>2</sub> offers the best compromise of the following requirements [222]:

- Good electrochemical voltage
- Good capacity retention
- High energy density, 400 Wh/L
- Highest electronic conductivity
- Excellent shelf life
- Safety issues manageable
- Industrial availability
- 10 years of safe usage

Its main disadvantages are:

- Restricted capacity, equivalent to only 0.5 Li/Co (130 mAh/g) [223], due to structural problems.
- Expensive
- Toxicity of Co
- Safety problems if used in large cells [223].
- Low tolerance for high discharge current due to overheating of the cell. This forces to limit charge and discharge rates to 1C.
- Low tolerance to charge and discharge cycles due to increasing internal resistance.

To sum up, LCO has excellent specific energy but offers moderate specific power, safety and life span. Consequently, cathodes with better safety as well as higher lifetime are important criteria for future markets.

- **LiMn<sub>2</sub>O<sub>4</sub> (LMO)**

Manganese is much cheaper than cobalt and the superior safety of manganese oxides compared with cobalt oxides renders manganese compounds attractive for use as cathodes in rechargeable lithium batteries [223]. LiMn<sub>2</sub>O<sub>4</sub> cathode was firstly designed in 1983, but it was not used in commercial batteries until 1996.

Lithium manganese oxide spinel provides a higher cell voltage than cobalt-based chemistries due to its three-dimensional spinel structure, which enables higher rate of ion exchange between electrodes. Moreover, the internal resistance of the battery is reduced and higher discharge rates are therefore possible.

The main disadvantages of this cathode are [224]:

- Its energy density is about 20% lower than of LCO [23].
- Reduced shelf due to poor thermal stability of LMO-based LIB. Capacity fading occur through a combination of various processes at elevated temperature:

- o dissolution of  $Mn^{+}$

Partial dissolution of manganese in the electrolyte may occur during charge and discharge cycles. Some strategies to overcome this problem are: replacing the electrolyte salts, partial substitutions of Mn by other elements in the cathode or surface modification of the LMO cathode.

- o irreversible phase and structure transition (*i.e.* Jahn-Teller distortion at the discharged state, transformation of an unstable two-phase structure in the high voltage region to a more stable single-phase structure through loss of MnO)
- o material loss of the loaded spinel.
- o polarisation loss due to cell resistance increase (*i.e.* high contact resistance at the spinel/carbon interface caused by Mn dissolution).

- **LiFePO<sub>4</sub> (LFP)**

Main advantages of phosphate-based technology are [23]:

- High specific capacity (170 mAh/g)
- Superior thermal and chemical stability, which provides better safety characteristics than those of other Li-ion technologies.
- They are incombustible, as they do not release oxygen (P-O bond is very strong).
- They are more stable under overcharge or short circuit conditions.
- They can withstand high temperatures without decomposing. Therefore, they are much less susceptible to thermal runaway.
- They offer a longer cycle life (1000-2500 cycles).

Moreover, cost, safety and toxicity have been significantly improved over LCO cells.

Main disadvantage of olivine LFP is that it has lower energy density than cobalt because the operating voltage is low: 3.5V vs. Li [23]. Nevertheless, they can support higher currents and thus greater power. On the other hand, LFP presents large intrinsic internal resistance, which requires special preparation for its minimisation: the most common solution is a carbon coating process so as to increase the conductivity, together with the reduction of particles size.

To sum up, the attributes of LFP are: excellent safety and long life span, but moderate specific energy and elevated self-discharge [18]. It is working on getting better performance derivative cathodes, like  $\text{LiMnPO}_4$  or  $\text{LiCoPO}_4$ .

- **Other oxides:  $\text{LiNi}_x\text{Mn}_y\text{O}_4$  (NMO),  $\text{LiNi}_x\text{Co}_y\text{Mn}_z\text{O}_2$  (NCM) or  $\text{LiNiCoAlO}_2$  (NCA)**

The development of materials with manganese partial substitution in LMO has led to two main ternary systems:  $\text{LiNi}_{0.5}\text{Mn}_{1.5}\text{O}_4$  and  $\text{LiNi}_{0.3}\text{Co}_{0.3}\text{Mn}_{0.3}\text{O}_2$ . Another used oxide is  $\text{LiNiCoAlO}_2$ .

$\text{LiNi}_{0.5}\text{Mn}_{1.5}\text{O}_4$  has spinel structure, like LMO, and reaches values of specific power in the same range as LCO: 146 mW/g. Its operating voltage is high, around 4.5 V vs. Li, so it is an interesting material to achieve higher energy density values, which currently is 30% higher than that of LMO. Nonetheless, it has to be highlighted that, even though a priori a greater potential may seem an advantage, it can sometimes destabilise the electrolyte because the organic carbonate present in it is not fully compatible with high voltages.

The other manganese cathode,  $\text{LiNi}_{0.3}\text{Co}_{0.3}\text{Mn}_{0.3}\text{O}_2$ , is of laminar structure and has specific power of 160-170 mW/g [224]. The main characteristics of NCM are good overall performance and excellent specific energy. It is the preferred candidate for electric vehicles [18]. Table A-2 shows different nickel, cobalt and manganese combinations of NCM cathode (NCM-xyz), with the corresponding masses proportions.

The Lithium Nickel Cobalt Aluminium Oxide cathode, NCA, shows high specific energy and specific power, as well as a long life span, which makes it to be widely used in the automotive industry. Less flattering are safety and cost.

**Table A-2.** Different NCM combinations of  $\text{LiNi}_x\text{Mn}_y\text{Co}_{1-x-y}\text{O}_2$  cathode. Theoretical calculations of Ni, Mn and Co metallic constituents proportions and ratios

$\text{LiNi}_x\text{Mn}_y\text{Co}_{1-x-y}\text{O}_2$				
	Atom	Molar mass [g/mol]		
Li(NMC)O <sub>2</sub>	1	Li	6.94	
		Ni	58.69	
	1	Mn	54.94	
	2	O	58.93	16

	Atom	Subtotal mass [g/mol]	Subtotal mass [%]	NMC [%]	
NMC-111	1	Li	6.94	7.19	
	0.33	Ni	19.56	20.28	34.01
	0.33	Mn	18.31	18.99	31.84
	0.33	Co	19.64	20.36	34.15
	2	O	32	33.17	
	TOTAL	96.46	100.00		

	Atom	Subtotal mass [g/mol]	Subtotal mass [%]	NMC [%]	
NMC-433	1	Li	6.94	7.19	
	0.40	Ni	23.48	24.31	40.73
	0.30	Mn	16.48	17.07	28.60
	0.30	Co	17.68	18.31	30.67
	2	O	32	33.13	
	TOTAL	96.58	100.00		

	Atom	Subtotal mass [g/mol]	Subtotal mass [%]	NMC [%]	
NMC-622	1	Li	6.94	7.16	
	0.60	Ni	35.21	36.33	60.73
	0.20	Mn	10.99	11.34	18.95
	0.20	Co	11.79	12.16	20.32
	2	O	32	33.01	
	TOTAL	96.93	100.00		

	Atom	Subtotal mass [g/mol]	Subtotal mass [%]	NMC [%]	
NMC-451	1	Li	6.94	7.25	
	0.40	Ni	23.48	24.51	41.30
	0.50	Mn	27.47	28.68	48.33
	0.10	Co	5.89	6.15	10.37
	2	O	32	33.41	
	TOTAL	95.78	100.00		

	Atom	Subtotal mass [g/mol]	Subtotal mass [%]	NMC [%]	
NMC-541	1	Li	6.94	7.22	
	0.50	Ni	29.35	30.52	51.29
	0.40	Mn	21.98	22.86	38.41
	0.10	Co	5.89	6.13	10.30
	2	O	32	33.28	
	TOTAL	96.15	100.00		

	Atom	Subtotal mass [g/mol]	Subtotal mass [%]	NMC [%]	
NMC-811	1	Li	6.94	7.13	
	0.80	Ni	46.95	48.27	80.48
	0.10	Mn	5.49	5.65	9.42
	0.10	Co	5.89	6.06	10.10
	2	O	32	32.90	
	TOTAL	97.28	100.00		

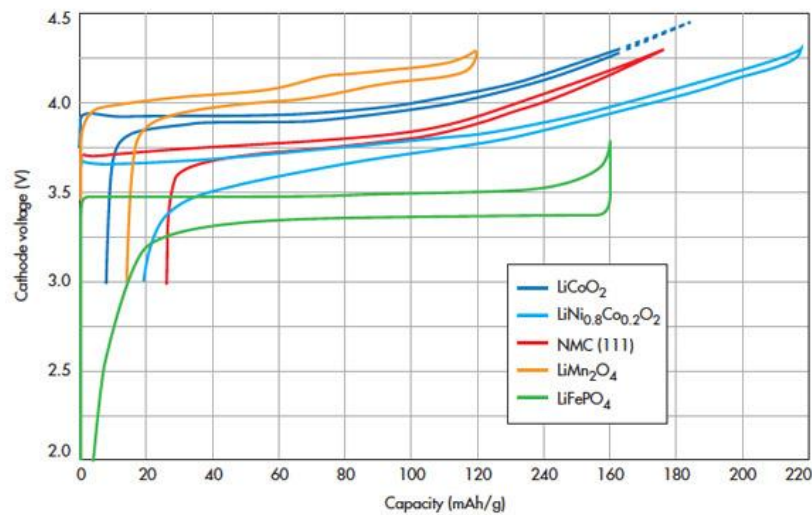
	Atom	Subtotal mass [g/mol]	Subtotal mass [%]	NMC [%]	
NMC-442	1	Li	6.94	7.22	
	0.40	Ni	23.48	24.41	41.01
	0.40	Mn	21.98	22.85	38.39
	0.20	Co	11.79	12.25	20.59
	2	O	32	33.27	
	TOTAL	96.18	100.00		

	Atom	Subtotal mass [g/mol]	Subtotal mass [%]	NMC [%]	
NMC-532	1	Li	6.94	7.19	
	0.50	Ni	29.35	30.39	50.93
	0.30	Mn	16.48	17.07	28.61
	0.20	Co	11.79	12.21	20.46
	2	O	32	33.14	
	TOTAL	96.55	100.00		

	Atom	Subtotal mass [g/mol]	Subtotal mass [%]	NMC [%]	
NMC-992	1	Li	6.94	7.23	
	0.45	Ni	26.41	27.52	46.31
	0.45	Mn	24.72	25.76	43.35
	0.10	Co	5.89	6.14	10.33
	2	O	32	33.34	
	TOTAL	95.97	100.00		

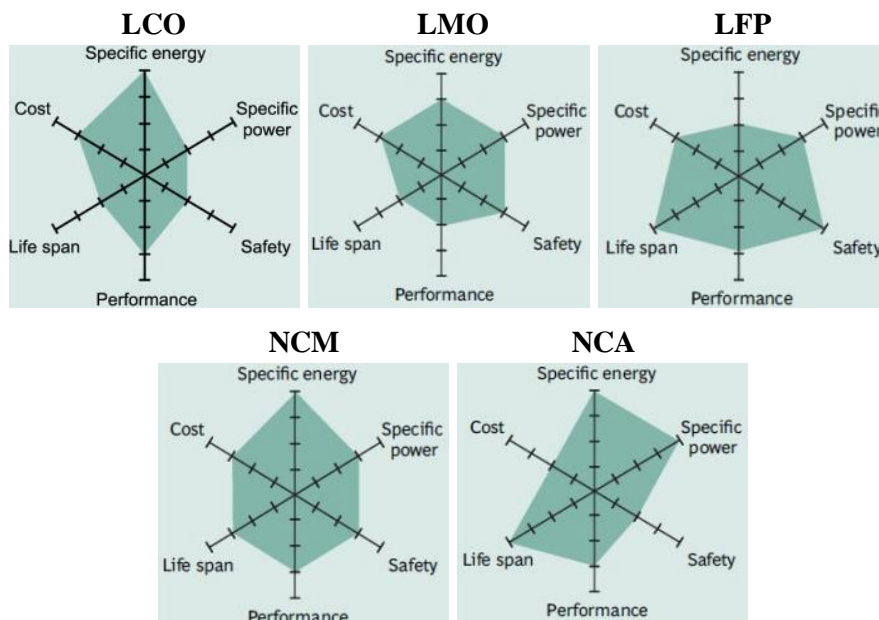
### A.2.1.1. COMPARISON OF CATHODES PROPERTIES

Figure A-4 shows intrinsic properties of main cathode materials. The voltage profiles against specific capacity only correspond to cathode material (tests carried out against lithium). LMO cathode will provide the largest instant power as it shows the largest nominal voltage. Specific capacity discharge from LNCO ( $\text{LiNiCoO}_2$ ) will be the largest, but the energy density of LCO will be larger. NCM in turn shows in between characteristics and it is a safer material.



**Figure A-4.** Voltage and specific capacity of different cathode materials

(Source: <http://electronicdesign.com/power/understanding-factors-lithium-battery-equation>)



**Figure A-5.** Trade-offs among the five principal cathode Li-ion battery technologies (Note: the farther the coloured shape extends along a given axis, the better the performance along that dimension) [18, 19]

Figure A-5 shows trade-offs among the five principal cathode Li-ion battery technologies. This comparison includes cost, safety and lifetime issues. The thermal stability is analysed in Figure A-6. It shows the energy released in the decomposition of different cathodes as a function of temperature. LFP is observed to be the cathode with the lowest energy release besides the temperature being above 300°C. Therefore, it is more stable than other cathodes.

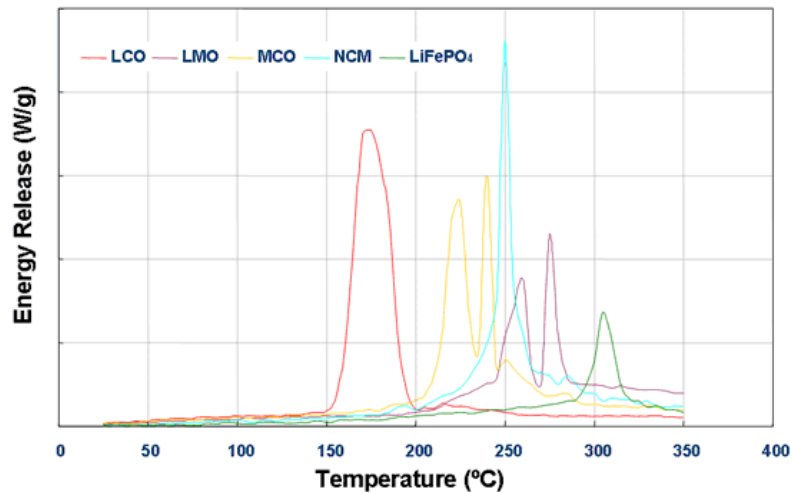


Figure A-6. Energy released in the decomposition of the different cathodes. Thermal stability [22]

Finally, Table A-3 and Figure A-7 show a more detailed comparison between the most common cathodes. The decision of the cathode to be used is a compromise between different properties and the importance range depends on application requirements.

Table A-3. Comparison of properties of the main cathodes [18, 23]

Cathodes	Cell level Specific Energy [Wh/Kg]	Cell level Energy Density [Wh/l]	Cycle Life (100% DOD) [No. cycles]	Price (estimate) [\$/Wh]	Safety Thermal Runaway Onset [°C]	Nominal Voltage [V]
LCO	150-190	450-490	500-1000	0.31-0.46	150	3.6
LFP	80-125	130-300	1000-2000	0.3-1.2	270	3.3
LMO	90-135	280	≥1000	0.45-0.55	250	3.8

NOTE: range of values correspond to different applications

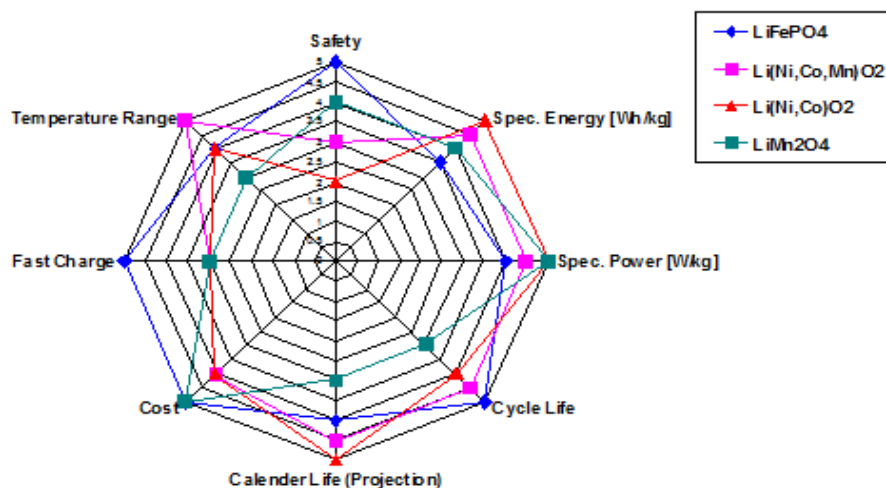


**Figure A-7.** Comparison of properties of different materials for cathodes  
(Source: <http://www.gaia-akku.com/en/technology/lfpnca.html>)

### A.2.2. ANODE

Secondary lithium battery development effort throughout the 1970s and 1980s focused on the use lithium metal as the negative electrode because of high specific capacity of the metal [219]. Nevertheless, safety issues caused the industry to concentrate on lithium intercalation into carbon at the negative electrode instead of using lithium metal. Safety properties of negative electrodes are correlated to their surface area. While the properties of lithium metal anodes change with use, carbon electrodes offer stable morphology [219].

The first Li-ion batteries in the market (Sony) had petroleum coke at the negative electrode. In the mid-1990s, most Li-ion cells utilised electrodes employing graphitic spheres, in particular a Mesocarbon Microbead (MCMB) carbon. Recently, a wider variety of carbon types has been used: natural graphite and hard carbon are the most common [219].

Even though carbon, usually graphite, remains as dominant anode material in commercial cells, Sony introduced Nexelion™ battery, a new generation of rechargeable lithium batteries [223]. Its anode is a nanostructure Sn-Co-C alloy, which increases by 30% the cell capacity compared to graphite. At present, nanoparticulate or nanostructure alloys are under investigation because they can better accommodate the volume changes on cycling without fracturing [223].

Lithium-silicon (Li-Si) and lithium-tin (Li-Sn) alloys are among the most promising anodes. Research for new anode materials is also addressed to titanium oxides: anatase titanium oxide, TiO<sub>2</sub> (TO), and lithium titanium oxide, Li<sub>4</sub>Ti<sub>5</sub>O<sub>12</sub> (LTO), are attractive for advanced Li-ion batteries [17].

- **Carbon anode**

The theoretical specific capacity of carbon ( $\text{LiC}_6$ ) is  $372 \text{ mAh}\cdot\text{g}^{-1}$  [219]. Hard carbon materials offer higher capacity, over  $1000 \text{ mAh}\cdot\text{g}^{-1}$ , but they have not achieved broad acceptance because they have greater irreversible capacity, are highly disorganised, and have higher voltage, ( $\sim 1\text{V}$  vs. Li) than graphitic materials [219]. Graphite shows five different plateaus on the potential profile that correspond to the coexistence of lithiated graphite at different stages [43]. Figure A-8 shows the potential of graphite against lithium during discharge.

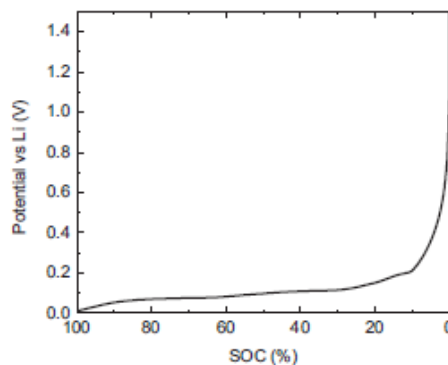


**Figure A-8.** C/20 discharge curves for graphitic carbon when measured against metallic lithium [67]

New graphite structures, such as nonotubes, are being developed to improve this material features. This way, potential use of multi-walled carbon nanotubes (MWCNTs), as conductive agents for electrodes in Li-ion batteries, is being under investigation. It has been demonstrated that, even in low amounts, it enables an increase in both energy and power densities of Li-ion battery [225].

Modifications of graphite by covering the surface with thin metal layers have been also performed. This treatment enhances the conductivity, so it may lead to improved electrode performance, especially in low temperatures [17].

- **Lithium-metal alloys**

Lithium-metal alloys have a specific capacity which largely exceeds that of lithium-graphite: about  $4000 \text{ mAh}\cdot\text{g}^{-1}$  for Li-Si and  $990 \text{ mAh}\cdot\text{g}^{-1}$  for Li-Sn, whereas it is  $370 \text{ mAh}\cdot\text{g}^{-1}$  for Li-C [17]. However, they do not have good cycling performance.

Nanostructure configurations, capable of assuring long cycle life combined with high specific capacity, have been developed. Electrode structures based on metal carbon nanocomposites, e.g. tin-carbon, have shown high chemical stability. Figure A-9 demonstrates high

electrochemical stability of Sn-C nanocomposite electrode, which undergoes deep discharge/charge cycles with no capacity fading for over two hundred cycles [17].

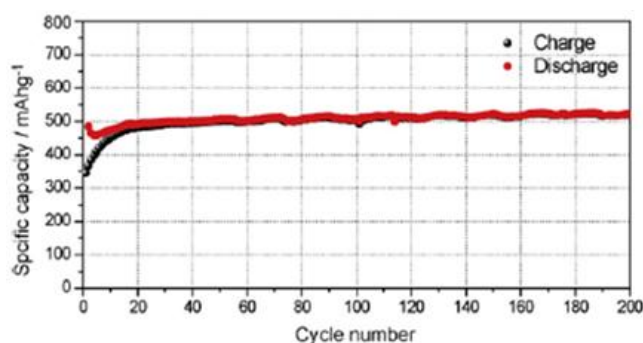


**Figure A-9.** Capacity delivery versus charge-discharge cycles of a Sn-C composite electrode [17]

Similar approaches have been adopted to promote the performance of Li-Si anodes. Long cycle lives can be achieved for instance by Si-C composites, nanowires morphologies or porous particles [17]. Thus, it has been possible the commercialisation of lithium metal anodes, as it is the case of Sn-Co-C anode battery.

- **Titanium oxides: titanium oxide (TO) and lithium titanium oxide (LTO)**

The lithium insertion potential of  $\text{TiO}_2$  (TO) and  $\text{Li}_4\text{Ti}_5\text{O}_{12}$  (LTO) is 1.2-2.0 V vs. Li, which is within the stability window of common organic electrolytes.

The capacity of spinel-framework LTO is  $170 \text{ mAh}\cdot\text{g}^{-1}$  and voltage level is 1.5 V vs. Li. Its highlighted advantages are [17]:

- Very low volume change (<1%) during cycling. Cycling stability.
- No electrolyte decomposition. No SEI formation.
- High rate charge/discharge capability at very low temperature.
- High thermal stability.

Enterprising manufacturers are considering the development of batteries using LTO anode. LFP/LTO combination maintaining the standard liquid electrolyte with  $\text{LiPF}_6$ -carbonate solvent would be the best option from safety, cycling capability and high power performance point of view. However, its voltage level would be lower than conventional systems (2 V). Figure A-10 shows different cathode and LTO combinations voltage profiles. LMO and  $\text{LiNi}_{0.5}\text{Mn}_{1.5}\text{O}_4$  are two possible candidates for higher voltage electrode combinations [17]. LMO/LTO batteries are widely used for PHEVs batteries at present (Altamiro and Ener1 (Enerdel/Enertch) batteries. See Appendix D).

The maximum theoretical capacity of TO with brookite structure is  $335 \text{ mAh}\cdot\text{g}^{-1}$ . It offers important advantages in terms of cost effectiveness, safety and environmental compatibility. Its performance depends on the morphology of particles (nanoforms are under investigation). Effective electronic conductive networks to increase mass utilisation and electrode kinetics are also being developed [17].

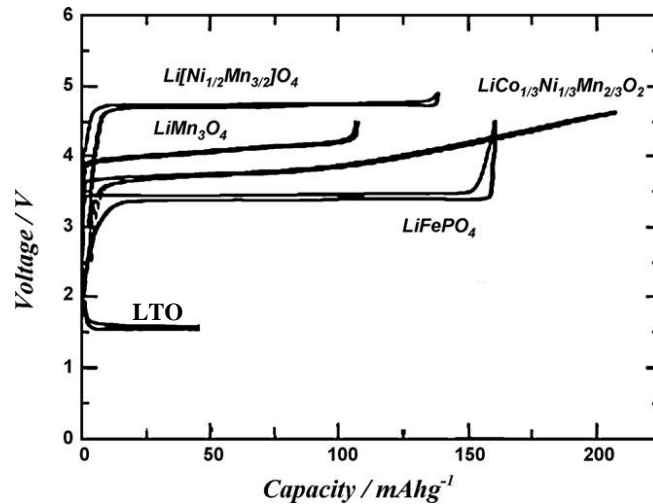


**Figure A-10.** Voltage charge-discharge profiles of a LTO anode and of various cathode materials [17]

### A.2.3. ELECTROLYTE

A safe and long-lasting battery needs a robust electrolyte that can withstand existing voltage and high temperatures, and that has a long shelf life, while offering a high mobility for lithium ions [226]. Four types of electrolytes have been used in Li-ion batteries: ceramic, liquid, polymer and gel electrolytes.

*Ceramic or solid electrolytes* are inorganic conductive crystals and ceramic glasses. They show very poor low-temperature performance because the lithium mobility in the solid is greatly reduced. In addition, they need special deposition conditions and temperature treatments to obtain acceptable behaviour, making them extremely expensive in use [226]. However, their inherent advantages are important: no need for separators, safety (no leakage and reduced flammability, with no risk of thermal runaway as consequence) and all-solid-state construction [227].

*Liquid electrolytes* are solutions of a lithium salt in organic solvents, typically carbonates [219]. The most important considerations are their flammability, which could cause explosion of the cell [224], and that they are almost completely absorbed into the electrode and separator materials [219] (lithium dissolution out of the anode). Moreover, “thermal runaway” may

happen as a consequence of electrolyte decomposition. Hence, the selection of an electrolyte often involves a trade-off between flammability (the best performing solvents have low boiling points and have flash points around 30°C) and electrochemical performance [224]. Typically used liquid organic electrolyte is a solution of lithium hexafluorophosphate (salt) in an ethylene carbonate dimethyl carbonate mixture (solvents), LiPF<sub>6</sub>-EC:DMC [224].

*Polymer electrolyte* is a liquid- and solvent-free material, where an ionic conducting phase is formed by dissolving a salt in a high molecular weight polymer [219]. They are often mixed in composites with ceramic nanoparticles, resulting in higher conductivities and resistance to higher voltages [226]. The most advanced ones are based on ethylene oxide solvents with lithium salts, such as LiCF<sub>3</sub>SO<sub>3</sub>. Potential advantages of polymer electrolytes are safety properties resulting from their low volatility and high viscosity: they could inhibit the growing of lithium dendrites. Consequently, it is possible their use with lithium metal anodes. The main drawback is their low conductivity due to the high ionic resistance below 70°C. This problem has been overcome by the new development of Bellcore Battery Technology (Valence): hybrid solid-liquid electrolytes, that is, gel electrolytes.

*Gel electrolytes* (PGEs) are typically ionic conductive films of PVDF-HFP, LiPF<sub>6</sub> or LiBF<sub>4</sub> salt, and carbonate solvent. That is, they are membranes formed by trapping a liquid solution in a polymer matrix [224]. The advantages of gel electrolytes are that there is no leakage risk because liquid phase is absorbed within the polymer [219] and that the conductivity is of the same order of magnitude of that of the liquid component [224].

Most Li-ion electrolytes use LiPF<sub>6</sub> as salt, since its solutions offer high ionic conductivity, >10<sup>-3</sup> S/cm, and acceptable safety properties. LiBF<sub>4</sub> is another salt that have attracted industrial interest. Salts commonly used in Li-ion cells are listed in Table A-4. Most common carbonate solvents are: ethylene carbonate (EC), dimethyl carbonate (DMC), ethyl methyl carbonate (EMC) and diethyl carbonate (DEC). And some additives are: alkyl pyrocarbonates, byphenil, sulfites, hexamethyldisilazane (HMDS), boron trifluoride (BF<sub>3</sub>) and related complexes, etc.

**Table A-4.** Salts used in electrolytes for Li-ion cells [219]

SALT	Comments
Lithium hexafluorophosphate, LiPF <sub>6</sub>	Most commonly used
Lithium tetrafluoroborate, LiBF <sub>4</sub>	Less hygroscopic than LiPF <sub>6</sub>
Lithium perchlorate, LiClO <sub>4</sub>	When dry, less stable than alternatives
Lithium hexafluoroarsenate, LiAsF <sub>6</sub>	Contains arsenic
Lithium triflate, LiSO <sub>3</sub> CF <sub>3</sub>	Al corrosion above 2.8V, stable to water
Lithium bisperfluoroethane-sulfonimide (BETI), LiN(SO <sub>2</sub> C <sub>2</sub> F <sub>5</sub> ) <sub>2</sub>	No Al corrosion below 4.4V, stable to water

Liquid electrolytes retain their importance in rechargeable Li-ion batteries because of their high conductivity [227]. Combination of graphite and unstable liquid electrolyte keeps safety risks for the overall battery: relatively narrow stability domain (thus high voltage cathodes cannot be used), high vapour pressure and flammability, and manipulation hazards due to incompatibility with both environment and human health [17]. No practical solvents are thermodynamically stable with lithium or  $\text{Li}_x\text{C}_6$  near 0 V vs. Li, and electrolyte domain extends from about 0.8 V vs. Li to 4.5 V vs. Li [17] (see Figure 1-6). However, many solvents undergo a limited reaction to form a passivation film, but ionic conductive, on the electrode surface: Solid Electrolyte Surface (SEI) [219]. It consists of reduction products of the electrolyte with either lithium or a lithiated specie such as  $\text{Li}_x\text{C}_6$ : lithium salts like LiF and  $\text{Li}_2\text{CO}_3$ , lithium alkoxides,  $\text{Li}_2\text{O}$ , LiOH, lithium alkyl carbonates, etc. [228] The SEI layer is composed of mainly two layers: the inner layer close to the electrode is more densified and comprises of lithium salts, while the outer layer is polymorphous and is comprised of lithium polymers, such as  $\text{Li}_2(\text{OCO}_2(\text{CH}_2)_2\text{OCO}_2)_2$  and  $(\text{CH}_2\text{OCO}_2\text{Li})_2$ .

PGEs appear particularly suitable in advance Li-ion batteries although safety is still a major issue (the solvent used in electrolyte must be stable at both anodic and cathodic potentials).  $\text{LiPF}_6$ -PC-EC-PVdF membrane is a very convenient electrolyte because it maintains high conductivity values over a temperature range exceeding from -10 to 80°C and has a wide electrochemical stability (0-5 V vs. Li) [224].

### A.3. CELLS CONSTRUCTION

#### A.3.1. CYLINDRICAL CELLS

Cylindrical cells are manufactured by spirally winding two electrodes, with a separator between them, into a bundle. This bundle is inserted into a metallic can, which is normally a nickel-plated steel can [229]. This cell construction is also called jelly-roll or swiss-roll.

The cylindrical cells are robust. The cylinder has the ability to withstand high internal pressures and usually have an overcharge protection (they are equipped with a venting mechanism to release pressure under extreme conditions) [18]. They have high power density: spiral construction of the electrodes maximises their surface area, which increases the cell current handling capability and reduces the internal impedance. Thus, the cell can deliver more power. Moreover, heat generation is reduced and charge/discharge rates are faster. The downside is that, since there is less room for the electrolyte within the can, the potential energy storage capacity of the cell is reduced.

The main disadvantages are that the cell size is bulky and packs use space inefficiently although the cavities created between cells allow air cooling.

Small cylindrical cells are easy to manufacture, so they are made in very high volumes and the price is low for standard shapes (high capacity cells are expensive). Typical applications are wireless communication, mobile computing, biomedical instruments, power tools and applications that do not demand ultra-small size [18]. The cell sizes are fixed and they are available with capacities up to 200 Ah [22].

### **A.3.2. PRISMATIC CELLS**

Prismatic cells are manufactured with spirally wounded rectangular electrodes, typically, or also with stacked electrodes in layers. The case can be metallic (nickel-plated steel, stainless steel or aluminium alloy) or plastic.

Prismatic cells can be packaged more efficiently than cylindrical ones and, therefore, the packaging density is higher (good space utilisation). Their energy density is also high, but slightly lower than that for cylindrical cells. They do not always have venting system, so heavier metallic can is used in order to prevent swelling due to pressure build up [18]. Thus, they are strong, robust and enable good heat dissipation.

The main disadvantage of these cells is their price (expensive systems). No standard cell size exists: they come in various sizes with capacities from 400 mAh to 200 Ah [18]. They are custom-made for cell phones and other high volume items.

### **A.3.3. POUCH CELLS**

The pouch cells, also known as LiPo cells, are typically used for solid electrolytes (polymer). Electrodes and electrolyte are stacked in layers or laminations and enclosed in a foil envelope. The electrical contacts consist of conductive foil tabs that are welded to the electrode and sealed to the pouch material [18].

The solid electrolyte makes cells safer and leak-proof. The foil construction makes possible very thin and light weight cells, with flexible construction. They make the most efficient use of available space and a packaging efficiency of 90-95% is achieved. Consequently, the pouch pack has lower weight and higher energy density.

They have good heat dissipation (large surface area). Nonetheless, they are hardly mechanically stable because of the lack of rigidity of the casing, which makes the cells to be prone to swelling as temperature rises. Swelling can be also a result of gas generation during charge and discharge. The pressure from swelling can crack a battery cover and even break the display or electronic circuit in some cases [229]. Therefore, the cells need some alternative support in the battery compartment to be protected from mechanical stress, which reduce the energy density. It is better not to stack pouch cells, but lay them side-by-side [18].

Manufactures can produce cells of different dimensions and forms for high power applications economically in high volumes (no standardised pouch cells exist). They are produced in sizes up to 240 Ah.

## APPENDIX B. STANDARDS AND MANUALS

---

Summary of Li-ion cells standards and manuals is shown in Table A-5 and Table A-6, respectively. Table A-7 gathers Li-ion cells Spanish standards that AENOR validated and CENELEC approved.

A number of battery safety standards and testing protocols, which are summarised in Table A-8, were developed to provide manufacturers with guidance on how to construct and use Li-ion batteries more safely. They incorporate a number of safety tests (in grey) designed to assess the ability of a battery to withstand certain abuse conditions. UL and ANL are considering translating battery safety research (such as UL1642) into ISC test methodologies for safety standards.

Table A-5. Summary and titles of all lithium-ion cells standards covered

<b>CERTIFICATION ORGANISATION</b>	<b>STANDARD NUMBER</b>	<b>TITLE</b>
International Organisation for Standardisation (ISO)	<b>ISO 12405-1: 2011</b>	Electrically propelled road vehicles -Test specification for lithium-ion traction battery packs and systems- Part 1: High-power applications
	<b>ISO 12405-2: 2012</b>	Electrically propelled road vehicles -Test specification for lithium-ion traction battery systems- Part 2: High-energy applications
	<b>ISO 12405-3: 2014</b>	Electrically propelled road vehicles -Test specification for lithium-ion traction battery packs and systems- Part 3: Safety performance requirements.
	<b>ISO 6469-1: 2009</b>	Electrically propelled road vehicles -- Safety specifications -- Part 1: On-board rechargeable energy storage system (RESS)
	<b>ISO 6469-2: 2001</b>	Electric road vehicles -- Safety specifications -- Part 2: Functional safety means and protection against failures
	<b>ISO 6469-3: 2011</b>	Electrically propelled road vehicles -- Safety specifications -- Part 3: Protection of persons against electric shock
International Electrotechnical Commission (IEC) European Norms (EN)	<b>IEC 62660-1: 2010 EN 62660-1: 2011</b>	Secondary lithium-ion cells for the propulsion of electric road vehicles – Part 1: Performance testing
	<b>IEC 62660-2: 2010 EN 62660-2: 2011</b>	Secondary lithium-ion cells for the propulsion of electric road vehicles – Part 2: Reliability and abuse testing
	<b>IEC 61982-1: 2006 EN 61982-1: 2006</b>	Secondary batteries for the propulsion of electric road vehicles – Part 1: Test parameters
	<b>IEC 61982-2: 2002 EN 61982-2: 2002</b>	Secondary batteries for the propulsion of electric road vehicles – Part 2: Dynamic discharge performance test and dynamic endurance test
	<b>IEC 61982-3: 2001 EN 61982-3: 2001</b>	Secondary batteries for the propulsion of electric road vehicles – Part 3: Performance and life testing (traffic compatible, urban use of vehicles)
	<b>IEC 61982-4: 2008</b>	Secondary batteries for the propulsion of electric road vehicles – Part 4: Performance testing for lithium-ion cells
	<b>IEC 61960: 2011 EN 61960: 2011</b>	Secondary cells and batteries containing alkaline or other non-acid electrolytes - Secondary lithium cells and batteries for portable applications
	<b>IEC 62133: 2002 EN 62133: 2003</b>	Secondary Cells and Batteries Containing Alkaline or Other Non-acid Electrolytes – Safety Requirements For Portable Sealed Secondary Cells, And For Batteries Made From Them, For Use In Portable Applications
	<b>IEC 62281: 2004 EN 62281: 2004</b>	Safety of Primary and Secondary Lithium Cells and Batteries During Transport
	<b>EN 50272-1: 2010</b>	Safety requirements for secondary batteries and battery installations - Part 1: General safety information
	<b>EN 50272-2: 2001</b>	Safety requirements for secondary batteries and battery installations - Part 2: Stationary batteries.
	<b>EN 50272-3: 2002</b>	Safety requirements for secondary batteries and battery installations - Part 3: Traction batteries
	<b>EN 50272-4: 2007</b>	Safety requirements for secondary batteries and battery installations - Part 4: Batteries for use in portable appliances
	Underwriters Laboratories Inc. (UL)	<b>UL1642</b>
<b>UL2054</b>		Household and Commercial Batteries
<b>UL2271</b>		Batteries For Use in LEV Applications
<b>UL2580</b>		Batteries For Use in Electric Vehicles
<b>UL2575</b>		Lithium Ion Battery Systems for Use in Electric Power Tool and Motor Operated, Heating and Lighting Appliances
Institute of Electrical and Electronics Engineers (IEEE)	<b>IEEE1625</b>	Rechargeable Batteries for Multi-Cell Mobile Computing Devices
	<b>IEEE1725</b>	Rechargeable Batteries for Cellular Telephones
Japanese Standards Association (JIS)	<b>JIS C8714</b>	Safety Tests For Portable Lithium Ion Secondary Cells and Batteries For Use in Portable Electronic Applications
Society of Automotive Engineers (SAE) International	<b>SAE J2464</b>	EV & HEV Rechargeable Energy Storage System (RESS) Safety and Abuse Testing Procedure
	<b>SAE J2288</b>	Life cycle testing of electric vehicle battery modules
	<b>SAE J2929</b>	Electric and Hybrid Vehicle Propulsion Battery System Safety Standard - Lithium-based Rechargeable Cells
National Electrical Manufacturers Association (NEMA)	<b>ANSI C18.2M.P2</b>	Portable Rechargeable Cells and Batteries – General and Specifications

**Table A-6. Summary and titles of all lithium-ion cells manuals and reports covered**

<b>ORGANISATION</b>	<b>MANUAL/REPORT NUMBER</b>	<b>TITLE</b>
U.S. Department of Energy (DOE)	<b>INL/EXT-07-12536</b>	Battery Test Manual for Plug-In Hybrid Electric Vehicles (INL)
	<b>INEEL/EXT-04-01986</b>	Battery Technology Life Verification Test Manual
	<b>DOE/ID-11069</b>	FreedomCar Battery Test Manual for power-assisted hybrid electric vehicles
	<b>DOE/ID-11070</b>	FreedomCar 42V Battery Test Manual
	<b>DOE/ID-10597</b>	PNGV Battery Test Manual
USABC	<b>USABC Battery Test Manual</b>	USABC Electric Vehicle Battery Test Procedures Manual
United Nations (UN)	<b>UN 38.3</b>	UN Manual of Tests and Criteria. Lithium Battery Testing Requirements
	<b>Manual of Tests and Criteria, PIIL, 38.3.</b>	Recommendations on the Transport of Dangerous Goods
Battery Safety Organisation (BATSO)	<b>BATSO 01</b>	Manual for Evaluation of Energy Systems for Light Electric Vehicle (LEV) – Secondary Lithium Batteries
Sandia National Laboratories (SNL)	<b>SAND 2005-3123</b>	FreedomCar Abuse test manual for electric and hybrid electric vehicles applications
	<b>SAND 99-0497</b>	FreedomCAR Electrical Energy Storage System Abuse Test Manual for Electric and Hybrid Electric Vehicle Applications
	<b>SAND 2010-0815</b>	Energy Storage for the Electricity Grid: Benefits and Market Potential Assessment Guide. A Study for DOE Energy Storage System Program
Pacific Northwest National Laboratory (PNNL) & SNL	<b>PNNL-22010</b>	Protocol for Uniformly Measuring and Expressing the Performance of Energy Storage Systems

**Table A-7. Spanish standards for lithium ion batteries**

<b>INTERNATIONAL STANDARD</b>	<b>Ratification by AENOR</b>
IEC 62660-1: 2010 / EN 62660-1: 2011	UNE-EN 62660-1:2011
IEC 62660-2: 2010 / EN 62660-2: 2011	UNE-EN 62660-2:2011
IEC 61982-1: 2006 / EN 61982-1: 2006	UNE-EN 61982-1: 2008
IEC 61982-2: 2002 / EN 61982-2: 2002	UNE-EN 61982-2:2004
IEC 61982-3: 2001 / EN 61982-3: 2001	UNE-EN 61982-3:2002
IEC 61960: 2011 / EN 61960: 2011	UNE-EN 61960:2004 UNE-EN 61960:2012
IEC 62133: 2002 / EN 62133: 2003	UNE-EN 62133:2004
IEC 62281: 2004 / EN 62281: 2004	UNE-EN 62281:2004
EN 50272-1: 2010	UNE-EN 50272-1:2011
EN 50272-2: 2001	UNE-EN 50272-2:2002
EN 50272-3: 2002	UNE-EN 50272-3:2004
EN 50272-4: 2007	UNE-EN 50272-4:2007

**Table A-8. Summary of safety testing protocols and abuse test for Li-ion (covered tests in grey)**

TEST CRITERIA	STANDARD NUMBER														
	UL					IEC			NEMA	SAE	UN	IEEE		JIS	BATSO
	1642	2054	2271	2580	2575	62133	62281	62660-2	C18.2M. P2	J2462	PIII, 38.3	1625	1725	C8714	01
External short circuit															
Overcharge															
Forced discharge															
Crush															
Impact															
Shock															
Vibration															
Heating															
Temperature cycling															
Low pressure (altitude)															
Projectile															
Drop															
Continuous low rate charging															
Molded casing heated test															
Open circuit voltage															
Insulation resistance															
Reverse charge															
Penetration															
Internal short circuit (ISC) test															

*NOTE. There is no generally accepted internal short circuit (ISC) specific test, but two tests are under consideration: Forced Internal Short Circuit Test and Indentation Induced Internal Short Circuit test. The latter has been developed by Underwriters Laboratories Inc. (UL) and adopted by NASA*

## APPENDIX C. EQUIPMENT AND ANALYTICAL SPECIFICATIONS

---

### a) Battery testers

- *DIGATRON MCT (Multiple Cell Tester)*, MCT 100-06-10 ME and MCT 50-06-24 ME models. Technical data is gathered in Table A-9.

**Table A-9.** Specific Technical Data of MCT100-06-10 ME and MCT 50-06-24 ME Digatron cell testers

	MCT 100-06-10 ME	MCT 50-06-24 ME
No. of channels	10	24
Current	0.1 - 100 A	0.05 – 50 A
Accuracy	±0.1% full scale	
Data Acquisition Rate	10 ms	
Voltage range	0 - 6 V	
PC Software	BTS-600	

- CSM CAN bus measurement module: temperature acquisition system with Type K thermocouples (a Type K thermocouple was placed on the cell surface for temperature recording during tests). Thermocouple grade: from -200°C to 1250°C. Standard limits of error: 2.2°C or 0.75% above 0°C and 2.0% below 0°C.
- *DIGATRON Safety Box*: cell voltage and temperature monitoring safety device.



**Figure A-11.** Digatron MCT cell tester (a), tests circuits in it (b) and safety box (c)

- *DIGATRON EISmeter* tester. Resistance range: 0.3-3000 m $\Omega$ . Maximum output alternative current (AC): 2 A with < 100  $\mu$ A resolution. AC current frequency range: 1  $\mu$ Hz - 6.5 kHz, with 0.005% accuracy from displayed value. Voltage range measurement: 0-20 V with 5  $\mu$ V accuracy. Measurement accuracy < 1%.



*Figure A-12. DIGATRON EISmeter Impedance Spectroscopy*

### a.1) Cells connections

Specific test assemblies design was carried out to ensure good contact and easy connection of cell terminal to the multiple cell tester circuit cables.

- For **cylindrical cells**, as shown in Figure A-13, the assembly consisted of four copper plates, which make pressure contact with cell terminals, and an insulating Teflon slab that gives rigidity to the system. The circuit power cables were connected to the copper plates and voltage sense cables were directly connected to other terminals welded to the cell, so that the measurements were carried out in four points (separate pairs of current-carrying and voltage-sensing electrodes). The key advantage of four-terminal sensing is that the separation of power and voltage sense electrodes eliminates the impedance contribution of the wiring and contact resistances.

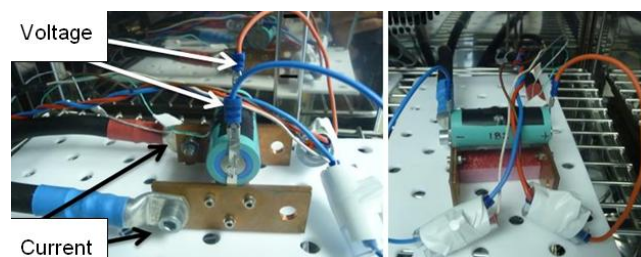


*Figure A-13. Cylindrical cells typical assembly and connections*

Before starting to test cells, assemblies validation was carried out to ensure that there was not any added resistance due to the connections, since it could lead to additional voltage drops or rises during cell discharging or charging, respectively. The validation of the assembly and connections was done measuring the internal resistance by means of EIS at 50% SOC and 25°C. If the measured value of internal resistance was equal to that obtained

by measuring it without the assembly, *i.e.* making direct contact in cell terminals, the testing assembly was considered to be valid. If not, the assembly had to be redesigned. The measured value was also compared with the one provided by the manufacturer (datasheet).

- **Pouch cells** terminals were placed between two copper plates with holes, which allowed screwing up the connection wires directly to the cell terminals, as shown in Figure A-14 (a). In case the terminals were short and there was no place for making holes in, it was used pressure contact between terminal and plates by means of larger plates, as shown in Figure A-14 (b), where the wires were screwed in holes that were made away from the terminals.

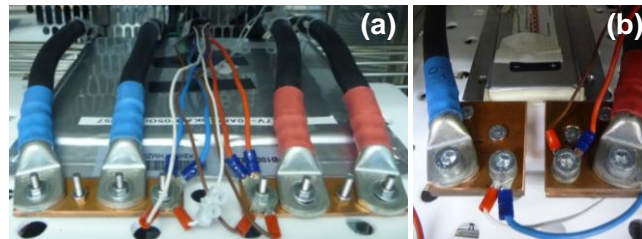


**Figure A-14.** Pouch cells connection. Cells with holes in terminals (a) and with short terminals without holes (b)

- **Prismatic cells** did not need any special assembly. Wires were directly connected to the torque terminals, as shown in Figure A-15. In this case, each electrode had a unique terminal connection for every wire.



**Figure A-15.** Prismatic cells connection

The multiple cell tester power cables were in all cases connected in the same way using a dynamometric torque wrench (5 Nm).

## b) Climate chambers

- *CTS (Clima-Temperatur-Systeme)*, *CTS/T-40/200/Li* and *CTS/T-40/600/Li*, temperature test cabinets (chemical resistance design test space) of 200 and 600 L with CO-sensor, N<sub>2</sub> flushing device and electromagnetical door locking. Operating temperature range: from

-40°C to +180°C, with  $\leq \pm 0.3$  K temporally temperature fluctuation and measurement accuracy of 0.35°C.



*Figure A-16. CTS climatic chambers*

- *Prebatem Selecta* Peltier effect 80 and 150 L temperature chambers. Operating temperature range: from 5°C to +50°C, with 0.045°C temporally temperature fluctuation and measurement accuracy of 0.225°C.



*Figure A-17. Prebatem climatic chamber*

- c) **Calorimeter** for tests at adiabatic environment: *THT EV-ARC Accelerating Rate Calorimeter (EV-esARC)* shown in Figure A-18. Type N tracking thermocouple. Standard limits of error: 5-10%.



*Figure A-18. THT EV-ARC Accelerating Rate Calorimeter*

- d) **Thermal imaging camera** for infrared radiation imaging: *FLIR Systems ThermoCAM P25* shown in Figure A-19.



**Figure A-19.** *FLIR Systems ThermoCAM P25 thermal imaging camera*

Thermograph images were taken at natural convection heat transport conditions and not in temperature-controlled environment (inside climate chambers).

e) **Post-mortem analysis**

- **Ar-atmosphere glove-boxes:** *Jakomex* (Type BS531) and *SylaTech* shown in Figure A-20. They are isolated devices with inert gas. Attainable cleanliness values:  $O_2 < 1\text{ppm}$ ,  $H_2O < 1\text{ppm}$ .



**Figure A-20.** *SylaTech glove-box (chemical lab of ISEA-RWTH Aachen University, Germany)*

- **Centrifuger** for liquid electrolyte extraction from cylindrical cells: *SIGMA 2-16 microcentrifuge No. 17140*, shown in Figure A-21.

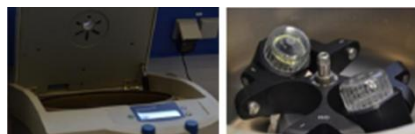


**Figure A-21.** *SIGMA 2-16 microcentrifuge No. 17140 and centrifuge containers (chemical lab of ISEA-RWTH Aachen University, Germany)*

- **Mercury Intrusion Porosimetry (MIP):** *Thermo Scientific Mercury Porosimeter PASCAL 140 and 440 Series*, shown in Figure A-22, with *Solid* software. Analytical conditions:

ambient temperature, 400 kPa parameters acquisition method and 6-8 penetration increasing-decreasing speed during pumping. Capacitive dilatometers that were used: CD3 and CD3P types shown in Figure A-23. Both types of dilatometers are for homogeneous samples, but CD3 type is for the solid ones with medium/low porosity, whereas CD3P type is for both solids and powders with medium/high porosity. Their specifications are gathered in Table A-10.



**Figure A-22.** Thermo Scientific Mercury Porosimeter PASCAL 140 and 440 Series (chemical lab of ISEA-RWTH Aachen University, Germany)

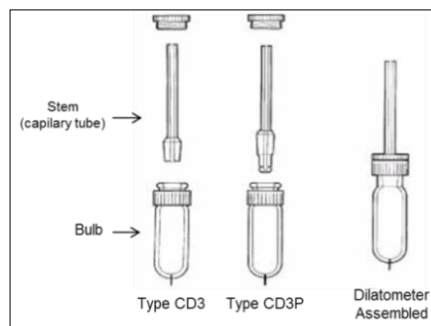


**Figure A-23.** CD3 and CD3P Dilatometers [230, 231]

**Table A-10.** Specifications of type CD3 and CD3P dilatometers [230, 231]

Parameter	CD3/CD3P Dilatometer
Maximum detection/measurable volume	0.5 cm <sup>3</sup>
Dilatometer internal total volume	15 cm <sup>3</sup>
Maximum size of sample (D x H)	1.2 cm x 4 cm
Internal radius of the capillary stem (CR)	1.5 mm
Volume size resolution	0.0001 cm <sup>3</sup>

Mercury porosimeters provide two sets of data, which are used for generating further data processing: the volume of mercury penetrated into the sample and the penetration pressure at the equilibrium [232]. Pore sizes are obtained from the former, whereas pore volume is given by the latter.

The total pore volume should lie within the recommended measuring range of the capillary tube and the apparatus . The maximum measureable volume using CD3 and CD3P dilatometers (see Table A-10) is 0.5 cm<sup>3</sup>, which means that this is the total volume of mercury available for the analysis, *i.e.* the maximum test filling volume. This is the volume of mercury in the stem after filling the dilatometer under vacuum conditions. The stem mercury height is given as Eq. A-1:

$$\text{Stem mercury height} = \frac{\text{Test filling volume}}{CR^2 \cdot \pi} \quad \text{Eq. A-1}$$

The optimal percentage of stem used for the analysis ought to be between 25 and 90%. The volume of mercury for filling the pores of the sample (in case all the porosity were open porosity) can be assessed according to Eq. A-2, where  $V_{\text{sample}}$  is the volume of the specimen to be tested,  $\varepsilon$  the porosity,  $m_{\text{sample}}$  the mass of the specimen to be tested and  $\rho_{\text{bulk}}$  the bulk density.

$$V_{Hg} = V_{\text{sample}} \cdot \frac{\varepsilon}{100} = \frac{m_{\text{sample}}}{\rho_{\text{bulk}}} \cdot \frac{\varepsilon}{100} \quad \text{Eq. A-2}$$

The mass of the sample is introduced in the software by the operator, whereas the volume is measured. The volume of the sample ( $V_{\text{sample}}$ ) is the total volume the material occupies in the bulb of the dilatometer including the void volumes. This parameter is computed by differential weight when the dilatometer is filled with mercury in vacuum conditions, surrounding the material without entering the pores. From the reported total intruded volume, *i.e.* total open pore volume ( $V_{\text{pores}}$ ), the measured volume of the sample can be obtained using calculated either porosity or density (bulk or apparent) data according to Eq. A-3, Eq. A-4 and Eq. A-5:

$$\varepsilon = \frac{V_{\text{pores}}}{V_{\text{sample}}} \cdot 100 \quad \text{Eq. A-3}$$

$$\rho_{\text{bulk}} = \frac{m_{\text{sample}}}{V_{\text{sample}}} \quad \text{Eq. A-4}$$

$$\rho_{\text{apparent/skeletal}} = \frac{m_{\text{sample}}}{(V_{\text{sample}} - V_{\text{pores}})} \quad \text{Eq. A-5}$$

- **Inductively Coupled Plasma-Optical Emission Spectrometry (ICP-OES)** for multi-element analysis of metallic compounds of the electrodes and electrolytes metals and

impurities detection: *ICP Optical Emission Spectrometer VARIAN 725-ES*, shown in Figure A-24, with ICP Expert II Agilent 725-ES Instrument Software (Version 1.1).



**Figure A-24.** *ICP Optical Emission Spectrometer VARIAN 725-ES*  
(chemical lab of ISEA-RWTH Aachen University, Germany)

ICP-OES technique consists on the elemental analysis of materials in aqueous solution, typically an acidic solution. It is a type of emission spectroscopy that uses the plasma to produce excited atoms and ions that emit electromagnetic radiation at wavelengths characteristic of a particular element. The intensity of this emission is indicative of the concentration of the element within the sample, which is compared to previously measured intensities of known concentrations of the elements. The concentrations are then computed by interpolation along the calibration lines.

#### - Calibration

In a complex matrix, the choice of internal standard is critical for achieving accurate results. Not only must the internal standard be absent from the sample but its emission spectra must be free from interference from the high concentrations of ions derived from the sample. Some metals have abundant spectral lines leading to significant peak overlaps and baseline shifts for some of the most commonly applied internal standards. The background matrix of the calibration standards should approximate as much as possible to the kind and quantity of elements in the samples to be analysed.

Merck XVI and Merck IV calibration standards were used (ICP multi Element Standard Solution XVI CertiPUR and ICP multi Element Standard Solution IV CertiPUR, respectively). The stock solutions were diluted in distilled water using dilution factors of: (i) 1:5, 1:10 and 1:20 for Merck XVI and (ii) 1:50 and 1:200 for Merck IV. Analytical samples were 10 ml in volume. Each analysis comprised 2 replicate analyses of the sample digest bracketed by standards and preceded with an analysis of the blank digest (diluted regia water).

- Analytical protocol

Samples need to be at least 10 ml in volume. It is generally possible to get by with 5 ml samples (sample volumes smaller than 5 ml will necessitate dilution with the corresponding change in reporting limits).

Each analysis comprises 2 replicate analyses of the sample digest bracketed by standards and preceded with an analysis of the blank digest (diluted regia H<sub>2</sub>O).

- **Microwave** for samples digestion: *CEM Mars 5 Microwave Accelerated Reaction System* shown in Figure A-25. It is designed for digesting, dissolving and hydrolysing a wide variety of materials in a laboratory setting. The system uses microwave energy to heat samples in polar or ionic solutions rapidly and at elevated pressures. Its main purpose is preparing samples for analysis by atomic absorption (AA), ICP and gas or liquid chromatography.

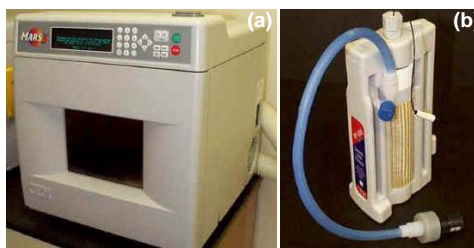


**Figure A-25.** *CEM Mars 5 Microwave Accelerated Reaction System. (a) Oven exterior and (b) Teflon reaction vessel in the support module with control parts assembled*

(Source: [http://www.ietltd.com/pdf\\_datasheets/Mars%205%20Data%20Sheet.pdf](http://www.ietltd.com/pdf_datasheets/Mars%205%20Data%20Sheet.pdf))

- **BaSyTec CTS** (Battery-System-Technology Cell **Test System**) for half-cell testing. Technical data is gathered in Table A-11.

**Table A-11.** *Specific Technical Data of BaSyTec CTS Standard*

Current range	0.001 - 5 A
Current precision	0.2 $\mu$ A
Current resolution	0.05 $\mu$ A
Time resolution	1 $\mu$ s
Voltage range	0 - 6 V
PC Software	Basytest software 5.5.6.0



**APPENDIX D. DATABASE OF LITHIUM-ION BATTERIES MARKET.  
WORLD-WIDE MANUFACTURERS AND TECHNOLOGIES**

---

Li-ion technology niche market was investigated and a database was created. Table A-12 compiles the most relevant information about Li-ion battery manufacturers, the technologies they work on and some of the applications are shown.

*Table A-12. Li-ion battery market database*

BATTERY COMPANY / JOINT VENTURES	COUNTRY	TECHNOLOGIES & PRODUCTS ACTIVITIES & SOME CUSTOMERS
<b>A123</b> ( <a href="http://www.a123systems.com">http://www.a123systems.com</a> )	USA	<ul style="list-style-type: none"> <li>- HP cylindrical and pouch cells</li> <li>- LFP-graphite cells</li> <li>- Nanophosphate based Li-ion batteries</li> <li>- Customers: BAE systems, THINK, Cessna, Delphi, Black&amp;Decker, AES, Daimler, SAIC, Better Place, General Motors, Volvo Truck, Magna, Chrysler, BMW</li> </ul>
<b>AESC</b> (Automotive Energy Supply Corporation) - joint venture between Nissan Motor Co., Ltd., NEC Corporation, and its subsidiary NEC TOKIN Corporation- ( <a href="http://www.eco-aesc-lb.com/en/">http://www.eco-aesc-lb.com/en/</a> )	Japan	<ul style="list-style-type: none"> <li>- Pouch cells</li> <li>- Laminated Li-ion cells using LMO and LMO/NCA cathode chemistries</li> <li>- Customers: Nissan (Leaf, NV200, Infiniti M35H), TEPCO (Subaru R1e, Subaru Plug-in Stella minicar), Renault, global OMS customers</li> </ul>
<b>Altairnano</b> ( <a href="http://www.altairnano.com">http://www.altairnano.com</a> )	USA	<ul style="list-style-type: none"> <li>- HP pouch cells</li> <li>- LMO-LTO (nano LTO technology)</li> <li>- Applications: industrial forklifts, elevators, locomotives, mining trucks, commercial trucks and buses, fast response solutions to grid stability</li> </ul>
<b>Amperex Technology Ltd., ATL</b> (Owned by TDK corp.) ( <a href="http://www.atlbattery.com/">http://www.atlbattery.com/</a> )	China	<ul style="list-style-type: none"> <li>- Large capacity prismatic cells, HP cells and pouch cells</li> <li>- NCM cathode</li> <li>- Customer: Valence</li> <li>- Applications: consumer electronics applications, HEV/PHEV and fully EVs, to large enterprise or utility level energy storage</li> </ul>
<b>BAK (China BAK Battery Inc.)</b> ( <a href="http://www.bak.com.cn/">www.bak.com.cn/</a> )	China	<ul style="list-style-type: none"> <li>- Cylindrical, prismatic case, polymeric and HP Li-ion cells</li> <li>- LFP cathode</li> <li>- Customers: Tier1 notebook computer OEM</li> <li>- Applications: E-bikes, power tools and UPS</li> </ul>
<b>Baoding Fengfan New Energy Co., Ltd.</b> -subsidiary wholly owned by Fengfan Co., Ltd.- ( <a href="http://en.sailli.cn/">http://en.sailli.cn/</a> )	China	<ul style="list-style-type: none"> <li>- HP and HE cylindrical and polymer batteries</li> <li>- Applications: notebook computer, digital products, electric tools, E-bikes, EVs, solar illumination, medical apparatus and national defense fields</li> </ul>
<b>Batscap</b> ( <a href="http://www.batscap.com/">http://www.batscap.com/</a> )	France	<ul style="list-style-type: none"> <li>- Prismatic lithium cells</li> <li>- Lithium metal polymer (LMP) batteries: metallic lithium anode, a polymer electrolyte and LFP cathode</li> <li>- Customers: Bluecar</li> </ul>

Table A-12. Li-ion battery market database (continued)

BATTERY COMPANY / JOINT VENTURES	COUNTRY	TECHNOLOGIES & PRODUCTS ACTIVITIES & SOME CUSTOMERS
<b>Blue Energy</b> -joint venture between GS Yuasa and Honda Motors- <a href="http://www.blue-energy.co.jp">http://www.blue-energy.co.jp</a>	Japan	<ul style="list-style-type: none"> <li>- Prismatic Compact, light and HP lithium cells</li> <li>- NCM cathode Li-ion battery for HEV and LMO cathode Li-ion battery for EV</li> <li>- Customers: Honda (Civic Hybrid, Accord hybrid and Plug-in hybrid)</li> </ul>
<b>Boston Power</b> <a href="http://www.boston-power.com/">http://www.boston-power.com/</a>	USA	<ul style="list-style-type: none"> <li>- HE cells, based on a flat, oval-shaped prismatic design (equivalent to two conventional 18650-type cells)</li> <li>- LCO and LMO cathodes</li> <li>- Customers: NASA, Asus and Electric Vehicle Automotive Industry, Saab</li> </ul>
<b>BYD Company</b> <a href="http://www.byd.com/">http://www.byd.com/</a>	China	<ul style="list-style-type: none"> <li>- Prismatic HP batteries</li> <li>- LFP-graphite</li> <li>- Customers: Volkswagen, Daimler, BYD (E-bus, F3DM and e6 EV), Nokia, Motorola, OEM, ODM</li> </ul>
<b>CALB</b> <a href="http://en.calb.cn/">http://en.calb.cn/</a>	China	<ul style="list-style-type: none"> <li>- Prismatic HE batteries with plastic and metallic case</li> <li>- LFP cathode</li> <li>- Applications: EV, E-bus, House-hold ESS, grid ESS and telecommunication power modules</li> </ul>
<b>CITIC GUOAN MGL</b> <a href="http://www.mgl.com.cn/http://en.mgl.com.cn/">http://www.mgl.com.cn/http://en.mgl.com.cn/</a>	China	<ul style="list-style-type: none"> <li>- Pouch and prismatic (stainless steel case) cells</li> <li>- LCO, LMO, <math>\text{LiMxCo}_{0.2}\text{Ni}_{0.8-x}\text{O}_2</math> and <math>\text{LiNi}_{1/3}\text{Co}_{1/3}\text{Mn}_{1/3}\text{O}_2</math> cathodes</li> <li>- Applications: E-bike, E-motorcycle, EVs, E-buses and electric field vehicles</li> </ul>
<b>Creup Technologies Ltd.</b> <a href="http://www.creup.com/">http://www.creup.com/</a>	China	<ul style="list-style-type: none"> <li>- Pouch, prismatic, cylindrical and coin cells. LiPo cells</li> <li>- LFP cathode</li> <li>- Applications: consumer electronics, battery pack for EVs and UPS</li> </ul>
<b>DLG Battery</b> <a href="http://www.dlgbattery.cn/">http://www.dlgbattery.cn/</a> Joint venture with K2 Energy Solutions	China	<ul style="list-style-type: none"> <li>- Cylindrical and pouch batteries. High capacity LiPo batteries</li> <li>- LFP and LCO cathodes</li> <li>- Applications: consumer electronics, UPS, power tools, E-bike, EV, solar energy storage, communication station energy storage and wind energy storage</li> </ul>
<b>Edan Technology Inc.</b> <a href="http://www.edan.com.tw/">http://www.edan.com.tw/</a>	Taiwan	<ul style="list-style-type: none"> <li>- Cylindrical, prismatic and pouch batteries. LiPo cells</li> <li>- LFP cathodes</li> <li>- Customers: BENQ, Lucent, Mustek, Inventek, Kodak and Asia Optical</li> </ul>
<b>EEMB Battery Co.</b> <a href="http://www.eemb.com">http://www.eemb.com</a>	China	<ul style="list-style-type: none"> <li>- Cylindrical and pouch cells</li> <li>- LCO, LFP pouch cells and LMO cells</li> <li>- Applications: Light EV, off-grid solar power and consumer electronics</li> </ul>

Table A-12. Li-ion battery market database (continued)

BATTERY COMPANY / JOINT VENTURES	COUNTRY	TECHNOLOGIES & PRODUCTS ACTIVITIES & SOME CUSTOMERS
<b>EIG</b> ( <a href="http://www.eigbattery.com">http://www.eigbattery.com</a> )	South Korea	<ul style="list-style-type: none"> <li>- Pouch cells (up to 20 Ah)</li> <li>- NCM- or LFP-based cathode with carbon anode cells and also LTO cells</li> <li>- Applications: HEV, EV, E-bikes, E-wheel chairs, defense and military markets, UPSs, mobile robots, residential and industrial ESS</li> </ul>
<b>Electrovaya</b> ( <a href="http://www.electrovaya.com/">http://www.electrovaya.com/</a> )	Canada	<ul style="list-style-type: none"> <li>- Pouch cells</li> <li>- LiPo nano-structured materials</li> <li>- Customers: Tata Motors and Miljø Grenland (partnership), Kongsberg, NASA, Scribbler (tablet PC), PowerPad and Nippon Kouatsu Electric Co. Ltd.</li> </ul>
<b>Eliiy power Co.</b> ( <a href="http://www.eliyypower.co.jp">http://www.eliyypower.co.jp</a> )	Japan	<ul style="list-style-type: none"> <li>- High capacity prismatic batteries</li> <li>- LFP cathode</li> <li>- Applications: indoor use ESS, stationary ESS and industrial use ESS</li> </ul>
<b>Enax</b> ( <a href="http://www.enax.jp">www.enax.jp</a> )	Japan	<ul style="list-style-type: none"> <li>- Pouch cells, LiPo cells, Laminated Sheet Battery (LSB)</li> <li>- Customers: Nissan, Hino Motors</li> </ul>
<b>Ener1-Enerdel</b> -Ener1 has purchased Enerdel and Enertech. The latter is the responsible for the fabrication of the batteries- ( <a href="http://www.ener1.com">http://www.ener1.com</a> )	USA	<ul style="list-style-type: none"> <li>- Pouch HP batteries. LiPo cells</li> <li>- LMO-LTO, NCM-Graphite and LMO-Hard Carbon cells</li> <li>- Customers: THINK, Fisher automotive (Karma), Volvo, Japan Post (Zero Sports), Toyota and Mazda</li> </ul>
<b>Energys</b> ( <a href="http://www.energys.com">http://www.energys.com</a> )	USA/ Switzerland/ Singapore	<ul style="list-style-type: none"> <li>- Cylindrical and prismatic cells</li> <li>- Applications: aerospace and defense, standby power and commercial markets (telecoms, UPS, robotics, renewable energy systems, etc.)</li> </ul>
<b>Envia Systems</b> ( <a href="http://www.enviasystems.com">www.enviasystems.com</a> )	USA	<ul style="list-style-type: none"> <li>- Pouch cells</li> <li>- Proprietary high capacity manganese rich cathode with its proprietary high capacity Si-based anode</li> <li>- Applications: EVs, HEVs and PHEVs</li> </ul>
<b>E-one Moli Energy Corp. (Molicell)</b> ( <a href="http://www.molicel.com/">http://www.molicel.com/</a> )	Taiwan/ Canada	<ul style="list-style-type: none"> <li>- Cylindrical, prismatic and HP cells</li> <li>- LCO, LMO, NCM and LFP cathode materials</li> <li>- Batteries for laptops, power tools, UPS systems, EVs and HEVs</li> <li>- Customers: laptops (Asus), power tools (TTI Group), EVs and HEVs (Ford and BMW MINI E)</li> </ul>
<b>ETV Motors</b> ( <a href="http://etvmotors.com/">http://etvmotors.com/</a> )	Israel	<ul style="list-style-type: none"> <li>- Pouch cells</li> <li>- High voltage spinel cathodes, High5ive battery: 4.7 V, 300-350 Wh/kg</li> <li>- Applications: EVs, HEVs and extended-range electric vehicles (EREVs)</li> </ul>

Table A-12. Li-ion battery market database (continued)

BATTERY COMPANY / JOINT VENTURES	COUNTRY	TECHNOLOGIES & PRODUCTS ACTIVITIES & SOME CUSTOMERS
<b>EVPST</b> (Electric Vehicle Power System Technology Co., Ltd.) <a href="http://www.evpst.com/">(http://www.evpst.com/)</a>	China	<ul style="list-style-type: none"> <li>- Cylindrical, prismatic and pouch batteries</li> <li>- LFP cathode</li> <li>- Applications: E-bike, EV, HEV, Electric Marine Propulsion system and UPS</li> </ul>
<b>EXA Energy, Ltd.</b> <a href="http://www.exa.com.tw/exa/">(http://www.exa.com.tw/exa/)</a>	Taiwan	<ul style="list-style-type: none"> <li>- Pouch cells</li> <li>- LFP cathode</li> <li>- Applications: EV, UPS, energy storage</li> </ul>
<b>Farasis Energy</b> <a href="http://www.farasis.com/">(www.farasis.com)</a>	USA	<ul style="list-style-type: none"> <li>- Prismatic cells</li> <li>- Manganese rich (MnR) cathode</li> <li>- Applications: consumer electronics, transportation and stationary energy storage</li> </ul>
<b>Foshan Gelong Energy Co., Ltd.</b> <b>Foshan U&amp;T battery Co., Ltd.</b> <a href="http://www.utbattery.com/">(http://www.utbattery.com/)</a>	China	<ul style="list-style-type: none"> <li>- Pouch cells. HP LiPo batteries</li> <li>- Applications: remote control air vehicles</li> </ul>
<b>FULLRIVER Battery</b> <a href="http://www.fullriver.com/">(http://www.fullriver.com/)</a>	China	<ul style="list-style-type: none"> <li>- Cylindrical steel shell and pouch packing batteries</li> <li>- LFP, LCO, LMO, Co-Mn mixture and ternary material series cathodes</li> <li>- Applications: communication, toys, digital products and transportation</li> </ul>
<b>Future synergy power source Co., Ltd.</b> <a href="http://www.synergy-power.com/">(http://www.synergy-power.com)</a>	China	<ul style="list-style-type: none"> <li>- Pouch and prismatic batteries. LiPo cells</li> <li>- Applications: consumer electronics</li> </ul>
<b>Gaia-LTC (Lithium Technology Corp.)</b> <a href="http://www.gaia-akku.com/">(http://www.gaia-akku.com)</a>	Germany/ USA	<ul style="list-style-type: none"> <li>- Large format cylindrical cells</li> <li>- LFP-graphite (from SüdChemie) and NCA</li> <li>- Customers: Quicc DiVa, ArvinMeritor Inc. (NYSE: ARM), Designline International (bus manufacturer -US and New Zealand-), EnerSys (battery packs using LTC batteries), VW (Golf Twin Drive)</li> </ul>
<b>GBP Battery</b> <a href="http://www.gbp-battery.com/">(http://www.gbp-battery.com/)</a>	China	<ul style="list-style-type: none"> <li>- Cylindrical and HP pouch batteries</li> <li>- LFP &amp; LMO cathode cells</li> <li>- Applications: RC &amp; Toy, EVs and industrial</li> </ul>
<b>Gold Peak Industries NA</b> <a href="http://gpina.com/">(http://gpina.com/)</a>	USA	<ul style="list-style-type: none"> <li>- Prismatic, cylindrical and LiPo pouch cells</li> <li>- LFP and LMO cathodes</li> <li>- Applications: portable electronics and EVs</li> </ul>

Table A-12. Li-ion battery market database (continued)

BATTERY COMPANY / JOINT VENTURES	COUNTRY	TECHNOLOGIES & PRODUCTS ACTIVITIES & SOME CUSTOMERS
<p><b>GP battery</b> (<a href="http://www.gpbatteries.com">http://www.gpbatteries.com</a>) Member of Gold Peak Industries. <i>Ningbo GP Sanyo Energy Co Ltd.</i> joint venture with Sanyo Energy (a subsidiary of Sanyo Electric Co. Ltd.)</p>	China	<ul style="list-style-type: none"> <li>- LiPo pouch, cylindrical and prismatic cells</li> <li>- HP batteries. LFP cathodes</li> <li>- Applications: consumer electronics</li> </ul>
<p><b>GS Yuasa</b> (created from Yuasa Corp and Japan Storage Battery Co. (JSB)) (<a href="http://www.gs-yuasa.com/us/">http://www.gs-yuasa.com/us/</a>) <i>Lithium Energy Japan</i> joint venture with Mitsubishi <i>Blue Energy</i> joint venture with Honda</p>	Japan	<ul style="list-style-type: none"> <li>- Prismatic cells</li> <li>- LMO-Graphite, NCM-LFP, LFP-Graphite and LCO cells</li> <li>- Applications: EV (Honda and Mitsubishi), E-bikes, computers, military and stationary applications</li> </ul>
<p><b>Halise</b> (<a href="http://www.halisebattery.com">http://www.halisebattery.com</a>)</p>	China	<ul style="list-style-type: none"> <li>- Cylindrical and prismatic cells</li> <li>- LFP cathode</li> <li>- Applications: consumer electronics, power tools, wind &amp; solar complementary hybrid system, street lighting system, photovoltaic pump system, photovoltaic rural program-controlled telephone, solar power station and EVs</li> </ul>
<p><b>Hangzhou Future Power Technology Co., Ltd.</b> -subsidiary of FUTONG GROUP- (<a href="http://www.ftbattery.com">http://www.ftbattery.com</a>)</p>	China	<ul style="list-style-type: none"> <li>- Pouch cells. LiPo cells</li> <li>- LCO/carbon cells</li> </ul>
<p><b>Headway</b> (<a href="http://www.chinaheadway.com">http://www.chinaheadway.com</a>)</p>	China	<ul style="list-style-type: none"> <li>- Cylindrical, prismatic and pouch cells. LiPo cells</li> <li>- LFP cathode</li> <li>- Applications: consumer electronics, EV, E-bike and ESS</li> </ul>
<p><b>Henan Bideli New Technology Co., Ltd. (BDL)</b> (<a href="http://www.bideli.com.cn">http://www.bideli.com.cn</a>)</p>	China	<ul style="list-style-type: none"> <li>- Cylindrical and prismatic cells</li> <li>- HP LFP, LMO and NCM cylindrical batteries</li> <li>- Applications: EV, E-bike, E-motor, consumer electronics, ESS</li> </ul>
<p><b>Heter</b> (<a href="http://www.heterbattery.com">http://www.heterbattery.com</a>)</p>	Thailand	<ul style="list-style-type: none"> <li>- Cylindrical and prismatic cells</li> <li>- LFP cathode</li> <li>- Applications: utilities, government agencies and transport</li> </ul>

Table A-12. Li-ion battery market database (continued)

BATTERY COMPANY / JOINT VENTURES	COUNTRY	TECHNOLOGIES & PRODUCTS ACTIVITIES & SOME CUSTOMERS
<b>Highpower International Hong-Kong High Power</b> <a href="http://www.highpowertech.com/">(http://www.highpowertech.com/)</a> <i>Subsidiaries; Shenzhen Highpower Technology Co., Ltd. and Springpower Technology (Shenzhen) Co., Ltd.</i>	China	<ul style="list-style-type: none"> <li>- Prismatic, cylindrical and pouch cells. LiPo cells</li> <li>- Applications: E-bike, GPS, military lighting, E-toy, vacuum cleaner and notebook</li> </ul>
<b>Hitachi Maxell Ltd. -Hitachi Vehicle Energy, Ltd.</b> <a href="http://www.hitachi-ve.co.jp">http://www.hitachi-ve.co.jp</a>	Japan	<ul style="list-style-type: none"> <li>- Prismatic and cylindrical HP batteries</li> <li>- Manganese-based cathode</li> <li>- Customers: Nissan, Isuzu, Mitsubishi, General Motors (EVs) and JR East (Trains)</li> </ul>
<b>Hubey Camel Special Power</b> <a href="http://www.chinacamel.com">http://www.chinacamel.com</a>	China	<ul style="list-style-type: none"> <li>- Prismatic and pouch cells</li> <li>- LFP cathode</li> </ul>
<b>HYD Battery Co., Ltd.</b> <a href="http://www.hyb-battery.com">http://www.hyb-battery.com</a>	China	<ul style="list-style-type: none"> <li>- Li-ion prismatic and pouch cells</li> <li>- Applications: portable devices</li> </ul>
<b>JiangXi JinGang Energy Technology Co., Ltd.</b> <a href="http://www.kingcell.com.cn">http://www.kingcell.com.cn</a>	China	<ul style="list-style-type: none"> <li>- Cylindrical cells</li> <li>- LFP, NCM and LCO cathode</li> <li>- Applications: E-bus, E-cycle, E-motor and electric tools</li> </ul>
<b>JMEnergy</b> <a href="http://www.jmenergy.co.jp/en/">http://www.jmenergy.co.jp/en/</a>	Japan	<ul style="list-style-type: none"> <li>- Pouch and prismatic cells</li> <li>- Li-ion capacitors</li> <li>- Customers: Meidensha, M-Tec Co. Ltd., Hokusho, Smart Hawk, Konica Minolta, Kictec and Jamstec</li> </ul>
<b>Johnson Controls</b> <a href="http://www.johnsoncontrols.com">http://www.johnsoncontrols.com</a>	USA	<ul style="list-style-type: none"> <li>- Cylindrical and prismatic</li> <li>- NCA-Graphite and NMC-Graphite chemistries</li> <li>- Customers: Ford (Escape PHEV), FedEx, Chevy, GMC, Daimler, BMW, Jaguar/Land Rover, Torqeedo and Azure Dynamics (converter of delivery vehicles for UPSs)</li> </ul>
<b>K2 Energy Solutions Inc.</b> <a href="http://www.K2battery.com">www.K2battery.com</a>	USA	<ul style="list-style-type: none"> <li>- Cylindrical cell</li> <li>- LFP technology</li> <li>- Customers: FIAT 500EV, Shelby, Chevy Aveo EV and E-bike manufacturers</li> </ul>
<b>Kayo battery Co., Ltd.</b> <a href="http://www.kayobattery.com/">http://www.kayobattery.com/</a>	China	<ul style="list-style-type: none"> <li>- Pouch, prismatic and cylindrical cells. LiPo cells</li> <li>- LCO and LFP chemistries</li> <li>- Applications: consumer electronics, power tools, E-bike, E-chair and UPS</li> </ul>

Table A-12. Li-ion battery market database (continued)

BATTERY COMPANY / JOINT VENTURES	COUNTRY	TECHNOLOGIES & PRODUCTS ACTIVITIES & SOME CUSTOMERS
<b>Kokam/Dow Kokam</b> ( <a href="http://www.kokam.com">www.kokam.com</a> )	Korea/USA (Kokam America Inc., subsidiary of Kokam Korea)	<ul style="list-style-type: none"> <li>- Pouch cells</li> <li>- NCM-Graphite LiPo, proprietary technology Superior Lithium Polymer Battery (SPLB)</li> <li>- Customers: consumer electronics, Safra, ZeroTruck, MotoCzysz, eCamion Inc., Corvus Energy, Motiv Power Systems, Quantum, Smith Electric Vehicles, Akasol and ads-tec</li> </ul>
<b>LG Chem</b> ( <a href="http://www.lgchem.com/">http://www.lgchem.com/</a> ) ( <a href="http://lgcpi.com/">http://lgcpi.com/</a> )	South Korea	<ul style="list-style-type: none"> <li>- Prismatic and cylindrical cells. LiPo cells</li> <li>- LMO-hard carbon, LFP-Graphite, NCM cathode</li> <li>- Applications: EVs, global leader in small-sized Li-ion batteries for IT products</li> <li>- Customers: GM -Chevrolet Volt-, Cadillac -ELR-, Ford -Ford Focus-, KIA Motors Corp. -KIA Forte Hybrid-, Hyundai Motor Co. -Hyundai Avant Hybrid (Accent), Hyundai Sonata-, Volvo -V70, V60 diesel, XC60 T8, XC90-</li> </ul>
<b>Leclanché</b> ( <a href="http://www.leclanche.eu/">http://www.leclanche.eu/</a> )	Switzerland & Germany	<ul style="list-style-type: none"> <li>- Pouch cells</li> <li>- LTO anode, LFP and NCA cathodes, ceramic based Leclanché Separator (patented technology). Doped and non doped cobalt oxide materials</li> <li>- Applications: home storage, industry storage, grid stabilisation, HEV, EV, medical devices, defense systems and mobile office units</li> </ul>
<b>Leyden Energy</b> ( <a href="http://www.leydenenergy.com/">http://www.leydenenergy.com/</a> )	USA	<ul style="list-style-type: none"> <li>- Pouch and cylindrical cells</li> <li>- Patented Lithium Imide electrolyte salt and graphite foil current collectors</li> <li>- Applications: EVs, consumer electronics, grid storage and UPSs</li> </ul>
<b>LiFeBatt</b> ( <a href="http://www.lifebatt.com/">http://www.lifebatt.com/</a> )	Taiwan	<ul style="list-style-type: none"> <li>- Cylindrical and metallic case prismatic cells</li> <li>- LFP cathodes</li> <li>- Applications, wind and solar back-up systems, auxiliary power tools, military and homeland security, marine applications and Light-EV</li> </ul>
<b>Lionik battery</b> ( <a href="http://www.lionik.com/">http://www.lionik.com/</a> )	China	<ul style="list-style-type: none"> <li>- Prismatic and cylindrical cells</li> <li>- LFP, LMO and NCM</li> <li>- Applications: consumer electronics</li> </ul>
<b>Lishen</b> (Tianjin Lishen Battery Joint-Stock Co., Ltd.) ( <a href="http://en.lishen.com.cn">http://en.lishen.com.cn</a> )	China	<ul style="list-style-type: none"> <li>- Prismatic, cylindrical and pouch cells</li> <li>- NCM and LFP cathode</li> <li>- Applications: consumer electronics, EV (Coda), HEV, PHEV, E-bikes and power tools</li> </ul>

Table A-12. Li-ion battery market database (continued)

BATTERY COMPANY / JOINT VENTURES	COUNTRY	TECHNOLOGIES & PRODUCTS ACTIVITIES & SOME CUSTOMERS
<b>Lithion</b> <a href="http://www.yardney.com/">(http://www.yardney.com/)</a>	USA	<ul style="list-style-type: none"> <li>- Prismatic batteries</li> <li>- Mixed Metal Oxide and LNCO cathodes with graphite anode</li> <li>- Applications: Aerospace (NASA-Mars Rover), undersea, naval and military applications</li> </ul>
<b>Lithium Energy Japan</b> -joint venture between GS Yuasa and Mitsubishi- <a href="http://www.lithiumenergy.jp/en">www.lithiumenergy.jp/en</a>	Japan	<ul style="list-style-type: none"> <li>- Prismatic cells</li> <li>- Mixed LMO/NMC cathode</li> <li>- Customer: Mitsubishi Motors (EV/MiEV)</li> </ul>
<b>Mitsubishi Batteries industrial</b> <a href="http://www.mhi.co.jp/en/power/lithium/index.html">http://www.mhi.co.jp/en/power/lithium/index.html</a>	Japan	<ul style="list-style-type: none"> <li>- Prismatic cells</li> <li>- Lithium compound oxide (nickel, manganese, and cobalt) for the cathode material, along with a graphite anode</li> <li>- Applications: HEVs, EVs and power tools</li> </ul>
<b>Mottcell Battery Technology Co., Ltd.</b> <a href="http://en.mottcell.com/">http://en.mottcell.com/</a>	China	<ul style="list-style-type: none"> <li>- Prismatic and cylindrical cells</li> <li>- LiPo and LFP</li> <li>- Applications: E-bike, EV and ESS</li> </ul>
<b>Narada Licom Power</b> <a href="http://www.naradabattery.com.cn/">http://www.naradabattery.com.cn/</a>	China	<ul style="list-style-type: none"> <li>- Prismatic and pouch cells. LiPo cells</li> <li>- LFP cathode</li> <li>- Applications: consumer electronics, military devices, power tools, radio control models, telecommunications, UPS, back-up system and ESS</li> </ul>
<b>Ningbo Veken Battery Co., Ltd.</b> <a href="http://www.vekenbattery.com">http://www.vekenbattery.com</a>	China	<ul style="list-style-type: none"> <li>- Prismatic and pouch cells. LiPo cells</li> <li>- Applications: consumer electronics and E-bikes</li> </ul>
<b>PanasonicEV Energy-Co., Ltd.</b> <a href="http://industrial.panasonic.com/">http://industrial.panasonic.com/</a> -Panasonic-Sanyo joint venture- -Joint venture with Toyota- -Joint venture with Tesla-	Japan	<ul style="list-style-type: none"> <li>- Coin, cylindrical and prismatic cells</li> <li>- LNO-Graphite, NCM-Graphite, NCA-Graphite and LMO-Graphite</li> <li>- Applications: consumer electronics manufacturers, power tool, portable computer and telecommunications industries</li> <li>- EV-Customers: Toyota, Ford (C-max), Honda (Insight, Civic), VW (E-Up!, Beetle, Golf, Toureg), Audi (A1 e-tron, R8 e-tron, A6, A8, Q5), Porsche (Cayenne, Panamera), Suzuki (Swift) and Tesla (Model S, Model X, Roadster)</li> </ul>

Table A-12. Li-ion battery market database (continued)

BATTERY COMPANY / JOINT VENTURES	COUNTRY	TECHNOLOGIES & PRODUCTS ACTIVITIES & SOME CUSTOMERS
<b>PHET Pihsiang Energy</b> ( <a href="http://www.phet.com.tw">http://www.phet.com.tw</a> )	China	<ul style="list-style-type: none"> <li>- 18650 cylindrical cells</li> <li>- LFP cathode</li> <li>- Applications: power tools, E-bikes and EV</li> <li>- Customer: Pihsiang Machinery Manufacturing Co.</li> </ul>
<b>Phylion battery (Suzhou)</b> ( <a href="http://www.phylion.com/">http://www.phylion.com/</a> )	China	<ul style="list-style-type: none"> <li>- Prismatic cells</li> <li>- LFP cathode</li> <li>- Applications: E-bikes, E-scooter, EV/HEV, power tools, trains standby battery, wind and solar energy storage</li> </ul>
<b>Q-Lite Industrial</b> ( <a href="http://www.q-liteindustrial.com/">http://www.q-liteindustrial.com/</a> )	China	<ul style="list-style-type: none"> <li>- Hard plastic prismatic cells, coin type cells and cylindrical cells</li> <li>- Polymer spiral and bobbin technology, and LFP-based cells</li> <li>- Applications: consumer electronics</li> </ul>
<b>Quallion</b> ( <a href="http://www.quallion.com">http://www.quallion.com</a> )	USA	<ul style="list-style-type: none"> <li>- Metallic case prismatic and cylindrical cells, and pouch cells</li> <li>- NCM, spinel and LFP batteries</li> <li>- Applications: medical, military and aerospace industries, and HEV / EV / PHEV batteries</li> </ul>
<b>Saft</b> ( <a href="http://www.saftbatteries.com/">http://www.saftbatteries.com/</a> )	France	<ul style="list-style-type: none"> <li>- Cylindrical and prismatic cells</li> <li>- LFP and NCA cathodes</li> <li>- Applications: grid, HP UPS systems, photovoltaics and other renewable energies (load shifting, load shaving), portable applications and vehicles (hybrid military vehicles, underwater, electric bicycles, etc.). EV and HEVs</li> </ul>
<b>Samsung SDI Co. Ltd.</b> ( <a href="http://www.samsungsdi.com">www.samsungsdi.com</a> )	South Korea	<ul style="list-style-type: none"> <li>- Prismatic and cylindrical cells</li> <li>- LCO-Graphite, LFP-Graphite, LMO-Graphite, NCM-Graphite</li> <li>- Applications: laptops, mobile phones and power tools, EV</li> </ul>
<b>Shenzhen B&amp;K Technology Co.</b> ( <a href="http://www.bkbattery.com">http://www.bkbattery.com</a> )	China	<ul style="list-style-type: none"> <li>- Pouch, prismatic and cylindrical cells</li> <li>- LiPo cells</li> <li>- Applications: consumer electronics</li> </ul>
<b>Shenzhen Cham Battery Technology Co.</b> ( <a href="http://www.cham.com.cn">http://www.cham.com.cn</a> )	China	<ul style="list-style-type: none"> <li>- Cylindrical cells. LiPo cells</li> <li>- LFP cathode</li> <li>- Applications: consumer electronics, E-bike and UPS</li> </ul>

Table A-12. Li-ion battery market database (continued)

BATTERY COMPANY / JOINT VENTURES	COUNTRY	TECHNOLOGIES & PRODUCTS ACTIVITIES & SOME CUSTOMERS
<b>Shenzhen Eastar Battery</b> <a href="http://www.eastarbattery.com/">(http://www.eastarbattery.com/)</a>	China	<ul style="list-style-type: none"> <li>- Pouch, cylindrical and prismatic HE cells</li> <li>- LiMnO<sub>2</sub> and LFP</li> <li>- Applications: consumer electronics, E-bike, electric golf vehicle and EV</li> </ul>
<b>Shenzhen Free Technology Co., Limited</b> <a href="http://www.chinafreepower.com/">(http://www.chinafreepower.com)</a>	China	<ul style="list-style-type: none"> <li>- Pouch, cylindrical and prismatic cells. LiPo cells</li> <li>- LFP cathode</li> <li>- Applications: EV/HEV, UPS, consumer electronics, power tools, and emergency or security applications</li> </ul>
<b>Shenzhen Yiklik Energy Limited</b> <a href="http://www.yiklik.com/">(http://www.yiklik.com)</a>	China	<ul style="list-style-type: none"> <li>- Cylindrical, prismatic and pouch cells. LiPo cells</li> <li>- LFP cathode</li> <li>- Applications: lighting, EV and UPS</li> </ul>
<b>Sony Energy Devices</b> <a href="http://www.sony.net/">(http://www.sony.net/)</a>	Japan	<ul style="list-style-type: none"> <li>- Coin, cylindrical and prismatic cells</li> <li>- LFP and, LiMnO<sub>2</sub> cathodes</li> <li>- Applications: consumer electronics, power tools and grid storage</li> </ul>
<b>SouthRiver Products Ltd.</b> <a href="http://www.southriverproducts.com/">(http://www.southriverproducts.com)</a>	China	<ul style="list-style-type: none"> <li>- Cylindrical and pouch cells. LiPo cells</li> <li>- LFP cathode</li> <li>- Applications: consumer electronics</li> </ul>
<b>SinoPoly</b> <a href="http://www.sinopolybattery.com/">(http://www.sinopolybattery.com)</a>	China	<ul style="list-style-type: none"> <li>- Prismatic plastic case cells</li> <li>- LFP batteries</li> <li>- Applications: EV and ESS</li> </ul>
<b>SK innovation SK mobile energy</b> <a href="http://www.skme.co.kr/">(http://www.skme.co.kr/)</a>	Korea	<ul style="list-style-type: none"> <li>- Pouch cells</li> <li>- NCM cathode</li> <li>- Customers: Mercedes S400 BlueHYBRID, KIA Soul EV, Continental, ads-tec</li> </ul>
<b>Sunhigh Battery</b> <a href="http://sunhighbattery.diytrade.com/">(http://sunhighbattery.diytrade.com/)</a>	China	<ul style="list-style-type: none"> <li>- Cylindrical and prismatic cells. LiPo cells</li> <li>- LFP cathode</li> </ul>
<b>TCL High Power Batteries</b> <a href="http://www.tclbattery.com/">(http://www.tclbattery.com)</a>	China	<ul style="list-style-type: none"> <li>- Pouch cells. LiPo cells</li> </ul>
<b>Tenergy</b> <a href="http://www.tenergybattery.com/">(www.tenergybattery.com/)</a>	USA	<ul style="list-style-type: none"> <li>- Cylindrical, prismatic and pouch cells. LiPo cells</li> <li>- LFP cathodes</li> <li>- Applications: consumer electronics products, E-bikes, miner lamps, UPS, backup power, EV and satellite communication systems</li> </ul>

*Table A-12. Li-ion battery market database (continued)*

BATTERY COMPANY / JOINT VENTURES	COUNTRY	TECHNOLOGIES & PRODUCTS ACTIVITIES & SOME CUSTOMERS
<p><b>Toshiba</b> (<a href="https://www.toshiba.com/tic/">https://www.toshiba.com/tic/</a>)</p>	Japan	<ul style="list-style-type: none"> <li>- Slim, small-sized prismatic batteries</li> <li>- LMO-LTO cells. Negative electrode uses new nano-particles to prevent organic liquid electrolytes from reducing during battery recharging</li> <li>- Customers: Honda (Fit EV), Mitsubishi (I MiEV-M, MiniCab, Fuso, Outlander Sport) and Fiat)</li> </ul>
<p><b>Valence</b> (<a href="http://www.valence.com/">http://www.valence.com/</a>)</p>	USA	<ul style="list-style-type: none"> <li>- 18650 Cylindrical Energy Cells and 26650 Cylindrical Power Cells</li> <li>- Proprietary lithium iron magnesium phosphate (LiFeMgPO<sub>4</sub>) active material</li> <li>- Customers: Mercedes Benz eVito, , Submergence Group, Beneteau, Electric Vehicles International, Enova Systems, Epyon, Optare Buses (Optare Solo), Oxygen Scooters (Oxygen Cargoscooter), Paneltex, Royal Huisman, Segway, Siemens hybrid marine drive, Smith Electric Vehicles, Tennant Ecolab Company, Wrightbus, ZF Marine and ZYTEK Systems</li> </ul>
<p><b>Varta AG</b> -Joint venture with Volkswagen- (<a href="http://www.varta.com/">http://www.varta.com/</a>)</p>	Germany	<ul style="list-style-type: none"> <li>- Cylindrical, prismatic and pouch cells</li> <li>- LiPo LMO batteries</li> <li>- Customers: VW, Engion</li> </ul>
<p><b>Winston Battery Limited</b> (<a href="http://en.winston-battery.com/index.php">http://en.winston-battery.com/index.php</a>)</p>	China	<ul style="list-style-type: none"> <li>- Plastic case prismatic cells</li> <li>- LFP cathode</li> <li>- Applications: submarine ESS, UPS and EV (FAW)</li> </ul>
<p><b>Yoku Energy (Shenzhen Co.)</b> (<a href="http://www.yokuenergy.com/en/">http://www.yokuenergy.com/en/</a>)</p>	China	<ul style="list-style-type: none"> <li>- Cylindrical, prismatic and pouch cells. LiPo cells</li> <li>- NCM and LFP cathode cells</li> <li>- Applications: consumer electronics and E-bikes</li> </ul>
<p><b>Yuntong Power Co.</b> (<a href="http://www.yuntong-batt.com">http://www.yuntong-batt.com</a>)</p>	China	<ul style="list-style-type: none"> <li>- Cylindrical and pouch cells</li> <li>- LiPo and LFP cathode cells</li> <li>- Applications: consumer electronics, Golf Trolley, RC Toys, power tools and E-bikes</li> </ul>

## APPENDIX E. SAFETY ANALYSIS FOR CELLS SELECTION

---

Safety is a serious issue in Li-ion battery technology. Much work has been done to improve batteries reliability, both adopting safer cell chemistries and better control of the cell manufacturing process, as well as by external cell protection electronics incorporated into the battery packs [22]. Nonetheless, all approaches are expected to depress the specific energy, so an acceptable compromise between energy and safety has to be achieved. Hence, Li-ion systems can still be hazardous.

The most common strategies regarding the safety of the cell are outlined next [17]:

- *Cell chemistries and structures*

Electrolyte and electrode combinations have to operate within the stability windows of all cell components (Figure 1-6) and all components may not contain toxic metals. In addition, non-cobalt based Li-ion alternatives may be found. Valence, for instance, has patented Saphion technology (Table A-12), which is made using a phosphate based cathode material (they are stable in overcharge or short circuit conditions).

At present, the concept of a fully solid lithium metal polymer battery is very appealing and it is being considered in industrial laboratories involved in electric transportation. An approach has been to consider solvent-free lithium conducting solid membranes, based on homopolymers (*e.g.* lithium trifluoromethanesulfonate,  $\text{LiCF}_3\text{SO}_3$ ), as electrolyte. Many studies are still however being carried out as the ionic conductivity of these membranes remains at high levels only at temperatures above 70°C. Regarding the metallic lithium anode, it could be used with no dendrite formation risk if ceramic stiffening additives (*e.g.* silica powder) were added to solid polymer electrolyte.

The intrinsic value of polymer electrolyte continues to hold industrial interest and PGEs are the most used ones. Currently, poly (vinylidene-co-hexafluoropropylene) (PVDF-HFP) copolymer matrix and polyalkaline oxide polymers, which are under production in Japan, are relevant.

Another emerging electrolyte is based on ionic liquids (ILs): low temperature molten salts. Nevertheless, it is likely that they will be used as additives to common organic liquid electrolyte solutions given to their high cost.

- *Additives* to make SEI more stable and enhance its thermal stability.

They cause the polymerisation of monomers that exist within the cells, which stops the charging process, when high values of voltage or pressure inside the cell are reached.

- *Redox shuttles* to protect from overcharge.

They are inactive materials that are added to the electrolyte to maintain cell potential within operating ranges and prevent damaging reactions. They provide a current bypass mechanism when the cell exceeds a certain voltage. The ideal redox or chemical shuttle operates at or near the voltage of the fully charged cell and takes up the extra charge passed during overcharge. That is, it is oxidised to be thereafter diffused through the electrolyte into the negative electrode, where it is reduced to return finally to the cathode, where continues the redox process. This strategy is restricted by the ability of the electrolyte to absorb the current, *i.e.* by rate of diffusion of the material.

- *Shut-down separators* to prevent thermal runaway.

These separators are designed to soften at high temperatures, normally above 130°C, so that the pores are closed. This way, the current flow is blocked in order to prevent overheating. There might be however a problem if temperature keeps rising and separators collapse. For this reason, the ongoing investigations are focused on polymer blending, so that one of them softens at 130°C but the other is stable up to 200°C.

- *Oversizing*

This safety and/or operating margin is used to prevent potential problems. Nonetheless, the main handicap of this strategy is the cost.

- *External electronic circuits (Battery Management System, BMS)*

They control the cell by cutting the power when voltage and temperature go over the upper operating limits. It is an efficient method, but it is external to the cell, so any circuit failure (*e.g.* misuse, inappropriate connection, etc.) makes the cell not to be protected.

There is high innovation pressure by legislation and competition, but reliability problems dismiss profit and market reputation. Even though Li-ion cells are designed with integrated passive safeguards, the complexity of the cell and the numerous conditions of use present challenges, both for designing safe cells and also for battery safety testing standards [233].

Test programs for new systems and applications (operation modes), which are capable to demonstrate reliability targets (especially in abusive conditions), are therefore impending. Thus, optimisation of tests time and resources, as well as estimation of all factors (especially the accelerated ones), are required. There are different approaches for system safety analysis, such as:

- Figure A-26 shows an alternative approach for functional safety evaluation and improvement of batteries. It is a systematic methodology to optimise the testing plan. A battery is demonstrated to be reliable when all the tests run without failure.
- C. J. Mikolajczak *et al.* [79] developed a scientific methodology for the investigation of Li-ion battery failures, which includes: collecting information about the incident; dissecting the remains of the incident device and battery pack; conducting visual, X-ray, and SEM examinations of failed and exemplar cells; and electrical testing of charging and battery protection system components.

These two approaches [79, 234] are a great help for the construction of a Failure Modes and Effects Analysis (FMEA, see following section) matrix. Selection of relevant components and key failures,  $F_i$ , make possible the definition of the operation dimensions for each application.

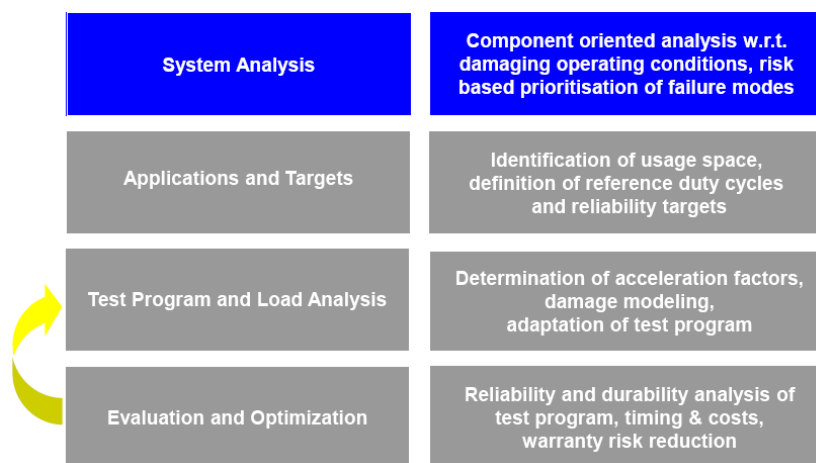


**Figure A-26.** Load matrix process [234]

## **E.1. FAILURE MODES AND EFFECTS ANALYSIS (FMEA) [22]**

### **E.1.1. FAILURE MODES**

Battery failures are usually defined in terms of the lifetime of the battery, as failure mechanisms not always lead to immediate and complete breakdown of the cell. The inability of a battery to fully meet its specified performance is considered a failure even if the battery

is still working. This performance degradation is due to constant and gradual deterioration of the active chemicals, which depends on the operation conditions (T, C-rate and DOD) over the lifetime of the battery. In these cases, measurement of SOH can provide an advance warning of impending failure.

Unfortunately, several failure mechanisms may exist simultaneously in a battery. Short circuits, open circuits and external faults can also cause failures:

- *Short circuits* can be a result of contaminated materials, mechanical tolerance problems (manufacturing defects), vibrations, changes in active materials, such as presence of dendrites or lithium plating, etc. Internal shorts are of particular concern, as they can lead to catastrophic failure.

Most Li-ion cells are designed with integrated safety devices that respond to open external electrical load when they detect over current or excessive pressure build up in the cell. These safety devices cannot mitigate all internal cell fault situation and, consequently, an internal short circuit may take place. In case it is located in a very small area, the heat of abnormal electrical current flow and the subsequent heat of the exothermic chemical reaction, together with an inability to transfer sufficient heat away, cause the internal cell temperature and pressure to increase rapidly, which can end in cell rupture. Moreover, thermal runaway can occur and combustible materials inside the cell may be therefore ignited [235].

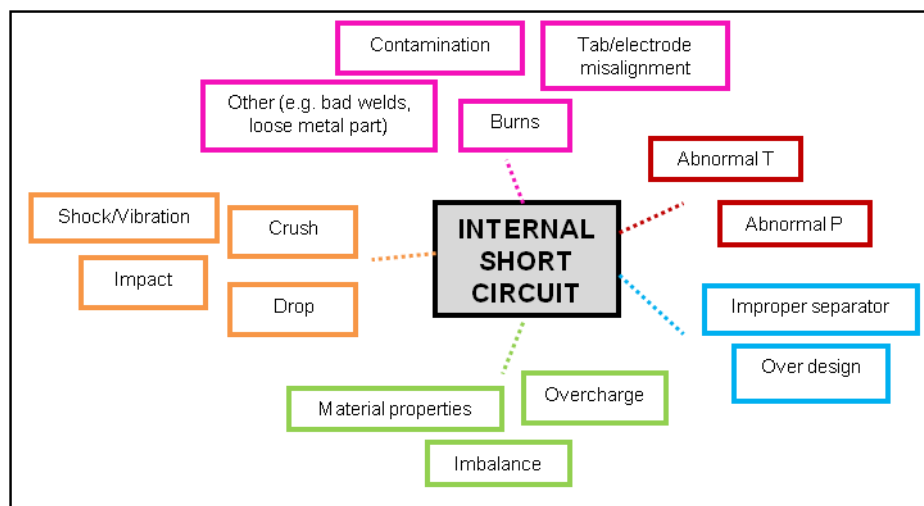


**Figure A-27.** Some root causes of internal short circuits

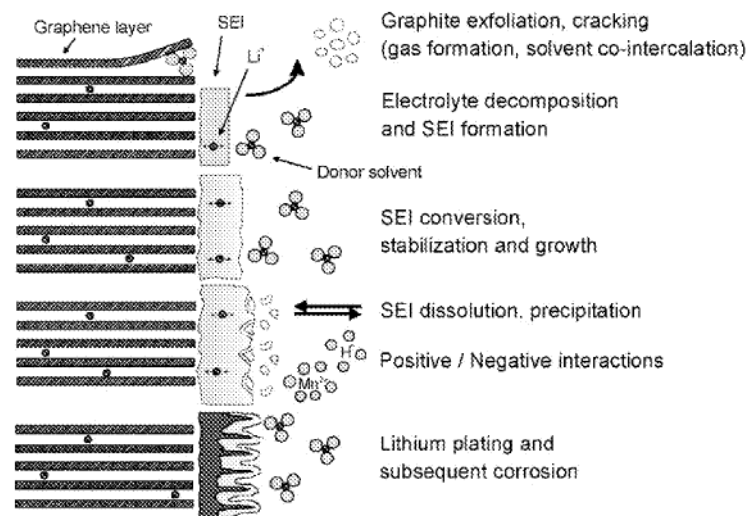
Figure A-27 shows some drives that can engender localised internal short circuits. However, they mainly occur due to a pathway between the cathode and anode that starts with an unintended highly localised charge flow. This results in joule heating, owing to the internal resistance, with subsequent heating of the active materials. These latter may be

therefore destabilised, starting, in turn, a self-sustaining exothermic reaction. As mentioned before, this may lead to catastrophic structural failure of the battery casing and the risk of additional combustion, as a result of exposure to outside air.

- *Open circuits* can be caused by broken welds, loose connections or cracks.
- *External faults*, such as BMS failures, can lead to problems instead of protecting the cells.

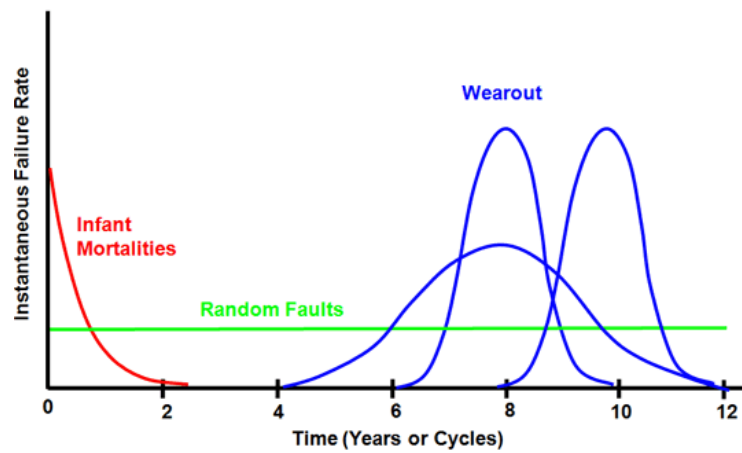
Early failures, commonly called “*infant mortalities*”, may be also brought about due to random latent defects in the components of the battery, such as contamination of active materials, or manufacturing defects. These failures are more difficult to characterise.

Gradual deterioration of cell chemicals, as shown in Figure A-28 for instance for graphite anode-electrolyte interface (e.g. loss of electrolyte due to chemical breakdown or leaks, dendrite growth and lithium plating at the anode, etc. or dissolving of the cathode material, etc.), can lead to *wearout failures*. This results in loss of capacity, which in turn may cause out of tolerance performance of the cell. These failures may be due to operational conditions/pattern.



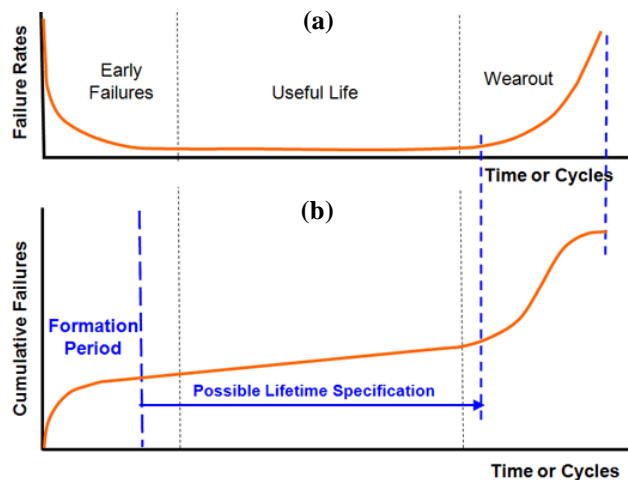
**Figure A-28.** Processes that take place on the graphite anode-electrolyte interface layer [150]. Reactions of the anode with the electrolyte are considered to be the major source of aging at the negative electrode

Figure A-29 shows cell failure distributions due to a variety of failure modes (several distributions may exist simultaneously). The curves represent histograms showing number of units failing at different times. Wearout failures (in blue) may occur either over a short period or be spread over longer time and they may also appear after different periods. Each wearout failure has its own characteristic distribution.



**Figure A-29.** Cell failure distributions [22]

The failure distribution for the cell is the sum of every distribution of all contributing factors, as it can be seen in Figure A-30. Instantaneous failure rate curve (Figure A-30 (a)) shows the combination of all the failure mechanisms over time. The cumulative failure distribution corresponding to the instantaneous failure rates (Figure A-30 (b)) indicates possible lifetime specification.



**Figure A-30.** Instantaneous failure rate curve (a) and cumulative failure distribution of a cell (b) [22]

Some of most common failure modes are summarised in Table A-13.

**Table A-13. Selected key failure modes of lithium ion cells [234]**

FAILURE MODE	CAUSE OF FAILURE	INFLUENCE FACTORS	
Increased internal resistance  Reduced capacity	Degradation of SEI at negative electrode	SOC	High @ low SOC and discharging Medium @ other conditions
		DOD	High
		T	High
		Power	Medium
		Vibration /Shock	Medium
Increased self-discharge  Hard short-circuit and subsequent cell venting	Lithium plating at negative electrode	SOC	High @ low SOC and charging at low T Low @ other conditions
		DOD	Low
		T	High
		Power	Medium
		Vibration /Shock	Low
Increased resistance  Cell swelling and subsequent venting	Decomposition of electrolyte	SOC	High @ low SOC and charging at low T Low @ other conditions
		DOD	Low
		T	High
		Power	Medium
		Vibration /Shock	Low
Increased resistance and reduced power  Reduced capacity	Crack of conducting paths	SOC	Low
		DOD	Medium
		T	Low
		Power	Low
		Vibration /Shock	High

## E.1.2. CAUSES AND EFFECTS

### E.1.2.1. CELL DESIGN

Weak mechanical design, inadequate pressure seals and vents, poor quality materials and improperly specified tolerances can be responsible for many potential failures.

Lack of precision and repeatability, as well as out of tolerance components when manufacturing, means potential short circuits, leaks, unreliable connections and contamination:

- Vibrations on the electrode current collector foils give rise to short circuits.
- Cavities reduce cell capacity, increase impedance and hinder heat dissipation.
- Contamination of the active chemicals could result in overheating, pressure build up, reduced capacity, increased impedance, self-discharge and short circuits.
- Poor control of electrode particle morphology. Particle size needs to be very small and uniform to achieve the specified cell power handling capability.

- Variable coating thicknesses of the active components on the electrodes. This could affect cell capacity, impedance and self-discharge.
- Sealing quality. This can result in localised heat accumulation and poor connections. Therefore, in leakage and/or ingress of outer undesirable components, such as water, and potential safety problems in consequence. Besides, loss of active chemicals may be observed.
- Mechanical weaknesses. The most likely outcomes would be leakage of the electrolyte, cracking or splitting (which also causes leakage), or distortion.

Moreover, unsuitable cell design for the application (even though it is a good battery) can provoke failure. The first step is hence to ensure that the most appropriate battery is chosen.

### **E.1.2.2. UNCONTROLLED OPERATING CONDITIONS**

Performance of Li-ion cells depends strongly on temperature and operating voltage. Figure A-31 shows the behaviour of this technology at different voltage and temperature ranges. These two parameters must be kept, as indicated with the green box, within 1.5-4.2 V and (-20)-(+80) °C, respectively, in order the cell not to be damaged.

#### **a. Voltage**

##### **a.1. Over-voltage**

Unsuitable charging profile can lead to failure. If the charging voltage is increased beyond the recommended upper cell voltage, typically 4.2 V, it can be lead to:

##### *- Lithium plating*

With excessive current, lithium ions cannot be accommodated quickly enough between the intercalation layers of the anode and they accumulate on the surface of the anode as metallic lithium, as shown in Figure A-32. As a result, there are less free lithium ions for chemical reactions and capacity is lost irreversibly. Furthermore, short circuit between the electrodes may take place as lithium plating can be in dendrite form that can fracture the separator.

##### *- Gas formation*

Overcharging can cause gas formation with the consequent loss of active materials, resulting in capacity loss.

##### *- Chemical breakdown of the electrolyte*

- *Overheating*

Excessive current also increases temperature (Joule effect).

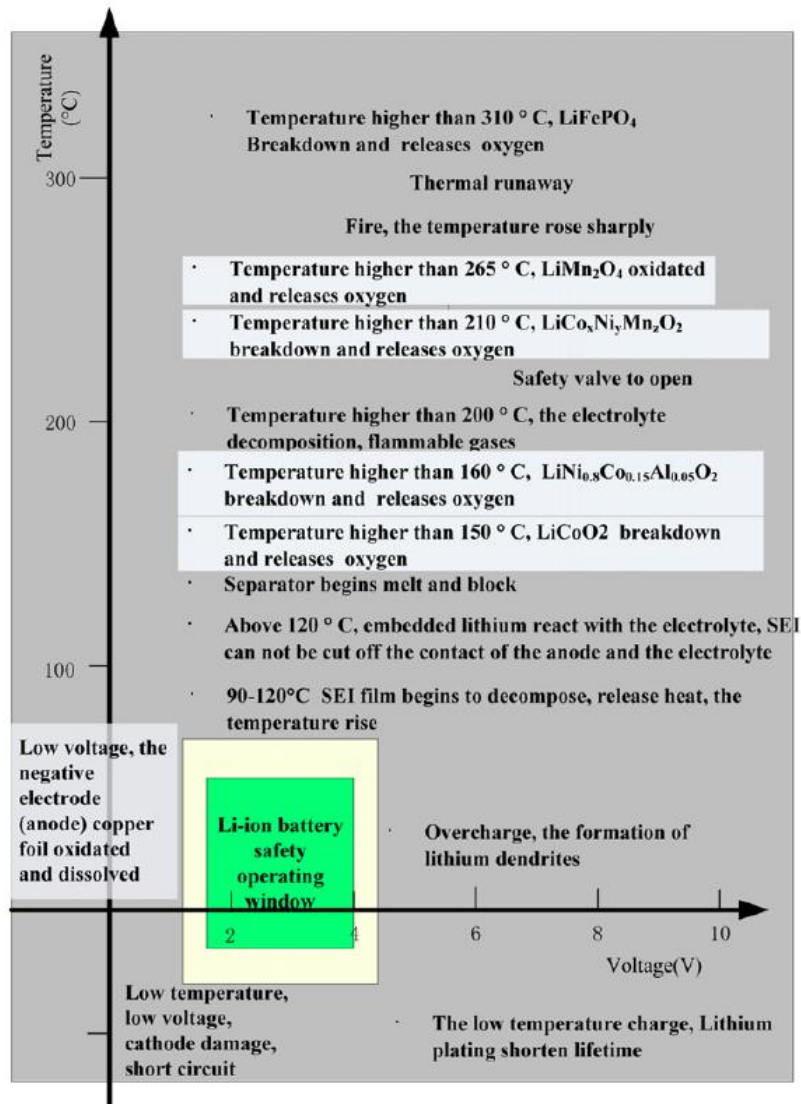
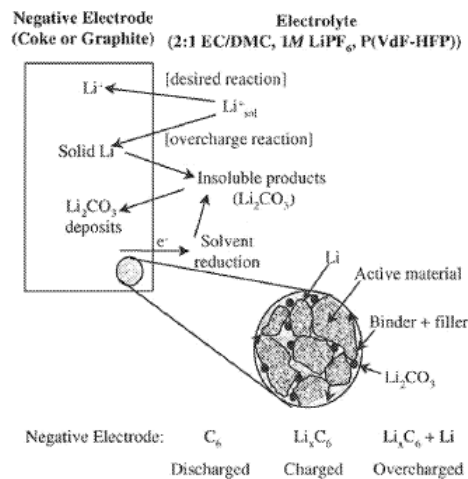


Figure A-31. Lithium-ion cell safety operating window [236]



**Figure A-32.** Reactions occurring on carbon based negative electrode during charge and overcharge [151]

### a.2. Over-discharge

Li-ion cells should never be discharged too low. Anodic dissolution of copper current collector can take place when Li-ion cells are discharged to voltages below 1.5 V, which causes oxidation of Cu atoms to Cu<sup>2+</sup> ions. These ions could reduce to Cu metal again when cell recovers normal voltage range, but they might disperse on the surface of the anode active materials [237]. If cell voltage falls below the cut-off voltage (either by over-discharging or because of storage for extended periods), they ought not to be recharged because copper shunts, which may have formed inside the cells, can lead to an electrical short [237]. If so, the cells might become unstable, causing excessive heat, gas generation and swelling. Moreover, the reaction of copper foil would greatly deteriorate the recharge and discharge performance [238].

#### - Anodes

Anode copper current collector can be dissolved into the electrolyte, which increases the self discharge rate of the cell. Furthermore, it can cause an internal short circuit.

#### - Cathodes

Cathodes that contain oxygen (LCO, LMO) can deteriorate over cell cycling with oxygen release and consequent permanent capacity loss.

### b. Temperature

Environmental conditions are very important. High ambient/storage temperature accelerates any process that makes the cell to fail.

### **b.1. Low temperature operation**

Low temperatures might cause electrode materials to shrink. In addition, the reduced reaction rate makes more difficult the insertion of the lithium ions into the intercalation spaces. Thus, not only is the power reduced, but anode plating is also enhanced with irreversible capacity loss in consequence.

### **b.2. High temperature operation**

Problems due to operation at high temperature can result in the destruction of the cell. Raising the reaction rate increases the power output, but higher currents also enhance internal heat generation (highly localised joule heating), therefore leading to even higher temperatures. Unless heat is removed faster than it is generated, thermal runaway will take place.

Several stages are involved in the progress to thermal runaway and each one results in increasingly permanent damage to the cell:

- The first stage is the breakdown of the thin passivating SEI layer on the anode, due to overheating or physical penetration.

The initial overheating may be caused by excessive currents, overcharging or high external ambient temperature. The breakdown of the SEI layer starts at the relatively low temperature of 80°C and once this layer is breached the electrolyte reacts with the anode in an uncontrolled way.

- As the temperature increases, heat from anode reaction causes the breakdown of the organic solvents used in the electrolyte releasing flammable hydrocarbon gases. This typically starts at 110 °C but with some electrolytes it can be even at 70°C.

The cells are normally fitted with a safety vent, which makes possible the controlled release of gases to relieve the internal pressure in the cell. This way, the possibility of an uncontrolled rupture of the cell is avoided.

- At around 135 °C, the polymer separator melts, which leads to the short circuits between the electrodes.
- Eventually heat from the electrolyte decomposition causes breakdown of the cathode with oxygen release. This can burn both the electrolyte and gases inside the cell.

The breakdown of the cathode is also highly exothermic.

### **c. Pressure**

Internal pressure may increase due to raised temperature and decomposition of the material. It favours chemical reaction, but side reactions are also enhanced. Excessive pressure can cause mechanical failure of the cell: short circuit, cell distortion and, ultimately, breakdown.

High pressure and temperature could compromise the integrity of the cell casing, violently releasing volatile gases which may further ignite [233]. Pouch cells are prone to swelling due to overheating before dangerous pressure limits are reached. This can contribute to problems in fitting the cell into the battery enclosure.

### **E.1.2.3. MECHANICAL FATIGUE**

The electrodes of Li-ion cells expand and shrink during charging and discharging due to the effect of the intercalation of the lithium ions into and out of the crystal structure of the electrodes. The cyclic stresses on the electrodes can eventually lead to cracking of the particles, which results in increased internal impedance or, in the worst case, in the breakdown of anode SEI layer, which could lead to cell overheating and immediate cell failure.

### **E.1.2.4. SELF-DISCHARGE**

Self-discharge depends on cathode and cell preparation, nature and purity of the electrolyte, temperature and time of storage [239].

Self-discharge contributes to either reversible or irreversible capacity losses because of consumption of active lithium. The extent to which capacity loss is irreversible depends on the charge and discharge rates used on the subsequent cycling. Nevertheless, self-discharge has to be taken into account particularly when storing at high temperature.

## **E.2. TESTS AND PATENTS**

Safety testing protocols and abuse tests for Li-ion battery are gathered in Appendix B. The main lithium battery patents that address battery safety are gathered in Table A-14.

**Table A-14. Lithium battery safety patents**

<b>PATENT ISSUE</b>	<b>DETAILS</b>	<b>DESCRIPTION</b>
<b>Battery electrode structure</b>	<i>Patent No.:</i> US 2009/0142659 A1 <i>Assignee:</i> BYD	This patent describes an electrode structure which is connected to the terminal by means of a pressure heat treatment or a mechanism of compression. Besides, in order to reduce internal resistance (greater safety), the connection is reinforced by welding.
<b>Battery cell of improved safety</b>	<i>Patent No.:</i> WO 2008/130148 A1 <i>Inventors:</i> You, Scungjae; Chonggu Narae Apt.; <i>et al.</i> <i>Assignee:</i> LG Chem, Ltd.	The invention relates to a battery cell of improved safety and, more particularly, to a battery cell constructed in a structure in which an electrode assembly is mounted in a battery case made of a laminate sheet including a metal layer and a resin layer. The battery case is thermally welded along edge of a receiving part thereof to form a sealing part.
<b>Battery Pack</b>	<i>Patent No.:</i> US 7,088,075 <i>Inventors:</i> Baba; Makoto (Kanagawa, JP), Sugita; Hidehisa (Fukushima, JP) <i>Assignee:</i> Sony Corp. (Tokyo, JP)	This patent describes a battery pack and an external protection circuit (it has a function that measures the performance of the batteries), which are housed in a case but are independent one another.
<b>Battery protection mechanism</b>	<i>Patent No.:</i> US 2009/0108808 A1 <i>Assignee:</i> BYD	This patent describes a system and methodology for detecting an internal failure of the cell while charging/discharging. The system includes circuits to determine and characterise: SOC, voltage evolution, voltage drop, etc.
<b>Cathode Materials for Lithium batteries</b>	<i>Patent No.:</i> US 2009/0142658 A1 <i>Assignee:</i> BYD	This patent describes the developed LFP cathodes that enhance thermal stability.
<b>Lithium Ion Battery</b>	<i>Patent No.:</i> US 2009/0142658 A1 <i>Assignee:</i> BYD	This patent describes the design of a battery with better performance at high current discharge rates in terms of mechanical stability and heat dissipation.
<b>Lithium Ion Battery Containing an Electrolyte Comprising an Ionic Liquid</b>	<i>Patent No.:</i> US 2010/029783 A1 <i>Assignee:</i> SAFT	This patent describes the design of a non-flammable electrolyte for Li-ion batteries.
<b>Lithium Secondary Battery Pack having Internal Protection Circuit</b>	<i>Patent No.:</i> US 7,701,169 B2 (2010) <i>Assignee:</i> BYD	This patent describes the design of a battery with internal protection circuit to prevent short circuit, overload, over-discharge and overcurrent.
<b>Rechargeable battery with charge control</b>	<i>Patent No.:</i> US 2006/0186857 A1 <i>Assignee:</i> SAFT	This patent describes the control strategy of the current external regulator. The regulator limits the charge current (loading/unloading) depending on both the amount of Ah consumed and temperature.
<b>Safety Device for a Sealed Cell</b>	<i>Patent No.:</i> US 2006/0019150 (2006) <i>Assignee:</i> SAFT	This patent describes the safety system of a sealed cylindrical or prismatic cell. When the pressure builds up inside the cell, a security system enables the expulsion of generated gas so that internal pressure does not exceed the security limit. This way, explosion is prevented.
<b>Secondary battery</b>	<i>Patent No.:</i> US 2006/0008699 A1 <i>Assignee:</i> LG Chemical, Ltd.	This patent describes the development of a battery with an external temperature gauge. This indicator alerts the user by changing colour.

**Table A-14. Lithium battery safety patents (continued)**

PATENT ISSUE	DETAILS	DESCRIPTION
<b>Secondary Battery with Protective Circuit</b>	<p><i>Patent No.:</i> US 7,079,003  <i>Inventors:</i> Furuta; Kazutaka (Kanuma, JP), Kawazu; Masami (Kanuma, JP)  <i>Assignee:</i> Sony Corp. (Tokyo, JP)</p>	<p>This patent describes a secondary battery, a heat-sensitive element which varies in resistance value due to a change in temperature. It can happen when charge or discharge current flows into or out of the battery. Accordingly, when a main switch element generates heat due to an overcurrent, a change in resistance value of the battery will allow an auxiliary switch to be turned on, thereby causing first and second auxiliary fuses to be blown. The charge or discharge current causes no power consumption at the battery, so high efficiency is provided. It is suitable for compact design.</p>
<b>Separator Including Electroactive Material for Overcharge Protection</b>	<p><i>Patent No.:</i> US 2009/0029261 A1  <i>Assignee:</i> A123</p>	<p>This patent describes the separator designed by A123 for Li-ion batteries.</p>
<b>System and Method for Efficiently Implementing a Battery Controller for an Electronic Device</b>	<p><i>Patent No.:</i> US 7,091,697  <i>Inventors:</i> Mader; Urs H. (Cupertino, CA), Sato; Hideyuki (Chiba, JP)  <i>Assignee:</i> Sony Electronics, Inc. (Park Ridge, NJ).</p>	<p>This patent describes a system and method for managing effectively the operating power of an electronic device that may include a coupled battery pack. A battery controller may be configured as a single integrated-circuit device (that may include a charge pump device) to alternately manage the battery pack either in a single-cell implementation or in a dual-cell implementation.</p>
<b>Vent for an Electrochemical Cell</b>	<p><i>Patent No.:</i> US 4,664,287 (1987)  <i>Assignee:</i> SAFT</p>	<p>This patent describes a vent system to minimise pressure inside the cell in order not to generate gases.</p>

## APPENDIX F. PUBLICATIONS AND PARTICIPATION IN CONFERENCES

---

### *Papers:*

- E. Sarasketa-Zabala, E. Martinez-Laserna, M. Berecibar, I. Gandiaga, L. M. Rodriguez-Martinez and I. Villarreal, *Realistic lifetime prediction approach for Li-ion batteries*, under preparation (2014).
- E. Sarasketa-Zabala, F. Aguesse, I. Villarreal, L.M. Rodriguez-Martinez, C.M. López and P. Kubiak, *Understanding lithium inventory loss and sudden performance fade in cylindrical cells with deep-discharge steps*, submitted to The Journal of Physical Chemistry (2014).
- E. Sarasketa-Zabala, I. Gandiaga, E. Martinez-Laserna, L. M. Rodriguez-Martinez and I. Villarreal, *Cycle ageing analysis of a LiFePO<sub>4</sub>/graphite cell with dynamic model validations: towards realistic lifetime predictions*, Journal of Power Sources (2014). DOI: 10.1016/j.jpowsour.2014.10.153
- E. Sarasketa-Zabala, I. Gandiaga, L. M. Rodriguez-Martinez and I. Villarreal, *Calendar ageing analysis of a LiFePO<sub>4</sub>/graphite cell with dynamic model validations: towards realistic lifetime predictions*, Journal of Power Sources 272 (2014) 45-57. Impact factor: 5.257.
- E. Sarasketa-Zabala, I. Laresgoiti, I. Alava, M. Rivas, I. Villarreal and F. Blanco, *Validation of the methodology for lithium-ion batteries lifetime prognosis*, EVS27 conference paper (2013).
- E. Sarasketa-Zabala, L. Otaegi, L. M. Rodriguez-Martinez, M. A. Alvarez, N. Burgos, F. Castro and I. Villarreal, *High temperature stability of porous metal substrates under highly humidified hydrogen conditions for metal supported Solid Oxide Fuel Cells*, Solid State Ionics 222-223 (2012) 16-22. ISSN: 0167-2738. Impact factor: 2.564.
- L. M. Rodriguez-Martinez, M. Rivas, L. Otaegi, N. Gomez, M. A. Alvarez, E. Sarasketa-Zabala, J. Manzanedo, N. Burgos, F. Castro, A. Laresgoiti and I. Villarreal, *Tubular metal supported solid oxide fuel cell manufacturing and characterization*, ECS Transactions, 35 (1) (2011) 445-450.

- L. M. Rodriguez-Martinez, L. Otaegi, E. Sarasketa, N. Gomez, N. Arizmendiarieta, M. A. Alvarez, M. Rivas, N. Burgos, F. Castro, I. Villarreal and A. Laresgoiti, *Influence of interconnects in long term stability of tubular metal supported SOFCs*, Proc. 9th Eur. Solid Oxide Fuel Cell Forum (2010) 34-43.

***Participation in conferences:***

- **Oral presentation** in lecture: E. Sarasketa-Zabala, I. Gandiaga, E. Martinez-Laserna, L.M. Rodriguez-Martinez and I. Villarreal, *Realistic approach to lifetime prediction for Li-ion batteries*, Power Our Future 2014, 2-4 Apr. 2014, Vitoria-Gasteiz, Spain.
- **Oral presentation** in lecture: E. Sarasketa-Zabala, I. Laresgoiti, I. Alava, M. Rivas, I. Villarreal and F. Blanco, *Validation of the methodology for lithium-ion batteries lifetime prognosis*, EVS27, Nov. 17-20 2013, Barcelona, Spain.
- E. Sarasketa-Zabala, J. Münnix, A. Warnecke and D.U. Sauer, *Methodology for lithium-ion cylindrical cells post-mortem-analysis*, **poster** exhibition in 5<sup>th</sup> Kraftwerk Batterie, 26-27 Feb. 2013, Aachen, Germany.
- **Oral presentation** in lecture: E. Sarasketa-Zabala, I. Laresgoiti, I. Gandiaga, I. Villarreal and F. Blanco, *A new multidisciplinary methodology for lithium-ion cells selection for novel applications*, Power Our Future 2012, 20-21 Mar. 2012, Vitoria-Gasteiz, Spain.
- E. Sarasketa-Zabala, I. Gandiaga, I. Villarreal and F. Blanco, *Methodology for the selection of lithium-ion cells to meet the requirements of energy and transport applications*, **poster** exhibition in 4<sup>th</sup> Kraftwerk Batterie, 6-7 Mar. 2012, Münster, Germany.

